ISSN 1849–0751 (On–line)
ISSN 0013–7448 (Print)
UDK 621.31

# Journal of Energy

VOLUME 68 Number 2–3 | 2019 Special Issue



ENERGIJA

# Journal of Energy

**Scientific Professional Journal Of Energy, Electricity, Power Systems**

Online ISSN 1849–0751, Print ISSN 0013–7448, VOL 68

**Published by**

**HEP d.d.,** Ulica grada Vukovara 37, HR–10000 Zagreb

**HRO CIGRÉ,** Berislavićeva 6, HR–10000 Zagreb




# EDITORIAL

Journal of Energy special issue: Papers from 12th International Conference of the Croatian Nuclear Society "Nuclear Option for CO2 Free Energy Generation".

Welcome to this special issue, which is based on selected papers presented at the 12th International Conference of the Croatian Nuclear Society "Nuclear Option for CO2 Free Energy Generation", held in Zadar, Croatia, on June 3rd–6th, 2018.

This International Conference was organized by the Croatian Nuclear Society in cooperation with International Atomic Energy Agency (IAEA), Croatian State Office for Nuclear Safety and University of Zagreb, Faculty of Electrical Engineering and Computing. The goal of the Conference was to address the various aspects of the implementation of nuclear energy as CO2 free electricity source in the countries with small and medium electricity grids and in power system in general. The conference also focuses on the exchange of experience and co-operation in the fields of the plant operation and maintenance, nuclear fuel cycle, nuclear safety and safety upgrades, spent fuel and radioactive waste management, regulatory practice and environment protection.

The conference was organized in nine oral sessions and one poster session. In addition, round table on "Knowledge Management's Challenges and Opportunities in Nuclear Safety, Security, Safeguards and Engineering" and IAEA Panel on „Technology Developments in Small Modular Reactors and Prospects in Europe as an Emission Free and Flexible Electricity and Heat Source" were held. In three Conference days authors presented 48 papers orally and 38 papers in poster session. 127 participants came from 25 countries representing equipment manufacturers and utilities, universities and research centres, and international and government institutions. Seven invited lectures were held and 86 papers were accepted by international programme committee.

The importance of international cooperation for the assessment of the nuclear option has been recognized by everybody planning to introduce nuclear power plant to the grid. That is even more important for small and medium countries having limited resources and specific requirements due to limited grid size. The Conference topics reflect some current emphasis, such as possible role of nuclear energy as a CO2 free energy source in country's energy strategy and in general, new reactor technologies (especially small reactors), maintenance, operation and safety of the current nuclear power plants, move of the focus in nuclear safety toward severe accidents and accident management strategies for both reactor and spent fuel pool, improvement in nuclear safety, reactor physics and radiation shielding calculation tools and ever increasing requirements for minimization of environmental impact.

From 86 papers presented at the Conference, 20 papers were accepted for publication in this issue of Journal of Energy after having undergone the additional peer-review process. We would like to thank the authors for their contributions and the reviewers who dedicated their valuable time in selecting and reviewing these papers, both during the Conference and during the preparation of this special issue of Journal of Energy. It was very challenging to collect a balanced overview of the entire Conference. We believe that 20 papers which were selected for this issue represent some of the best research related to nuclear plant operation, maintenance and safety upgrades, energy planning, development of new reactors and technologies, reactor physics and radiation shielding, plant simulation, nuclear safety (both reactor and spent fuel pool), severe accident management, and risk and hazard assessment. We hope this special issue will provide a valuable insight into different aspects of nuclear and electrical engineering and reactor physics, as well as a pleasant and inspiring reading.

Guest Editors


**Dubravko Pevec**
**Davor Grgić**
University of Zagreb, Croatia

Journal of Energy
VOLUME 68 Number 2-3 | 2019 | Special Issue
journal homepage: http://journalofenergy.com/

# Electricity Market and Energy Policies Uncertainties for Investment in Life Time Operation of Nuclear Power Plants

**Željko Tomšić, Ivan Rajšl**
University of Zagreb Faculty of Electrical Engineering and Computing
Unska 3, 10000 Zagreb, CROATIA
Email: zeljko.tomsic@fer.hr; ivan.rajsl@fer.hr

## ABSTRACT

In the electricity sector, market participants must make decisions about capacity choice in a situation of radical uncertainty about future market conditions. Electricity sector is characterized by non-storability and periodic and stochastic demand fluctuations. Capacity determination is a decision for the long term, whereas production is adjusted in the short run. Today decisions pertaining to investment in new capacity or life time extension are surrounded by considerable uncertainties about the future economics of the projects. One reason is that in a deregulated market private investors typically have to bear a greater portion of the investment risk compared to a monopoly utility in a regulated market. This favours flexible investment alternatives with short-lead times and low capital requirements. Moreover, energy and climate policy – with feed-in tariffs for RES or green certificate system and the EU $CO_2$ ETS may add to investment uncertainties. From the economic point of view, the costs of LTO are usually lower than the construction of any other source of electricity. But in the aftermath of the Fukushima accident, policies towards nuclear energy in some countries were changed. Because of that economic life decisions are plant specific. In evaluating the future economic prospects of existing plant, the owners/utility focus on the unique circumstances of that plant and its cost and performance, and the future demand for electricity, and value of electricity. Nevertheless, quantification of the LTO costs is not an easy task. It is recognized that LTO costs are highly dependent on specific conditions related to each NPP, such as: design of the plant; NPP operating history including ageing conditions; regulatory requirements; full or partial replacement of components; refurbishment for LTO; accounting methodologies; etc. The risks that may have an impact on the economic case for the long term operation of NPP should be identified with pre mitigation impact and probability assessment.

**Keywords:** *Life Time Operation Nuclear Power Plant, Electricity Market, Energy Policies, Economic Analysis, Costs of Nuclear Power Plant.*

## 1 INTRODUCTION

NPP operating costs, capital investment costs in addition to decommissioning costs may decrease "profitability" of the NPP eventually to the extent that it could prove to be above projected wholesale electricity price on accessible markets. Therefore there are the following major tasks for economic assessment for LTO of NPPs: Evaluate the facts and circumstances that define the boundary conditions for the economics and long-term operation of NPP; ultimately marginal cost of electricity from NPP shall be determined to represent the justification of investments in all strategic upgrades required to continue operation in extended lifetime; identify scenarios that might lead to loss of competitiveness of NPP power generation; assess the risk of early closure i.e. not to continue operation after year the original lifetime of NPP; perform sensitivity analyses for the contributing parameters with the highest identified risk.

All, including additional capital expenditure necessary to meet regulatory requirements, have significant impact on the cost of nuclear power generation to the extent that is prudent to reconfirm/check the continuity of economic sustainability of NPP continues operation. The economic assessments of NPP operation for long term operation are necessary due to: required capital investment into upgrading the safety level of the plant, potential increase of operation & maintenance (O&M) costs, limited existing capacities for storage of low level and intermediate waste and spent nuclear fuel, regulation framework that may require additional capital investments, Potential increase of annual charges into national decommissioning funds, volatility of electricity market prices.

Each nuclear power plant has its own unique history of costs and performance. Large year-to-year fluctuations in costs are common for most NPPs as capital additions are undertaken and completed. Plant availability also varies from year to year as the plants undergo refuelling and planned maintenance during refuelling cycles. Also, unplanned repair outages contribute to cost and performance fluctuations.

Three types of nuclear power plant costs can have important and distinct roles in determining the economic life of individual units: historical capital costs, future capital additions (for regular operating time and for LTO), annual O&M and fuel costs.

It is important to stress that the economic evaluation of LTO measures is complicated and depends on the concrete circumstances for each plant.

Deregulation of electricity market is increasing competition and eliminating monopolies and guaranteed sales at fixed rates defined usually by government. Therefore, nuclear power plant owners endeavour to reduce the cost of plant life management.

The choice between LTO and building a new power plant, fossil-fuelled or nuclear or renewable, is influenced also by the size of the investment which is smaller for refurbishment than for a new construction.

To support the business case for extending the operating life of NPP (and delaying the start of decommissioning activities) it is need to undertake an independent economic assessment of the life extension.

Indeed, extending the operating lives of existing plants provides clear advantages. High capacity factors and low operating costs make nuclear plants some of the most economical power generators. And even when major plant components must be upgraded to extend operating life, these plants represent a cost effective, carbon-free asset that is critical to energy future. Extending the life of a major generating asset avoids the need for immediate investment in new generating capacity. The capital costs of plant life management for LTO will be smaller than investment in any type of replacement capacity, although there might be a need for additional investment in plant upgrading and safety improvements. Combining the plant upgrading and safety improvements with power uprating made lifetime extension even more cost effective. In addition, the kWh costs for waste management and decommissioning can be reduced.

In a deregulated electricity market power plant lifetime extension and upgrading are driven by cost and revenue consideration. Decision to continue operating an existing plant is based on its marginal generation cost, i.e., operation & maintenance, fuel cycle cost, taxes and capital cost compared to generation costs of other options. The marginal cost is lower for existing nuclear power plants than for most alternatives, therefore LTO is a lucrative option.

In case of Europe lifetime extension and uprating of NPPs are going hand in hand together with safety improvements. The cost for lifetime extension and consequently necessary safety upgrading are in the average €400 million per unit despite of the size.

For the purpose of economic analysis, can be identified two NPP operational life scenarios:
Scenario 1 – NPP operation to planned operating life and
Scenario 2 – Full life extension up to 20 years.

To make decision at least should be assessed the cost of each of these two scenarios to determine the most economically viable scenario. It is also need to understand the risks associated with these scenarios and the alternate power options that may be included in scenarios 1 and 2.

In addition to ranking the different NPP scenarios and alternate power options based on their LCOE, analysis of the risks associated with each option should be undertaken. This analysis should be considered along with the LCOE ranking of the options considered.

Future revenue and expenses can be determined by based on actual historic data, known future plans and the experience of NPP. Investment plan data is based, where possible, on indicative quotations that NPP has obtained for the major capital works.

## 2 ECONOMIC ANALYSIS FOR DECISON ON LTO OF NPP

### 2.1 Introduction

Responsibility for the economic performance of existing nuclear power plants and decision on life time extension lies with the utilities owning and operating them.

The objectives in nuclear plant life operation (LTO) decisions stem from broader electricity power system objectives, including the following:

- assuring adequate supplies to meet demand; minimizing the costs of electricity (including, increasingly, environmental costs);
- equitably treating both electricity consumers and plant owners in the recovery of costs; and increasingly, responding to intensifying market forces in the electric power industry.

The nuclear power plants represent a technical and financial asset with strategic significance for both the utility/corporation and the country.

Decision on life time extension includes many of the tasks associated with LTO that includes input to the corporate strategy and interaction with many corporate elements not directly associated with plant operations. These activities include economic evaluations of alternatives for major refurbishment or replacement projects as well as strategic decisions regarding use and disposition of the plant.

Today, elements for decision for LTO also depend of electricity market structure: regulated or deregulated market.

To assess the economic benefits of life time extension the following factors should be considered at regulated market:

- LTO economic dependence on a many ‘power system-level’ characteristics, including alternatives options for replacement capacity, short-term replacement energy costs during nuclear plant outages, corporate financial situation, and accounting policies
- LTO uncertainties: the long planning horizon determined by the licensing lead time, the lead time for possible replacement capacity and the period of actual operation. Furthermore the lack of industry large experience with LTO creates uncertainty about capital and operating costs, regulatory requirements and long-term plant performance.
- LTO should present interest for both customers and investors. From the viewpoint of investors and owners, the operating life of a nuclear unit will be determined primarily by its profitability rates relative to other available generation options. With respect to the customers, their major interest will be the minimisation of electricity rates.

It is not enough just to assess independently NPP and comprehensive approach in assessing the economic viability of actual operational lifetime should include a power system analysis. This means that in order to decide on economic viability of extended nuclear power generation, it should be compared the costs (or rather the present value) of this generation with the costs of replacement power. As replacement power alternatives can be generation on conventional or

innovative power sources, power purchases from power exchange, contracts with independent power producers or demand side management. Based on the power system analysis, utility selects the adequate grid development scenario for the next period (usually the time interval considered is 10-20 years) to meet the demand for electricity at the minimum cost, subject to a set of financial, resource, technical, environmental and political constraints.

## 2.2 Cost in existing nuclear power plant

Each nuclear power plant has its own unique history of costs and performance. Large year-to-year fluctuations in costs are common for most nuclear plants as capital additions are undertaken and completed. Plant availability also varies from year to year as the plants undergo refuelling and planned maintenance during 12, 18 or 24-month refuelling cycles. Also, unplanned repair outages contribute to cost and performance fluctuations.

Because of that economic life decisions are plant specific. In evaluating the future economic prospects of existing plant, the owners/utility focus on the unique circumstances of that plant and its cost and performance, and the future demand for electricity, and value of electricity in the country.

Three types of nuclear power plant costs can have important and distinct roles in determining the economic life of individual units:

1. historical capital costs,
2. future capital additions (for regular operating time and for LTO)
3. annual O&M and fuel costs.

It is important to stress that the economic evaluation of LTO measures is complicated and depends on the concrete circumstances for each plant.

## 2.3 Methodology for LTO economic analysis

Nuclear power plant lifetimes are, for the most part, driven by cost and revenue consideration. In most cases, the decision to continue operating an existing plant is based upon its marginal generation cost, i.e., operation, maintenance and fuel cycle cost, and amortisation of the investment required for lifetime extension if applicable, as compared with the marginal generation costs of other options. The marginal cost is lower for existing nuclear power plants than for most alternatives. Therefore, lifetime extension generally is an attractive option from an economic viewpoint.

Deregulation of electricity market is increasing competition and eliminating monopolies and guaranteed sales at fixed rates defined usually by government. Therefore, nuclear power plant owners endeavour to reduce the cost of plant life management.

The choice between LTO and building a new power plant, fossil-fuelled or nuclear or renewable, is influenced also by the size of the investment which is smaller for refurbishment than for a new construction. The refurbishment cost of major components are in the order of tens to a few hundred million US dollars per net GWe capacity [1] but these costs are relatively smaller compared to new plant investment, but still can be significant from financing point of view.

Nuclear LTO brings additional benefits in term of electricity cost, and price, stability since fuel cycle costs represent only a small share (typically around 15-20%) of total generation costs, and are not as volatile as gas prices for example.

### 2.3.1 Concept of Cost

Cost is a difficult concept, as there is a whole variety of different types of costs, each meaningful and applicable in a certain context. It is important to distinguish between bookkeeping cost, opportunity cost, average cost, marginal cost, sunk cost, investment cost, variable and operational O&M costs, fuel cost, operational cost, decommissioning cost, resource cost, fuel-cycle cost, refurbishment costs, private cost, social cost, external cost, etc.

Also there is requirement that for costs should be always identified the year of the currency quoted, or mention whether the quotation is in nominal or real currency, and what the reference year is in case of the real currency.

As a second important element in the discussion on nuclear costs, it must be recognized the difference between the cost of existing plants as seen today (only marginal cost and fixed O&M costs, since the investment cost is a repaid) and a new plant (whereby the investment cost must be taken into account). It means that the cost of nuclear electricity should be compared to the cost of other generation types, like coal, gas and renewables. Theoretically speaking, economic cost is reflected by the *opportunity cost* which is the value of the best alternative good or service foregone, or still differently, a measure of what has been given up when we make a decision. [2][3].

To cover full range of the cost for nuclear electricity generation, it must be calculated total cost - the *social cost*; which is equal to the sum of private and external cost.

- *Private costs*: costs that show up in the profit-and-loss statement at the end of the year
- *External costs*: or externalities, "are costs that arise when the social or economic activities of one group of persons have an impact on another group and when that impact is not fully accounted, or compensated, for by the first group" [4]

Cost is somewhat untouchable: it varies in time, it is geographically different (e.g., the OECD versus the non-OECD countries) [5], it furthermore depends on the viewpoint of the investor because the opportunity cost may be different - a private versus a public investor, versus a (private) concession holder in a regulated market.

The fact that investors expect a return on investment (whereby this investment competes with other possible investment choices) and that interest is to be paid on loans means that money has a *time value*, usually expressed by a *discount rate*. The discount rate, usually considered as the opportunity cost of capital.

### 2.3.2 Cost Elements of Nuclear Generation

The cost elements constituting a "full" cost of electricity (i.e., EUR or USD per MWh) for nuclear power plants consist of following:

a. Private costs
   i. Investment cost
   ii. Decommissioning cost
   iii. Operation & Maintenance (O&M cost)
   iv. Fuel-cycle (including the back-end) cost
b. External Costs

When looking at external costs in the nuclear area it is important to recognize that a considerable fraction of the costs linked to the harmful nature of radioactive substances basically has already been internalized, and should thus no longer be considered as an externality. Typical examples are levies that have been and are being charged both for radioactive-waste management and final disposal, and for decommissioning, for the purpose of feeding long-term funds.

A few remaining externalities (where depending on the situation they may still be part of the externalities; in other cases they should be deleted from the list).

(1) Radioactive emissions
(2) Long-term waste disposal (sometimes part of fuel cycle; often already internalized)
(3) Accidents – liability
(4) Proliferation
(5) Avoided $CO_2$ emissions – a positive externality?
(6) System effects

## 2.4 Overview

Originally, NPP was designed to operate until original planed operating life (POL). Power generation would cease in year and decommissioning would immediately commence.

Owner is considering the economic case for extending the generating life of NPP beyond its POL. NPP must, with the nuclear regulator, undertaken a technical review of NPP and determined that significant engineering works are required to support the safety case, the safety case upgrades needed to the plant to operate to planned operating life (following the post Fukashima recommendations and stress test in EU) and to meet the regulators requirements for a life extension of up to 20 years. This may require significant investment.

To support the business case for extending the operating life of NPP (and delaying the start of decommissioning activities) it is need to undertake an independent economic assessment of the life extension.

# 3 NPP'S REVENUE AND EXPENSES

For the purposes of economic analysis, the costs for NPP, which are required to be covered by the price that is charged for electricity, should be divided into the following categories:

1. **Nuclear fuel:** This is expected to include the cost for uranium and enrichment under the existing contract with supplier.
2. **Water tax:** Tax for use of water, including river water for cooling, by NPP.
3. **Materials and Services:** This cost line covers all the costs associated with services carried out at the NPP and materials used at the NPP. This is expected to cover the cost of spare parts, maintenance (planned and unplanned) of fixed assets, other material, services in the production process and other miscellaneous services. Salaries and related costs, as well as fuel and depreciation charges are excluded.
4. **Depreciation charge/investment costs**: The cost line covers major investment in NPP. It is identified in the NPP accounts as the depreciation charge. The depreciation charges are not calculated on the basis of amortisation rates and asset values. The depreciation charge represents the sum of the amount of investment expected to be made in a specific year (as stated in the long term investment plan) and the amount relating to repayment of the principal outstanding for the long term bank loan facility (if any). This charge also includes an amount for small scale investments relating to investment in small assets like furniture, re-roofing etc.
5. **Insurance:** This includes all insurance costs (both nuclear and non-nuclear) associated with the ongoing operation of NPP.
6. **Salaries and related costs (labour costs):** This covers basic salaries of the NPP employees along with social contributions, taxes attributable to the employees and paid by NPP, and pensions insurance.
7. **Compensation to Local Communities (CLC) paid directly by NPP (Contributions to LC)**: This represents the contribution that NPP makes directly towards the local communities for restricted use of the land, in line with government legislative requirements.
8. **All other expenses:** Includes expenses of supplementary activities; financial expenses; revaluation/withdrawals; and other expenses as included in the NPP management accounts.

## 4 ECONOMIC ANALYSIS BY COMPARING LTO OF NPP WITH ALTERNATE POWER GENERATION OR IMPORT OF ELECTRICITY

When considering the economics of nuclear power, it is instructive not only to focus on new build, but to reflect on the desirability, from an economics point of view, to consider *long-term operation* of existing plants, likely after appropriate refurbishment to keep the safety level of the plants in line with current expectations. Electricity generation system is currently going through almost revolutionary changes on its path towards a zero $CO_2$ emission target which is expected to cost considerably, it may be an interesting option to extend the operational life of NPPs beyond their originally 'estimated' design life, so as to keep a dispatchable and firm $CO_2$-free electricity generation technology on line at reasonably low cost. This would give the electric power sector more time to thoroughly analyse the transitional aspects of system integration with ample intermittent, decentralized and centralized, generation, with substantial non-dispatchable overcapacity. In addition, it gives reactor developers some breathing space to reflect on design changes that meet the challenges of future electricity systems, such as load-following participation, whilst still guaranteeing sufficient rotational inertia into the system to support grid stability.

Different aspects of prolonged operation of nuclear power plants is discussed in several sources in the literature ([6], [7], [8], [9], [10]), but the most updated, timely and comprehensive document on the economics of LTO has been published late 2012, by the Nuclear Energy Agency of the OECD. [11].

## 5 INVESTMENT COST FOR MAJOR REFURBISHMENTS FOR LTO

Plants that have been built in the past, whether or not depreciated in a bookkeeping sense, are characterized by a "sunk" investment cost. Such plants will keep operating as long as the marginal operational cost (consisting of the O&M cost and the fuel cost) is lower than the electricity market prices.

If operational costs are too high in comparison with other generation means and the market price, then it may be that owners/operators decide to shut down plants for pure economic reasons, regardless of the technical end/or safety related status of the plant. Such early retirement has taken place on May 07 2013 in the state of Wisconsin, USA, where the Kewaunee nuclear plant was shut down, even though it had received a regulatory operational extension by the NRC until 2033, because of low market prices mostly driven by cheap shale-gas electricity generation.

In other markets and circumstances, especially in Europe, where a possible shale-gas breakthrough is not obvious, it certainly makes economic sense to continue operation of existing plants. Even if safety concerns become an issue so that major refurbishment investments are necessary, it may still be advantageous in several markets to consider prolonged operation. A precondition for operational extension after refurbishment, however, is a stable political decision climate. When substantial investments are made to refurbish a plant, then an expected operational period must be part of the regulatory operational license (clearly always subject to the future safety status of the plant). The possibility for changes in future standpoints of the authorities must be foreseen in the LTO-related agreement with government authorities, with possible (contractual) compensation when a premature shutdown would be enforced.

The crucially important parameter for prolonged operation is the investment cost for refurbishment. This investment is to a large extent determined by the overnight refurbishment cost (ORC).

A set of specific overnight refurbishment costs has recently been obtained for a variety of countries by the NEA, as shown in Table 1. [11] As shown in the table post-Fukushima upgrades have been included in the numbers given.

Table 1: Cost summary of specific 'overnight refurbishment investment cost' in some OECD countries [11]

| Country | Specific investment in LTO | Comment |
|---|---|---|
| Belgium | USD2010 650/kWe | Including ~11% increase due to post-Fukushima measures. |
| France | USD2010 1 090/kWe | Including all investments from 2011 to 2025: maintenance, refurbishment, safety upgrades, performance improvement; and ~10% increase due to post-Fukushima measures. |
| Hungary | USD2010 740-792/kWe | Including 10-17% increase due to post-Fukushima measures. |
| Korea, Republic of | USD 500/kWe | Including ~10% increase due to post-Fukushima measures. |
| Switzerland | USD2010 490-650/kWe | Specific future investment in NPP refurbishment and maintenance (approximately the double of the specific LTO investment) is USD2010 980-1 300/kWe. |
| United States | About USD2010 750/kWe | Electric Power Research Institute (EPRI) survey data and current spending on capital improvement. |
| | | |
| Russian Federation | About USD2010 485/kWe | Data for Novovoronezh 5 unit (first series of VVER-1000: V-187). |
| Ukraine | About USD 300-500/kWe | Public statements by Energoatom and Ukrainian prime minister. |

### 5.1 Economics in the decision between LTO versus new building replacement

Indeed, extending the operating lives of existing plants provides clear advantages. High capacity factors and low operating costs make nuclear plants some of the most economical power generators. And even when major plant components must be upgraded to extend operating life, these plants represent a cost effective, carbon-free asset that is critical to energy future.

Extending the life of a major generating asset avoids the need for immediate investment in new generating capacity. The capital costs of plant life management for LTO will be smaller than investment in any type of replacement capacity, although there might be a need for additional investment in plant upgrading and safety improvements. Combining the plant upgrading and safety improvements with power uprating made lifetime extension even more cost effective. In addition, the kWh costs for waste management and decommissioning can be reduced.

Nevertheless, quantification of the LTO costs is not an easy task. It is recognized that LTO costs are highly dependent on specific conditions related to each NPP, such as: design of the plant; NPP operating history including ageing conditions; condition of the critical SSCs; regulatory requirements; full or partial replacement of components; refurbishment for PLIM versus refurbishment for LTO; accounting methodologies; etc.

### 5.2 Economics of lifetime extension and safety improvements

In a deregulated electricity market power plant lifetime extension and upgrading are driven by cost and revenue consideration. Decision to continue operating an existing plant is based on its marginal generation cost, i.e., operation & maintenance, fuel cycle cost, taxes and capital cost compared to generation costs of other options. The marginal cost is lower for existing nuclear power plants than for most alternatives, therefore LTO is a lucrative option.

In case of Europe lifetime extension and uprating of NPPs are going hand in hand together with safety improvements. The cost for lifetime extension and consequently necessary safety

upgrading are in the average €400 million per unit despite of the size. These large costs increase the generation cost during the amortisation period by 0.2 – 0.6 eurocent/kWh [8].

## 6 EXAMPLE OF SCENARIOS FOR ECONOMIC ANALYSIS FOR LTO

For the purpose of economic analysis, can be identified two NPP operational life scenarios:

**Scenario 1** – NPP operation to planned operating life:

- NPP is partially refurbished to provide for ongoing operation to planned operating life (e.g. implementation of safety upgrade work that the regulator requires).
- Decommissioning of the NPP will commence in year after planned operating life.
- Alternate power source(s) that could be available from the start of in year after planned operating life.

**Scenario 2** – Full life extension up to 20 years:

- An investment programme is implemented that allows NPP subject to ongoing regulatory requirements, to extend operational life for up to 20 years.
- Decommissioning of NPP will commence in year after extended life.
- Alternate power sources that could be available after year of extended life have not been considered as these are outside the scope of this economic analysis.

To make decision at least should be assessed the cost of each of these two scenarios to determine the most economically viable scenario. It is also need to understand the risks associated with these scenarios and the alternate power options that may be included in scenarios 1 and 2.

As a baseline to the two scenarios mentioned above, is assessed the expenses associated with NPP ongoing generating activities. The expenses include NPP's operating expenses together with remaining contributions that will need to be paid into the decommissioning fund.

The contributions that need to be paid into the decommissioning fund will vary depending on the operating lifetime of NPP in each scenario and in terms of a Levelized Cost of Electricity (LCOE) will be significantly higher in the scenarios where NPP has a shorter remaining operating life.

In order to assess the two scenarios on an equalised basis, the LCOE generation can be used to compare the cost of electricity generation (in $/MWh terms) across the different scenarios. The LCOE approach is established and widely used across the electricity industry, to compare the economics of different generating options, particularly where alternate power generation options have differing operational lives.

Once the costs of NPP's ongoing generating activities (including the payments into the decommissioning funds) for scenarios 1 and 2 is established, it should be considered the alternative power sources that may be available in the market and the costs of implementing the alternative power sources (excluding grid and infrastructure associated with the power source outside of the plant itself). For scenarios 1 and 2, a long list of alternate power options can be determined. Alternate power options SHOULD BE determined on the basis of their suitability for use as base load electricity supply from the date that NPP is assumed to cease generation. Suitability should be determined on the basis of the alternate power generation technology being in use, on a commercial basis for base load generation, at any other site in the world.

In addition to ranking the different NPP scenarios and alternate power options based on their LCOE, analysis of the risks associated with each option should be undertaken. This analysis should be considered along with the LCOE ranking of the options considered.

Future revenue and expenses can be determined by based on actual historic data, known future plans and the experience of NPP. Investment plan data is based, where possible, on indicative quotations that NPP has obtained for the major capital works.

The inputs for the decommissioning fund are based on data sources that have been previously defined by the regulator or government.

### 6.1 Alternate power options

When considering alternate power options, it should be noted that a replacement scheme would be likely to include a mix of alternate power generation technologies, rather than a single replacement option. For the purposes of the economic analysis, however, each alternate power option should be considered on its own, recognising that the combined impact on the LCOE would result in an LCOE for the combined alternate power generation that would be higher than the LCOE for the more economically viable alternate power source if it were to be installed on its own. Therefore, by looking at the economic viability of the alternate power options when installed independently of one another, their economic viability may be compared with the NPP life extension case.

Where alternate power could be installed, the LCOE has been determined over the stated useful economic life of that alternative power option. For example, where an alternate power option has a useful operating life of 20 years then the economic analysis has been determined over the combined duration of NPP operation in the scenario and the 20 years operational life of the alternate power option. The use of LCOE equalises this difference as for each case being considered the full useful operating life of the alternate power plant is considered.

In the case of import of electricity, the LCOE can be calculated over a period to planned operating life (POL) so that it aligns with the NPP life extension scenario (Scenario 2). In the case of import of power there are many influences that may result in changes to the real cost of imported electricity over the duration being considered in the analysis. Review of historic baseload energy prices from the surrounding region should be undertaken to identify and confirm correlating regional electricity markets that may be used as a source of traded futures price data.

For each alternate power generation option, the development period has to be stated, along with the overnight investment cost per MW of installed capacity.

For the purpose of this economic analysis, alternate power options should be sized to deliver similar baseload electricity. Based on the future assumed capacity factor for NPP the equivalent annual electricity production should be, Which has been used as the required total useful energy production from alternate power options. The required installed plant size (or combined plant size where multiple plant is required) should be determined so that an annual amount of electricity that is equivalent to NPP is achieved. Import of electricity should be assessed on the same basis.

Where alternate power generation capacity of the required size is not available, i.e. in the case of new nuclear power plant, then it is assumed that additional capacity may be installed and that the spare capacity may be sold to other buyers for the same price.

The costs that are included in the LCOE calculation shall include all costs associated with generation of electricity, but shall not include costs associated with electricity grid infrastructure, supporting infrastructure and transmission charges. For all alternate power options there is likely to be a varying degree of additional grid infrastructure and associated infrastructure costs, and for certain options there will be ongoing costs for the grid operator as a result of incorporation of the alternate power option into the grid.

LCOE is not a complete and single method of assessing the economic benefit of an electricity source for the following reasons:

(a) The LCOE approach does not adequately reflect the market realities characterised by uncertainties and dynamic pricing.
(b) The LCOE approach provides generation costs at the plant level and does not include the network costs of a power system.
(c) The LCOE approach reveals little information on the contribution of a given technology to addressing energy.
(d) The LCOE does not indicate the relative likely stability of production costs over a plant's lifetime, and therefore the potential contribution to cost and possibly price stability.

### 6.2 Imported baseload electricity

Historic power price data should be used, with caution, as a general indicator of possible future prices. Where liquid power exchanges exist, and futures prices are available, this provides the best indication of short term future trends. Analysis of recent historic data may also be used to identify correlated markets.

It should be taken into account when considering cases that assume the use of imported electricity that the generating capacity of countries with ability to supply base load electricity on a long term basis should be assessed.

## 7 REPLACEMENT POWER GENERATION

Potential replacement power generation options should be considered. A long list of alternate power generation options should be determined, that may provide direct replacement of NPP for the purposes of baseload electricity generation. An equivalent annual electricity production requirement should be also assumed.

In the first instance, the long list of alternate power options can be prepared, along with an initial qualitative assessment of each alternate power option against a set of criteria that are considered likely to influence the successful implementation of that power option from a non-economic perspective.

Source for Replacement Power: New Solar, New Wind, Biomass, New CCGT, New Hydro, New Coal, New nuclear Power Plant.

Needed Characteristic for Replacement Power: required energy output (GWh/y); capacity factor assessment; required installed power (in MW); construction duration (initial decision to commercial operation).

It should be developed criteria for qualitative assessment of alternate power options: For example some criteria can be: is alternate power suitable for base load electricity (is it dispatchable), alignment with policy on $CO_2$ emissions, including national targets, aligned with other environmental policy, technically feasible within country, alignment with policy around high reliance on imported fuel, aligned with policy on diversity of supply.

The carbon cost, per tonne of $CO_2$ produced as a result of generation, for relevant generation technologies, should be stated and be on a consistent basis for all applicable energy sources.

Incentive payments are not included in the current LCOE calculations and should not be included unless there is long term contractual certainty regarding their payment.

Transmission costs, grid infrastructure and other external costs associated with grid enhancement works or ongoing grid stability operations may be included in the scope of analysis. There may also be additional costs associated with achieving a similar level of grid stability to that achieved currently, with NPP operational on the grid. These costs would be incurred under certain alternate power options and it is likely that the grid operators would look to recover these costs

through grid connection charges. These costs should be taken into account as additional costs, when considering decisions related to alternate power sources.

National policy should be considered, with a particular focus on areas of policy which are considered likely to have an influence on the economic and risk analysis project.

Before any formal investment decision on alternate options is taken, a full review of the prevailing policy and regulatory framework should be undertaken to confirm that the policy and regulation has not been updated or superseded.

The decline in the demand for energy generally causes the price for energy to drop. As the recession, technologies with improved energy efficiency, energy efficiency policies lift the demand for energy and electricity it is likely to decrease the price of electricity.

For the purpose of analysis, it should be performed detailed analysis on the impact of different sensitivities on the LCOE for each scenario.

### 7.1 New nuclear plant to replace NPP

As it may not be possible to build a power plant that is smaller than 1,000 MW in today's market, there would be a surplus generating capacity at beginning of operation. This spare generating capacity will need to be sold to a third party. The LCOE calculation in this case assumes that the additional capex and the operating costs associated with the spare capacity will be covered by long term power purchase agreements with third parties.

There is a risk however that it may not be possible to obtain long term power purchase agreements for this additional capacity. If this is the case, then the additional investment cost and O&M costs associated with the spare capacity would have to be included in the LCOE calculation and would significantly increase the LCOE further.

The availability of finance to support the significant investment associated with new nuclear power plant construction, and the impact on the sponsors balance sheet and credit rating should be considered in this analysis.

## 8 DECOMMISSIONING COSTS

The different costs associated with decommissioning of the NPP and the disposal of low and intermediate level waste (LILW) and spent fuel should be considered. It can be assumed that all decommissioning and waste management costs will be funded by decommissioning fund.

For the purposes of the economic analysis, two scenarios can be considered:

1. Shutdown as envisaged in original licence (Scenario 1)
2. Changes to the quantum and the timing of decommissioning costs if the life extension works are completed and the NPP shuts down is posponed (Scenario 2).

Definitions for the sub categories that make up the total decommissioning cost:

1. NPP dismantling (or NPP Decommissioning): This is assumed to reflect the costs associated with the onsite transportation, storage, decontamination and removal of the main components and the reactor vessel, demolishing of the buildings and complete restoration of the site.
2. Spent Fuel (SF) disposal: This is assumed to include the construction costs associated with building the SF repository (and/or the deep geological repository for High Level Waste (HLW)).
3. SF Storage and transport to disposal site: This is assumed to reflect costs for construction of the dry storage facility if needed, procurement of any containers and the transportation of spent fuel from the spent fuel pit to the dry storage facility at generic site.

## 9 RISK ANALYSIS

The risks that may have an impact on the economic case for the long term operation of NPP should be identified. A list of risks has to be prepared. The list of risks has to be prepared with pre mitigation impact and probability assessment. Mitigating actions has also to be proposed where considered appropriate.

1. **Political and policy risks*:*** These risks cover the impact of changes in policy relating to the use of nuclear power plants to operate. Other policy changes may include changes to the national radioactive waste and used fuel management/ decommissioning. There is also a risk that NPP may be required to pay additional taxes as a result of changes to the tax regime that adversely impact nuclear power compared to other sources making NPP a more expensive source of electricity.
2. **Business and economic risks*:*** These risks broadly relate to unexpected adverse changes in the national economy, risks with regards to the projections data/assumptions that have been provided by for the purposes of this economic analysis and also risks relating to the base decommissioning costs for NPP. Another key risk is the impact that fluctuating inflation.
3. **Social risks:** These risks relate to impact of stakeholders on the NPP life extension option. There is a risk that the general public and other stakeholders may set requirements for NPP that are difficult to meet due to the perceived radiological risks.
4. **Technical risks:** These risks relate to the safety status of the power generation technology, ability of the plant to operate at high availability and capacity factors, duration for construction and commercial operation given the programme requirement, extreme weather conditions etc. i.e., any risks resulting in mechanical or safety issues which affect the operation of the plant.
5. **Legal and regulatory risks:** These risks relate to the impact of changes in national or other international laws and regulations with respect to use of nuclear energy or the impact that implementation of additional safety upgrade requirements will have on the life extension of NPP.

The majority of the risks identified in the list of risks, under the above categories, may have an impact on the costs for NPP. The key risks are:

1. NPP's capacity factor will decline over NPP's extended life.
2. Base decommissioning cost assumptions that were originally agreed may have changed significantly.
3. NPP's projected operating cost uncertainty.
4. NPP's projected investment costs may vary over the next 30 years.

Once ranked by LCOE, a qualitative assessment of risks associated with each option should be undertaken. This assessment has to consider a series of risks, including the following:

- Political and policy risks
  - Whether the alternate power option would have an impact on national commitments to climate change
  - Whether the alternate power option is aligned with security of supply and diversity of supply policy for the Ultimate Owners and the European Union
  - Long term availability of subsidies or incentives
  - Future environmental charges, such as carbon charges
- Economic risks
  - Inflation of costs
  - Discount rates
  - Electricity prices in neighbouring countries or attainable markets as well as price of services and materials
- Technical risks
  - Availability of suitable/ technically feasible sites

    - Availability of sites for building a (or multiple) power plant(s) to match the scale required to replace NPP.
    - The likely amount of additional grid investment required to incorporate the alternate power option
    - Whether the alternate power option can be constructed in the time available prior to NPP stopping generation for the given scenario
- Legal and legislative
    - Existing contract durations and contract replacement
    - Legislative changes
    - Risk associated with expiry of nuclear fuel contracts.

## 10 CONCLUSION

Capacity determination is a decision for the long term, whereas production is adjusted in the short run. Paper looks on the main contributions in investment planning under uncertainty, in particular in the electricity market for capital intensive investments like NPP. The relationship between market and non-market factors in determining investment signals in competitive electricity markets is analysed. Paper analyse the ability of competitive electricity markets to deliver the desired quantity and type of generation capacity and also investigates the variety of market imperfections operating in electricity generation and their impact on long-term dynamics for generation capacity.

Today decisions pertaining to investment in new capacity or life time extension are surrounded by considerable uncertainties about the future economics of the projects. One reason is that in a deregulated market private investors typically have to bear a greater portion of the investment risk compared to a monopoly utility in a regulated market. This favours flexible investment alternatives with short-lead times and low capital requirements. Moreover, energy and climate policy – with feed-in tariffs for RES or green certificate system and the European emission trading systems for $CO_2$ (EU ETS) - may add to investment uncertainties. Delayed and uncertain permitting processes also increase investors' risks.

Competitive wholesale markets for electricity and energy often fail to provide adequate net revenues to attract investment in generation to meet reliability criteria. In addition, it is also argued that short-term price volatility is more extreme and frequent than in other commodity markets, because storage for electricity is too costly for commercial application. The liberalization of electricity markets shows that the fate of nuclear is strongly affected by energy market structure. In liberalized markets investments are profit motivated, with the choice of technology left to the market. The redistribution of risk among the different stakeholders is likely to make nuclear generation unattractive for an investor, even when its levelized costs are similar to the levelized costs of the dominant technology, for several reasons.

Current electricity price on EU Power Exchanges and CO2 allowances are so low that no new power plant even life time extension of NPP can be competitive on electricity market and that almost all investment will be in renewable energy sources because of support schemes.

From the economic point of view, the costs of LTO are usually lower than the construction of any other source of electricity. But in the aftermath of the Fukushima accident, policies towards nuclear energy in some countries were changed.

All, including additional capital expenditure necessary to meet regulatory requirements, have significant impact on the cost of nuclear power generation to the extent that is prudent to reconfirm/check the continuity of economic sustainability of NPP continues operation. The economic assessments of NPP operation for long term operation are necessary due to: Required capital investment into upgrading the safety level of the plant, Potential increase of operation & maintenance (O&M) costs, Limited existing capacities for storage of low level and intermediate waste and spent nuclear fuel, Regulation framework that may require additional capital investments,

Potential increase of annual charges into national decommissioning funds, Volatility of electricity market prices.

Each nuclear power plant has its own unique history of costs and performance. Large year-to-year fluctuations in costs are common for most NPPs as capital additions are undertaken and completed. Plant availability also varies from year to year as the plants undergo refuelling and planned maintenance during refuelling cycles. Also, unplanned repair outages contribute to cost and performance fluctuations.

Because of that economic life decisions are plant specific. In evaluating the future economic prospects of existing plant, the owners/utility focus on the unique circumstances of that plant and its cost and performance, and the future demand for electricity, and value of electricity in the country.

Three types of nuclear power plant costs can have important and distinct roles in determining the economic life of individual units: historical capital costs, future capital additions (for regular operating time and for LTO), annual O&M and fuel costs.

It is important to stress that the economic evaluation of LTO measures is complicated and depends on the concrete circumstances for each plant.

The choice between LTO and building a new power plant, fossil-fuelled or nuclear or renewable, is influenced also by the size of the investment which is smaller for refurbishment than for a new construction.

To support the business case for extending the operating life of NPP (and delaying the start of decommissioning activities) it is need to undertake an independent economic assessment of the life extension.

Indeed, extending the operating lives of existing plants provides clear advantages. High capacity factors and low operating costs make nuclear plants some of the most economical power generators. And even when major plant components must be upgraded to extend operating life, these plants represent a cost effective, carbon-free asset that is critical to energy future.

Extending the life of a major generating asset avoids the need for immediate investment in new generating capacity. The capital costs of plant life management for LTO will be smaller than investment in any type of replacement capacity, although there might be a need for additional investment in plant upgrading and safety improvements. Combining the plant upgrading and safety improvements with power uprating made lifetime extension even more cost effective. In addition, the kWh costs for waste management and decommissioning can be reduced.

Nevertheless, quantification of the LTO costs is not an easy task. It is recognized that LTO costs are highly dependent on specific conditions related to each NPP, such as: design of the plant; NPP operating history including ageing conditions; condition of the critical SSCs; regulatory requirements; full or partial replacement of components; refurbishment for PLIM versus refurbishment for LTO; accounting methodologies; etc.

In a deregulated electricity market power plant lifetime extension and upgrading are driven by cost and revenue consideration. Decision to continue operating an existing plant is based on its marginal generation cost, i.e., operation & maintenance, fuel cycle cost, taxes and capital cost compared to generation costs of other options. The marginal cost is lower for existing nuclear power plants than for most alternatives, therefore LTO is a lucrative option. Lifetime extension and uprating of NPPs are going hand in hand together with safety improvements.

For the purpose of economic analysis, can be identified two NPP operational life scenarios:

Scenario 1 – NPP operation to planned operating life and Scenario 2 – Full life extension up to 20 years.

To make decision at least should be assessed the cost of each of these two scenarios to determine the most economically viable scenario. It is also need to understand the risks associated with these scenarios and the alternate power options that may be included in scenarios 1 and 2.

In addition to ranking the different NPP scenarios and alternate power options based on their LCOE, analysis of the risks associated with each option should be undertaken. This analysis should be considered along with the LCOE ranking of the options considered.

Future revenue and expenses can be determined by based on actual historic data, known future plans and the experience of NPP. Investment plan data is based, where possible, on indicative quotations that NPP has obtained for the major capital works.

The risks that may have an impact on the economic case for the long term operation of NPP should be identified. A list of risks has to be prepared. The list of risks has to be prepared with pre mitigation impact and probability assessment: Political and policy risks; Business and economic risks; Social risks; Technical risks; Legal and regulatory risks, Mitigating actions has also to be proposed where considered appropriate.

## REFERENCES


[1] OECD/NEA, Statis Report on Nuclear Power Plant Life Management, NEA/SEN/NDC (2000)6, Paris, 2000; Available at: https://www.oecd-nea.org/ndd/docs/2000/sen-ndc2000-6.pdf

[2] Paul A. Samuelson and William D. Nordhaus, "Economics", 19-th Ed., MacGraw-Hill, New York,

[3] François Lévêque, "Estimating the cost of nuclear power: benchmarks and uncertainties", Working Paper 13-ME-01, Interdisciplinary Institute for Innovation /CERNA, MINES ParisTech, May 2013; Available at: http://www.cerna.ensmp.fr/images/stories/Cerna_Working_Papers/I3WP_13-ME-01.pdf

[4] Commission of the European Union, "External Costs – Research results on socio-environmental damages due to electricity and transport", Report EUR 20198, Brussels, 2003.

[5] OECD/NEA, "Cost Estimation for Decommissioning – An international Overview of Cost Elements, Estimation Practices and Reporting Requirements", NEA Report Nr 6831, Paris, 2010

[6] "Cost drivers for the assessment of nuclear power plant life extension", IAEA-TECDOC-1309, IAEA, Vienna, September 2002;Available at: http://www-pub.iaea.org/MTCD/publications/PDF/te_1309_web.pdf

[7] "Aging Management and Life Extension in the US Nuclear Power Industry", Frank Gregor and Alan Chockie, authors, Chockie Group International, Seattle, WA, October 2006 188

[8] "Country Experience in relation to PLEX costs in view of the updating of the PINC document", Bernhard Elsing and Antonio Ballesteros, authors, JRC Report EUR 24400 EN-2010, 2010 197

[9] "Power uprates in nuclear power plants: Guidelines and experience", IAEA, NP-T-3.9, Vienna, 2011 195

[10] "DOE-NE Light Water Reactor Sustainability Program and EPRI Long-Term Operations Program – Joint Research and Development Plan", Report INL/EXT-12-24562, Revision 2, Washington, D.C., April 2013; Available at: http://energy.gov/sites/prod/files/2013/05/f0/LWRS-LTO_Joint_R%26D_Plan_Rev_2.pdf

[11] Nuclear Energy Agency, "The Economics of Long-Term Operation of Nuclear Power Plants", NEA/OECD Report, No. 7054, Paris, 2012; Available at: http://www.oecd-nea.org/ndd/reports/2012/7054-long-term-operation-npps.pdf.

Journal of Energy
VOLUME 68 Number 2-3 | 2019 | Special Issue
journal homepage: http://journalofenergy.com/

# Hazard Assessment of NPP Krško for Republic of Croatia

**Mr.sc. Saša Medaković, dr.sc. Davor Rašeta**
State Office for Radiological and Nuclear Safety
Frankopanska 11, 10000 Zagreb, Croatia
sasa.medakovic@dzrns.hr, davor.raseta@dzrns.hr

**Dr.sc. Davor Grgić**
University of Zagreb, Faculty of Electrical Engineering and Computing
Unska 3, 10000 Zagreb, Croatia
davor.grgic@fer.hr

## ABSTRACT

While Croatia does not have nuclear power plant on its territory, NPP Krško in Slovenia is just 10 km from the Croatian border. It is important for Croatia to include NPP Krško in comprehensive hazard assessment. This article will present hazard assessment based on calculations using RODOS. Real-time weather prepared by Croatian National Weather Service and collected by the State Office for Radiological and Nuclear Safety over the years will be used. Scenario resulting in the large release from the NPP will be analysed. Results from hundreds of calculations will be statistically analysed and compared to the current protection zones in Croatia around the NPP Krško.

***Keywords:*** *emergency, protective actions, planning zones, NPP, hazard assessment*

## 1 INTRODUCTION

Nuclear power plants are safe facilities, with probability of serious accident in range of once every 20 000 years or less. However, the impact of such serious accident can be severe, so, despite very low probability, risk of such an accident is moderate, and warrants mitigation measures, especially for the protection of the population.

Urgent protective actions are primarily evacuation, sheltering and iodine thyroid blocking. Their aim is to reduce or prevent external exposure to the radioactive cloud, as well as external exposure to the deposited radioactive material and internal exposure through inhalation. Urgent protective actions include also decontamination of individuals, urgent medical assistance, prevention of inadvertent ingestion of radionuclides and prevention of ingestion of contaminated food and drinks.

This article will consider only first group of urgent protective actions, evacuation, sheltering and iodine thyroid blocking.

### 1.1 Description of protective actions

Evacuation is protective action where the whole population from affected area is urgently relocated to a safer area. Evacuation needs to be done in a matter of hours and usually is performed by the people themselves, with authorities ensuring open roads and evacuation of vulnerable individuals.

Sheltering is protective action where people shelter themselves in their own homes or in predefined shelters. It is more effective in big buildings with thick walls. Thick walls should reduce cloud-shine, and people should close all ingresses (duck-taping doors and windows, for example) to prevent or reduce internal exposure by inhalation.

Sheltering cannot last longer than 48 hours.

Iodine thyroid blocking (ITB) is protective action where high amount of stable iodine is taken in order to saturate the thyroid gland and prevent the accumulation of radioactive iodine that enters the body through inhalation.

Current IAEA recommendations and Croatian legislature do not have intervention levels for urgent protective actions, instead relying on overarching strategy based on reference levels. This strategy will be developed in Croatian Emergency preparedness and response plan for nuclear and radiological emergencies. Until then, IAEA recommendations valid before reference levels were developed have to be used. Intervention levels considered in this paper are set in Table 1.

Table 1: Intervention levels for urgent measures

| Measure | Level (mSv) |
|---|---|
| Evacuation | 100, averted over 7 days |
| Sheltering | 10, averted over 2 days |
| ITB, adults | 100, thyroid dose averted over 7 days |
| ITB, children | 100, thyroid dose averted over 7 days |

## 1.2 Protection zones

In order to ensure proper effectiveness, all the urgent protective measures have to be activated and implemented as soon as possible, ideally close before or just after the release of radioactive cloud. For that to be possible, both authorities and people need to know in advance what are actions to be performed, where are locations affected and when to perform the actions. For that reason, protection zones (and distances) are set. In each protection zone prospective protective actions should be known in advance, as well as triggers to start the actions. International organizations work on establishing optimal zones, especially after the Fukushima [1], [2].

### 1.2.1 Protection zones in Croatia

Closest Croatian territory to the NPP Krško is 10 km from the reactor. That means that Croatia does not need to have the first recommended zone, *Precautionary Action Zone*, PAZ, that is typically up to 5 km from the NPP.

*Urgent Protective Action Zone* (UPZ) in Croatia is set up to the distance of 20 km form NPP Krško. This is the zone where sheltering and ITB are expected in case of serious accident, and evacuation should be planned.

*Extended Planning Distance* (EPD) in Croatia is set between 20 km and 100 km from NPP Krško. In this zone evacuation is not expected, except for the hot spots, and general plans exist for sheltering and ITB.

*Ingestion and Commodities Planning Distance* (ICPD) is zone where only agricultural measures are expected.

Immediate restriction of use of drinking water from open sources (wells and similar) as well as restriction of consummation of fresh food and feed exposed to open air is expected for all the zones.

Distance is first parameter in determination of the zones. Actual zones follow municipal boundaries.

# 2 HAZARD ASSESSMENT

Protective zones presented in Chapter 1.2.1 were set based on international recommendations ([1], [2]). The aim of this article is to repeat calculations similar to the ones made by international organizations, but for Croatian specific situation, and to see if internationally recommended

protection zones are adequate. Maximum sheltering time is 48 hours, but usually sheltering is considered for 24 hours (time used in calculation is this paper).

As a tool in emergencies, Croatia uses RODOS (Real-time On-line DecisiOn Support) system. One of the capabilities of RODOS system is calculation of spread of radioactive cloud based on the meteorological data. One of the functions of RODOS system is the ability to continuously run calculation for selected NPP, using selected source-term data and up-to-date weather prognosis.

State Office for Radiological and Nuclear Safety has an agreement with Croatian Meteorological and Hydrological Service to get prognosis for the next 48 hours in RODOS-usable format. The past agreement assumed availability of new prognosis every 12 hours, and since 2018 it has changed to the new prognosis every 6 hours.

To check the validity of current protection zones, this article will simulate release from NPP Krško for all prognosis available for the year 2017. Maximum distance predicted for sheltering, ITB and evacuation will be collected, analysed and compared to current zones.

## 3 INPUT DATA FOR CALCULATION

### 3.1 Source Term

Specific source terms prepared for NPP Krško were not available for this paper. Instead, generic source term was taken. Source term was selected from program InterRAS. Source term was for generic PWR, 1994 MWt, for scenario core melt – dry containment leak. Source term consists of 47 radionuclides.

#### 3.1.1 InterRAS

InterRAS (International radiological assessment system) was developed for IAEA by the US NRC. It is a version of NRC RASCAL (**R**adiological **A**ssessment **S**ystem for **C**onsequence **A**na**L**ysis) code prepared for international use. InterRAS is simple to use with limited options, but quite powerful. Weather has to be set manually and it uses Gaussian puff atmospheric dispersion model. It has generic core inventories for major reactor types, expected release coefficients based on the scenario (conservative ones) and calculates decay.

### 3.2 Weather

Meteorological data used was received from Croatian Meteorological and Hydrological Service. Every day prognoses were received after 06:00 UTC and 18:00 UTC, consisting of last 6 hours of real meteorological data and 48-hour prognosis. Since data were collected and stored automatically, some data were not stored because of server error.

For this paper, calculations were started at 06:00 UTC every day for which data exists. In all, 341 calculations were made.

### 3.3 Scenario

Standard release scenarios, including the most severe ones, last for days. On one hand, it is important to simulate longer-time release, because of changing weather conditions. On the other hand, this article is considering only measures that need to be implemented as soon as possible, and calculations were set up so that protection measures started at the ideal time – at the start of release. Since only urgent protective actions are assessed, the calculation time was set at 24 hours.

Five-hour uniform release interval was selected as interval large enough to enable effects from changing weather, while still short enough that the whole inventory can be released and transferred

through the atmosphere. Five-hour uniform interval was realized as 10 half-hour intervals with same source term, meaning that there is no decay calculated for any of the intervals up to the time it is released from the NPP.

Recently, Germany and Sweden analysed their protective zones using similar method. Selected source term compares well to the data available for Swedish and German ones ([3], [4]). The most significant difference, from radiological point of view, is around 3 times higher iodine release than Swedish case, relative to NPP power.

## 4 RODOS

RODOS (Real-time On-line DecisiOn. Support) system is system designed for off-site nuclear emergency management. In case of nuclear emergency in Europe, RODOS provides consistent and comprehensive information on the present and future radiological situation, the extent and the benefits and drawbacks of emergency actions and countermeasures, and methodological support for taking decisions on emergency response strategies. The RODOS system is the result of a close collaboration between almost 40 institutes from about 20 countries within the European Union, Eastern Europe and the former Soviet Union. The RODOS project was funded by the German Ministry of Environment, the European Commission and the participating institutes [5].

RODOS system has many features, functions and capabilities. Only some are presented in this article.

### 4.1 Selected RODOS features

RODOS system has two main operation modes, automatic and continuous mode:

- Automatic mode enables automatic calculation whenever real-time meteorological and radiological data is present. This mode can use user-defined source term, and between calculations with real data it can run calculations with prognostic data, but it cannot be set up without access to real-time meteorological data.
- In continuous mode RODOS automatically starts calculation for defined source term in defined intervals (default is 1 hour), changing start of the release to match time of the start of the calculation. User has to ensure that new meteorological data is regularly fed into RODOS. This mode enables the user to see at any time possible spread and consequences of sudden release of radioactive material.

RODOS has internal data for core inventories for various burnups for select NPPs, including generic inventories for LWR. User can add plant specific core inventories. RODOS is capable to calculate decay from the time designated as reactor shutdown and includes progeny in the analysis.

EMERSIM model is used for simulating urgent protective actions and calculating doses with and without those actions. The code calculates deposition of radioactive materials, and can calculate effects and costs of different clean-up measures. The food contamination and received dose from eating it, are calculated for variety of food and feedstuff.

New version of RODOS, JRodos, works with GIS database and results can be exported as .shp files.

RODOS includes three models for atmospheric dispersion of radioactive material. One of them RIMPUFF, is puff model, while the other two, DIPCOT and LASAT, are particle models.

### 4.2 DIPCOT

DIPCOT model was created during the development of RODOS system. DIPCOT is a dispersion model, which simulates the motion of air pollutants over complex terrain, based on a 3-D Lagrangian particle scheme. In order to build up a picture of the concentration distribution the total

mass of the pollutant is assigned to a certain number of computational particles. Each particle is "moved" with a velocity which takes account of two basic components: the transport due to the mean wind velocity, provided by meteorological pre-processors, and the random turbulent fluctuations are estimated by the Langevin equation. The knowledge of the spatial and temporal distribution of the particles allow the calculation of the mean ensemble concentration of the pollutants. DIPCOT utilizes topographical and meteorological information given at a 3-D grid and is capable of simulating dispersion from multiple point sources, at all atmospheric conditions. In the case of buoyant point sources, the model performs plume rise calculations. [6].

DIPCOT is of particular interest because, depending on the direction, plume from the NPP Krško is expected to start over hilly areas, continuing either over mountains or over low-lends. DIPCOT should handle such a terrain better then puff model.

DIPCOT has been validated against experimental data [6], [7].

### 4.3 Calculation spatial mesh

RODOS uses mesh of square cells. Calculations were done for the distance up to 400 km from the NPP, to allow for extreme cases. That means that calculation mesh was square with side length of 800 km and NPP Krško in the centre.

RODOS uses five different sizes of squares in calculation area, depending on the proximity to the NPP. Up to 10 km from the NPP, cell size is 1 km. From 10 to 40 km, it is 2 km. From 40 to 104 km from the NPP, cell size is 4 km, from 104 to 208 km it is 8 km and from 208 km to the end of the calculation area (400 km) it is 16 km.

## 5 RESULTS

From each calculation the furthest point from the NPP where action was implemented in the calculation was selected (tip of the cell that is furthest from the NPP). Tip of the cell, as opposed to the centre, was selected because it is easier to select on the graphical display of the results. Coordinates of that point were taken and distance was calculated, using "haversine" formula:

$$a = \sin^2(\Delta\varphi/2) + \cos\varphi_1 \cdot \cos\varphi_2 \cdot \sin^2(\Delta\lambda/2) \quad (1)$$

$$c = 2 \cdot \arctan\left(\sqrt{a}/\sqrt{(1-a)}\right) \quad (2)$$

$$d = R \cdot c \quad (3)$$

, where:
$\varphi$ is latitude,
$\lambda$ is longitude,
R is earth radius (calculated with mean radius of 6371 km).

For each calculation the procedure was repeated four times, once for each urgent protective action considered.

For each urgent protective action one other parameter was determined – does the area where protective action is implemented in RODOS cover any part of Croatia (is the centre of any cell on Croatian territory).

### 5.1 Actions on Croatian territory

The parameter whether measure needed to be implemented on Croatian territory is interesting, but not really important for decision-making. This parameter just states if measure was implemented on any area in Croatia, not the size of the area, so there are plenty of calculations where measure is implemented just between Kumrovec and Hum na Sutli in Croatia, but is implemented up to 100 km in Slovenia and Austria. Also, there were instances where measure is implemented just up to Croatian

border. Since border in RODOS is smoothed actual border, this may mean that measure was actually implemented on Croatian territory, but the program does not show it. The other way around is also valid, that is, measures where cell is just over the border may actually be implemented fully in Slovenia, but because of smoothing of the border are presented in RODOS as if they are in Croatia.

Number of calculations when measure needed to be implemented in Croatia is shown in Table 2.

Table 2: Is measure implemented in Croatia

| Measure | Yes (number of calculations) | No (number of calculations) |
|---|---|---|
| Evacuation | 159 | 182 |
| Sheltering | 132 | 209 |
| ITB, adults | 236 | 105 |
| ITB, children | 248 | 93 |

Calculations where ITB for children is not implemented in Croatia indicate that radioactive plume is going away from Croatia or that plume is going towards Gorski Kotar or Istria and is well dispersed. Calculations where ITB for children is implemented, but one or more of other measures is not indicate that plume is going towards Croatia, but meteorological conditions are such that it is dispersed well enough that high doses are not reached in Croatia.

## 5.2 Distance of implemented actions

In Table 3 selected calculated distances are given for each measure. Distances in table are minimum, mean, median and maximum.

Table 3: Distances where measures are implemented (in km)

| Distance | Evacuation | Sheltering | ITB, adults | ITB, children |
|---|---|---|---|---|
| Minimum | 8.5 | 7.0 | 19.6 | 22.7 |
| Median | 25.0 | 19.9 | 62.1 | 93.4 |
| Mean | 30.5 | 23.5 | 71.5 | 104.3 |
| Maximum | 107.9 | 94.7 | 303.6 | 351.8 |

In most cases maximum distances are relatively close together, but in small number of cases maximum distances are extremely far. This can be seen in Figures Figure 1 toFigure 8, and Table 4. Difference between $90^{th}$ and $100^{th}$ percentile for all measures is larger than absolute distance for $90^{th}$ percentile. In such circumstances expecting protective actions to be fully prepared and planned for the whole area of 100% of cases would be very expensive and counterproductive. Such an extension of protective zones would increase their area enormously. At the same time, people living so far from the NPP need first to be awoken to the fact that they need to plan some actions. In such circumstances, most of resources would need to be spent in the areas furthest from the NPP, potentially hurting the ability to protect the people closest to the NPP, those who may be in danger in non-extreme cases.

Also, implementation zones for extreme distances are not continuous – for extreme cases, implementation zones are usually up to the median continuously distributed and several distant cells are located where meteorological conditions stop the plume for a few hours over one location.

All the results of the calculations are shown in Figure 1 (evacuation), Figure 2 (sheltering), Figure 3 (ITB), and Figure 4 (ITB for children).

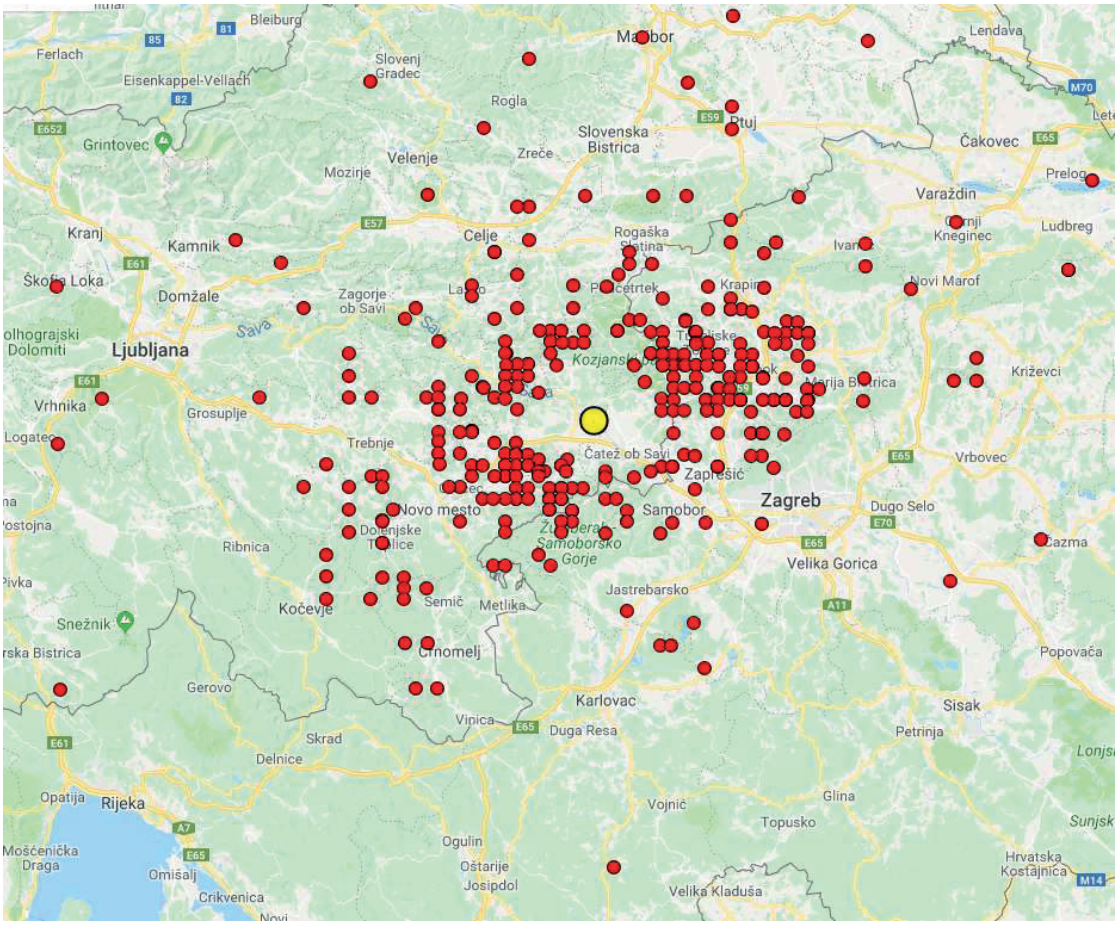


Figure 1: maximum distances for evacuation, all calculations

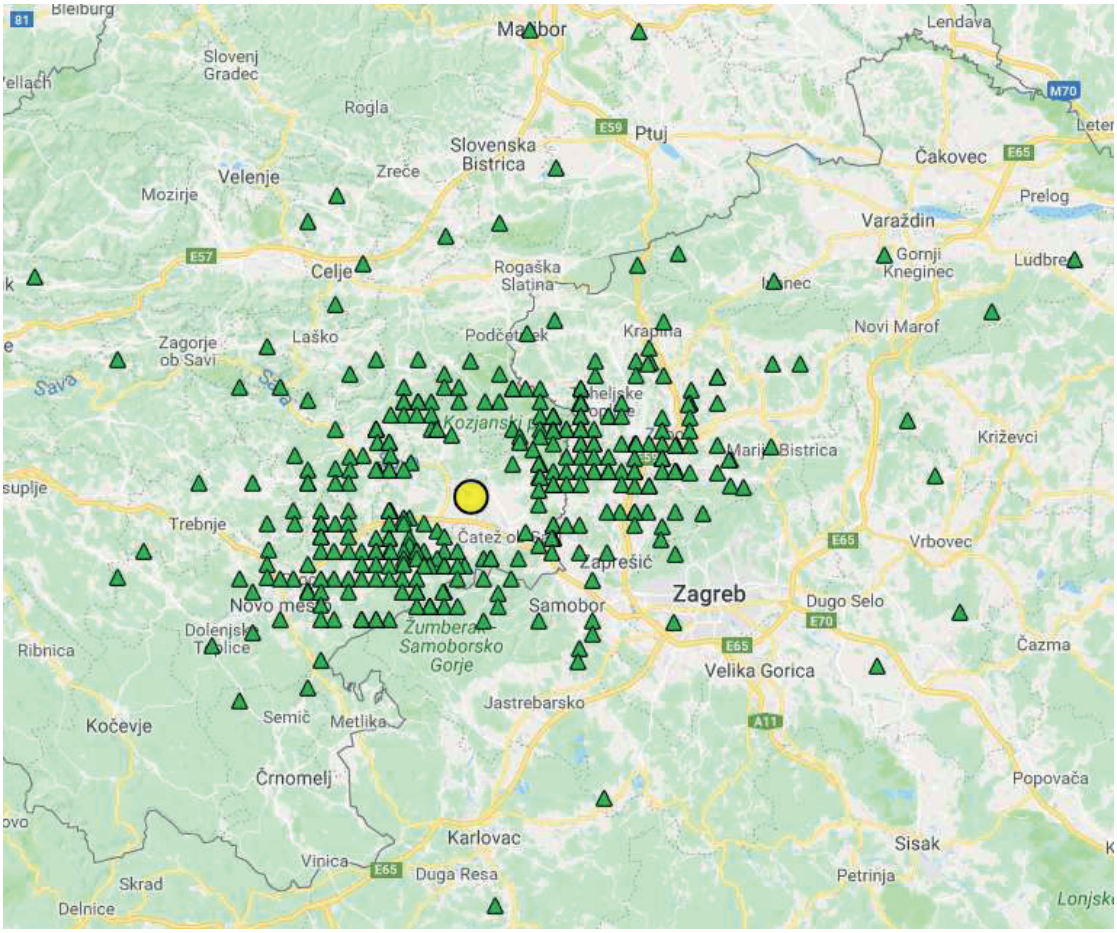


Figure 2: maximum distances for sheltering, all calculations

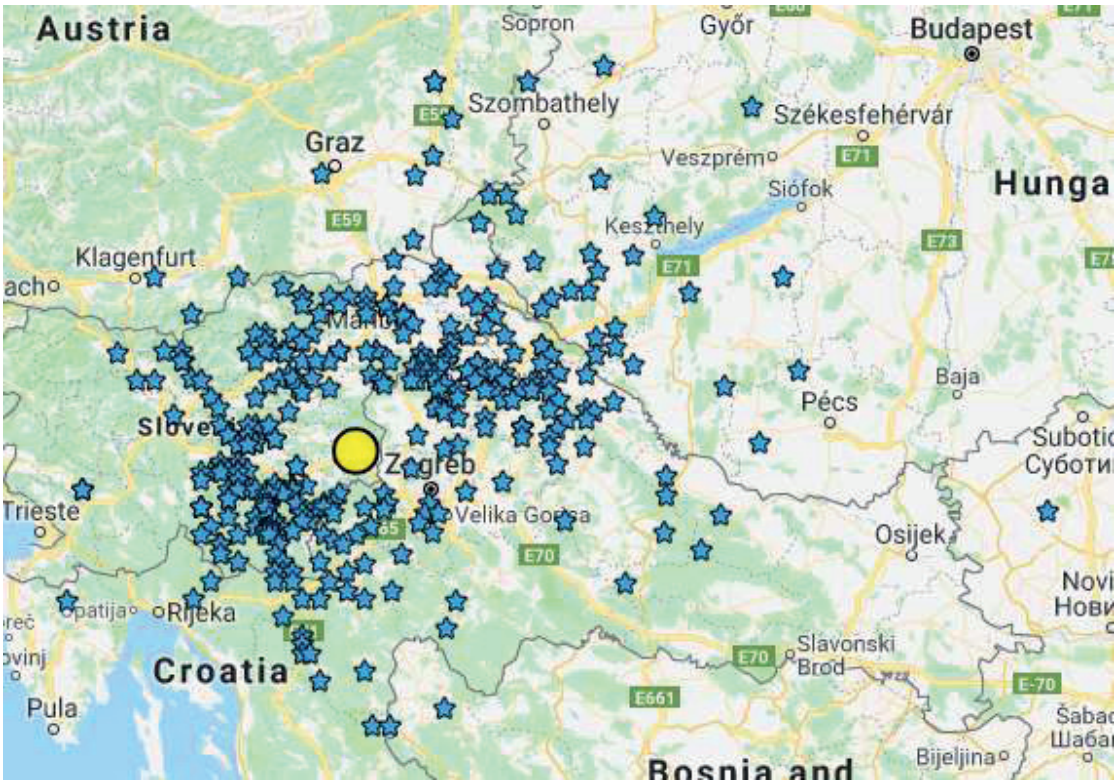


Figure 3: maximum distances for ITB, all calculations

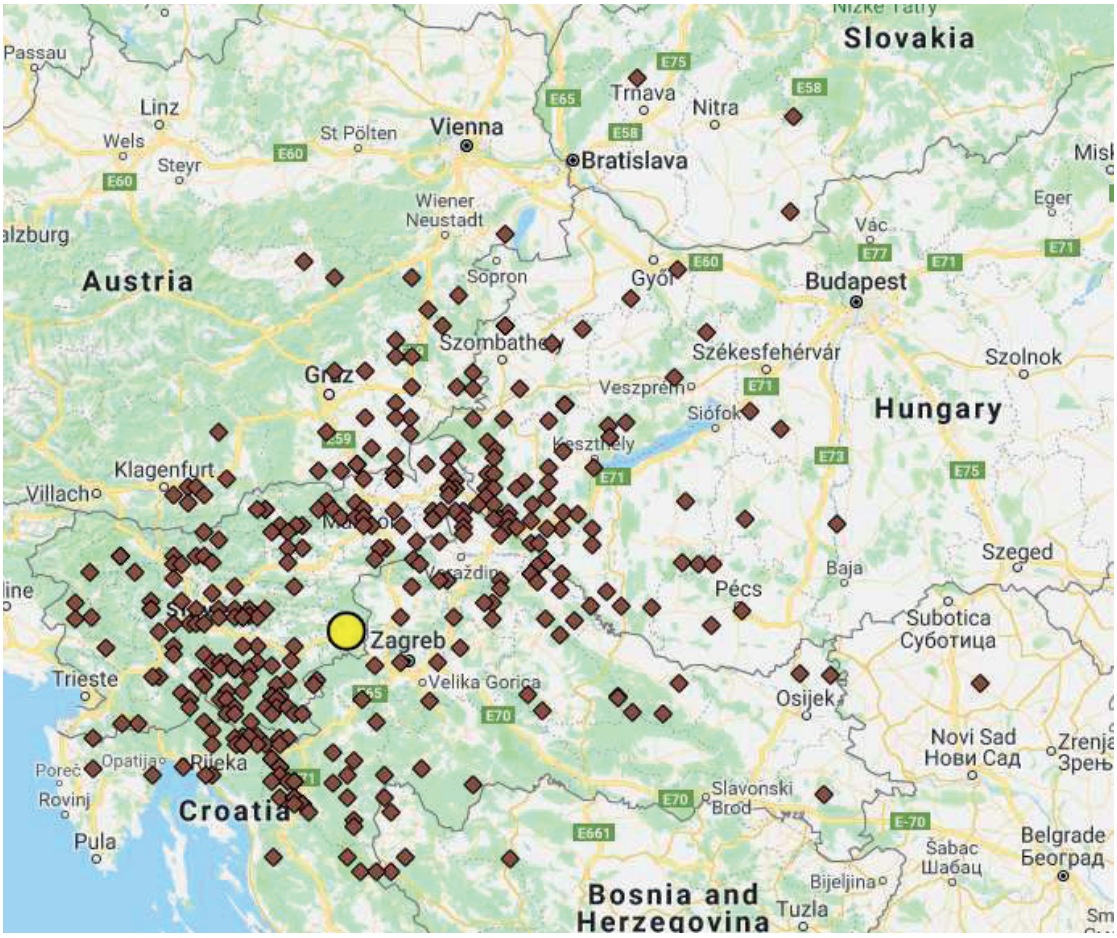


Figure 4: maximum distances for ITB for children, all calculations

While protection zones should not cover every case, question is how many cases they should cover. It is important to remember that Germany and Sweden selected for their calculations most extreme release for the NPPs they consider possible. German experts decided that 80% of analysed cases is enough, while Swedish experts displayed results for 70$^{th}$, 80$^{th}$ and 90$^{th}$ percentile, with 70$^{th}$ being considered good enough. Protection zones that cover 70% or 80% of possible outcomes for largest predicted release would cover well over 90% of possible outcomes for other large release scenarios and 100% possible outcomes for any accident that does not result in large release.

Source term selected in this paper is even more extreme than source terms selected in German and Swedish calculations, because the whole released inventory is released in the first five hours. Therefore, it should be expected that protection zones of similar dimension like in Germany and Sweden should cover less possible outcomes.

Distances for percentiles are given in Table 4.

Table 4: Distance percentiles (in km)

| Percentile (%) | Evacuation | Sheltering | ITB, adults | ITB, children |
|---|---|---|---|---|
| 10 | 14,4 | 11,2 | 36,6 | 52,4 |
| 20 | 16,5 | 13,4 | 44,6 | 64,5 |
| 30 | 18,8 | 15,9 | 49,6 | 76,3 |
| 40 | 22,0 | 17,1 | 55,7 | 83,5 |
| 50 | 24,9 | 19,9 | 62,1 | 92,8 |
| 60 | 29,6 | 22,7 | 68,3 | 103,5 |
| 70 | 34,5 | 26,0 | 80,5 | 114,2 |
| 80 | 41,0 | 30,9 | 91,9 | 131,0 |
| 90 | 53,5 | 38,0 | 120,6 | 167,1 |
| 100 | 107,0 | 94,7 | 303,6 | 351,8 |

Distances and percentiles are shown in Figure 5 (evacuation), Figure 6 (sheltering), Figure 7 (ITB), and Figure 8 (ITB for children).

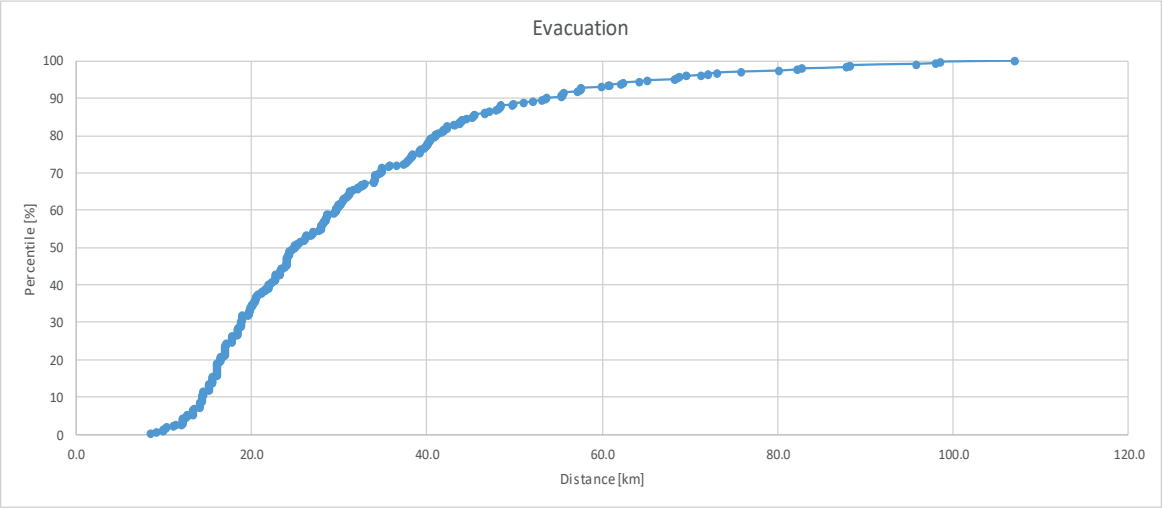


Figure 5: Percentiles for evacuation.

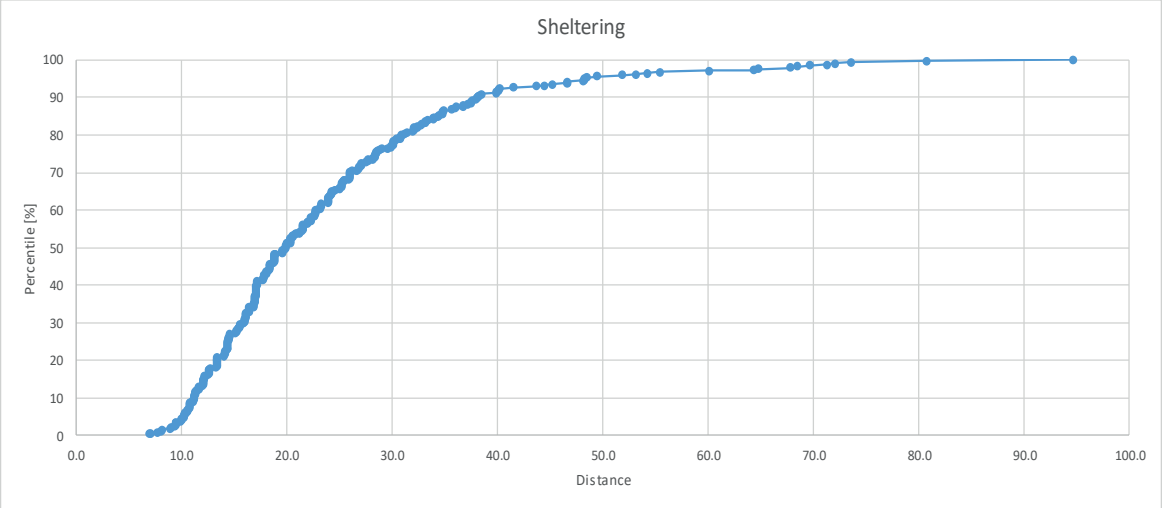


Figure 6: Percentiles for sheltering

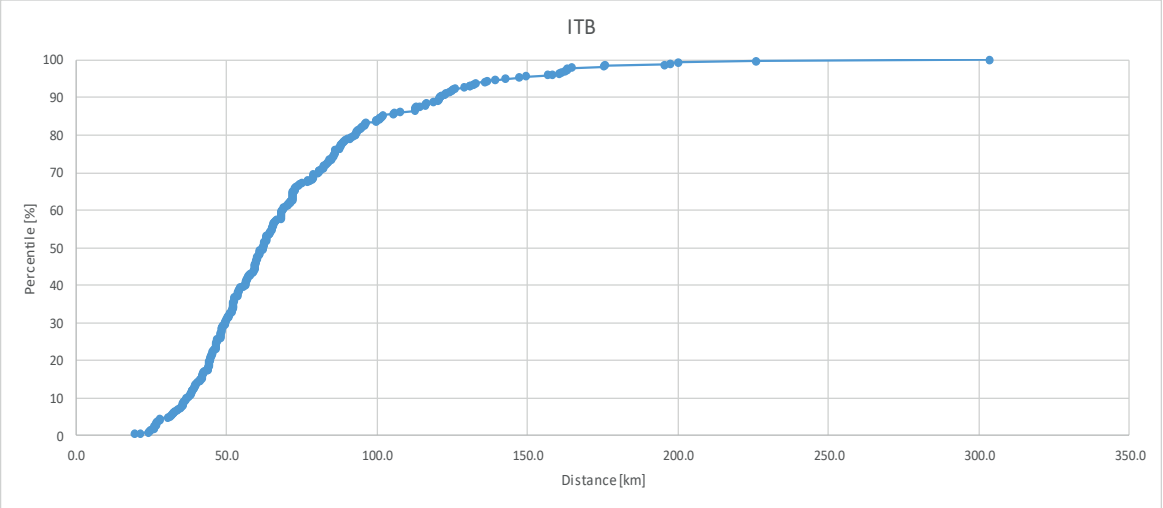


Figure 7: Percentiles for ITB

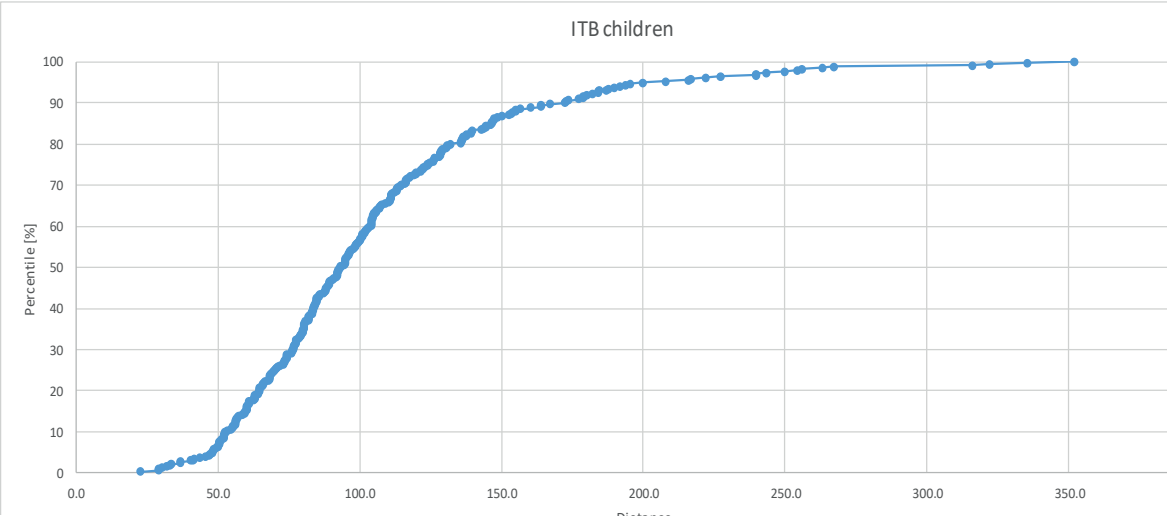


Figure 8: Percentiles for ITB for children

## 5.3 Comparison with current Croatian zones

Current Urgent Protective Zone (UPZ) covers over 30% of cases where evacuation is needed and over 50% of cases where sheltering is needed. These results are immediately interesting: area where sheltering is considered useful (it will reduce effective dose received by at least 10 mSv) is in all calculations smaller than the area where evacuation is considered useful (reducing effective dose received by at least 100 mSv over seven days). Sheltering protects from cloudshine and from inhalation during the passage of radioactive cloud. Evacuation, if implemented before the arrival of the cloud (for this set of calculations both sheltering and evacuation are expected to be fully implemented at the time of the release), protects from cloudshine, from inhalation during the passage of radioactive cloud and from groundshine. RODOS assesses need for each protective action individually. Area where evacuation is needed, but not sheltering, means that avoided dose from groundshine and inhalation is less than 10 mSv, but total dose from cloudshine, inhalation and groundshine is at least 100 mSv over 7 days. There are three possible explanations for such a situation: radioactive plume does not pass during first 24 hours, reduction coefficients for sheltering are very low, or deposition is very high.

There are some cases where meteorological situation is such that radioactive cloud circles over one area. However, such conditions are anomaly, not standard and cannot explain why all calculations show that evacuation area is larger than sheltering area.

Croatia is just outside of the Central European area that is fully characterized in RODOS. Most of the population living between 20 and 50 km from the NPP Krško live in cities and sheltering factors should be fairly high. If population density and cities are not properly entered in RODOS for area in question, RODOS may use lower sheltering factors. If that is the case, it should be obvious soon. Announced update expected in July should bring the whole Europe to the level of detail of Central Europe in current version.

Groundshine in calculations is very high. It can be explained by source term. Since no specific source terms were available, source term was taken from InterRAS (very large release) and released during 5 hours without additional decay calculated (see 3.3). Around 80% of groundshine comes from I-132, I-133 and I-135, isotopes with half-life of 2.3 hr, 20.8 hr and 6.6 hr respectively. Plant-specific source term, including realistic release intervals, should be used to check realistic groundshine.

Current Extended Planning Distance (EPD) covers over 80% of cases where ITB for adults is needed and over 50% of cases where ITB for children is needed. Considering number of cases and area covered, it is not advisable or even useful to extend EPD nor to plan pre-distribution of iodine tablets outside of EPD. Instead, it would be advisable to create several (2-4) regional storages from which iodine tablets can be quickly distributed to selected points (schools, kindergartens, hospitals) in areas where they may be needed outside of EPD. Because of time constraints, it is advisable to plan pre-distribution if not for the whole EPD, then at least for UPZ.

### 5.4 Comparison with other works

As has been previously said, Sweden and Germany did similar calculations as input for regulatory purposes. Both have used scenarios and source terms specific to their NPPs.

Swedish analysis in [3] shows that evacuation of up to 20 km is enough to prevent population receiving more than 100 mSv in 70% of cases. Because of different criteria for other protective actions, they cannot be directly compared.

German analysis in [4] shows that evacuation up to 26 km is enough to prevent population receiving more than 100 mSv in 80% of cases for all analysed NPPs, and only NPP Phillipsburg (1400 MWe PWR) needs evacuation of more than 20 km to cover more than 80% of the cases. As with Swedish analysis, criteria for other protective actions is sufficiently different that they cannot be directly compared.

Both previous analyses performed with similar tools (Germany used RODOS, Sweden ARGOS) show much smaller evacuation zones needed than the calculation in this paper, even though power plants analysed have higher power. There are several possible reasons for such discrepancy.

Source term selected for this paper released maximum inventory in five hours. Plant-specific source terms release radionuclides over a period of days. Longer release time in most cases ensures larger dispersion. Also, it means significant reduction in the activity of short-lived radionuclides. Both factors should reduce doses in areas with highest doses.

Sweden used ten years of data for calculations, Germany five. This paper only uses one year. Less data means more possibility for extremes.

### 5.5 Further work

These calculations need to be repeated when better local data is available in RODOS. It would be advisable to extend the calculations to larger time period (not just 2017, but also previous years) and to start release at different time of day (if possible, doing several calculations for each day). It would be especially useful if specific source terms for specific large release scenarios (like station blackout or steam generator tube rupture) were available.

## 6 CONCLUSION

This paper presents calculations made with large release source term and real weather data in order to assess current emergency preparedness zones in Croatia. Calculations show that EPD covers over 80% of cases that need ITB for adults and over 50% of cases that need ITB for children. At the same time, current UPZ covers only 34% of cases analysed that need evacuation, lower percentage than for sheltering (50%). This is not in line with other internationally performed calculations, which showed that UPZ of similar size completely covers of 70% of cases that need evacuation. The main difference in the setup of this calculation compared the other international calculations is that other calculations used plant-specific source terms, with both release and calculation lasting up to days, depending on the scenario.

In other internationally performed calculations distance where sheltering should be initiated is between 2 and 7 times larger than distance where evacuation should be initiated (this paper uses same criteria for evacuation and sheltering as Germany and Sweden). If supposition that too high source term is responsible for such large evacuation areas is correct, and we use the lowest factor from other calculations (sheltering distance is two times higher than evacuation distance), Croatian UPZ would cover over 90% of cases that need evacuation. This number is also in line with expectations based on the results of German and Swedish calculations, taking into account power of their NPPs compared to the power of NPP Krško.

This paper should be expanded using weather data from multiple years, modelling release at different times of day and using plant-specific source terms for large release scenarios.

## REFERENCES


[1] Actions to Protect the Public in an Emergency due to Severe Conditions at a Light Water Reactor, EPR-NPP Public Protective Actions, IAEA, 2013.

[2] HERCA-WENRA Approach for a better cross-border coordination of protective actions during the early phase of a nuclear accident, HERCA/WENRA, 2014.

[3] Review of Swedish emergency planning zones and distances, Strålsäkerhetsmyndigheten Sweden, Report number: 2017:27e, 2018.

[4] Simulation potentieller Unfallszenarien für den Notfallschutz in der Umgebung von Kernkraftwerken mit RODOS, Bundesamt für Strahlenschutz Germany, BfS-SCHR-55/14, 2014

[5] RODOS home-page: https://resy5.iket.kit.edu/RODOS/Overview/index.html

[6] S. Andronopoulos, E. Davakis, J.G. Bartzis, RODOS-DIPCOT Model Description and Evaluation, RODOS report RODOS(RA)-TN(09)-01, 2009.

[7] E. Davakis, S. Andronopoulos, J.G. Bartzis, S. Nychas, Stavros. Validation study of the dispersion Lagrangian particle model DIPCOT over complex topographies using different concentration calculation methods, *International Journal of Environment and Pollution*, Vol. 20 No. 1-6, pp. 33-46, 2003.

Journal of Energy
VOLUME 68 Number 2-3 | 2019 | Special Issue
journal homepage: http://journalofenergy.com/

# Possibilities of Reliable Ultrasonic Detection of Subwavelength Pipework Cracks

**Ivan Hrabar**
INETEC–Institute for Nuclear Technology Ltd.
Dolenica 28, Lučko, Croatia
ivan.hrabar@inetec.hr

**Antonio Petošić, Petar Franček**
University of Zagreb, Faculty of Electrical Engineering and Computing,
Department of Electroacoustics
Unska 3, 10000 Zagreb, Croatia
antonio.petosic@fer.hr, petar.francek@fer.hr

**Marko Budimir**
INETEC–Institute for Nuclear Technology Ltd.
Dolenica 28, Lučko, Croatia
marko.budimir@inetec.hr

## ABSTRACT

An occurrence of cracks in pipework could lead to potentially very dangerous malfunction in some critical engineering systems such as power plants. There is a clear trend of replacing traditional manual testing with non-invasive in-situ methods that should detect crack formation in its early stage. Such as approach would enable replacing of unhealthy pipe components during the regular periodic outages. Ultrasonic testing is known to be a rather mature and reliable technology. However, it suffers from serious problems in detection of the cracks of subwavelength size. This paper attempts to soften aforementioned problems by investigating the influence of a duration of the unipolar excitation signal on the achieved resolution. In addition, the transducer input electrical-impedance of NDT transmitter was measured by using different excitation pulses and their levels and the results are compared with those obtained using traditional frequency sweeping method at low excitation levels. Finally, use of some advanced signal processing algorithms that might lead to the automatic detection of subwavelength voids, in scenarios with low signal-to-noise ratio, is discussed.

***Keywords:*** *ultrasonic testing, NDT, subwavelength, transducer self-impedance*

## 1 INTRODUCTION

Detection of damaged pipelines is a major concern in the power generation industry. Pipeline failure is a serious problem which leads to unpredicted power plant outages and an unplanned increase of operational costs. Therefore, it is important to regularly inspect critical components and to detect cracks in the earliest possible stage. A wide range of non-destructive testing (NDT) techniques can be used for pipe health monitoring (ultrasound, eddy current, surface replication …) [1]. Ultrasonic examination of critical components is a common practice in a variety of applications: aerospace industry, railway industry, quality control, critical nuclear power plant components, etc. In order to be able to detect small defects, in any material, it is needed to transfer as much as possible energy to the ultrasound wave in the component under test. Most commonly, single element ultrasound transducers are used [1]. The same active element is transmitting and receiving the ultrasound signal.

It is needed to design excitation signal in the way that we can get the best possible reflection from the early staged crack. Early stage cracks are small in dimensions and are usually smaller than half of the ultrasound wavelength. Importance of NDT early detection of possible defects in a pipeline is especially visible in nuclear power plant industry [2].

Ultrasound NDT transducers are usually characterized using low voltage (1 $V_{RMS}$) frequency sweeping signals around resonance of interest [3]. Electrical characterization is performed by measuring impedance magnitude and phase at a different frequency or amplitude ranges covering resonance and anti-resonance frequencies. But, on the field, operators most commonly use rectangular or spike excitation pulse signal of around 100 $V_{peak}$ up to 200 $V_{peak}$ with a duration determined from resonant frequencies of NDT transducer (around 200 ns) [1][4].

## 2 EXPERIMENTAL SETUP AND MEASUREMENT METHODS


Figure 1: Part of the experimental setup for testing detection algorithm: Krautkramer 2.25 MHz ultrasound transducer on SS 1018 calibration block

The experimental setup is constructed with commercial NDT Krautkramer 2.25 MHz transducer. Arbitrary waveform generator Keysight 33520b [5] is used for generation of different types of impulse excitation. Signal designed by waveform generator is amplified by E&I 2100L RF Power Amplifier [6]. The current is measured with Tektronix TCP312 current probe (range: 1 mA - 30 A, frequency range up to 100 MHz) [7]. Tektronix TCP312 current probe has integrated its own amplifier TCPA300. The current probe was auto-calibrated, before every measurement session, accordingly to the manual. Voltage is measured using Testec TT-SI9001 Differential Voltage probe.

Voltage probe Testec TT-SI 9001 is connected to coaxial cables right next to the current probe. Testec TT-SI 9001 has a frequency range up to 25 MHz and levels up to 700 $V_{pp}$ [7]. Signals from probes are acquired by Agilent MSO-X 3024A oscilloscope [8]. Acquired signals are analysed in MATLAB by using own developed functions. Signals in experimental setup propagate through coaxial cables except on measuring spot where small modification was made to accommodate current and voltage probe one next to another. Measuring spot is placed as close to the transducer as possible. As sample of material, with the known defect, PH Tool calibration block IIW type 2 reference block made from 1018 steel is used. Repetition frequency is set to a low value to avoid heating of examined ultrasound transducer. Scheme of the experimental system is shown in Figure 2.

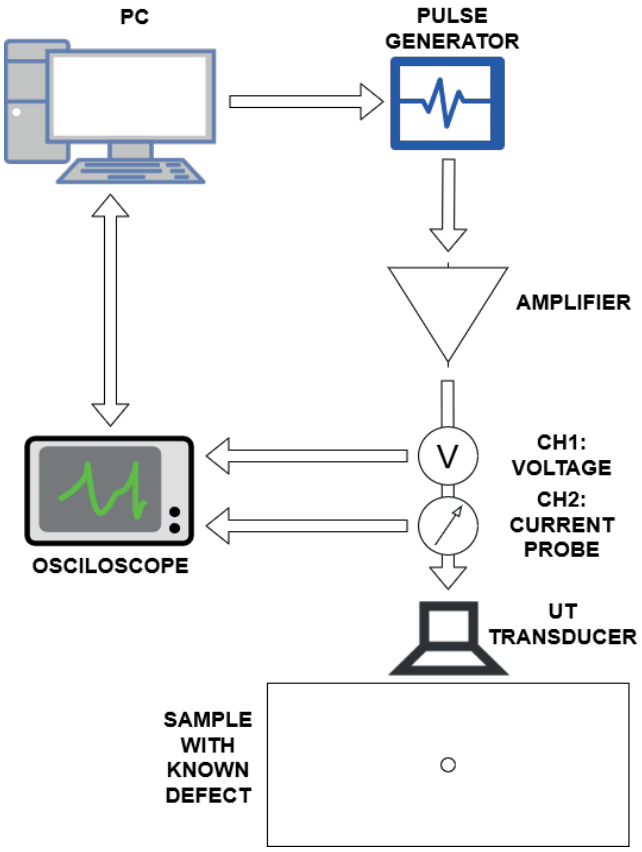


Figure 2: A schematic preview of the experimental setup

Parameters of a pulse generator and oscilloscope can be selected from a computer via standard USB communication. Aforementioned equipment is controlled by MATLAB R2010b programming package [9]. MATLAB script was developed in which computer sequentially sets parameters to pulse generator and acquire data from an oscilloscope. The BODE 100 impedance analyser is used for measuring impute impedance of selected transducer. The BODE impedance analyser is using low voltage (1 $V_{rms}$) frequency sweeping signal. Before every measurement, short, open and load circuit calibration of measurement system was performed in accordance with the manual [10].

## 3 REFLECTION DETECTION ALGORITHM

Algorithm for automatic detection of reflection in low signal to noise ration A-scan was constructed. Acquired A-scans has noticeable quantization noise. A measurement was performed on calibration block with a hole in it (Figure 1.).

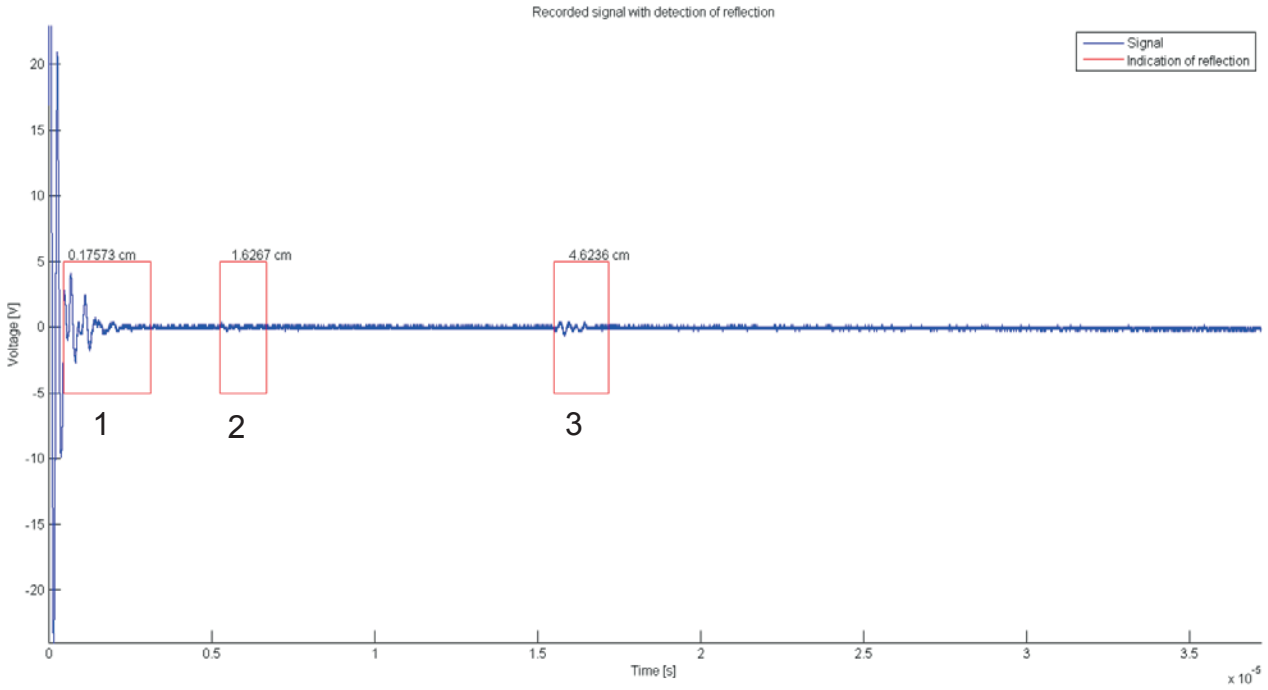


Figure 3: Acquired A-scan with algorithm indicated reflectors (surface reflection, 1 mm hole reflection and bottom reflection)

The diameter of a hole is 1 mm which is below half of the wavelength (1.28 mm) at the declared working frequency of considered transducer at 2.25 MHz of the used ultrasonic wave in calibration block. The hole is placed 1.5 cm from a surface. The algorithm was developed in MATLAB R2010b [9] programming package using built in mathematical and signal processing functions. The bottom surface is placed 4.5 cm from a surface.

Example of acquired A-scan with the result of the algorithm is shown in Figure 3. and part of the setup for algorithm validation can be seen in Figure 1. As it is seen acquired A-scan had high noise presence and reflection from 1 mm hole defect is barely recognizable even for a skilled operator. The goal of the developed algorithm is to soften aforementioned challenge. The amplitudes of both reflections (1 mm hole reflection and bottom reflection) are small. Classical filtering techniques were examined in order to find distinguishing feature which will enable automatically reflection detection in a signal.

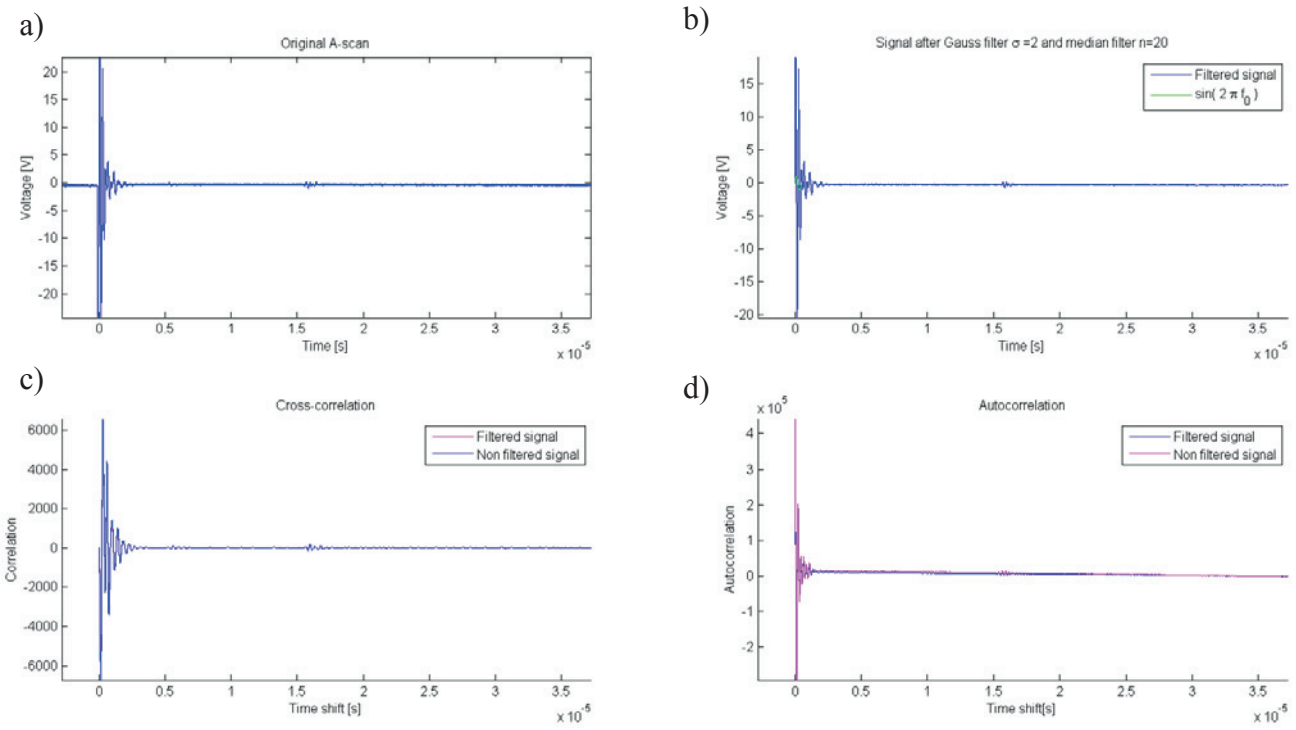


Figure 4: Comparison of classical filtering techniques on acquired A-scan.
a) Original acquired A-scan
b) Signal filtered with low pass Gauss filter ($f_p$= 2.25 MHz, σ=2) and median filter (n=20). One period of sin signal with frequency 2.25 MHz is plotted for comparison.
c) Comparison of cross-correlation of constructed one period of sine signal (amp=1, f=2.25 MHz) and acquired and filtered signal
d) Comparison of an autocorrelation of a filtered and non-filtered signal

From Figure 4. is seen that best results were achieved with cross-correlation of one period of sine signal, at working frequency of the transducer (2.25 MHz), and acquired signal. Classical filtering did not provide desired information for distinguishing feature of reflection. Hilbert transformation was performed on filtered signal (Equation 1).

$$H(u)(t) = \frac{1}{\pi}\int_{-\infty}^{\infty}\frac{u(\tau)}{t-\tau}d\tau \qquad 1)$$

An absolute value of the result of Hilbert transform is an envelope of the transformed signal [11]: Figure 5a).

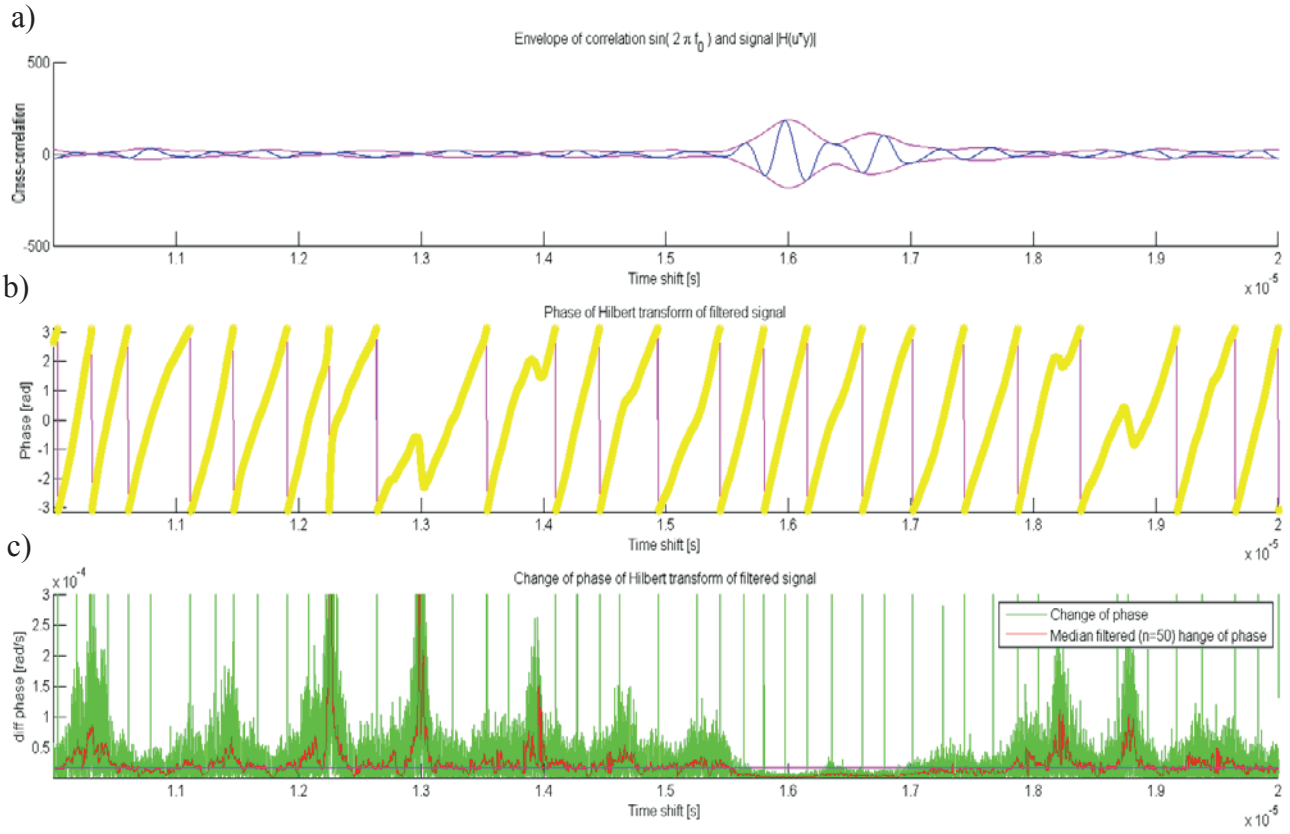


Figure 5: Comparison of part of the signal (1 mm hole reflection) with results of the Hilbert transform

It has been noticed that phase of Hilbert transformation with reflection changes constantly: Figure 5b). In Figure 5c) change of phase of the Hilbert transform is shown. Change of Hilbert transform has frequent, periodic, high pikes caused by phase "jumping" from +π to –π. Other pikes are probably caused by noise. Change of phase of Hilbert transform was filtered by a median filter (n=50) to get rid of all pikes. It is seen, Figure 5c), that after filtering change of phase is almost zero. This showed to be easily distinguishing feature useful for automatic detection of a reflected signal [12]. Criteria of 40% of the mean value of phase change in whole signal and minimal duration of zero phase change (one period, $T = \frac{1}{f}$) were selected for reflection detection.

In Figure 3., the result is shown: red boxes enclosing detected reflections in acquired A-scan. The algorithm had detected and noted three reflections in acquired A-scan. First one is caused by front surface reflection. An ultrasonic gel is applied on ultrasonic transducer before use, to make the transition of ultrasonic waved, to a target material, easier. If a transducer is not firmly placed on the sample, the ultrasonic gel forms a thick layer in between. The second reflection is hard to notice. It is the reflection from subwavelength reflector: 1 mm diameter hole. The third reflection is caused by bottom surface reflection. Based on known sound velocity in used calibration block, the algorithm calculates a position of the reflector in a material. Positions are acceptably correct calculated. Error in position calculation is caused by thickens of the ultrasonic gel layer. Described criteria showed the excellent result of detecting subwavelength reflector in signal with a high signal to noise ratio.

## 4 MEASURING THE INPUT ELECTRICAL IMPEDANCE OF USED TRANSDUCER

Ultrasound transducer from manufacturer Krautkramer, model B 00WT5F with a declared working frequency of 2.25 MHz is used [13]. Ultrasound transducer was characterized in a range from 1.75 MHz to 6.75 MHz. Aforementioned ultrasound transducer was electromechanically characterized using BODE 100. Impedance response of ultrasound transducer can be seen in Figure 6. It is visible that the series resonant frequency of the whole transducer is not on the declared frequency of 2.25 MHz. It is assumed that ultrasound transducers have incorporated impedance matching circuit (RLC circuit to adjust impedance of active element to impedance of cable) inside. Electromechanical characterization of the whole transducer does not necessarily describe behaviour of the active element itself because the resonant frequency of assembled transducer is changed due to added masses (backing and front layers) [1].

Sound speed in used calibration block is 5760 m/s. Calibration block has few through holes that are used as known defects. For frequency of 2.25 MHz and sound velocity of 5760 m/s wavelength in calibration block is 2.56 mm. A hole with the diameter of 2 mm is used in the experiment, which is about 78% of the used wavelength at the declared series resonance frequency ($f_{sr}$) of 2.25 MHz.

$$PW = \frac{1}{2} \cdot \frac{1}{f_{sr}} \tag{2}$$

The input electrical impedance of the used transducer around resonance mode of interest is shown in Figure 6.

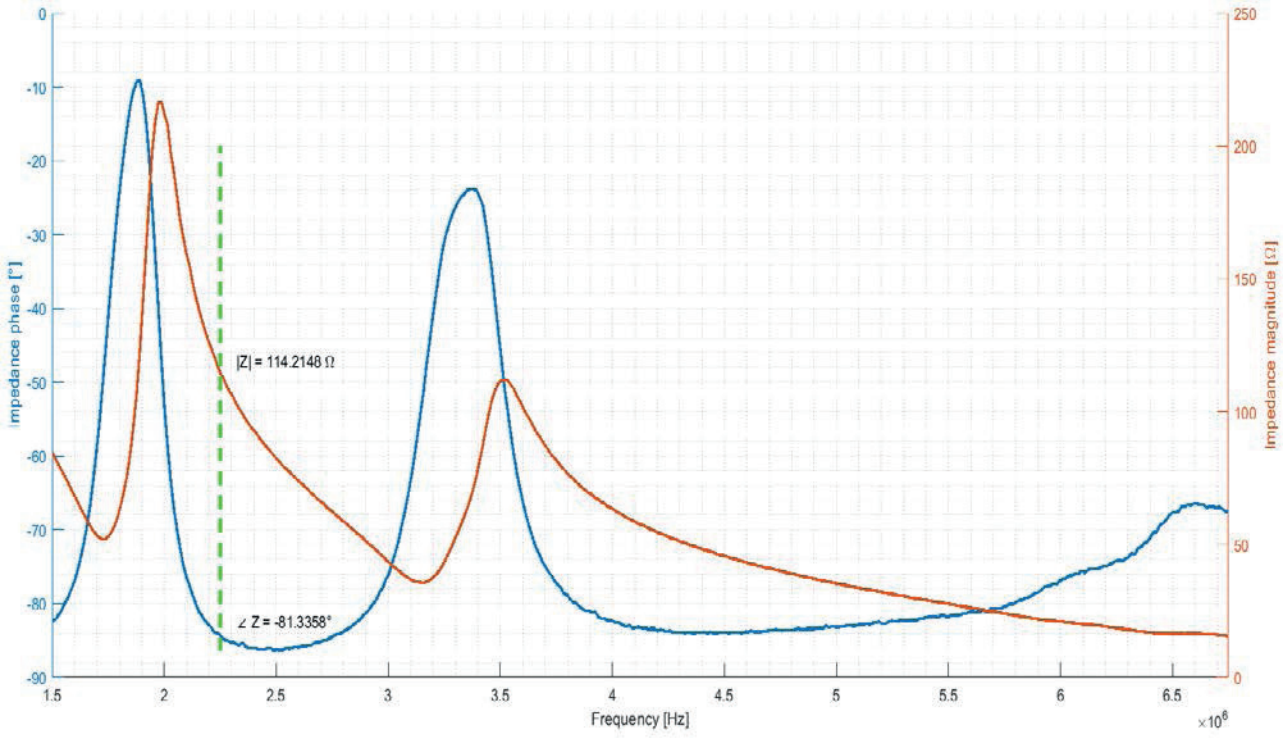


Figure 6: Impedance characteristics of ultrasound transducer Krautkramer B 00WT5F with the specified frequency of 2.25 MHz and accompanying values of impedance magnitude and phase.

In field operations, an ultrasound transducer is excited by a rectangular pulse which duration is determined, in accordance with Equation 2., on declared frequency. The rectangular unipolar excitation signal is constructed in the generator with repetition frequency f=100 Hz. The perfect rectangular signal is not possible to construct on used waveform generator. Minimal feasible rising and falling time of 8.6 ns is used. The duration of the unipolar signal is varied around the declared best duration of excitation signal (222.2 ns) with quantization of 0.1 ns.

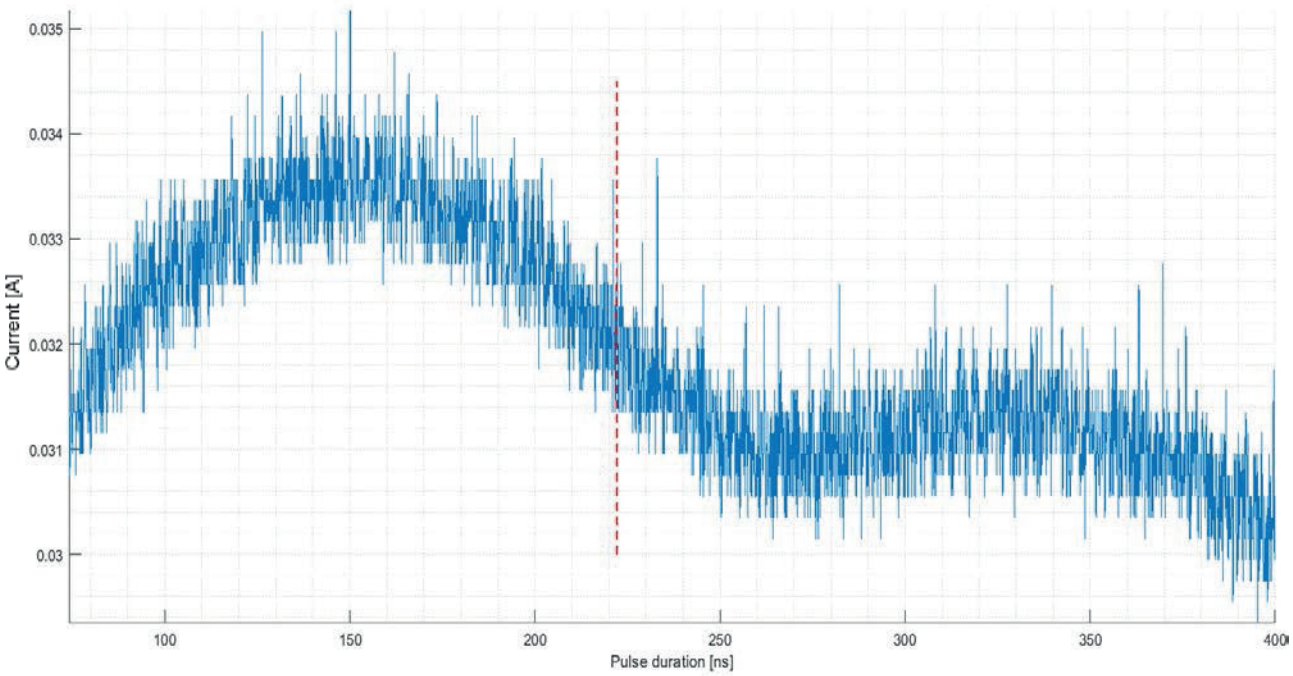


It is visible in Figure 7. That better intensity of reflection from known defect, in this case, can be achieved by shortening pulse duration around the 150 ns which gives excitation frequency of 3.33 MHz.

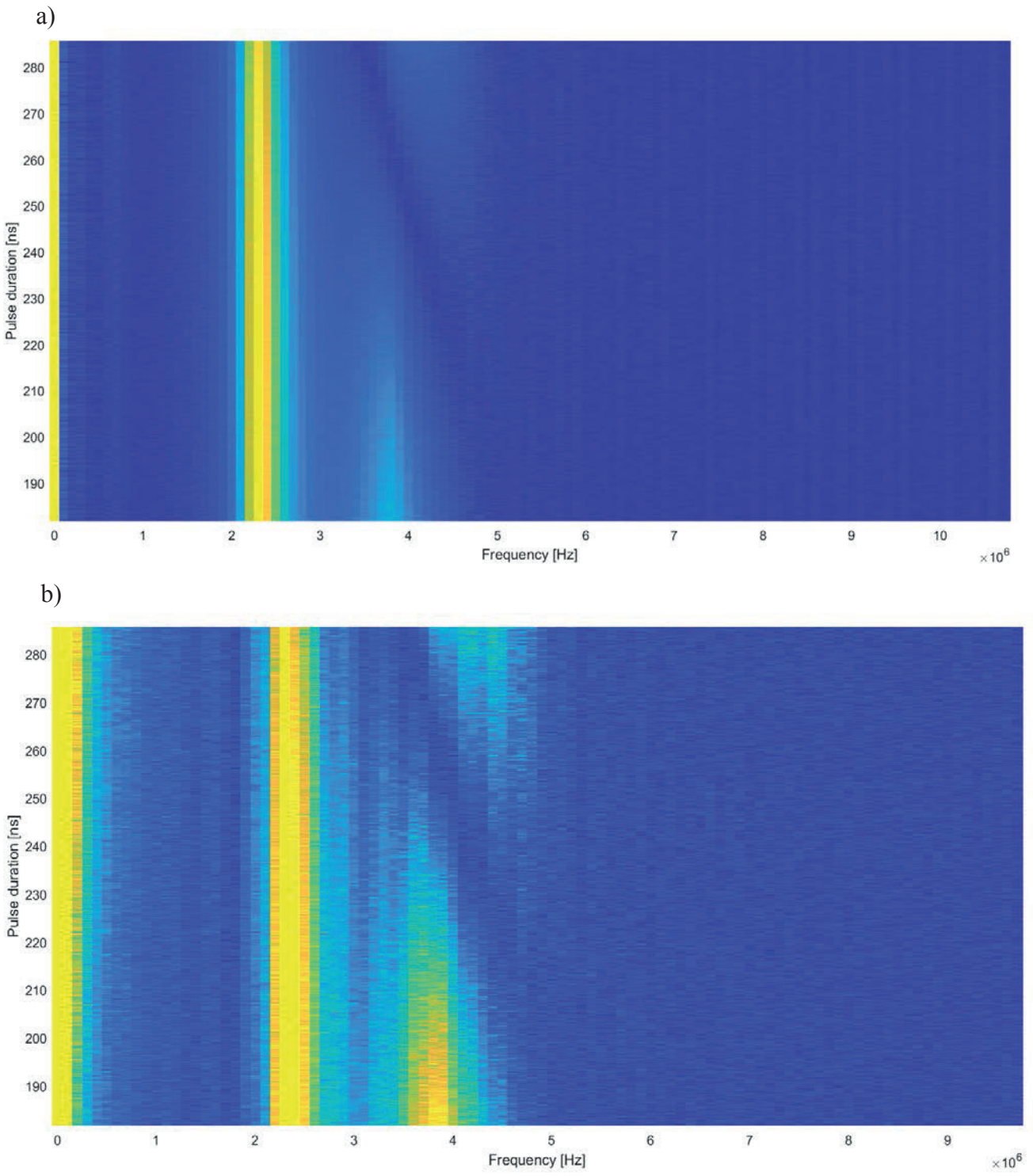


Figure 8. Comparison of lower parts of single side amplitude spectrums of current (a) and voltage (b) of reflection from known defect to the duration of rectangular pulse excitation signal. Warmer colour indicates a higher value of the spectral component.

From Figure 8., it is seen that active element always oscillates on its own resonant frequency of 2.25 MHz and duration of excitation unipolar signal does not make any visible impact on the self-resonant frequency of active element of the examined ultrasonic transducer.

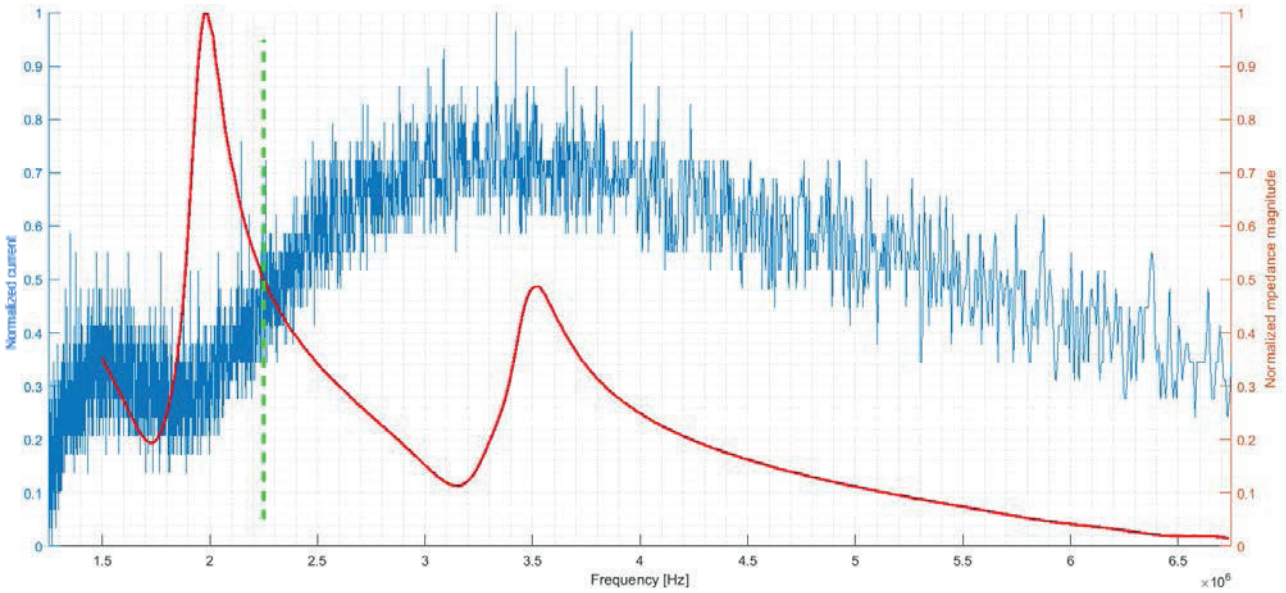


Figure 9: Comparison of the normalized impedance of transducer and normalized intensity of reflection form known defect whit specified declared frequency of 2.25 MHz

From Figure 9. it is seen that shape of the normalized intensity of reflection and shape of normalized impedance magnitude do not match in shape or inverse of shape.

The excitation signal is, by changing the duration of the excitation signal, adjusted not only to the active element but to the impedance of the overall transducer (piezo-electrical element loaded with front and backing layers and) electrical matching network of the transducer as well [1].

## 5 CONCLUSION

The experimental setup for testing the influence of different unipolar pulse duration on the reflection detection is designed by using laboratory setup.

The input electrical impedance of NDT transducer is measured by using BODE 100 Vector/Network analyser and additional electrical characterization of commercial ultrasound transducer was performed with a rectangular unipolar excitation signal before RF amplifier. Dependencies of reflection intensity, form known defect, is measured in dependence with the duration of a unipolar excitation pulse of the same amplitude. Duration of excitation signal was varied around typical duration (Equation 2) determined from the low level series resonance frequency. The intensity of reflection from known subwavelength defect (defect diameter 2 mm, wavelength 2.56 mm, frequency 2.25 MHz) was maximized by shortening duration of excitation rectangular pulse.

Algorithm for automatic detection of subwavelength defects based on the change of A-scan Hilbert transform phase derivation was constructed and experimentally validated. Algorithm showed a very positive result on detection subwavelength reflector (reflector diameter 1 mm, wavelength in material 2.56 mm, Figure 1.).

The input electrical impedance does not depend on the pulse duration when it is determined by using unipolar excitation signals. It is possible to determine the optimal duration of excitation unipolar pulse signal by using pulse excitation, compared with the situation when pulse duration is determined by widely used expression (Equation 2.), when commercial transducer declared series resonance frequency is used as input parameter for optimal pulse width. Described characterization with unipolar excitation pulse of optimal duration enables more reliable early stage crack detection due to higher reflection amplitude.

**ACKNOWLEDGMENTS:**

This work has been partially funded by the European Commission Horizon 2020 Fast Track for Innovation CreepUT project, grant number 760232.

**REFERENCES**

[1] Mark V. Brook, Ultrasonic Inspection Technology Development and Search Unit Design, John Wiley & Sons, Hoboken, 2012.

[2] A. Ballesteros, R. Sanda, M. Peinador, B. Zerger, P. Negri, R. Wenke, Analysis or events related to cracks and leaks in the reactor coolant pressure boundary, *Nuclear Engineering and Design*, Vol. 275, pp. 163-167, 2014.

[3] A. Petošić, M. Budimir, N. Pavlović, Comparison between piezoelectric material properties obtained by using low-voltage magnitude frequency sweeping and high-level short impulse signals, *Ultrasonics*, Vol. 53, No. 6, pp. 1192-1199, 2013.

[4] L. Svilainis, V. Dumbrava, S. Kitov, A. Aleksandrovas, P. Tervydis, D. Liaukonis, Electronics for Ultrasonic Imaging System, *Electronica ir elektrotechnika*, Vol. 20, No. 7, pp. 51-56, 2014

[5] 33500B Series Waveform Generators – Data Sheet, Keysight Technologies, 2017.

[6] 2100L Broadband Power Amplifier – Product Manual, Electronics & Innovation Ltd., Rochester, 2008.

[7] AC/DC Current Measurement Systems – Probes Datasheet, Tektronix, Inc., 2007.

[8] Agilent InfiniiVision 3000 X-Series Oscilloscopes User's Guide, Agilent Technologies, Inc., Colorado Springs, 2013.

[9] MATLAB primer, The MathWork, Inc., Natick, 2018.

[10] Bode 100 User Manual, OMICRON Lab, 2010.

[11] A. B. Ming, W. Zhang, Z. Y. Qin, F. L. Chu, Envelope calculation of the multi-component signal and its application to the deterministic component cancellation in bearing fault diagnosis, *Mechanical Systems and Signal Processing*, Vol. 50-51, pp. 70-100, 2015.

[12] S. Purves, Phase and the Hilbert transform, *The Leading Edge*, Vol. 33, No. 10, pp. 1164-1166, 2014.

[13] Ultrasonic Transducers for Non-destructive Testing, Krautkramer, Lewistown, 2001.

Journal of Energy
VOLUME 68 Number 2-3 | 2019 | Special Issue
journal homepage: http://journalofenergy.com/

# Ensuring Electromagnetic Compatibility in Nuclear Power Plant beyond Equipment Qualification Tests

**Hrvoje Grganić**
Nuclear Power Plant Krško
Vrbina 12, 8270, Krško
hrvoje.grganic@nek.si

**Marko Valjak**
Nuclear Power Plant Krško
Vrbina 12, 8270, Krško
marko.valjak@nek.si

**Gregor Škorc**
Nuclear Power Plant Krško
Vrbina 12, 8270, Krško
gregor.skorc@nek.si

**Luka Romac**
Nuclear Power Plant Krško
Vrbina 12, 8270, Krško
luka.romac@nek.si

## ABSTRACT

Electromagnetic compatibility (EMC) is defined as the capability of equipment or system to function satisfactorily in its electromagnetic environment without introducing intolerable electromagnetic disturbances to anything in that same environment [1]. EMC regulatory requirements for instrumentation and control (I&C) equipment were not developed or in effect until the last few years. Therefore, there is a considerable number of plant equipment that has not been qualified for EMC. The current EMC regulatory requirements address new and modified equipment only, and do not call for testing of existing equipment. There is a gap, which has to be overcome, in order to understand the current level of EMC within the plant.

Equipment qualification normally implies formal tests in EMC chambers, which is not practical for the equipment already installed. This paper is a short overview of the preparation phase of a project that includes various EMC-related activities currently being performed in Krško nuclear power plant (NPP). The activities are categorized into two main groups: equipment immunity (susceptibility) tests, used as an assessment of the immunity of the existing equipment such as process cabinets, transmitters and similar, and zone mapping measurements, which are performed to record the electromagnetic environment of the selected plant areas.

There is no clear, detailed and unambiguous guidance on how to perform any of these tests. It takes a lot of engineering judgement to optimize them for a specific plant. Some of the most important questions addressed in this paper are 1) the selection of the plant areas for zone mapping measurements and susceptible equipment to be tested for immunity, 2) choice of electromagnetic disturbances, which shall be simulated during those tests, and 3) practical performance, i.e. harmonization of immunity tests with operation of other plant systems. It is necessary to decide which operation mode poses the "worst-case", i.e. how and when the immunity tests and zone mapping measurement should be performed.

The paper also addresses troubleshooting of poor EMC design and installation practices, which can significantly reduce the number of EMC-related problems in a plant.

***Keywords:*** *electromagnetic compatibility, electromagnetic interference, equipment testing, site surveys, in-situ tests*

## 1 INTRODUCTION

Regulatory Guide 1.180 [2][1] endorses test methods for evaluating electromagnetic emissions and immunity of new safety-related systems and modifications to existing safety-related systems. Revision 1 of this document was published in 2003. The average age of U.S. commercial reactors is around 36 years [3]. That means that most of the power plants have a significant portion of different I&C systems, which were installed prior to the publication of RG-1.180. Therefore, the existing equipment is not addressed by the regulatory requirements. It would be highly impractical to perform the same tests on existing equipment, as required for the new and modified equipment, including emission and immunity tests in an anechoic chamber. Hence, in order to assure that the existing process and control cabinets, pressure transmitters, positioners and similar equipment do not emit excessive emissions well above the limits defined in military and commercial standards, and that they can withstand expected noise levels, it is necessary to define a customized set of in-situ EMC tests.

This paper presents additional measures that can be taken in order to address the existing equipment. It describes the preparation phase of such an assessment, supported with the examples from the Krško NPP.

## 2 MOTIVATION FOR EMC ASSESSMENT

There are different results, which an assessment of this type can yield. Some power plants have recognized the benefits of wireless technologies [4], which can be used for online monitoring and transfer of operational parameters in inaccessible locations, remote controls of cranes and robots, communication systems and other. In that case, it is necessary to prove that the wireless signals will not interfere with the existing plant equipment.

Power plants commonly experience EMC related problems. The most relevant are spurious occurrences of alarms, but more serious consequences, like reactor scrams, are possible. The root cause for these problems and the associated equipment can't be determined. In that case, it is possible to target the specific equipment and thoroughly analyze its immunity.

Plant radios are commonly used in plants, but often they interfere with susceptible instrumentation. Their impact can be characterized with testing that can help to determine whether the existing exclusion zones are properly defined. It might be desirable to eliminate these exclusion zones, in order not to rely on administrative controls.

The results of the immunity tests and zone mapping can be used as input data for the EMC qualification tests of new equipment, instead of relying on generic data that can be found in the existing guidance [5]. Test and measurements of such type will help identify electromagnetic energy (EM) hotspots, which should be avoided as installation locations, or even as the potential health hazards. Other motives are possible as well.

## 3 IN-SITU IMMUNITY TESTS

In-situ immunity tests, performed on the equipment located in the plant areas, correspond to immunity tests performed in (semi)anechoic (reverberation) chambers or Open Area Test Sites (OATS), with some differences, which are discussed below.

In-situ immunity tests can be performed almost exclusively during the outage, when the impact to plant operation is minimized. For the same reason, it is further recommended to limit these tests to the core offload window only. This limit could possibly interfere with the requirement that the equipment must be energized and have meaningful (nominal if possible) indications that

can be observed. In addition, it is advisable to perform tests during the night shifts, not only for the above presented reasons, but also to be confident with a greater level of certainty that the equipment response is a result of the intentional electromagnetic and radio frequency interference (EMI/RFI) interference, and not some unrelated activity.

The first task is to decide which equipment should be tested. It should be based on the project motives, industry operational experience, importance of the equipment for plant safety and power production, estimation of the equipment susceptibility and severity of the EM environment, quantity of similar or identical components in the plant (discussed later) and other factors. The total number of the equipment must be limited due to the substantial duration of each test.

The monitored outputs for the equipment under test can be defined arbitrarily, but they mostly depend on the significance of the particular outputs. In the simple case of a pressure transmitter, it is reasonable to monitor the pressure value, locally or remotely. It is less straightforward what should be observed in case of complex process cabinets, but usually the choice is reduced to the local indications and displays, alarms, different parameters available on the plant computer and/or recorders in main control room (MCR). The acceptance criteria can also be arbitrarily defined, e.g. a predefined percentage of the process range for the monitored signals.

The injected EMI/RFI test levels can correspond to those defined for the MIL-STD-461 RS103 test (10 V/m over the whole frequency range), but it is possible to apply higher levels as well, in order to minimize test uncertainty, or to prove that it is possible to use different devices, like plant radios or tablets, within a closer distance of cabinets and other equipment.

In-situ immunity tests are intended to determine the response of the tested equipment, but not affect other equipment located in vicinity of the Equipment under Test (EUT). Thus, they are limited to the radiated immunity tests only. The radiated noise can be localized more easily compared to the conducted noise (also, some conductive immunity tests are defined as destructive). In order to do that, it is possible to reduce the distance between the emitting antenna and EUT, thereby reducing the effective radiated area of the EUT (sometimes this is inevitable because of lack of space), or simply by shielding the other equipment in the vicinity. The latter should include the equipment behind the antenna, as some antennas could have radiation patterns with significant back lobes. Shielding can be achieved by using copper nickel or similar fabric, which offers good shielding effectiveness up to the highest frequencies of interest. If it is recognized that the other equipment could cause any unwanted actuation, it should be disabled by putting it to test mode or by directly disabling executive components (for example, putting pump switches to pull-out positions).

The frequency range of in-situ immunity tests depends on the plant motives. It could be for troubleshooting of problems with plant radios, in which case the focus will be on 400 – 500 MHz range. If the plant wants to examine implementation of new wireless technologies, it will more closely study higher frequencies. The most common wireless data standards include Bluetooth and Wi-Fi, where it is important that both the existing equipment is not vulnerable in those frequency ranges, and also that all equipment that utilizes wireless technology can coexist in the same frequency band.

Different wireless technologies are characterized by different signal modulations. In order to shorten the test time, which can be crucial for realization of the tests during short system windows, it is practical to use conservative modulation schemes taken from military EMC tests. It can be assumed that it is more severe than all commercially used modulations. The RS103 test uses 1 kHz pulse modulation, 50% duty cycle, where the fast rise and fall time of the pulse produce significant harmonic content that affects analog and digital circuits. The more detailed explanation for why this modulation was chosen can be found in MIL-STD-461G [6].

In-situ immunity tests should be performed for different polarizations (vertical and horizontal) of the emitting antenna, although the worst case is usually the vertical polarization. Other polarizations between the horizontal and vertical one can be used as well, especially if it is dictated by the layout of the tested components, such as cables within the cabinet. By selecting only frequencies of interest, worst-case polarizations and modulations, reducing the dwell time (time at

which the interfering signal is injected for a particular frequency), and by testing more components at the same time, it is possible to significantly reduce the total test duration (from a couple of hours to approximately 30 – 40 minutes per test), and to test more equipment in a given period, without making any compromise on trustworthiness of the results. The minimum dwell time is limited by the response time of the equipment and sampling time of the recording system (local recorder, plant computer or other). Additionally, the test should be automated by using a single signal generator and predefining the test frequencies. In that case, it is only necessary to change the emitting antennas depending on the frequency range, and change their polarization.

In case that susceptibility is identified, several options are possible. If the equipment was conservatively tested with the doors open, or without its enclosure in general, it is possible to retest it in a less vulnerable configuration, which is usually the default one. Another option is to modify the equipment in order to improve its immunity. This includes the use of additional shielding, gaskets, EMC cable glands, ferrites, filters and other methods. Abovementioned methods of improvement of the equipment immunity are presented later in more details. If none of those measures is effective, it is always possible to define an exclusion zone around the susceptible equipment.

One of the most important advantages of these tests, compared to the EMC qualification tests, is that they reflect the authentic installation, whereas qualification tests only try to replicate it. It is common that the equipment itself is designed in accordance with the best EMC practice, but it fails immunity or emission tests due to the poor installation. Although it is a general rule to perform qualification tests in the same configuration, as it will be installed, and to install it in the same configuration as it will be tested, there are usually deviations from the rule. For that reason, it makes sense even to perform in-situ immunity test of the equipment that has been previously qualified, in case that there are large concerns over the way the installation was performed.

On the other hand, in-situ test repeatability is limited because the background emissions can vary, the equipment and structures in vicinity can affect results, and because the in-situ tests do not follow well-defined test setups and procedures, like qualification tests.

It is possible to test one representative component and assume that other identical or comparable equipment will behave similarly. If possible, it is recommended to choose one, which is assumed the most susceptible in its installation configuration, for example, because it contains the largest portion of exposed cables. Another criterion for the electronic equipment could be aging, whereby the older components may be more susceptible.

Figure 1 shows an example of an immunity test performed in NEK. It illustrates the statements presented above. The cabinet is tested with the doors open, which is a conservative assumption. The antenna is directed toward the cabinet cards that are assumed to be the most susceptible. The injected field strength is measured using an electric field probe in the cabinet's front plane. This cabinet is tested from both the front and back side. The same figure also shows that the equipment in vicinity is properly shielded using conductive fabric.

Figure 1 Immunity Test of Solid State Protection System (SSPS) Cabinet in MCR

## 4 BENCH IMMUNITY TESTS

Sometimes it is not possible, or desirable, to test equipment in-situ in the plant. In that case, it is possible to perform an alternative bench test, either in a laboratory, or in a workshop. Again, there are several advantages and disadvantages of this approach.

The positive side is that bench tests offer better flexibility, as they are not time limited, and therefore, it is possible to compare different installation configurations. However, they do not reflect the existing plant location. Similar to qualification tests, bench tests will likely identify potential problems of the component itself, but they will fail to answer whether the installation is adequate.

Bench tests are limited to components that can be found in the plant warehouse. Plant cabinets, on the other hand, are usually unique components, and they can only be tested in-situ.

Some of-the-shelf products could be already qualified, and their qualification reports are readily available. In that case, it is important to check whether the test methods, test scope, test levels, acceptance criteria and other factors are appropriate for the intended use. The highest test frequency increases as the new wireless standards emerge, and it is possible to find equipment that was tested, but up to only 1 GHz.

## 5 ZONE MAPPING

Zone mapping, sometimes also referred to as site survey, is a passive measurement of the electromagnetic environment levels in a power plant. It is not reasonable nor possible to perform it in all plant areas. The areas of interest include rooms where the susceptible I&C equipment is located, as well as areas with potentially excessive EM emissions. In addition to that, it is important to include areas where the related plant modifications, especially digital upgrades, are foreseen. The tests are based on emission tests described in MIL-STD-461 (CE101, CE102, RE101 and RE102) and corresponding commercial standards, yet they are slightly modified to fit the zone mapping purpose.

In contrast to in-situ immunity tests, zone mapping should be performed during on line operation. Otherwise, during outage, a large number of equipment is de-energized and does not contribute to the plant EM emission levels.

The plant EM environment is never in a steady state. Infrequent EM phenomena and/or transients could appear during plant startup, surveillance tests and while starting significant loads. Thus, zone mapping should be scheduled simultaneously with these activities. These kind of measurements are always challenging to perform. Measurement of the plant emissions in the

different frequency ranges requires use of different measuring equipment, in particular various antennas. The main reason is that different antennas have different gain profiles across different frequency ranges. Often, it is necessary to decide which phenomena shall be recorded during the short duration of the transients. Some (un)intentional emitters, such as plant radios and welding machines, can also easily be included in this survey.

Radiated emissions are preferably made with two opposite antenna directions. Firstly, in direction away of the equipment, to measure emissions seen by a cabinet or instrumentation. Second measurement would be in the opposite direction toward the equipment, in order to measure emissions of that same equipment. In both cases, it should be accounted that there is background emission level, i.e. the hypothetical cabinet is not the only contributor.

Zone mapping is not strictly related to radiative emissions. It is possible to obtain conductive emissions in an unobtrusive way as well, by using current clamps. Transient phenomena should be captured in the time domain, in contrast to the other measurements for which frequency domain is more suitable.

Although it could be said that each new modification affects the plant EM environment, it is not intention to repeat this assessment too often, except in case of major changes.

## 6 TROUBLESHOOTING

Electromagnetic interference can affect a victim in many ways, but usually the majority of the problems can be associated to a smaller number of causes, as the famous Pareto principle states.

As already indicated in previous sections, there are several options when susceptibility has been detected, whether during an immunity test or simply identified as a deviation from good practice by visual inspection. In the first case, before taking any corrective measures, it is advisable to repeat the portion of test during which the susceptibility was detected and to confirm that it was caused by the immunity test. The exact frequency for which the interference occurred should be determined.

It is possible to modify the installation or even the equipment itself to address the susceptibility. One of the simplest troubleshooting steps and tools to reduce or isolate most radiated emissions is to apply additional shielding. There are several different ways to use shielding to reduce interference caused by radiated emissions. For cabinets with glass doors, or different indicators, it is possible to apply metallic transparent foil. If there is a susceptible transmitter, it could be possible to put it in a metallic enclosure. Furthermore, it is desirable to replace nonmetallic enclosures with metallic. If it is necessary to protect equipment from magnetic fields, a material with high permeability should be used.

One of the most common examples of vulnerable equipment are pressure transmitters, which are, according to reports, often susceptible to radiated emissions in frequency range of plant radios. There are several identified mechanisms for how the radiated emissions can affect such instrumentation. It is possible that the EM noise penetrates the enclosure of the transmitter, which usually have a lid that is tightened to its body. The second mechanism is indirect. It involves noise coupled to the cables that enters equipment as a conductive interference, and possibly reradiates noise within its enclosure. The exact mechanism for a specific case can be determined by retesting the EUT in different configurations.

Depending on the identified failure, it could be adequate to shield the cables (as in Figure 2), the transmitter, or both. Shielding of the cables is usually the simplest solution, and it can be done by using metallized flexible conduit.


Figure 2 Retesting of the Pressure Transmitters with Provisionary Shielded Flexible Conduit

It is important to check whether EMC gaskets installed on the cabinet doors, or on the instrumentation lids, are installed appropriately. Large apertures, those used for ventilation, or simply consequence of a door design, can significantly reduce the shielding effectiveness.

Another simple fix could be the installation of ferrites around the cables. Such a fix can decrease the noise coupling, as well as the radiation of EM energy from the cables on which the ferrites are installed. Basically, a ferrite acts as a low-pass filter that blocks high-frequency current, thus attenuating the high-frequency noise. The frequency characteristics depend on selection the of the ferrite material.

Other methods could be more intrusive and it is not necessary advantageous to apply them, even if they can improve equipment immunity. For example, varistors can protect equipment from overvoltages, but they can also fail shorted and make the equipment inoperable. It is necessary to determine in advance which modifications are acceptable. The last solution, if none of discussed methods gives adequate results, is to declare an exclusion zones, or to replace the equipment with an alternative, immune model.

Following the implementation of one or more solutions discussed above, it is necessary to repeat the immunity test at least for the frequency and polarization for which the interference was detected.

## 7 CONCLUSION

Electromagnetic compatibility involves numerous different phenomena in a typical nuclear power plant. The consequences of interference range from nuisance to plant personnel up to reactor scrams and large economical losses. Existing regulation only partially addresses this problem.

There are different methods that concentrate on the existing I&C systems. They are categorized, similar to the EMC qualification tests, to immunity tests and emission tests.

It is challenging to develop a procedure for such in-situ tests. They have to take into account that it is not acceptable to affect the normal operation of the power plant. For now, there is no strict guidance on how to perform these tests, hence each power plant will come up with a unique plan. This paper presents some of the factors that should be taken into consideration for a successful performance of such an EMC assessment.

The test scope depends on the plant motives. Usually these are the implementation of wireless technologies, troubleshooting of specific EMC-related problems or gathering of input data for qualification tests. It is crucial to harmonize it with other plant activities, and be aware that the majority of the in-situ immunity tests can be performed during the outage period only, which is usually short.

The suggestions given in this paper are based on a similar project that is currently in progress at Krško NPP. Most of the recommendations are general and they can be applied on the other plants as well. Once the tests are finished, the results and conclusions will be presented in later papers. The described tests will help Krško NPP to be more confident that the tested equipment is immune to a specific EM interference, but it does not encompass all possible cases.

The electromagnetic environment is continuously changing, and there are new technologies on the horizon. It is important to keep pace with them in order maintain an appropriate level of electromagnetic compatibility in the plant, once it is established.

## REFERENCES


[1] International Technical Commission, IEC 60050-161:1990, "International Electrotechnical Vocabulary", Area 161: Electromagnetic compatibility, 1990

[2] United States Nuclear Regulatory Commission, Regulatory Guide 1.180 rev.1, "Guidelines for Evaluating Electromagnetic and Radio-Frequency Interference in Safety-Related Instrumentation and Control Systems ", ML032740277, 2003

[3] United States Energy Information Administration, https://www.eia.gov/tools/faqs/faq.php?id=228&t=21, last updated on July 21, 2017, accessed on April 2, 2018

[4] Kiger, C. J. et al., Harnessing wireless data from the containment of a nuclear power plant, Instrumentation & Measurement Magazine IEEE, vol. 16, pp. 18-23, 2013, ISSN 1094-6969.

[5] Electric Power Research Institute, TR-102323 rev.4, "Guidelines for Electromagnetic Interference Testing in Power Plants", 2013

[6] Department of Defense, MIL-STD-461G, Requirements for the Control of Electromagnetic Interference Characteristics of Subsystems and Equipment, 2015

Journal of Energy
VOLUME 68 Number 2-3 | 2019 | Special Issue
journal homepage: http://journalofenergy.com/

# Sludge Removal at Krško NPP Steam Generators during Outage

**Robert Kelavić, Marko Turalija**
Krško Nuclear Power Plant
Vrbina 12, 8270 Krško, Slovenia
Robert.Kelavic@nek.si, Marko.Turalija@nek.si

## ABSTRACT

Sludge removal is performed on two steam generators (SG's) at the Krško Nuclear Power Plant (NEK) during every outage. SG's are a meeting point of four major plant systems: Reactor Coolant System (RC) on the primary side and three systems on the secondary side – Auxiliary Feedwater System (AF), Main Feedwater System (FW) and Main Steam System (MS).

Sludge removal activities take place on the secondary side of the SG's on the top of the tube sheet. It consists of classical Sludge Lancing (SL) which is done by spraying water at different angles (30°, 90°, 150°) between the tube gaps in the steam generator tube bundle with a pressure around 220 bars. Another method is Inner Bundle Lancing (IBL) which means spraying water at a much higher pressure (NEK's contractor reached a pressure of approximately 590 bars). Such water is sprayed directly on the top of the tube sheet with a robot guided lance which is placed inside a steam generator. The robot is controlled by an operator and at times fully autonomous to provide the highest protection measures possible. After these activities, a televisual inspection (TVI) of the top of the tube sheet is performed to access the hard sludge area and to search for potential foreign objects in the SG's. If an object is found, an attempt to retrieve it would usually take place. Other methods of sludge removal as upper bundle flushing or chemical cleaning have not been implemented in NEK thus far.

Since the power plant uprate in May 2000, NEK conducted SL on both SG's every outage with IBL in 2013 and 2015 and the same method was used in the 2018 outage. The purpose of these activities is mainly to extend the full load operation of the plant, prevent denting processes in the SG's from occurring, stop the buildup of hard sludge area to increase/sustain efficiency and remove foreign objects found in the SG's.

SG's U-tubes are a barrier between the primary side coolant and the secondary side of NEK and the environment. Therefore, it is crucial to keep the highest level of integrity of the U-tubes because any leak could potentially mean a release of radioactive material to the atmosphere.

This paper describes the purpose and workflow of sludge removal in NEK.

***Keywords:*** *steam generators (SG's), Sludge Lancing (SL), Inner Bundle Lancing (IBL), televisual inspection (TVI), Foreign Object Search and Retrieval (FOSAR), Krško Nuclear Power Plant (NEK)*

## 1 INTRODUCTION

Sludge removal activities are performed on two steam generators (SG's) during every outage. SG's are a meeting point of four major systems which are Reactor Coolant System (RC) on the primary side and the three systems on the secondary side: Auxiliary Feedwater System (AF), Main Feedwater System (FW) and Main Steam System (MS).

Steam generators are safety related components that are required to operate during normal, abnormal and emergency conditions. During normal power operation steam from steam generators is supplied to the turbine. During shutdown conditions, they are a vital component in decay heat removal process. Additionally, steam generators act as a third barrier for preventing radioactive releases into the environment. Due to this the cleanliness and operability of steam generators is vital for safe operation.

Sludge removal activities take place on the secondary side of the SG's on the top of the tube sheet. It consists of classical Sludge Lancing (SL) which is done by spraying water at different angles (30°, 90°, 150°) between the tube gaps in the steam generator tube bundle with a pressure around 220 bars. Another method is Inner Bundle Lancing (IBL) which means spraying water at a much higher pressure (NEK's contractor reached a pressure of approximately 590 bars). Such water is sprayed directly on the top of the tube sheet with a robot guided lance which is placed inside a steam generator. The robot is controlled by an operator and at times fully autonomous to provide the highest protection measures possible. After these activities, a televisual inspection (TVI) of the top of the tube sheet is performed to access the hard sludge area and to search for potential foreign objects in the SG's. If an object is found, an attempt to retrieve it would usually take place.

This paper describes the sludge removal process in NEK from start to finish. Descriptions from setting up the equipment, differences between Sludge Lancing and Inner Bundle Lancing, and the purpose of TV inspection and FOSAR attempts will be included. The paper will offer an insight into the results of this year's outage as well.

## 2 SETUP OF EQUIPMENT

Arrival of equipment and its radiological check take place about 7-10 days prior the start of operations. After the arrival of personnel, a detailed pre-job briefing and basic general employee trainings are conducted. 1-2 days prior to start of operations, a rough setup of the equipment is done, which includes setting up the hoses, cables, control units etc. inside the reactor building (RB). For the SL/IBL activities, containment integrity is not required, so as soon that's the case, the equipment inside the RB and outside of it is connected and water is recirculated through the Sludge Lancing system. The first analysis must prove the cleanliness of the SL/IBL equipment prior to introduction of that water inside the NEK's SG's.

The equipment for SL/IBL consists of a Sludge Lancing robot, diaphragm drain pumps, buffer tank, filter units (mechanical), storage tank with bypass cooling and resin filter system, high pressure pumps, control unit and hoses and valves.

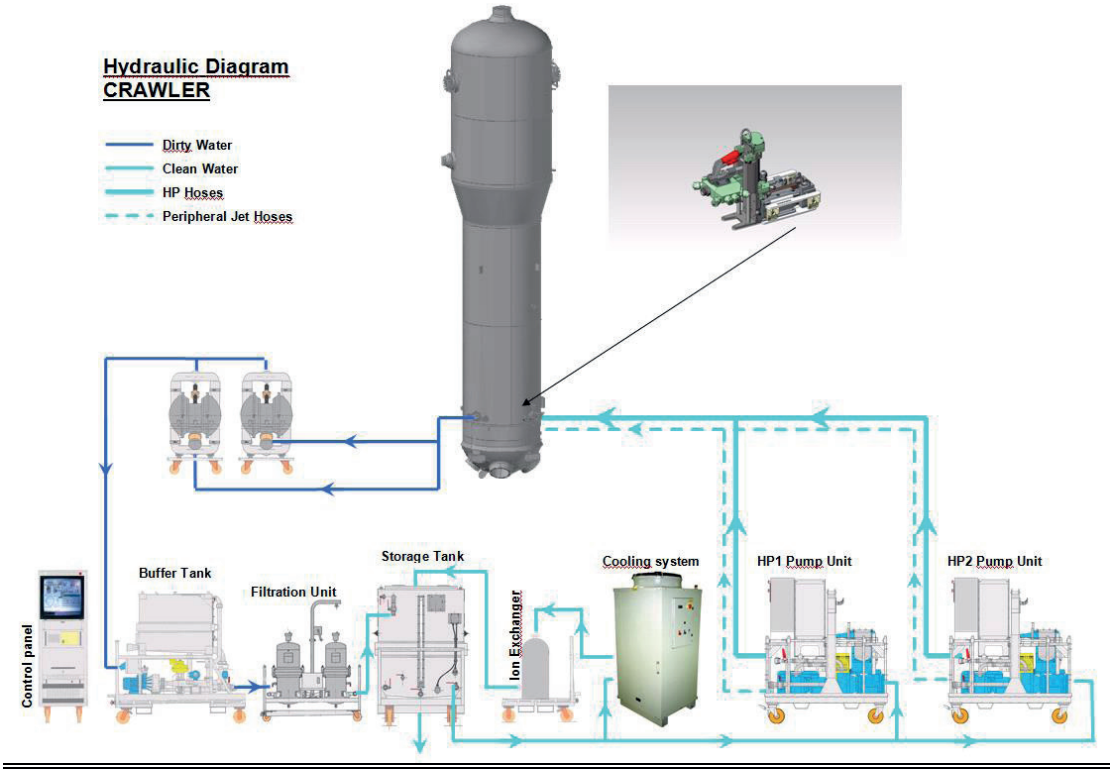


Figure 1[1]: Equipment setup for SL/IBL

## 3 OPERATION

### 3.1 Sludge Lancing (SL)

A SL robot is positioned and operated in the NO-Tube lane in order to remove the loosen sludge accumulated inside the hot leg (HL) and cold leg (CL) out of the tube bundle. The water is directed to the SG through high pressure (HP) pumps (200b and 250b). Then the mixture of water plus sludge is removed from the SG by diaphragm pumps and trapped by high performance filtering elements. The water is then conducted to a storage tank, to be re-injected into the steam generator by high pressure and peripheral jets pumps (see Figure 1). A bypass loop cools the water from the storage tank and purifies it so the SL cleaning process uses as neutral water as possible inside the SG's.

Because of the triangular pitch of the Krško SG's, the SL robot can be used in 90° direction and 30°/150° from the NO-Tube lane (see Figure 2). With the orientation of jet stream in the direction of 30°, 90° and 150°, it is possible to reach both higher number of passes of the HP jets and various areas of the tube bundle compared to cleaning only at 90°. In this manner, the "shadow areas" which are behind the U-tubes from perpendicular direction of the NO-Tube lane are also reached and cleaned.

[1] All pictures in the document are property of SUEZ RV OSIS SUD-EST.

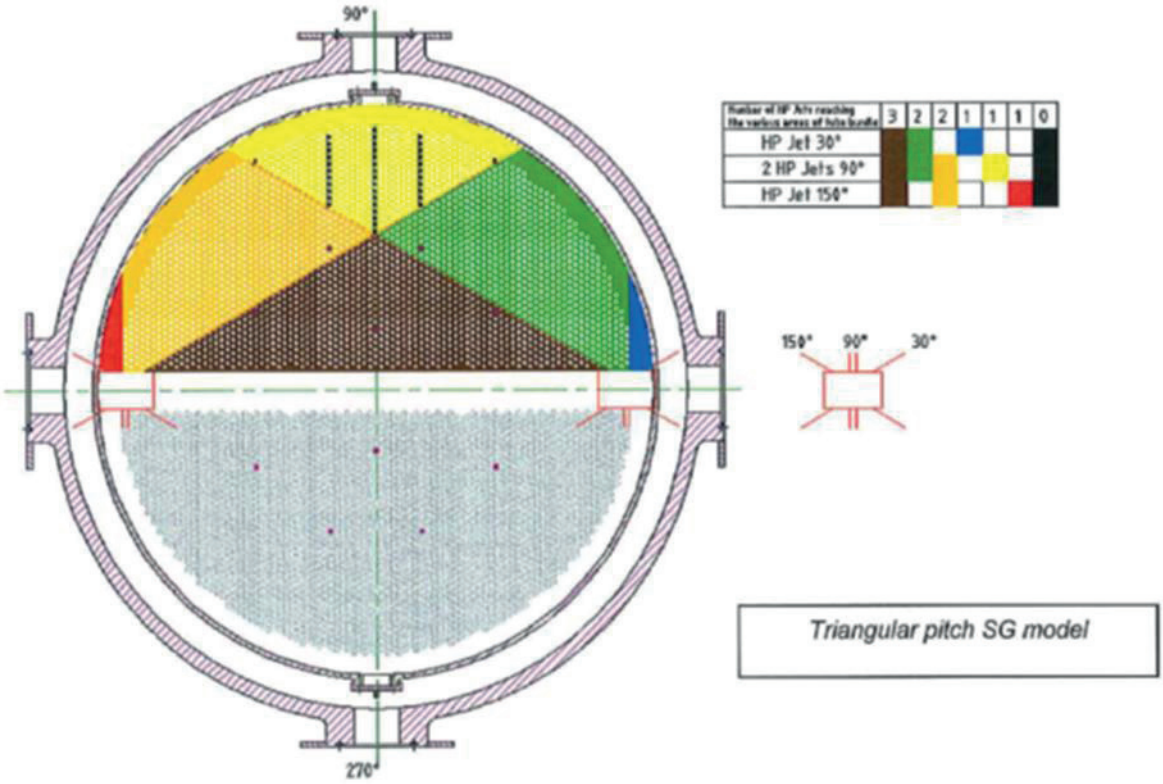


Figure 2: Direction of HP jets inside the SG during SL cleaning phase

### 3.2 Inner Bundle Lancing (IBL)

A crawler (see Figure 3) installed in the NO-Tube lane is equipped with a HP lance which can enter between tubes. Using a 590b pressure, it realizes the Inner Bundle Lancing (IBL). Its goal is to break hard sludge deposits inside the tube bundle in the very low velocity water area. Using two different heads, the lance can be guided at 90° and at 150°. By using different hand hole (HH), the HP jet can cover three directions of the triangular pitch. IBL lance travels between the tube bundle in two different heights: at 6 and 20 cm above the tube sheet. The head is self-balancing with a jet stream oriented directly down and up for counter balance.

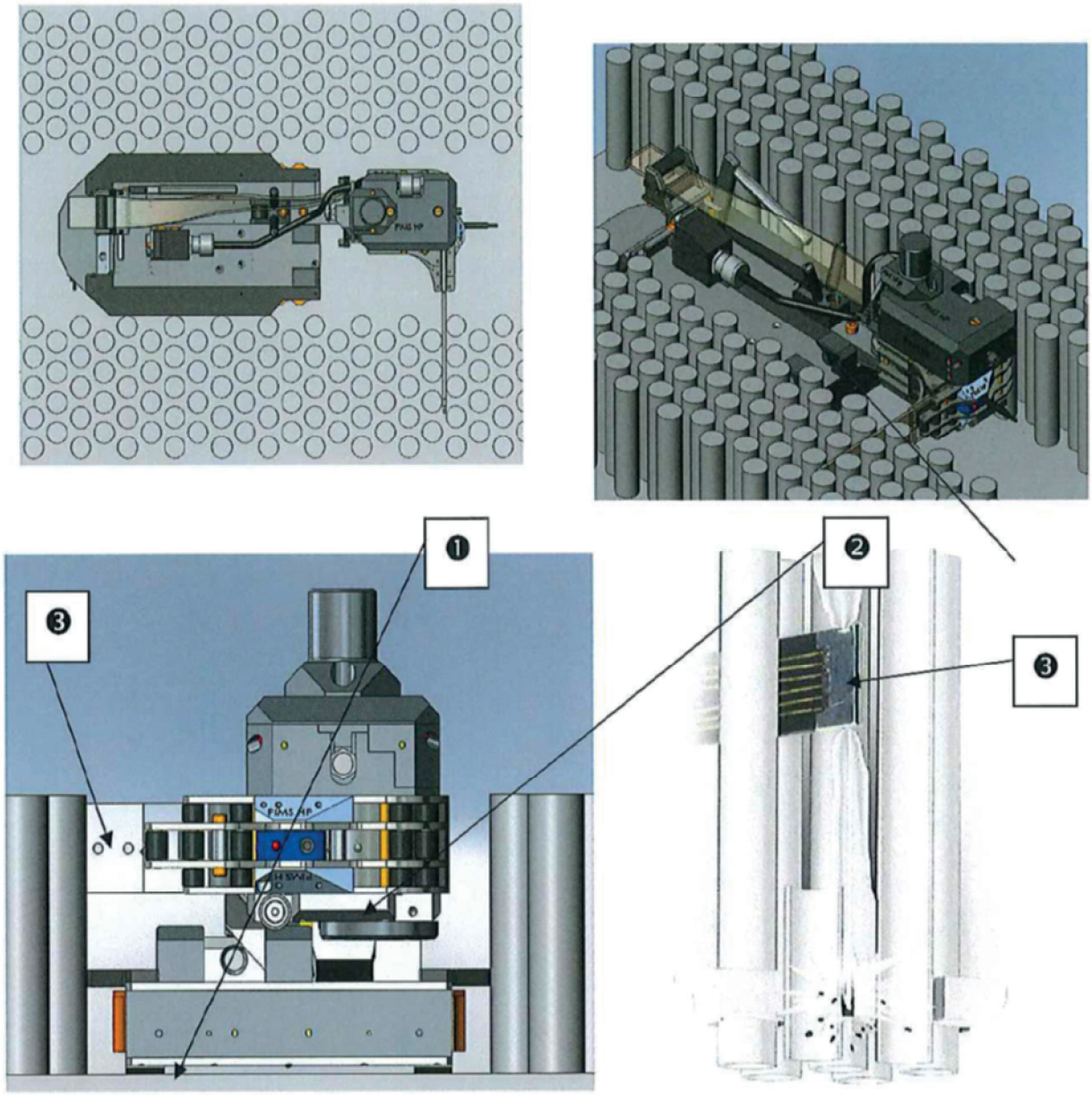


Figure 3: IBL crawler and HP jet position

1. Crawler moving straight in the NO-Tube lane
2. Push-pull system to guide the lance inside the tube bundle
3. Hard Sludge Lance with working jet, to the bottom, and counterbalanced jet, to the top

### 3.3 Drying

After SL, the SG must be prepared for TV inspection. Due to high humidity inside the SG after SL/IBL phase, the camera lens gets foggy and blurry, therefore the drying equipment is introduced. The drying equipment consists of two intake units with HEPA filters, double fan unit with heater and connection hoses. The discharge hoses are connected to the SG's inspection holes in the direction of the NO-Tube lane with the perpendicular inspection closed at the time. At least one secondary manway must be opened to effectively dry the SG prior to TV inspection. This process lasts about 10 hours.

### 3.4 TV inspection and FOSAR

Remote visual inspection is performed to inspect the inner tubes on the tube sheet, after the Sludge Lancing, to check the cleanliness, locate eventual foreign objects and check the result of the Sludge Lancing. A crawler starts moving in the NO-Tube lane (see Figure 4). It is equipped with a push-pull mechanism and a lance (or strip). The lance goes into each inter column at 90°, from the NO-Tube lane to the peripheral lane. The space between each U-tube is approximately 3.6 mm when the tubes are new and no sludge has been accumulated. Small layer of sludge on the tube can block a camera path regardless of the fact, that the lens is only 2.7 mm thick (see Figure 5). Another obstacle inside the SG is the space between a Tie-Rod and a U-tube.

Figure 4: Crawler moving in the NO-Tube lane

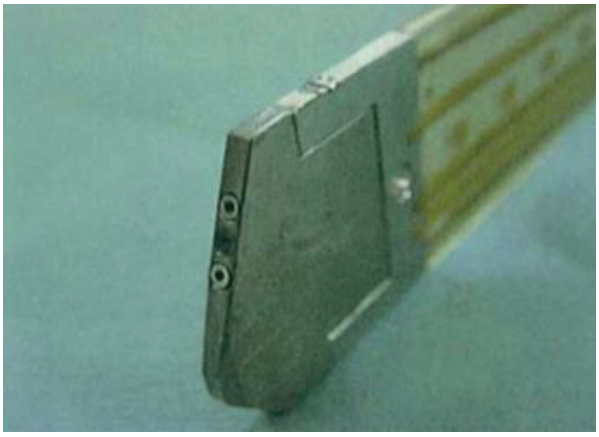

Figure 5: 2.7 mm camera strip with lens

If a foreign object is found inside the SG, its location is carefully noted, the object is categorized, the length is approximated, as is the weight and the material. The categorization is carried out using the EPRI Technical Report 1020989 Steam Generator Management Program: Foreign Object Prioritization Strategy for Triangular Pitch Steam Generators. Based on the shape, size and position of the object, its general location inside the SG and some other factors, a decision will be made if a retrieval attempt is performed. TV crawler in that case acts as a guide for the operator who manually inserts the tool and tries to grab the object stuck inside the SG. Success rate of these attempts varies and depends mostly on the skill of the operator of the FOSAR tool, experience and some luck. If an object is retrieved, a detailed analysis is conducted to determine its origin and structure. If the attempt fails, the location is reported and ECT inspection of the contact and surrounding tubes is performed at the shortest possible interval. Some objects are monitored during the entire time of operations in the SG's.

# 4 RESULTS

## 4.1 SG1 results after Sludge Lancing

In 2018 outage, NEK implemented SL only at SG1. No IBL on SG1 was performed. In the cold leg, the hard sludge area is difficult to characterize. The zone is extended (compared to the last TV inspection) but it is not important in height. No fixed foreign objects are present (see Figure 6).

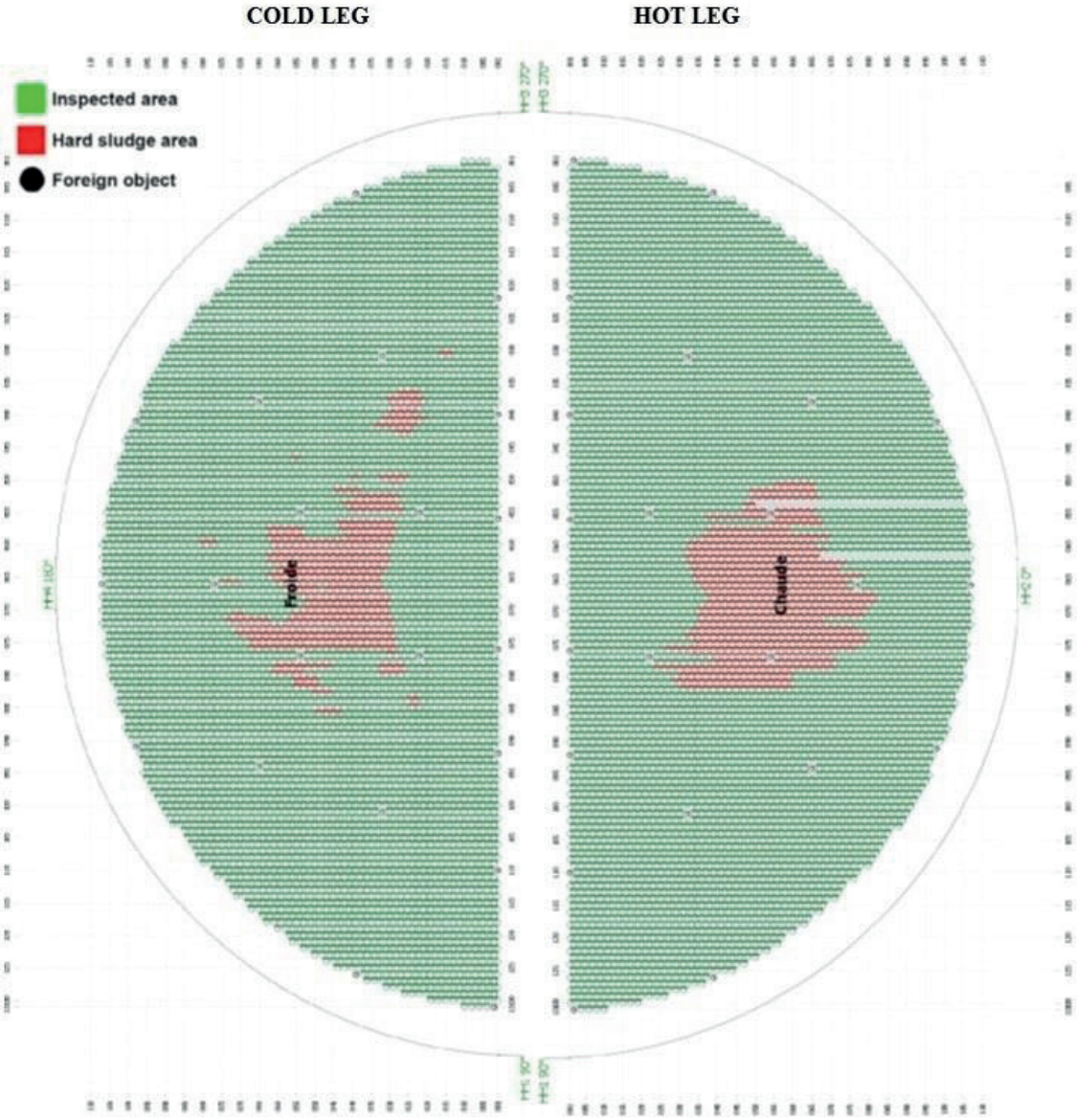


Figure 6: SG1 TV inspection results

## 4.2 SG2 results after first Sludge Lancing

In 2018 outage, NEK carried out the first SL on SG2 with a TV inspection, followed by IBL, second SL and another final TV inspection. During the first TV inspection, three old foreign objects were found in addition to a new one. It was believed that the new one would be destroyed during the IBL phase which was exactly what happened. In the cold leg, the hard sludge area is difficult to characterize. Only hard sludge with small elevations is noted.

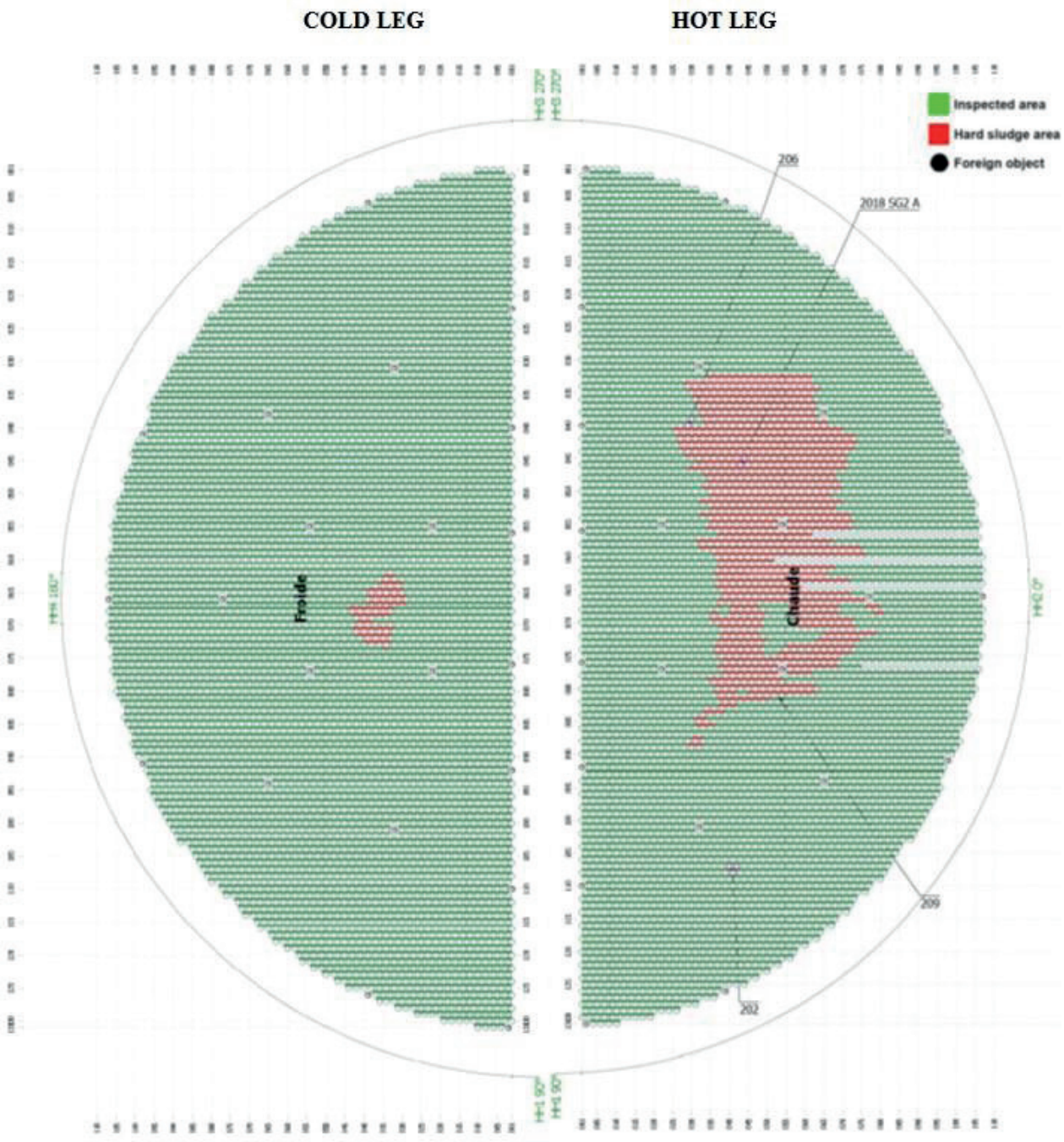


Figure 7: SG2 TV inspection results after the first SL

## 4.3 SG2 results after Inner Bundle Lancing

After the IBL phase in SG2 in both legs, the sludge height has decreased. IBL is oriented to hard sludge area only, so the second TV inspection only checks those areas. Two old foreign objects remained in place, one (new one) was destroyed as expected but one old object moved to another location. It will be closely monitored in the future.

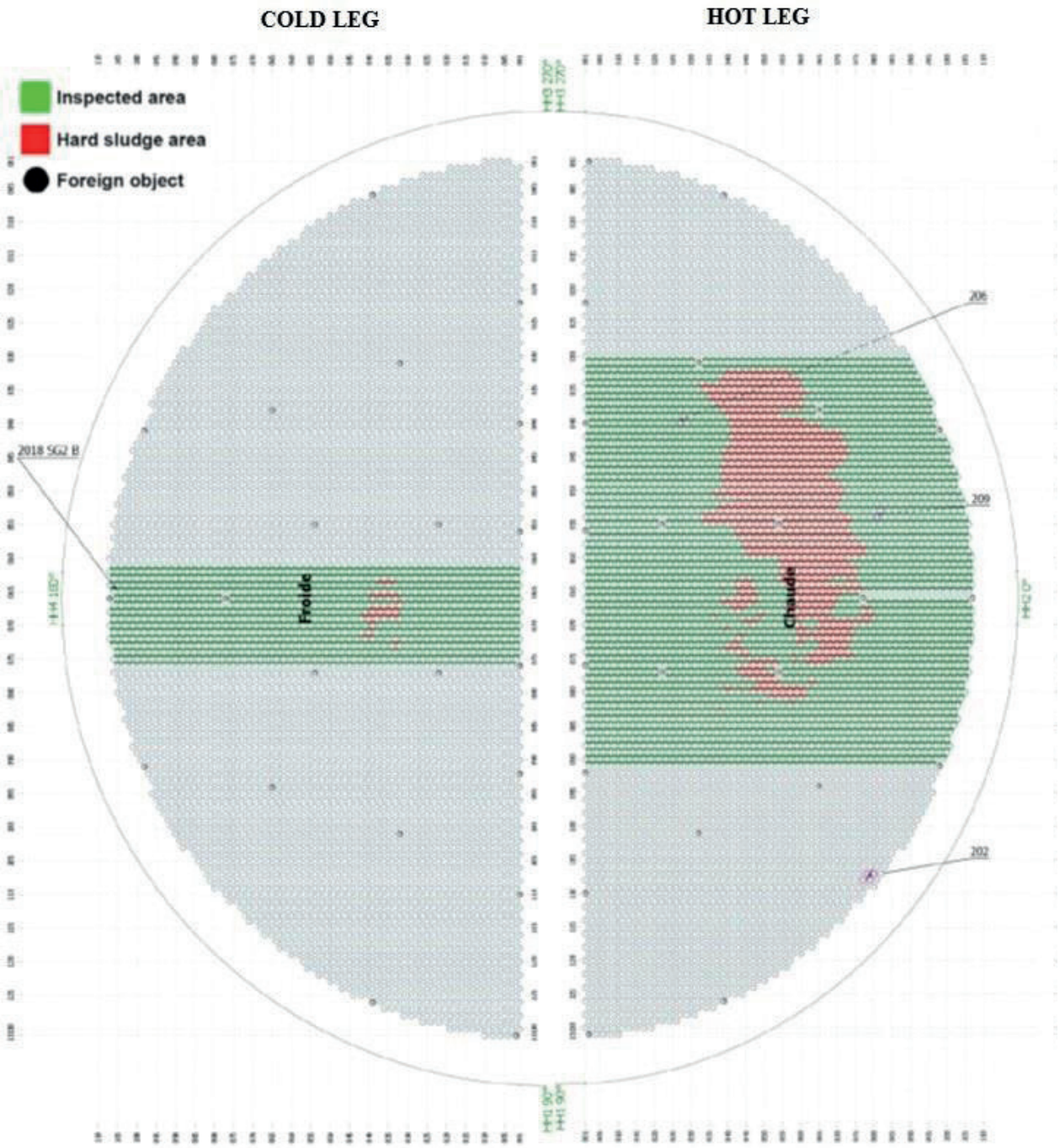


Figure 8: SG2 TV inspection results after IBL and second SL

## 4.4 Amount of sludge removed from the SG's at NEK in 2018

The weighing is performed after each SL for each steam generator separately. The process is strictly monitored, photographed, and noted. The scale is verified, calibration sheets are provided. The filter is weighed prior to start of operations and again at the end. The results on the amount of sludge are reported to Chemistry Department and the samples of the sludge are taken to determine the structure and to check the radiochemistry.

After the SL on SG1, a total of 40.7 kg of wet sludge which equals to 30.2 kg of dry sludge was removed.

On SG2 after the first SL, a total of 44.2 kg of wet sludge which is approximately equal to 33.0 kg of dry sludge was removed and after the IBL and second SL additional amount of 24.1 kg of wet sludge equal to 18.2 kg dry sludge was removed.

The total amount of the removed sludge was 109.0 kg (wet) which is equivalent to 81.4 kg of dry sludge.

Currently, three stuck foreign objects, which are closely monitored every outage, are inside SG2.

## 5 CONCLUSION

Steam generators are safety related components that are required to operate during normal, abnormal and emergency conditions. During normal power operation steam from steam generators is supplied to the turbine at a pressure of 66.9 kp/cm$^2$ and a flow of 3931 t/hr. During shutdown conditions, they are a vital component in decay heat removal process. In case of a station blackout, decay heat removal is ensured by maintaining auxiliary feedwater flow to both steam generators with auxiliary turbine driven feedwater pump. Additionally, steam generators act as a third barrier for preventing radioactive releases into the environment. Due to this the cleanliness and operability of steam generators is vital for safe operation.

Performance of SL and IBL cleaning methods, minimize the growth rate of sludge deposits on top of tube sheet. The benefit is mostly observed in the reduction of sludge height and area surface. Based on previous experience, each time the IBL is performed, the amount of sludge removed from steam generator increases by up to 40%. Therefore, it can be concluded that periodic IBL and SL should be performed each outage to decrease and remove sludge deposits in steam generators, therefore ensuring a longer operational lifetime of steam generators.

## REFERENCES

[1] NEK, "Updated Safety Analysis Report'', Rev. 24, December 2017.

[2] SUEZ "End of intervention report" Reference number: 18 RFI EC 001

Journal of Energy
VOLUME 68 Number 2-3 | 2019 | Special Issue
journal homepage: http://journalofenergy.com/

# Passive Autocatalytic Recombiners Periodic Testing Issue

**Violeta Čalić**
Krško Nuclear Power Plant
Vrbina 12, 8270 Krško, Slovenia
violeta.calic@nek.si

## ABSTRACT

During the refueling outage (RFO) 2013 at NPP Krško, the electric hydrogen recombiners, a system for the hydrogen control during severe accidents and design basis accidents, were replaced by passive autocatalytic recombiners (PARs).

During the next RFOs in 2015, 2016 and 2018, periodic tests of PAR cartridges were performed. The periodic testing of NIS-PARs shall prove that the catalytic reaction starts up as specified. According to the licenced testing procedure, each outage six cartridges were obtained and tested in the NIS PAR test device (TD). Randomly selected PAR cartridges did not pass the periodic test at room temperature (RT). Cartridges that do not pass the periodic testing have to be regenerated according to NEK procedure, followed again by a test in the TD to demonstrate the success of the regeneration. The effort of a full regeneration of all cartridges is not necessary and conservative. Due to significant unexpected workload during outages, the need for enhanced testing procedure with higher catalyst test temperature is priority. The concept for this is based on the conclusion that the PARs installed in NPP Krško were functional under accident conditions during the operational cycles (OL27, OL28 and OL29) even though PAR cartridges did not pass the periodic testing on RT (testing at higher but well below accident temperatures was successful). Revision of procedure and methodology in that direction requires development of the new TD. New TD will allow PAR cartridge measurements at defined elevated temperatures (range 40 - 70 deg C). It shall be vacuum oven type device or upgraded current NIS device. In both examples it shall provide testing of at least two cartridges at the same time, independently, however the whole cartridge shall be tested. Test gas remains 3 vol. % hydrogen in the air.

For a detailed plant specific investigation of this catalytic material behavior, increased testing of cartridges was developed. Additionally, testing of different batch behavior was performed.

***Keywords:*** *passive autocatalytic recombiners, PAR, NIS PAR, periodic test, testing temperature*

## 1 INTRODUCTION

NPP Krško is a two loop Westinghouse PWR with a reactor thermal power of 1994 MWt. The reactor containment building is a cylindrical steel shell enclosed within an outer concrete shield building. Because of accident management review and as a response on the Fukshima accident in Japan, NPP Krško is enhancing its current plant safety even beyond postulated design basis (severe) accidents in sight of its predicted lifetime safe operation and safe shut down. As a part of this comprehensive project, for the hydrogen control during design basis and severe accidents, passive autocatalytic recombiners (PARs) replaced the existing electric hydrogen recombiners.

PARs are simple and passive devices independent of the need for electrical power or any other support system thanks to self-actuated catalytic exothermic reaction between hydrogen/carbon monoxide and oxygen and natural convection. Their purpose is to prevent and mitigate the consequences of generation of explosive gases inside containment even in case of reactor core melt.

The following design bases apply for the PARs:

- The PARs are designed to sustain all normal loads as well as accident loads including

- The PARs are designed to survive and maintain required efficiency in the severe accident environment,
- The PARs are designed for a lifetime of 40 years, consistent with that of the plant,
- All materials used in the PARs are selected to be compatible with the environmental conditions inside the reactor containment during severe accident conditions.

The hydrogen accumulation in the containment atmosphere can be the result of production from several sources:
- Zirconium-steam reaction,
- Radiolysis of water,
- Post accident aluminum and zinc corrosion,
- Release of the hydrogen contained in the reactor coolant system,
- Molten core concrete interaction (MCCI) phenomenon

The following installation criteria apply for the PARs:
- The PARs are located in the containment such that they process a flow of containment air containing hydrogen at a concentration which is generally typical of the average concentration throughout the containment,
- The PARs are located away from high velocity air streams, such as could emanate from fan cooler exhaust posts, or they will be protected from direct impingement of high velocity air streams by suitable barriers such as walls or floors,
- The PARs are located in an area of the containment such that they will be protected from potential high energy missiles or jet impingement from broken pipes,
- The PARs are mounted on a substantial foundation with no ambient vibration,
- The PARs are located in such a manner that there is adequate area around the units for maintenance,
- The PARs arranged and other related equipment accounts for the fact that there may be very high local temperatures in the area of exhaust gas from the recombiners.

Data about PAR locations in NPP Krško are given in Table 1. An example of installed PAR is presented in Figure 1. The cartridge is shown in Figure 2.

The PAR technology uses hydrogen recombination to prevent the build-up of hydrogen gas, or other flammable gases like carbon monoxide that can collect and create an explosive atmosphere. The function is completely passive and self-starting at low temperatures and in steam environments. It is driven by natural convection generated by the heat from the hydrogen recombination. Chimney elongation of the PAR devices boosts the depletion rate. Each PAR has a hood to protect against containment spray.

Catalytic cartridges, which are inserted into the housing, could be removed and replaced without removal and replacement of the housing. The cartridge are fabricated from perforated stainless steel plates which hold the catalyst pellets. Catalytic element consists of a ceramic (aluminum oxide) sphere coated with a catalyst material (palladium) and hydrophobic polymer.

Table 1: PAR locations in NPP Krško

| PAR No. | Safety related | RB elevation | Mounting |
|---|---|---|---|
| GHPARS01 | Yes | 115.55 | SG1 mall |
| GHPARS02 | Yes | 115.55 | RCP2 wall |
| GHPARS03 | No | 107.62 | Clamped on CV37 |
| GHPARS04 | No | 107.62 | HVAC chase wall |
| GHPARS05 | No | 107.62 | HVAC chase wall |
| GHPARS06 | No | 107.62 | Clamped on CV41 |
| GHPARS07 | No | 132.75 | Platform VA101AHU-02A |
| GHPARS08 | No | 132.75 | Platform VA101AHU-02A |
| GHPARS09 | No | 132.75 | Platform VA101AHU-01A |
| GHPARS10 | No | 132.75 | Platform VA101AHU-01A |
| GHPARS11 | No | 132.75 | Platform VA101AHU-02B |
| GHPARS12 | No | 132.75 | Platform VA101AHU-02B |
| GHPARS13 | No | 132.75 | Platform VA101AHU-02B |
| GHPARS14 | No | 132.75 | Platform VA101AHU-01B |
| GHPARS15 | No | 132.75 | Platform VA101AHU-01B |
| GHPARS16 | No | 132.75 | Platform VA101AHU-01B |
| GHPARS17 | No | 107.62 | Clamped on CV35 |
| GHPARS18 | No | 107.62 | Platform at SIATA02 |
| GHPARS19 | No | 100.30 | SG1 wall |
| GHPARS20 | No | 100.30 | SG2 wall |
| GHPARS21 | No | 123.00 | Platform VA111PLM-001 |
| GHPARS22 | No | 123.00 | Platform VA111PLM-001 |

Figure 1: An example of the installed PAR unit in NPP Krško

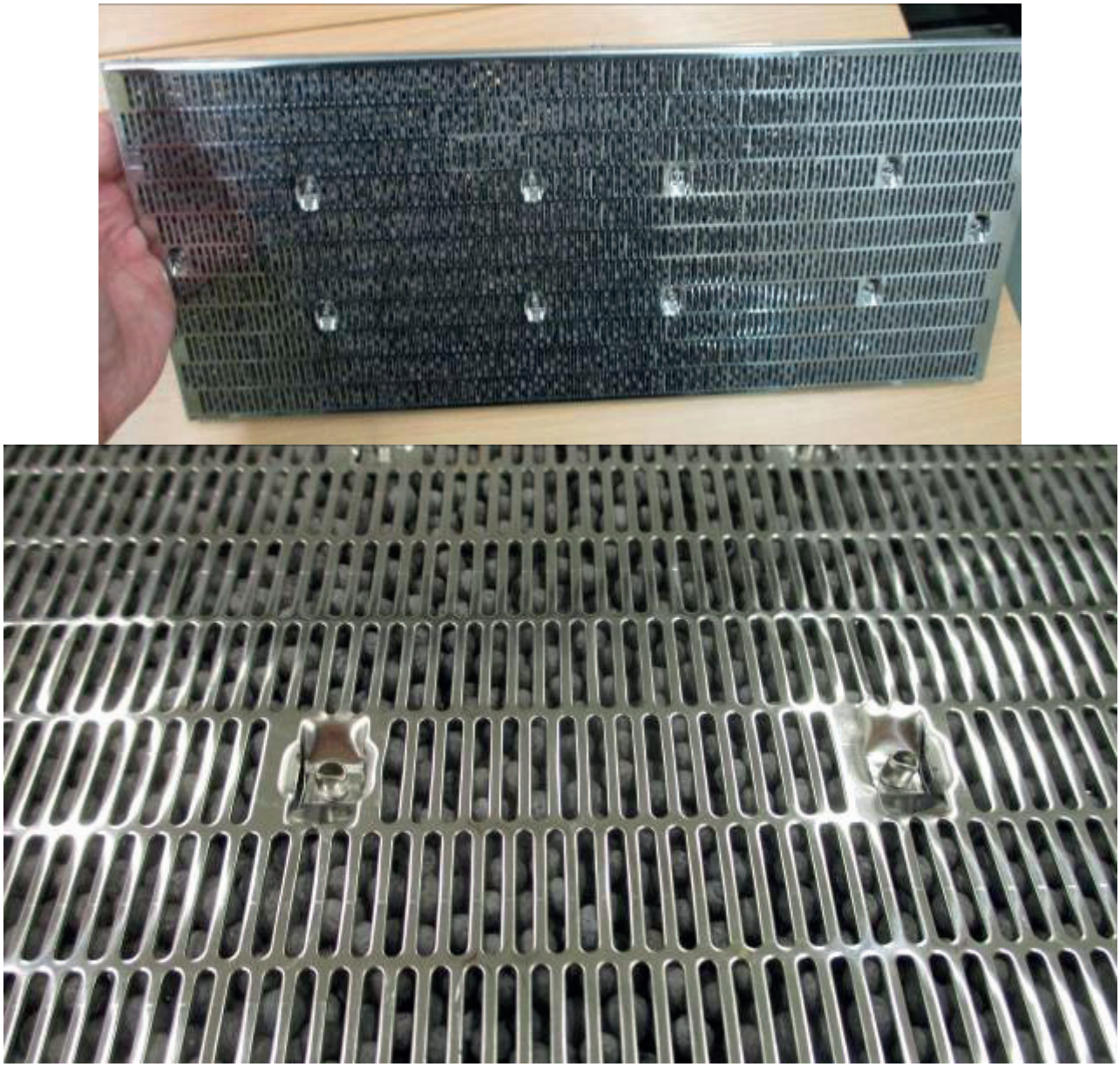

Figure 2: PAR cartridge with catalytic material

## 2 TESTING METHODOLOGY OF NIS PAR

Inspection and testing program for PARs provides 18 months inspection intervals (ones per each refueling) in compliance with the requirements of technical specification surveillance testing.

The reaction products of the catalytic recombination of hydrogen with the oxygen contained in the air are water and reaction heat. The heat of reaction results in a heat-up of the structure and the test gas. The respective temperature increase is determined by the amount of hydrogen converted. The converted amount of hydrogen depends essentially on the offered hydrogen and the efficiency of the conversion. At a constant gas flow rate and constant gas concentration the resulting heat is determined by the efficiency of the recombination. The relation of the heat entering into the structure and the heat entering into the gas flow is essentially constant for the same test conditions. Therefore, the temperature increase in the gas flow is proportional to the efficiency of the recombination.

The temperature increase in the test gas is determined by thermocouples and is used as an evaluation criterion for the efficiency of the hydrogen recombination.

## 2.1 Standard testing procedure

The operability of the PAR cartridges is determined with the functional test using NIS test device and demonstrated by a certain temperature increase of the cartridges within a certain time interval when exposed to a test gas with specified hydrogen concentration and gas flow.

The testing device consists of two test channels with a flap to insert a cartridge; two flow meters at front; four thermocouples mounted in each flow channel; a gas connection nozzle on the backside and a data logger with a PC-interface cable (Figure 3). The cartridge, which is to be tested (one PAR cartridge from each of the two safety-related PARs and from four non-safety related PARs), is inserted in the NIS PAR TD and creates a flow channel in it which is representative for a flow channel in PAR. Test gas with constant hydrogen concentration of about 3 (± 0,25 abs.) vol. % in air is used preferably from pressurized bottles with pre-mixed gas to obtain constant conditions. The temperature increase in the gas flow is measured by 4 thermocouples about 10 cm away from the gas entrance. The 4 temperatures are averaged and the rate of temperature increase is the criterion of the correct NIS-PAR function.

The standard NIS cartridge test is performed at a flow rate of 1500 l/h, room temperature and an input pressure of max. 1.5 bar differential pressure. In these conditions, it shall be demonstrated that the start-up behavior is acceptable. The acceptance criteria are to reach a temperature increase of 10 °C within 20 minutes or for delayed start-up 20 °C within 30 minutes.

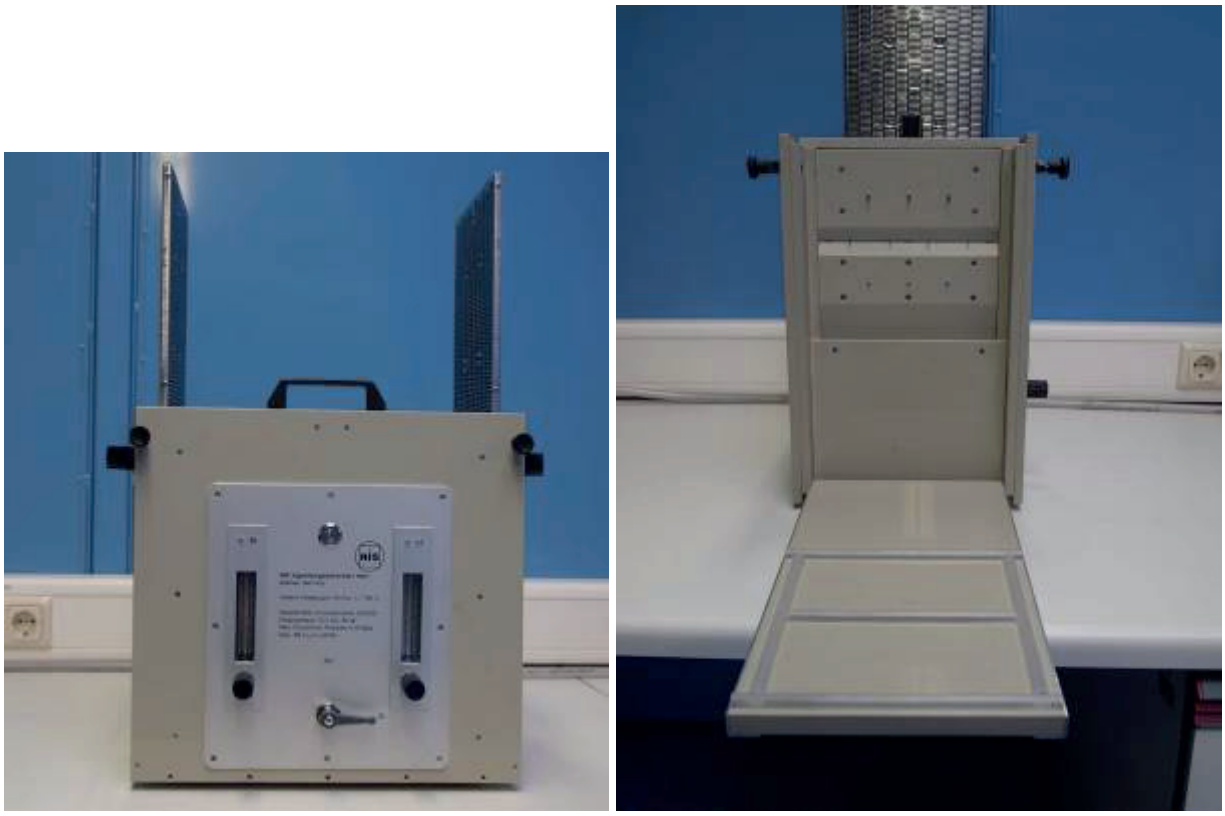

Figure 3: NIS PAR testing device

## 2.2 Additional test

Randomly selected PAR cartridges at NEK site did not pass the periodic test at room temperature during RFOs in 2015, 2016 and 2018.

Regeneration is prescribed in case of failure of the test. Regeneration takes place in an oven at elevated temperature and under low pressure conditions to accelerate the desorption process. The temperature for regeneration is chosen based on practical reasons: a higher temperature speeds up the desorption of any components that are adsorbed at the catalytic surface and reduces the time,

which is necessary for regeneration. However, the temperature has to be below a level that could cause damage to the hydrophobic coating. A temperature chosen is 180 °C at a pressure level of a few mbar. The retesting of cartridges after the regeneration was performed to proof that the cartridge starts up again as specified.

The contractor coordinated investigation of the unexpected PAR testing results. Still a root cause for such a behavior of cartridges is not clearly identified. The purpose of the additional testing was to provide an apparent cause, analyse why the PAR cartridges did not pass the periodic testing and give recommendations for the future actions for testing the NIS-PARs at the NPP Krško.

Specific ageing testing program was developed [5]. Determination of the plant specific ageing characteristics of PAR is necessary to form a basis for a prediction of the behaviour of the cartridges. These tests were necessary in order to validate and define the new test procedure, and new temperature value for PARs testing. A test series were performed at different elevated starting temperatures to show whether the catalyst still works under accident conditions.

The goal of these additional tests was to reduce the effort in future outages. The concept for this is based on the conclusion that the PARs installed in NPP Krško were functional under accident conditions during the operational cycles even though PAR cartridges did not pass the periodic testing on RT (testing at higher but well below accident temperatures was successful) [2]. For a detailed plant specific investigation of this behavior, several cartridges have been tested at different starting temperatures. The elevated starting test temperature was obtained with two methods: preheating the cartridges in the oven and testing with the modified thermally isolated NIS TD, heated with the stream of preheated compressed air.

## 3 TEST RESULTS

During periodic testing, the cartridges taken from containment did not pass the test in the NIS testing device on room temperature according to SCP-6.630 [3] (Figure 4). As a consequence for 3 subsequent outages all cartridges had to be regenerated according to procedure COP-6.500 [4]. Regeneration was successful and all re-tested cartridges passed the test (Figure 5).

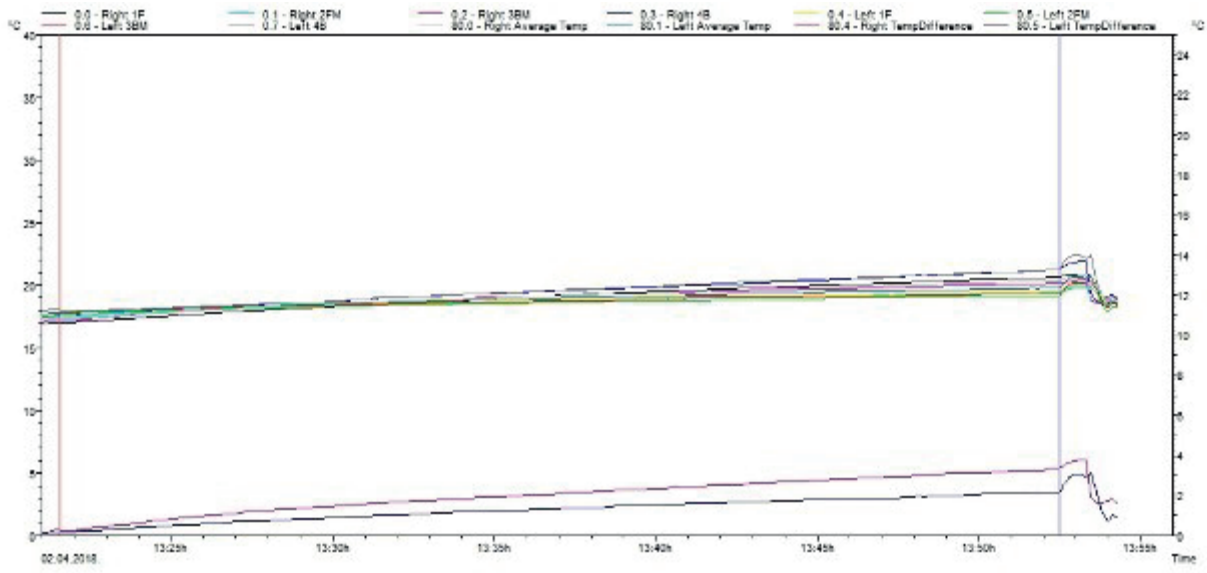


Figure 4: Standard periodic test of NIS PAR at NPP Krško

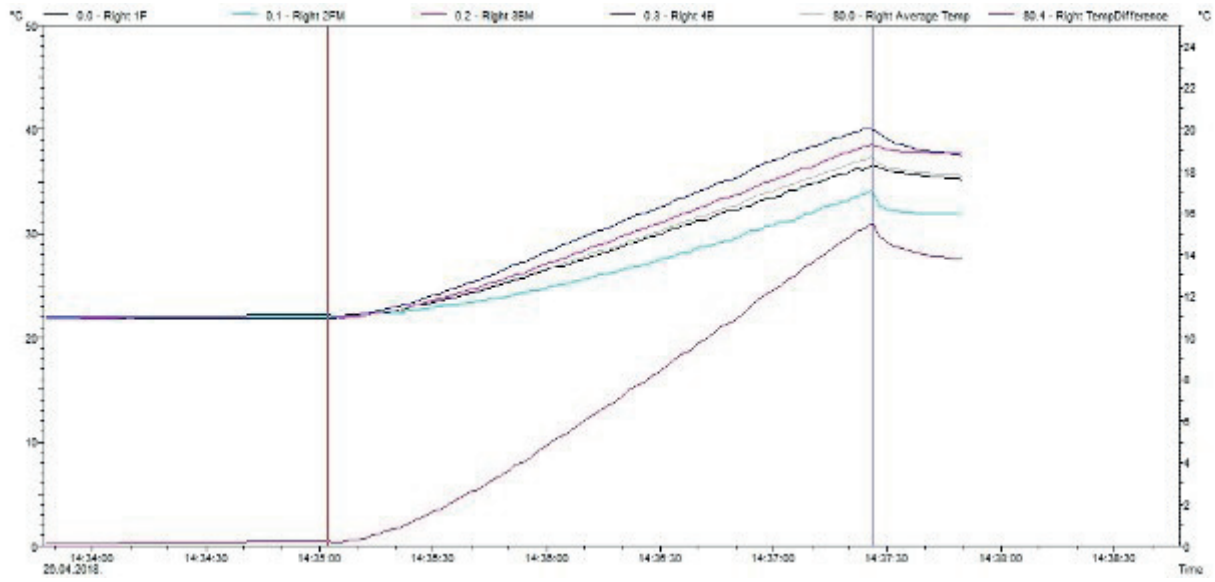


Figure 5: Test after regeneration of NIS PAR cartridge

The failure to pass the test was an unexpected behavior, given the operating experience of NIS-PARs: under normal containment conditions the start-up behavior of cartridges does not deteriorate to an extent that the test criteria are not met, even for many years of exposure to the containment atmosphere.

Specific testing program was suggested by contractor in technical document WEG-EEA-16-006 [5]. These tests were necessary in order to validate and define the new test procedure, and temperature value for PARs testing. The tests have been performed in 2016, just before and during the RFO, as well during outage in 2018.

The behavior of PAR during testing indicates that the one of the reasons for the failed tests could be a soiling. An investigation was coordinated by WEG. The catalyst material was tested in chemical laboratories to determine the exact source of soiling, based on the information which was available from NPP Krško. The exact source of soiling is still not identified and no root cause for such a behavior of cartridges could be clearly identified. To prevent exposure to any potential soiling agent, the cartridges had been inserted into the PARs and thus subjected to containment atmosphere only at the end of the outage, and were hence not exposed to the most of outage works nor have any such works been done in the current outage prior to the testing of the cartridges. It should be noted that a certain amount of reactor coolant pump (RCP) oil has been lost into the containment in the cycle before PARs had been installed in 2013 and during OL29. Confusing fact is that in the outage 2018, the only cartridge that passed the periodic test successfully according to SCP-6.630, was the one from GHPARS02 placed directly above reactor coolant pump RCP2.

Furthermore, the finding from the tests in NPP Krško is that the soiling is not localized but global effect, i.e. that PARs from all locations in the containment are affected.

In 2016 tests with cartridges preheated in an oven were conducted. Different starting temperatures were applied for testing (45, 50, 55, 60 deg C). Results showed the following: difficult manipulation of the heated cartridges; variable initial decrease of temperature caused by the transport of the heated cartridge from oven to TD, dependent on ambient temperature and on human performance. Conclusion was that the testing method and the system should be isolated and not influenced by human performance and ambient conditions [6].

In 2018 two parallel sets of test were performed: on room temperature with standard NIS TD and on elevated temperature using new experimental NIS TD (Table 2) [7].

The majority of cartridges failed the acceptance test at room temperature.

Unlike other batches (8989 and 7471), cartridges from batch 8770, from all 22 GHPARS units (meaning from different elevations and positions, see Table 1), have had successful test results on RT. The successful tests included as well three cartridges that were unregenerated and placed in the containment for two cycles. All the tests from batch 8770 showed delayed start up time (temperature increase) compared to a new cartridges (Figures 6 and 7). Furthermore, by selecting NIS-PARs at different elevations, it was shown that the cause for this PAR problem at NPP Krško is not just a soiling phenomenon. There has to be some influence of quality of catalytic material.

All tested cartridges on elevated temperature successfully passed the test. The new experimental PAR-TD device showed an initial heat-up time of about 8 hours and a heat up time to an steady state cartridge temperature on average about 20 min (Figure 8). The temperature measurements of the thermocouples in the device showed uncertainties in acceptable range. All these properties should be improved by the design of an industrial commercial test device.

Table 2: Summery of test results

| | BATCH | NO OF TESTS | SUCCESSIFUL | FAILED |
|---|---|---|---|---|
| **Test on room temperature** | 8989 | 66 | 3 | 63 |
| | 8770 | 36 | 35 | 1 |
| | 7471 | 8 | 0 | 8 |
| **Test on elevated temperature** | 8989 | 44 | 44 | 0 |
| | 8770 | 11 | 11 | 0 |
| | 7471 | 12 | 12 | 0 |

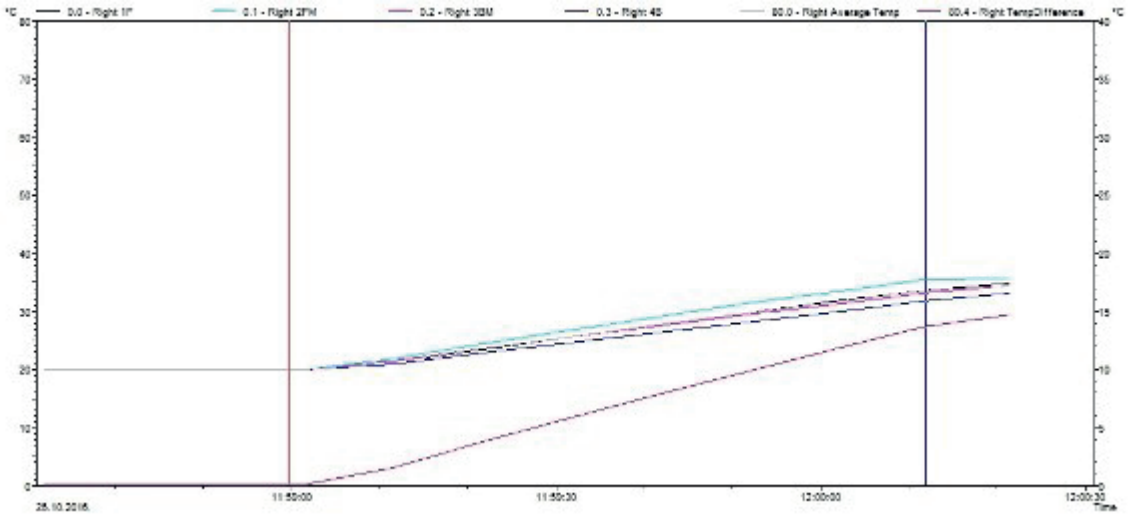

Figure 6: Standard test of the new cartridges

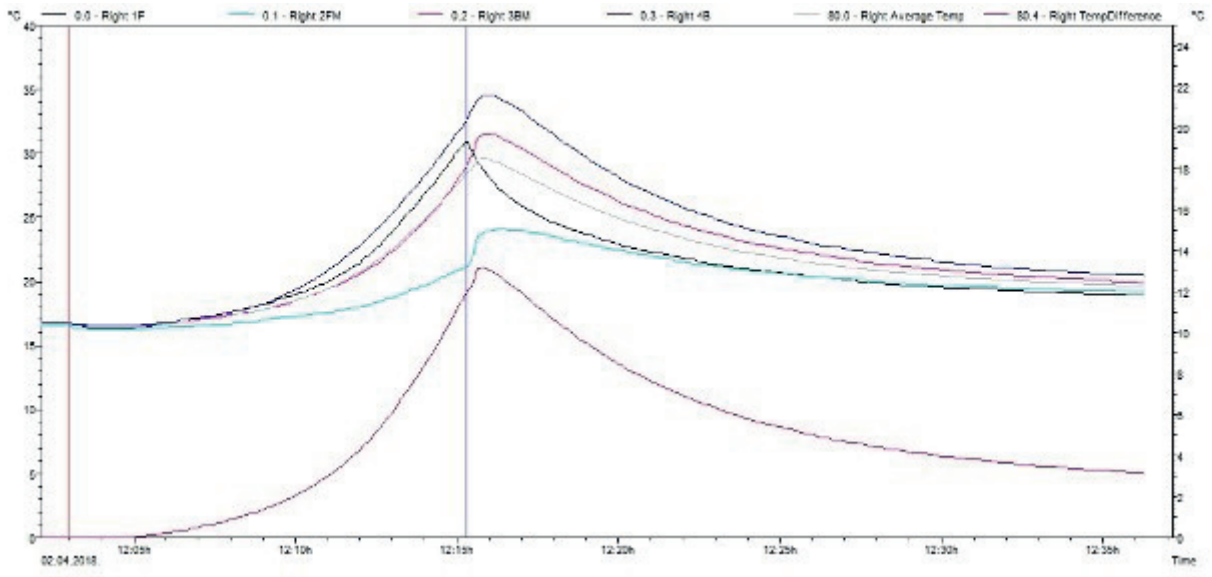

Figure 7: Standard test with the cartridge from batch 8770/C/xxxx

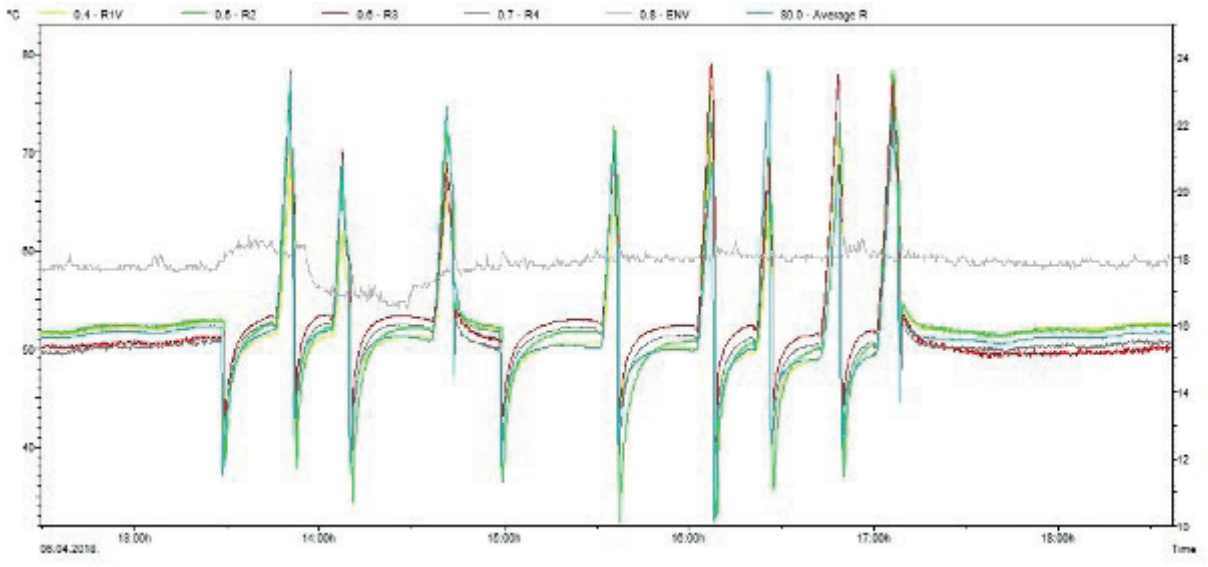

Figure 8: Test at elevated temperature with the modified TD

## 4 CONCLUSION

Based on the test results the following conclusions are derived:

- The PAR cartridge periodic tests showed a high failure rate for the tested cartridges on room temperature.
- Regarding possible soiling agent in NPP Krško containment, the evaluation of the performed tests did not show any spatial dependence nor identify a location of the soiling agent(s).
- Regeneration of the cartridges is successful and reduces the start-up time of reaction.
- Comparison of test data between different batches indicate that reasonable suspicion on the deficiencies in the series of autocatalytic material may exist. An investigation of the manufacturing process for all batches shall be done to investigate if there are significant differences.
- Successful PAR test at NPP Krško showed a delayed heat up rate compared to the tests of new cartridges.

- All cartridges tested on elevated temperatures passed the test. For testing of PAR cartridges on elevated temperatures (40-70 deg C) new testing device is required (a testing method and system should be isolated and not influenced by human performance and ambient conditions)
- A detailed analysis of the cartridge test data has to be performed for a definite root cause analysis of NPP Krško PAR testing issues.

## REFERENCES


[1] Krško Severe Accident Hydrogen Control, Krško USAR Chapter 19 for the PARs Installation, WENX 13-12, rev. 1 (2013)

[2] Krško NPP NIS Passive Autocatalytic Recombiners Periodic Testing Issue - Summary Report, WEG-PEA-15-021, rev. 1.1 (2015)

[3] SCP-6.630, rev. 1: 18-MONTH OPERABILITY TEST OF PASSIVE AUTOCATALITIC RECOMBINERS (PAR)

[4] COP-6.500, rev. 0: CLEANING OF CATALITIC CARTRIDGES FROM PASSIVE AUTOCATALITIC RECOMBINERS (PAR)

[5] Krško NPP NIS Passive Autocatalytic Recombiners Periodic Testing Issue, Development of Plant Specific PAR Ageing Characteristics Test Program, Technical Report WEG-EEA-16-006, rev. 5 (2018)

[6] Supporting Tests and Measurements for Development of Plant Specific PAR Ageing Characteristics Test Program, NEK ESD-TR-19/16, rev. 0 (2017)

[7] Documentation of PAR-Cartridge-Test Results obtained in the Outage 2018, Test results, WEG-EEA-18-40, rev. 1 (2018)

Journal of Energy
VOLUME 68 Number 2-3 | 2019 | Special Issue
journal homepage: http://journalofenergy.com/

# Krško NPP Experience with RTD Bypass Elimination

**Gordan Janković**
Nuclear Power Plant Krško
Vrbina 12, 8270 Krško, Slovenia
gordan.jankovic@nek.si

## ABSTRACT

This paper describes Krško experience and problems that had to be resolved with RTD Bypass Elimination project (RTDBE). Following RTD bypass manifold isolation valve leak in 2008, Krško decided to perform RTDBE modification on reactor coolant system narrow range temperature measurement system. The installation was performed during Outage 2013. Soon after the plant returned to power, newly configured measurement channels showed that OPΔT reactor trip was oversensitive to spikes caused by auxiliary relay operation in the cabinets nearby. The solution was to reconfigure OPΔT trip filtering constants to filter out short-term spikes in the signal. After almost full operating cycle of trouble-free operation, RTD failures started occurring on reactor coolant system cold leg, which was caused by the high frequency vibrations (3-5 kHz) induced by reactor coolant pumps. To resolve RTD failures, Krško ordered re-design of the RTDs to add robustness and specific qualification in high-frequency vibration operating environment. Improved RTDs were installed in Outage 2016 and were operating one full cycle with minor deviations.

***Keywords:*** *RTD, RTDBE, high-frequency vibration, reactor coolant pump*

## 1 INTRODUCTION

Narrow range temperature measurement system of reactor coolant system (RCS) cooling water at Krško, which is used to calculate reactor protection and control signals, was originally implemented by using three flow scoops in the hot legs, bypass piping, isolation and flow regulation valves, and RTD manifolds with directly immersed RTDs (see Figure 1). This mechanically rather complex system addressed hot leg streaming phenomena (see Figure 2) by taking several samples of hot leg water using three scoops with five flow holes each, mixing it hydraulically in the bypass piping and measuring single water temperature in a manifold with two redundant RTDs. Spare RTDs were also installed and wired to protection cabinets in case one of the RTDs would fail. In order to enable RTD replacement without fully depressurizing the primary system, bypass piping was equipped with isolation valves, which acted as a crud trap and became highly radioactive over time, which resulted in high doses for the workers during outage maintenance on the RCS system and components. There were also problems with isolation valves leaking which forced plants to shutdown to replace the valve. These problems motivated most of the similar plants in the world to perform RTD Bypass elimination (RTDBE) project, usually in the early life of the plant. Krško had one of the isolation valves leaking in 2008, and decided to performed RTDBE project, which was done in Outage 2013.

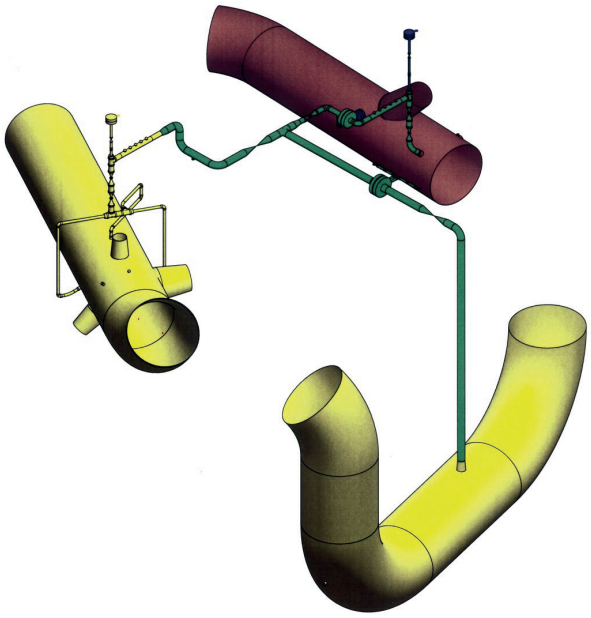

Figure 1: 3-D model of Krško RCS RTD Bypass piping (left: hot leg, right: cold leg, bottom: intermediate leg)

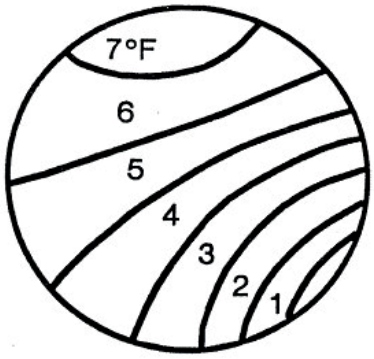


Figure 2: Hot leg streaming – typical pattern

## 2 DESCRIPTION OF RTD BYPASS ELIMINATION PROJECT

The project generally consisted of existing bypass components removal, installation of new thermowell-mounted RTDs directly into the RCS piping, instrument channel reconfiguration and testing, and revision of the safety analyses.

### 2.1 Mechanical scope of the project

Mechanical scope of the project was very demanding in terms of high-radiation work environment, radiation shielding installation and limited space. The work consisted of demolition and installation phase. Within the demolition phase, existing bypass piping and components were removed, which became radioactive waste. They were placed in containers and transported outside of the reactor building. Table 1 provides overview of radwaste amounts [1].

Table 1: Overview of radwaste

| Waste type | Amount [pieces] | Volume [m3] |
|---|---|---|
| Reflective metal insulation | 120 | 7 |
| Snubbers and supports | 54 | 1.7 |
| Piping | N/A | 1.7 |
| Valves | 26 | 1.7 |

Installation phase of the mechanical scope consisted of six new thermowells installed in each hot leg, two thermowells installed in each cold leg, welding of cap on the intermediate leg piping, and new reflective metal insulation installation. For hot legs, three thermowells were placed inside exiting scoops, which were left inside the pipe. Three new holes had to be drilled at 60° to the scoops (see Figure 3). Since drilling into RCS piping represents Foreign Material Exclusion (FME) issue because of the metal residue, pipes were first drilled to about 90% of the pipe wall thickness with standard drilling bits, and the last 10% was drilled using Electrical Discharge Machining EDM technique. With EDM, only metal droplets less than 20 μm in diameter [2] may remain in the RCS, and they have been proven not to adversely affect nuclear fuel cladding.

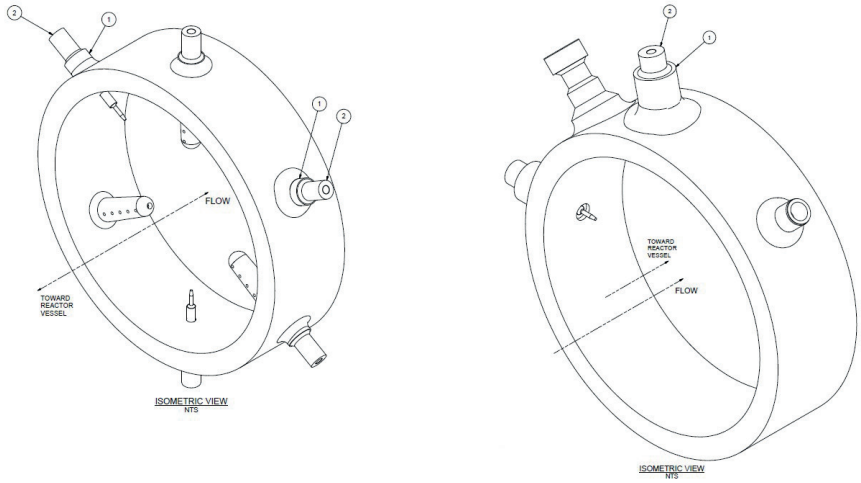


Figure 3: Isometric view of hot leg RTDs installation (left) and cold leg RTDs installation (right)

For cold leg thermowell installation, Krško used NPP Vandellos experience [3], where multiple RTD failures occurred in the cold leg due to flow-induced vibrations of the thermowell in the cold legs. This problem was resolved by removing thermowell outwards by 1 inch, which reduced vibrations, and the plant did not report any more RTD failures since. Identical design was used at Krško.

## 2.2 I&C scope of the project

Krško reactor protection system consists of 4 independent measurement channels for each critical parameter, which means that 2 independent narrow range temperature channels had to be installed per RCS loop. To address the hot leg streaming phenomena, 3 RTDs were used per hot leg per channel, with second channel also having 3 RTDs in the same hot leg which were 60° apart (see Figure 3). Each channel then averaged 3 RTDs to obtain single Thot-average signal, as shown on

Figure 4. In order to exploit six-point measurement in each hot leg, but with channel independency rule, a bias circuitry was installed, which enabled correction of Thot-average to the average of six RTDs. Once set the bias is a fixed value (it is not connected to other protection channel) and is checked periodically by manual calculation, and reset if necessary. It is also reactor-power dependent (using ΔT signal), so that it does not give false offset when the reactor is shut down.

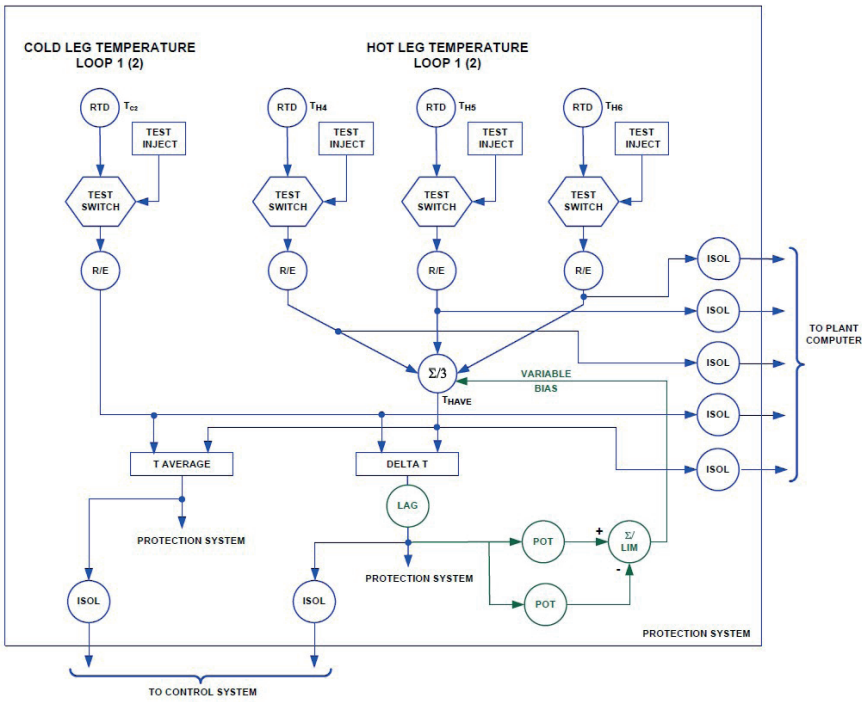


Figure 4: Thot-average and bias signal diagram

Streaming phenomena in cold legs is only marginal due to good mixing of RCS coolant by the reactor coolant pump (RCP) impeller, so 1 RTD per measurement channel was installed.

To add some redundancy in case of RTD failure, dual RTD units were used (Weed/Ultra electronics model N9004, see Figure 5), with two platinum coils inside each RTD assembly, as shown on Figure 6, and both wired individually to the protection cabinets. New thermowell-mounted RTDs have guaranteed response time of 4 seconds [4], with additional 1 second allowed in the safety analyses for conservatism and maintenance flexibility [5].

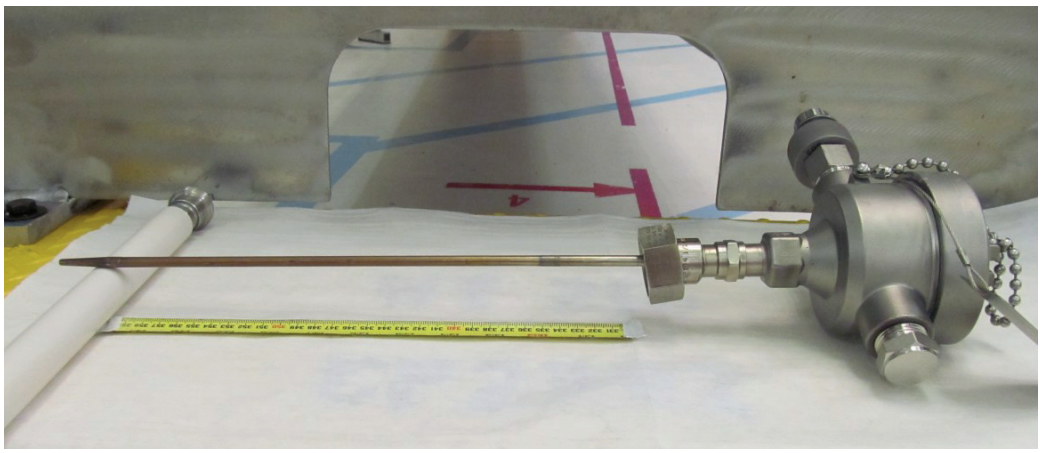

Figure 5: Weed/Ultra Electronics RTD model N9004

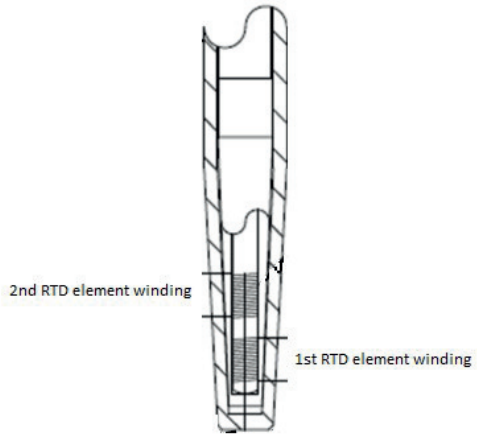


Figure 6: Dual RTD configuration

The biggest concerns for the post-RTDBE plant operation were hot leg streaming distribution and margin to OPΔT/OTΔT turbine runback and trip.

Hot leg streaming phenomena occurs due to imperfect mixing of the RCS coolant after it exits fuel elements' channels with temperature differences of more than 30°C. Because of that, temperature distribution in the hot legs has layers with significant temperature differences, so point temperature measurements inherently contain uncertainties that had to be evaluated for (primarily) RCS flow calculation. Originally, hot leg streaming data from Vandellos Unit 2 (3-loop) and Beznau Unit 2 (2-loop) plants were used to asses Krško streaming [6], but the adequacy of those plants as references for Krško was questionable. This phenomenon was considered to be more pronounced on 2-loop plants with reactor power uprate performed and with low load leakage pattern, which is the situation at Krško. In order to estimate streaming magnitude, Krško-specific CFD simulation was performed with ANSYS thermo-hydraulic code [7], which then served for input data for streaming uncertainty calculation. As power operation after the RTDBE showed, results from the simulation were very conservative in estimating more than 13°C temperature difference between highest and lowest RTD reading, which are typically 6°C to 8°C and quite stable, see Figure 7.

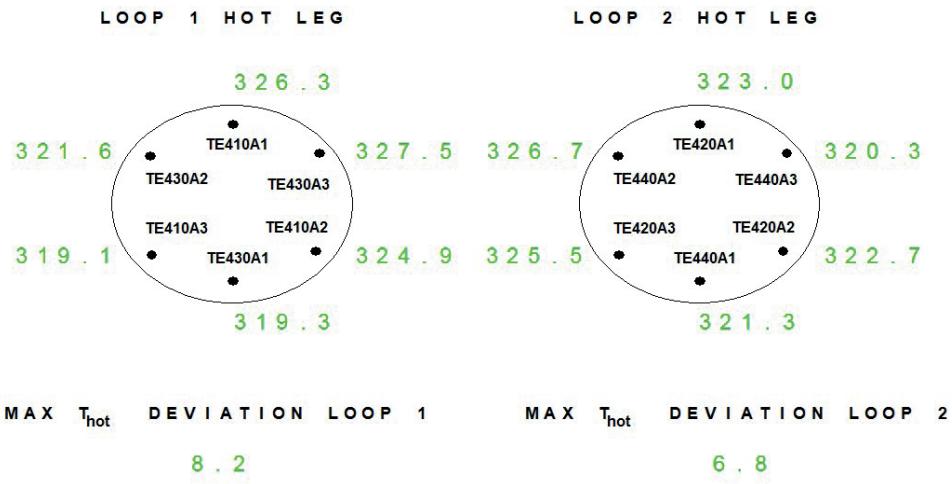


Figure 7: Typical RTD measurements with the plant at full power

Direct RCS coolant temperature measurement after the RTDBE modification was expected to result in increased fluctuations of Thot and possible rod control movement or even OPΔT/OTΔT

runback/reactor trip. The designer proposed adding lag filter to Thot signal and lead/lag filter to Tcold signal, as implemented on Tihange Unit 2 plant [6]. Placing the lead/lag on Tcold preserves or even increases the efficiency of the protection for secondary accidents, while suppressing hot leg fluctuations. The resulting OPΔT/OTΔT trip function diagram can be seen on Figure 8.

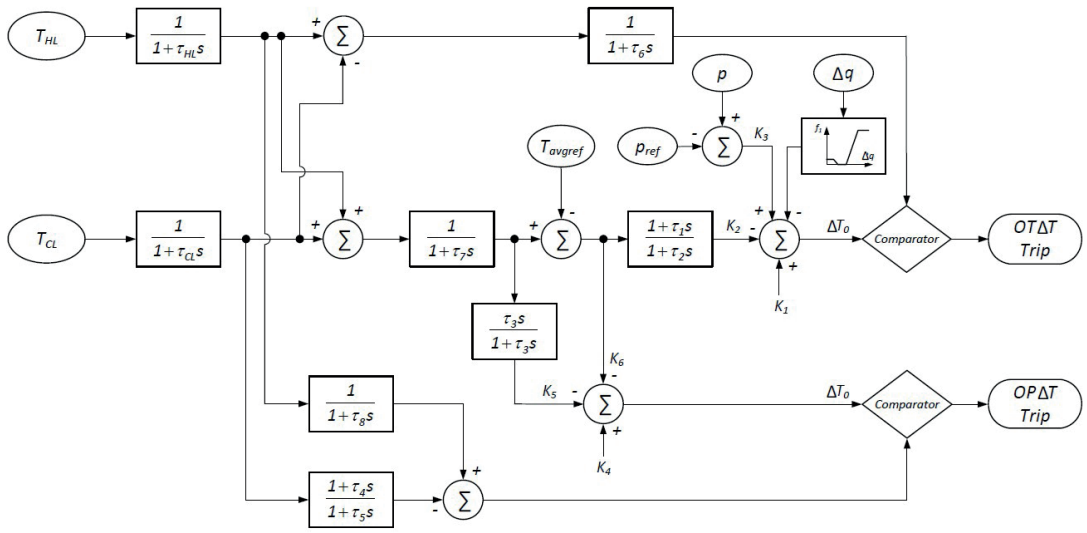


Figure 8: OPΔT/OTΔT trip function diagram

The OTΔT trip calculation expression was changed as follows:

$$\text{Delta T}\left(\frac{1}{1+t_6 S}\right) \le \text{Delta T}_0\left\{K_1 - K_2\left(\frac{1+t_1 S}{1+t_2 S}\right)\left[T_{avg}\left(\frac{1}{1+t_7 S}\right) - T^0_{avg}\right] + K_3(p - p_0) - f_1(\text{Delta q})\right\} \tag{1}$$

The OPΔT trip calculation expression was changed as follows:

$$\text{Delta T}_{OP} = T_{hot}\frac{1}{1+t_8 S} - T_{cold}\frac{1+t_4 S}{1+t_5 S}$$
$$\le \text{Delta T}_0\left\{K_4 - K_5\left(\frac{t_3 S}{1+t_3 S}\right)\left(\frac{1}{1+t_7 S}\right)T_{avg} - K_6\left[T_{avg}\left(\frac{1}{1+t_7 S}\right) - T^0_{avg}\right]\right\} \tag{2}$$

## 2.3 Revised analyses of record

Following analyses of record had to be updated because of the new RCS coolant temperature measurement system and OPΔT/OTΔT reactor protection changes [8]:

- Revised Thermal Design Procedure Uncertainty Analysis
- Integrated Core Design
- Margin to DNB
- Containment Response to Steamline Break
- Increase in Heat Removal by the Secondary System
- Reactivity and Power Distribution Anomalies
- Decrease in Reactor Coolant Inventory
- Radiological Consequences

- RCL Branch Nozzle Analysis
- Class 1 Lines Reconciliation Analysis Summary

### 2.4 Post-installation testing

After all the installation works were completed complex testing of all components were performed per Site Acceptance Tests Program [9]. These include new temperature channels calibration, calibration of channels affected by rack card relocation, response time measurements of all branches of new temperature channels, RTDs response time testing, RTDs cross-calibration, deltaT and bias calibrations at power, and RCS flow calculation.

## 3 PLANT TRIP ON OPΔT

As the plant was performing an initial power increase after the outage, at about 90% power, the reactor tripped on OPΔT protection signal. By looking at the trends on the plant computer (as shown on Figure 9 and Figure 10), it could be seen that all temperature signals coming from the field had downward spike. Lag filters filtered out these spikes for the Thot signal, but strong lead/lag filters amplified the spike on Tcold signal, which resulted in large spikes on ΔT signal, so that it went above the OPΔT trip setpoint on 2 out of 4 channels. Reactor operator on shift noted that the trip coincided with reactor makeup water selector switch operation, which was known to sometimes cause irregularities on control equipment, but plant did not have any record of spikes or any irregularities in reactor protection instrumentation. With reactor tripped, the troubleshooting team was able to reconstruct the spikes of varying amplitude on resistance-to-voltage cards (NRA cards) whenever the reactor makeup water selector switch was operated. The cause for that was determined to be operation of up to 12 auxiliary relays that are located in auxiliary relay racks nearby temperature channels. The relays are powered by 118 VAC power source. Since relays did not have any surge protection, whenever a relay was energized or de-energized, voltage spikes of sometimes more than 1000 volts occurred (see Figure 11), which emitted electro-magnetic (EM) pulse. EM pulse is believed to be picked-up by the interconnecting cables and transferred from auxiliary relay racks to reactor protection cabinets, where temperature channel cards were located. Since NRA cards operate with relatively small field signals of about 300 mV, which is then amplified with large gains, they were most susceptible to picking up the EM pulse.

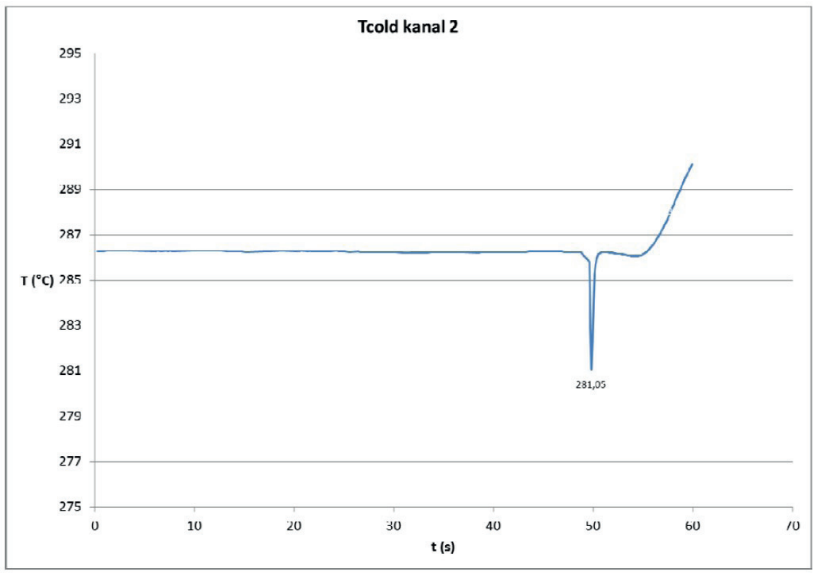


Figure 9: Plant computer trend for protection channel 2 Tcold

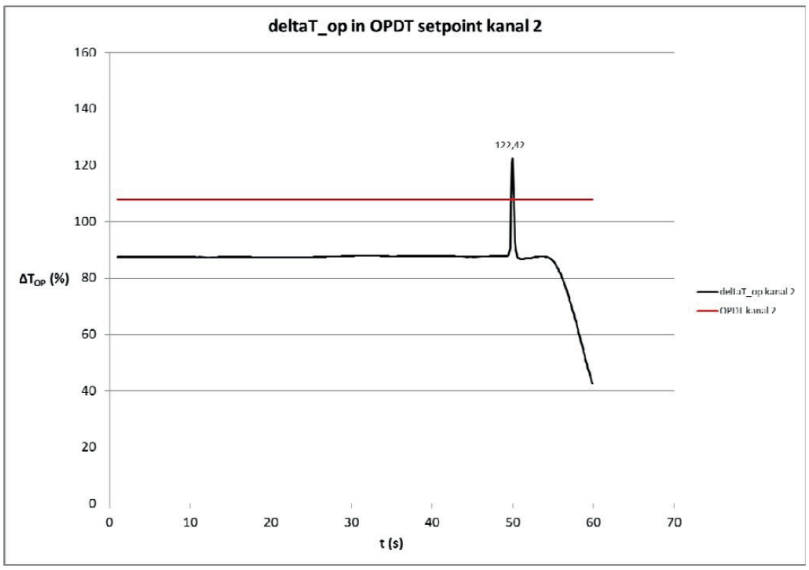


Figure 10: Plant computer trend for ΔT signal for OPΔT reactor trip (black) and OPΔT setpoint (red) for protection channel 2

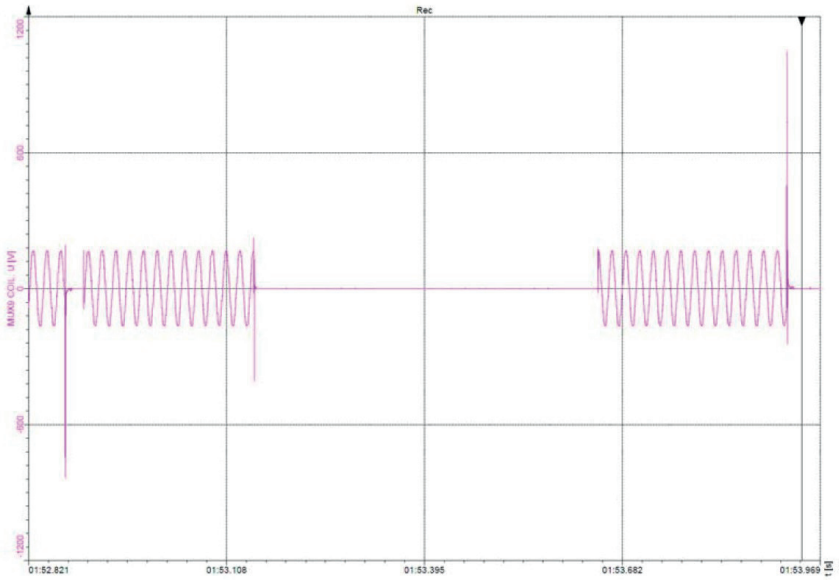


Figure 11: Voltage spikes on auxiliary relay coils

The root cause analysis was performed which identified four contributing causes for the trip: the EM pulse generation by the auxiliary relays, the transfer path for the pulses, the NRA cards input stage susceptibility to EM noise, and OPΔT protection reconfiguration that made the channel vulnerable to short-term spikes in field signal. In order to prevent such events in the future, three contributing causes were addressed and resolved or mitigated. It was judged that resolution of EM noise transfer to protection cabinets would require significant effort without further improvement to temperature channels noise immunity, and possibly creating new problems.

The EM pulse generation was greatly reduced by installation of the surge protectors an all affected relays, which limit the voltage spikes on the relay coils to 200 volts. These are passive metal oxide varistors, which do not require any maintenance.

It is believed that the EM spike transmission is through interconnecting cables (cables can generally act as an antenna) from auxiliary relay racks to protection cabinets, where the pulse can be re-emitted and picked up again by RTD field cables in the protection cabinets. The NRA card

supplier modified the card design to include a filter in order to mitigate card output variations due to short-term input signal disturbances. This card design upgrade now normally comes with the NRA card available on the market.

The most complex contributing cause to address was OPΔT protection change that would remain efficient for the mitigation of design accidents and not be over-sensitive to short-term signal disturbances. A sensitivity study [10] was performed where a series of Tcold lead/lag or lag-only filters were compared with magnitude of the Tcold signal disturbance they can filter out without generating a trip signal, and compared with the departure from nucleate boiling ration (DNBR) they still attain (as a measure of reactor protection efficiency). This showed that the implemented aggressive Tcold lead/lag filtering was very conservative and that DNBR margin remains with lag filter on the Tcold signal, while it offered maximum disturbance rejection. Based on this conclusion, Tcold lead/lag filter was replaced with lag-only filter.

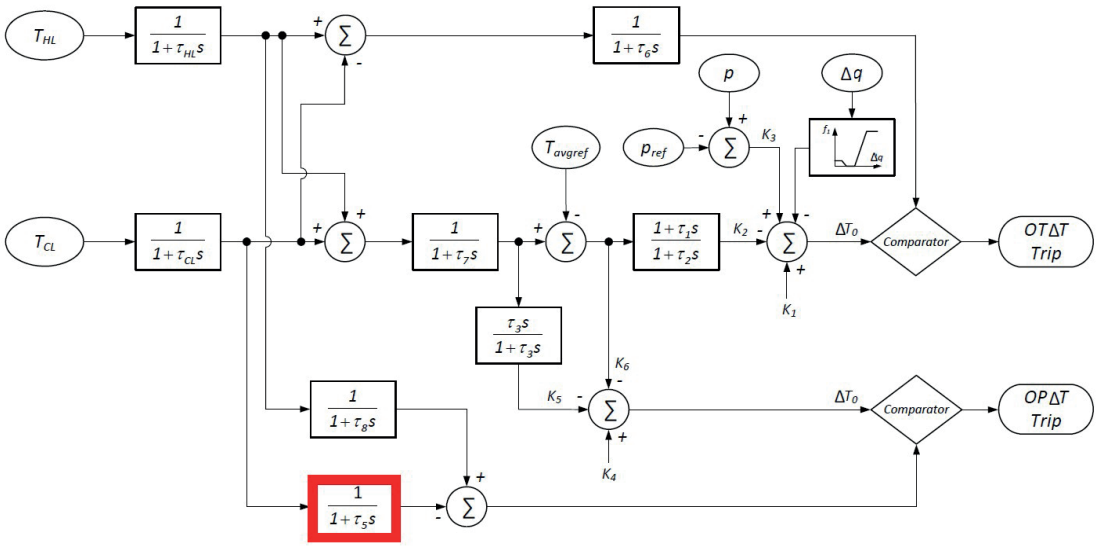


Figure 12: OPΔT/OTΔT trip function diagram after Tcold filter change (in red)

The time constant reduction on Thot signal lag filter did not make significant impact to DNBR for affected accident analyses, so it remained unchanged to keep the filtering capacity of possible Thot fluctuations (Thot indications have been very steady since RTDBE). Accident analyses in which OPΔT is actually actuated were impacted and had to be repeated. Those are Hot Full Power Steam Line Break and Decrease in Feedwater Temperature.

Tcold filter change also affected trip response time, which had to be re-calculated and measured again on each protection channel as an acceptance test.

## 4 COLD LEG RTD FAILURES

After about 17 months of stable operation of temperature channels, one of the cold leg RTDs indication started drifting upwards. The troubleshooting team checked all channel components that could cause the rise in the indication and narrowed it down to actual resistance coming from the RTD and connecting wires (including wire splices). One of the possible causes for this behaviour was assumed to be platinum wire cracks due to vibratory load, but not much testing was possible with the plant at power due to neutron radiation, noise and heat at the RTD location. Ultimately the RTD failed open completely, so the plant used spare RTD in the dual-RTD unit, and continued operation until nearing outage.

In Outage 2015 the vibration levels were measured at and near the RTDs with readily available equipment, finding significant levels of high-frequency vibrations within 3-5 kHz [11],

which were also measured on and believed to originate from reactor coolant pumps (RCP). Failed RTD was removed from the thermowell and significant rub marks were observed on several places on RTD sheath (see Figure 14), which supported the assumptions about vibratory environment. The plant conservatively decided to replace all four cold leg RTDs in outage 2015 with spares. The failed RTD unit was shipped to the manufacturer for examination and determination of root cause for the failure. After one cycle of operation in a neutron flux environment the RTD was slightly activated so the manufacturer was only able to perform visual and x-ray examination, because he did not have means to contain radioactive debris that would form with destructive examination. Nevertheless, the cause for the RTD failure was clearly visible as platinum lead wire breaks on the x-ray shots (see Figure 13). The causes for the break however could only be assumed.

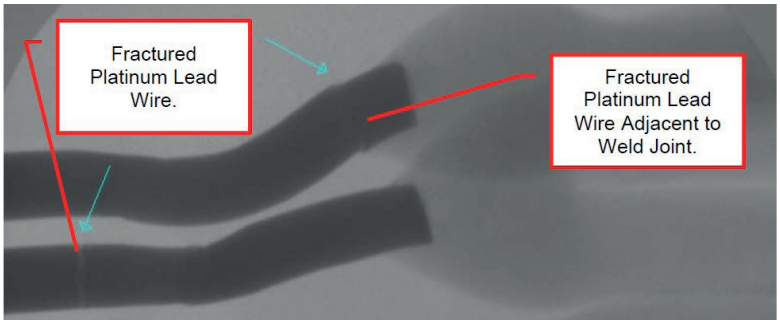


Figure 13: X-ray of RTD platinum lead wire fractures

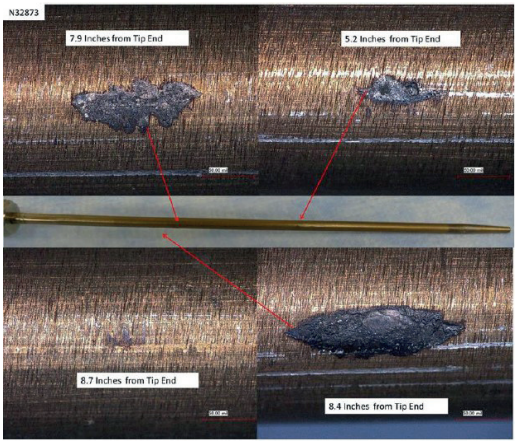


Figure 14: Rub marks on the RTD sheath

Just a few weeks into the following on-line operation, second active RTD failed, followed by failure of a spare unit in dual-RTD (with similar drifting behaviour preceding the failure). The plant resumed power operation since Technical Specifications allow normal plant operation with one failed protection channel in safe (trip) position. This however made the OPΔT and OTΔT reactor trip actuate on 1 out-of 3 coincidence, which significantly decreased the plant operating margin to human errors or equipment failures. Since more information about the vibration environment of the RTDs were needed for the failure root cause determination, the vibration measurement campaign was organized with the RTDBE project contractor and RTD manufacturer. Similar campaign was performed with the same companies involved in order to resolve failures on Vandellos plant, so that experience served as a basis for Krško.

In order to measure vibrations inside thermowell, a special dummy RTD was manufactured which was instrumented with two accelometers in the RTD tip (x and y direction) and two accelometers in the RTD head. The RTD was inserted into the thermowells and the accelometers were wired to the data acquisition station just outside of the RCP cubicles in the reactor building.

Simultaneously RCP vibration data was recorded with second data acquisition system. The measurements started on second RCS loop. Close to completion of second locations of loop 2, the RTD tip broke when extracting the dummy RTD from the thermowell and the measurement campaign was stopped. Since the manufacturer was only able to supply one dummy RTD in the given timeframe, the measurement of vibrations on loop 1 had to be cancelled. It was judged however that vibration level on loop 2 was bounding due to lower vibrations level on RCP no. 1.

The contractor analysed the vibration data and concluded following [12]:

- the RTD sheath has higher resonant modes in 3-5 kHz region
- the measured vibrations in the RTD tip spectre had peaks in the same 3-5 kHz region
- comparison between RTD tip and RCP vibrations proved RCP to be the source of the vibrations
- the vibration data indicates that excitation by flow turbulence is not a large contributor to RTD tip vibrations.

In the meantime, both failed RTD units were shipped to the laboratory capable of performing destructive examination of activated materials. These were most important conclusions of the analysis [13]:

- failed RTD units had insufficient powder potting in the RTD tip region, which resulted in excessive platinum lead wire mechanical loading and failure
- the cross-section of the most of the failed wires showed typical signs of metal fatique.

Based on conclusions from both vibration data and destructive examination analyses, and since RTD dimensions are bounded by the existing thermowells, Krško decided to invest into following:

- redesign of the internals of the RTDs, so that vibratory loading on the critical RTD components would be as low as achievable
- qualification programme for plant-specific high frequency vibration operating environment
- to order the high frequency vibration root cause study from RCP OEM, in order to suggest methods to reduce or eliminate vibrations generation from the pump.

The allowed time for completion of all tasks was Outage 2016, which imposed very demanding schedule for all parties. RTD manufacturer and the RTDBE contractor analysed the possible improvements to the RTD design and manufacturing process within given boundaries and proposed following:

- Instead of pure platinum, a higher strength platinum-rhodium alloy material shall be used for RTD lead wires
- The RTD manufacturing process was revised so that better potting was assured
- RTD tip was slightly redesigned to support better potting.

The same two companies worked together on a qualification programme for improved RTDs. The most important goals of the programme were finding RTD resonant frequency(es) and to simulate 20 years (which was guaranteed RTD lifetime) of operation at that frequency environment without failures. Since this type of qualification was unique in the industry, it was difficult to both contract the laboratory with appropriate capabilities and to execute the programme with confidence in results. The available high-frequency shaking tables had very strict mass limits for equipment under test so manufacturer had to adapt their RTD test setup considerably, reducing the overall mass by the factor of 100. To cover complete frequency spectre recorded at Krško several shakers had to be used, with results on some of them being inconclusive and thus discarded. Eventually with much effort testing was completed, results reviewed and the RTDs were considered to have been qualified to Krško specific high frequency environment.

Concurrently RCP OEM was contracted to perform a root cause analysis for the generation of the high frequency vibrations. Normally vibrations in this spectre do not affect pump operation or behaviour at all and are therefore not even measured, so very little data was available from the industry. For this reason, the analysis was based primarily on the experience and expertise of the author, who used all available information from testing and measurements performed at the plant. The conclusion of this analysis [14] was that the high frequency vibrations are generated due to some sort of acoustic resonant effect in the pumped coolant, excited by the diffuser vane pass harmonics. The possible mitigation actions would be RCP internal design modifications, which were not further considered due to cost and the complexity.

## 5 CONCLUSION

Following isolation valve leak in 2008, Krško decided to perform RTD Bypass Elimination project. The project was very complex to design and perform, and included significant effort in mechanical, instrumentation and safety analyses area. Although design team resolved many expected negative influences in advance, some plant conditions, that only had minor impact to plant operation before, caused plant trip and major equipment failures during operation of the new system. Krško invested many resources into resolving all the issues and making the new RCS temperature measurement system operate trouble-free.

## REFERENCES


[1] RTDBE-RWM, Nuclear Power Plant Krško RTDBE Radwaste Minimization, Revision 03

[2] FME Plan for Project 716-RC-L RTDBE, Revision 0

[3] STR-NEK-10-04, Vandellos Weed Experience, Revision 0, August 2010

[4] 0337-P000393094-001, N9004 Fast Time Response RTD with Bayonet Connector Assembly, Revision 2

[5] RTDBE-NEK-AR-01, Analyses Program and Evaluations, Revision 5, February 2013

[6] RTDBE-NEK-DR-01, Functional Design, Revision 10, August 2013

[7] FER-ZVNE/SA/DA-TR02/13-0, Assessment of NPP Krsko Hot Leg Streaming Profiles Using CFD Calculations, Revision 1

[8] RTDBE-NEK-AR-01, Analyses Program and Evaluations, Revision 10, March 2014

[9] RTDBE-NEK-TP-01, Site Acceptance Tests Program, Revision 3

[10] RTDBE-NEK-LR-05, Optimization of OPΔT Protection, Revision 2, March 2014

[11] PDM-4.100, Cold Leg RTD vibration measurement, 13.4.2015

[12] CN-ARIDA-15-1, Krško RTD Vibration Data Evaluation, Revision 0

[13] MCOE-LTR-15-99, Examination of Krško Cold Leg RTDs, Revision 0

[14] CPS-16-012, A Reviee of the Krško RTD Vibration Evaluation Provided in Westinghouse Report CN-ARIDA-15-1, June 30, 2016

Journal of Energy
VOLUME 68 Number 2-3 | 2019 | Special Issue
journal homepage: http://journalofenergy.com/

# Innovation in Power Maneuvering Mode for NPP Hanhikivi with WWER-1200 reactor

**Grigory Ponomarenko**,
"Fennovoima Oy"Company
Salmisaarenaukio 1, 00180 Helsinki, Finland
grigory.ponomarenko@fennovoima.fi

## ABSTRACT

The possible innovative methods of maneuvering are investigated on the example of NPP Hanhikivi with WWER-1200 reactor in a frame of AES-2006 project. Stationary fuel loading analysis was performed for the for the most significant graph of daily manoeuvring (100-50-100)% Nnom with the rate of power change 1-5 % Nnom per minute, that are the European Utility Requirements. The improvement is ensured by maintaining a constant average coolant temperature in the core "Tav = const" (by changing the pressure in SGs) and a constant boron content in the primary coolant "CB = const". The change of power and Xenon concentration during power manoeuvring is compensated by special movement of the special chosen grey CRs in the core instead of CB change. CB is changed in usual way only for fuel burnup compensation during reactor campaign. The mode "Tav = const" is normally used for the control of power of PWRs in wide diapason and it reduces the amount of radioactive primary water discharges and the mechanical fatigue of the RCS components. Implementation of both – main mode "Tav = const" and auxiliary mode "CB = const" leads to positive effect of synergy. The mode "Tav = const" facilitates the implementation of the mode "CB = const" very much, and they together allow to completely eliminate the production of liquid waste during maneuvering and ensure load following practically for the full length of reactor campaign. Presence of large CRs quantity (121 pieces) in the WWER-1200 allows using part of them as grey CRs without safety violation due to small decrease of EP efficiency. The efficiency of grey CRs is 2-3 times less than of usual black CRs that allows more softly maintain criticality, AO and power peaking factors in their acceptable diapasons at CB = const. Analysis is performed with Russian 3D code BIPR-7 only for neutronics aspects without considering strength cyclic characteristics of the equipment and nuclear fuel.

***Key Words:*** Maneuvering modes, Boron-free control, grey absorbing rods, advantages of WWER-1200.

## 1 INTRODUCTION

1.1 Two different main modes for power maneuvering can be used in WWER (PWR):

- mode "$P_2$ = const". The maintenance of constant secondary pressure at the normal operation with power rising or decreasing is traditionally used for WWERs. It naturally spread initially on the conditions with power maneuvering. At this the temperature at the core input tin decreases (increases) with a decrease (increase) in power by about 0.2 °C /% $N_{nom}$. For example, for the graph (100-50-100) % $N_{nom}$, the corresponding coolant temperature jumps (affecting the mechanical fatigue) reach 24.8 °C (Table 1), which is considered as disadvantage of this mode. Another disadvantage of this mode is the need to introduce an additional absorber (boron in water and CRs). It

is needed to compensate for reactivity due to decrease in the coolant temperature with decrease in power (about 1% Δk/k for 50% $N_{nom}$) and vice versa, to withdraw an additional absorber for power increase (Table 2). This additional reactivity is substantially greater than the reactivity required to compensate for the power change and current non-stationary Xenon poisoning. This is presented in Table 2 and more clearly in the figures below.

- mode "Tav = const". Maintaining a constant coolant temperature in the core eliminates both of the above mentioned disadvantages of the mode $P_2$ = const. This can be achieved by increasing the pressure in the SGs. The pressure in the SG should increase (decrease) with a decrease (increase) in power by about 0.020-0.025 MPa /% $N_{nom}$. For the graph (100-50-100)% $N_{nom}$, the corresponding jumps in the coolant temperature reach lower values (see Table 1) that should reduce the mechanical fatigue of the RCS components in comparison with mode $P_2$ = const. An additional absorber is also not required (Table 2). This mode reduces the amount of primary water discharges and less perturbs the power distribution by the movement of the CRs CPS in comparison with mode $P_2$ = const. Moreover, a need in the small operative reactivity margin makes it possible to use the so-called grey CRs to control power and xenon. Grey absorber has 2-3 times less efficiency than the commonly used black absorber. Grey CRs even less disturb the power distribution and make it easier to implement the auxiliary mode "CB = const" during power maneuvering. Figure 2 shows the number, location and mutual movement of grey CRs in the core which should be most effective in ensuring that the acceptance criteria are met (item 2.3). Grey CRs CPS are installed in the cells instead of a part of the usual black CRs CPS (see item 3.1). The maximum number of 121 CRs was specifically set initially in the AES-2006 project, including possible replacing some part of the black CRs by the grey ones. Therefore, there is some freedom of their reasonable choice.

1.2 Requirements of EUR [1] in relation of power maneuvering and goals, which are achieved in this paper:

1) Load following operation for graph 100-50-100 with rate of power change (1-5) % $N_{nom}$/minute has to be ensured during as long as possible, but not less than 90% of the whole reactor campaign.

2) This should be achieved in PWRs without adjusting soluble boron concentration during the manoeuvre.

3) The average coolant temperature is normally the parameter of the PWR. Mode Tav = const have to be ensured for the range between 50% and 100% $N_{nom}$ [1]. A constant coolant temperature over a wide range up to 100% load favours Load Following operation. It reduces the amount of the primary water discharges and the mechanical fatigue of the RCS components [1].

Table 1: Temperature changes (jumps) which realized at Power change

| Place in the Reactor Plant equipment | Temperature changes (jumps) which realized at Power change from 100 till 50 %$N_{nom}$ (and back) for two modes, $^oC$ | |
|---|---|---|
| | $P_2$=const | $T_{av}$=const |
| RPV inlet | 10 | 9.2 |
| RPV outlet | **24.8** | **5.6** |
| SG inlet | **24.8** | **5.6** |
| SG outlet | 10 | 9.2 |

1.3 Figure 1 demonstrates the changes of AO and Ro vs. time at free Xenon oscillations after single power maneuvering for different moments (BOC, EOC) of reactor campaign and different core lengths (375 cm (AES-2006), 355 cm (WWER-1000) and 250 cm [2, 3] ). A relatively small power change excites Xenon oscillations. They are increased with increasing core height and move from self-attenuation (for BOC) to self-amplification (for EOC) of the amplitude of oscillations.

However, the remarkable intrinsic property of the WWER (PWR) core is the coincidence of the phases of oscillations AO and Ro [7]. It is displayed in the fact that the APC work, while maintaining a constant power (zero reactivity), has addition side effect of suppress "in the bud" amplification of AO oscillations. It is interesting that this coincidence of phases is an indirect consequence of negative TCR - another important intrinsic property of the WWER (PWR) core.

Table 2: Reactivity changes (jumps) which realized at Power change

| Rate of power change, $\%N_{nom}$ per minute | Moment of reactor campaign | Power decrease or increase | Average reactivity changes (jumps) which realized at Power change from 100 till 50 $\%N_{nom}$ (and back) for two modes, $\%\Delta k/k$ | | Reference Figure number |
|---|---|---|---|---|---|
| | | | $P_2$=const | $T_{av}$=const | |
| 5 | BOC (0FPD) | decrease | 1.32 | 0.46 | 6 |
| | | increase | -1.36 | -0.48 | |
| 5 | EOC*(280 FPD) | decrease | 1.71 | 0.47 | 4 |
| | | increase | - | -0.50 | |
| 0.83 | EOC*(280 FPD) | decrease | 1.62 | 0.41 | 5 |
| | | increase | -1.58 | -0.34 | |

*280 FPD is about 81% of full reactor campaign lengths (347 FPD). 280 FPD was used for EOC because calculation with 347 FPD (CRs are fixed) is stopped due to very large power nonuniformity Kv.

## 2 DESIGN MODELING AND ACCEPTANCE CRITERIA

2.1 Initial state. Analysis is carried out only for neutronics aspect without consideration of the strength cyclic characteristics of the equipment and nuclear fuel. As a reference, the calculation of neutronics, developed by Kurchatov Institute - the scientific supervisor of the Hanhikivi project, was used. By the code BIPR-7 was simulated a simplified stationary fuel loading for the symmetry sector $60^o$ (reference calculation is performed for the full core $360^o$ due to the lack of strict symmetry $60^o$). Satisfactory results for the purposes of this paper were achieved, close to the reference calculation: the duration of the reactor campaign, fuel burn-up, effects and coefficients of reactivity, power peaking factors, etc. Figure 2(a) presents Power distributions (for BOC and EOC) in the core (for symmetry sector $60^o$) for stationary loading of Hanhikivi NPP. Initial (before start of power maneuvering) grey RGs heights partially inserted into the core for creation of operation reactivity margin are presented in Table 3.

2.2 The following improvements were modelled in this paper during power maneuvering in the power range (50-100) $\%N_{nom}$:

1) maintaining the constant average coolant temperature in the core "$T_{av}$ = const". This may be achieved by changing the pressure in SGs;

2) maintaining the constant boron content in the primary coolant "CB = const". This may be achieved by movement of the CRs in the core for compensation of reactivity change. Boron concentration is changed as usual only for fuel burn-up compensation during reactor campaign, but not for change of power and Xenon concentration during maneuvering;

3) replace of part of the usual black CRs by grey CRs. Presence of large CRs quantity (121 pieces) in the WWER-1200 allows to use part of them as grey CRs without safety violation. The efficiency of grey absorber is 2-3 times less than of usual black absorber that allows more softly maintain criticality, AO and power peaking factors in their acceptable diapasons at "CB = const" (see item 2.3).

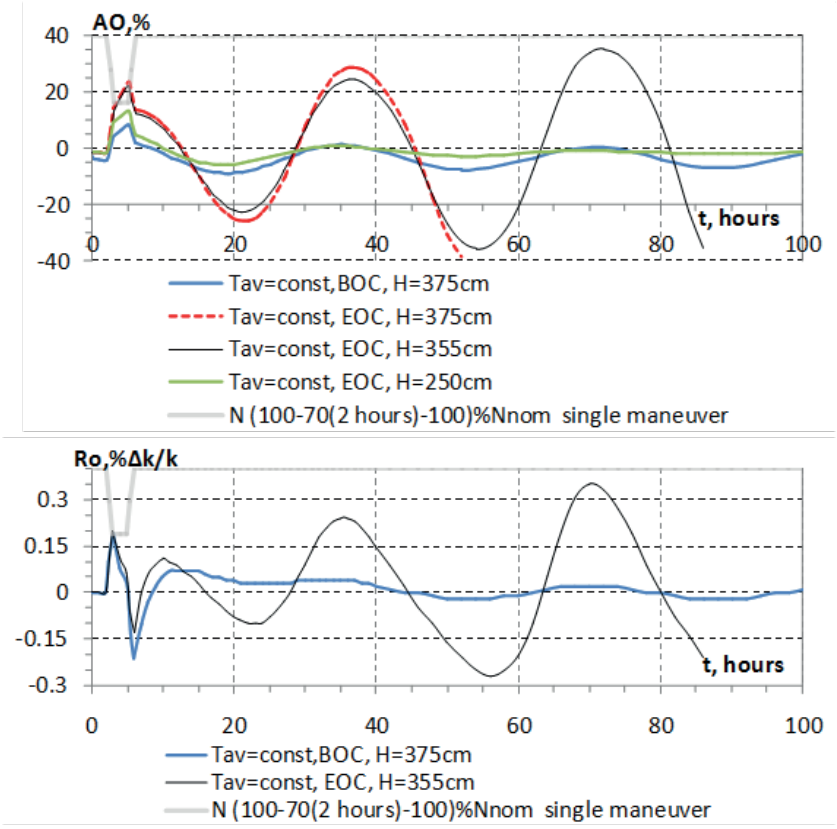


Figure 1: Axial power offset (AO) and reactivity (Ro) vs. time at free Xenon oscillations after single power maneuver *(background grey semitransparent line (N))* for different moments (BOC, EOC) of reactor campaign and different core lengths (375, 355 and 250 cm)

2.3 Acceptance criteria for calculations are maintaining the AO, Kv, Kq, criticality (Ro=0) for CB=const and some specific preliminary data for subsequent safety substantiation in their permissible ranges:

- AO should have as minimal deviation as possible from initial equilibrium value;
- Kv has not to exceed 1.9 for 100% $N_{nom}$ and 2.1 for 50% $N_{nom}$;
- Kq has not to exceed 1.40 for 100% $N_{nom}$ and 1.45 for 50% $N_{nom}$;
- Insertion of reactivity at fall of half-length grey RG has not to exceed 0.23 % Δk/k;
- Decrease of EP efficiency due to replacement of part black CRs by grey ones and after account of partially inserted grey CRs (for creation of operation reactivity margin which is required for maneuvering with CB=const), and due to burn-out of grey CRs, has not to exceed 5-10 % (rel.).

## 3 RESEARCH RESULTS

3.1 Figure 2(b) presents placement of Black and Grey groups of CRs in the core cells. RG_17&24 (placed in the core periphery) are mutually balanced with RG_3 (placed in the central part of the core) and therefore their movement is approximately the same. When maneuvering, their height remains well above 50% from the core bottom (see Figures 4-6 (d) and 7 (g)). Their bottom parts work as grey absorber during maneuvering. When the EP actuates, their upper parts with a black absorber work more efficiently.

RG_10&19 contains grey CRs of half-length in the bottom part and intended for effective suppression of big negative AO in the core. RG_6 is intended for fine regulation.

As a result we have 18 Grey&Black CRs, which weakly decrease the EP, 6 Grey CRs and 12 Grey CRs of half length. Part of Grey CRs is partially inserted into the core for creating the required operative margin for maneuvering with CB=const. Grey CRs also fall with EP actuation.

The results of calculations show that overall decrease in the EP efficiency due to the replacement of a part of the black CRs by the grey ones and after account of partially inserted the grey CRs, and due to burn-out of grey CRs, does not exceed 10 % (rel.). Small share of the EP efficiency loss is explained by the following: when all 121 CRs are inserted into the core by EP signal, each weakened grey CR is surrounded by powerful black CRs without formation of zones of potential local criticality.

The interesting effect was revealed in the calculations: in the contrary to black CRs the prolonged presence of grey CRs in the core which were chosen for operative reactivity margin weakly distorts the distributions of power and fuel burnup. No need even correct the stationary fuel loading pattern during and after several loadings with inserted grey CRs. It is explained by the rather big quantity of grey CRs uniformly distributed in the core.

Let's compare with some other PWR designs which have significantly less quantity of CRs, that allow to expect the sufficient EP efficiency for WWER-1200 for conditions with rather large quantity of grey CRs (36 ps.), considered in this paper:

- Reactor EPR (http://www.tvo.fi/uploads/julkaisut/tiedostot/ydinvoimalayks_OL3_ENG.pdf).

4300 MW (thermal), 1600 MW (el.). The core contains 241 FAs and totally 89 CRs. 53 CRs of them are black CRs intended for EP. Remaining 36 consist of the grey (12 ps.) and black (24 ps.) CRs, which are intended to control power and AO. However the CB is changed during maneuvering.

- Reactor AP-1000 (https://www.ipen.br/biblioteca/cd/genes4/2003/papers/1030-final.pdf). The core contains 157 FAs and totally 69 CRs. 16 CRs of them are grey CRs intended for control of power and AO. In that paper it is declared that there is possibility to achieve CB=const during maneuvering, but this is raw result obtained on the base of very simplified calculations – one-dimensional diffusion theory.

Also, the big quantity of neutron and thermal sensors in the core of WWERs [4-6], including WWER-1200 of NPP Hanhikivi (much more than in PWRs, including the above mentioned PWRs) facilitates adequate on-line monitoring and control of power distribution by the movement of grey CRs in the core during the power maneuvering with CB=const.

Therefore one can conclude that just the presence of so big numbers of CRs and neutron and thermal in-core detectors in WWER-1200 are the unique cases that makes it possible to realize mode CB=const by the grey CRs. Moreover such big quantities of CRs and sensors in the core is the most reasonable only for this case, whereas the maneuvering with change of CB and less movement of CRs may uses the less quantities of CRs and detectors.

3.2 The following side effect arises. The fall of RG of "half-length" grey CRs from the height of 50% from the core bottom can introduce positive reactivity. For example, when operating at rated power, a large positive AO can sometimes be compensated by such RG_10 at a height of 50%. Its fall to the core bottom will introduce a positive reactivity about 0.2% $\Delta k / k$ during about 1 s, which is comparable to the reactivity inserted during the design basis accident "the ejection of one CR CPS". This RIA should be analyzed within the framework of the further safety justification. It is not expected the safety violation in this event.

```
28
4year
0.258
0.328
26     27
1year  3year
1.153  0.449
1.208  0.550
23     24     25
3year  1year  1year
1.036  1.263  0.926
0.977  1.361  1.041
19     20     21     22
2year  3year  2year  1year
1.218  1.049  1.193  0.927
1.107  1.015  1.185  1.042
14     15     16     17     18
2year  1year  3year  1year  3year
1.135  1.202  1.020  1.266  0.452
1.067  1.240  0.990  1.362  0.554
8      9     10     11     12     13
2year  2year2year  3year  1year  4year
1.248  1.133  1.216  1.066  1.164  0.268
1.164  1.069  1.105  0.998  1.215  0.340
1      2      3      4      5      6      7 - FA's Number
4year  3year  1year  3year  2year  2year  4yearof work
0.685  0.996  1.232  1.029  1.361  1.271  0.522 - BOC Kq
0.719  0.970  1.288  0.946  1.168  1.169  0.586 - EOC Kq
```

a – Power distribution by FAs (Kq for **BOC** and **EOC**) in the core (symmetry sector 60°). Grey CRs are partially inserted into the core to create operational margin for maneuvering with CB=const

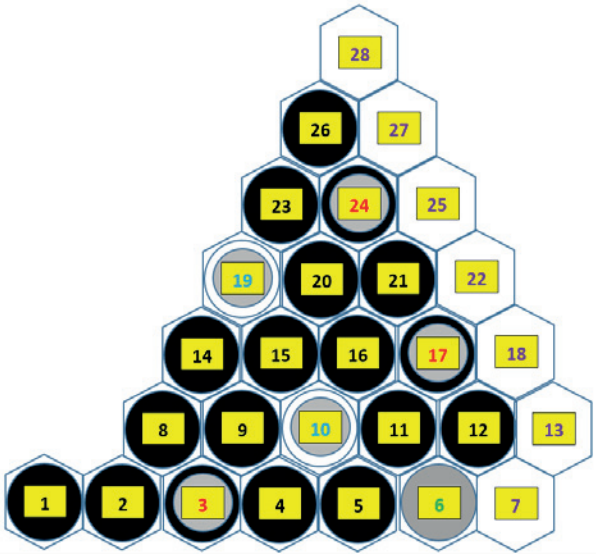



- Grey and Black (G&B) absorbers on the Bottom and Top halves of CRs accordingly (Cells 3, 17,24)
- Grey and Zero (G&Z) absorbers on the Bottom and Top halves of CRs accordingly (Cells 10, 19 without absorber on the Top half)
- Grey (G) absorber on all length (Cell 6)
- Black absorber (B) on all length (Cells 1,2,4,5, 8,9,11,12,14,15,16,20,21,23,26)
- No absorber on all length (Cells 7,13,18,22,25,27,28)

b –allocation of Black and Grey absorbers in the core cells. The CR CPS group's number is the same as the cell number (if CR CPS is there in this cell)

Figure 2: Cartogram of the core symmetry sector 60°

3.3 Grey absorbers are simulated in this paper in such a way that their efficiency (in the form of the difference $K_{eff}$ in their absence and in their presence in the FA $\Delta K_{eff} = K_{eff}^{(without\ absorber)} - K_{eff}^{(with\ absorber)}$) is equal to half (1/2) of the efficiency of the commonly used black absorbers. Grey absorbers with a lower efficiency – 1/3 of black absorber, were also examined to evaluate approximately their performance with significant absorber burn-out over several years of operation, and also to have an idea about the sustainability of the results and conclusions in the presence of

uncertainty and calculation code accuracy. Grey absorbers can be realized on the basis of some (n-γ) absorbers that remain effective during prolonged burn-out, such as hafnium (Hf) and dysprosium (Dy).

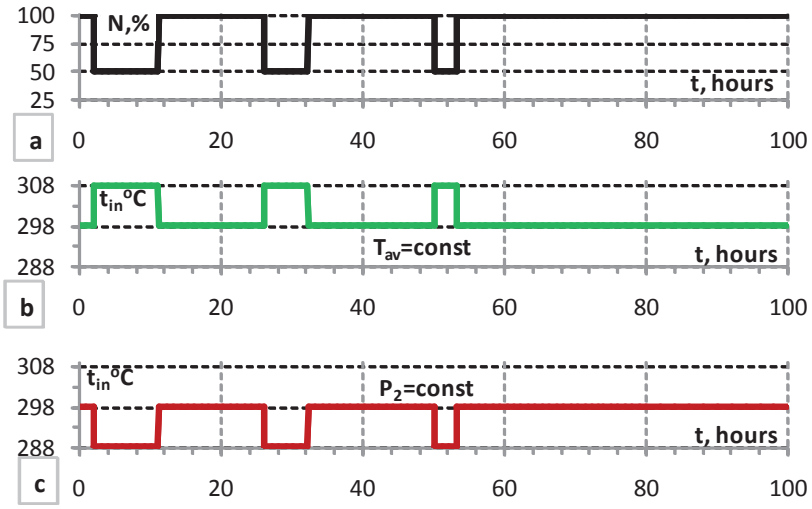


Three daily power decrease for 9, 6 and 3 hours to 50 % $N_{nom}$ and subsequent increase to 100 % $N_{nom}$ occur during 10 minutes and then till 100 hours – the period of stabilization at nominal power

Figure 3: N (a) and $t_{in}$ vs. time for modes $T_{av}$=const (b) and $P_2$=const (c) at daily maneuvering (100-50-100) % $N_{nom}$ at rate of power change 5 % $N_{nom}$ per minute

3.4 Figures 4-7 show the maneuvering characteristics of Ro, AO, Kv, Kq, H_RG for different states and conditions.

The common thing for Figures 4-7 is that the main case on them is the mode "Tav = const, CRs are moving" (see the notation in Figure 4-6 (a-c)) in which $T_{av}$ = const and criticality (Ro = 0), AO, $K_v$, $K_q$ are maintained in their acceptable diapasons by special movement of special selected Grey CRs and partially by black RG_15 (see Figures 4-6(d, e)). Figures 4-6 (a - c) also provide auxiliary additional information for modes $T_{av}$ = const and $P_2$ = const: Ro, AO, Kv without any compensation by CRs movement. In these conditions, CRs are fixed in the initial position.

This information together with attachment of power changes graph is very demonstrable for comparison with the main case and understanding of proposed strategy. In particular, it is clear from such a comparison that the mode $T_{av}$ = const can be realized with grey CRs without CB changing.

It was also showed that the mode $P_2$ = const make it hardly achievable or even impossible to realize CB = const because it requires the insertion of black CRs (with big negative reactivity) for power decrease. It greatly distorts the power distributions on the 50 % $N_{nom}$directly and also (with delay) on the 100 % $N_{nom}$due to the distortion of the latent Xenon distribution.

Figures 4 and 6 correspond to the maneuvering graph depicted in Figure 3a with a power change of 5% $N_{nom}$ per minute. Figure 4 corresponds to EOC, and Figure 6 – to BOC, where some lower maximum values of $K_v$ (1.8) are achieved than for EOC (1.9) at 100% $N_{nom}$. At the same time, it should be noted that the CRs movements presented in Figures 4-7 were chosen "in first approximation" and can be considered conservative (suitable as initial data for safety analysis), but in the future they can be optimized with attainment of smaller values of $K_v$ , for example, not more than 1.8-1.85. In addition one can visually note that RGs movement for EOC is simpler and therefore it can be easier controlled than RGs movement for BOC (compare Figure 4(e) with 6(e)). The reason of this simpler movement is more flatten axial distribution of power at the EOC in comparison with sinusoidal axial power distribution at the BOC. It make CRs more effective near the core top and bottom for EOC. The use of axial profiling of BA in the FAs, for example excluding of BA from the 15-20% of the fuel length at the very top and very bottom parts of FAs can ensure more flatten axial distribution of power and facilitate control during the full reactor

campaign. Similar axial profiling of the BA and sometimes of the fuel enrichment is used in some PWRs (WWERs) to get small positive effects in improvements of fuel utilization and Kv. But the use of this BA profiling for simplification of control of maneuvering mode "CB = const" by the grey CRs can be a new and more significant its additional application.

Table 3: The positions of the working group (RG_15) and grey RGs in the initial state (before maneuvering) and at the moments of the first, second and third power raises from 50% to 100% $N_{nom}$

| Rate of power change, %$N_{nom}$ per minute | RG'sNumber | Initial RG's heights, % from the core bottom | RG's heights at the first power raise to 100 % $N_{nom}$, % from the core bottom | | RG's heights at the second power raise to 100 % $N_{nom}$, % from the core bottom | RG's heights at the third power raise to 100 % $N_{nom}$, % from the core bottom | Figures' Number (and moments of 100 % $N_{nom}$ achieving) |
|---|---|---|---|---|---|---|---|
| 5 | 15 | 90 | 98 | | 98 | 96 | Fig 4 (11.3, 32.3 and 53.3 hours) |
| | 17&24 | 96 | 100 | | 100 | 100 | |
| | 3 | 96 | 100 | | 100 | 100 | |
| | 10&19 | 26 | 88 | | 82 | 84 | |
| | 6 | 100 | 100 | | 100 | 100 | |
| 0.83 | 15 | 90 | 96 | 98 | 96 | - | Fig 5 (12.0 and 33.0 hours) |
| | 17&24 | 96 | 100 | 100 | 100 | - | |
| | 3 | 96 | 100 | 100 | 100 | - | |
| | 10&19 | 26 | 76 | 100 | 100 | - | |
| | 6 | 100 | 100 | 36 | 24 | - | |

3.5 The peculiarity is that when the reactor is returned to 100% $N_{nom}$, it is required to introduce more positive reactivity (i.e. to achieve greater RG's heights in comparison with the initial RG's heights, see Table 3), than negative reactivity which was introduced before that to reduce the power from 100 to 50 % $N_{nom}$. This is necessary for compensation of the additional Xenon poisoning accumulated when operating at reduced power during several hours. That is why, for the maneuvering mode with CB = const, it is necessary to create a certain operative reactivity margin by partially inserted grey CRs CPS into the core.

Figure 5 corresponds to a power change 0.83% $N_{nom}$ per minute.

Comparison of Figure 4 and 5 shows that, as expected, a smaller rate of power change requires a slightly smaller introduction of positive reactivity (i.e. lower RG's heights, see Table 3) for the reactor to achieve 100% after 50% $N_{nom}$ and vice versa with a power decrease from 100 to 50% $N_{nom}$.

Figure 7 simulates daily maneuvering, which differs from Figure 4 in that grey absorbers have a lower efficiency - 1/3 from the black one, in contrast to Figure 4 (with grey absorbers with 1/2 of black efficiency). The maneuvering graph was also slightly changed in comparison with Figure 4. It can be seen that grey absorbers with less efficiency can successfully ensure the maneuvering regimes. As a result, it can be concluded that the grey CRs can maintain their performance in the long-term burn-out of the absorber (over several years of operation) in a maneuverable regime.

3.6 In summary one can conclude that all acceptance criteria (see item 2.3) are met including AO, Kv, Kq and criticality (Ro=0) for CB=const. Safety analyzes have to be fulfilled on the next stage of work for CPS efficiency with grey CRs and for the fall of half-length grey RG_10 or 19.

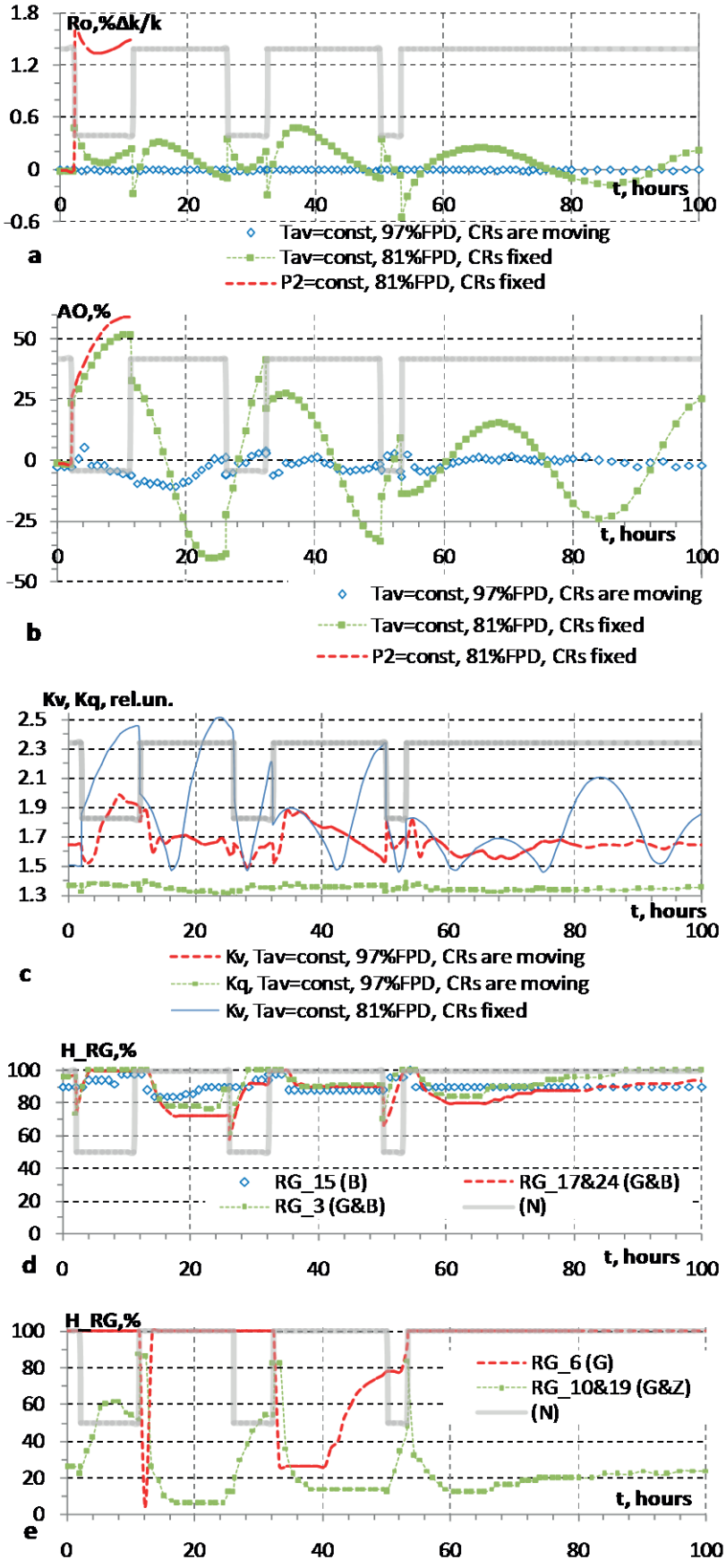


Figure 4: EOC. *5% $N_{nom}$/min*

**a** – change of reactivity for:
**-main** mode $T_{av}$=const and criticality (Ro=0) is ensured mainly by movement of Grey CRs (see below Figures d and e);
-reactivity which should be compensated when CRs are fixed in initial position for modes $T_{av}$=const and $P_2$=const (calculation of the last one was stopped due to very large power nonuniformity Kv).

**b**– change of axial offset due to Xe oscillations for the same modes as on Figure a. Movement of Grey CRs (Figures d and e) smooth Xe oscillations for main mode $T_{av}$=const;

**c** – change of power peaking factors Kv, Kq for main mode and Kv for fixed CRs;

**d, e** – change of heights of RGs 15, 17, 3, 6, 10, 19 for main mode $T_{av}$=const to ensure criticality and allowable values of AO and power peaking factors.

*Note: Background grey semitransparent line (N) facilitate understanding of process due to attachment of power change (100-50-100)%$N_{nom}$(at rate 5%/min) on all Figures.*

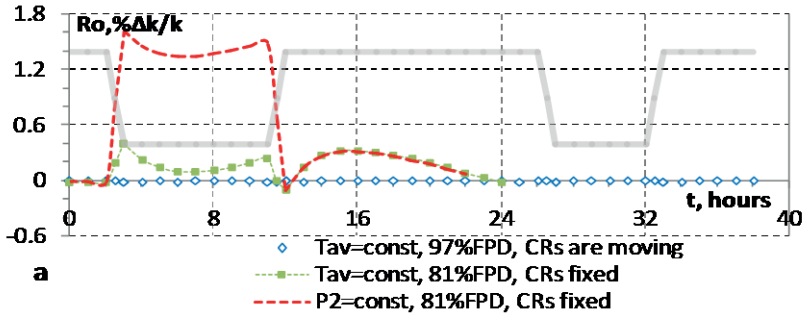


**a** – change of reactivity for:
-main mode $T_{av}$=const and criticality (Ro=0) is ensured mainly by movement of Grey CRs (see below Figures d and e);
-reactivity which should be compensated when CRs are fixed in initial position for modes $T_{av}$=const and $P_2$=const.

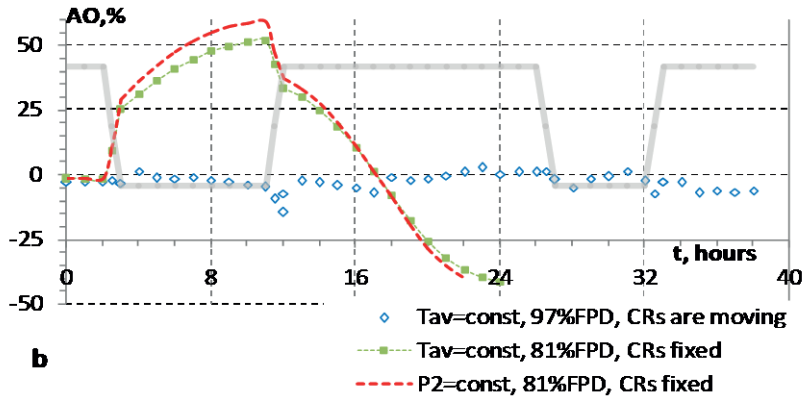


**b** – change of axial offset due to Xe oscillations for the same modes as on Figure a. Movement of Grey CRs (Figures d and e) smooth Xe oscillations for main mode $T_{av}$=const;

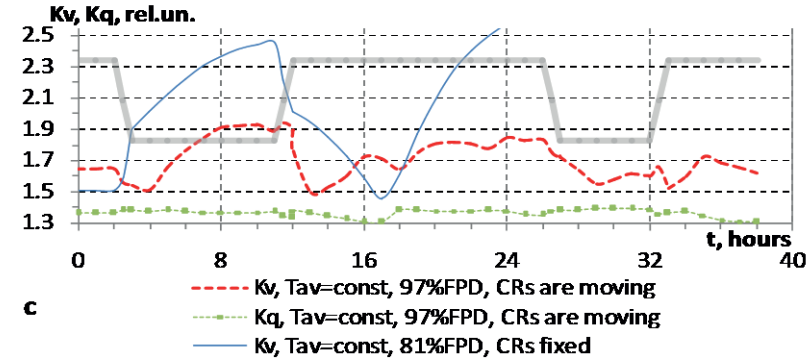


**c** – change of power peaking factors Kv, Kq for main mode and Kv for fixed CRs;

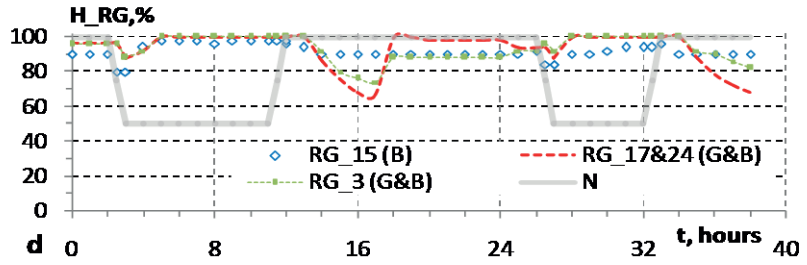


**d, e** – change of heights of RGs 15, 17, 3, 6, 10, 19 for main mode $T_{av}$=const to ensure criticality and allowable values of AO and power peaking factors.

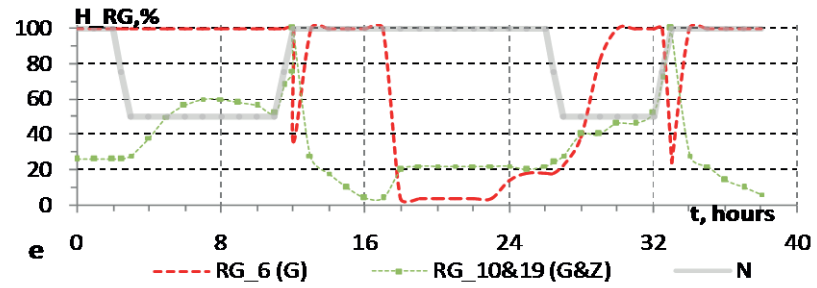


*Note: Background grey semitransparent line (N) facilitate understanding of process due to attachment of power change (100-50-100)%$N_{nom}$(at rate 0.83%/min) on all Figures.*

Figure 5:EOC *0.83% $N_{nom}$ /min*

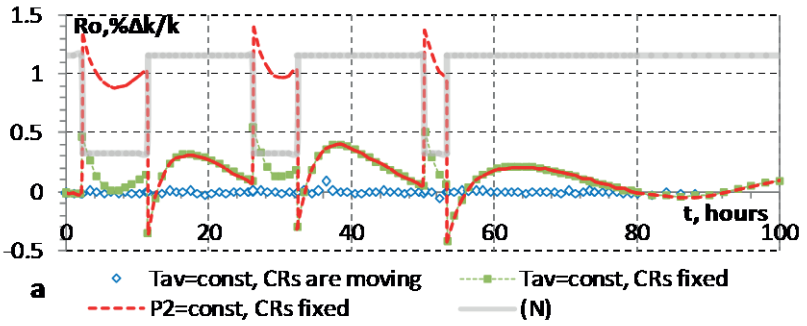


**a** – change of reactivity for:
-main mode $T_{av}$=const and criticality (Ro=0) is ensured mainly by movement of Grey CRs (see below Figures d and e);
-reactivity which should be compensated when CRs are fixed in initial position for modes $T_{av}$=const and $P_2$=const.

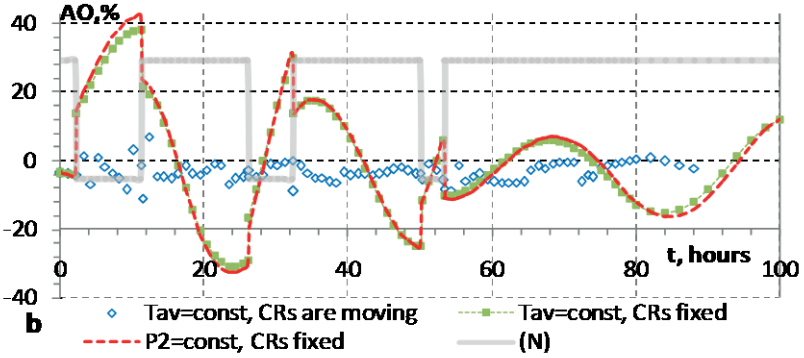


**b** – change of axial offset due to Xe oscillations for the same modes as on Figure a. Movement of Grey CRs (Figures d and e) smooth Xe oscillations for main mode $T_{av}$=const;

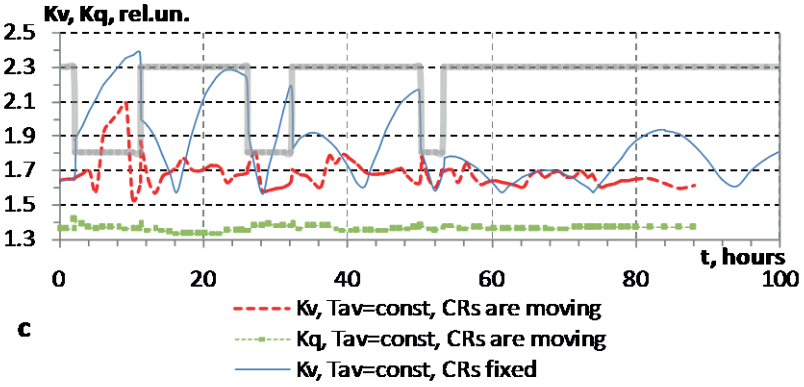


**c** – change of power peaking factors Kv, Kq for main mode and Kv for fixed CRs;

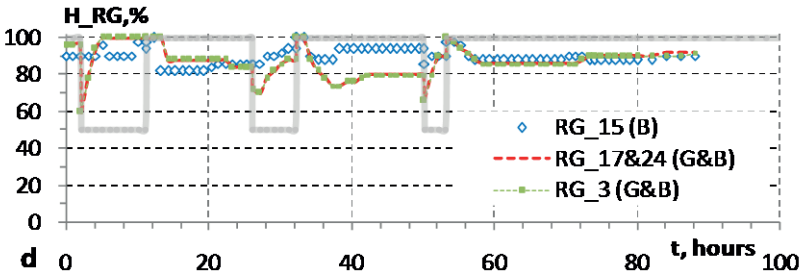


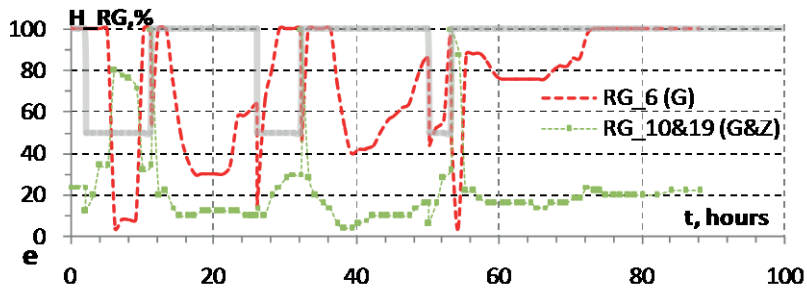


**d, e** – change of heights of RGs 15, 17, 3, 6, 10, 19 for main mode $T_{av}$=const to ensure criticality and allowable values of AO and power peaking factors.

*Note: Background grey semitransparent line (N) facilitate understanding of process due to attachment of power change (100-50-100)%$N_{nom}$(at rate 5%/min) on all Figures.*

Figure 6: BOC *5% $N_{nom}$/min*

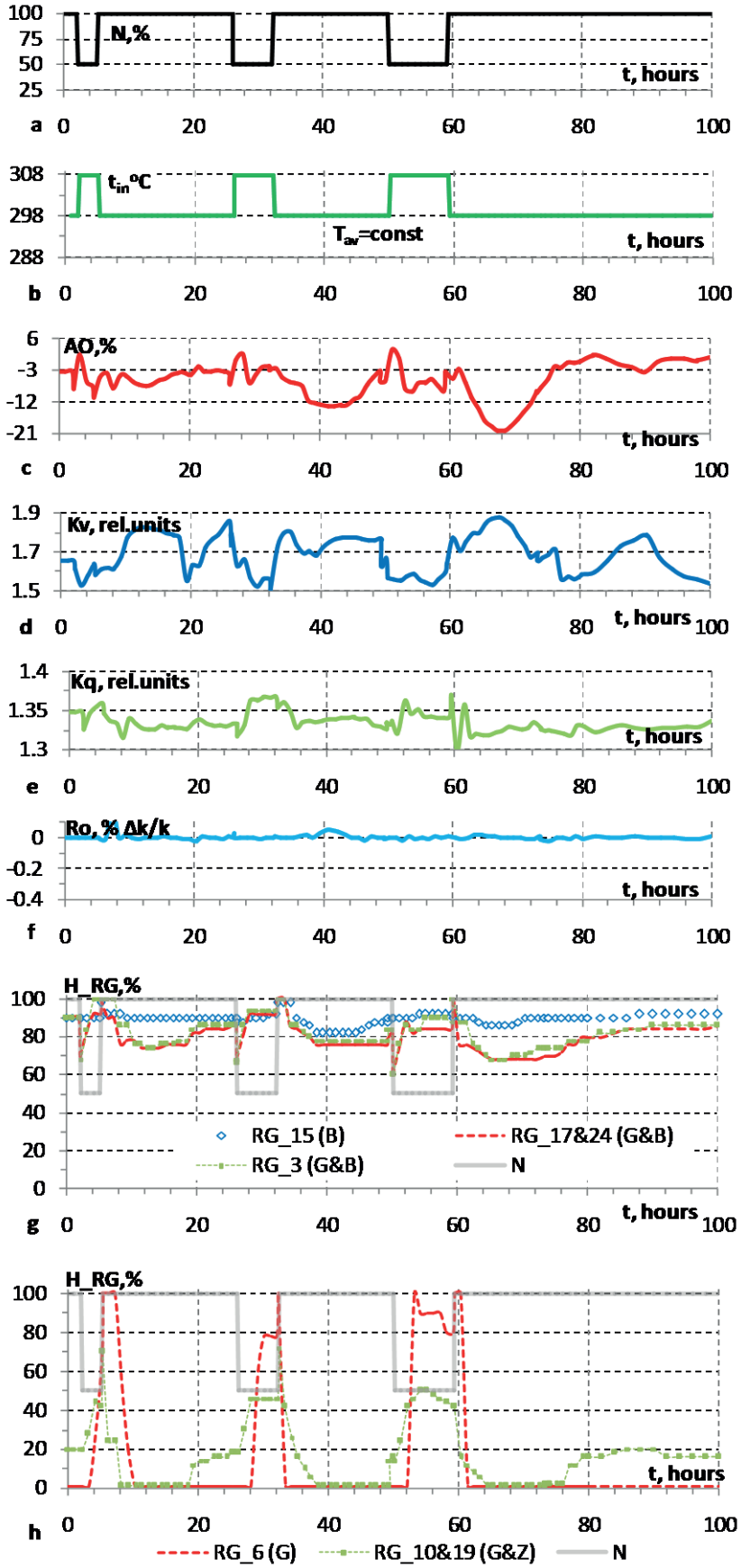


**a, b** – N and $t_{in}$ vs. time for mode $T_{av}$=const at daily maneuvering (100-50-100) % $N_{nom}$ at the rate of power change 5 % $N_{nom}$ per minute

**c** – change of axial offset due to Xe oscillations. Movement of Grey CRs (Figures g and h) smooth Xe oscillations for main mode $T_{av}$=const;

**d, e** – change of power peaking factors Kv, Kq for main mode;

**f**– change of reactivity for main mode $T_{av}$=const and criticality (Ro=0) is ensured mainly by movement of Grey CRs (see below Figures g and h);

**g, h** – change of heights of RGs 15, 17, 3, 6, 10, 19 for main mode $T_{av}$=const to ensure criticality and allowable values of AO and power peaking factors.

Figure 7: EOC decreased efficiency of grey absorber (1/3 of the black one) for RG_10&19

## 4 CONCLUSION

The possibility of satisfying the increased modern requirements of the operators (EUR) to the maneuvering regimes for NPP Hanhikivi was investigated for neutronics aspects. The analysis was fulfilled on the example of the daily maneuvering (100-50-100) % $N_{nom}$ with the rate of power change 1-5 % $N_{nom}$ per minute.

The obtained results demonstrate that maneuvering is possible practically during the full length of reactor campaign without water exchange (at CB=const) in the primary coolant.

For this it is necessary to implement mode of maintaining of the average coolant temperature ($T_{av}$=const) during power maneuvering and replace part of usual black CRs by the grey ones. In the paper it is described the proposed characteristics of grey absorbers: quantity, effectiveness, placement in the core, approximate algorithms of their mutual movement and is demonstrated the satisfaction of the preliminary acceptance criteria (item 2.3) during maneuvering.In the contrary to black CRs the prolonged presence of grey CRs in the core which were chosen for operative reactivity margin weakly distort the distributions of power and fuel burnup.It is recommended also to use the axial profiling of BA in the FAs, for more flatten power distribution that facilitate control of CRs movement during full reactor campaign.

It was also showed that the mode $P_2$ = const make it hardly achievable or even impossible to realize mode CB = const, because it requires the insertion of black CRs (with big negative reactivity) for power decrease. It greatly distorts the power distributions on the 50 % $N_{nom}$directly and also (with delay) on the 100 % $N_{nom}$due to the distortion of the latent Xenon distribution.

The key conditions of successful solution of the problem of power maneuvering with CB=const is the presence of big quantities of CRs and neutron and thermal sensors in the core of WWER-1200 of NPP Hanhikivi (much more than in the PWRs). This allows to choose the grey CRs, the quantity, placement and movement of which is sufficient and effective to ensure the adequate on-line monitoring of power distribution and safe control of power and Xenon changes.

## 5 ACRONYMS AND CONVENTIONAL SYMBOLS

APC – automated power controller
BOC – beginning of cycle
BA – burnable absorber
CB – boron concentration
CPS – control and protection system
CR – control rod
EOC – end of cycle
EP – emergency protection
EUR – European Utilities Requirements
FA – fuel assembly
FPD – full power days
FR – fuel rod
NPP – nuclear power plant
PWR – pressurized water reactor
RP – reactor plant
RPV – reactor pressure vessel
TCR – temperature coefficient of reactivity
WWER – water-water energy reactor

AO – axial offset of power in the core, %
H – height of the core, % from the bottom
H_RG – height of RG in the core, % from the bottom
$K_{eff}$ – effective multiplication factor, rel. units
$K_q$ – power peaking factor by FAs in the core, rel. units
$K_v$ – power peaking factor by the nodes in the core, rel. units
N – neutron power of reactor, % of nominal power
"$P_2$=const" – mode of power maneuvering with maintaining of constant secondary pressure
RG_*i* – regulative group of CRs CPS with number *i*
Ro – reactivity, %Δk/k
t – time of Xenon transient during power maneuvering, hours
$t_{in}$ – coolant temperature at the core entrance, $^oC$
"$t_{av}$=const" – mode of power maneuvering with maintaining of constant average by the core coolant temperature

## REFERENCES


[1] EUR. European Utility Requirements for LWR Nuclear Power Plants. Volumes 1, 2&4 Rev. D, October2012.

[2] G.L. Ponomarenko, Peculiarities of Neutronics Characteristics of Integral Reactor WWER-I of Small Capacity. *In Proceedings of the 11th International Conference of the Croatian Nuclear Society*, Zadar, Croatia, 5-8 June, 2016.

[3] G.L. Ponomarenko, D.O. Veselov, D.N. Ermakov,Peculiarities of Neutronics Characteristics of Integral Reactor WWER of Small Capacity. (In English). *VANT*, *Problems of Atomic Science and Engineering*. Series: Physics of Nuclear Reactors, Issue 2, pp. 77-86, 2016.http://www.nrcki.ru/files/pdf/1506084143.pdf.

[4] G.L. Ponomarenko, Substantiation of WWERs Uprating with Usage of Neutronics, Thermo-Hydraulics and Probabilistic Calculating Methods, *Dissertation* for the degree of Doctor of Engineering Science Podolsk, 2011.

[5] G.L. Ponomarenko, V. Ja. Berkovitch, M.A. Bykov et.al. Innovative Experimental Study of Coolant Mixing and its Results Obtained Using Standard Monitoring System Complex at Operating WWER-1000 unit Bushehr NPP// *VANT*, Series: Safety of NPPs. Issue 31. Nuclear Installations with WWER, Podolsk, RF, p. 91-102, 2012.

[6] G.L. Ponomarenko, V. Ja. Berkovitch, M.A. Bykov et.al. New method of coolant mixing studies at the operating WWER-1000 units. *In Proceedings of the 21st International Conference on Nuclear Engineering, ICONE21-15251*, Chengdu, China, July 29 - August 2, 2013.

[7] Averyanova S.P. et al., Superposition of integral and axial xenon oscillations and stability of energy distribution of the WWER-1000 core, *Atomic Energy*, Vol. 111, issue 1, pp.8-13, 2011.

Journal of Energy
VOLUME 68 Number 2-3 | 2019 | Special Issue
journal homepage: http://journalofenergy.com/

# Dose Calculation for Emergency Control Room HVAC Filter

**Davor Grgić, Štefica Vlahović, Mario Matijević, Paulina Dučkić**
Faculty of Electrical Engineering and Computing, University of Zagreb
Unska 3, Zagreb, Hrvatska
davor.grgic@fer.hr, stefica.vlahovic@fer.hr, mario.matijevic@fer.hr, paulina.duckic@fer.hr

**Srđan Špalj**
*Nuclear Power Plant Krško*
*Vrbina 12, 8270 Krško, Croatia*
srdjan.spalj@nek.si

## ABSTRACT

NPP Krsko is introducing Emergency Control Room (ECR) as part of safety upgrades. According to 10CFR50 Appendix A, GDC 19, both main control room and emergency control room should have adequate radiation protection to permit operators to shutdown the plant and keep it in safe shutdown conditions without receiving more than 50 mSv effective whole body dose, within 30 days from accident initiation. One of the important prerequisites to achieve that is proper operation of control room HVAC. In this work we are focused to calculation of gamma doses from radioactive materials accumulated in HEPA and charcoal filters during 30 days of HVAC operation. The dose at selected points around the filter was calculated using Microshield 10.0 point kernel code. The radioactive gamma source is calculated using RADTRAD 3.03 for plant's severe accident SGTR sequence calculated with MAAP 4.0.7 code. Calculated dose rates at peak filter activity are compared against results obtained with SCALE 6.2 MAVRIC shielding sequence (Monaco Monte Carlo functional module and CADIS methodology). The reasonable agreement between point kernel and hybrid Monte Carlo results was obtained.

***Keywords:*** *Emergency Control Room, HVAC filter, gamma dose, point kernel, Monte Carlo*

## 1 INTRODUCTION

Based on Slovenian nuclear regulation related to Plant Life Extension and consequences after the Fukushima accident, Slovenian Nuclear Safety Administration (SNSA) requested the NEK to reassess the existing Severe Accident Management strategy. Afterwards, the NEK shall implement necessary safety improvements for prevention of severe accidents and mitigation of their consequences. This modernization will extend capability of plant to cope with different internal and external events resulting in so called Design Extension Conditions (DEC). As a part of the NEK Plant Safety Upgrade, the Bunkered Building (BB1) was constructed where the ECR, the Technical Support Center (TSC) and third emergency diesel generator are located, [1], [2].

The ECR is located on the second floor of the BB1 above the new diesel generator. The existing spare room on the second floor was used to construct the ECR and TSC. This project also included the relocation and upgrade of existing Remote Shutdown Panels (SDP) to the new Remote Shutdown Control Board (RSCB) and the construction of a new Design Extension Conditions Control Board (DECCB). The function of DECCB Panels will be to enable the operation of specially provided equipment for preventing and mitigation of Potential Severe Accidents.

The function of the RSCB in the ECR is to provide the necessary resources for the NPP operators to achieve and maintain safe shutdown following the evacuation of the Main Control

Room (MCR). The purpose of the relocated and centralized RSCB is to provide Plant Hot Stand-by and Cold shutdown capabilities in a centralized location.

Taking into account its importance, ECR has to be equipped with the communication, habitability capabilities and other equipment to enable continuous occupation of the operating crew 30 days after the postulated accident. Additionally, it is important that operators do not receive more than 50 mSv effective whole body dose, within 30 days from accident initiation, according to 10CFR50 Appendix A, GDC 19. Therefore, the most important is to achieve the proper operation of room HVAC. In this paper, we will focus to calculate the gamma doses from radioactive materials accumulated in HEPA and charcoal filters during 30 days of HVAC operation.

## 2 MODELS AND CALCULATION TOOLS

In order to assess maximum possible doses in ECR, the conservative release of radioactive material is assumed. We were more focused on equipment doses, especially related to the influence of radioactive source in HVAC filters.

Selected sequence for radioactivity release is SGTR severe accident as calculated by MAAP code using NEK standard parameter input file (Individual Plan Examination (IPE) release category 8B SGTR).

MAAP is fully integrated code that couples thermal-hydraulics with fission product release and transport [3]. It is developed by EPRI as the fast-running, integral severe accident analysis code, soon after the TMI-2 accident. It simulates the accident progression from a set of initiating events to either safe and stable state or containment failure leading to radioactive releases to the environment. In this paper, the version MAAP 4.0.7 is used.

Core uncover was calculated at 69529 s, HL creep rupture at 77959 s, first core relocation to the lower plenum at 79567 s and vessel failure at 84428 s. First release to the environment was predicted at 72730 s (from first release category different from zero), Figure 1. In Figure 2, release fractions are shown together with liquid and gas flow through SG valve. We can see gas flow rate (steam) relevant for transport of radioactivity. Using upstream gas density, volumetric flow rate is calculated in MAAP and corresponding leakage flow rate (in percent of containment free volume released per day). The volumetric flow rate is required for RADTRAD calculation procedure. It is assumed that release is from the containment volume to simplify calculation (in MAAP calculation it is SGTR containment bypass). The same amount of fluid is released in both cases (MAAP and RADTRAD).

RADTRAD was developed for the U.S. Nuclear Regulatory Commission (NRC) Office of Nuclear Regulatory Research to estimate transport and removal of radionuclides and dose at selected receptors [4]. The code uses a combination of tables and numerical models of source term to determine the time dependent dose at user-specified locations for a given accident scenario. In this paper, the version RADTRAD 3.03 is used. The program takes output data from MAAP to calculate radioactive gamma source.

Core source term is based on ORIGEN 2.2 plant (102% core power) and cycle specific calculations (NEK cycle 26-29) [5]. It is decayed in ORIGEN till the time of release (72730 s). Alternative Source Term (AST) fuel release fractions are assumed [6]. RADTRAD uses 8 chemical and 4 transport groups. Transport groups are noble gases, elemental iodine, organic iodine and aerosols. The fractions of iodine are according AST specification. Transport groups from the containment atmosphere are calculated using MAAP SG SV/RV volumetric flow after start of radioactivity release. It is assumed that start of calculation and start of the release are at the same time point (0 s).

RADTRAD code uses automatic integration time stepping in order to capture both flow and decay phenomena. First time steps are 2 s, then 10 minutes till 12.6 hours and after that 1 hour. In order to simplify calculation, time dependent flow rate calculated by MAAP was approximated with three release intervals having the same total release as MAAP calculation. Up to 2 hours, the

leakage rate is 180% of Vc per day, after that up to 7 days, it is 18% of Vc per day, and then 1% of Vc per day. Environment is approximately treated in RADTRAD and it has not specific volume assigned, but it is included in mass and radioactivity conservation. Any specific point within the environment or the point where any other volume has intake is related to the concentration at the release point using predetermined X/Q values (ARCON96 for building locations close to release point). The activity present in the environment during any time step is determined by release from the containment during the same period and any outflow to other compartments in the model. It is assumed that at the end of time step, due to plume transport, all radioactivity leaves environment volume. Amount of released material, and in the same time amount of radioactivity present in the environment, is product of concentration in the containment, leakage flow rate and time step length. Global reactivity balance is shown in Figure 3. Total activity released is activity measured at release point (after that there is no decay) and activity in the environment is total activity present in the environment at any time (released + decay). The radioactivity present in RADTRAD environment is just part of that activity (close to the release point between two plume transport events).

General layout of RADTRAD model used in calculation of doses in BB1 rooms is shown in Figure 4. Compartment number 1 is containment and that is the only compartment where radioactivity is directly released. In this case, it is used to release radioactivity which is consequence of SGTR accident. Compartment number 2 is environment and compartment number 3 is used to model room where immersion doses are needed (as shown for ECR). There is no deposition assumed in compartments. That is conservative for containment (more material is released). For the environment, it is conservative because all radioactivity is in the air (immersion and intake) and not conservative because all radioactivity is removed by plume transport (no deposits). It is again conservative for immersion dose in rooms (everything is in the air) and not conservative from point of view of surface contamination. Overall effect is that more conservative doses are predicted. There are 4 explicit paths in the model. Path number 1 is used to model release to the environment. It is based on volumetric flow calculated by MAAP code (total release is reproduced). The flow should be in units of percent of upstream compartment volume per day. Path number 2 is for uncontrolled inflow from the environment to the calculated room. It is 6% of room free volume per hour (Campe). Path 4 is used to model HVAC air intake in the room and path number 3 is modeling air exhaust from the model. It is assumed that in all situations exhaust flow is equal to the sum of inflow and intake flows. Activity obtained from paths 2 and 4 is related to release activity rate using X/Q factors calculated by ARCON96 [7]. It is assumed that filter can exist in all of the flow paths 2 to 4. The only filter with non-zero efficiency is on intake flow path (4). It is implicit assumption (no matter what is entered as filter efficiency) of the model that radioactivity is kept in virtual filter F3 (there is no return of radioactivity to the environment). In RADTRAD code recirculation filters are attached to the compartments and there is no explicit flow path for them. In NEK case, recirculation filters F1 and intake filter F4 are the one filter having function of filtration of the intake air or recirculation of ECR/TSC air, depending on HVAC line-up. Radioactivity is removed from the environment compartment at the end of each calculation step to simulate plume transport.

X/Q factors needed for paths 2 and 4 are calculated using ARCON96 code. That is for location called ECR/TSC intake. For shine dose at the BB1 roof (close to the IB building) X/Q factors are calculated for location called ECR/TSC roof. Relative positions of release and receptor points used in ARCON96 code are shown in Figure 5.

RADTRAD 3.03 is used for calculation of immersion doses in BB1 rooms. As already said, the same nodalization is used in all calculations, Figure 4. What is changed from calculation to calculation is volume of compartment 3, Figure 6, inflow rate (6% of free volume per hour), and HVAC operation.

BB1 rooms 011A (ECR), 011B (TSC) and the rooms sharing the same protective pressure barrier (011C, D, E and F, 012 Utility and 013 Toilet, 019 Machine Room MR), Figure 6, have assumed volume of 1665 $m^3$. The inflow is 99.9 $m^3$/h. Four different HVAC scenarios are analysed.

The first one (case01) is referent or design scenario. The filtered air intake (600 $m^3$/h) is present all the time. The HVAC is in recirculation mode (internal recirculation flow rate is 19800 $m^3$/h) during whole 720 days. The filter (in RADTRAD case filter F1 is recirculation and F4 intake) has efficiency 99.97% for aerosols and 95% for elemental and organic iodine. The outflow is always sum of inflow and HVAC intake flow. The second case (case02) is the same as case01 except for uncontrolled inflow which is assumed to be zero (reasonable due overpressure produced by filtered intake). In case03 HVAC isolation is assumed from 0 till 1.7 hours. The recirculation flow is 20400 $m^3$/h. From 1.7 till 2.7 hours HVAC is purge mode (filtered intake at 10200 $m^3$/h) and inflow is present. From 2.7 h till 720 hours filtered intake is 600 $m^3$/h, recirculation flow is 19800 $m^3$/h and there is no uncontrolled inflow (established room overpressure). That is called improved scenario and it is optimized to decrease the dose to the ECR operators. Due to different assumptions on radioactivity release and other timing differences, the time to end isolation (intake activity less than room activity) is not the same in this calculation as in operator dose calculation. In case04, isolation time is between 0 and 2.7 h, and purge interval is from 2.7 to 3.7 hours. All other assumptions are the same as for case03. The case04 is called optimized HVAC scenario. The doses calculated in this calculation are beta and gamma air immersion doses to the equipment. The doses to ECR personnel are calculated, but are not shown here. Beta and gamma air immersion doses are shown in Figure 7 for referent case01. Gamma dose suppression is based on whole protected volume and not on separately on ECR, or TSC or any other separate room volume from protected pressure boundary, and that is conservative. The doses calculated for HVAC scenario case01 are highest and the doses calculated for case04 are lowest. Gamma doses depend on number of air exchanges (free volume and HVAC intake flow rate) and volume used in calculation of reduction factor compared to infinite hemisphere immersion. For beta doses most important factor is concentration of radioactive material in air of the room. All rooms are well ventilated and doses are similar. The size of the volume is not important due to limited range of beta rays. For all rooms without filtered HVAC, immersion is dominant source of equipment exposition to radiation. The shine dose from external sources through the building walls is negligible. For rooms within pressure envelope, mainly ECR and TSC, it is required to check for the influence of shine doses from environment, from neighbouring rooms without air filtration, and from concentrated source in HVAC filter.

The dose from the radioactive material kept within HVAC filter is analysed first. As part of already described RADTRAD compartment calculation some radioactive material, depending on selected HVAC scenario, is deposited within HVAC filter. Original RADTRAD code was modified to enable access to deposited activity and to make possible decay calculation of that deposit. The activity of the recirculation filter (F1) and intake filter (F4), for all four cases, is shown in Figure 8. As said earlier, one actual HVAC filter is in RADTRAD treated as two separate filters. That way it is possible to see amount of the material removed from intake flow and during recirculation. Noble gases are not affected by filter operation. As expected, most of the deposit is due to intake flow and recirculation deposit is mainly due to uncontrolled inflow. As can be seen the accumulation of radioactive material depends on HVAC scenario. It is smallest for case02 and largest for case03. The design scenario and final optimized scenario have similar accumulated activities. ECR atmosphere activity, for all four cases, are shown in Figure 9. It is clear that decision to operate HVAC in purge mode should be planned depending on timing of the accident. 30-days immersion air dose is, depending on HVAC case, between 25 and 37 mGy for gamma, and between 1.6 and 2.2 Gy for beta. Calculated immersion beta and gamma doses can be conservatively used for any room within pressure protective envelope, including Machine Room (MR, New HVAC room).

Position of HVAC filter within MR is shown in Figure 10. It is directly above TSC room. Microshield 10 code was used in calculation of gamma shine dose from radioactive material accumulated within filter [8]. The inventory of radioactive material (isotopic activities) is saved from RADTRAD run at selected times. Filter geometry for calculation of shine doses through ECR/TSC ceiling is shown in Figure 11. Green box (assumed dimensions are 3x3x8m) contains radioactive source homogenously distributed within air. Blue box is side shielding (0.5 cm filter wall and 1 m concrete floor/ceiling toward TSC). The dose rates are calculated, for prescribed time

points (15), at the middle bottom side of the filter, at the distance 1 cm, 70 cm, 210 cm, and 350 cm from bottom of TSC ceiling. The gamma dose rates are integrated using central integration (dose rate is constant within time interval at the arithmetic average of the dose rates at interval ends) for 720 hours (30 days). Gamma dose from HVAC filter to ECR through ECR/MR ceiling is below 1 mGy, Figure 12. Gamma doses are for referent HVAC scenario (case01) and for optimized scenario (case04). Due to slightly higher radioactive inventory, doses are always higher for improved HVAC scenario.

The filter doses are calculated in the middle of longer side, Figure 13, at the distances 1, 10, 50, 100 and up to 800 cm from filter surface, Figure 14. 30-days filter surface dose is 240 Gy and dose at the distance of 100 cm is around 120 Gy. The integrated dose is below 100 Gy at distance of 500 cm. The doses are given for referent and improved HVAC scenario. The calculated doses can be problem for electronic equipment used for control of HVAC components.

In order to get spatial dependence of dose rates, Figure 15, at peak filter activity (120 h), additional calculation is performed with SCALE 6.2 MAVRIC shielding sequence (Monaco Monte Carlo functional module and CADIS methodology) [9]. The dose rates perpendicular to the longer filter side are shown in Figure 16. The dose rates are similar but higher than corresponding Microshield doses. The improved calculation methodology can be used to determine local dose rates or to calculate local shielding of sensitive parts.

## 3 CONCLUSION

The methodology starting with reactor core source term calculation and calculation of release of radioactive materials to the environment and ending with calculation of transport of radioactive materials within emergency control room and related HVAC filter was presented. For radioactive materials deposited within HVAC filter shine gamma dose was calculated for period of 30 days after accident using point kernel code Microshield. The shine doses to operators and equipment within ECR is rather small, but the doses to the equipment located within machine room can be limiting for electronic control equipment and some kind of shielding can be needed for absorbed doses above 100 Gy. In that case more detailed Monte Carlo calculation can be used. The reasonable agreement between point kernel and hybrid Monte Carlo results was obtained for simple filter geometry without shielding.

**Acknowledgements:**

We would like to express our gratitude to the NPP Krško for providing relevant input data used in calculation and for supporting whole activity.

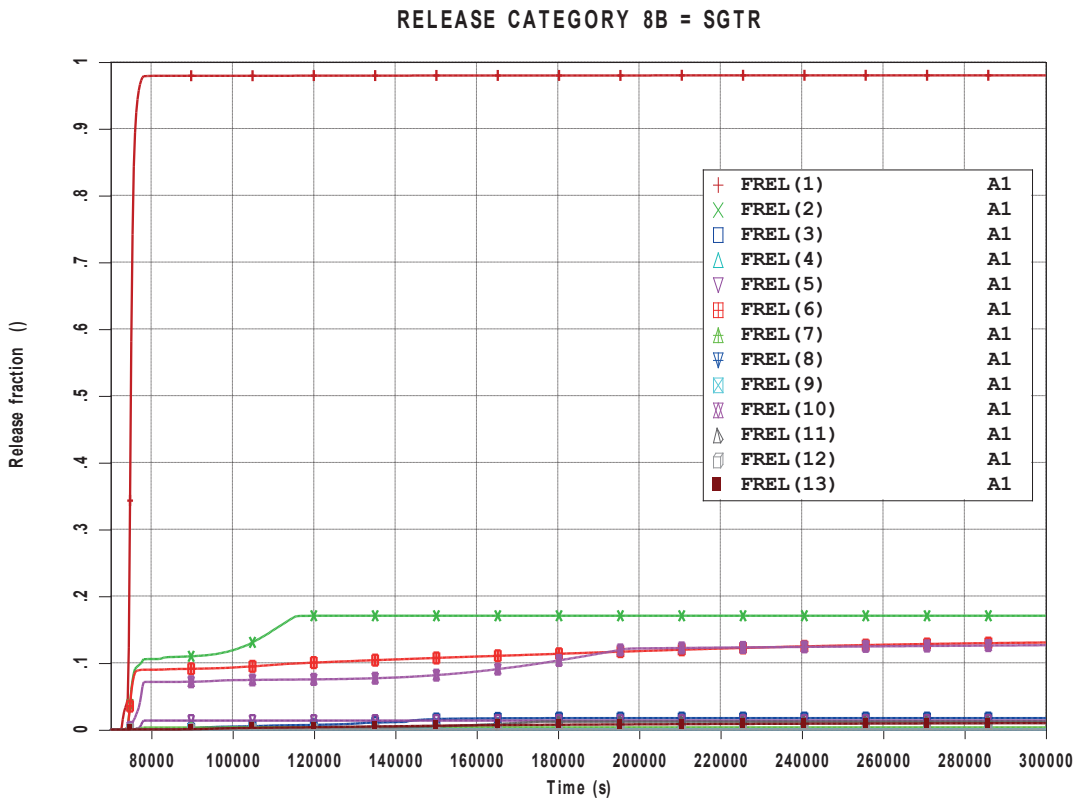


Figure 1: MAAP release categories

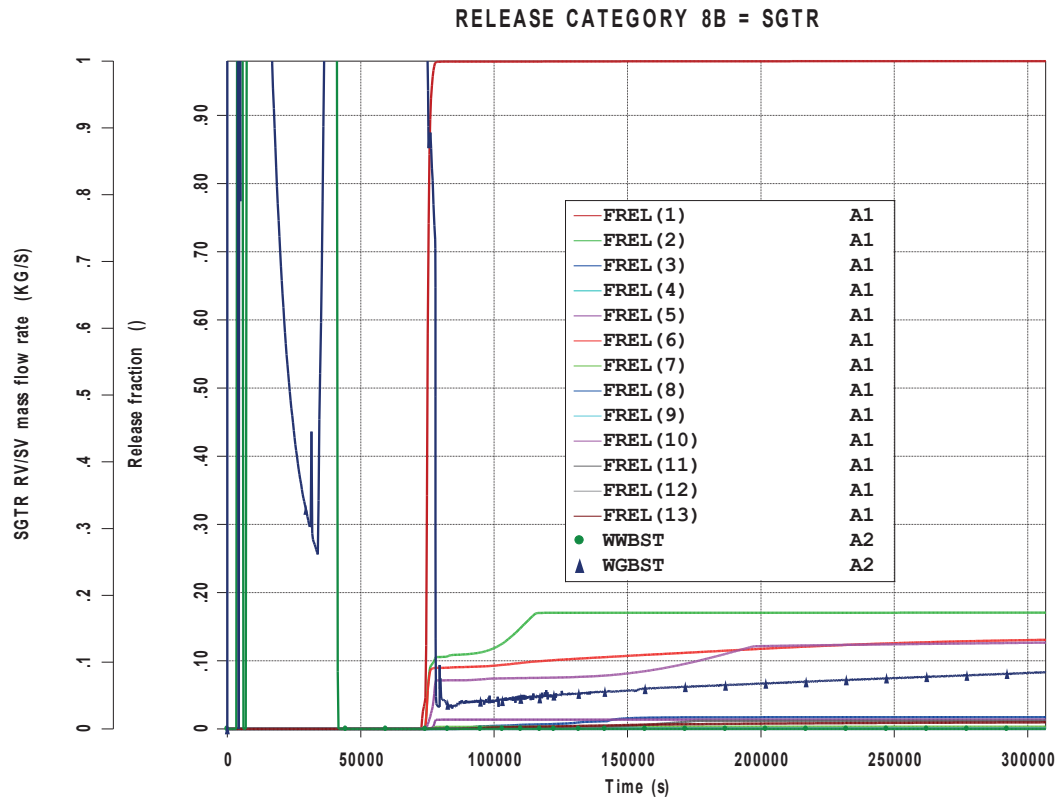


Figure 2: SG SV/RV mass flow rate and release categories

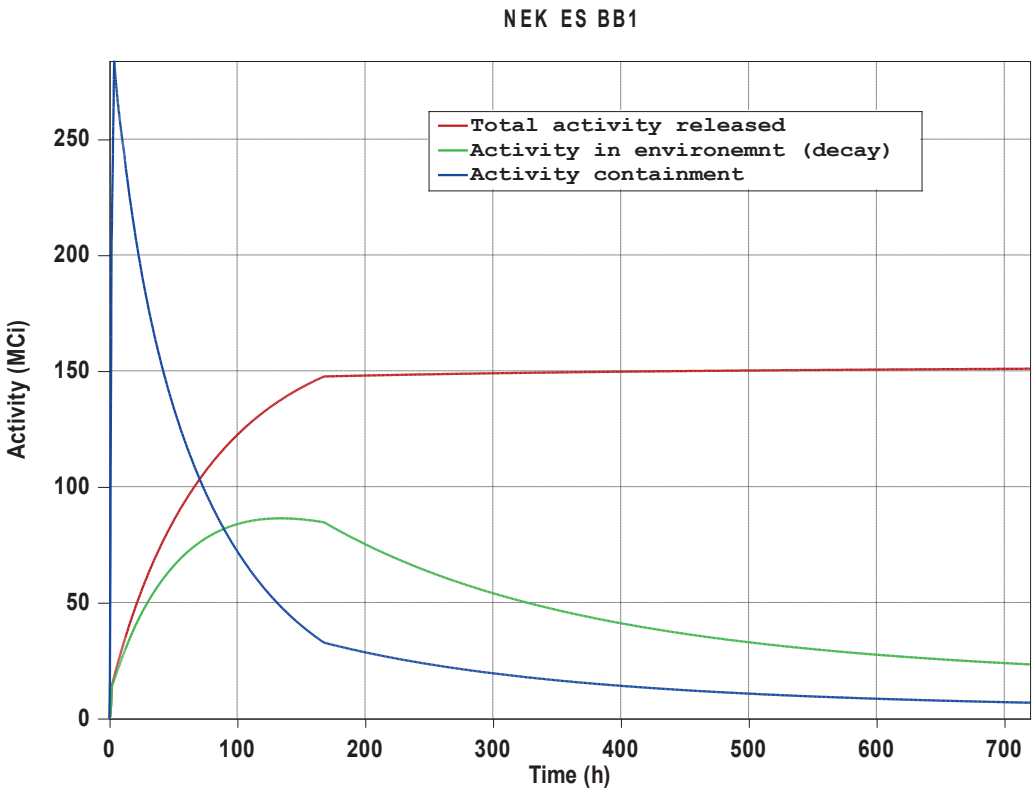


Figure 3: Activity released and activities left in the containment and present in environment

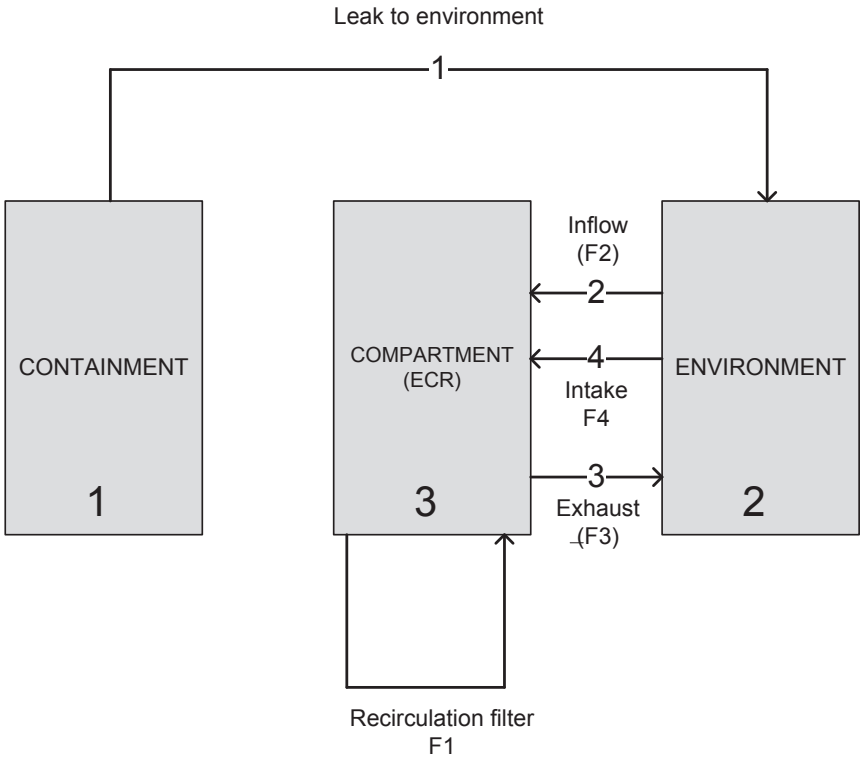


Figure 4: RADTRAD compartment used in calculation of BB1 rooms


Davor Grgić, Štefica Vlahović, Mario Matijević, Paulina Dučkić, Srđan Špalj, Dose Calculation for Emergency Control Room HVAC Filter, Journal of Energy, vol. 68 Number 2–3, Special Issue (2019), p. 98–111

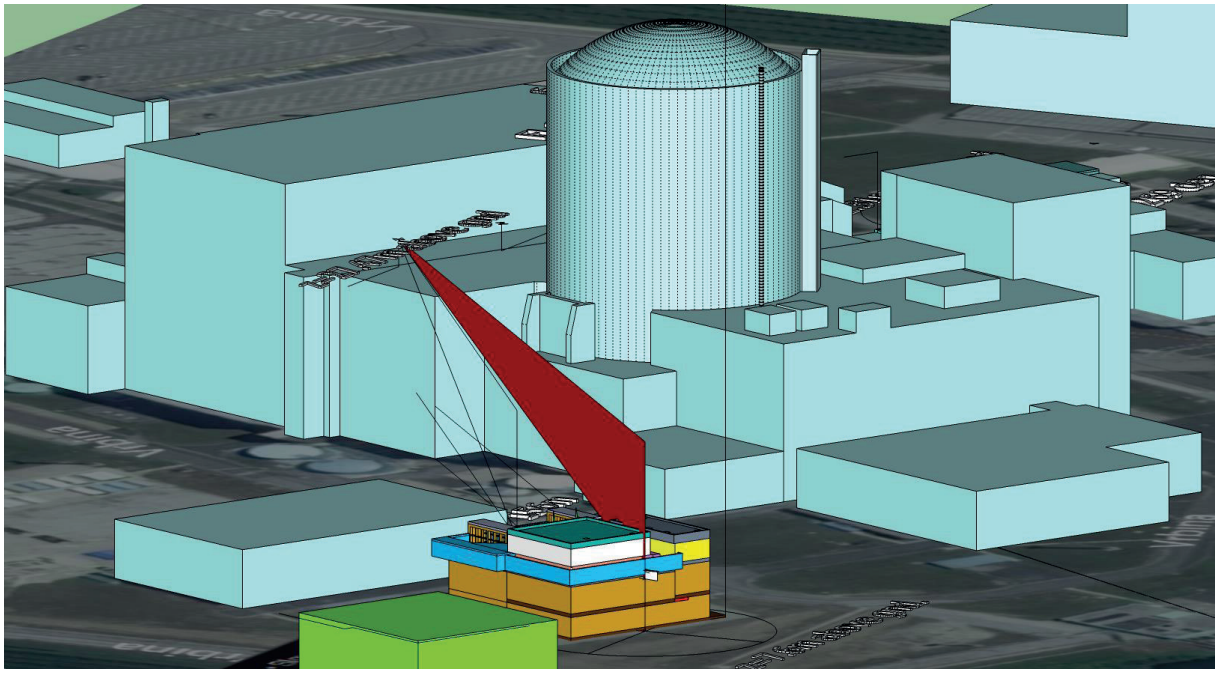

Figure 5: Geometry for ECR/TSC HVAC intake

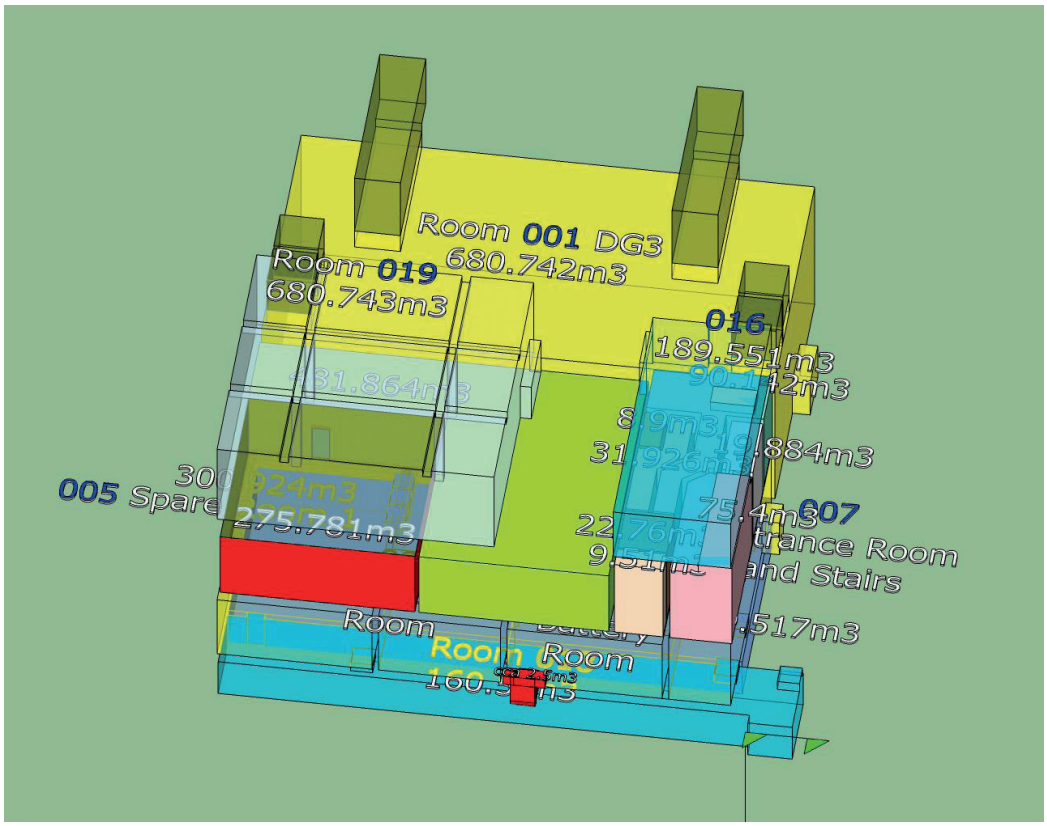


Figure 6: BB1 empty room volumes


Davor Grgić, Štefica Vlahović, Mario Matijević, Paulina Dučkić, Srđan Špalj, Dose Calculation for Emergency Control Room HVAC Filter, Journal of Energy, vol. 68 Number 2–3, Special Issue (2019), p. 98–111

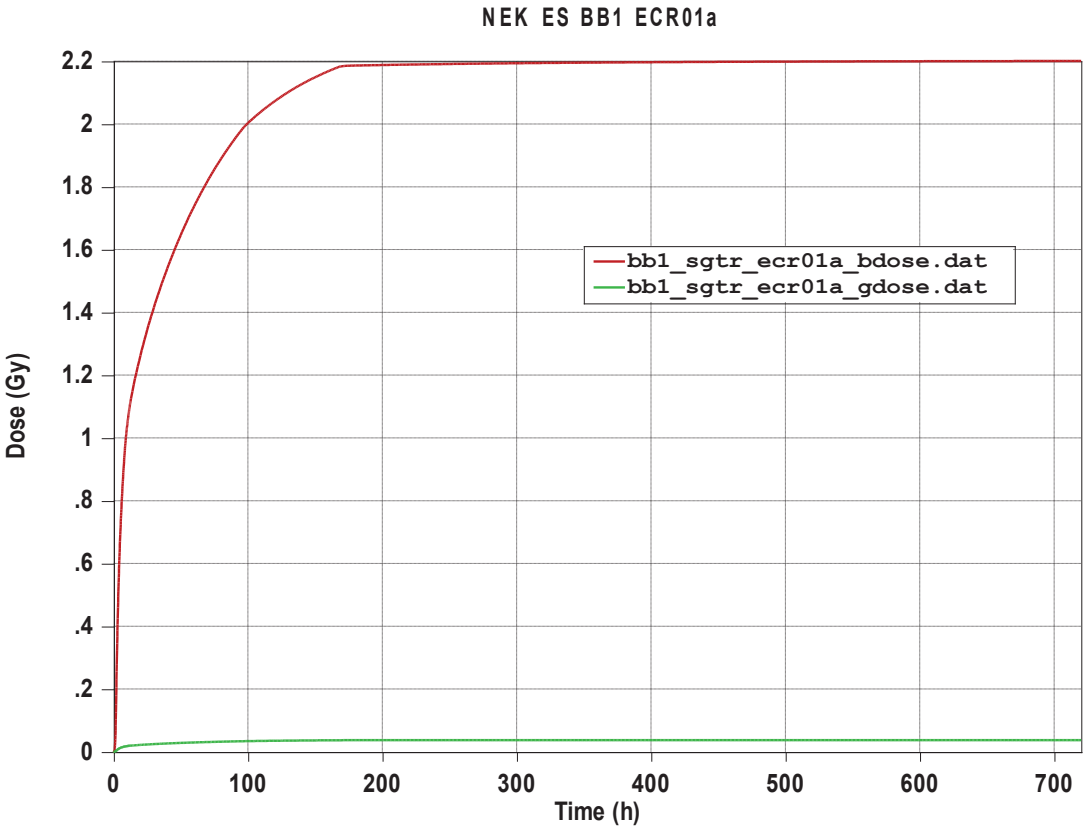


Figure 7: ECR beta and gamma immersion dose

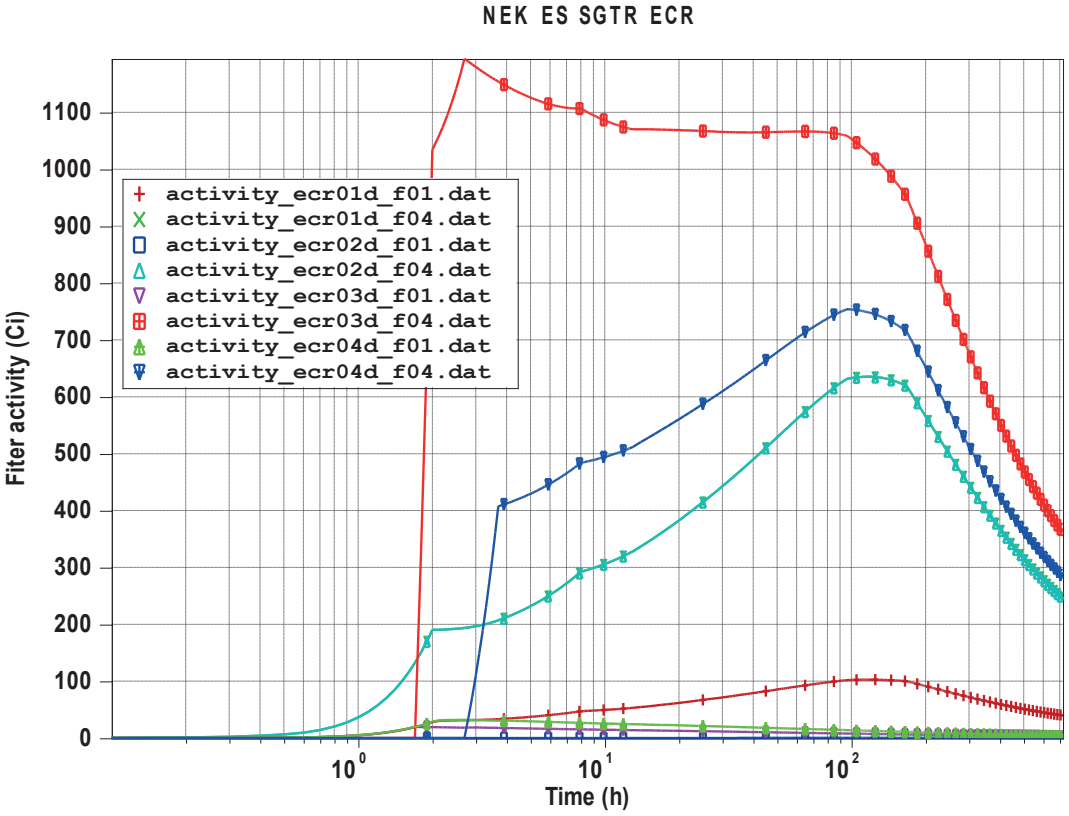


Figure 8: Recirculation and intake filter activity, case01-04

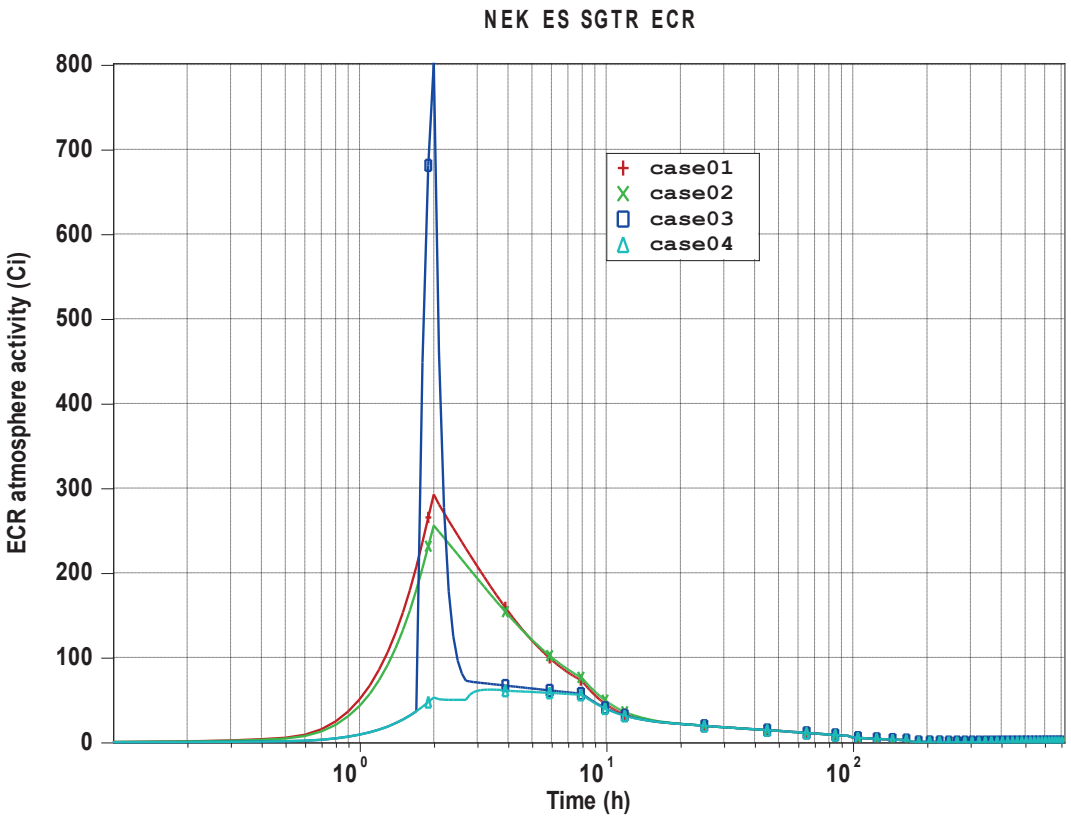


Figure 9: ECR/TSC air activity, case01-04

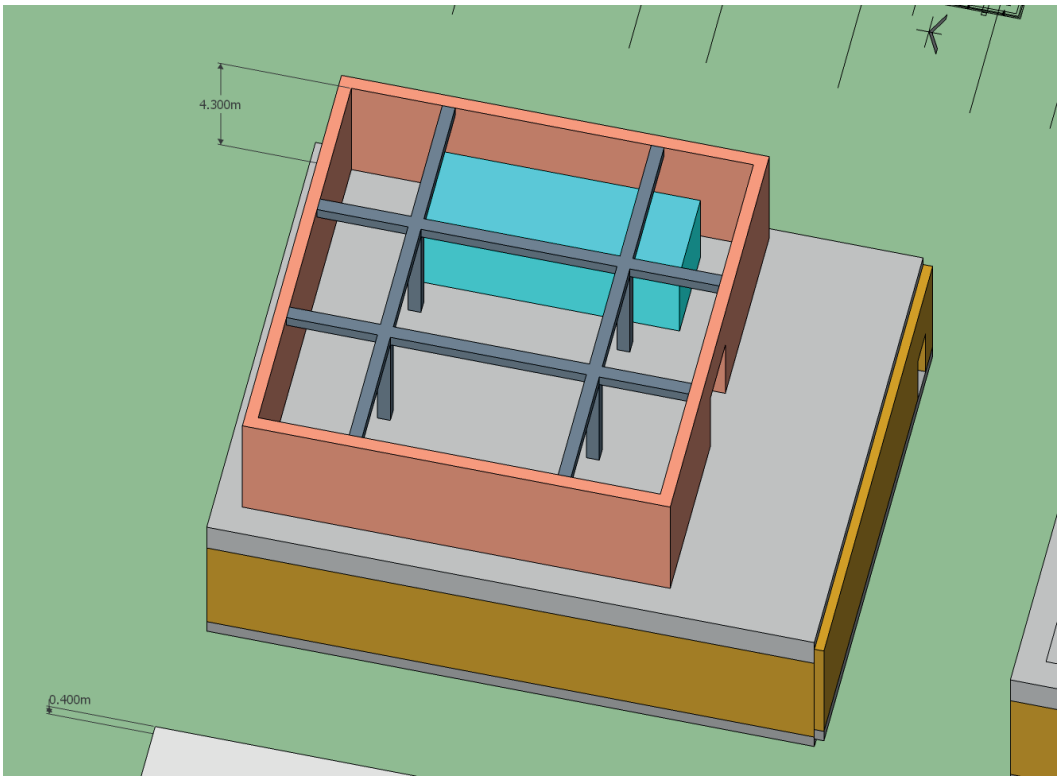


Figure 10: Position of ECR/TSC HVAC filter


Davor Grgić, Štefica Vlahović, Mario Matijević, Paulina Dučkić, Srđan Špalj, Dose Calculation for Emergency Control Room HVAC Filter, Journal of Energy, vol. 68 Number 2–3, Special Issue (2019), p. 98–111

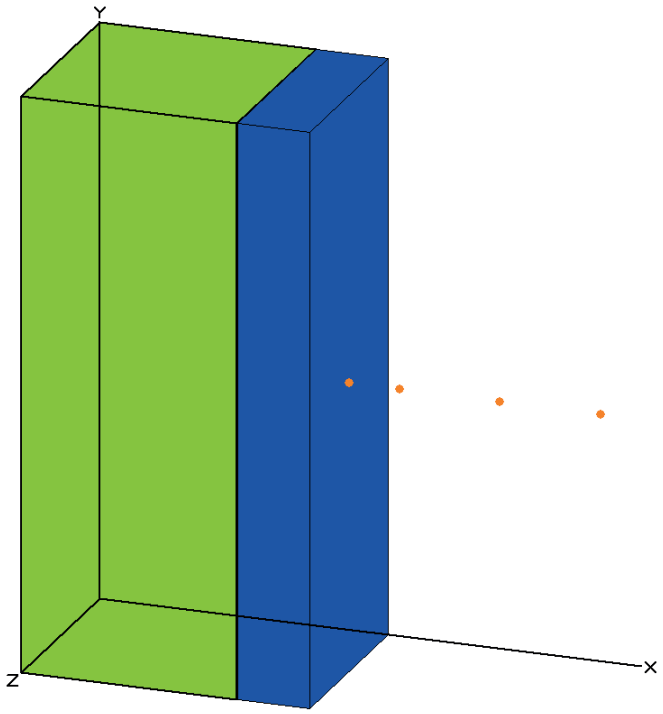


Figure 11: ECR filter geometry layout for dose calculated in upper part of ECR/TSC

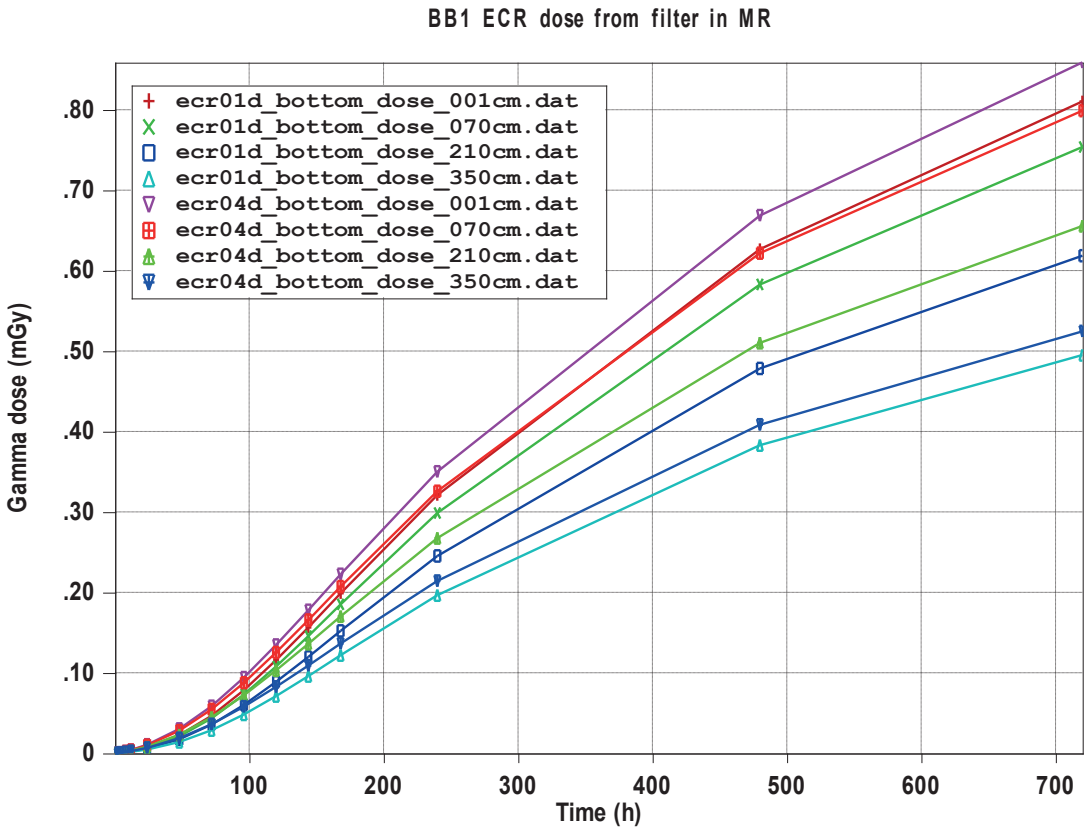


Figure 12: Gamma dose in ECR/TSC upper part from filter in MR

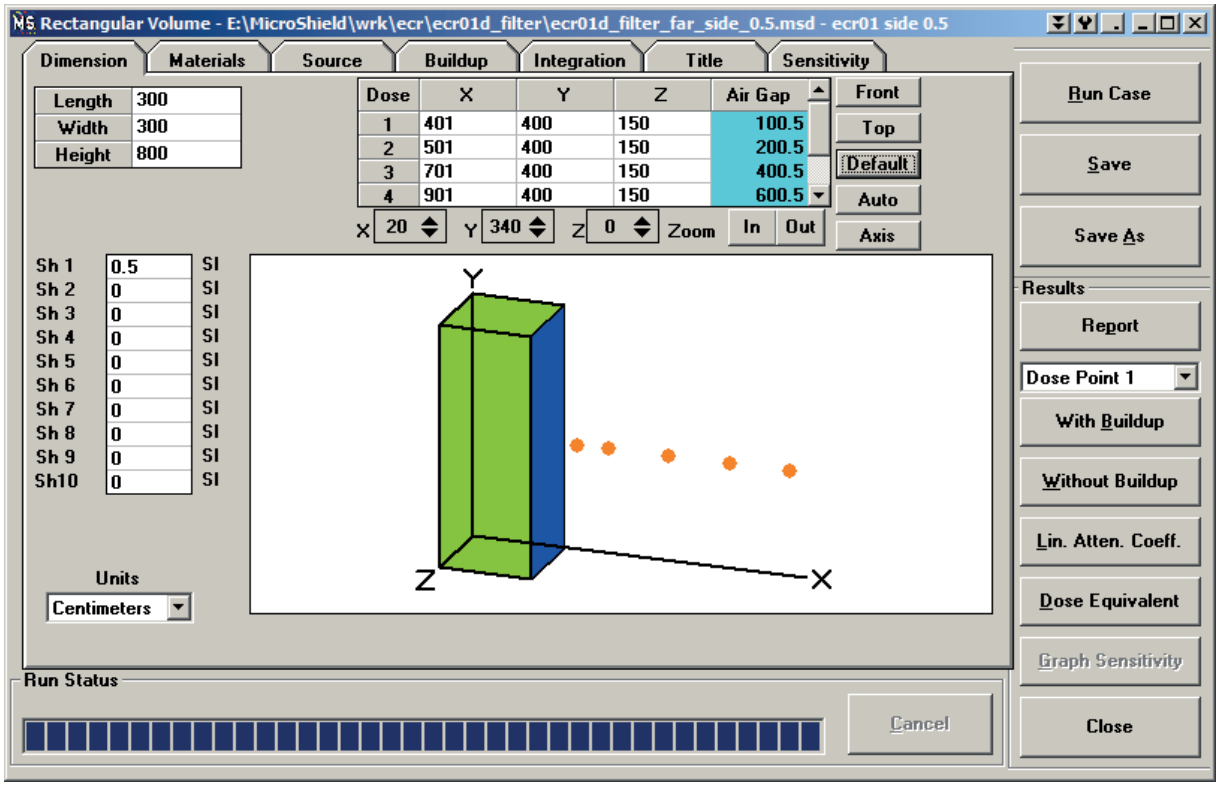


Figure 13: Problem layout for Microshiled dose calculation from filter longer side

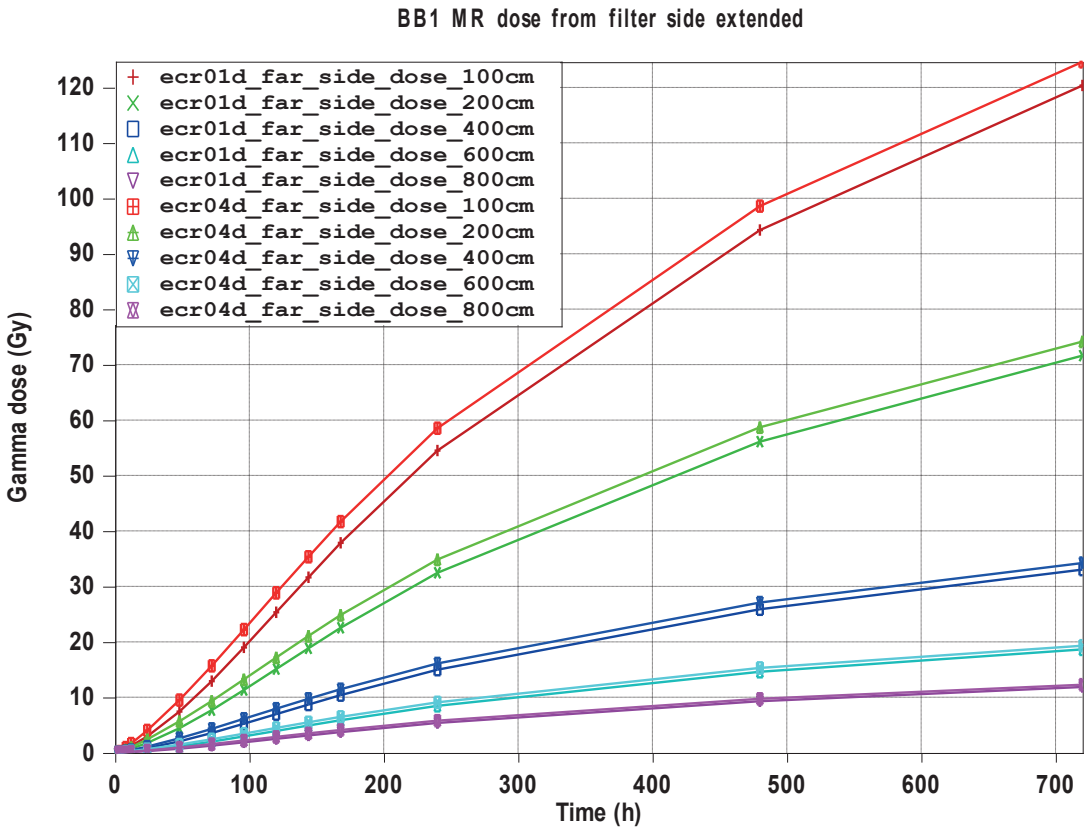


Figure 14: Gamma doses in BB1 MR – filter side


Davor Grgić, Štefica Vlahović, Mario Matijević, Paulina Dučkić, Srđan Špalj, Dose Calculation for Emergency Control Room HVAC Filter, Journal of Energy, vol. 68 Number 2–3, Special Issue (2019), p. 98–111

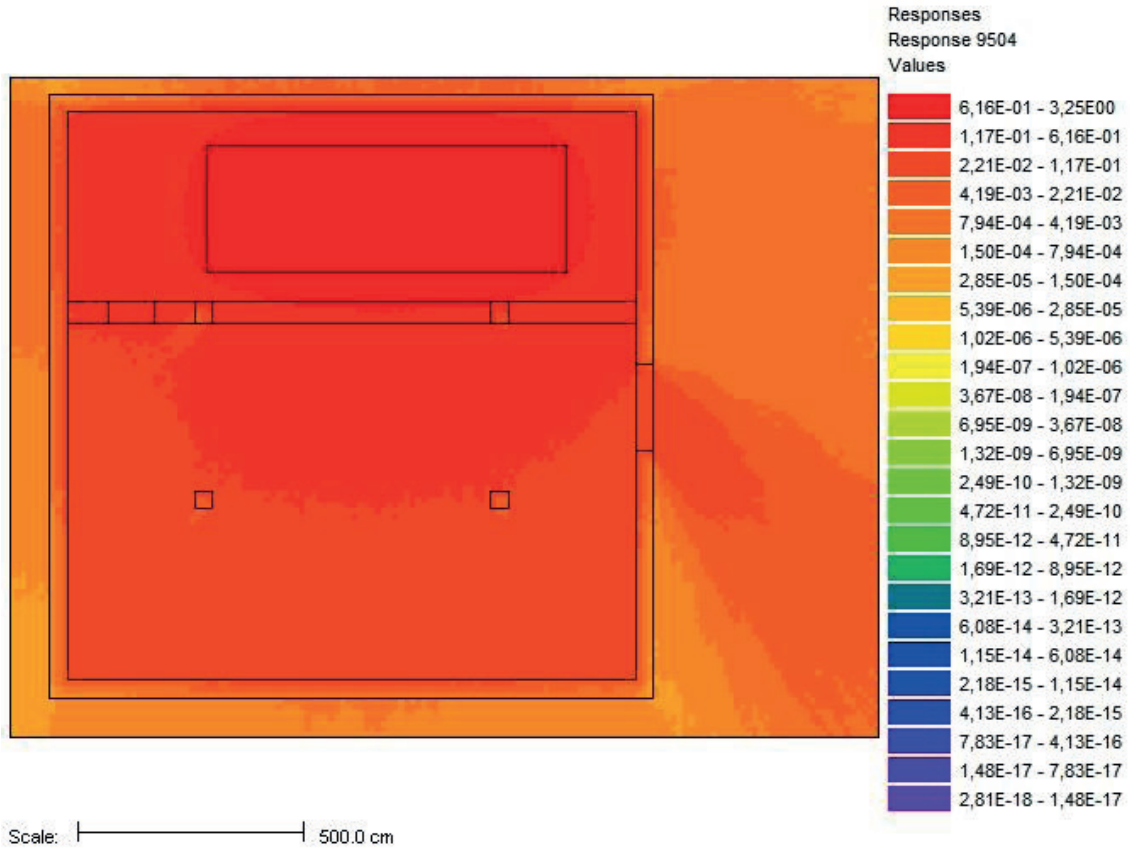


Figure 15: Monte Carlo calculation of dose rate at 120 h

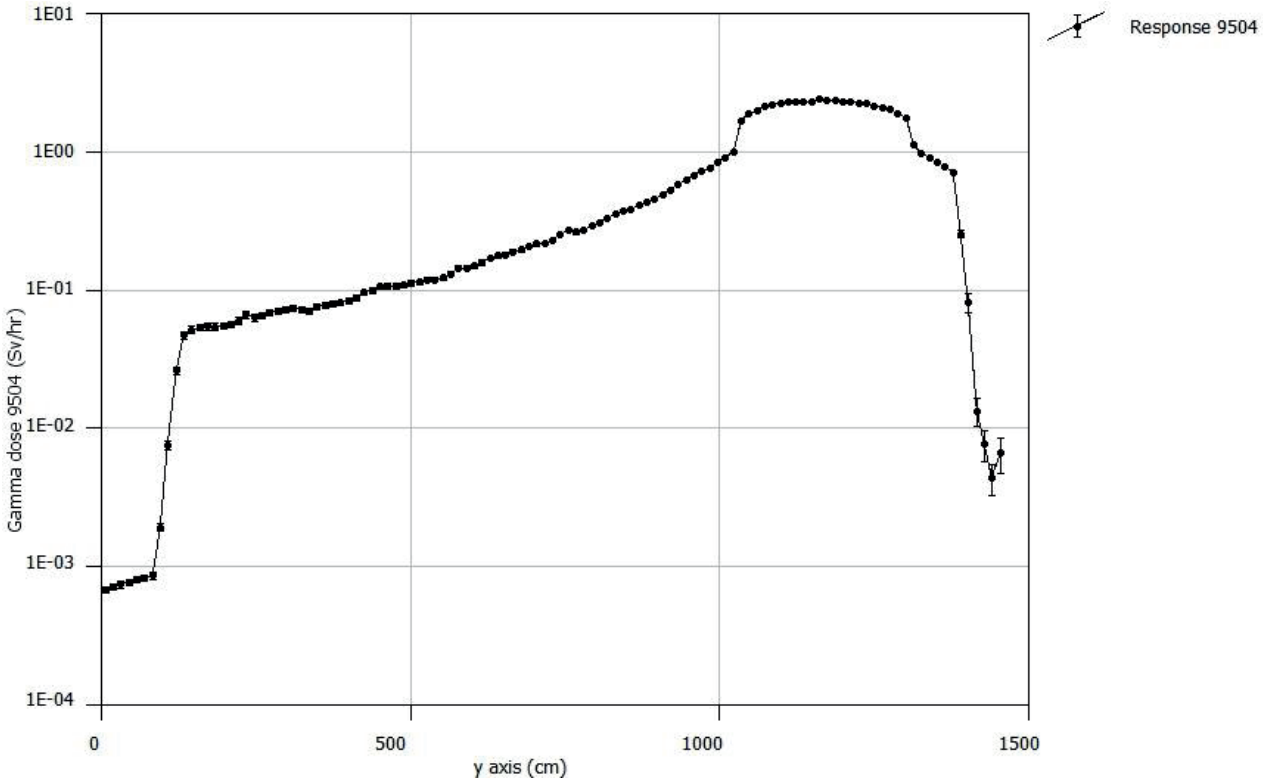


Figure 16: Monte Carlo calculation of dose rate at 120 h – perpendicular to filter side

## REFERENCES


[1] NEK Safety Upgrade Project Design Input and Interfaces, Rev.6

[2] STR-NEK-12-04, “NEK SUP equipment under DEC survivability concept”, Rev.1 (contains Third Party Proprietary documents)

[3] MAAP4 User Manual, Electric Power Research Institute

[4] NUREG/CR-6604, “RADTRAD: A Simplified Model for RADionuclide Transport and Removal and Dose Estimation,” U.S. NRC, December 1997.

[5] ORIGEN 2.1 Isotope Generation and Depletion Code, ORNL, CCC-371

[6] NUREG-1465 “Accident Source Term for Light Water Reactors”, 1995

[7] Atmospheric Relative Concentrations in Building Wakes, NUREG/CR-6331, 1997

[8] MicroShield User's Manual, Version 10, Grove Software, 2014.

[9] "SCALE: A comprehensive Modeling and Simulation Suite for Nuclear Safety and Design", ORNL/TM-2005/39, Version 6.1, June 2011. Available from Radiation Safety Information Computational Center at Oak Ridge National Laboratory as CCC-785.

Journal of Energy
VOLUME 68 Number 2-3 | 2019 | Special Issue
journal homepage: http://journalofenergy.com/

# Review of Design Extension Conditions Experiments and Analyses for Non-degraded Core

**Andrej Prošek, Mitja Uršič**
Jožef Stefan Institute
Jamova cesta 39, SI-1000 Ljubljana, Slovenia
andrej.prosek@ijs.si, mitja.ursic@ijs.si

## ABSTRACT

The second generation nuclear power plants were designed and built to withstand without loss to the systems, structures, and components necessary to ensure public health and safety during design basis accidents (DBAs). In the transient and accident analysis the effects of single active failures and operator errors were considered. There are also accident sequences that are possible but were judged to be too unlikely and therefore were not fully considered in the design process of second generation reactors. In that sense, they were considered beyond the scope of design-basis accidents that a nuclear facility must be designed and built to withstand. Such accident sequences have been analysed in the past to fully understand the capability of a design.

The requirements to analyse such sequences for existing reactors have been introduced after Fukushima Dai-ichi accident. In 2012 the design extension conditions (DECs) were introduced in the International Atomic Energy Agency (IAEA) requirements for the design of nuclear power plants (NPPs). Western European Nuclear Regulators Association (WENRA) requirements of existing reactors for DEC were introduced in 2014. The purpose of considering DEC is to further improve safety by enhancing the plant's capability to withstand the conditions generated by accidents that are more severe than DBAs. This concept by IAEA and WENRA (WENRA definition of DEC is consistent with IAEA definition from 2012, in which DEC with prevention of core melt is called DEC A) is not completely new, since some multiple failures have already been considered in the design of existing reactors, for example anticipated transients without scram and station blackout. The research for beyond design basis accidents with non-degraded core (i.e. DEC A) for existing reactors has been already done in 80's and 90' of the previous century. The purpose of this paper is to review that research. The tests performed include total loss of feedwater, station blackout, small break without high pressure safety injection, steam generator tube rupture with no high pressure safety injection etc. Besides review of experiments performed on integral test facilities, examples of DEC A tests, which have been analysed at Jožef Stefan Institute using RELAP5 or TRACE computer code in the last three decades, will be presented too.

***Keywords:*** *design extension conditions, RELAP5, TRACE, safety analysis*

## 1 INTRODUCTION

The existing reactors were designed and built to withstand without loss to the systems, structures, and components necessary to ensure public health and safety during design basis accidents (DBAs). In the transient and accident analysis the effects of single active failures and operator errors were considered. There are also accident sequences that are possible but were judged to be too unlikely and therefore were not fully considered in the design process of second generation reactors. In that sense, they were considered beyond the scope of design-basis accidents that a nuclear facility must be designed and built to withstand. Such accident sequences have been

analysed in the past to fully understand the capability of a design. They were called beyond design basis accidents (BDBA). However, after Fukushima Dai-ichi accident the International Atomic Energy Agency (IAEA) adopted term design extension conditions (DEC) [1].

The term "design extension conditions" has rather long history and was introduced during the design of the reactors of third generation. The DEC was introduced to define some selected accident sequences due to multiple failures. The design extension conditions were introduced as preferred method for giving due consideration to the complex sequences and severe accidents at the design stage without including them in the design basis conditions [3]. On the other hand, the Western European Nuclear Regulators Association (WENRA) recommended a "design extension" analysis in 2007 [4] and they proposed a list of events to be analysed at minimum. By its meaning this list corresponds to DEC without core melt. WENRA reference levels (RLs) from 2014 [5] introduced DEC term. The WENRA guidance document for issue F [6] explains that DEC in WENRA RLs are consistent with the definition of DEC in IAEA SSR-2/1 [1], published in 2012. DEC are more complex and/or more severe than conditions postulated as design basis accidents [6].

The paper [7] recommends that the IAEA requirements and guidelines keep up the definition of severe accidents so that this type of accident be clearly identified, linked to the partial or complete melting of reactor core. The IAEA DEC term has been redefined in 2016 as follows: "Postulated accident conditions that are not considered for design basis accidents, but that are considered in the design process for the facility in accordance with best estimate methodology, and for which releases of radioactive material are kept within acceptable limits." WENRA did not follow the new IAEA DEC, which modification is significant.

The DEC concept by IAEA and WENRA (DEC with prevention of core melt is called DEC A) is not completely new, since some multiple failures have already been considered in the design, for example anticipated transients without scram (ATWS) and station blackout (SBO). Also, the research for beyond design basis accidents with non-degraded core (i.e. DEC A) for existing reactors has been already done in 80's and 90' of the previous century.

In this paper review of that research is done. Besides review of experiments performed on integral test facilities, examples of DEC A tests, which have been analysed at Jožef Stefan Institute using RELAP5 or TRACE computer code in the last three decades, will be presented too.

## 2 INITIATING EVENTS FOR DEC A

WENRA guidance document [6] for issue F provides the following list of DEC A (with a note that final sets of conditions selected for DEC A analysis will be plant and site specific, developed on the basis of the following non-exhaustive list, which applies mainly to pressurized water reactors (PWR) and boiling water reactors):

- Initiating events induced by earthquake, flood or other natural hazards exceeding the design basis events (see Issue T [5]);
- Initiating events induced by relevant human-made external hazards exceeding the design basis events;
- Prolonged station black out (SBO; for up to several days);
    - SBO (loss of off-site power and of stationary primary emergency alternate current (AC) power sources)
    - total SBO (SBO plus loss of all other stationary AC power sources), unless there are sufficiently diversified power sources which are adequately protected
- Loss of primary ultimate heat sink, including prolonged loss (for up to several days);
- Anticipated transient without scram (ATWS);
- Uncontrolled boron dilution;
- Total loss of feed water;

- Loss of coolant accident (LOCA) together with the complete loss of one emergency core cooling function (e.g. high pressure injection (HPI) or low pressure injection (LPI));
- Total loss of the component cooling water system;
- Loss of core cooling in the residual heat removal mode;
- Long-term loss of active spent fuel pool cooling;
- Multiple steam generator tube ruptures (PWR, pressurized heavy water reactors);
- Loss of required safety systems in the long term after a design basis accident.

The IAEA document [8] states that the list of DEC may include:

- ATWS;
- SBO;
- Loss of core cooling in the residual heat removal mode;
- Extended loss of cooling of fuel pool and inventory;
- Loss of normal access to the ultimate heat sink.

The IAEA document [8] further provides an example list of additional DECs derived from probabilistic safety assessment (PSA):

- Total loss of feed water;
- LOCA plus loss of one emergency core cooling system (either the high pressure or the low pressure emergency cooling system);
- Loss of the component cooling water system or the essential service water system (ESWS);
- Uncontrolled boron dilution;
- Multiple steam generator tube ruptures (MSGTR) (for PWRs);
- Steam generator (SG) tube ruptures induced by main steam line break (MSLB) (for PWRs);
- Uncontrolled level drop during mid-loop operation (for PWRs) or during refuelling.

When comparing the WENRA and IAEA list, first major difference is that WENRA list includes initiating events induced by earthquake, flood or other natural hazards exceeding the design basis events. However, IAEA document [8] stressed that "some Member States tend to include in the list of DECs also some external hazards that were not considered in the past (e.g. earthquake exceeding the design basis earthquake, commercial air craft impact, etc.). In the IAEA terminology, a DEC is a postulated plant state (see Table 1) that is determined by a postulated sequence of events, and for the same reasons that design basis hazards are not considered DBAs, more severe hazards are not considered DECs although they might result in a DBA or possibly in DEC." Second difference is that IAEA provides deterministically and probabilistically identified list.

## 3 REVIEW OF RESEARCH ON BDBA WITHOUT CORE DEGRADATION FOR EXISTING REACTORS

In this section selected BDBA experiments without core degradation are briefly described in Tables 1 and 2.

Table 1 shows tests for accident management in PWRs, in which operator actions were studied for BDBA with non-degraded core (DEC A). Experiments were mainly selected from cross-reference matrix for accident management for non-degraded core, which has been created in the frame of OECD/NEA [9].

Table 1: Accident management in PWRs for BDBA with non-degraded core (DEC A)

| Test No. | Test type | Brief description |
|---|---|---|
| PKL Ill B1.2 | Total loss of feedwater with secondary side feed and bleed | Total loss of feedwater (loss of main and auxiliary feedwater) with no core cooling systems (high and low pressure injection pumps and accumulators) was studied. Secondary side bleed and feed was performed. Injection of water was due to flashing in feedwater line and subsequent injection by a mobile pump [9]. |
| BETHSY 5.2c2 | Total loss of feedwater | During BETHSY (Boucle d'Etudes Thermohydrauliques de Systemes) test 5.2c2 [10], the emergency operating procedure (EOP) was conducted in accordance with the rules presently implemented in plant control rooms, which allow operators more time for the recovery of feedwater systems: it consisted in manually starting the high pressure injection system (HPIS) as soon as 2 SG liquid levels reached 3 m; as a consequence, primary pressure slowly increases up to 16.3 MPa, and is then maintained at this value through pressurizer power operated relief valves (PORVs) automatic operation. 30 minutes after EOP initiation, or earlier if the core outlet fluid temperature reaches 603 K, the pressurizer PORVs are actuated at full discharge capacity. |
| BETHSY 6.2TC | 6” cold leg break without HPIS and LPIS | BETHSY 6.2TC test was a 15.24 cm (6 inch) cold leg break in the loop one without available high pressure and low pressure safety injection system. Accumulators were available in the intact loops. The main aims of this test were to compare the counterpart test data from BETHSY and Large Scale Test Facility (LSTF) facilities and qualification of CATHARE 2 computer code. |
| BETHSY 9.1b | 2" cold leg break without HPIS and with delayed ultimate procedure | BDBA involves two failures: a break on the cold leg together with a complete failure of the HPIS, combined with a human error regarding the conditions in which the operators start the Ultimate Operating Procedure (UOP). The UOP then consists in depressurizing the primary circuit by means of a full opening of the 3 SG atmospheric steam dumps. |
| BETHSY 9.3 | SGTR with HPIS and AFW unavailable | The simultaneous failure of the high pressure safety injection and auxiliary feedwater systems is a Beyond Design Basis Accident, which leads to core heat up, if no additional measures are taken. During the test 9.3 the efficiency of both the steam generator atmospheric steam dump and the depressurization of the primary circuit via the pressurizer relief valve is investigated [11]. |
| LSTF | PWR Cold-Leg small-break LOCA with total HPI failure | Cold-leg break tests were conducted at the LSTF for five break areas 0.5%, 1%, 2.5%, 5 and 10% of the scaled cold-leg flow area, with totally failed HPI [12]. |
| LSTF | 0.5% cold leg small-break LOCA total failure of the HPI and auxiliary feedwater (AFW) systems | The depressurization procedure was simulated in a 0.5% cold-leg break LOCA experiment [13]. |
| LSTF SB-SG-11 | SGTR concurrent with secondary break | In this experiment, the pressure difference between the primary side of the steam generator (SG) and the secondary side of SG is kept so high that the two-phase critical flow is observed for a long time. The secondary break was simulated for the feedwater line because this was the only line which can be connected to the break catch tank (ST). The secondary initial level for the affected SG was lowered to 4.3m to scale the inventory. The recovery action was simulated by depressurizing, starting 600 s after scram. Also, the pressurizer auxiliary spray was activated subsequently [9]. |

New design includes design features aimed at preventing the onset of a severe accident, including severe accident precursors identified in SECY-90-016 [18] and SECY-93-087 [19]: ATWS, mid-loop operation, station blackout (SBO) event, fire, and an intersystem loss of coolant accident (ISLOCA). Similarly WENRA [20] provides examples of multiple failure scenarios (DEC A) to be prevented in new designs: LOCA, station blackout, total loss of feedwater and ATWS.

Table 2 shows typical multiple failure scenarios (ATWS, mid-loop operation, SBO and LOFW followed by small break LOCA).

Table 2: BDBAs with non-degraded core (DEC A), which typically need to be prevented

| Test No. | Test type | Brief description |
|---|---|---|
| LSTF TR·LF-06 | Pump seal leak following station blackout | The test simulated a pump seal leak following a station blackout (or TMLB', where T = transient event, M = failure of the secondary system steam relief valves and power conversion system, L = failure of secondary system steam relief valves and auxiliary feedwater system, and B' = failure to recover onsite and offsite AC power) transient. The test was initiated with an "accelerated transient" which was designed to obtain primary and secondary states including: steam generator (SG) secondary sides dried out; primary side reached saturation at the pressurizer power operated relief valve (PORV) opening setpoint pressure. After these states were reached, at a scaled core power of 1.2%, a cold leg break, with an area of 0.1% of the scaled cold leg cross-sectional area, was opened to simulate a pump seal leak [9]. |
| LOBI A2-90 | SBO-ATWS | LONOP-ATWS or "SBO" anticipated transient caused by loss of offsite and normal onsite electrical power (LONOP) with failure to scram [17]. |
| BETHSY 6.9c* | Loss of RHR at mid-loop operation with pressuriser and SG manways open | The test includes a loss of residual heat removal (RHR) system during mid-loop operation at 0.5% of nominal value core power. Initial liquid level in reactor coolant system (RCS) was at horizontal axis of the hot legs. Pressurizer and steam generator manways were opened 1 s after the transient was initiated [9]. |
| LOFT L9-1 / L3-3 | Total loss of feedwater (LOFW) accident followed by small break LOCA | Experiment L9-1 was the first anticipated transient with multiple failures performed at Loss-of-Fluid-Test (LOFT), and consisted of a simulated LOFW accident with delayed reactor scram and no auxiliary feedwater injection.<br>Experiment L3-3 simulated two independent recovery procedures from the LOFW accident L9-1, without engaging the emergency core coolant (ECC). |
| LOFT L9-3 | Loss of feedwater without reactor trip | Experiment L9-3 conducted in the LOFT facility was a unique one simulating an ATWS event in pressurized water reactor. The experiment simulated a loss of feedwater induced ATWS in a commercial plant. The experiment consisted of two parts: the ATWS itself, which lasted about 600 s, and the plant recovery [15]. |
| LOFT L9-4 | Loss-of-offsite-power accident without reactor trip | This was an anticipated-transient-without-scram test initiated from typical commercial PWR operating conditions in which the primary coolant and main feedwater pumps, the steam generator main feedwater discontinued, and the main steam-outlet valve closed. Auxiliary feedwater was initiated after a delay of 10 s to simulate the start-up time of the diesel generators, and the pressuriser PORV and spray were both inoperative throughout the transient [16]. |

* - low power operation

## 4 REVIEW OF BDBA (DEC A) SIMULATIONS AT JOŽEF STEFAN INSTITUTE

Results of selected simulations of experiments described in Tables 1 and 2 are presented. This includes BETHSY 9.1b, 6.2TC and 6.9c tests, and LOFT L9-1/L3-3 test. The scenarios with multiple failures simulated for Krško Nuclear Power Plant are not in the scope of this paper (e.g. references [21] through [27]).

BETHSY was an integral test facility, which was designed to simulate most pressurized water reactor accidents of interest, study accident management procedures and validate the computer codes. It was a scaled down model of three loop Framatome (now AREVA NC) nuclear power plant with the thermal power 2775 MW.

The LOFT facility was a 50 $MW_{th}$ two-loop PWR, which was designed to study the thermo-hydraulic response of the system to a variety of simulated LOCA scenarios. The facility incorporated similar hydraulic components to those in commercial PWRs, although the components were volumetrically scaled by a ratio of 1/60 in comparison to a full-scale commercial PWR with a power of 3000 $MW_{th}$. Inherent in the scaling are some compromises in the geometric similarity. In particular, the 1.7m-long LOFT reactor core was around half the length of that of a commercial PWR, but the Emergency Core Coolant (ECC) system was designed to inject a similar amount of core coolant in the event of an LOCA.

### 4.1 Simulation of BETHSY 9.1b

The Bethsy 9.1.b test is a scaled 5.08 cm cold leg no. 1 break without high pressure safety injection and with delayed operator action for secondary system depressurization. Due to core heatup the operator depressurized the secondary side by atmospheric relief steam dump valves. In the simulation this operator action was delayed. The test was analyzed in the frame of international standard problem 27 (ISP-27) performed to validate the thermalhydraulic computer codes. The test scenario was the following: break was opened in the cold leg no. 1 (initiation of the transient). When the maximum heater rod cladding temperature reaches 723 K, the ultimate procedure was started by opening three steam line dumps to atmosphere. When pressurizer pressure dropped below 4.2 MPa accumulators started to inject and they stopped to inject below 1.46 MPa. The low pressure safety injection system was activated when the primary pressure was below 0.91 MPa. When stable residual heat removal system operating conditions prevail, the transient was terminated.

The aim of the study [28] was to perform calculations with to Jožef Stefan Institute (JSI) available RELAP5 versions using as much as possible the same input model in order to see the differences between the code versions. As it is difficult to compare so many calculations, line colors are selected in such way that MOD3.3 versions have green color palette, MOD3.2 are in red and pink and MOD3.1 has blue palette. Pressurizer pressure and maximum heater rod temperature are shown in Figure 1 and Figure 2, respectively. As high pressure injection is not available, the core starts to uncover and when maximum heater rod cladding temperature reaches 723 K, the ultimate procedure was started by opening three steam line dumps to atmosphere, in the calculations a bit earlier than in the experiment. This causes secondary pressure decrease, followed by primary system pressure decrease. When primary system dropped below the accumulator injection setpoint, the injection started and soon the clad temperature started to decrease. Again the heatup in the calculation is earlier than in the experiment. Later the accumulators are emptied, however cooling is established through the secondary side, and therefore the primary pressure is decreasing. When reaching the low pressure injection system setpoint, the low pressure injection started and the experiment lasted until the stable residual heat removal system conditions were reached. From results it may be seen that secondary side depressurization prevented core heatup as primary pressure drops below accumulator injection.

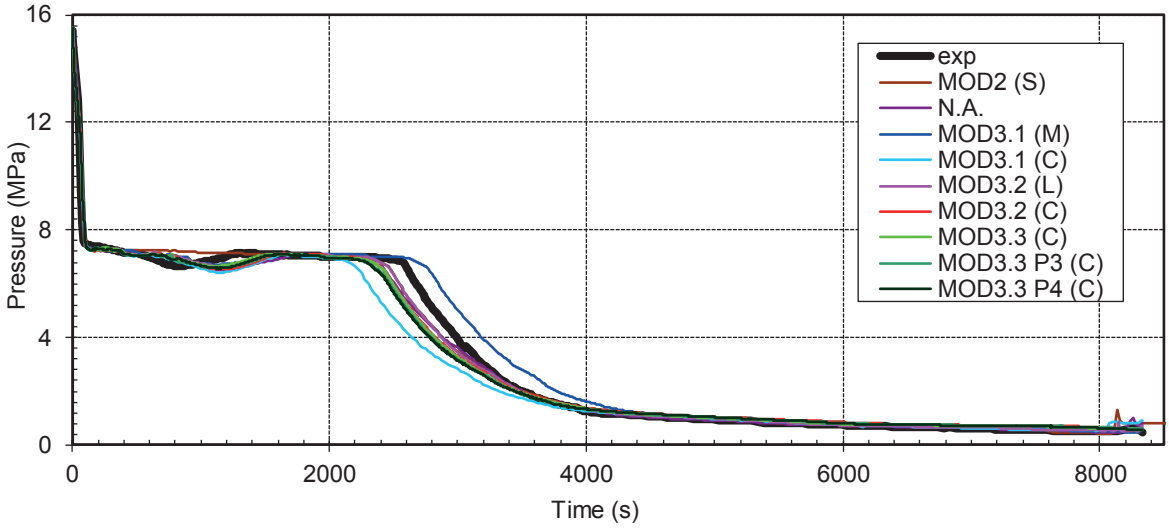


Figure 1: Pressurizer pressure – BETHSY 9.1b

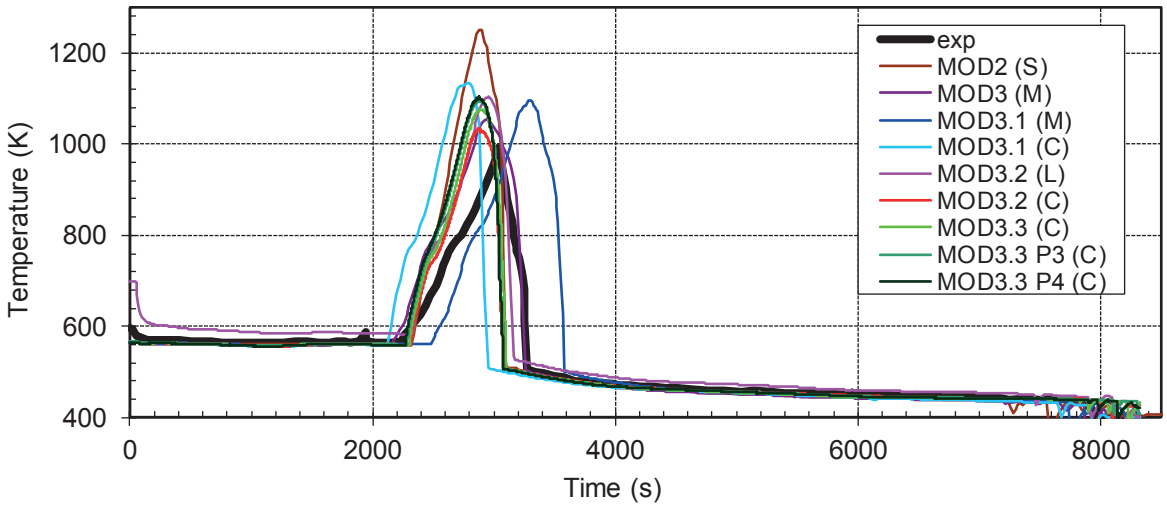


Figure 2: Maximum heater rod cladding temperature – BETHSY 9.1b

### 4.2 Simulation of BETHSY 6.2TC

BETHSY 6.2TC test was a 15.24 cm (6 inch) cold leg break in the loop no. 1 without available high pressure and low pressure safety injection system. The experiment started with opening of the valve simulating the break in the cold leg no. 1 at the time 0 s. Sudden primary pressure drop caused scram signal when pressure was below 13.0 MPa and safety injection (SI) signal was generated, when primary pressure was below 11.7 MPa. At scram signal all three primary pumps were stopped and natural circulation regime took over the primary system. The hot parts of the primary circuit (upper head, upper plenum, SG U-tubes) started to boil. The formation of loop seal caused the core level depression. The drop in the core collapsed liquid level was stopped at 134 s by loop seal clearance on the three loops. The loop seal clearance occurred at the same time on all three loops. After loop seal clearance the core liquid level rose again due to pressure balances and then started to drop again due to inventory loss through the break. When primary pressure dropped below 4.2 MPa, the accumulator injection started, which recovered the core. The accumulator injection was stopped on the basis of low level criterion. After it stopped, in the absence of high pressure injection, the primary circuit emptied through the break and third core uncovery occurred. The low pressure injection was not activated by assumption. The test was ended when the primary pressure dropped below 0.7 MPa.

The results of simulation [29] are shown for pressurizer pressure and maximum heater rod temperature in Figure 3 and Figure 4, respectively. For RELAP5 original Ransom-Trapp break flow model the values of 0.85, 1.25 and 0.75 were used for subcooled, two phase and superheated discharge coefficient, respectively. For TRACE break model the values of 0.8 and 0.9 were used for subcooled and two phase discharge coefficients, respectively. The pressure drop (see Figure 3) is faster in case of TRACE calculation than in the experiment, while in the case of RELAP5 is slower. In the case of heater rod surface temperature (see Figure 4) the timing of heatup prediction was better in the case of TRACE, while heatup rate was better predicted in the case of RELAP5. It may be seen that due to unavailability of high and low pressure injections systems the core heatup would continue, if test would not be ended. In such a case new engineered safety feature for primary injection would be needed to prevent core heatup.

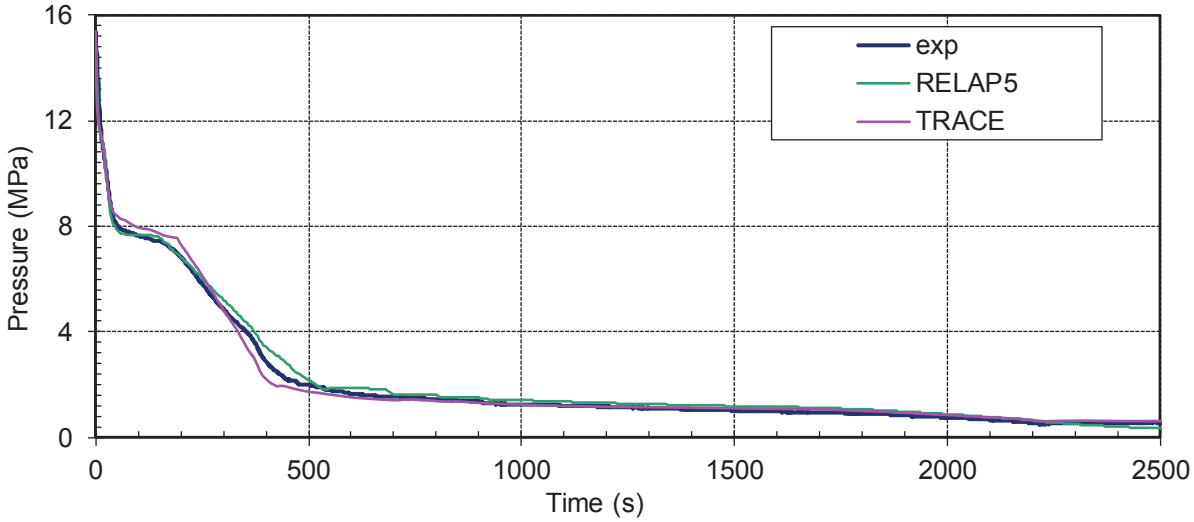


Figure 3: Pressurizer pressure – BETHSY 6.2TC

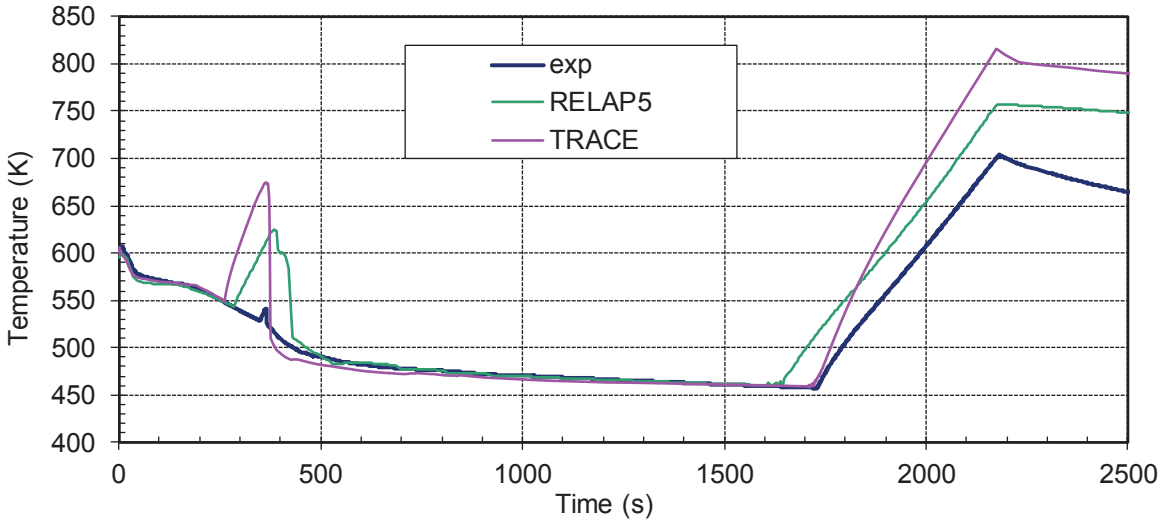


Figure 4: Maximum heater rod cladding temperature – BETHSY 9.1b

### 4.3 Simulation of BETHSY 6.9c

Test 6.9c OECD ISP-38 includes a loss of RHR system during mid-loop operation at 0.5% of nominal value core power. Initial liquid level in RCS was at horizontal axis of the hot legs. Pressurizer and steam generator manways were opened 1 s after the transient was initiated. Boil away and liquid entrainment through manways are in that case the physical phenomena which

mainly determine the RCS behaviour while both the presence of non condensable gas above the liquid level and heat removal by SG's play a minor role. The initial conditions for this tests are: RCS at atmospheric pressure with a liquid level at mid height of hot legs, fluid and structure temperatures close to 373 K in the whole RCS (the liquid heat up phase was ignored in test), and the SG secondary sides are filled with air and isolated. Manways are simulated by geometrically scaled orifices with the same form loss coefficient.

At the start of the test the water in the primary circuit was at the centre line level of the hot legs and very close to the saturation temperature. The manways in the pressuriser and steam generator were opened and the core power increased to 140kW. Boiling occurred almost immediately.

Over the first 3000 s of the transient, water was entrained into the surgeline and then carried on up into the pressuriser by the high steam flow rate. It accumulated in the pressuriser. The accumulated water was not held there continuously, but twice it flowed back to the hot leg and then partially refilled. Finally as the mixture level in the vessel fell the pressuriser and surge line emptied completely.

During this period also there was water entrained into the vertical part of the hot leg and the steam generator inlet plenum and tubes. These also emptied when the mixture level fell below the hot legs.

After about 6000 s the level fell sufficiently for the core to become uncovered and the temperature of the fuel rod simulators to rise. When the temperature rose above 523 K, emergency core cooling was initiated by a (simulated) gravity driven feed. This was sufficient to halt the core heat-up and re-establish the primary circuit inventory. The test was stopped when the level in the vessel reached the mid loop condition. The total test time was nearly 10000 s. The simulated mass calculated by different computers is shown in Figure 5. The experimental line is blue.

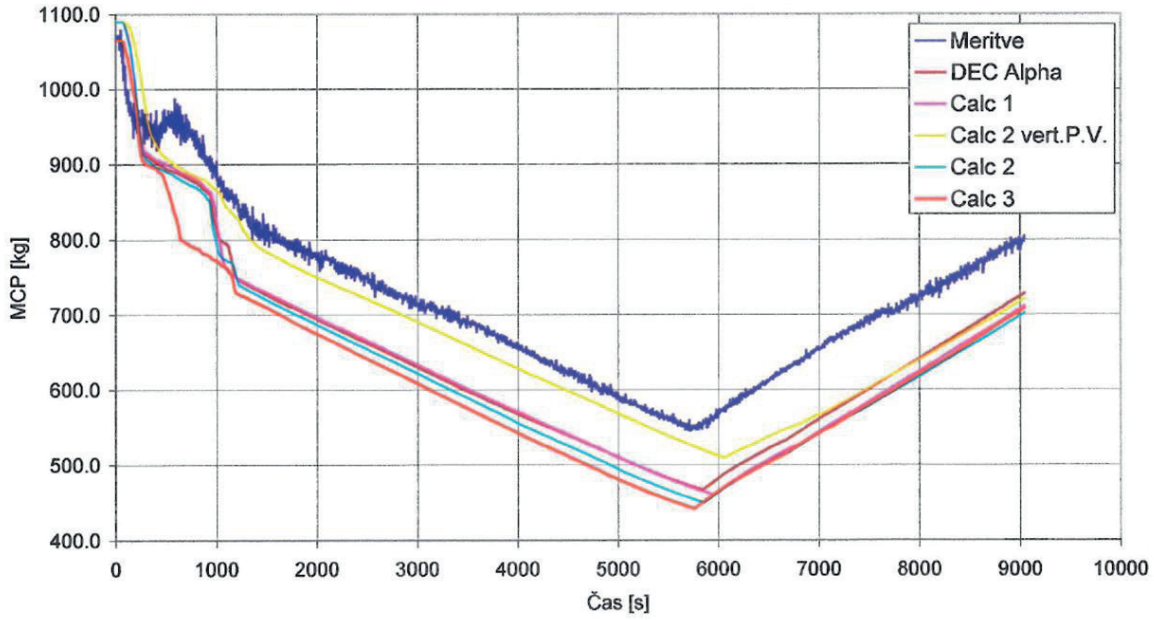


Figure 5: Mass in primary system – BETHSY 6.9c

The calculations were performed on DEC Alpha and SUN Sparc workstation (labelled “DEC Alpha” and “Calc1”) using base input deck and modified input models (“Calc 2 vert.P.V”, “Calc 2” and “Calc 3”). From the experiment and simulated results it may be seen that without gravity driven injection the core would continue to uncover. By GL 88-17 [30] the following enhancements have been recommended for mid-loop operation such as training, temperature and level indications, implementation of procedures and controls, and at least two available or operable means of adding inventory to the RCS that are in addition to pumps that are a part of the normal RHR systems.

## 4.4 Simulation of LOFT L9-1/L3-3

The LOFT experiment L9-1/L3-3 tested the system response to an anticipated transient with multiple failures (L9-1) followed by a small-break LOCA (L3-3) due to the failure of a power-operated relief valve (PORV).

Experiment L9-1 was the first anticipated transient with multiple failures performed at LOFT, and consisted of a simulated LOFW accident with delayed reactor scram and no auxiliary feedwater injection. The LOFW accident was initiated due to the failure of the main feedwater pump, leading to the loss of coolant through the PORV, which resulted in a LOCA.

Experiment L3-3 simulated two independent recovery procedures from the LOFW accident L9-1, without engaging the emergency core coolant (ECC). The first recovery mode involved latching open the PORV to depressurize the primary system whilst simultaneously turning off the primary coolant pumps. The second mode consisted of refilling the steam generator (SG) and removing excess decay heat through a feed-and-bleed operation of the SG secondary side.

In short, the LOFT experiment L9-1/L3-3 was conducted to evaluate the effectiveness of the PORV cycling and the subsequent feed-and-bleed operation using the secondary side for removal of decay heat.

The simulation was performed by RELAP5/MOD3.3 Patch 04. The transient conditions at 1690 s is displayed in Figure 6, clearly indicating that the pressurizer has completely filled with fluid when the PORV cycling is initiated. Figure 7 depicts the system at 7050 seconds, upon the initiation of the feed-and-bleed operation in the secondary loop.

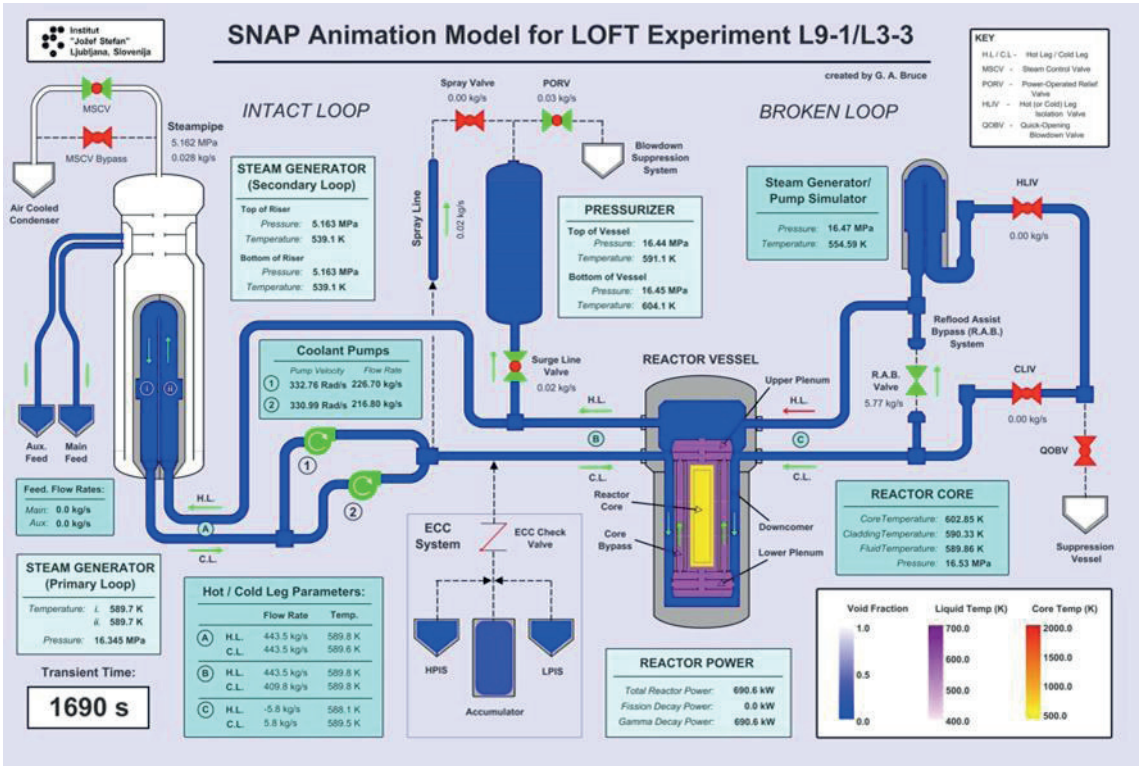


Figure 6: Spray valve closed and PORV cycling initiated (t=1690 s)


Andrej Prošek, Mitja Uršič, Review of Design Extension Conditions Experiments and Analyses for Non–degraded Core, Journal of Energy, vol. 68 Number 2–3, Special Issue (2019), p. 112–125

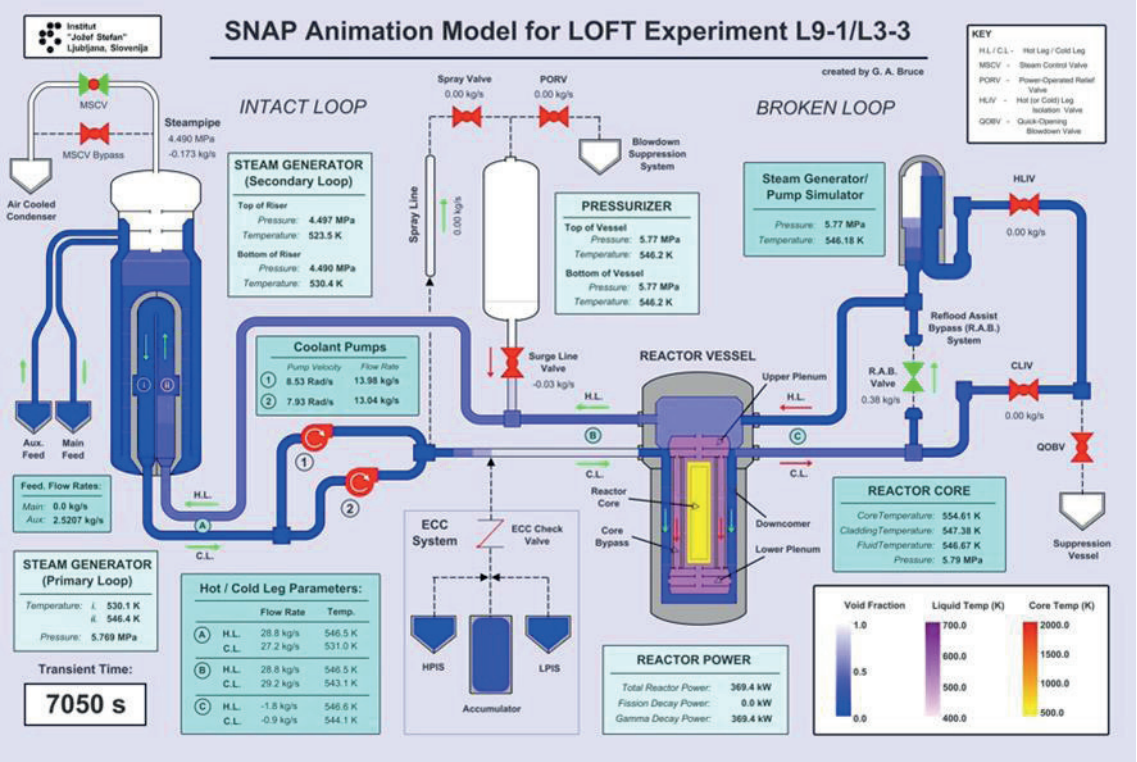


Figure 7: SG secondary refilled, feed-and-bleed operation initiated (t=7050 s)

## 5 CONCLUSIONS

The requirements to analyse design extension conditions for existing reactors have been introduced after Fukushima Dai-ichi accident. The purpose of considering design extension conditions (DEC) is to further improve safety by enhancing the plant's capability to withstand the conditions generated by accidents that are more severe than design basis accidents (DBAs). The paper first provides example lists of DEC proposed by International Atomic Energy Agency (IAEA) and Western European Nuclear Regulators Association (WENRA). Then, research for beyond design basis accidents with non-degraded core (i.e. DEC A) for existing reactors done in 80's and 90' of the previous century is presented. The tests performed include total loss of feedwater, station blackout, small break without high pressure safety injection, steam generator tube rupture with no high pressure safety injection etc. Finally, simulations of few experiments (representing DEC A) tests performed on integral test facilities, which have been analysed at Jožef Stefan Institute using RELAP5 or TRACE computer code in the last three decades, have been presented. The review of beyond design basis accidents performed on integral test facilities and simulations suggest that selected DEC scenarios were studied well before the requirements on DEC analyses have been made. Also, before the Fukushima Dai-ichi accident several existing plants have already implemented certain measures to prevent severe accidents from multiple failures (e.g. station blackout or anticipated transients without reactor scram).

## ACKNOWLEDGMENTS

The author acknowledges the financial support from the Slovenian Research Agency (research core funding No. P2-0026 "Reactor engineering"). The Krško nuclear power plant (NPP Krško) and Slovenian Nuclear Safety Administration (SNSA) supported this research through CAMP project no. POG-U3-KE-R4/104/12 (NEK no. 3180019).

## REFERENCES


[1] International Atomic Energy Agency (IAEA), Safety of Nuclear Power Plants: Design, Specific Safety Requirements No. SSR-2/1, January 2012.

[2] International Atomic Energy Agency (IAEA), Safety of Nuclear Power Plants: Design, Specific Safety Requirements No. SSR-2/1 (Rev. 1), February 2016.

[3] European Utility Requirements, Volumes 1 and 2, Rev C., April 2001.

[4] WENRA, WENRA Reactor Safety Reference Levels, January 2007.

[5] WENRA, WENRA Safety Reference Levels for Existing Reactors, September 2014.

[6] WENRA, Guidance Document Issue F: Design Extension of Existing Reactors, 29 September, 2014.

[7] M.A.B. Alvarenga, P.F. Frutuoso e Melo, Including severe accidents in the design basis of nuclear power plants: An organizational factors perspective after the Fukushima accident, *Annals of Nuclear Energy* Vol. 79, 68–77, 2015.

[8] International Atomic Energy Agency (IAEA), Considerations on the Application of the IAEA Safety Requirements for the Design of Nuclear Power Plants, IAEA TECDOC No. 1791, Vienna, 2016.

[9] A. Annunziato, H. Glaeser, J. Lillington, P. Marsili, C. Renault, A. Sjöberg, CSNI Integral Test Facility Validation Matrix for the Assessment of Thermal-Hydraulic Codes for LWR LOCA and Transients, NEA/CSNI/R(96)17, July 1996.

[10] P. Clement, T. Chataing, R. Deruaz, PWR accident management related tests: Some Bethsy results, *In Proceedings of the 6th Int. Topical Meeting on Nuclear Reactor Thermal Hydraulics, NURETH6*, Grenoble, France, October 5-8, 1993.

[11] F. Schafer, E. Krepper, F.-P. Weiss, Post-Test Analysis of Two Accident Management Experiments Performed at the BETHSY Test Facility using the Code ATHLET, *In Proceedings of ICONE - Ninth International Conference on Nuclear Engineering*, Nice, France, April 8-12 2001.

[12] H. Kumamaru, Y. Kukita, PWR Cold-Leg Small-Break LOCA with Total HPI Failure, *Journal of Nuclear Science and Technology*, Vol. 29, No. 12, pp. 1162-1172, 1992.

[13] H. Asaka, Y. Kukita, Intentional Depressurization of Steam Generator Secondary Side during a PWR Small-Break Loss-of-Coolant Accident, *Journal of Nuclear Science and Technology*, Vol. 32, No. 2, 1995.

[14] J. M. Putney, R. J. Preece, Assessment of PWR Steam Generator Modelling in RELAP5/MOD2, NUREG/IA-0106, June 1993.

[15] J.K. Suh, Y.S. Bang, H.J.Kim, Assessment of RELAP5/MOD3.2.2 Gamma with the LOFT L9-3 Experiment Simulating an Anticipated Transient Without Scram (NUREG/IA-0192), January 2001.

[16] R.C. Kern, D.A. Rautmann, R.O. Anderson, Best-Estimate Analyses of LOFT Anticipated Transients with and without Scram Using DYNODE-P, Anticipated and Abnormal Plant Transients in Light Water Reactors, American Nuclear Society, New York and London, 1984.

[17] C. Addabbo, A. Annunziato, The LOBI Integral System Test Facility Experimental Programme, *Science and Technology of Nuclear Installations*, Volume 2012, Article ID 238019.

[18] SECY-90-016, Evolutionary Light Water (LWR) Certification Issues and Their Relationship to Current Regulatory Requirements," Nuclear Regulatory Commission, issued January 12, 1990, and the corresponding SRM, issued June 26, 1990.

[19] SECY-93-087, Policy, Technical, and Licensing Issues Pertaining to Evolutionary and Advanced Light-Water (ALWR) Designs," Nuclear Regulatory Commission, issued April 2, 1993, and the corresponding SRM, issued July 21, 1993.

[20] WENRA, Safety of new NPP designs, Study by Reactor Harmonization Working Group RHWG, March 2013.

[21] A. Prošek, A. Volkanovski, RELAP5/MOD3.3 analyses for prevention strategy of extended station blackout, *Journal of nuclear engineering and radiation science*, Vol. 1, No. 4, pp. 041016-1-041016-10, 2015.

[22] A. Prošek, L. Cizelj, Long-term station blackout accident analyses of a PWR with RELAP5/MOD3.3, *Science and Technology of Nuclear Installations*, Vol. 2013, pp. 851987-1-851987-15, 2013

[23] A. Prošek, B. Mavko, Estimation of operator action success criteria time windows by RELAP/MOD3.3 during total loss of all feedwater Spring CAMP 2008 meeting: code applications and maintenance program: Pisa, Italy, 28-30 May, 2008.

[24] A. Prošek, B. Mavko, S. Petelin, Decay heat removal during SB LOCA with loss of all feedwater. Power Plant Transients 1994: 1994 International Mechanical Engineering Congress and Exposition, Chicago, November 6-11, 1994: FED-Vol. 204. New York: American Society of Mechanical Engineers. 1994, pp. 83-88.

[25] S. Petelin, B. Mavko, O. Gortnar, I. Parzer, An ISP-27 accident scenario for analysis of Krško nuclear power plant SBLOCA, *Transactions of the American Nuclear Society*, Vol. 70, pp. 435-437, 1994.

[26] I. Parzer, S. Petelin, B. Mavko, Feed-and-bleed procedure mitigating the consequences of a steam generator tube rupture accident, *Nuclear Engineering and Design*, Vol. 154, pp. 51-59, 1995.

[27] G. Černe, I. Tiselj, I. Parzer, ATWS analyses for Krško Full Scope Simulator verification, *In Proceedings of International Conference Nuclear Energy in Central Europe 2000*, Bled, Slovenia, 11 - 14 September 2000.

[28] A. Prošek, RELAP5 Calculations of Bethsy 9.1b Test, *Science and Technology of Nuclear Installations*, Vol. 2012, Article ID 238090, 11 pages, 2012.

[29] A. Prošek, O. A. Berar, Advanced Presentation of BETHSY 6.2TC Test Results Calculated by RELAP5 and TRACE, *Science and Technology of Nuclear Installations*, Vol. 2012, Article ID 812130, 15 pages, 2012.

[30] U.S. Nuclear Regulatory Commission, Loss of Decay Heat Removal, GL 88-17, October 17, 1988.

Journal of Energy
VOLUME 68 Number 2-3 | 2019 | Special Issue
journal homepage: http://journalofenergy.com/

# NPP Krško 3 inch Cold Leg Break LOCA Calculation using RELAP5/MOD 3.3 and MELCOR 1.8.6 Codes

**Vesna Benčik, Davor Grgić, Siniša Šadek, Štefica Vlahović**
University of Zagreb, Faculty of Electrical Engineering and Computing
Unska 3, 10000 Zagrerb, Croatia
vesna.bencik@fer.hr, davor.grgic@fer.hr, sinisa.sadek@fer.hr, stefica.vlahovic@fer.hr

## ABSTRACT

NPP Krško input deck developed at Faculty of Electrical Engineering and Computing (FER) Zagreb, for severe accident code MELCOR 1.8.6 is currently being tested. MELCOR is primarily used for the analyses of severe accidents including in-vessel and ex-vessel core melt progression as well as containment response under severe accident conditions. Accurate modelling of the plant thermal-hydraulic behaviour as well as engineering safety features, e.g., Emergency Core Cooling System, Auxiliary feedwater system and various containment systems (e.g., Passive Autocatalytic Recombiners, Fan Coolers and Containment spray) is necessary to correctly predict the plant response and operator actions. For MELCOR input data verification, the comparison of the results for small break (3 inch) cold leg Loss of Coolant Accident (LOCA) for NPP Krško using MELCOR 1.8.6 and RELAP5/MOD 3.3 was performed. A detailed RELAP5/MOD 3.3 model for NPP Krško has been developed at FER and it has been extensively used for accident and transient analyses. The RELAP5 model has been upgraded and improved along with the plant modernization in the year 2000. and after more recent plant modifications. The results of the steady state calculation (first 1000 seconds) for both MELCOR and RELAP5 were assessed against the referent plant data. In order to test all thermal-hydraulic aspects of developed MELCOR 1.8.6 model the accident was analysed, and comparison to the existing RELAP5 model was performed, with all engineering safety features available. After initial fast pressure drop and accumulator injection for both codes stable conditions were established with heat removal through the break and core inventory maintained by safety injection. Transient was simulated for 10000 seconds and overall good agreement between results obtained with both codes was found.

***Keywords:*** *MELCOR, RELAP5, code comparison, input data verification, small break Loss of Coolant Accident*

## 1 INTRODUCTION

Calculation models for NPP Krško for computer codes RELAP5/MOD 3.3 and MELCOR are being developed at FER. Usually, these two codes are used for different purposes; RELAP5/MOD 3.3, ref. [1], is used as a best-estimate calculation tool for analysis of postulated accidents, whereas MELCOR, ref. [2] and [3] is used to model progression of severe accidents in light water reactors. After Fukushima accident in 2011. development of strategies for management of severe accidents as well as Beyond Design Basis Accidents (BDBAs) has gained awareness worldwide. The Slovenian Nuclear Safety Administration (SNSA) has issued a request for Safety Upgrade Program (SUP) for NPP Krško in relation to Plant Life Extension as well as new requirements regarding Design Extension Conditions (DEC – the conditions that are more challenging/severe than original conditions used in plant design) and BDBA. The program consists in a reassessment of Severe Accidents strategy and implementation of necessary safety improvements. As a part of this

program, in 2013. the electrical hydrogen recombiners were replaced by Passive Autocatalytic Recombiners (PARs) and the Passive Containment Filtered Vent (PCFV) system were installed at NEK. During the upcoming second phase of the program RCS and containment alternate long term cooling will be installed. In case of event (BDBA) Alternate Residual Heat Removal Pumps (ARHR) will be used to either supply the water for RCS safety injection or for containment spray. ARHR pumps can take the suction either from the Refueling Water Storage Tank (RWST) or from RCS hot/cold legs or from containment sump. Water taken from sump will be cooled in existing RHR or in Mobile Heat Exchangers (MHX).

At FER a detailed RELAP5/MOD 3.3 model for NPP Krško is being developed, ref. [4] and [5]. The model is being constantly updated to reflect changes after plant modernization and modifications, e.g., Steam Generators (SG) replacement and power uprate in 2000., Resistance Temperature Detector Bypass Elimination (RTDBE) in 2013. and Up-Flow Conversion (UFC) in 2015. RELAP5 model contains detailed nodalization of NPP Krško Safety Injection (SI) system, Main feedwater and Auxiliary feedwater (AFW) system as well as models of protection and control systems including the detailed models of automatic control rod, pressurizer pressure and level control, steam generator level control and steam dump control with realistic steam dump valves.

NEK data base that has been used for development of the RELAP5 model is being used for development of MELCOR model for NPP Krško, ref. [6] and [7], as well. Recently, MELCOR 1.8.6 was used to analyse Station Blackout (SBO) accident at NEK, ref. [8] and [9]. Transient scenario assumed that Engineering Safety Systems (ESF); e.g., safety injection, auxiliary feedwater system, containment fan coolers and containment spray system were not available. The calculation model includes the latest plant safety upgrade with addition of Passive Autocatalytic Recombiners (PAR) and the Passive Containment Filter Venting (PCFV) system. The results with MELCOR 1.8.6 were compared with the MAAP 4.0.7 calculation of the same transient scenario. The SBO sequence included core degradation, reactor vessel failure, release of corium to containment, Molten Core Concrete Interaction (MCCI), production of hydrogen and containment pressurization. The PCFV system provided controlled release of containment inventory to atmosphere thus maintaining the containment pressure at design limits whereas the PARs have reduced hydrogen concentration by controlling the chemical reaction between hydrogen and oxygen.

In this paper the part of our work at developing and verification of MELCOR input deck for NPP Krško is presented. In order to model the plant behaviour under non-severe accident conditions as well as planned mitigation actions, MELCOR input deck has been updated with realistic models of plant safety systems. For verification purposes, a Small Break LOCA (SB LOCA) consisting in a 3 inch break in cold leg 1 (loop with pressurizer) was analysed. In the analysis it was assumed that all the Engineering Safety Features are available and operating. The results of both steady state and transient calculation were assessed against RELAP5/MOD 3.3 analysis for the same transient scenario.

## 2 CALCULATIONAL MODEL FOR NPP KRŠKO

The schemes of NPP Krško nodalization for RELAP5/MOD 3.3 and MELCOR 1.8.6 are shown in Figure 1 and Figure 2, respectively. Both nodalizations have been updated according to the recent plant modifications; i.e., RTDBE (Resistance Temperature Detector Bypass Elimination) in 2013. and UFC (Up Flow Conversion) in 2015. The UFC modification was performed in order to minimize the baffle jetting across the baffle-barrel bypass and the core. The modification consisted in altering the reactor vessel internals in such way that the coolant downflow path in the baffle-barrel region was converted to an upflow path. The RELAP5 nodalization consists of 506 thermal-hydraulic volumes, 543 junctions, 383 heat structures with 2127 mesh points, 732 control variables and 197 variable and 221 logical trips.

MELCOR 1.8.6 nodalization consists of 123 thermal-hydraulic control volumes, 174 flow paths and 100 heat structures. There are 189 real valued and 91 logical valued control functions

aimed to model the artificial steady state control as well as protection and ESF (Engineered Safety System) behaviour, e.g., Auxiliary Feedwater, Safety Injection, Containment fan coolers and Containment spray control. So far, MELCOR 1.8.6 model does not contain realistic models of plant control systems (pressurizer pressure and level control, SG level control, automatic rod control system and steam dump).

Reactor pressure vessel (RPV) is modelled with 40 control volumes. The lower plenum is represented with 3 CVs, the downcomer with 5 CVs, the upper plenum with 4 CVs and the upper head with 2 CVs. Reactor core is represented with 12 control volumes (CV 007-018), as well as the baffle-barrel region (CV 067-078). The guide tubes bypass is represented with CV 079.

Reactor core and lower plenum for MELCOR COR package are represented with 7 radial rings, 12 axial levels in reactor core, 2 axial levels in lower plenum and 10 axial segments in non-cylindrical part of lower head, respectively. Five radial rings are used to represent the active core, one ring for the region between the baffle and the barrel, and one additional ring in the lower plenum as requested by the code. The lower head is represented with 10 radial rings for better prediction of the RPV wall temperature which is used to calculate the RPV rupture.

The NEK containment model for MELCOR code is based on the NPP Krško containment nodalization notebook, ref. [10] which contains detailed calculations of containment volumes and heat structures' dimensions. Containment nodalization is shown in Figure 3. The containment building is represented with 12 control volumes. There are four additional volumes:

1. CV 706 – refuelling water storage tank
2. CV 707 – connection between the upper compartment and the environment, added to control opening/closing of the PCFV valve.
3. CV 716 – RHR heat exchanger volume
4. CV 900 (environment) – a large volume ($10^8$ $m^3$) at constant temperature (307 K) and pressure ($10^5$ Pa)

Containment control volumes are connected by 30 flow paths. Heat sinks representing outside containment wall, internal walls, floors, polar crane, fan coolers, platforms and other miscellaneous stainless and carbon steel structures are modelled with 20 heat structures.

During steady state, both in RELAP5 and MELCOR, control systems for artificial steady state maintain the pressurizer pressure as well as pressurizer and SG level at their setpoint values. On the secondary side, turbine valve opening is controlled in order to maintain the RCS average temperature at its setpoint value (578.15 K). Steady state was simulated for 1000 seconds for both RELAP5 and MELCOR 1.8.6. The results for relevant physical parameters are summarized in Table 1. A very good agreement for both RELAP5 and MELCOR 1.8.6 calculation with NEK referent data were obtained.

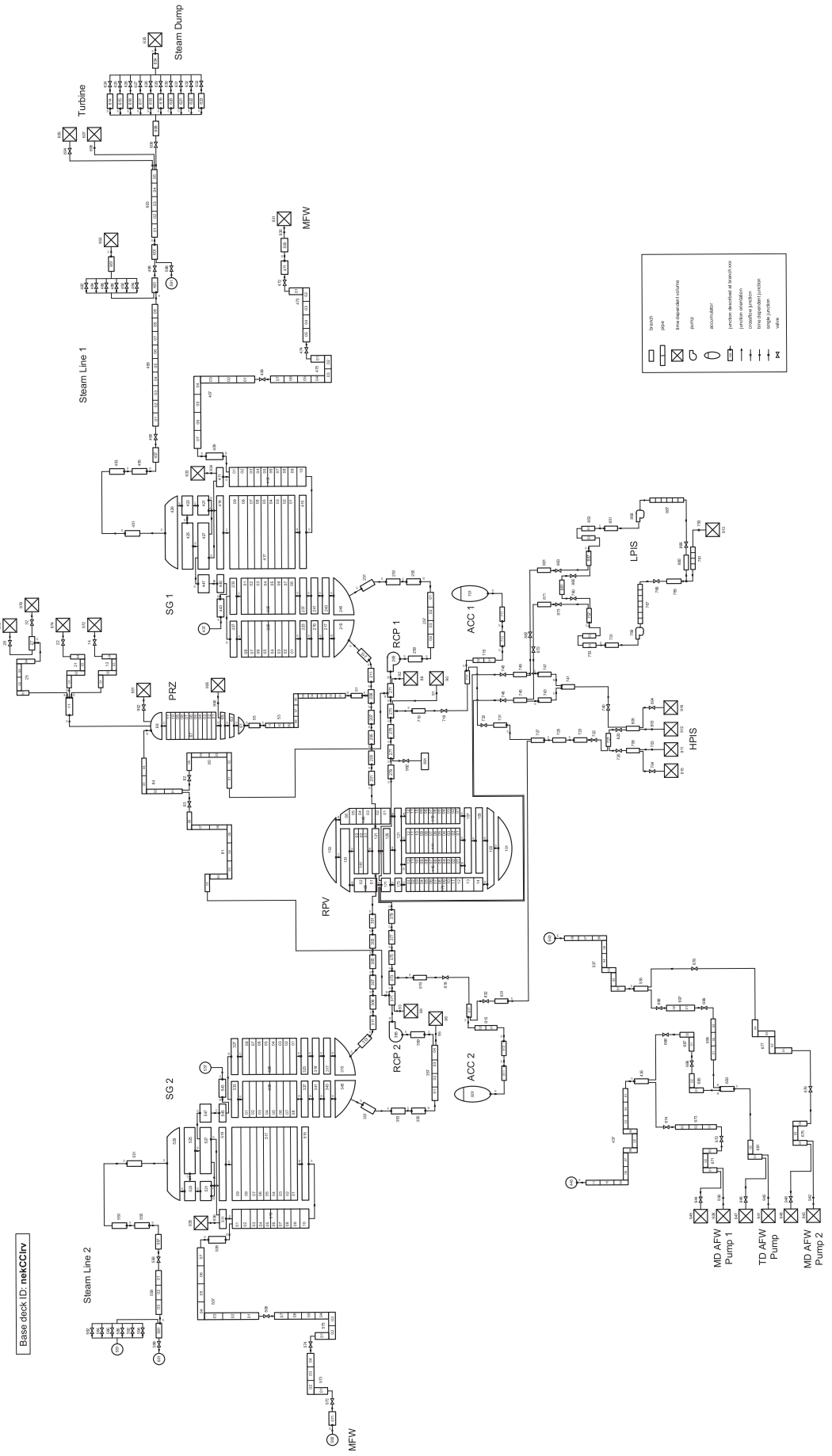


Figure 1: RELAP5/MOD 3.3 nodalization scheme for NPP Krško



Vesna Benčik, Davor Grgić, Siniša Šadek, Štefica Vlahović, NPP Krško 3 inch Cold Leg Break LOCA Calculation using RELAP5/MOD 3.3 and MELCOR 1.8.6 Codes, Journal of Energy, vol. 68 Number 2–3, Special Issue (2019), p.126–139

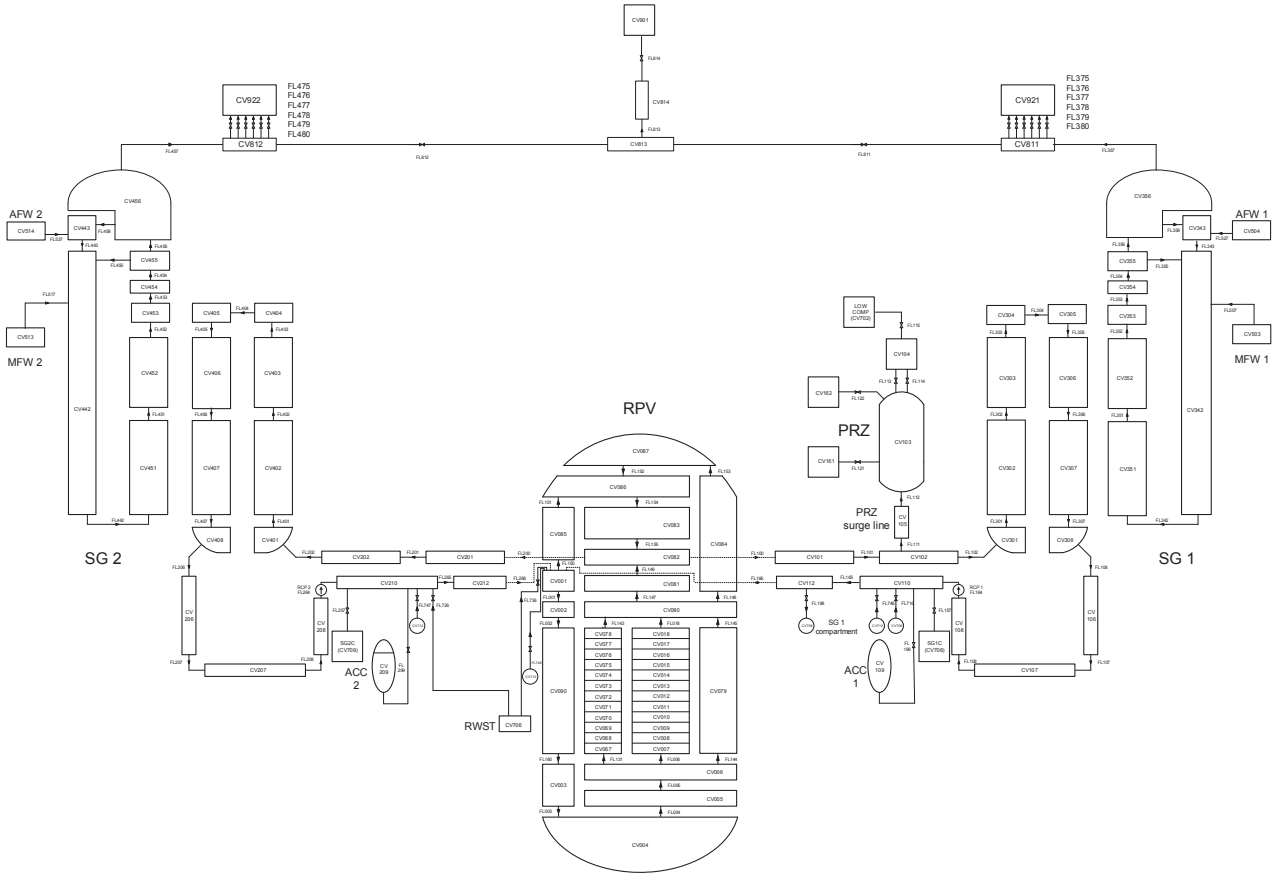


Figure 2: MELCOR 1.8.6 nodalization scheme for NPP Krško

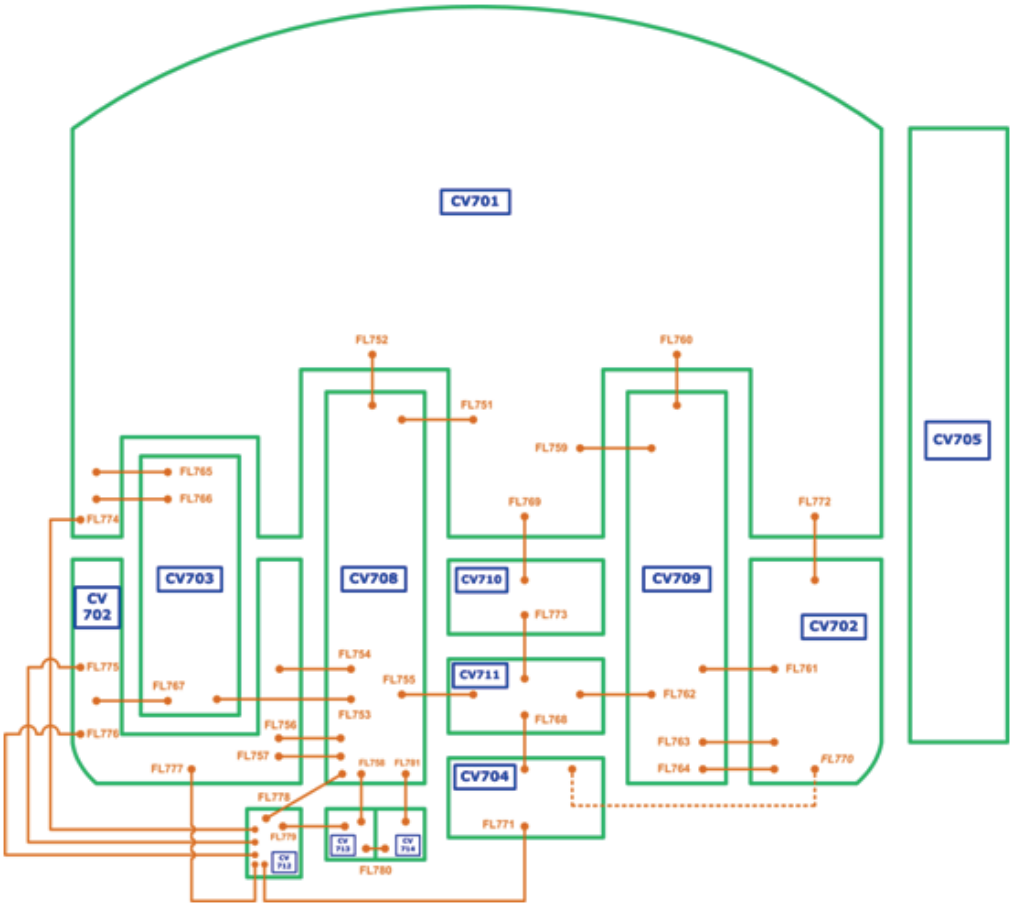


Figure 3: MELCOR 1.8.6 nodalization scheme for NPP Krško containment



Vesna Benčik, Davor Grgić, Siniša Šadek, Štefica Vlahović, NPP Krško 3 inch Cold Leg Break LOCA Calculation using RELAP5/MOD 3.3 and MELCOR 1.8.6 Codes, Journal of Energy, vol. 68 Number 2–3, Special Issue (2019), p.126–139

Table 1: Results of steady state calculation (1000 s)

| Parameter | NEK referent data, cycle 28 | RELAP5/MOD 3.3 | MELCOR 1.8.6 |
|---|---|---|---|
| **1. Pressure (MPa)** | | | |
| Pressurizer | 15.513 | 15.513 | 15.517 |
| Steam generator | 6.281 | 6.275/6.286 | 6.19/6.16 |
| Accumulator | 4.93 | 4.93 | 4.93 |
| **2. Fluid Temperature (K)** | | | |
| Cold leg | 558.75 | 559.49/559.25 | 559.36/559.15 |
| Hot leg | 597.55 | 596.82/596.82 | 596.94/596.94 |
| Feedwater | 492.6 | 492.7 | 492.6 |
| **3. Mass Flow (kg/s)** | | | |
| Core | 8899.7 | 8925.3 | 8876.4 |
| Cold leg | 4697.4 | 4711.7/4710.7 | 4683.7 /4686.2 |
| Main feedwater | 544.5 | 540.9/544.7 | 538.9/541.8 |
| Main steam line | 544.5 | 540.9/544.7 | 538.9/541.8 |
| DC-UP bypass | 0.0% | 0.0% | 0.0% |
| DC-UH bypass | 0.346% | 0.371% | 0.346% |
| Baffle-barrel flow | 1.0939% | 1.094%% | 1.094% |
| RCCA guide tubes | 3.32% | 3.81% (includes core cavity flow) | 3.83% (includes core cavity flow) |
| Core cavity (0.5067%) | 0.5067% | - | - |
| **4. Liquid level (%)** | | | |
| Pressurizer | 55.7 | 55.8 | 55.8 |
| Steam generator narrow range | 69.3 | 69.3/69.3 | 69.2/69.2 |
| **5. Fluid Mass (t)** | | | |
| Primary system | - | 131.3 | 131.8 |
| Steam generator (secondary) | 47.0 | 49.1/48.9 | 48.08/48.07 |
| **6. Power (MW)** | | | |
| Core | 1994.0 | 1994.0 | 1994.0 |
| Steam generator | 1000.0 | 995.9/1003.0 | 997.1/1002.6 |

## 3 ANALYSIS OF 3 INCH COLD BREAK LOCA

The analysed accident is the 3 inch Loss of Coolant Accident (LOCA) in the cold leg 1 (loop with pressurizer. Transient is actuated after 1000 seconds steady state calculation. Small break LOCA is initiated in cold leg volume 275 by opening the valve 992 (RELAP5) to containment (volume 991). In MELCOR, valve simulating the break is opened in FL 198 connecting cold leg volume 112 and SG 1 compartment volume 708. Main events for both RELAP5 and MELCOR calculations are summarized in Table 2. Reactor trip is initiated on low pressurizer pressure signal. Thereupon, turbine trip and main steam isolation valve (MSIV) closure are actuated. Until trip, turbine valve opening in both RELAP5 and MELCOR is maintained at the value that would result in steady state turbine flow. In the analysis it was assumed that pressurizer pressure and level as well as SG level control are not active after transient begin. Under realistic conditions main feedwater is usually isolated on reactor scram & low-1 RCS average temperature. Here, trip of main FW as well as trip of both reactor coolant pumps are actuated on reactor trip. In the analysis all ESF systems are assumed available with minimum delay. Thus, Safety injection pumps are available with 5 seconds and auxiliary feedwater with 60 seconds delay. In MELCOR safety injection pumps

initially take suction from Refueling Water Storage Tank (RWST). In the analysis it was assumed that upon the signal: RWST empty (RWST level equal to 38.6%) operator stops the injection from RWST and switches to recirculation mode with LPIS pumps only, taking suction from containment sump (CV 712). Before it is injected in reactor vessel, pumped water is cooled in the Residual Heat Removal (RHR) heat exchangers. Assumed delay for operator action (stopping the suction from RWST and realigning to containment sump) is 5 minutes. Water level in containment sump has to be monitored in order to assure the required Net Pump Suction Head (NPSH) of LPIS pumps. In RELAP5 calculation an uninterrupted supply from RWST to HPIS and LPIS pumps is assumed.

Following the break opening, Figure 4 RCS rapidly depressurizes, Figure 6 and its inventory decreases. Reactor trip is actuated on low pressurizer pressure (12.995 MPa) at 12.8 s for RELAP5 and at 14.5 s for MELCOR code, respectively. Following actions are performed following reactor trip: turbine trip, MSIV isolation, trip of both RC pumps and main feedwater trip. Auxiliary feedwater will be enabled 60 seconds after trip of main feedwater pumps. Heat produced in the core is primarily removed through the break although in the first phase of the transient heat is also removed in steam generators thus coupling primary and secondary pressure during the first 600 seconds, Figure 6. However, along with the RCS inventory depletion heat transfer in steam generators ceases and the primary pressure decouples from the secondary pressure and begins to decrease more rapidly. At the very beginning of the transient, SG safety valves (SG relief valves are assumed unavailable) open for a short time after turbine trip since the steam dump was assumed unavailable. As a consequence, steam generator mass slightly decreases since the main feedwater is isolated along with reactor trip, Figure 11. Auxiliary feedwater is actuated 60 seconds after main feedwater isolation (72.8 s in RELAP5 and 74.5 s in MELCOR). It is aimed to maintain SG narrow range level in the range (60, 70 %). After decoupling the primary and secondary pressure secondary pressure is affected by auxiliary feedwater injection only in a way that its decrease is stopped first after terminating the auxiliary feedwater flow.

Accumulators open about 11 minutes after transient begin (at 655 s in RELAP5 and at 649 s in MELCOR) and their inventory is injected into RCS approx. for the next 20 minutes. Safety injection signal is initiated on low-2 pressurizer pressure (12.27 MPa) signal in both RELAP5 (17.4 s) and in MELCOR (18.8 s). Safety injection with its full capacity (two High head – HPIS and two Low head – LPIS Safety Injection pumps) is enabled with minimum delay (5 s), Figure 8. In MELCOR, water source for safety injection is Refueling Water Storage Tank (RWST) until RWST empty signal (RWST level less than 38.6%) is generated (at 5391 seconds). Thereafter, the operator starts (with 5 minutes delay) the recirculation phase by switching the suction of LPIS pumps from the RWST to containment sump. After 2200 s the average break flow in MELCOR becomes larger than in RELAP5. Consequently, the primary pressure continues to decrease in MELCOR, whereas in RELAP5 primary pressure slightly increases. This results in a larger amount of injected SI flow in MELCOR and in lower cold leg temperature than in RELAP5, Figure 6, Figure 8 and Figure 10. Accumulator flow in MELCOR is also considerably larger than in RELAP5, Figure 8 and the accumulators have emptied earlier than in RELAP5, as well. After terminating the injection from RWST and by starting the recirculation from containment sump using LPIS pumps only, cold leg temperature in MELCOR increases to a new higher average value. Water from the sump is cooled in RHR heat exchangers before it is injected into RCS, but its temperature is still higher than the RWST temperature. In RELAP5 an oscillatory behaviour of safety injection flow was obtained after approx. 7000 seconds. This is due to the fact that in RELAP5 HPIS pumps are in operation throughout the simulation while the sufficient cooling can be achieved with LPIS pumps only. Oscillations of safety injection flow have caused the oscillations of other parameters, e.g., break flow, RCS temperature and pressure as well as fuel cladding temperature.

In a long term, stable conditions with break flow equal to safety injection flow as well as stable average hot and cold leg temperature for both RELAP5 and MELCOR have been established, Figure 4, Figure 8, Figure 9 and Figure 10. Core dry-out (max. cladding temperature=823 K) occurred in MELCOR during a short period, Figure 12, but fuel cladding oxidation did not occur. Containment pressure increases following the break opening, Figure 7. In MELCOR, containment

pressure is being reduced due to heat removal by fan coolers (1 train available, 35 sec delay). In RELAP5 the simple one-volume containment model is used. Despite of the lack of ESF systems in containment (fan coolers and containment spray) containment pressure in RELAP5 is reduced in the long term due to condensation on containment inner surfaces and convective heat transfer loss from containment outer surface to atmosphere.

Table 2: Time sequence of the main events (3 inch cold leg 1 LOCA)

| Event | RELAP5/MOD 3.3 | MELCOR 1.8.6 |
|---|---|---|
| Transient begin | 0 s | 0 s |
| Reactor trip | 12.8 s (on low PRZ pressure) | 14.5 s (on low PRZ pressure) |
| Turbine trip, MSIV isolation, Main feedwater isolation, RCP trip | 12.8 s (on reactor trip signal) | 14.5 s (on reactor trip signal) |
| Safety injection signal | 17.4 s (on low-2 PRZ pressure) | 18.8 s (on low-2 PRZ pressure) |
| Safety injection enabled | 22.4 s (5 s delay) | 23.8 s (5 s delay) |
| AFW enabled | 72.8 s (60 s delay) | 74.5 s (60 s delay) |
| Start of containment fan coolers | - | 75.0 s (35 s delay) |
| Start of accumulator injection | 655.0 s | 649.0 s |
| Accumulators empty | 1990.0 s | 1670.0 s |
| RWST empty | - | 5391.0 s |
| Start of recirculation from sump | - | 5991.0 s (5 minutes delay) |
| Maximum fuel cladding temperature | 610 K (steady state value) | 823 K (430 s) |
| End of transient | 10000 s | 10000 s |

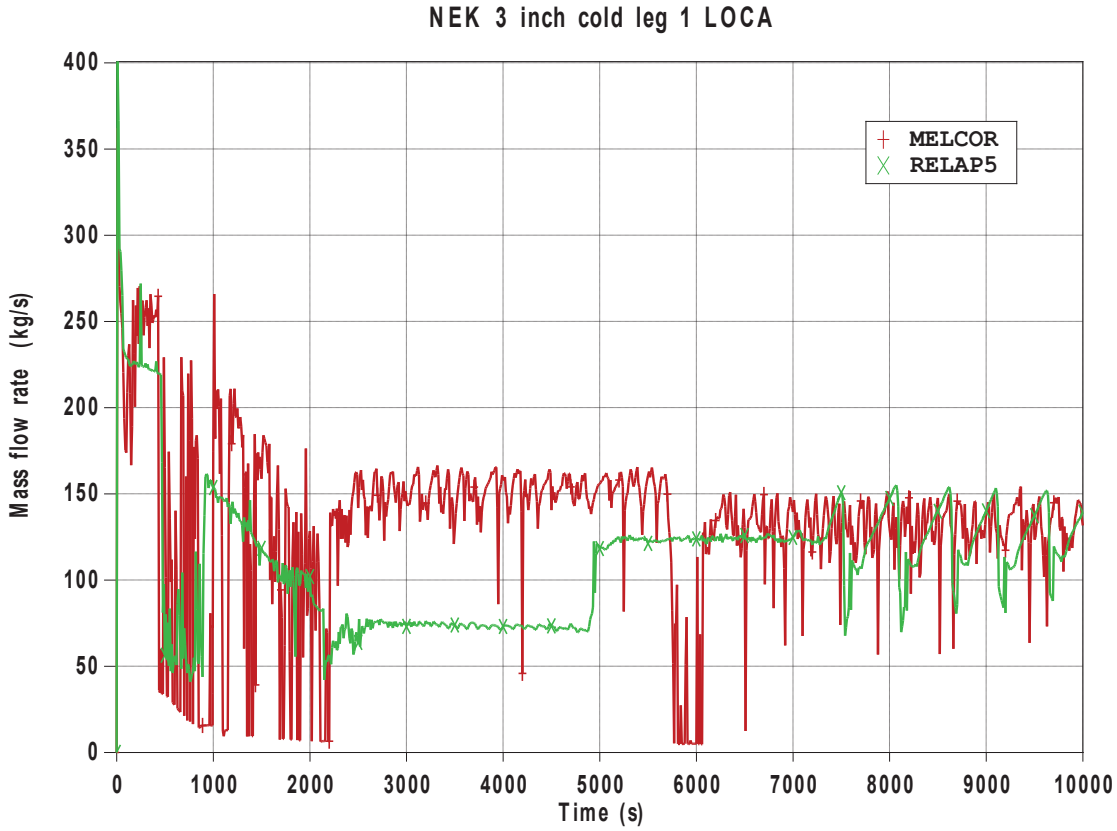


Figure 4: 3 inch cold leg 1 LOCA: Break mass flow rate

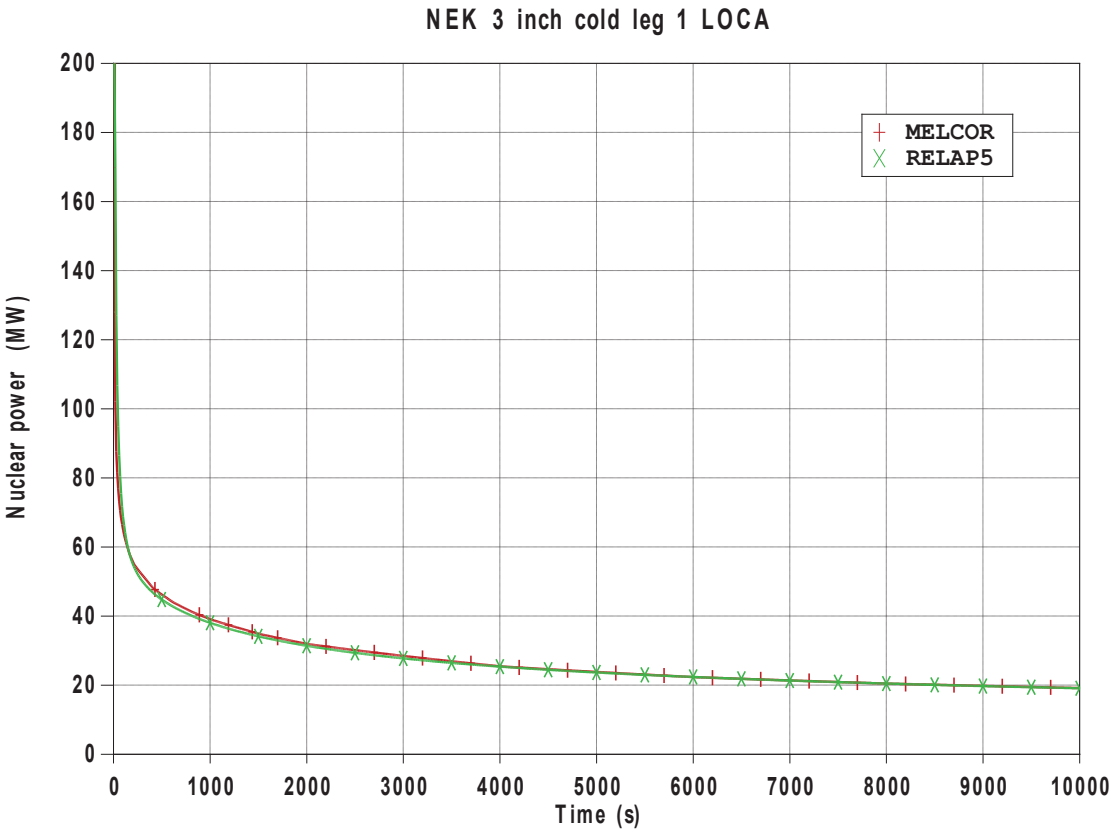


Figure 5: 3 inch cold leg 1 LOCA: Nuclear power (0-200 MW)

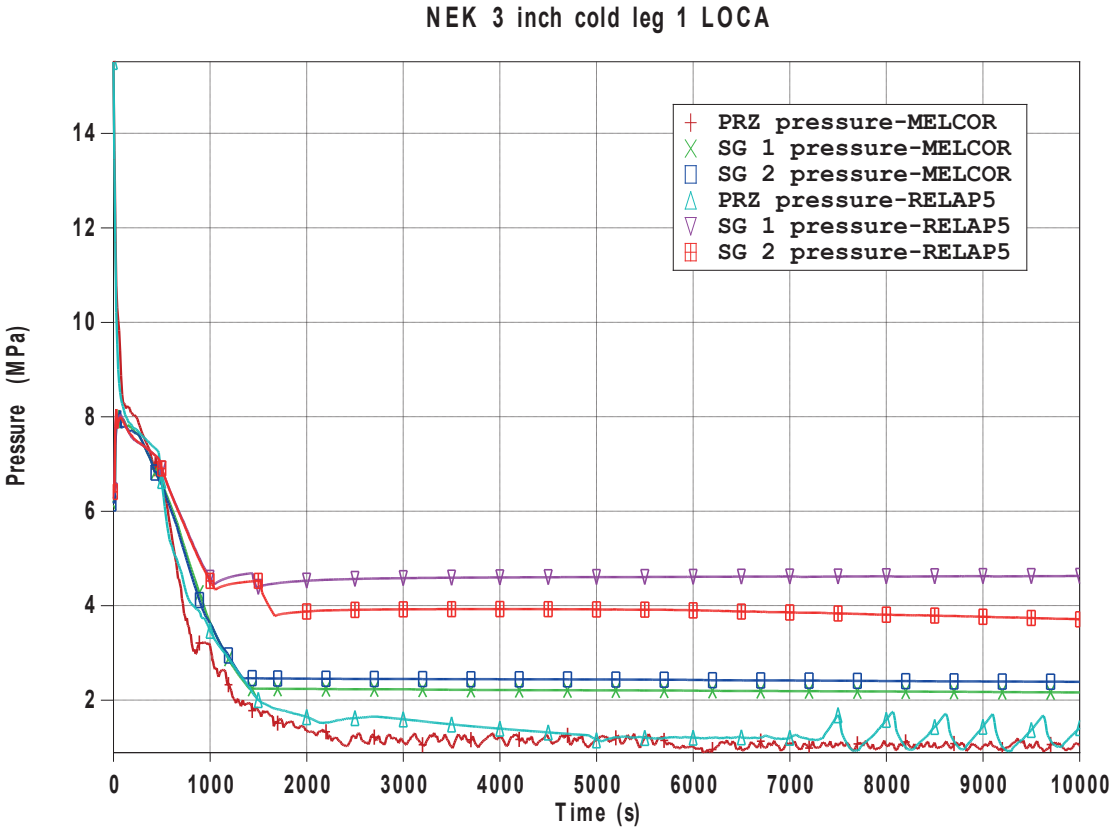


Figure 6: 3 inch cold leg 1 LOCA: Pressurizer and SG pressure

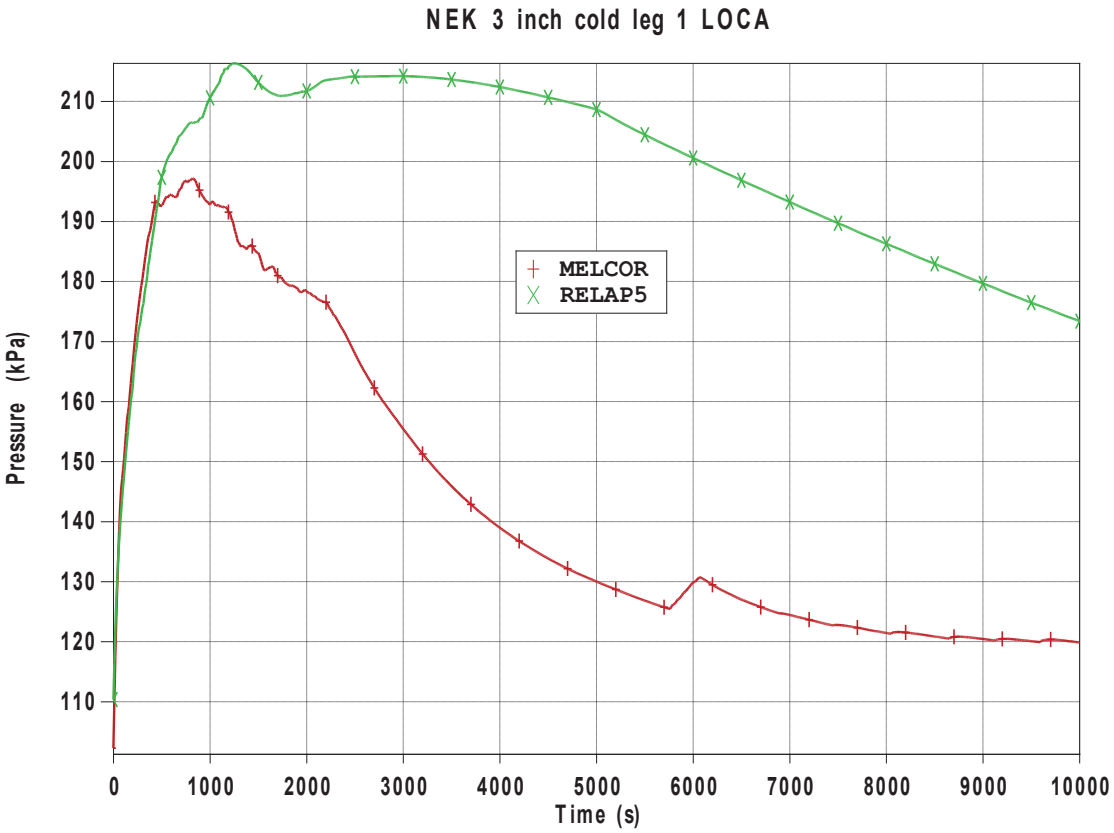


Figure 7: 3 inch cold leg 1 LOCA: Containment pressure

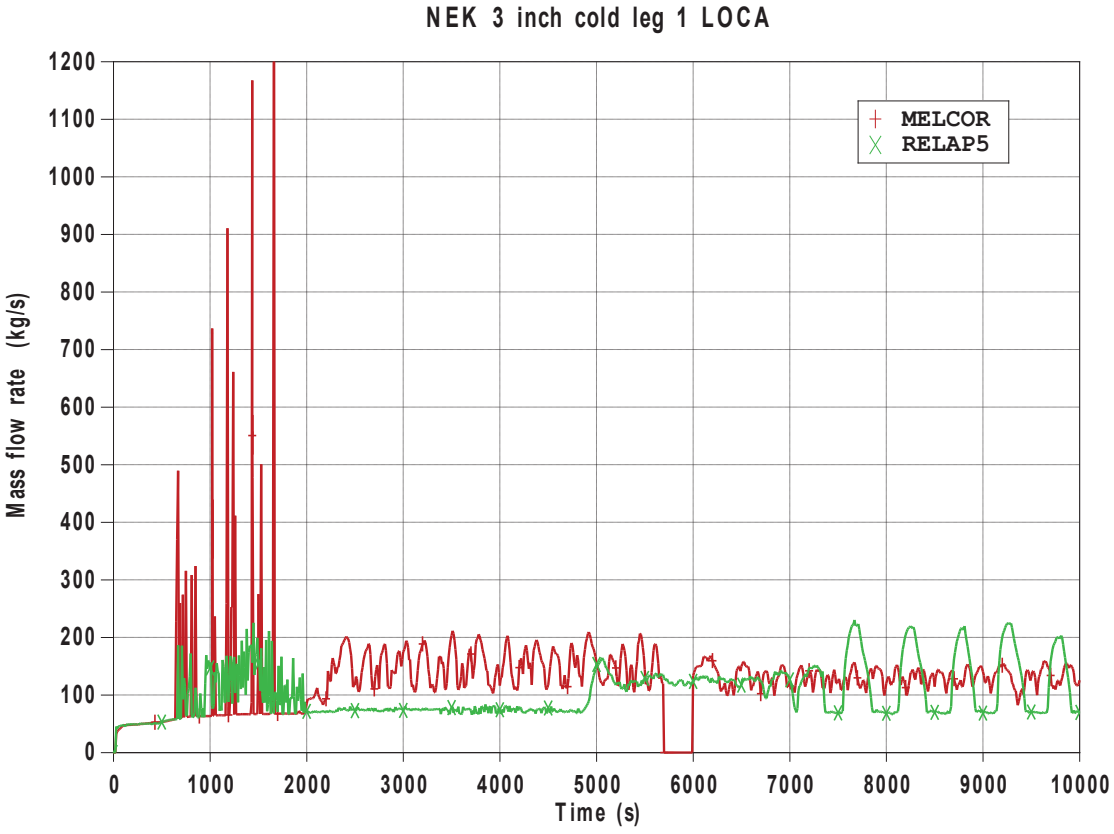


Figure 8: 3 inch cold leg 1 LOCA: ECCS flow

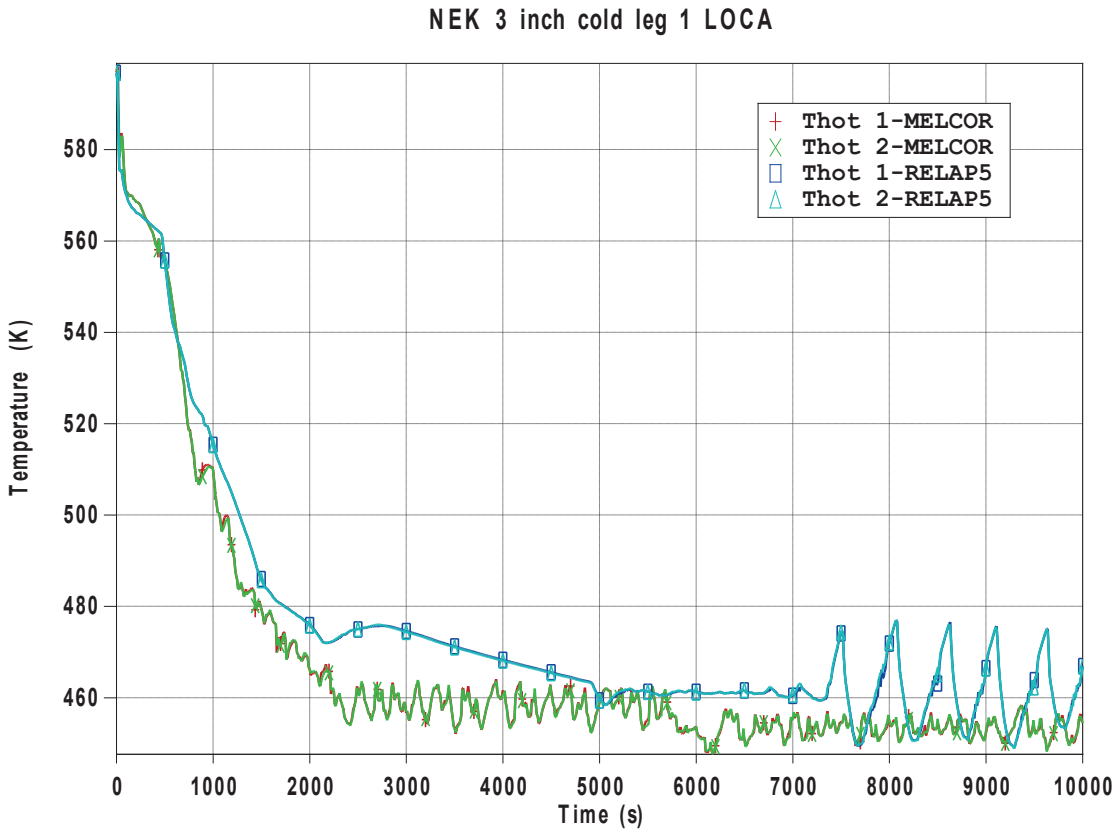


Figure 9: 3 inch cold leg 1 LOCA: RCS hot leg temperature

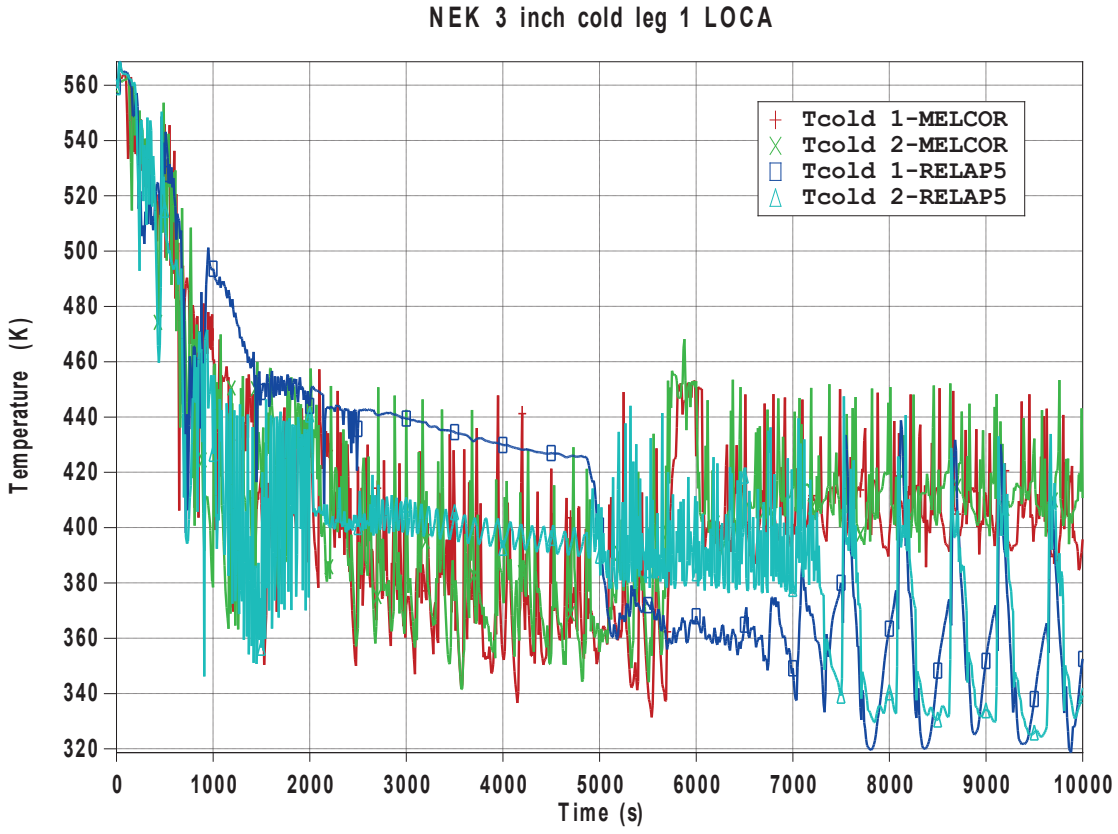


Figure 10: 3 inch cold leg 1 LOCA: RCS cold leg temperature

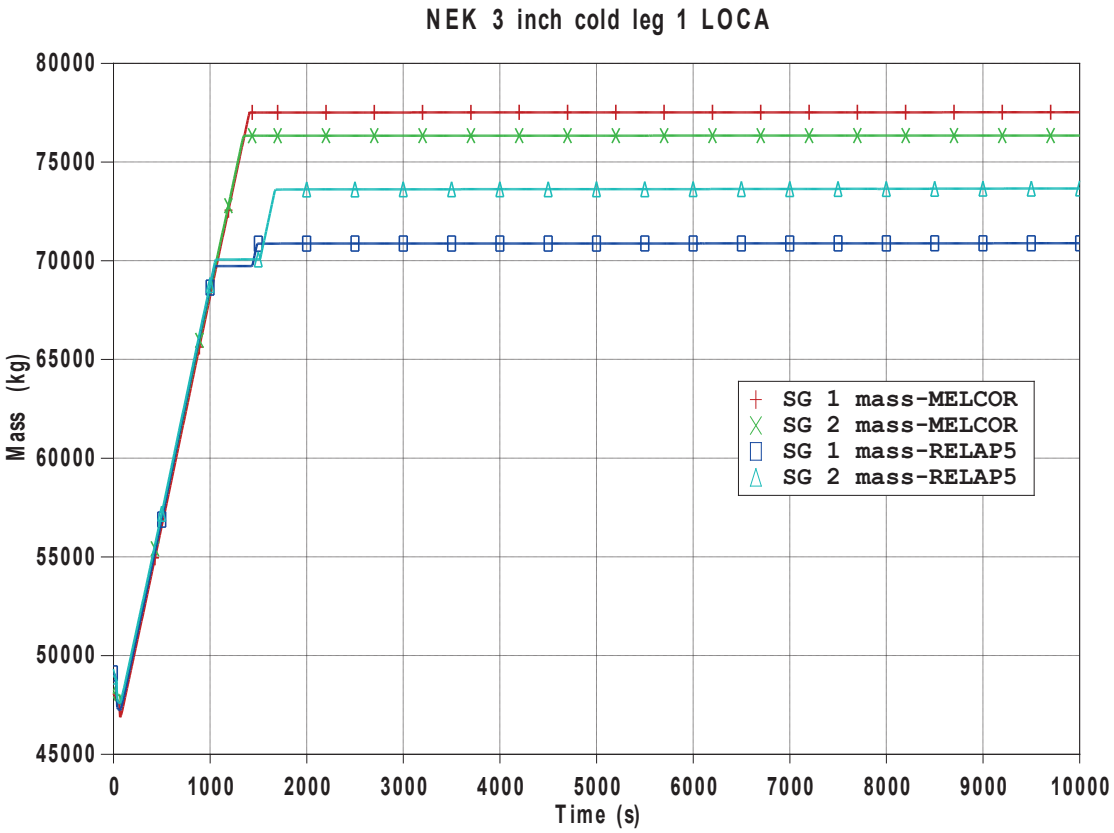


Figure 11: 3 inch cold leg 1 LOCA: SG mass

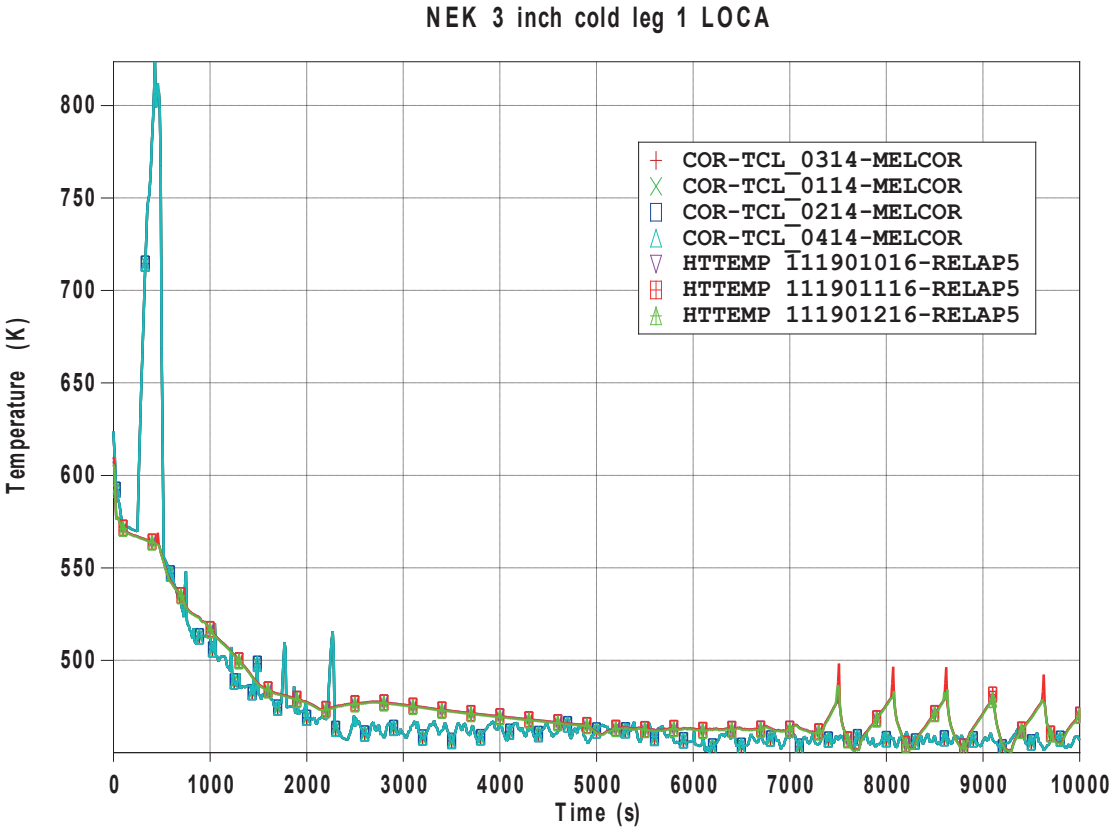


Figure 12: 3 inch cold leg 1 LOCA: Fuel cladding temperature

## 4 CONCLUSION

As a part of verification of developed MELCOR 1.8.6 model for NPP Krško, SB LOCA (3 inch cold leg LOCA) with all the engineering safety features available was analysed. The results were assessed against the RELAP5/MOD 3.3 analysis for the same transient scenario. Following conclusions can be drawn from the presented RELAP5/MOD 3.3 and MELCOR 1.8.6 analyses:

- Steady state calculation has been performed for 1000 seconds. Very small differences between the results for both RELAP5/MOD 3.3 and MELCOR 1.8.6 and the referent data were obtained.
- In MELCOR calculation, a larger break flow than in RELAP5 was obtained. This difference is mainly caused by different choked flow models in the two codes. Containment back pressure is lower in MELCOR than in RELAP5 due to fan coolers operation, but this had a small influence on break flow in MELCOR.
- Larger break flow in MELCOR has led to larger safety injection flow than in RELAP5. As a consequence, lower RCS temperatures were obtained in MELCOR than in RELAP5. After RWST depletion in MELCOR operator switched the suction of LPIS pumps to containment sump. Since the HPIS pumps did not operate further in MELCOR and the temperature of injected water is higher than the RWST temperature, cold leg temperature stabilized at a new higher value. In RELAP5 a continuous operation of HPIS pumps led to ON/OFF operation of LPIS pumps what on the other hand has caused the oscillatory behaviour of break flow as well as primary pressure and temperature.
- Core dry-out occurred for a short time period in MELCOR before the beginning of accumulator injection (max. temperature=823 K), but fuel cladding oxidation did not occur. In a long term, stable conditions were established for both codes with heat removal through the break and core inventory maintained by safety injection. The presented analyses have demonstrated the capability of available safety systems to ensure adequate core cooling as well as containment integrity.
- Similar trends of main physical parameters for both codes were obtained and the differences were identified and mainly well understood. One part of the obtained differences can be assigned to the differences in codes' physical models and numeric procedure as well as user effect. The rest of the differences can be assigned to phenomena that are transient specific; e.g., here, the break flow sustained by safety injection flow that has influence on other variables, e.g., RCS pressure and temperature.

## REFERENCES


[1] RELAP5/mod3 Code Manual Volume II: User's Guide and Input Requirements, NUREG/CR 5535-Vol II, SCIENTECH, Inc., Rockville, Maryland, June 1999.

[2] Gauntt, R. O., Cash J. E., Cole R. K., Erickson C. M., Humphries L.L., Rodriguez S. B., Young M. F., MELCOR Computer Code Manulas, Vol. 1: Primer and Users' Guide, Version 1.8.6, Sandia National Laboratories, Albuquerque, September 2005.

[3] Gauntt, R. O., Cash J. E., Cole R. K., Erickson C. M., Humphries L.L., Rodriguez S. B., Young M. F., MELCOR Computer Code Manulas, Vol. 2: Reference Manuals, Version 1.8.6, Sandia National Laboratories, Albuquerque, September 2005.

[4] NEK RELAP5/MOD3.3 Post-RTDBE Nodalization Notebook, NEK ESD TR 02/13, Revision 1, Krško 2014.

[5] NEK RELAP5/MOD3.3 Steady State Qualification Report for Cycle 29, NEK ESD TR 13/16, Revision 0, Krško 2017.

[6] NEK MELCOR 1.8.6 Nodalization Notebook, FER-ZVNE/SA/DA-TR03/16-0, 2017.

[7] NEK Steady State Qualification Report for MELCOR 1.8.6 Code, FER-ZVNE/SA/DA-TR04/16-0, 2017.

[8] S. Šadek, D. Grgić, V. Benčik, Analysis of the NPP Krško Station Blackout Accident with PAR and PCFV Using MELCOR 1.8.6 Code, FER-ZVNE/SA/DA-TR01/15-1, Revision 1, 2015.

[9] S. Šadek, D. Grgić, V. Benčik, NPP Krško Station Blackout Analysis after Safety Upgrade Using MELCOR Code, *In Proceedings of the 11th International Conference of the Croatian Nuclear Society*, Zadar, Croatia, 5-8 June 2016, pp. 058-1 – 058-13.

[10] T. Fancev, D. Grgić, NEK Containment Nodalization Notebook, NEK ESD-TR18/00, FER-ZVNE/SA/DA-TR49/00-0, Revision 0, 2000.

Journal of Energy
VOLUME 68 Number 2-3 | 2019 | Special Issue
journal homepage: http://journalofenergy.com/

# Use of Simplified Nuclear Power Plant Simulator

**Marko Čepin**
University of Ljubljana, Faculty of Electrical Engineering
Tržaška cesta 25, 1000 Ljubljana, Slovenia
marko.cepin@fe.uni-lj.si

## ABSTRACT

Simplified nuclear power plant simulator is a tool for simulating normal, abnormal and emergency operation of a nuclear power plant. The nuclear power plant with two loop pressurized water reactor and with inverted U-bend steam generators and dry containment system is considered. One loop with the pressurizer is modeled separately from the other loop without it. The model deals with 138 main input parameters related with the plant parameters such as pressures, temperatures, levels, power, setpoints, concentrations, capacities, masses and dimensionless numbers. The initial conditions contain 110 parameters. 18 initiating events from the set of internal initiating events can be considered. The objective of the work is to show the applicability of the simplified nuclear power plant simulator for modelling of the selected scenarios from a set of selected design basis accidents for the education purposes. Selected initiating events and scenarios have been identified and the data about them was collected. The simulation of the scenarios was performed. The initial conditions have been determined and the operational characteristics were modelled in sense to timely model plant automatic actuations and manual actions of plant operators. The results have been obtained in sense of time dependent curves of the main parameters of interest for showing the state of the plant itself and its systems and subsystems. The obtained results have been compared with the results of other simulations. The differences and the similarities have been discussed. The comparison of the results with some measurements and mostly with other simulations shows some degree of similarity and some differences, which differ among the parameters of interest. In general, the resulted comparisons show acceptability of simulator for education purposes.

***Keywords:*** *nuclear power plant, simulator, safety, human reliability*

## 1 INTRODUCTION

Simplified nuclear power plant simulator is a tool for simulating normal, abnormal and emergency operation of a nuclear power plant. The nuclear power plant with two loop pressurized water reactor and with inverted U-bend steam generators and dry containment system is considered. One loop with the pressurizer is modeled separately from the other loop without it. The model deals with 138 main input parameters related with the plant parameters such as pressures, temperatures, levels, power, setpoints, concentrations, capacities, masses and dimensionless numbers. The initial conditions contain 110 parameters. 18 initiating events from the set of internal initiating events can be considered. The details of the modelling within the simulation are collected in ref. [1], [2], [3].

The objective of the work is to show the applicability of the simplified nuclear power plant simulator for modelling of the selected scenarios from a set of selected design basis accidents for the education purposes.

## 2 METHODS AND MODELS

Simplified simulator contains a reduced-node approach used to model the primary coolant system. A non-equilibrium model of the pressurizer handles its normal controls by the pressurizer sprays, pressurizer heaters and pressurizer relief valves. It allows sudden changes of related parameters and extreme conditions such as two-phase mixture in the reactor core and pressurizer filled rigid with water. The steam generators (two of them in the model) are modeled as homogeneous equilibrium two-phase volumes. Heat transfer from the primary system (reactor coolant system) to the secondary system (power conversion system) is treated rigorously during both forced and natural circulation. A point kinetics model is used for the reactor power calculation. The model of large containment is included. Major plant control systems are modelled. Improved heat transfer correlation for the steam generators is included. The discharge rates of fluids due to breaks use typical critical flow models. A mechanistic model of the reactor coolant flow covering both forced and natural circulation provides temperature distribution in the primary coolant. The conditions of the containment are calculated based on a homogeneous equilibrium model with participation of non-condensable air and hydrogen. If the core would be exposed to steam for extended period of time, the core may become overheated and melted consequently. If the zirconium in the cladding reacts with steam then a calculated amount of hydrogen is generated. The mass and energy balance equations with correlations in momentum and heat transfer are solved for all control volumes simultaneously. The progress of transients is dealt with by using Euler integration over every time step increment [1], [2], [3].

### 2.1 Work procedure

Selected initiating events and scenarios have been identified and the data about them was collected. The initial conditions have been determined and the operational characteristics were modelled in sense to timely model plant automatic actuations and manual actions of plant operators. The simulation of the scenarios was performed. The timing of operator actions was studied for some of the scenarios in order to assess the time window for the operator action before the core gets damaged. The criteria for the core damage is exceedance of the temperature in the reactor core of 923 K for more than 30 minutes or exceedance of the temperature of the core of 1348 K [4].

For some of the simulations, the reference literature has been collected and compared [5], [6], [7], [8], [9].

The small loss of coolant accident, the steam generator tube rupture and the steam line break are selected for presentation of the results.

### 2.2 Small loss of coolant accident

Initial conditions for the simulation before t=0 were the following: reactor was at full power, 1800 MWt, which suits 600 MW electrical for pressurized water reactor with two loops. The end of fuel cycle is assumed. The location of small loss of coolant accident is in hot leg towards the steam generator A. The extent of the break was 2 inch, where the considering break relate to affected area of 20.25 $cm^2$ (the simulation software requires the input of the area of the break). It is assumed that the break occurs instantly. Different timings of operator establishing high pressure safety injection are compared assumed that it does not start automatically. When started, both pumps are at times after 30 min, after 40 min, after 50 min and after 1 hour started instantly.

## 2.3 Steam generator tube rupture model

Initial conditions for the simulation before t=0 were the following: reactor was at full power, 1800 MWt. The end of fuel cycle is assumed. The 100 % break of one tube of steam generator A is assumed ruptured instantly.

## 2.4 Steam line break model

Initial conditions for the simulation before t=0 were the following: reactor was at full power, 1800 MWt. The end of fuel cycle is assumed. The location of steam line break is outside of containment. The extend of the break was varied as diameter of the break: 8 inch, 9 inch, 10 inch and 11 inch, where the considering breaks relate to affected area of 324.1 $cm^2$, 410.2 $cm^2$, 506.4 $cm^2$ and 612.8 $cm^2$, respectively. It is assumed that the break occurs instantly.

# 3 ANALYSES AND RESULTS

The results have been obtained in sense of time dependent curves of the main parameters of interest for showing the status of the plant itself and its systems and subsystems.

## 3.1 Small loss of coolant accident – results

The results of timely response of 92 parameters was collected. The focus was placed to the water level in the core, high pressure safety injection flow (which gives the timing of success of the related operator action), cladding temperature and the void of reactor coolant system.

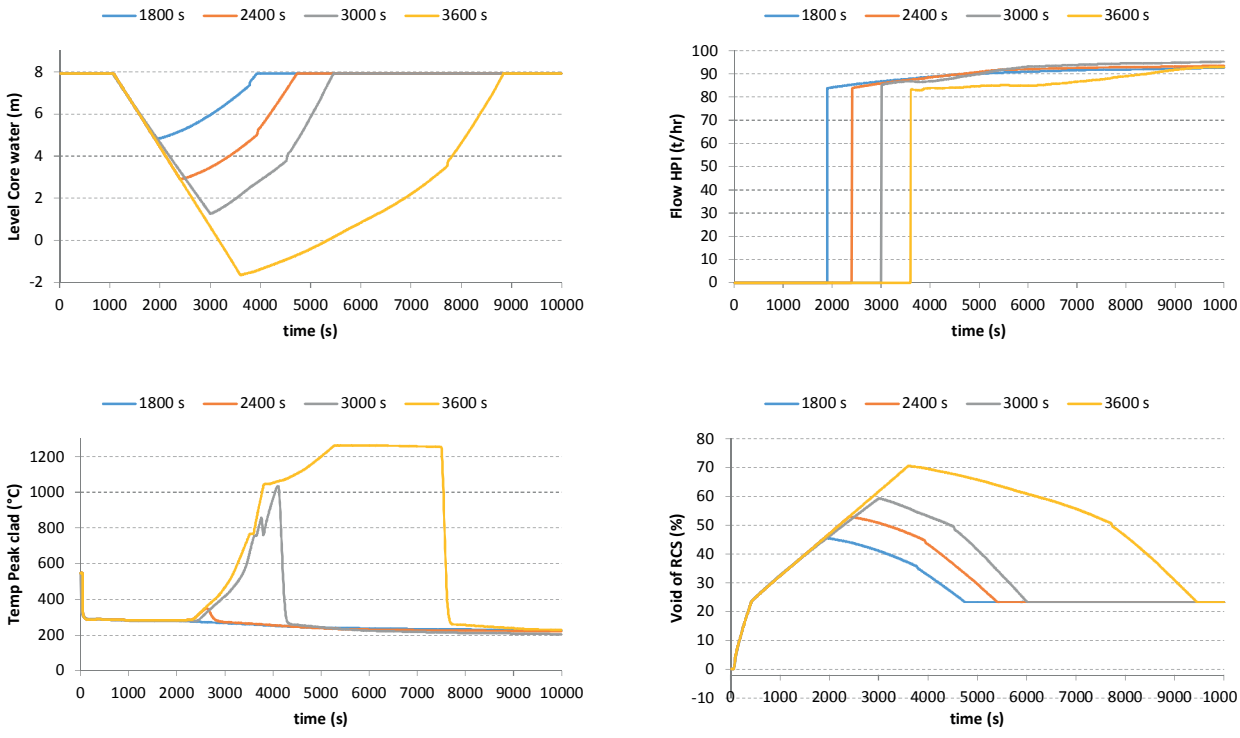


Figure 1: Small loss of coolant accident, 2 inch, timing of establishing high pressure safety injection manually (after 1800 s, after 2400 s, after 3000 s and after 3600 s) vary for 4 cases as indicated at legend, parameters of interest: water level in the core, high pressure safety injection flow (which gives the timing of success of the related operator action), cladding temperature and the void of reactor coolant system

Figure 1 shows the results, which indicate that the lack of the high pressure safety injection for 40 minutes does not result in core damage if soon after that time the high pressure safety injection is restored. The amount of water in the system is assumed rather large (reactor coolant system volume without pressurizer is assumed 180 $m^3$).

Such sensitivity curves are interesting for strengthening the knowledge about the mutual cross connection of various plant parameters and for feedback to engineering students about behaviour of the plant systems, which can be obtained relatively quickly (the simulation runs 16 times faster than the real time).

Such sensitivity curves may help in determining the operator time windows which are in addition to the determination of the time needed for operator action needed for evaluation of human error probability. The time available equals the difference between the time window and the time needed for the operator action. The larger is the time available, the smaller is the human error probability [4]. The ref. [4] focused to consideration of timing of auxiliary feedwater system actuation if the automatic action has failed.

### 3.2 Steam generator tube rupture - results

The focus of the 92 observed parameters was placed to the reactor coolant system pressure, high pressure safety injection system flow, rupture mass flow and steam generator levels.

The results depend largely on the amount and the timing of high pressure safety injection to the primary system. The sensitivity analyses for different simulations with different timing of faulted steam generator isolation and injecting water flow revealed difficulties with steam generator level, which can be raised in faulted steam generator far more than expected. Our simulations revealed much larger reactor coolant system pressure decrease and consequently smaller safety injection flow and rupture flow compared to ref. [6] in some of the simulations. Although, if the operator actions are done in the appropriate way the transient is more comparable to the literature [10].

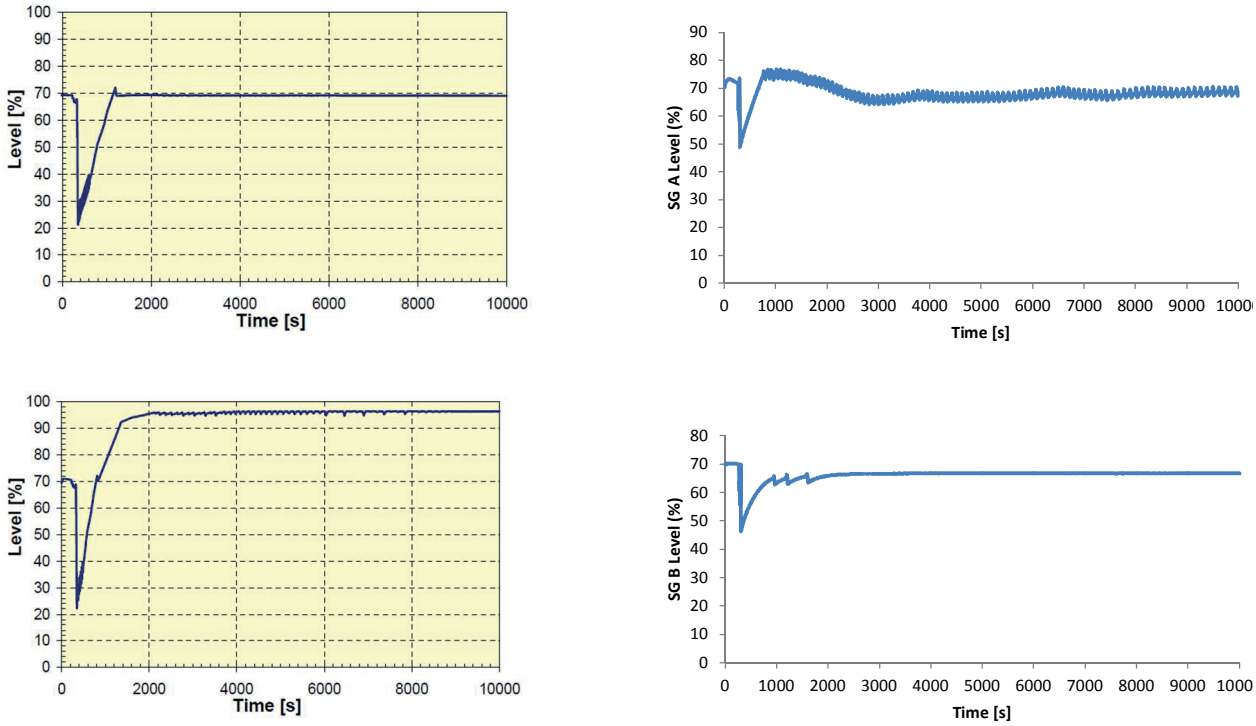


Figure 2: Steam generator tube rupture – steam generator levels, compared with ref. [6]

### 3.3 Steam line break - results

The parameters such as pressurizer pressure, core thermal power, departure from nucleate boiling, primary side coolant temperatures, steam generator flow rate are selected for presentation of the results of the simulation and for the comparison with the reference literature [5]. The steam line break simulation results differ by the timing of automatic events, which depends on the size of the break. Reactor trip due to high neutron flux (stated at 118 %) occurs at 24 s (116 % of power), 13 s (114 % of power), 9 s (111 % of power) or 7 s (107 % of power) for 8 inch, 9 inch, 10 inch or 11 inch break respectively. Reference [5] reports the reactor trip at 121 % of reactor power after 14.5 s, but the power of the plant is significantly higher 2815 MW of thermal power and two cold legs per one hot leg of each loop, while our plant has one cold leg per one hot leg within each loop.

The following figures show comparison of performed simulations for 9 inch break with the reference [5]. The selection of parameters on those figures was made based on the figures shown in the literature to enable comparison. Figure 3 shows pressurizer pressure. The pressure decreases slowly and with higher rate after the plant trip, similarly as in reference [5]. Figure 4 shows total core power, which increases firstly, and decreases after reactor trip. The power curve is similar as in reference [5].

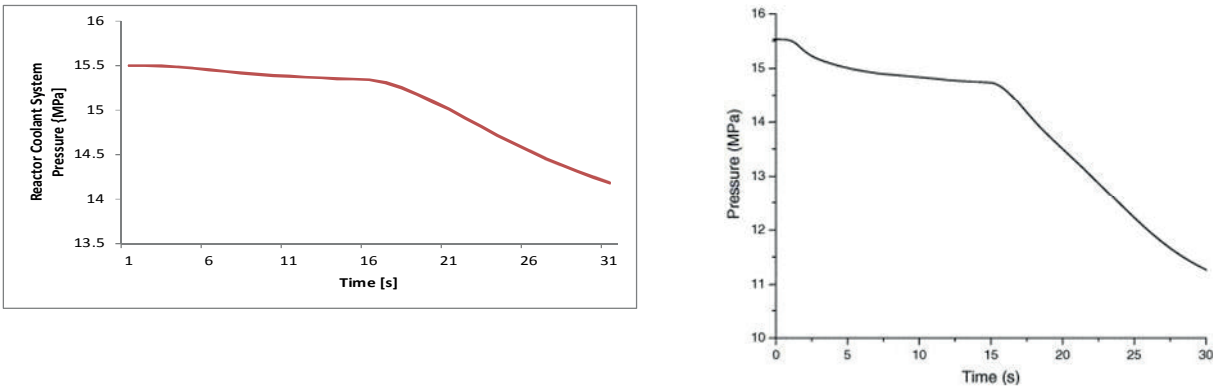


Figure 3: Steam line break outside of containment - pressurizer pressure, comparison with ref. [5]

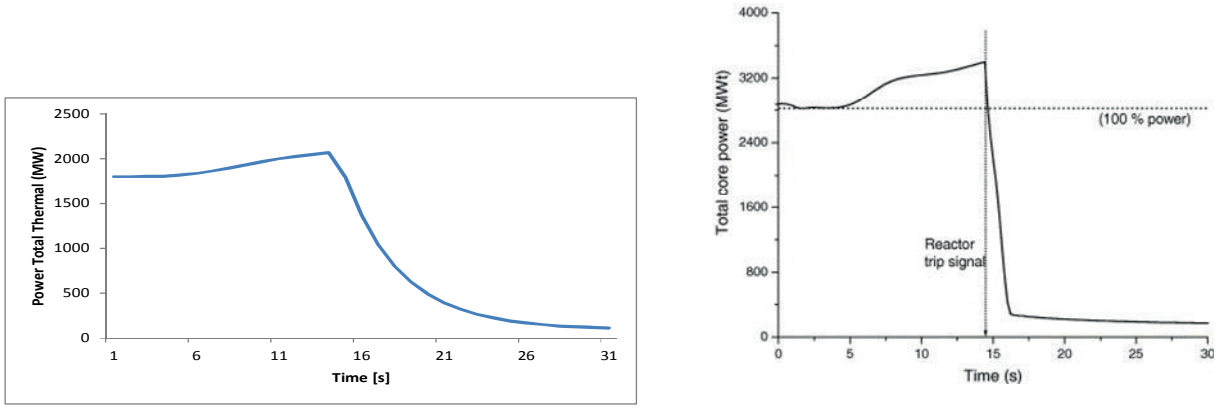


Figure 4: Steam line break outside of containment - power, comparison with ref. [5]

Figure 5 shows minimum departure from nucleate boiling (DNBR), which decrease firstly and increase fast after reactor trip. The curve is similar as in reference [5]. Figure 6 shows primary side coolant temperatures. The hot leg temperatures at our simulations decrease slowly after the reactor trip than in reference [5]. The cold leg temperature at our simulations decrease slowly compared to reference [5].

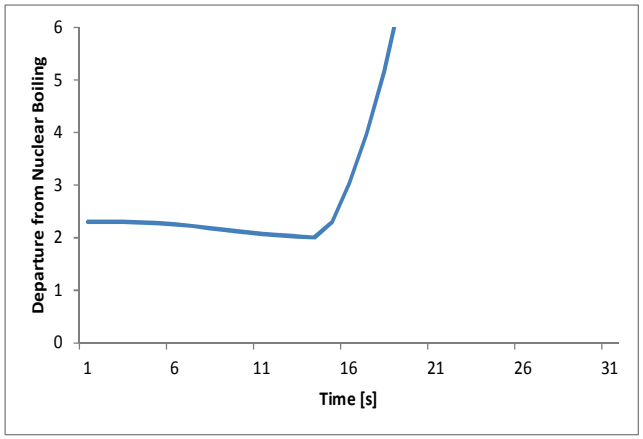


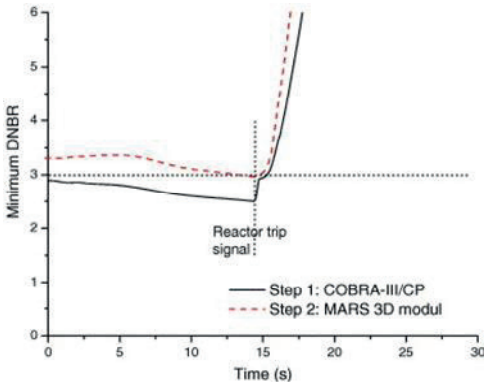


Figure 5: Steam line break outside of containment - minimum DNBR, comparison with ref. [5]

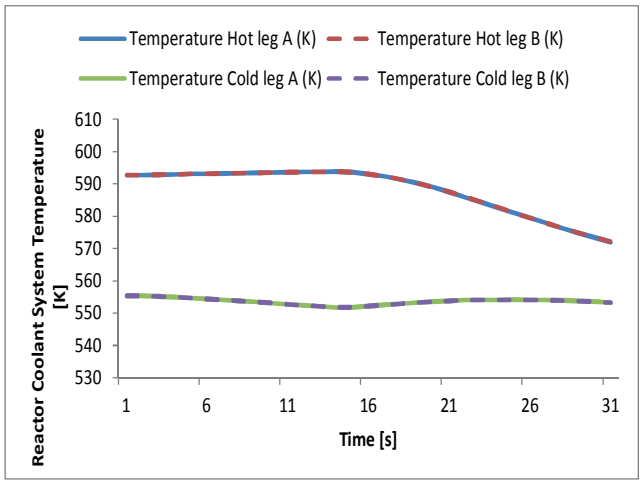


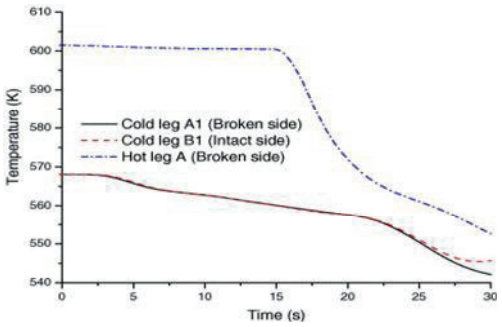


Figure 6: Steam line break outside of containment - primary side coolant temperatures, comparison with ref. [5]

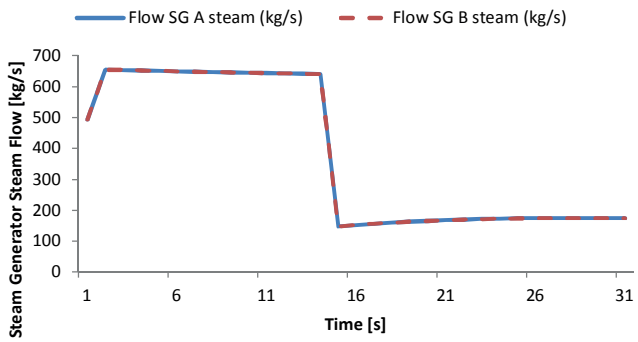


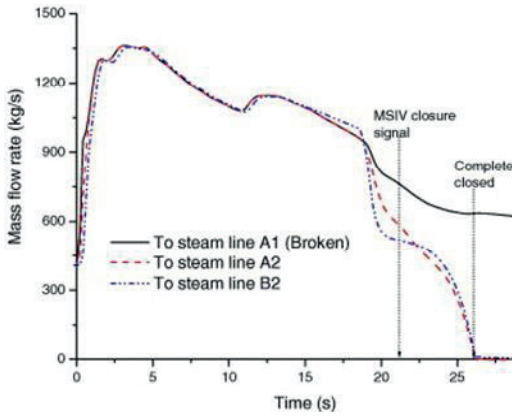


Figure 7: Steam line break outside of containment - steam flow rate at the steam generator exit, comparison with ref. [5]

Figure 7 shows steam flow rate at the steam generator exit. Our simulations shows generally more flat curve, which show significant reduction of flow shortly after trip and final reduction after longer time (see Figure 8) if compared to the ref. [5]. Both times largely depends on the size of the break, which is in more details shown on Figure 8.

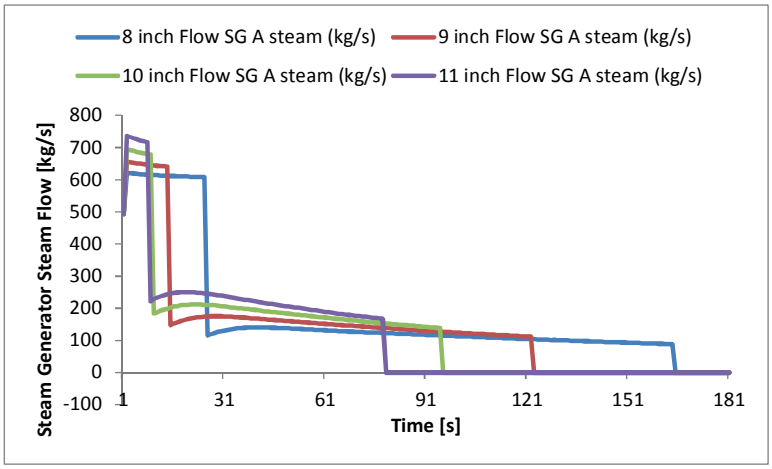


Figure 8: Steam line break outside of containment - steam flow rate at the steam generator exit, extended time to observe the closure time of the main steam isolation valve

Several other simulations of other initiating events were performed [10], [11], including various losses of coolant accidents [12] and the scenario as happened at Three miles island in 1979.

The overall impression about the results obtained is positive. The simplified simulator is simplified enough that engineering students can use it together with studying the theory of reactor systems and their behaviour and can quickly get the results (several times faster than the real time). The differences regarding the simulator results and the scenarios timing from the safety analysis report can differ significantly for some of the parameters and can be very similar for other parameters, so the scenarios need to be carefully selected and prepared. But general connections between parameters of interests support the initial expectation about usability of the simulator.

## 4 CONCLUSION

The simplified nuclear power plant simulator was tested in sense of observing the timely behaviour of the plant parameters at various plant conditions. Selected initiating events were analysed and the related plant behaviour was observed accordingly and some simulations were compared with the references reporting similar scenarios. Small loss of coolant accident, steam line break and steam generator tube rupture have been selected for analysis, in spite of the fact that several other simulations have been performed. In general, the resulted comparisons show acceptability of simulator for education purposes.

## REFERENCES

[1] L. C. Po, Analysis of the Rancho Seco Overcooling Event Using PCTRAN, Nuclear Science & Engineering, 98, 154-161, 1988.

[2] L. C. Po, IAEA Activities in Advanced Reactor Simulation, paper S1, the Fifth International Topical Meeting on Nuclear Thermal Hydraulics, Operations and Safety (NUTHOS-5), Beijing, China, April 14-18, 1997.

[3] L. C. Po, PCTRAN-Personal Computer Transient Analyzer For a Two-loop PWR and TRIGA Reactor, International Atomic Energy Commission, Micro-Simulation Technology, 2011.

[4] A. Prošek, M. Čepin, Success criteria time windows of operator actions using RELAP5/MOD3.3 within human reliability analysis, Journal of loss prevention in the process industries, 2008, vol. 21, no. 3, p. 260-267.

[5] Jae Jun Jeong, Won Jae Lee, Bub Dong Chung, Simulation of a main steam line break accident using a coupled ‘‘system thermal-hydraulics, three-dimensional reactor kinetics, and hot channel analysis’’ code, Annals of Nuclear Energy, Volume 33 (9), June 2006, Pages 820-828.

[6] Iztok Parzer, Boštjan Končar, SGTR Analysis for Krško Full Scope Simulator Validation, International Conference Nuclear Energy for New Europe, Institut Jožef Stefan, Bled 2005.

[7] J. L. Rempe, D. L. Knudson, Instrumentation Performance During the TMI-2 Accident, Idaho National Laboratory, 2015, str. 1-4.

[8] J. K. Hohorst, S. T. Polkinghorne, L. J. Siefken, C. M. Allison, C. A. Dobe, TMI-2 analysis using SCDAP/RELAP5/MOD3.1, Idaho National Engineering Laboratory, 1994, str. 25-26.

[9] C. M. Allison, J. K. Hohorst, An assessment of effectiveness of core exit temperatures with respect to PWR core damage state using RELAP/SCDAPSIM/MOD3.4, Nuclear Engineering and Design, Vol. 238, Issue 7, julij 2008, str. 1547-1560.

[10] B. Štih, Simulacija zloma cevi uparjalnika v jedrski elektrarni, Diplomsko delo, Univerza v Ljubljani, 2013.

[11] S. Kastrevc, Simulacija zloma parovoda v jedrski elektrarni, Diplomsko delo, Univerza v Ljubljani, 2013.

[12] M. Macario, Evaluation of Simplified Nuclear Power Plant Simulator in Case of a Main Steam Line Break, University of Coimbra, 2016.

Journal of Energy
VOLUME 68 Number 2-3 | 2019 | Special Issue
journal homepage: http://journalofenergy.com/

# Comparing Analysis of Loss of Coolant Accident on Bethsy Facility with Apros 6.05 and 6.06

**Klemen Debelak, Luka Štrubelj**
*GEN energija, d.o.o*
Vrbina 17, 8270 Krško, Slovenija
klemen.debelak@gen-energija.si, luka.strubelj@gen-energija.si

## ABSTRACT

In this paper, the comparison of analysis of international standardized problem ISP 27 using two versions of APROS process simulation software 6.05 and 6.06 is presented. Numerical simulation of experiment Bethsy 9.1b, also known as ISP 27 was performed on a scaled down model of a three loop, 900 MWe Framatome PWR. In the test a small LOCA, with 2-inch cold leg break, combined with High pressure Injection System (HPIS) failure is simulated. State oriented approach, which requires operators to start an Ultimate Procedure were used. Model was first built in APROS 6.05 using standard modules in order to describe the volumes, heat structures and regulation of the test facility and was then exported to APROS 6.06.

The results from both versions showed all the processes such as loop seal clearing, core uncover and rise of cladding temperature and other processes taking place in the experiment were in a good agreement with experimental data. However even though results were similar some differences were noticeable. The differences in core cladding temperature, time integrated break mass flow, core liquid level and pressurized pressure were analysed in more detail in this paper.

***Keywords:*** *APROS, Loss of Coolant Accident, Bethsy, ISP 27*

## 1 INTRODUCTION

Betsy is an integral test facility which was constructed for research of PWR accident transients. It is placed at the Nuclear Center of Grenoble in France. The Bethsy design aims to contribute to validating computer safety code and to check the relevance of the physical bases of the Emergency Operating Procedures (EOP). It represents a scaled down Framatome PWR, with three loops and thermal power of 2775 MW (900MWe) [1].

In this paper, the comparison of results of simulation of the test 9.1 b, using APROS 6.05 and APROS 6.06 computer code are presented. The test 9.1 b (ISP-27) involves a 2-inch cold leg break, combined with the High Pressure Injection System (HPIS) failure. The model for the facility was first built in APROS 6.05 and was latter exported to APROS 6.06. The expected differences in results were investigated in more detail.

## 2 BETHSY MAIN FEATURES

BETHSY facility is a 3-loop replica of a reference 2857 MW thermal (900 MWe) FRAMATOME PWR, with following characteristics [2], [3]:

- 428 heater rod core simulation, electrically heated,
- 3 secondary steam generators designed with 34 U-tubes of original dimensions,
- primary system pressure up to 17.2 MPa, secondary side pressure up to 8 MPa,

• initial power level of test section allows for 10 % of scaled nominal full power,
• heat losses controlled by external heater system,
• HPIS and LPIS available (HPIS not available in test 9.1b).

Scaling Information:
• power and volume scaling is 1/100,
• full length core simulator, decay power level and nominal flow rates scaled are 1/100,
• geodetical elevations of all components preserved 1/1 to simulate gravitational head
• loop piping diameter of hot legs dimensioned to preserve FROUDE number criterion of full size plant

## 3 APROS MODEL DESCRIPTION

The thermohydraulcal model consists of: 760 Points, 60 Nodes, 71 Branches, 159 Heat structures X (1D heat structures), 48 Heat pipes (Thermal-hydraulic large volumes divided into many smaller volumes in one direction with pipe walls heat structures), 18 Pipes (Thermal-hydraulic large volumes divided into many smaller volumes in one direction), 38 Heat transfer modules (Heat transfer coefficients defined), 3 pumps with defined head curve, 5 valves, 2 Accumulators and 3 Steam generators. Volume is represented by 293 volumes with 6-equation model.

**Reactor pressure vessel**

The volumetric model of Reactor pressure vessel was built using nodes and branches. Wall materials are represented with HEAT_STRUCTURE_X module. Core, which are electrical heaters at Bethsy facility are also represented with HEAT_STRUCTURE_X. Their relative power is regulated according to events and time tables in order to follow the power of the experiment.

**Reactor cooling system**

Reactor cooling system consists of three loops. In comparison to loop one, loops two and three have accumulator and low pressure injection, whereas pressurizer is connected to loop one. The break is located 332 mm downstream of the outlet flange of the pump in loop one. For the break, which is represented by a branch, critical flow feature was enabled. Reactor coolant pumps are represented with common pipe module in combination with calculation level modules for electrical motor and pump. Heat structures are simulated within heat pipes and are connected with heat transfer coefficient module to point that represents environment. Accumulators are modelled using ACCUMULTOR module and are using Calculation mode 1 of node velocity.

**Pressurizer**

Pressurizer volumetric model was built using nodes and branches. Wall materials and electrical heaters are represented with HEAT_STRUCTURE_X module. Spray system is not modelled.

**Steam generator**

The model consist of three advanced steam generator modules. Heat structures (except for u-tubes) are modelled using HEAT_STRUCTURE_X. Due to limitations of the module advanced steam generator additional two branches and one node was added to simulate upper part of the node. This was done in order to minimize the difference of volumes that are above the riser, compared to the real Bethsy steam generator.

**Feedwater and auxiliary feedwater**

Feedwater and auxiliary feedwater are modelled using pipes and pipes with heat structures.

**Main steam and steam dump**

Main steam and steam dump are modelled using pipes, pipes with heat structures and basic valves.

**Regulation**

Regulation was built in order to initiate and simulate events in timely manner that is in compliance with experiment. There are three separate automations: for pressurizer power, for core

power and one that is responsible for controlling all other system. The last is responsible for control of feedwater, auxiliary feedwater, accumulator injection, reactor coolant pump trip, low pressure injection, main steam, steam dump and safety valves on main steam.

Regulation for pressurizer power is used only for achieving steady state. After the simulation start the pressurizer heaters are switched off. Core power regulation enables to simulate decay heat according to the table that was obtained during experiment [2], [3], [4].

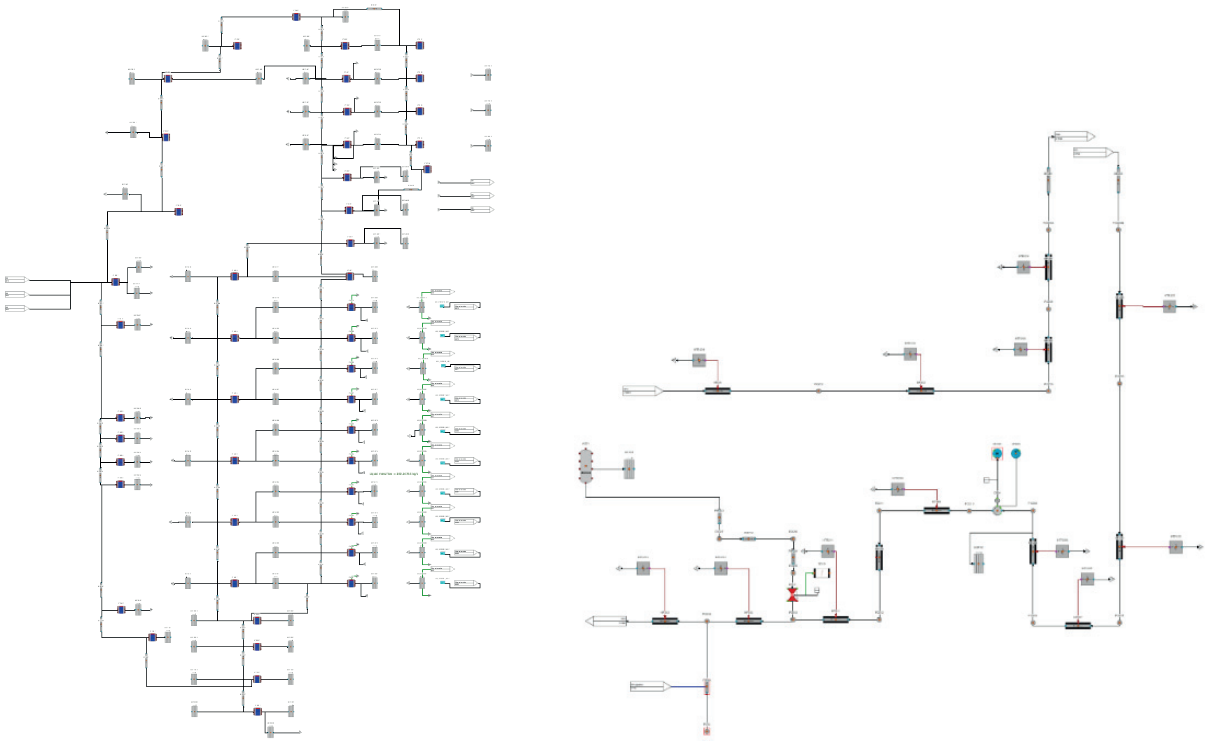

Figure 1: Reactor pressure vessel (left); Cooling loop 2 (right)

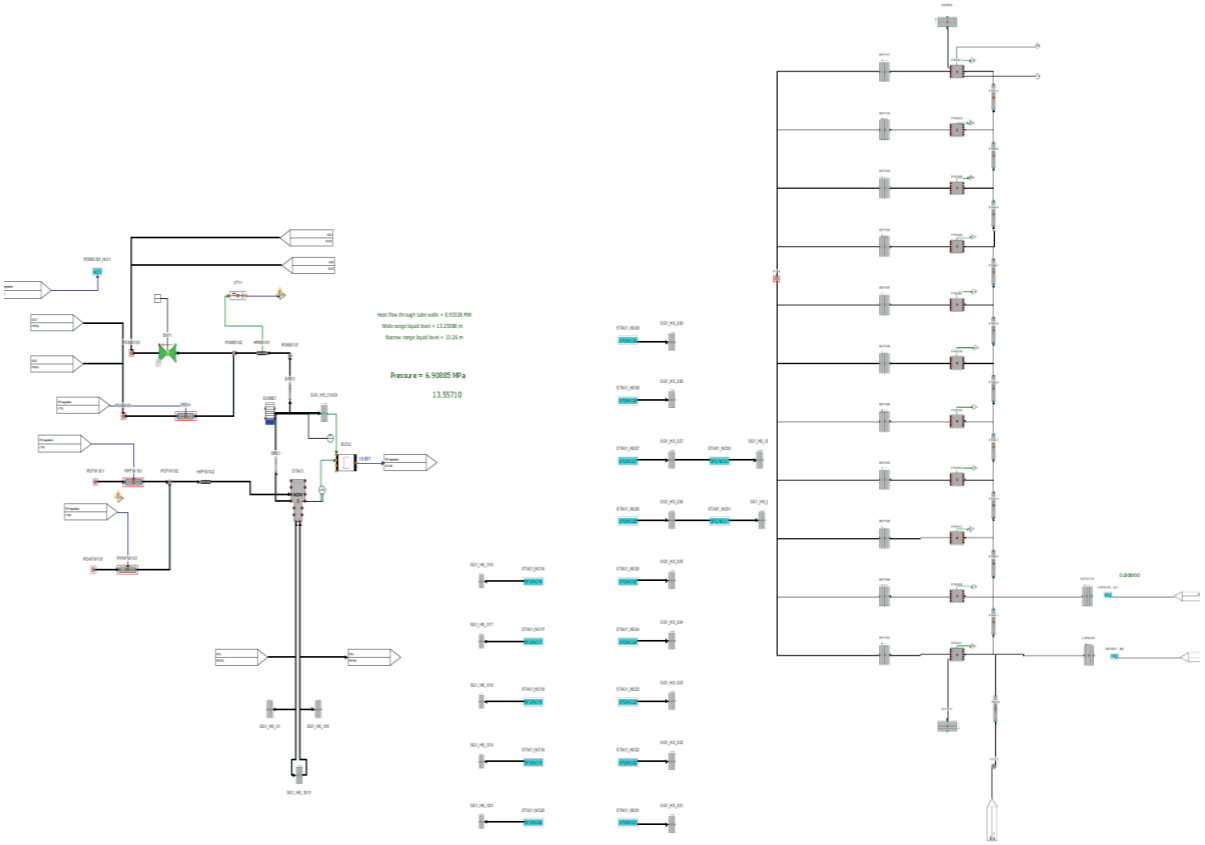

Figure 2: Steam generator with main steam, Feedwater and Auxiliary feedwater system (left); Pressurizer (right)

The verification of APROS model was made on heights, volumes and mass of heat structures.

## 4 BETHSY 9.1B TEST DESCRIPTION

Test 9.1 b is categorized as multiple failure transient (Beyond Design Basis Accident), and is involved in Accident Management studies. According to newer (IAEA, EUR) terminology the transient is categorized as Design Extension Condition A – complex sequence without core damage. The test begins with a 2 inch cold leg break, while high pressure safety injection system (HPIS) is assumed to be unavailable. This leads to a large core uncovery and fuel heat-up, requiring the implementation of an Ultimate Procedure.

In the 9.1b scenario, the start of the procedure is delayed. When the maximum heater rod cladding temperature reaches 723 K (trigger criterion), the 3 steam generator steam dumps to atmosphere are fully opened (condenser is unavailable). This cause the depressurization of the primary coolant circuit, up to the accumulator injection threshold, then to LPIS actuation. The test ends as soon as a safe state of the primary coolant circuit is recovered, i.e. when the conditions required for the actuation of the Residual Heat Removal System (RHRS) are obtained [1].

Electrical trace heating in experiment, located on almost every component and piping of the primary coolant system is provided until accumulator injection starts. In model trace heating is considered in the way heat transfer to the environment starts after injection (before there is no heat transfer to the environment).[2]

## 5 COMPARISON OF RESULTS

The model was first brought to steady state in APROS 6.05 and was in good agreement with the experimental data. When imported in APROS 6.06 the model did not show any deviation from the previous version.

The simulation results of both version of APROS were in a good agreement with the experimental data. Comparison of timing of major events is shown in Table 1. Processes such as loop seal clearing, core uncover and rise of cladding temperature, which are taking place in the experiment can also be seen in both simulations. However a minor deviations of results from experimental data can be seen in both cases (Figure 3, Figure 4, Figure 5, Figure 6, Figure 7 and Figure 8). The simulation results are almost identical to the time of maximum core clad heatup (Figure 5) and minimum primary mass inventory (Figure 8). After the behaviour is a bit different.

Table 1: Table of events

| Events | Time | | |
|---|---|---|---|
| | Experiment | APROS 6.05 | APROS 6.06 |
| Transient initiation : Break opening | 0 s | 0 s | 0 s |
| * P+P = 13.1 MPa : Scram Signal (AU) | 41 s | 32 s | 32 s |
| Pressurizer is empty | 50 s | 82 s | 82 s |
| * P+P = 11.9 MPa : Safety Injection Signal (IS) | 54 s | 62 s | 62 s |
| Main feedwater off, turbine bypass | 59 s | 67 s | 67 s |
| Core power decay starts (17 s after AU signal) | 58 s | 49 s | 49 s |
| Auxiliary feedwater on (30 s after IS signal) | 82 s | 92 s | 92 s |
| Pump coastdown starts 300 s after IS signal | 356 s | 362 s | 362 s |
| Start of the first core level depletion | 1830 s | 1800 s | 1800 s |

| | | | |
|---|---|---|---|
| First loop seal clearing in loop 2 | 1944 s | 1874 s | 1874 s |
| Start of the second core uncovery | 2180 s | 1968 | 1964 s |
| • Ultimate procedure initiation by | 2562 s | 2453 | 2453 s |
| atmospheric steam dump opening (3 SG) | 2567 s | 2458 s | 2458 s |
| Loop seal reformation in loop 2 | 2750 s | 2510 s | 2510 s |
| • P+P = 4.2 MPa : Accumulator injection starts | 2962 s | 2890 s | 2894 s |
| Primary mass inventory is minimum | 2970 s (400 kg) | 2890 s (465 kg) | 2890 s (465 kg) |
| Second loop seal clearing in loop 2 | 3040 s | 3036 s | 3041 s |
| Maximum core clad heatup | 3053 s (995 K) | 3013 s (1031 K) | 3027 s (1038 K) |
| Loop seal reformation in loop 2 | 3680 s | 3593 s | 3605 s |
| • P+P = 1.5 MPa : Accumulator isolation | 3831 s | 3817 s | 3849 s |
| * P+P = 0.91 MPa : LPIS starts | 5177 S | 5209 s | 5357 s |
| * End of the test (RBRS stable operating condition) | 8200 s | 8537 s | 8566 s |

The pressurizer pressure is almost identical with both versions of results. As it can be seen from Figure 3 the simulation results are in good agreement with the experiment. Only the pressure drop between time 500 s and 1100 is not big enough.

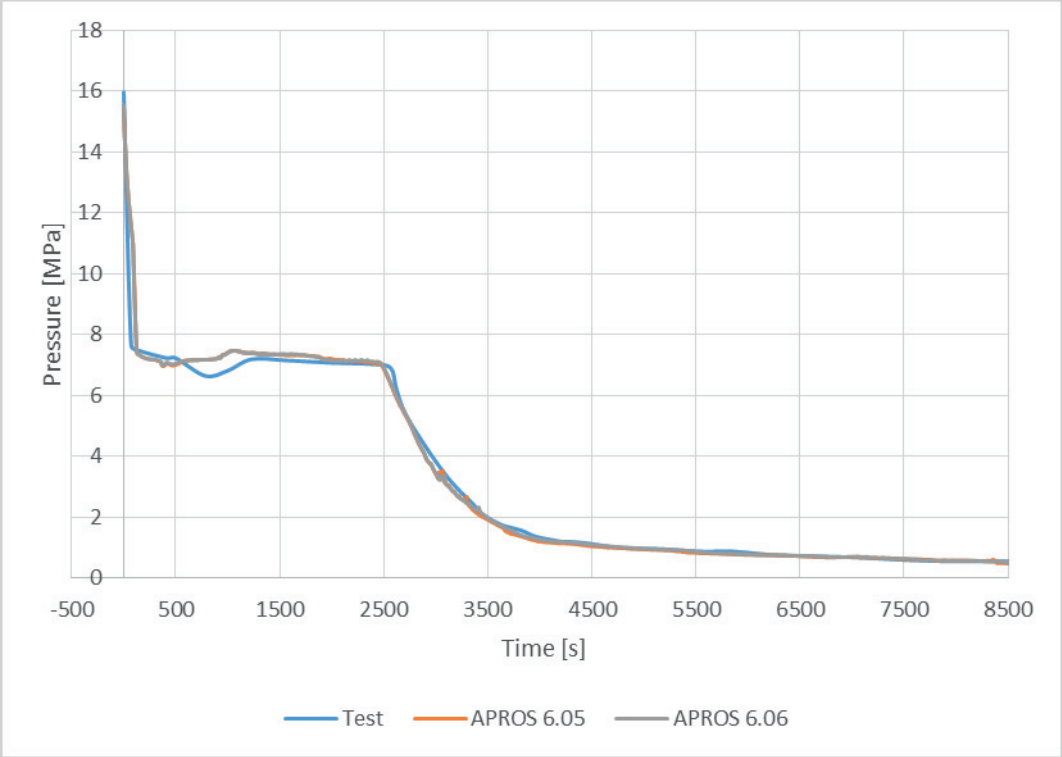


Figure 3: Pressurizer pressure

The minimal core liquid level and the maximum cladding temperature of core is higher in both versions of APROS compared to experiment (Figure 4, Figure 5). The difference between APROS 6.05 and 6.06 core liquid level can be seen between 3000 s and 3500 s. Higher core liquid level in APROS 6.05 results in faster cooldown of the maximum cladding temperature (Figure 5) and better alignment with experiment. The temperature rise of the core cladding begins earlier in both simulation cases (Figure 5).

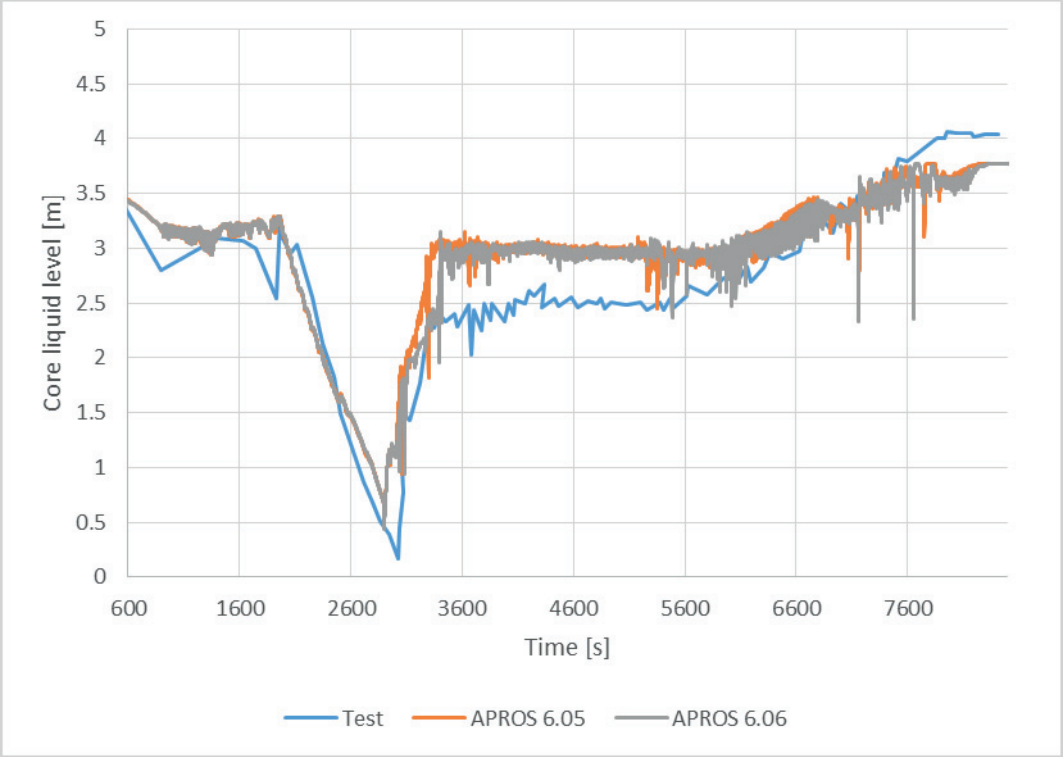


Figure 4: Core liquid level

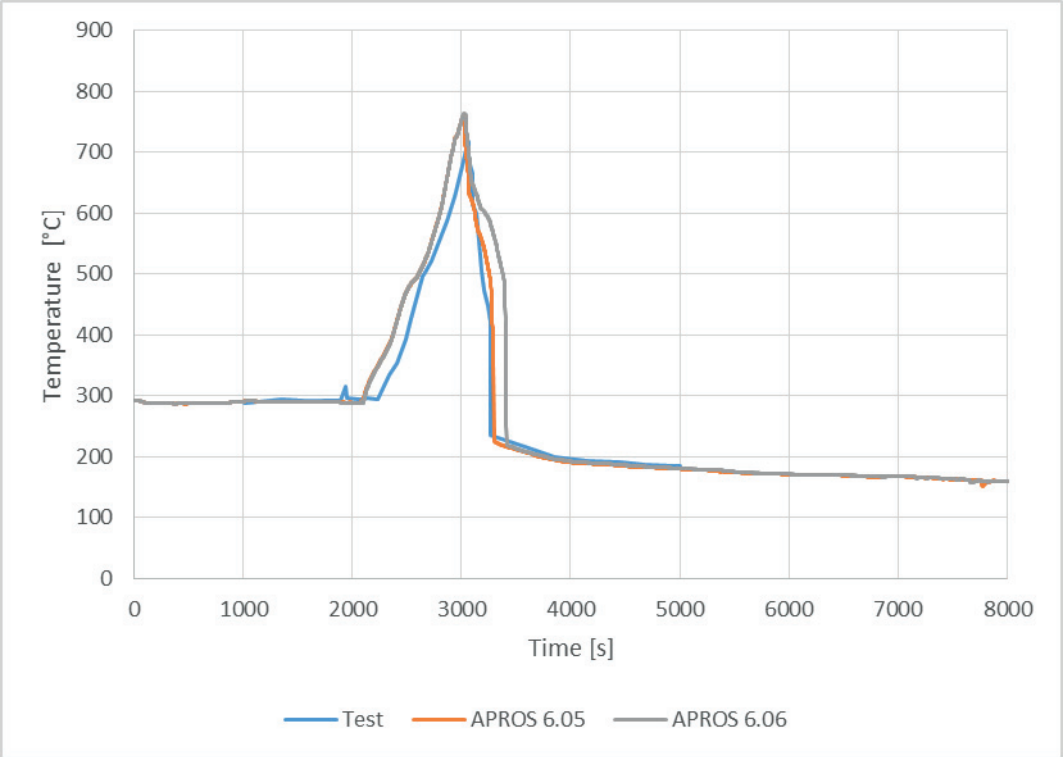


Figure 5: Maximum cladding temperature

The integral break flow in APROS 6.05 is in very good agreement with the experiment up to time 3300 s and is also identical to APROS 6.06 results (Figure 6). From this point the flow in AROS 6.05 is higher but becomes almost identical to test results at the end of the experiment. Integral break flow in APROS 6.06 is in very good agreement with the experiment up to time 5400 s, but after it is too small compared to the test.

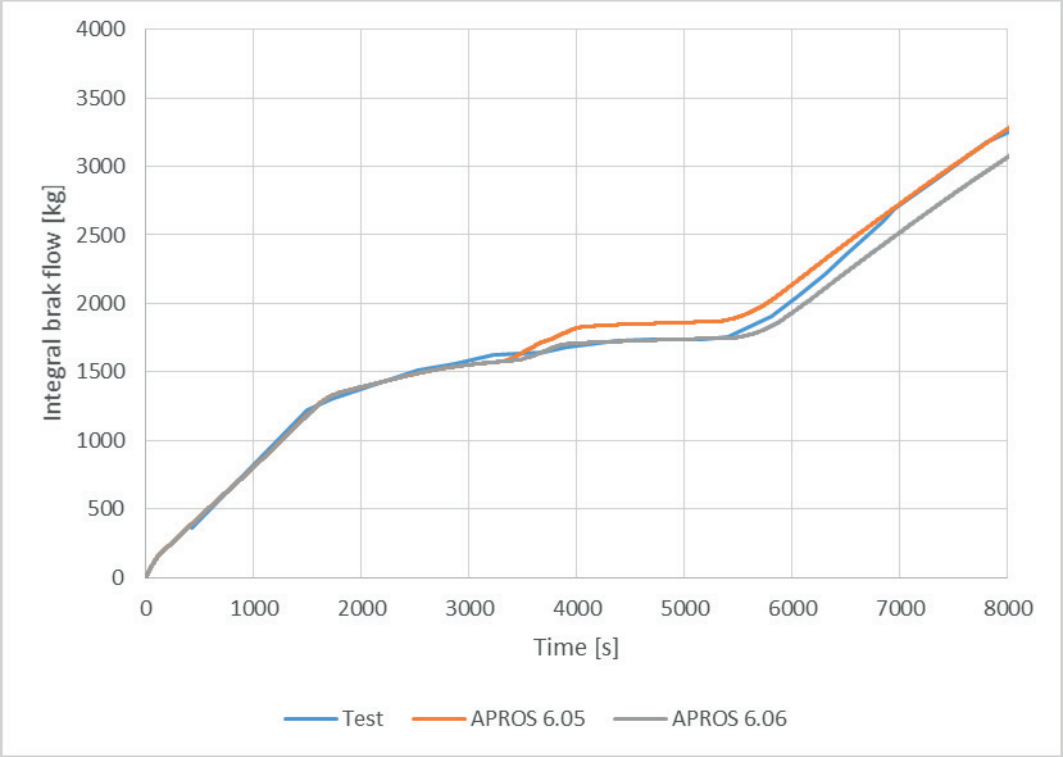


Figure 6: Integral break flow

The Simulation results for the steam generator 2 mass of both APROS versions are almost the same (Figure 7). However there is a difference compared to the experiment in steam generator mass inventory in time between 500 s and 3000 s. This is the consequence of limitation of advance steam generator module, which has a displacement of volumes above riser in regard to experiment steam generator.

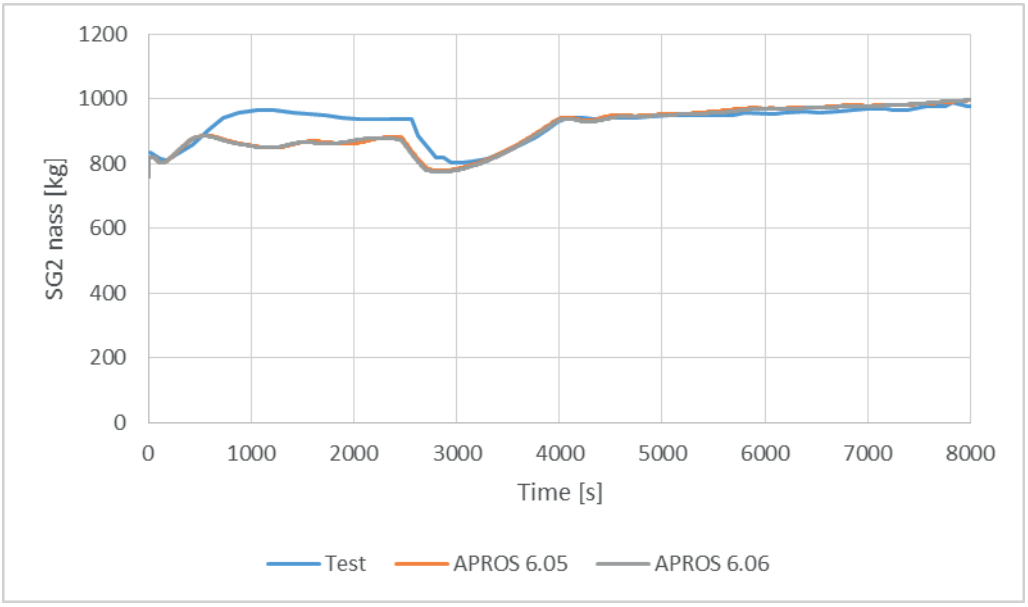


Figure 7: Steam generator 2 mass

The biggest deviation in the primary mass inventory can be observed in APROS 6.05 results between time 3600 s and 4100 s (Figure 8).

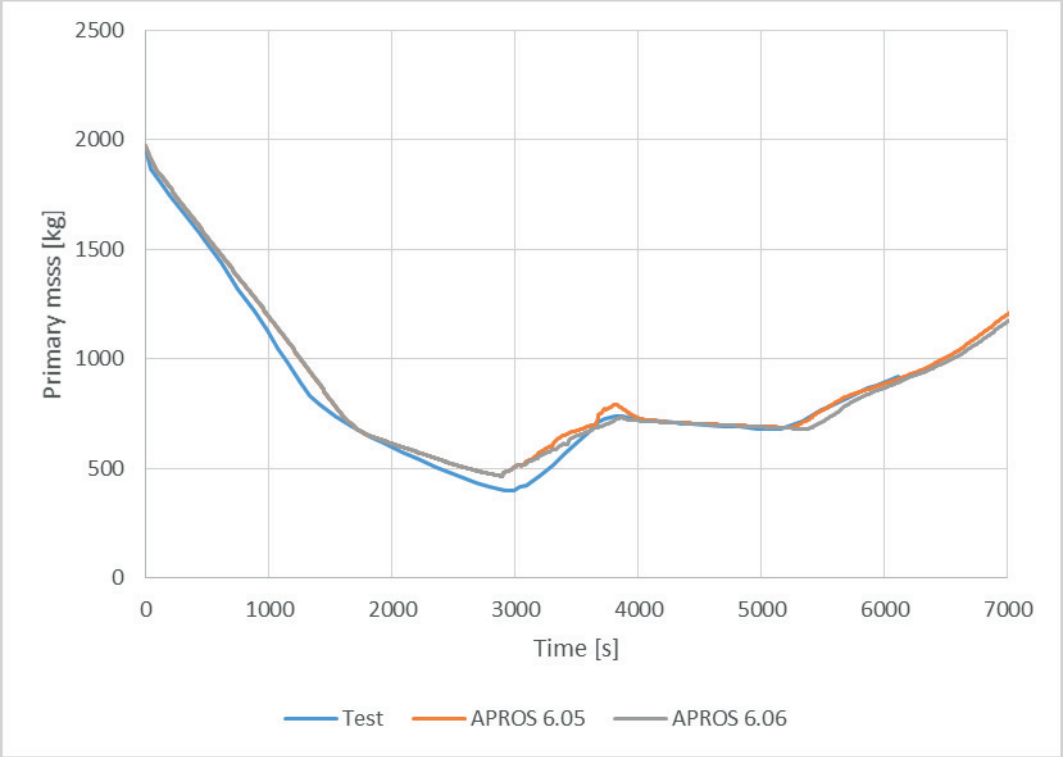

Figure 8: Primary mass inventory

## 6 CONCLUSION

In this paper, the comparison of analysis of international standardized problem ISP 27 using two versions of APROS process simulation software 6.05 and 6.06 is presented. Numerical simulation of experiment Bethsy 9.1b, also known as ISP 27 was performed on a scaled down model of a three loop, 900 MWe Framatome PWR. Model was first built in APROS 6.05 using standard modules in order to describe the volumes, heat structures and regulation of the test facility and was then exported to APROS 6.06.

The results from both versions showed all the processes such as loop seal clearing, core uncover and rise of cladding temperature and other processes taking place in the experiment were in a good agreement with experimental data. The simulation results were very similar to the point of maximal cladding temperature. After some differences were observed. When comparing the APROS 6.05 results to the APROS 6.06 results, it is not obvious which is in better alignment with the experiment. In some cases one is better in others the other one, however both are in relative good agreement with the experiment and can be used for simulations of such scenarios in nuclear power plants

## REFERENCES

[1] CEA, “BETHSY, General Description,” Note SETh/LES/90-97, CEA (Commissariat `a l’´energie atomique et aux ´energies alternatives), Grenoble, France, April 1990

[2] Klemen Debelak, Luka Štrubelj, Modeling of Loss of Coolant Accident on Bethsy Facility with Apros Software, NENE 2017 – 26th International Conference Nuclear Energy for New Europe, 2017

[3] NEA/OECD, CSNI0076 BETHSY/6.9C., WWW: http://www.oecd-nea.org/tools/abstract/detail/csni0076/, Accessed on 2.2.2016.

[4] APROS 6 Nuclear documentation, VTT and Fortum, 2015

Journal of Energy
VOLUME 68 Number 2-3 | 2019 | Special Issue
journal homepage: http://journalofenergy.com/

# Point Kernel Modification Including Support Vector Regression Neutron Buildup Factor Models

**Paulina Dučkić, Krešimir Trontl, Davor Grgić, Mario Matijević**
University of Zagreb, Faculty of Electrical Engineering and Computing
Unska 3, 10000 Zagreb, Croatia
paulina.duckic@fer.hr, kresimir.trontl@fer.hr, davor.grgic@fer.hr, mario.matijevic@fer.hr

## ABSTRACT

This work presents the results of radiation shielding calculations using modified point kernel code QAD-CGGP. The modification includes a new approach to neutron buildup factor estimations based on machine learning technique called Support vector regression (SVR). SVR neutron buildup factor models for common shielding materials are developed and built into the QAD-CGGP. The development of the models consisted of acquiring the data to be used for learning the model, optimizing the SVR parameters, and application of active learning methods for improving the learning process. The modified code is tested, and the results are compared with the MCNP6 results.

***Keywords:*** *point kernel, neutron buildup factor, support vector regression, shielding*

## 1 INTRODUCTION

Point kernel method is an approximate approach to radiation shielding analysis, involving the calculation of the direct component of radiation and a buildup factor to correct the direct component for the secondary radiation produced within the shield. In general, the direct component of radiation from an extended source at a detector point is obtained by assuming that the extended source consists of many point isotropic sources and that the resulting radiation is obtained by summing the contributions of the individual point sources. If the source is a plane emitting parallel beam of monoenergetic neutrons, the direct component is calculated using an exponential law:

$$\phi(x) = \phi_0 e^{-\Sigma x} \tag{1}$$

where $\phi$ is the total flux at a distance $x$ from the source, $\phi_0$ is the incident flux, and $\Sigma$ is the macroscopic cross section. The point kernel method is widely used in gamma ray shielding analysis, but for neutrons somewhat different approach based on the removal cross section has been used [1]. This is due to variety of interactions neutrons may undergo with the shielding media, as well as a strongly non-linear dependence of the total macroscopic cross section on the incident neutron energy. It has been shown that the behaviour of the buildup factors is led by the macroscopic cross sections [2], thus the non-linearity of the macroscopic cross sections is transferred to the buildup factors making the use of the point kernel method in neutron shielding analysis impractical. This problem may be overcome because with the development of machine learning techniques, the determination of the neutron buildup factors can be simplified.

Support Vector Regression (SVR) is a machine learning technique that has been used in different fields of study, including medicine, pharmacy, engineering, etc. [3][4][5][6][7][8]. Its main characteristics are a) learning from data, b) structural risk minimization, c) convex optimization problem d) partial solution e) mapping in the features space. In the simplest form, the model developed by the SVR is a linear function, also called the target function (Eqn. 2), which is based only on the so called training set involving input vectors and corresponding output values:

$D: \{(\vec{x}_1, y_1), (\vec{x}_2, y_2), \ldots, (\vec{x}_n, y_n)\} \subset R^n \times R.$

$$f(\vec{x}) = \langle \vec{w}, \vec{x} \rangle + b \quad \vec{w} \in R^N, b \in R \tag{2}$$

The target function is obtained by minimizing structural risk composed of prediction error and model complexity (Eqn. 3)

$$\begin{aligned} &\min \quad \frac{1}{2}\|w\|^2 + C\sum_{i=1}^{l}(\xi_i + \xi_i^*) \\ &\text{with respect to} \begin{cases} y_i - \langle w, x_i \rangle - b \leq \varepsilon + \xi_i \\ \langle w, x_i \rangle + b - y_i \leq \varepsilon + \xi_i^* \\ \xi_i, \xi_i^* \geq 0 \end{cases} \\ &i = 1, 2, \ldots, l \end{aligned} \tag{3}$$

Real life problems are usually non-linear, therefore, SVR solves non-linear problems by mapping the input vector in a higher dimensional features space. There are many mapping functions, also called the kernel functions, that can serve this purpose (Eqn. 4 – Eqn. 7). The commonly used kernel function is Gaussian Radial Basis Function (Eqn. 4).

$$K(\vec{x}_i, \vec{x}) = e^{-\frac{\|\vec{x}_i - \vec{x}\|^2}{2\sigma^2}} \tag{4}$$

$$K(\vec{x}_i, \vec{x}) = ((\vec{x}_i \cdot \vec{x}) + \theta)^d \tag{5}$$

$$K(\vec{x}_i, \vec{x}) = \tanh(\kappa(\vec{x}_i \cdot \vec{x}) + \theta) \tag{6}$$

$$K(\vec{x}_i, \vec{x}) = \frac{1}{\sqrt{\|\vec{x}_i - \vec{x}\|^2 + c^2}} \tag{7}$$

Using a kernel function to transfer an input vector in a features space, an SVR model for non-linear problems is also a liner function, but in a features space (Eqn. 8).

$$f(\vec{x}) = \sum_{i=1}^{l}(\alpha_i - \alpha_i^*)K(\vec{x}_i, \vec{x}) + b \tag{8}$$

Support vectors (SV) are those input vectors for which $\alpha_i$ and $\alpha_i^*$ are non-zero. That is why it is said that the solution is partial [9]. The number of SVs strongly depends on the selection of SVR parameters $C$, $\varepsilon$, and $\sigma$. Constant $C$ determines the balance between the complexity of the function and prediction error. The larger the constant $C$, the model is more accurate in predicting the labels of the data that have been included in the learning process and the target function is much complex (more SVs form the solution). However, this may lead to an overfitting effect and poor prediction of the outputs of the data that have not been included in the learning process. Constant $\varepsilon$ is a loss function parameter which represents the radius of the tube surrounding the target function. Lower $\varepsilon$ value results in a lager number of SV forming the target function. On the other hand, lower $C$ and higher $\varepsilon$ values may result in an underfitting effect which also results in poor prediction. Parameter $\sigma$ is the width of the Gaussian kernel function. Thus, the selection of SVR parameters affects the accuracy of the model and users must approach to this problem very carefully [10]. Optimization techniques are very popular for selecting SVR parameters due to their efficiency [11][12][13][14].

Active learning is a subfield of machine learning developed with the aim to speed up the learning process by selecting the training data carefully. This is very desirable in situations when obtaining the training data is time, resource and finance consuming. The goal of active learning is to develop an accurate SVR model with as low as possible training data. Different active learning algorithms have been developed and adopted for developing an SVR models [15] and it has been shown that such models achieve good accuracy in predicting labels as it would have been achieved with having so called full training (including all data).

In this work a point kernel code QAD-CGGP [16] is modified by including SVR models for total neutron buildup factors determination. The models are developed for materials usually encountered in radiation shielding problems. The training data for model development have been calculated using MCNP6 [17] and different optimization techniques have been investigated for selecting the SVR parameters, as well as different active learning algorithms have been considered to improve the learning process. The modified QAD-CGGP is tested and the obtained results have been compared with the ones obtained using MCNP6.

The rest of the paper is organized as follows. In Section 2 total neutron buildup factor modelling details are provided. Section 3 presents the obtained SVR models. In Section 4 QAD-CGGP is explained. In Section 5 final testing is made. Conclusions are given in Section 6.

## 2 TOTAL NEUTRON BUILDUP FACTOR MODELLING

### 2.1 Total neutron buildup factor

Total neutron buildup factor is defined as the ratio of the total dose (neutron and secondary gamma rays) and the direct neutron dose (Eqn. 9) [2]:

$$B = \frac{D_{total}}{D_{n,\,direct}} = \frac{D_n + D_g}{D_0 e^{-\Sigma_T z}} \tag{9}$$

where $D_n$ is the neutron dose, $D_g$ is the secondary gamma ray dose, $D_0$ is the incident dose, $\Sigma_T$ is total macroscopic cross section, and $z$ is the shielding thickness. In this work total neutron buildup factors are defined in terms of ambient dose equivalent with the corresponding conversion coefficients taken from ICRP Publication 74 [18]. The process of calculating buildup factors is two-step. Firstly, neutron and secondary gamma ray ambient dose equivalent is calculated using MCNP6 and in the second step direct component is calculated manually using an exponential law with the macroscopic cross section calculated using MCNP6.

The modelled geometry includes a plane source emitting parallel beam of monoenergetic neutrons. The incident flux of 1 n/cm$^2$/s is normally directed to the slab of finite thickness and infinite width and height. MCNP calculations are performed using cross section from ENDF/B-VII.1 library, as well as S($\alpha, \beta$) to account for thermal scattering. The number of particles run is one million and weight window generator is used to obtain results with acceptable statistics.

### 2.2 Training data

To learn an SVR model, a training set that describes the problem of interest well is required. In the case of total neutron buildup factor modelling, three features are selected to form an input vector, namely, shielding thickness $z$, incident neutron energy $E$, and total macroscopic cross section $\Sigma_T$ (Eqn. 10), while output vector is the total ambient dose equivalent buildup factor (Eqn. 11).

$$x = \{z, E, \Sigma_T\} \tag{10}$$

$$y = \{B\} \tag{11}$$

Considered shielding thicknesses depend on the material. The calculations are run for seven commonly used shielding materials, namely, aluminum, carbon steel, iron, lead, Portland concrete, stainless steel and water. For each material 40 different shielding thicknesses are being observed. For all materials except concrete, shielding thicknesses vary up to 20 cm and for concrete up to 200 cm. From the incident neutron energy range [0.025 eV – 14 MeV] 30 different energies are considered. Thus, having 40 different shielding thicknesses and 30 different incident neutron energies, for each material, initial set is composed of 1200 samples. These samples are divided in several subsets:

- Training set (90 samples)
- Test set (240 samples)
- Validation set (120 samples)

- Unlabeled set (7500 samples)

Training set samples are selected in a manner to cover the edges and the middle of the shielding thickness domain at all energies. Test set includes uniformly distributed samples over the shielding thickness domain at all energies. Validation set is randomly selected, and the unlabeled set consists of the samples that are to be selected and added to the training set in active learning process. It is important to note that for the initial set of data output values are unknown. After dividing the samples into different subsets, MCNP calculation are run for training, testing and validation samples and in each iteration of active learning, samples are firstly selected from the unlabeled set, and then labeled.

## 2.3 SVR modelling

For SVR modelling LibSVM (Library Support Vector Machine) [19] is used. LibSVM is a computer code used for classification and regression model development. The two main functions of the code are svm-train used for learning the model, and svm-predict used for predicting the output values for new input vectors based on the developed model. The options of the svm-train and svm-predict functions are shown in Figure 1 and Figure 2, respectively. LibSVM requires train set in .train format and test set in .test format. To obtain a better correlation between the feature of the input vector, it is recommended to scale input vector. In this case, due to a large range of the incident neutron energies, as well as a large range of the buildup factors, the input vector and the output vector are scaled using natural logarithm (ln) function. Therefore, the input vector has the form (ln(x), ln(y)).

```
D:\libsvm-3.20\windows>svm-train
Usage: svm-train [options] training_set_file [model_file]
options:
-s svm_type : set type of SVM (default 0)
        0 -- C-SVC              (multi-class classification)
        1 -- nu-SVC             (multi-class classification)
        2 -- one-class SVM
        3 -- epsilon-SVR        (regression)
        4 -- nu-SVR             (regression)
-t kernel_type : set type of kernel function (default 2)
        0 -- linear: u'*v
        1 -- polynomial: (gamma*u'*v + coef0)^degree
        2 -- radial basis function: exp(-gamma*|u-v|^2)
        3 -- sigmoid: tanh(gamma*u'*v + coef0)
        4 -- precomputed kernel (kernel values in training_set_file)
-d degree : set degree in kernel function (default 3)
-g gamma : set gamma in kernel function (default 1/num_features)
-r coef0 : set coef0 in kernel function (default 0)
-c cost : set the parameter C of C-SVC, epsilon-SVR, and nu-SVR (default 1)
-n nu : set the parameter nu of nu-SVC, one-class SVM, and nu-SVR (default 0.5)
-p epsilon : set the epsilon in loss function of epsilon-SVR (default 0.1)
-m cachesize : set cache memory size in MB (default 100)
-e epsilon : set tolerance of termination criterion (default 0.001)
-h shrinking : whether to use the shrinking heuristics, 0 or 1 (default 1)
-b probability_estimates : whether to train a SVC or SVR model for probability estimates, 0 or 1 (default 0)
-wi weight : set the parameter C of class i to weight*C, for C-SVC (default 1)
-v n: n-fold cross validation mode
-q : quiet mode (no outputs)
```

Figure 1: Options of the svm-train function

```
D:\libsvm-3.20\windows>svm-predict
Usage: svm-predict [options] test_file model_file output_file
options:
-b probability_estimates: whether to predict probability estimates, 0 or 1 (default 0); for one-class SVM only 0 is supported
-q : quiet mode (no outputs)
```

Figure 2: Options of the svm-predict function

## 2.4 SVR parameters optimization

Selecting SVR parameters is not a simple task due to their mutual dependency, i.e. all three parameters must be selected at the same time. Lately, optimization algorithms play an important role in selecting SVR parameters due to their performance capabilities and efficiency.

In this work four different optimization techniques are considered and adopted to select SVR parameters for the problem of total neutron buildup factors determination, namely, Differential Evolution (DE), Genetic Algorithm (GA), Particle Swarm Optimization (PSO), and Sine Cosine Algorithm (SCA). The optimization procedure of each technique is given in the references [13],[14],[20],[21]. The criteria for selecting an optimization technique are the accuracy of the developed models with the optimized SVR parameters and the run time of the optimization algorithm.

The performance of the SVR models combined with different optimization techniques for SVR parameters selection is given in Figure 3. The accuracy of the models is expressed in terms of MSE (Eqn. 12). In Table 1 times and the accuracy of the models combined with different optimization techniques in predicting output values of the validation and test set are presented. The accuracy is expressed in terms of Relative Average Deviation – RAD (Eqn. 13). From these results it can be seen that SVR model combined with PSO gives the smallest error in predicting output values of the validation set, as well as on the test set. Although less computational time is required for the GA method, an increase of about 65% time for PSO results in about two and a half times better accuracy.

$$MSE = \frac{\sum_{i=1}^{n}(y_i - f_i)^2}{n} \tag{12}$$

$$RAD = \frac{\sum_{i=1}^{n}\frac{|y_i - f_i|}{y_i} \cdot 100\%}{n} \tag{13}$$

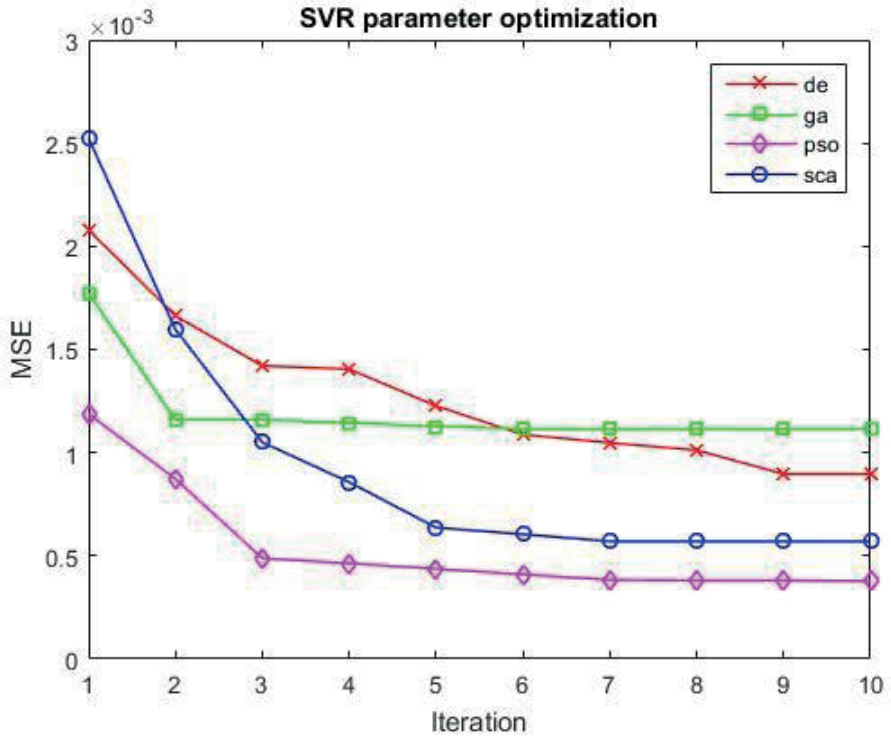


Figure 3: Comparison of the optimization techniques

Table 1: The average computational time of the optimization techniques, validation and testing of the developed models

| Method | Run time (s) | RAD (%) validation | RAD (%) testing |
|---|---|---|---|
| DE | 270±120 | 1.08±0.79 | 1.72±0.72 |
| GA | 119±48 | 1.35±0.81 | 2.8±1.7 |
| PSO | 196±41 | 0.54±0.20 | 1.15±0.17 |
| SCA | 336±69 | 0.83±0.42 | 1.51±0.51 |

## 2.5 Active learning algorithm selection

Active learning algorithms are developed with the aim to select the most valuable data that are to be included in the train set. In this way, the model is learned using as least as possible training samples, which in turns results in a reduction of an effort involved in obtaining the training samples (time, computational resources, finances, etc.).

In the case of buildup factor modelling, for each combination of incident neutron energy and shielding thickness, MCNP6 is engaged for obtaining the total ambient dose equivalent. Thicker shields require more computational time. Thus, it is presumed that involving active learning in the SVR model development could save computational time.

Three different active learning algorithms are investigated, namely, Differential Evolution Active Learning (DEAL), K-Nearest Neighbor (KNN), and Query By Committee (QBC). Active learning algorithm based on DE is derived from DE optimization algorithm [20] with a following modification. A new input sample is formed by combining two support vectors and then the nearest sample from the unlabeled set is selected for labelling. That input vector and the corresponding output value is added to the training set. In the KNN method [22], around the sample for which the model had the largest prediction error, K nearest samples are selected for labelling and those samples and the corresponding labels are added to the training set. QBC method [23] is based on developing two or more models. The models are then used for prediction of the labels of each sample in the unlabeled set. Those samples for which the models give the largest disagreement in predicted label are selected for labeling and adding to the training set.

The initial conditions are the same for every method. The size of the initial training set is 9 samples and in each iteration 10 most informative samples are selected and added to the training set. The stopping criterion is either maximal number of iteration (in this case 75) or the accuracy of the model prediction RAD=5%.

The results of the methods are given in Table 2 and compared with passive learning and full training results. From these results it can be seen that KNN method has the least computation time but has unacceptable prediction error on the test. DE method has the best prediction result but has the larger computation time. QBC method is a compromise between these two, with the reduction of time by a factor of about two, the prediction error increases about 23%, but it is below the allowed limit. Therefore, QBC is selected as an active learning algorithm suitable for total ambient dose equivalent buildup factor modelling. Compared to passive learning, a significant increase in computational time is observed, due to larger amount of training samples required. However, in this case less prediction error is obtained than with the active learning. The full training case is characterized by the lowest prediction error, but the computational time is about an order of magnitude higher compared to QBC.

Table 2: Comparison of the active learning algorithms

| Method | Training set size | Time (s) | RAD validation (%) | RAD evaluation (%) |
|---|---|---|---|---|
| DEAL | 273±19 | 780±210 | 2.30±0.81 | 2.64±0.97 |
| KNN | 178±22 | 87±51 | 2.98±0.62 | 6.3±1.0 |
| QBC | 220±21 | 360±160 | 2.90±0.58 | 3.26±0.66 |
| PASS | 319±50 | 1200±1100 | 2.04±0.93 | 2.33±0.95 |
| FULL | 960 | 3378 | - | 0.39 |

## 2.6 SVR model development procedure

SVR model development procedure is given in Figure 4. Based on the conducted investigation, the procedure of the SVR model development is as following. Firstly, it is necessary to obtain the training, testing, validation and unlabeled sets. PSO method is engaged for SVR parameters optimization. Having the training set and the corresponding SVR parameters, the SVR model is developed using LibSVM code. The accuracy of the model is tested in terms of RAD. If RAD>5%, QBC is engaged to select new samples from the unlabeled set. In the first iteration 20 samples are selected, in the second 10 and in the following iterations 5 samples are selected to be labeled and added to the training set. These steps are repeated until there are samples in the unlabeled set or stopping criterion is met.

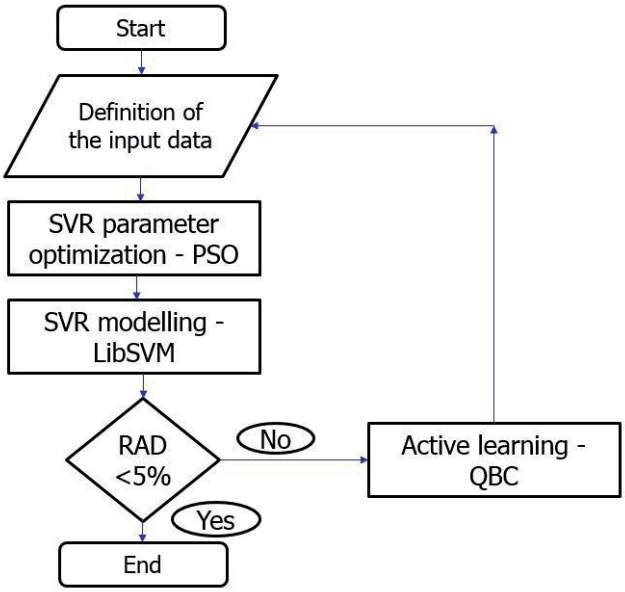


Figure 4: SVR model development procedure

## 3 SVR MODELS

In the following figures and tables, the results of the SVR model development for commonly used shielding materials are given. Figure 5 a) - Figure 11 a) show the learning process in terms of RAD of the validation set for each material, respectively, while in Figure 5 b) - Figure 11 b) the model testing in terms of Relative Error – RE (Eqn. 14) is given. Table 3 provides the details of the developed models: final training set size, the number of support vectors and the computational time. Exceptionally, for iron a comparison is made with the full training to check the assumption of computational time saving when active learning is involved in the process of SVR model development (Table 4). From these results it can be seen that all models have good generalization capabilities, i.e. the models can predict output values of the samples that have not been included in the model development process with generally low relative error. Exceptionally, somewhat higher relative errors for a few samples are observed in the prediction of SVR model for lead. This can be resolved by including more samples in the training set.

$$RE = \frac{|y_i - f_i|}{y_i} \cdot 100\% \tag{14}$$

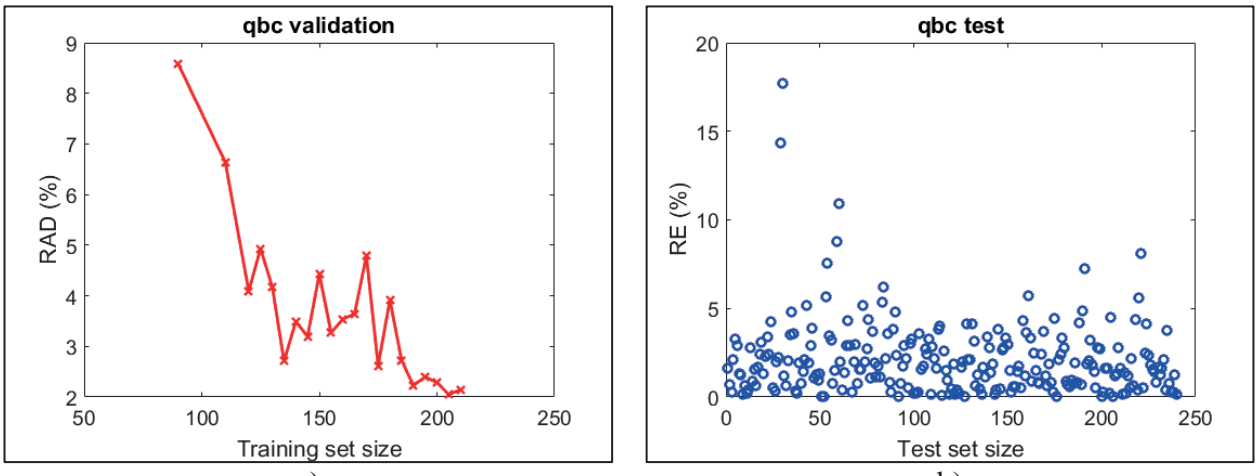


a) b)

Figure 5: SVR model for aluminum: a) model development b) final testing

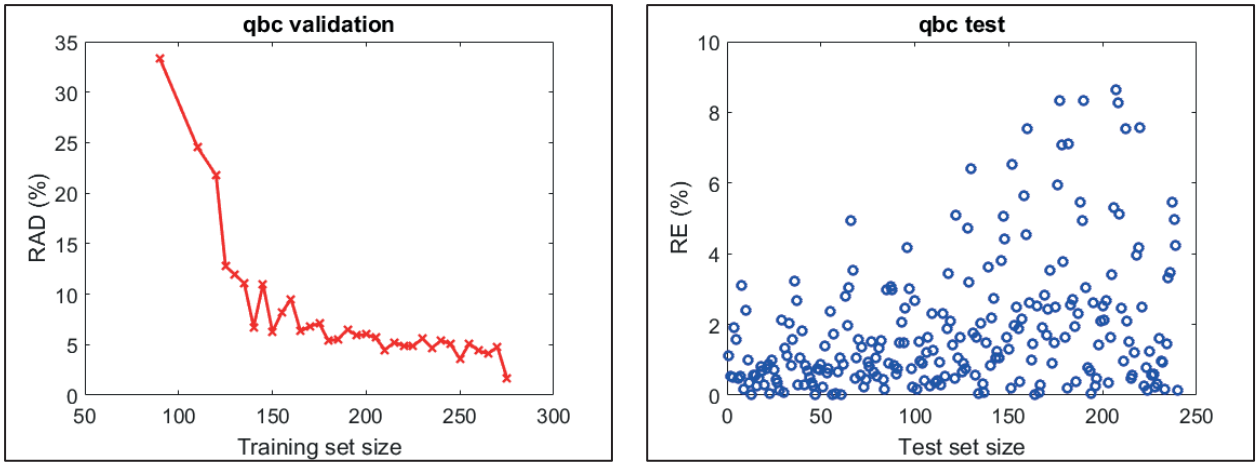


a) b)

Figure 6: SVR model for carbon steel: a) model development b) final testing

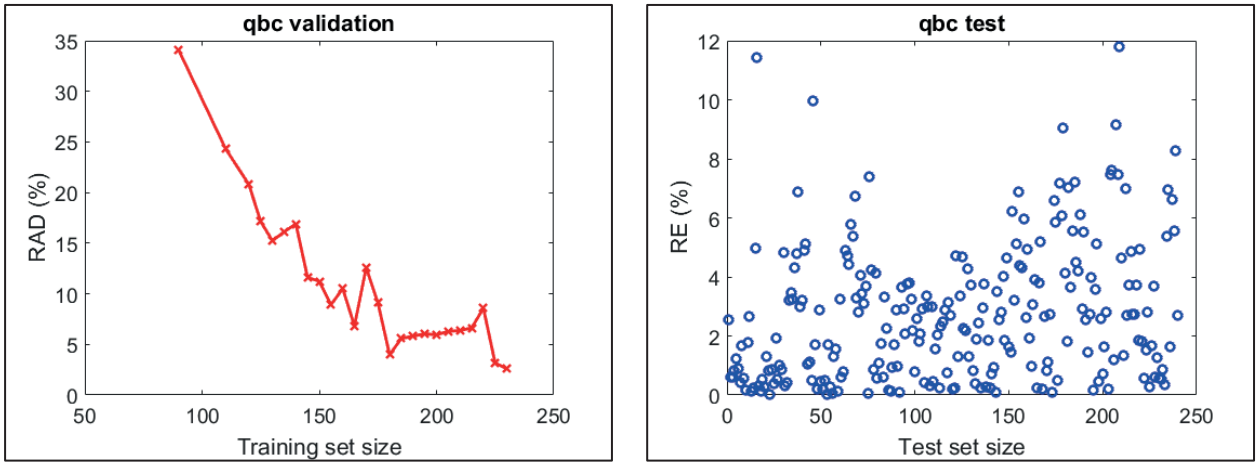


a) b)

Figure 7: SVR model for iron: a) model development b) final testing

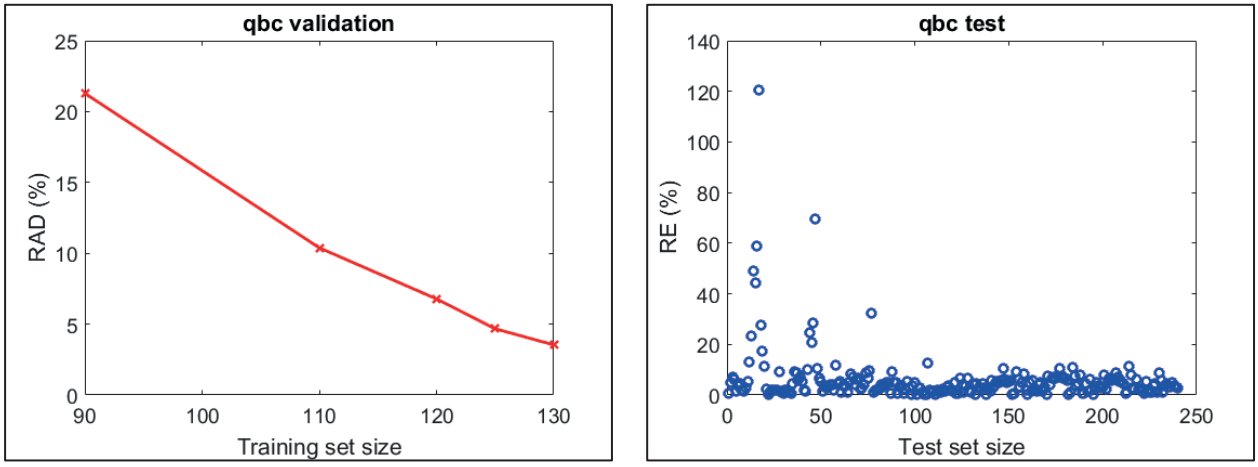


a) b)

Figure 8: SVR model for lead: a) model development b) final testing

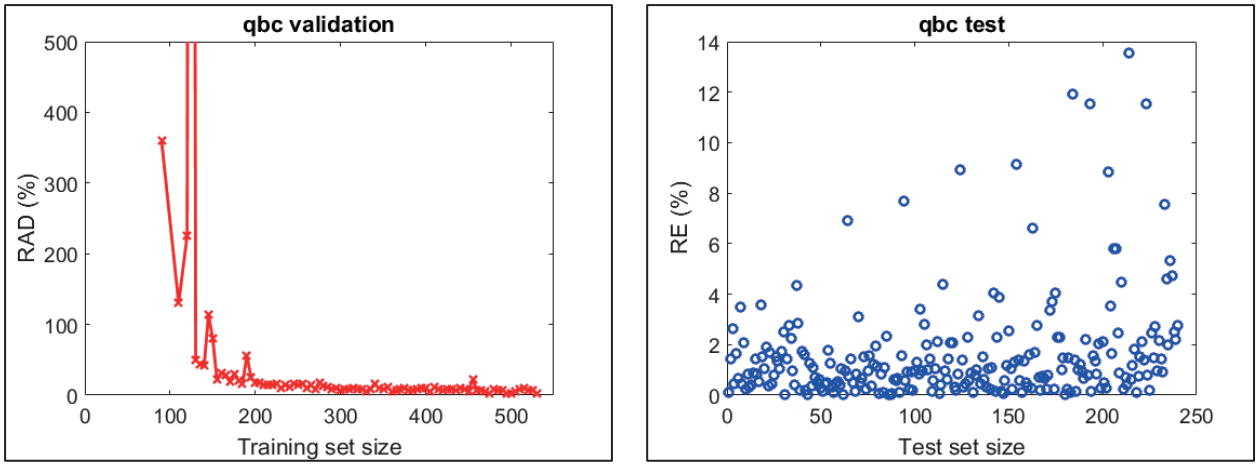


a) b)

Figure 9: SVR model for concrete: a) model development b) final testing

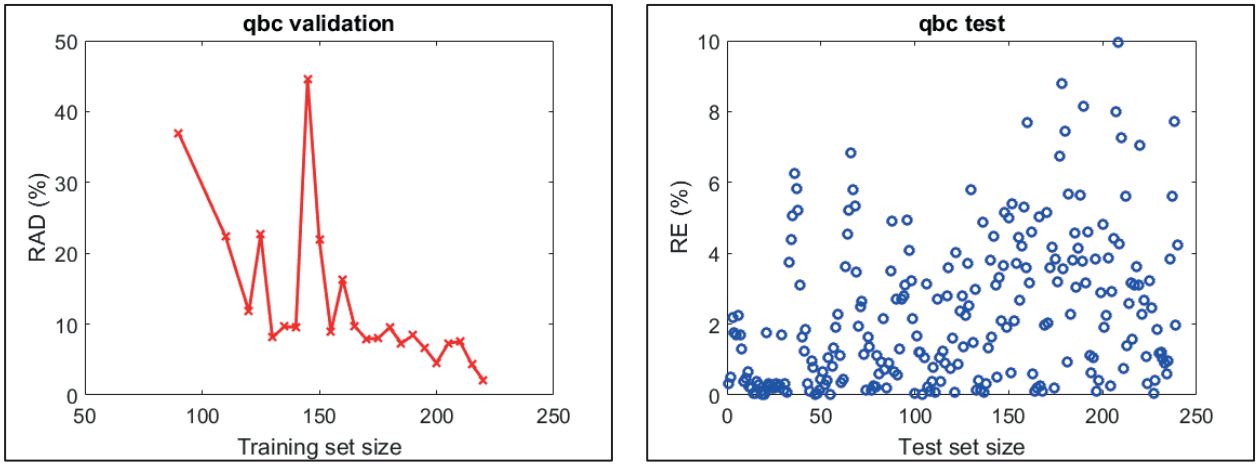


a) b)

Figure 10: SVR model for stainless steel: a) model development b) final testing

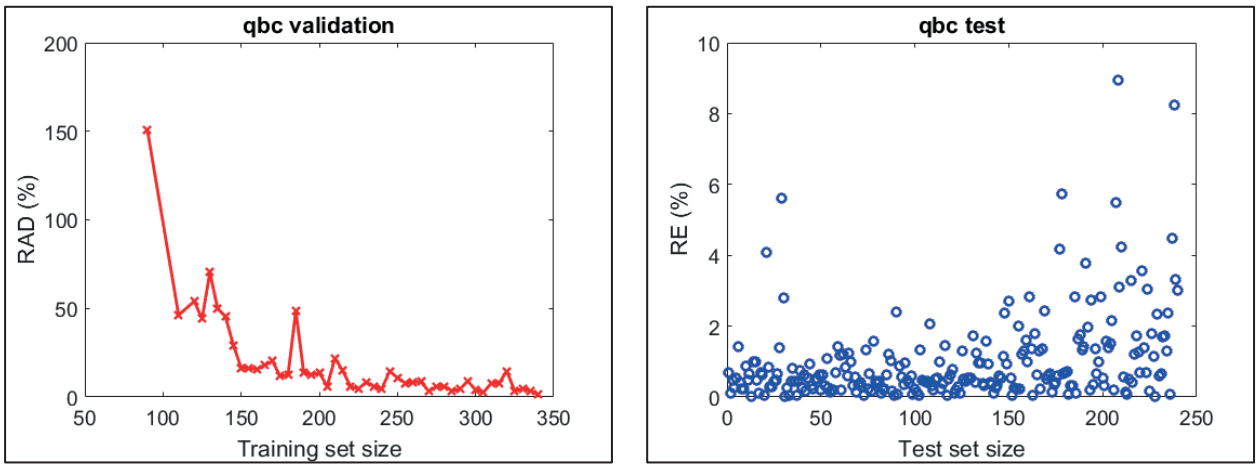


a) b)

Figure 11: SVR model for water: a) model development b) final testing

Table 3: Training set size, number of support vectors, and computation time for all shielding materials

| Material | Training set size | Number of SVs | Time (h) |
|---|---|---|---|
| Aluminum | 210 | 97 | 7.36 |
| Carbon steel | 275 | 159 | 26.57 |
| Iron | 230 | 172 | 24.47 |
| Lead | 130 | 79 | 7.25 |
| Concrete | 530 | 416 | 160.21 |
| Stainless steel | 220 | 220 | 34.19 |
| Water | 340 | 304 | 35.83 |

Table 4: Comparison between active learning and full training for iron

| Method | Training set size | Number of SVs | Time (h) | RAD (%) - test |
|---|---|---|---|---|
| QBC | 230 | 172 | 24.47 | 2.72 |
| FULL | 960 | 410 | 49.40 | 0.58 |

## 4 QAD-CGGP MODIFICATION

QAD-CGGP is a point kernel code used for calculating fast neutron and gamma ray shielding problems. The code includes combinatorial geometry to make various shielding configurations. The preparation of an input file is simple, and the running time of the code is very fast, which make the use of the code in shielding analysis very practical.

Gamma ray shielding calculations require buildup factor data which in QAD-CGGP is resolved using Geometric Progression (GP) fitting function. Neutron shielding calculations are performed using Albert-Welton kernel or kernels obtained from the moments method solution of the Boltzmann equation.

QAD-CGGP was validated for shielding analyses of intermediate and low level waste drums by Šmuc et. al. [24]. Trontl et. al. modified QAD-CGGP to include a multi-layer option [25]. Baće et. al. introduced a multisource option in QAD-CGGP [26]. Baće et. al performed radiation shielding analyses for a dry storage facility using modified QAD-CGGP [27]. Trontl et. al used QAD-CGGP for a radiation dose evaluation of a hypothetical accident with transport package containing Iridium-192 [28].

At this stage of the research the primary goal was to develop the SVR neutron buildup factors models and test their applicability on realistic shielding problems. Therefore, the modifications performed on the QAD-CGGP code were as simple as possible without any code performance optimization being pursuit. Changes have been made to FORT10 library and gamma cross sections have been replaced with appropriate total neutron cross sections. In addition, minor modifications have been introduced into LENGTH and KERNEL subroutines in order to calculate neutron attenuation and appropriate neutron buildup factors.

## 5 TESTING

The testing of the modified QAD-CGGP code has been performed on the concrete spent fuel cask containing ten PWR spent fuel assemblies with the initial enrichment of 4.304 w/o U-235, burnup of 45,000 MWd/tU and a cooling period of 10 years. The total mass of the fuel in a fresh fuel assembly was presumed to be 412 kg of uranium (cca. 467 kg of UO2) with the density of 10.41 g/cm3 (95% of the theoretical density). The density of the moderator has been set to 0.709 g/cm3 as a result of the pressure of 150 bar (2,250 psi) and the temperature of 308°C (581 K, 586.2°F). The

rest of the input data regarding fuel assembly, used for isotopic inventory calculation and neutron source spectrum calculation by ORIGEN-S as a part of the SCALE SAS2H sequence, are based on a typical 16×16 Westinghouse fuel assembly.

To simplify the modelling only the construction materials and most important uranium and plutonium isotopes have been used in MCNP and modified QAD-CGGP calculations. The entire content of the cask basket containing the spent fuel assemblies has been homogenized. The dimensions and materials of the cask are the following. The inner radius is 48 cm and the outer radius is 104 cm. The first layer of the cask is 2 cm of stainless steel, the second layer is 52 cm of Portland concrete and the third layer is 2 cm of carbon steel. A point detector is placed at the surface of the cask radially and in the middle of the cask axially. The final MCNP model of the problem is depicted in Figure 12.

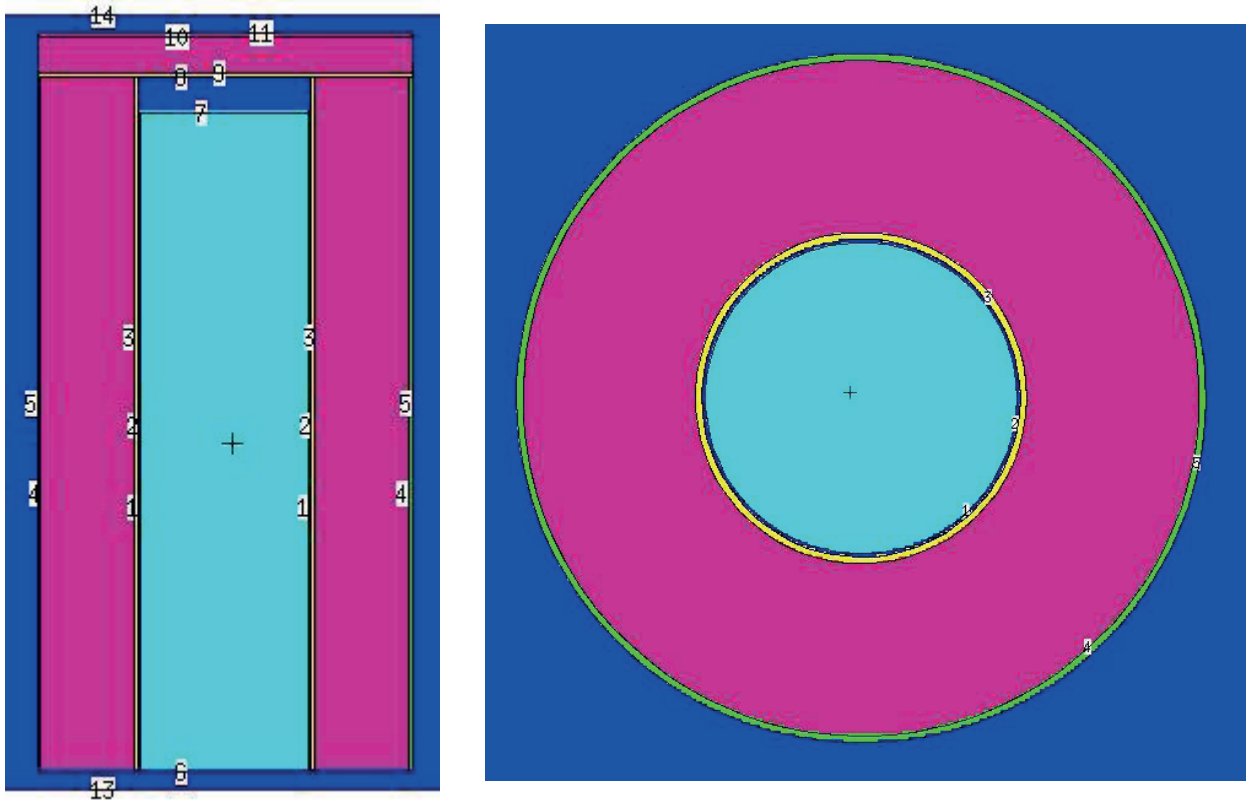

a) b)

Figure 12: MCNP model of the cask a) axially b) radially

The results of the test case calculated using the modified QAD-CGGP and MCNP are given in Table 5. From these results it can be seen that the modified QAD-CGGP and MCNP agree well at 1.2 MeV. It is interesting to note that at energies higher than 1.2 MeV QAD-CGGP results are higher than MCNP results, while at energies lower than 1.2 MeV QAD-CGGP produces lower results than MCNP. This can be attributed to the complexity of the test case geometry, which includes multiple layer shielding. The SVR models used for buildup factors calculation are developed for a simple geometry including a planar source and a monolayer slab shield. Since in multilayer configuration neutrons pass through layers of different materials having different cross sections, neutron spectrum is affected. Therefore, applying the buildup factors for a layer in the middle of the sandwich type shield (steel-concrete-steel) is inappropriate.

Table 5: Test case results

| Energy (MeV) | MCNP NEUTRON REL. ERR. (%) | MCNP GAMMA REL. ERR. (%) | MCNP TOTAL REL. ERR. (%) | QAD-CGGP |
|---|---|---|---|---|
| 14 | 3.73E-09<br>3.39 | 5.31E-10<br>9.48 | 4.26E-09<br>10.07 | 1.25E-06 |
| 4.5 | 2.17E-08<br>2.48 | 3.70E-09<br>5.59 | 2.54E-08<br>6.12 | 1.56E-06 |
| 2.5 | 1.36E-08<br>4.07 | 3.49E-09<br>3.97 | 1.71E-08<br>5.69 | 1.61E-07 |
| 1.5 | 1.89E-09<br>6.06 | 1.56E-09<br>6.91 | 3.45E-09<br>9.19 | 1.20E-07 |
| 1.2 | 1.48E-09<br>4.78 | 1.75E-09<br>6.68 | 3.23E-09<br>8.21 | 5.75E-09 |
| 0.5 | 1.51E-09<br>5.13 | 2.32E-09<br>12.35 | 3.83E-09<br>13.37 | 1.22E-11 |

## 6 CONCLUSION

In this work, total ambient dose equivalent buildup factors are calculated using SVR method. The steps of the SVR model development procedure are determined, including optimization techniques for SVR parameters selection and active learning. The SVR models are developed for commonly used shielding materials and embedded in the point kernel code QAD-CGGP. At this stage of research, the modifications of the code are as simple as possible.

The ambient doses obtained by modified QAD-CGGP code with integrated SVR neutron buildup factor model agree well at 1.2 MeV. At energies higher than 1.2 MeV, the modified QAD-CGGP results are conservative compared to MCNP results. However, at energies lower than 1.2 MeV, the modified QAD-CGGP results are lower than the MCNP results. The differences between the modified QAD-CGGP and MCNP results reach about two orders of magnitude. Although a certain level of conservatism was expected and is welcomed when an engineering approach is evoked, the difference of approximately two orders of magnitude, is a reason for concern which requires additional research. Prior testing as well as model development were performed on a pure single layer shield configuration with a planar source and a slab shield in monolayer configuration. The cask model is a multi-layer shield problem with neutrons passing through fuel assembly material and the sandwich type shield (steel-concrete-steel) which influences the neutron spectrum. The obtained results indicate that additional effort is required in developing an SVR model capable of handling multi-layer shields. To treat such a shielding configuration, redesign of an input vector is required accompanied by multi target SVR modelling.

## REFERENCES


[1] J. Wood, Computational Methods in Reactor Shielding, Pergamon, London, 1982.

[2] P. Dučkić, R. B. Hayes, „Total ambient dose equivalent buildup factors determination for NBS04 concrete“, *Health Physics*, Vol. 114(6), pp. 569-581, 2018.

[3] J. D. Sousa de Almeida, A. C. Silva, J. A. Meireles Teixeira, A. Cardoso Paiva, M. Gattass, “Surgical planning for horizontal strabismus using Support Vector Regression,” *Computers in Biology and Medicine*, Vol. 63, pp. 178-186, 2015.

[4] R. Sałat, K. Sałat, "Modeling analgesic drug interactions using support vector regression: A new approach to isobolographic analysis," *Journal of Pharmacological and Toxicological Method,* Vol. 71, pp. 95-102, 2015.

[5] N. Marković, S. Milinković, K. S. Tikhonov, P. Schonfeld, "Analyzing passenger train arrival delays with support vector regression," *Transportation Research Part C*, Vol. 56, pp. 251-262, 2015.

[6] L. Zhu, M. S. Li, Q. H. Wu, L. Jiang, "Short-term natural gas demand prediction based on support vector regression with false neighbours filtered," *Energy*, Vol. 80, pp. 428-436, 2015.

[7] G. Santamaría-Bonfil, A. Reyes-Ballesteros, C. Gershenson. "Wind speed forecasting for wind farms: A method based on support vector regression," *Renewable Energy*, Vol. 85, pp. 790-809, 2016, doi:10.1016/j.renene.2015.07.004.

[8] P. Vrablecova, A. B. Ezzeddine, V. Rozinajova, S. Šarik, A. K. Sangaiah, "Smart grid load forecasting using online support vector regression" *Computers and Electrical Engineering*, Vol. 65, pp. 102-117, 2018.

[9] A. Smola, B. Schölkopf: „A Tutorial on Support Vector Regression", *Statistics and Computing*, Vol. 14, pp. 199-222, 2004.

[10] V. Cherkassky and Y. Ma, "Selection of Meta-parameters for Support Vector Regression," *ICANN '02 Proceedings of the International Conference on Artificial Neural Networks*, pp. 687-693, 2002.

[11] C.L. Huang, C. J. Wang, "A GA-based feature selection and parameters optimization for support vector machines," *Expert Systems with Applications*, Vol. 31, pp. 231-240, 2006.

[12] Q. Yu, Y. Liu, F. Rao, "Parameter Selection of Support Vector Regression Machine Based on Differential Evolution Algorithm", Sixth International Conference on Fuzzy Systems and Knowledge Discovery, 2009.

[13] G. Ren, S. Wen, Z.Yan, R. Hu, Z. Zeng, Y. Cao, "Power Load Forecasting Based on Support Vector Machine and Particle Swarm Optimization", 12th World Congress on Intelligent Control and Automation (WCICA), June 12-15,2016, Guilin, China.

[14] S. Li, H. Fang, X. Liu, "Parameter optimization of support vector regression based sine cosine algorithm", Expert Systems With Applications, Vol. 91, pp. 63-77, 2018.

[15] B. Settles, “Active Learning Literature Survey”, Computer Sciences, Technical Report 1648, University of Wisconsin–Madison. 2009.

[16] Oak Ridge National Laboratory, RSICC Computer code collection: QAD-CGGP-A Point Kernel Code System for Neutron and Gamma-Ray Shielding Calculations Using the GP Buildup Factor, 1995.

[17] J. Goorley, M. James, T. Booth, F. Brown, J. Bull, L. Cox, J. Durkee, J. Elson, M. Fensin, R. Forster, MCNP$^{TM}$ user’s manual. D. B. Peplowitz, 2013.

[18] ICRP, “Conversion coefficients to Use in Radiological Protection against External Radiation. ICRP Publikacija 74”, Annals of ICRP, Vol. 26, No. 3/4, 1996.

[19] C. C. Chang, C. J. Lin, LIBSVM: a library for support vector machines. ACM Transactions on Intelligent Systems and Technology, Vol. 2, pp. 27:1-27:27, 2011.

[20] R. Storn, K. Price, “Differential Evolution-A Simple and Efficient Heuristic for Global Optimization over Continuous Spaces,” *Journal of Global Optimization*, Vol. 11, pp. 341-359,1997.

[21] D. Whitley, “A Genetic Algorithm Tutorial,” Statistics and Computing, Vol. 4, Issue 2, pp. 65-85, 1994.

[22] L. E. Peterson, “K-nearest neighbor,” Scholarpedia, Vol.4(2):1883.

[23] R. Burbidge, J. J. Rowland, R. D. King, “Active Learning for Regression Based on Query by Committee”, U: Yin H., Tino P., Corchado E., Byrne W., Yao X. (eds) Intelligent Data Engineering and Automated Learning - IDEAL 2007. IDEAL 2007. Lecture Notes in Computer Science, vol 4881. Springer, Berlin, Heidelberg.

[24] T. Šmuc, R. Ječmenica, K. Trontl, “Validation of QAD-CGGP for Shielding Analyses of Intermediate and Low Level Waste Drums”, Croatian Nuclear Society, pp. 456-463, 1998.

[25] K. Trontl, M. Baće, T. Šmuc, “Incorporation of multi-layer option into QAD-CGGP code”, International Conference Nuclear Energy in Central Europe ‘98, Terme Čatež, September 7-10, 1998.

[26] M. Baće, K. Trontl, D. Grgić, “Evaluation of a multisource option introduced into QAAD-CGGP code”, International Conference Nuclear Energy in Central Europe 2001, Portorož, Slovenia, September 10-13, 2001.

[27] M. Baće, K. Trontl, D. Pevec, “Model of a dry storage facility for a medium nuclear power plant”, Radioactive Waste Management and Environmental Remediation – ASME 2001, Bruges: ICEM, 2001. 185.1-185.6

[28] K. Trontl, M. Baće, D. Pevec, “Radiation dose evaluation for hypothetical accident with transport package containing Iridium-192 source”, International Conference Nuclear Energy for New Europe 2002, Kranjska Gora, Slovenia, September 9-12, 2002.

Journal of Energy
VOLUME 68 Number 2-3 | 2019 | Special Issue
journal homepage: http://journalofenergy.com/

# PCA Benchmark Analysis with ADVANTG3.0.1. and MCNP6.1.1b Codes

**Mario Matijević, Dubravko Pevec, Krešimir Trontl**
University of Zagreb, Faculty of Electrical Engineering and Computing
Unska 3, 10000 Zagreb, Croatia
mario.matijevic@fer.hr, dubravko.pevec@fer.hr, kresimir.trontl@fer.hr

**Bojan Petrović**
Georgia Institute of Technology, Nuclear and Radiological Engineering
770 State St., Atlanta, GA 30332-0745, USA
bojan.petrovic@gatech.edu

## ABSTRACT

The Pool Critical Assembly Pressure Vessel (PCA) benchmark is a well known benchmark in the reactor shielding community which is described in the Shielding Integral Benchmark Archive and Database (SINBAD). It is based on the experiments performed at the PCA facility in the Oak Ridge National Laboratory (ORNL) and it can be used for the qualification of the pressure vessel fluence calculational methodology. The measured quantities to be compared against the calculated values are the equivalent fission fluxes at several experimental access tubes (A1 to A8) in front, behind, and inside the pressure-vessel wall simulator. This benchmark is particularly suitable to test the capabilities of the shielding calculational methodology and cross-section libraries to predict in-vessel flux gradients because only a few approximations are necessary in the overall analysis. This benchmark was analyzed using a modern hybrid stochastic-deterministic shielding methodology with ADVANTG3.0.1 and MCNP6.1.1b codes. ADVANTG3.0.1 is an automated tool for generating variance reduction (VR) parameters for Monte Carlo (MC) calculations with MCNP5v1.60 code (and higher versions). It is based on the multigroup, discrete ordinates solver Denovo, used for approximating the forward-adjoint transport fluxes to construct VR parameters for the final MC simulation. The VR parameters in form of the weight windows and the source biasing cards can be directly used with unmodified MCNP input. The underlining CADIS methodology in Denovo code was initially developed for biasing local MC results, such as point detector or a limited region detector. The FW-CADIS extension was developed for biasing MC results globally over a mesh tallies or multiple point/region detectors. Both CADIS and FW-CADIS are based on the concept of the neutron importance function, which is a solution of the adjoint Boltzmann transport equation. The equivalent fission fluxes calculated with MCNP are based on several high-energy threshold reactions from international dosimetry libraries IRDF-2002 and IRDFF-2014, distributed by the IAEA Nuclear Data Section. The obtained results show a good agreement with referenced PCA measurements. Visualization of the deterministic solution in 3D was done using the VisIt code from the Lawrence Livermore National Laboratory (LLNL).

**Keywords:** *PCA benchmark, shielding, pressure vessel, Monte Carlo, variance reduction*

## 1 INTRODUCTION

Accurate knowledge of the reactor pressure vessel (RPV) irradiation with fast neutron fluence is one of the key safety requirements when determining the lifetime of a nuclear power plant. Another important aspect is the potential financial savings which could be achieved by approving nuclear power plant (NPP) lifetime extension. Modern calculational methods of reactor physics are successors of decades-long efforts to produce fast, reliable and predictive answers to challenging real-life problems, so any developed or analyzed calculation methodology requires comprehensive verification and validation against evaluated reference data. A large database of benchmarks aimed at validation of computer codes and nuclear data used for radiation transport and shielding problems is "Shielding Integral Benchmark Archive and Database (SINBAD)" [1]. One of the most widely used SINBAD benchmarks for qualification of radiation transport methods and evaluation of nuclear data for dosimetry calculations in Light Water Reactors (LWR) is the "Pool Critical Assembly Pressure Vessel Facility Benchmark" (PCA benchmark) [2].

The purpose of the PCA benchmark is to validate the capabilities of the computational shielding methodology to predict reaction rates in the regions outside of the reactor core when the neutron source, material compositions, and geometry are well defined. Over the years a number of PCA benchmark studies have been conducted using different calculational methods (discrete ordinates $S_N$ method or Monte Carlo MC method) and dosimetry data libraries [3][4][5][6][7]. This paper presents another effort of the PCA benchmark analysis by using modern hybrid shielding methodology, where fast deterministic solution via discrete ordinates is used as a means to accelerate the final MC answer. Dosimetry cross-section data were extracted from the international library IRDF-2002 [8] for all dosimeters in order to be used as response functions. Such response functions have a meaning of the adjoint source spectrum which is an important physical parameter for variance reduction (VR) parameters construction. This paper is organized as follows. The PCA benchmark is described in Section 2. The description of the hybrid shielding methodology implemented in ADVANTG/MCNP codes is given in Section 3. The analysis of the PCA benchmark, including results of the criticality eigenvalue and fixed-source shielding calculations, is presented in Section 4. Conclusions are given in Section 5 while the referenced literature is given at the end of the paper.

## 2 PCA BENCHMARK FACILITY DESCRIPTION

The fast neutron fluence induced embrittlement of the reactor pressure vessel (RPV) is for some reactors the main cause for limiting the PWR power plant lifetime. With the advances of computer computational power the reactor dosimetry calculations can now give better insight into radiation damage of the RPV when exposed to intense neutron flux environment. For such purposes various correlations between neutron flux and irradiation effects of detectors have been established, such as displacement per atom (DPA), helium accumulation in reactor baffle plates by $^{58}Ni(n,\gamma)^{59}Ni(n,a)^{56}Fe$ reaction sequence, etc. The current guideline for RPV dosimetry calculations is the U.S.NRC Regulatory Guide 1.190 [9], which states that calculational methods used to estimate RPV fast fluence should use the latest version of the Evaluated Nuclear Data File (ENDF/B) in the fast energy range (0.1–15) MeV. In accordance with this guideline, we present calculational results for the ORNL PCA Benchmark. The scope of PCA benchmark is to validate the capabilities of the calculational methodologies to predict the reaction rates in the region outside of the core when the neutron source, material compositions, and relatively simple geometry configuration are well defined and given. The PCA benchmark provides the calculated and measured reaction rates (C/M ratio) inside the simulated pressure vessel, as well as in the water gap in front of the pressure vessel. This allows an assessment of the accuracy with which the calculations predict the neutron flux attenuation inside the pressure vessel. The PCA benchmark

facility consists of the reactor core and the components that mock up the reactor-to-cavity region in typical light water reactors. These components are the thermal shield (TS), the reactor pressure vessel simulator (RPVS), and the void box (VB), which simulates the reactor cavity. The Monte Carlo simulation model of the PCA benchmark facility is shown in Figure 1.

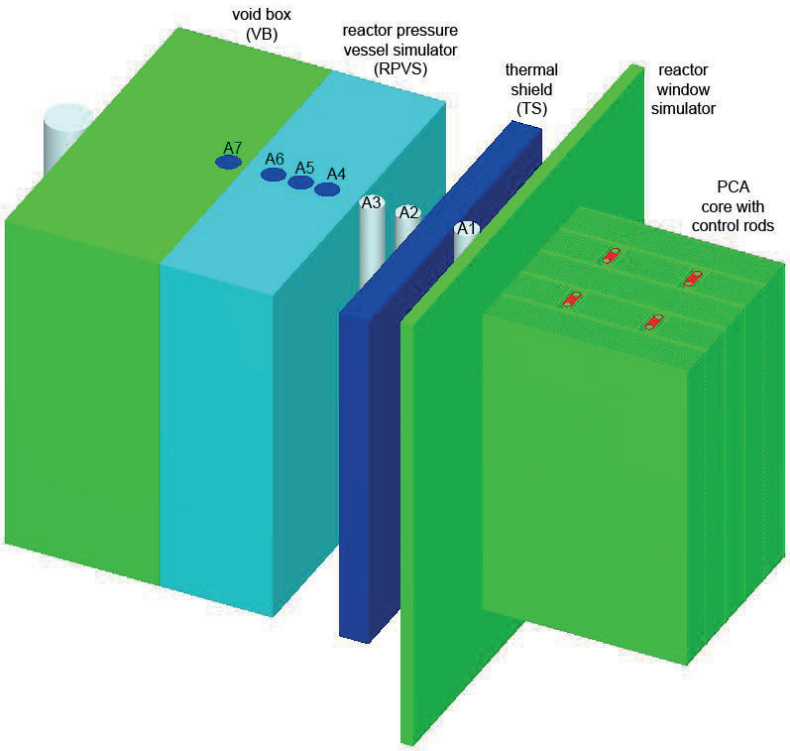


Figure 1: MC model of the PCA benchmark facility (water removed)

The large aluminum plate in front of the PCA core, referred to in Figure 1 as the reactor window simulator, was added to the facility for operational reasons. The thicknesses of the water gaps between the aluminum window and thermal shield and between the thermal shield and pressure vessel are approximately 12 cm and 13 cm, respectively. Such PCA configuration is known as "12/13" configuration. The materials used for the components outside the core were aluminum for the reactor window simulator, stainless steel for the thermal shield, and carbon steel for the pressure vessel. The PCA facility is located in a large pool of water (removed in Figure 1), which serves as reactor core coolant and moderator and provides extra shielding. The PCA benchmark facility core is a light water moderated, highly enriched uranium (e=93%) fueled critical assembly. It consists of 25 material test reactor (MTR) plate type elements. The standard MTR fuel element and control element are depicted in Figure 2.

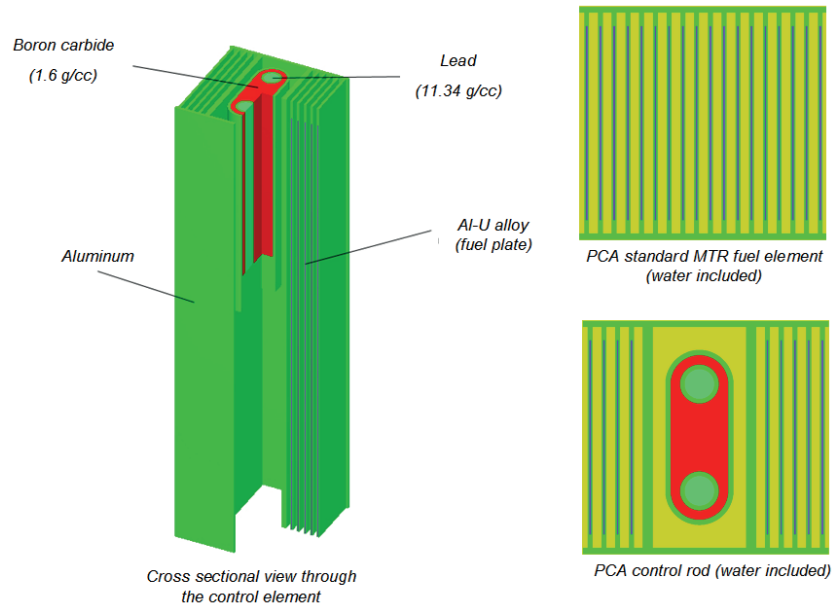


Figure 2: Standard MTR and control element of the PCA core

The eight vertical experimental access tubes (A1-A8) in which the measurements were done were filled with appropriate material (steel in the pressure vessel locations and Plexiglas in the in-water locations) in order to minimize the perturbations of the neutron field. Measured quantities, used in the PCA benchmark, are given in terms of the equivalent $^{235}U$ fission fluxes which were calculated by dividing the reaction rates with the cross-sections averaged over the $^{235}U$ fission spectrum [2]. All measured quantities provided for comparison with calculated DORT values are given per unit PCA benchmark facility core neutron source, meaning that they are normalized to a unit source. Therefore, the calculated results need to be normalized to the source strength of one fission neutron per second being born in the whole PCA core. The ratios of the calculated-to measured (C/M) equivalent fission fluxes for DORT libraries BUGLE-93, SAILOR-95, and BUGLE-96 are given in PCA benchmark reference [2]. Measurements were performed at the core midplane (z = 0) at several locations, labeled in Figure 3 as A1 to A7.

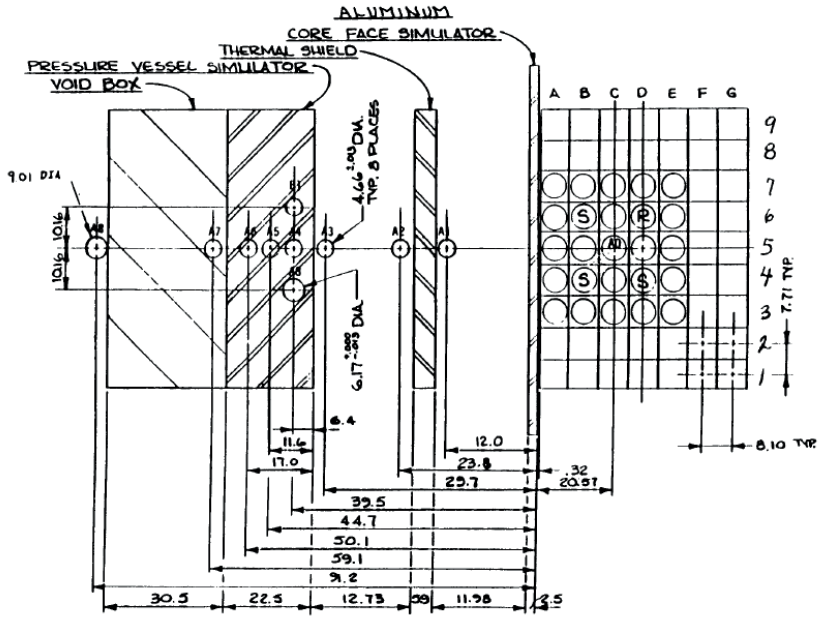


Figure 3: Horizontal cross section of the PCA pressure vessel benchmark facility "12/13" [2]


Mario Matijević, Dubravko Pevec, Krešimir Trontl, Bojan Petrović, PCA Benchmark Analysis with ADVANTG3.0.1 and MCNP6.1.1b Codes, Journal of Energy, vol. 68 Number 2–3, Special Issue (2019), p. 171–183

To complete the PCA benchmark analysis the analyst must determine the calculated-to-measured (C/M) ratios of the equivalent $^{235}U$ fission fluxes for all the locations and all the dosimeters for which the measured values are provided. The significance of the PCA Benchmark are the *experimental data measurements* inside the thick steel RPV in locations A4 to A6, that is, the neutron flux gradient inside the pressure vessel, which provides the means for verification of calculated neutron flux attenuation. This is in contrast to available data from existing operating reactors, which are typically addressing neutron flux for downcomer region internal to RPV and reactor cavity external to RPV wall [10].

## 3 HYBRID SHIELDING METHODOLOGY WITH ADVANTG/MCNP

The ADVANTG3.0.1 [11] is an automated tool for generating variance reduction parameters for fixed-source continuous-energy MC simulations with MCNP6.1.1b code [12], based on approximate 3D multigroup discrete ordinates forward-adjoint transport solutions generated by Denovo [13]. The Denovo is a structured, Cartesian grid $S_N$ solver based on the Koch-Baker-Alcouffe parallel transport sweep algorithm across the x-y domain blocks. Denovo is used in forward and adjoint mode to approximate the space-energy dependent flux across the $S_N$ mesh. These solutions are utilized to calculate space-energy dependent biasing parameters, biased source and transport importance map (weight windows), to be used as VR parameters in the MCNP. CADIS methodology [14] is used to optimize MC results in localized regions of phase-space, while FW-CADIS [15] is applied to obtain global uniform statistical uncertainty by weighting the adjoint source with expected detector response approximated with forward Denovo solution. CADIS and FW-CADIS are based on the adjoint function [16] (i.e., solution of the adjoint Boltzmann equation) which has long been recognized as the importance function for some objective function of interest. Detector response is found by integrating the product of the detector cross-section $\sigma_d(\vec{r},E)$ and flux over detector volume:

$$R = \int_{V_D}\int_E \sigma_d(\vec{r},E)\phi(\vec{r},E)dVdE \tag{1}$$

Alternatively, if we approximate the adjoint scalar flux with a quick Denovo solution, where the adjoint source is set as $q^\dagger(\vec{r},E) = \sigma_d(\vec{r},E)$, then the detector response is found by integrating the product of the normal source distribution $q$ and the adjoint flux over the source volume:

$$R = \int_{V_S}\int_E q(\vec{r},E)\phi^\dagger(\vec{r},E)dVdE\,. \tag{2}$$

The biased source distribution $\hat{q}(\vec{r},E)$ [11], which minimizes the variance of a user-desired response $R$, can be found by using the Lagrange multiplier $\lambda$ method [17],

$$L\left[\hat{q}(\vec{r},E)\right] = \int_V\int_E \frac{q^2(\vec{r},E)\left(\phi^\dagger(\vec{r},E)\right)^2}{\hat{q}(\vec{r},E)}dVdE + \lambda\int_V\int_E \hat{q}(\vec{r},E)dVdE\,, \tag{3}$$

giving the final expression for a biased source

$$\hat{q}(\vec{r},E) = \frac{\phi^\dagger(\vec{r},E)q(\vec{r},E)}{R} = \frac{\phi^\dagger(\vec{r},E)q(\vec{r},E)}{\int_{V_S}\int_E q(\vec{r},E)\phi^\dagger(\vec{r},E)dVdE}\,, \tag{4}$$

where $\phi^{\dagger}(\vec{r},E)$, $q(\vec{r},E)$ and $R$ are the scalar adjoint function, the source emission probability (forward source), and the total detector response, respectively. For transport biasing the weight window technique is employed, that is, space-energy dependent geometric splitting/roulette. Biased source and weight-window lower bounds are consistent, so the source particles are created with statistical weights within weight windows:

$$\bar{w}(\vec{r},E)=\frac{q(\vec{r},E)}{\hat{q}(\vec{r},E)}=\frac{R}{\phi^{\dagger}(\vec{r},E)}=\frac{\int_{V_S}\int_{E} q(\vec{r},E)\phi^{\dagger}(\vec{r},E)dVdE}{\phi^{\dagger}(\vec{r},E)}. \quad (5)$$

Inverse relationship between the particle statistical weight and adjoint function must be emphasized. Since the PCA Benchmark involves calculation of near and far detector reaction rates, this FW-CADIS methodology was a highly desirable choice. The VR parameters generated by ADVANTG consist of space-energy dependent weight-window bounds (WWINP file) and biased source distributions (SB cards in SDEF), which are outputted in formats that can be directly used with unmodified version of MCNP. ADVANTG has been applied to neutron, photon, and coupled neutron-photon simulations of real-world radiation detection and shielding scenarios. ADVANTG is compatible with all MCNP geometry features and can be used to accelerate cell tallies (F4, F6, F8), surface tallies (F1 and F2), point-detector tallies (F5), and Cartesian mesh tallies (FMESH).

The MCNP6.1.1b is a general-purpose Monte Carlo N-Particle code that can be used for neutron, photon, electron, or coupled neutron/photon/electron transport. The MCNP treats an arbitrary three-dimensional configuration of materials in geometric cells bounded by first- and second-degree surfaces and fourth-degree elliptical tori. For neutrons, all reactions given in a particular cross-section evaluation (such as ENDF/B-VI) are accounted for. Thermal neutrons are described by both the free gas and $S(\alpha,\beta)$ models. Important standard features that make MCNP very versatile and easy to use include a powerful general source, criticality source, and surface source; both geometry and output tally plotters; a rich collection of variance reduction techniques; a flexible tally structure; and an extensive collection of cross-section data. Energy ranges are from 1e-11 to 20 MeV for neutrons with data up to 150 MeV for some nuclides, 1 keV to 1 GeV for electrons, and 1 keV to 100 GeV for photons. Pointwise cross-section data were used within MCNP: auxiliary program MAKXSF prepares cross-section libraries with Doppler broadening.

## 4 ANALYSIS OF THE PCA BENCHMARK

The Monte Carlo calculational model of the PCA facility was developed using combinatorial geometry of the MCNP code. The model was verified with criticality eigenvalue calculation while the obtained equivalent fission fluxes have been compared with the referenced PCA benchmark data.

### 4.1 Criticality eigenvalue results

The criticality eigenvalue calculation of the PCA benchmark facility was performed using 350 active neutron cycles with 2000 neutrons per cycle. First 50 cycles were skipped in order for the fission source distribution to converge to the fundamental eigenmode, which was confirmed with the Shannon entropy check. Geometry of the system, materials, and critical control rod positions were verified yielding the effective neutron multiplication factor of the system $k_{\text{eff}}$ = (0.99924 ± 0.00100).

### 4.2 Fixed source shielding results

The FW-CADIS methodology of the ADVANTG code was used for the VR preparation in form of the consistent weight windows and biased source distributions for biasing neutron transport from the PCA core to eight detector locations in the experimental access tubes A1–A8. The equivalent fission fluxes in the PCA report were calculated by dividing the reaction rates by the cross-sections averaged over the $^{235}$U fission spectrum. Equivalent fission fluxes are thus defined as

$$\phi_{eq} = \frac{\int_E \sigma_i(E)\phi(E)dE}{\frac{\int_E \sigma_i(E)\varphi(E)dE}{\int_E \varphi(E)dE}} = \frac{\text{reaction rates}}{\bar{\sigma}_i} \tag{6}$$

where $\sigma_i(E)$, $\phi(E)$ and $\varphi(E)$ are dosimetry cross-sections for the reaction of interest, the Monte Carlo flux at the dosimetry location (center of experimental tubes), and weighting spectrum function, respectively. The spectrum-averaged cross-sections $\bar{\sigma}_i$ were taken from the referenced PCA benchmark Table 1.6 [2] for the sake of consistency, but they were independently cross-checked with our libraries. Seven point detector locations (A1 to A7) were tallied for total of six reaction rates of interest using IRDF-2002 library: $^{237}$Np(n,f)$^{137}$Cs, $^{238}$U(n,f)$^{137}$Cs, $^{103}$Rh(n,n')$^{103m}$Rh, $^{115}$In(n,n')$^{115m}$In, $^{58}$Ni(n,p)$^{58}$Co, and $^{27}$Al(n,α)$^{24}$Na. These reactions were used as response functions for the FW-CADIS methodology, corresponding to point adjoint source spectrum. The threshold energies for the $^{27}$Al(n,α)$^{24}$Na, $^{58}$Ni(n,p)$^{58}$Co, $^{238}$U(n,f)$^{137}$Cs, $^{237}$Np(n,f)$^{137}$Cs, $^{115}$In(n,n')$^{115m}$In, and $^{103}$Rh(n,n')$^{103m}$Rh reactions are 5.0, 2.05, 1.45, 0.69, 0.3, and 0.1 MeV, respectively. Even though majority of the reactions are in the fast neutron range, MCNP calculations were performed with full neutron spectrum using continuous energies.

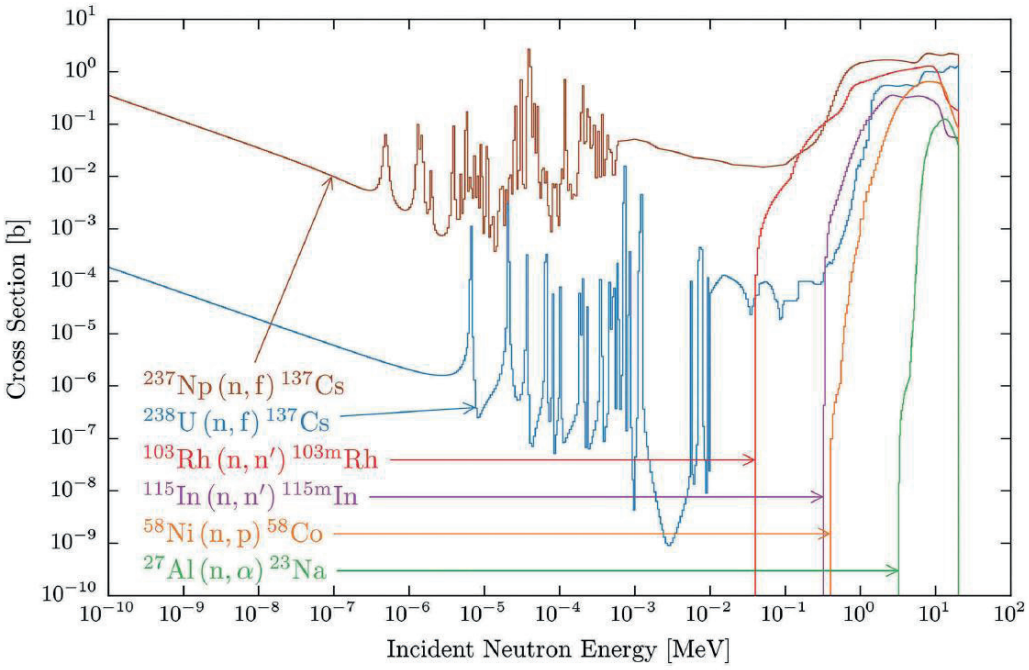


Figure 4: Reaction cross sections of interest in the PCA benchmark

The ADVANTG code with FW-CADIS methodology was used with updated "bplus" ANISN-type multigroup shielding library (47n/20g), containing 393 isotopes and based on the ENDF/B-VII.0 nuclear data [18][19]. The robust and flux-positive step characteristic (SC) spatial differencing scheme was used in $S_N$ calculations. The "macromaterial" option was used to mix 11 pure materials

into 26857 effective Denovo materials. Point detectors were placed in the center of void spheres which are located in the axial midplane of the experimental tubes. The Denovo $S_N$ mesh had 1.6e+06 cells covering the PCA facility model, that is, 160×100×100 cells in the *xyz* direction with average cell side of 1.0 cm. The same mesh size was used for the MCNP mesh tally. The quadrature set was quadruple QR (2 polar x 2 azimuth per octant) and Legendre order of scattering cross-section expansion was $P_1$ (upscattering was deactivated). Since the axial flux gradients inside tubes are confirmed to be sufficiently small, void spheres with 1.0 cm radius were also placed in the midplane (z = 0) of the access tubes, to verify point detector results. The ADVANTG memory consumption is highly dependent on the adjoint source spectrum function, so the forward run used 6-9 GB RAM and adjoint run used 10-14 GB RAM. The MCNP was run for 3 hrs in parallel mode utilizing PVM routine with 4 CPU cores which resulted in 2-4 million histories. Point detectors had on the average less than 1% statistical relative error (*RE*). Selected ADVANTG and MCNP results for $^{27}Al(n,\alpha)^{24}Na$ reaction are presented next. Figure 5 shows Denovo fast (7.4 – 6.1 MeV) and thermal (1e-05 – 0.1 eV) neutron flux solutions, with characteristic gradients in thick steel regions. Figure 6 shows Denovo total (integrated) adjoint flux where local maxima correspond to point detector locations. The most distant detector A8 has the highest peak, since the probability of neutron transport to that location is extremely low.

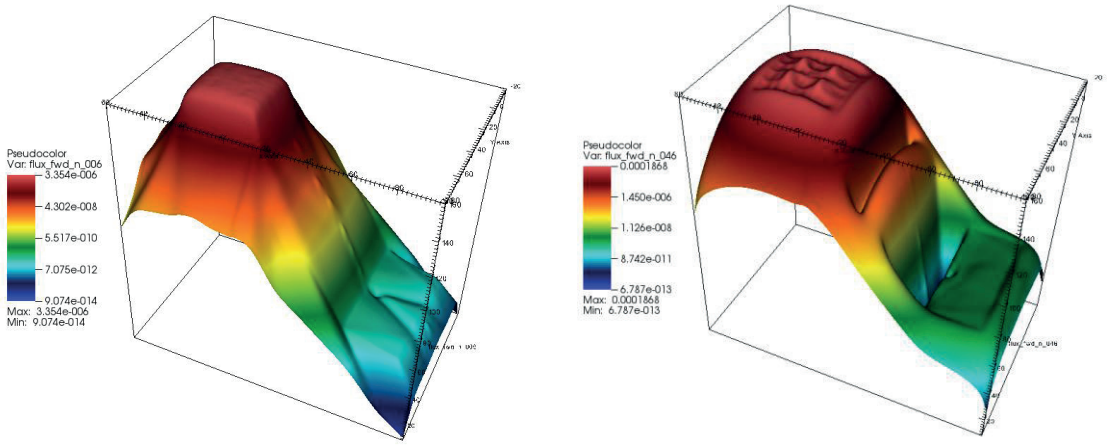


Figure 5: Denovo neutron flux solution in the PCA midplane
(left: fast group no. 6; right: thermal group no. 46)

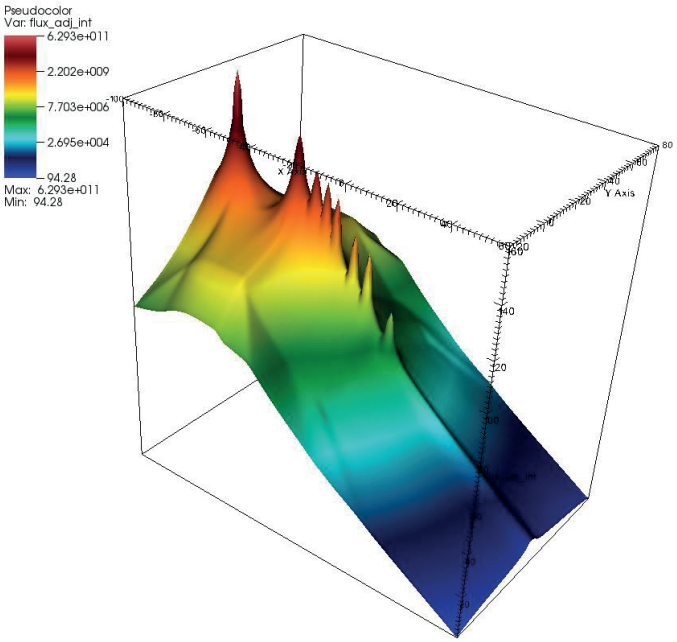


Figure 6: Denovo integrated total adjoint flux in the PCA midplane

The weight windows for the first energy group (17.3 – 14.2 MeV) are shown in Figure 7, where one can notice the expected $\bar{w}(\vec{r},E) = R / \phi^{\dagger}(\vec{r},E)$ behavior. Figure 8 and Figure 9 are depicting MCNP mesh tally solution in the PCA midplane with relative errors. One can notice that regions with smallest statistical error correspond to point detector locations.

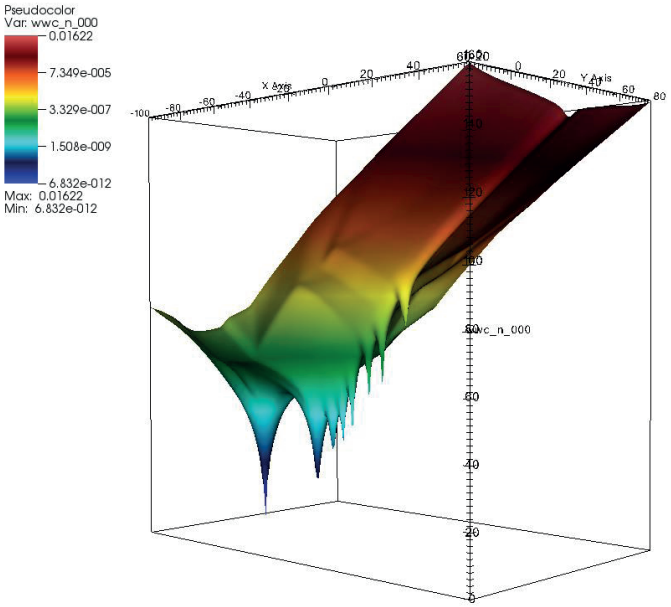


Figure 7: Denovo weight windows in the PCA midplane (fast group no. 1)

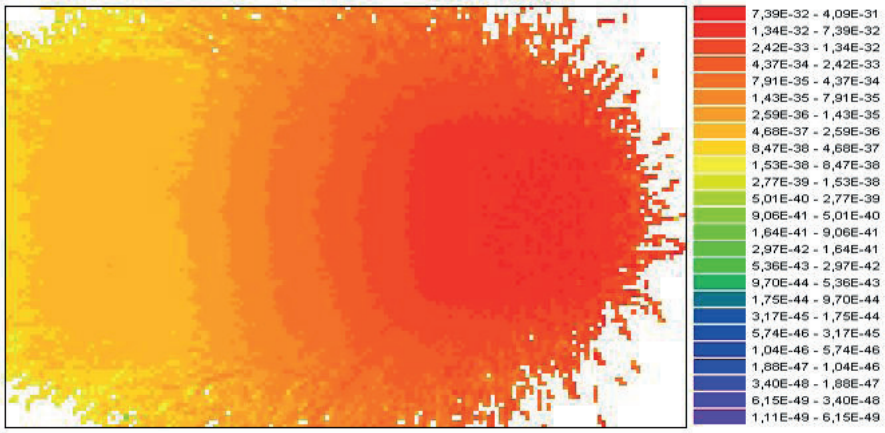


Figure 8: MCNP $^{27}Al(n,\alpha)^{24}Na$ reaction rates in the PCA midplane

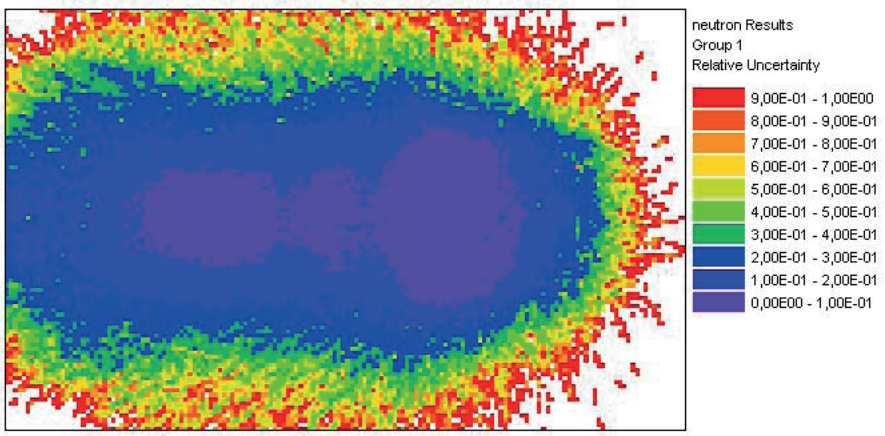


Figure 9: MCNP relative error of $^{27}Al(n,\alpha)^{24}Na$ reaction rates in the PCA midplane

The MCNP calculated equivalent fission fluxes C/M ratios are shown in Table 1. Average C/M per location is also shown with one standard deviation. Only the reactions for which the PCA measurements were reported are listed. These results are compared to the referenced DORT results [2], where one can notice high similarity between the stochastic and deterministic solution methods. Locations A4 to A6 highlighted in yellow are for the detectors placed inside the RPV simulator.

Table 1: Equivalent fission fluxes C/M ratios*

| Location | $^{237}$Np(n,f) | $^{238}$U(n,f) | $^{27}$Al(n,α) | $^{58}$Ni(n,p) | $^{115}$In(n,n') | $^{103}$Rh(n,n') | MCNP Avg ± sig | DORT Avg ± sig |
|---|---|---|---|---|---|---|---|---|
| **A1** | 0.86 | - | 0.85 | 0.99 | 1.01 | 1.01 | 0.94 ± 0.04 | 0.91 ± 0.02 |
| **A2** | - | - | 0.91 | 1.05 | 1.10 | - | 1.02 ± 0.06 | 0.92 ± 0.01 |
| **A3** | 0.91 | - | 0.80 | 0.90 | 0.93 | - | 0.89 ± 0.03 | 0.96 ± 0.02 |
| **A4** | 0.87 | 0.88 | 0.90 | 0.98 | 0.97 | 0.94 | 0.92 ± 0.02 | 0.94 ± 0.03 |
| **A5** | 0.91 | 0.88 | 0.96 | 1.02 | 0.99 | 0.95 | 0.95 ± 0.02 | 0.92 ± 0.03 |
| **A6** | 0.88 | 0.88 | 1.01 | 1.04 | 1.02 | 0.96 | 0.97 ± 0.03 | 0.91 ± 0.04 |
| **A7** | 0.94 | - | - | - | - | - | 0.94 ± 0.00 | 0.89 ± 0.00 |
| **A8** | - | - | - | - | - | - | - | - |

(*"-" experimental results were not provided in the PCA benchmark)

## 5 DISCUSSION OF RESULTS

The obtained MCNP results for the equivalent fission fluxes are in accordance with the calculational uncertainty criterion from the U.S.NRC Regulatory Guide 1.190, meaning that the calculated values agree with the measurements to within 20% for out-of-core dosimetry locations. Underprediction in the C/M ratio can be observed for the reaction $^{238}$U(n,f)$^{137}$Cs (1.45 MeV threshold) through the thick RPV simulator (locations A4 to A6), with 0.88 on average. High attenuation of the neutron flux in that area is causing softening of the neutron spectrum in the RPV simulator, which shifts neutrons in resonance regions for inelastic scattering on iron isotopes. Microscopic cross-section for neutron inelastic scattering on iron isotopes is shown in Figure 10 [20][21].

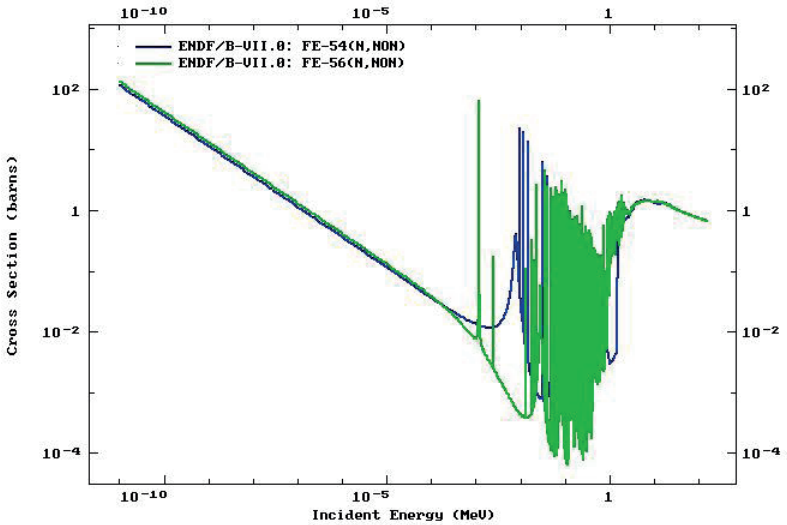


Figure 10: Inelastic scattering (MT=3) of iron isotopes

Results for $^{238}$U(n,f)$^{137}$Cs can indicate self-shielding effects and sensitivity of the multigroup shielding library "bplus" on the iron cross sections. Overprediction in results is highest for the

detector A2 with average C/M ratio of 1.02, immediately after the stainless steel thermal shield, which has large amount of iron. Again, self-shielding effects of iron cross-sections are pronounced, especially for $^{27}Al(n,\alpha)^{24}Na$ with C/M ratio of 0.91. The obtained MCNP results show an overall good agreement with the experimental results, however, for location A3 in front of the RPV simulator there is underprediction about 10% on average.

Another indicator of an efficient hybrid shielding MC simulation is the adjusted figure-of-merit (FOM) factor [11][12]. It is introduced to account for the time it takes to achieve a given level of uncertainty in a MC simulation

$$FOM = 1/RE^2(T_{MC} + T_{ADV}), \tag{7}$$

where $RE$ is the tally relative error (on 1 sigma level), $T_{MC}$ is the MCNP run time (in min), and $T_{ADV}$ is the ADVANTG run time (in min). This adjusted FOM factor can be used to determine whether ADVANTG-based VR parameters are worth the time that was required to generate them. This useful metric was a bit abused in this paper by making $T_{MC}$ larger than what is actually required in practical application. This is evident since the average point detector $RE$ is below 1 %, while an acceptable value by the MCNP manual is 5% or less. General trend of decreasing FOM factors on Figure 11 towards distant detectors means that it is a hard task to transport neutrons through thick layers of water and steel, so more histories (i.e. CPU time) is necessary to achieve the same level of uncertainty. In this paper all calculations have been performed on QuadCore Q6600 with 8GB of RAM.

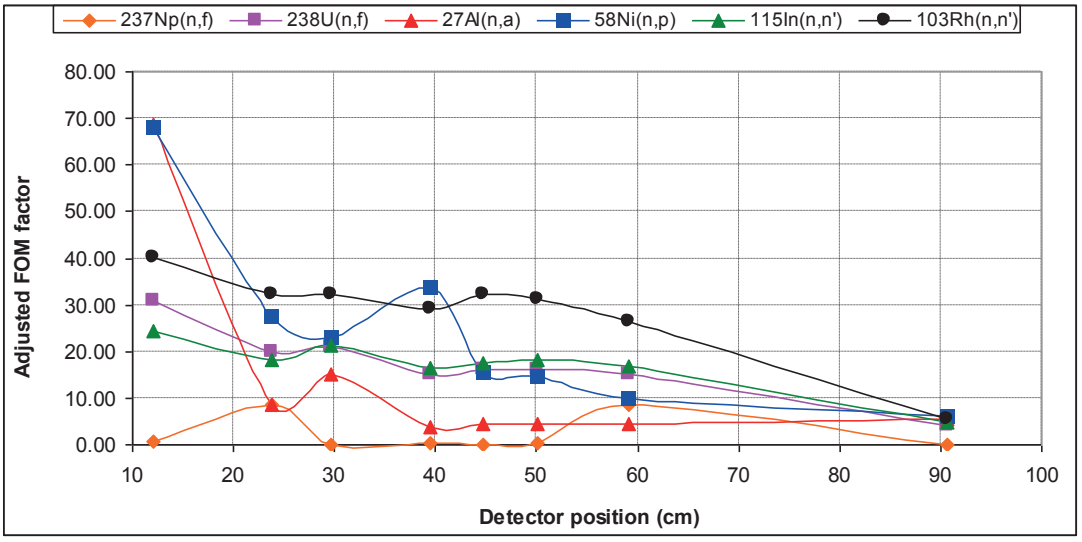


Figure 11: MCNP adjusted FOM factors for different detector locations

## 6 CONCLUSIONS

The simulation model of the PCA benchmark facility was developed using MCNP and ADVANTG codes, implementing modern hybrid shielding techniques. The results of shielding calculations in form of equivalent fission fluxes have been compared with PCA reference data. A good agreement of the calculated and measured equivalent fission fluxes has been obtained. No systematic decrease of agreements between calculations and measurements with increasing distance of detector from the PCA core was observed. This indicates that the shapes of calculated neutron spectra, in the energy range were dosimeters are sensitive, are properly determined. Application of the automated variance reduction technique based on FW-CADIS methodology removes the burden of manually tuning the VR parameters and significantly improves the quality of MC calculations.

## REFERENCES


[1] "Shielding Integral Benchmark Archive and Database," SINBAD Reactor Shielding Benchmark Experiments, OECD/NEA, 2011.

[2] I. Remec and F. B. Kam, "Pool Critical Assembly Pressure Vessel Facility Benchmark," NUREG/CR-6454 (ORNL/TM-13205), prepared for the U.S.NRC by Oak Ridge National Laboratory, August 1997.

[3] A.H. Fero, S.L. Anderson, and G.K. Roberts, "Analysis of the ORNL PCA benchmark using TORT and BUGLE-96," in Reactor Dosimetry: Radiation Metrology and Assessment, J.G. Williams, D. W. Vehar, F. H. Ruddy, and D. M. Gilliam, Eds., pp. 360–366, American Society for Testing and Materials, Philadelphia, Pa, USA, 2001.

[4] Y.K. Lee, "Analysis of the NRC PCA pressure vessel dosimetry benchmark using TRIPOLI-4.3 Monte Carlo code and ENDF/BVI.4, JEF2.2 and IRDF-90 libraries," Nuclear Mathematical and Computational Science: A Century in Review, A Century A new, " Gatlinburg, Tenn, USA, April 2003.

[5] T. Flaspoehler, B. Petrovic, "Validating Scale6.1/MAVRIC with Two Reactor Pressure Vessel Dosimetry Benchmarks," Trans. Am. Nucl. Soc., 106, (2012).

[6] M. Matijević, D. Pevec, K. Trontl, "Modeling of the ORNL PCA Benchmark Using SCALE6.0 Hybrid Deterministic-Stochastic Methodology," Science and Technology of Nuclear Installations, Vol. 2013, Article ID 252140, 2013.

[7] J.A. Kulesza and R.L. Martz, "Evaluation of the Pool Critical Assembly Benchmark with Explicitly Modeled Geometry Using MCNP6," Nuclear Technology 197:3, 284-295, 2017.

[8] International Atomic Energy Agency, Vienna, Austria, "International Reactor Dosimetry File 2002 (IRDF-2002)," 2006.

[9] U.S.NRC, "Calculational and Dosimetry Methods for Determining Pressure Vessel Neutron Fluence," Regulatory Guide 1.190, 2001.

[10] I. Remec and F. B. K. Kam, "H.B. Robinson-2 Pressure Vessel Benchmark," NUREG/CR-6453 (ORNL/TM-13204), prepared for the U.S.NRC by Oak Ridge National Laboratory, October 1997.

[11] S.W. Mosher, S.R. Johnson, A.M. Bevil et al., "ADVANTG – An Automated Variance Reduction Parameter Generator," ORNL/TM-2013/416, Rev. 1, August 2015.

[12] T. Goorley, "MCNP6.1.1-Beta Release Notes," LA-UR-14-24680, 2014.

[13] T.M. Evans, A.S. Stafford, R.N. Slaybaugh, K.T. Clarno, "Denovo: A New Three-Dimensional Parallel Discrete Ordinates Code in SCALE," Nuclear Technology, 171:2, 171-200, DOI: 10.13182/NT171-171, 2010.

[14] J.C.Wagner and A. Haghighat, "Automated variance reduction of Monte Carlo shielding calculations using the discrete ordinates adjoint function," Nuclear Science and Engineering, Vol. 128, no. 2, pp. 186–208, 1998.

[15] J.C. Wagner, E. D. Blakeman, and D. E. Peplow, "Forward weighted CADIS method for global variance reduction," Transactions of the American Nuclear Society, vol. 97, pp. 630–633, 2007.

[16] G.I. Bell and S. Glasstone, "Nuclear Reactor Theory," Van Nostrand Reinhold Company, Litton Educational Publishing, 1970.

[17] D.H. Kim, et al, "A proposal on multi-response CADIS method to optimize reduction of regional variances in hybrid Monte Carlo simulation," Annals of Nuclear Energy 104, 282-290, 2017.

[18] J.M. Risner, D.Wiarda, M.E. Dunn, T.M. Miller, D.E. Peplow, and B.W. Patton, "Production and Testing of the VITAMIN-B7 Fine-Group and BUGLE-B7 Broad-Group Coupled Neutron/Gamma Cross-Section Libraries Derived from ENDF/B-VII. 0 Nuclear Data," U.S.NRC NUREG/CR-7045, 2011.

[19] M.B. Chadwick, P. Obložinsky, M. Herman et al., "ENDF/B-VII.0: next generation evaluated nuclear data library for nuclear science and technology," Nuclear Data Sheets, Vol. 107, no. 12, pp. 2931–3060, 2006.

[20] A. Trkov, M. Herman, and D. A. Brown, "ENDF-6 Formats Manual," Data Formats and Procedures for the Evaluated Nuclear Data Files ENDF/B-VI and ENDF/B-VII, National Nuclear Data Center, Brookhaven National Laboratory, 2011.

[21] IAEA Nuclear Data Services, http://www-nds.iaea.org/, last accessed on May 2018.

Journal of Energy
VOLUME 68 Number 2-3 | 2019 | Special Issue
journal homepage: http://journalofenergy.com/

# Assessment of the Photon and Neutron Source Term for the NPP Krško Spent Fuel

**Marjan Kromar**
"Jožef Stefan" Institute
Reactor Physics Division
Jamova 39, 1001 Ljubljana, Slovenia
and University of Maribor
Faculty of Energy Technology
Hočevarjev trg 1, 8270 Krško, Slovenia
Marjan.Kromar@ijs.si

**Bojan Kurinčič**
Nuclear Power Plant Krško
Engineering Division - Nuclear Fuel & Reactor Core
Vrbina 12, 8270 Krško, Slovenia
Bojan.Kurincic@nek.si

## ABSTRACT

Accurate knowledge of the fuel nuclide inventory is important after reactor shut down, during the fuel storage and subsequent reprocessing or disposal to provide adequate shielding from the photon and neutron radiation. In this paper possibility to calculate the NPP Krško photon and neutron source term with the Serpent code has been analysed. Some deficiencies in the supplied ENDF/B-VII.0 decay library have been observed. In addition, Serpent reports only spontaneous fission rates without (α, n) and (β, n) contributions. To get neutron emission, spontaneous fission rates had to be multiplied with the average number of neutrons born for each particular nuclide manually. Comparison with the Origen code has shown acceptable agreement of the ENDF/B-VII.1 results. Influence of several factors such as fuel burnup, enrichment, temperature, moderator temperature (density), soluble boron concentration, average power, and burnable absorbers has been analysed. In addition, it was demonstrated that, except for the burnup and enrichment, averaging of all other parameters is acceptable approach. IFBA fuel should be accounted for explicitly due to relative high impact on the photon and neutron emissions.

***Keywords:*** *PWR fuel, photon source term, neutron source term*

## 1 INTRODUCTION

In a nuclear reactor, the fission of heavy atoms such as isotopes of uranium and plutonium results in the formation of highly radioactive fission products. Due to neutron capture higher actinides are formed, some of them being unstable. All these unstable isotopes radioactively decay and produce decay heat and radiation. Accurate knowledge of the nuclide inventory is important after reactor shut down, during the fuel storage and subsequent reprocessing or disposal. Namely, proper radiation protection is a primary objective in the transportation, storage or processing of irradiated nuclear fuel. The designing of adequate shielding to provide this protection requires appropriate knowledge of the radiation source in spent nuclear fuel.

In this paper possibility to calculate the fuel isotopic composition and determination of the photon and neutron source term with the Serpent code [1] is investigated. Serpent is a well-known

Monte Carlo code used primarily for the calculation of the neutron transport in the reactor. It has been validated for the burn-up calculations [2]. However, in the calculation of the photon and neutron source term different set of isotopes is important than in the neutron transport case. For the purpose of this evaluation only the radioactive decay of fission products and actinides is considered. A typical case of the NPP Krško fuel is selected for comparison with the Origen code [3]. Origen is a well-known computer code system for calculating the buildup, decay, and processing of radioactive materials. Comparison with the Serpent code is performed to verify that the Serpent is taking into account all isotopes important to assess photon and neutron radiation. A similar analysis comparing fuel radioactivity [4] and decay heat [5] has already been performed, showing promising results. After the code validation a sensitivity study is carried out. Fuel isotopic composition is namely pretty dependent on the neutron spectrum and consequently on fuel operating conditions. Influence of several factors such as fuel burnup, enrichment, temperature, moderator temperature (density), soluble boron concentration, average power, and burnable absorbers is analysed.

## 2 BRIEF CODE DESCRIPTION

### 2.1 Origen

The Oak Ridge Isotope Generation (ORIGEN) depletion/decay code was developed at ORNL in 1973. Since then, many new versions have been created [3] and are available from RSICC and NEA data bank. It is a well-known point-depletion inventory code and has been used to model nuclide transmutation with capability to generate source terms for accident analyses, characterize used fuel (including activity, decay heat, radiation emission rates, and radiotoxicity), activate structural materials, and perform fuel cycle analysis studies. Origen uses a matrix exponential method to solve a large system of coupled, linear, first-order ordinary differential equations with constant coefficients (Bateman equations). Version 2.1 with “pwrue” library has been used in this paper.

### 2.2 Serpent

Sensitivity study of the radiation source term is performed with the Serpent code [1, 2]. Serpent is a three-dimensional continuous-energy Monte Carlo reactor physics burnup calculation code, developed at the VTT Technical Research Centre of Finland. It is not a typical Monte Carlo code. While the majority of the other codes use the ray-tracing algorithm as a transport model, Serpent uses the Woodcock delta tracking method. In this way the geometry routines get simplified and calculations are faster compared to conventional Monte Carlo codes. The improved matrix exponential method CRAM (Chebyshev Rational Approximation Method) for solving the Bateman equations [6] has been implemented for the burnup applications. Serpent uses a continuous energy neutron cross section library in an ACE format. Libraries provided with the code distribution are based on the JEF-2.2, JEFF-3.1, JEFF-3.1.1, ENDF/B-VI.8 and ENDF/B-VII.0 evaluated nuclear data files [7]. The code is specialized for two-dimensional lattice physics calculations, but the universe-based geometry description allows the modelling of complicated three-dimensional geometries as well. Detailed geometrical modelling of the NPP Krško fuel assembly in the Serpent code enables accurate determination of fuel isotopics and consequently determination of the photon and neutron source term. In this analyses Serpent 2, version 2.1.28, has been used.

## 3 COMPARISON OF THE CODES AND LIBRARIES

The NPP Krško is a 2-loop Westinghouse PWR that began electricity production in 1981. The start-up core had a rated thermal capacity of 1,876 MWt, and a 626 MWe gross electric power. Currently, the thermal rating is 1,994 MWt with 727 MWe gross electric power. The core consists of 121 standard 16×16 fuel assemblies with some VANTAGE+ features. A typical fuel assembly with 4.95 % enrichment and no IFBA (Integral Fuel Burnable Absorber) rods was selected as a starting point. A reference case scenario consists of the following reactor operational parameters:

1. Fuel temperature 900 K,
2. Moderator temperature 580.46 K with density 0.70871 g/cm$^3$,
3. Soluble boron concentration of 1000 ppm.

Parameters are close to the average operational parameters applied in the last NPP Krško cycles. Comparison of several cases is presented in Fig. 1, where photon emission rate per kg of initial uranium fuel is plotted for the burnups up to 60000 MWd/tU. Emissions calculated with the ENDF/B-VII.0 library are almost 40 % lower than emissions predicted with the Origen code. This is somehow in contradiction with the [4] where predicted activities were higher compared to the Origen results. Closer examination has shown that the ENDF/B-VII.0 decay library supplied with the code contains some dubious photon data for some nuclides. For example, there are no photon data for the $^{240}$Np, resulting in a zero emission, although $^{240}$Np substantially contributes to the total photon emissions. Situation is a little better with the JEFF-3.1.1 library, but the discrepancy with the Origen is still relatively high. Because of that, it was decided to implement ENDF/B-VII.1 library supplied with the MCNP code [8]. Comparison with the Origen shows much better agreement. However, differences are mainly in short lived isotopes as can be seen from Fig. 2, where all 3 libraries give almost identical results after a few days of fuel cooling.

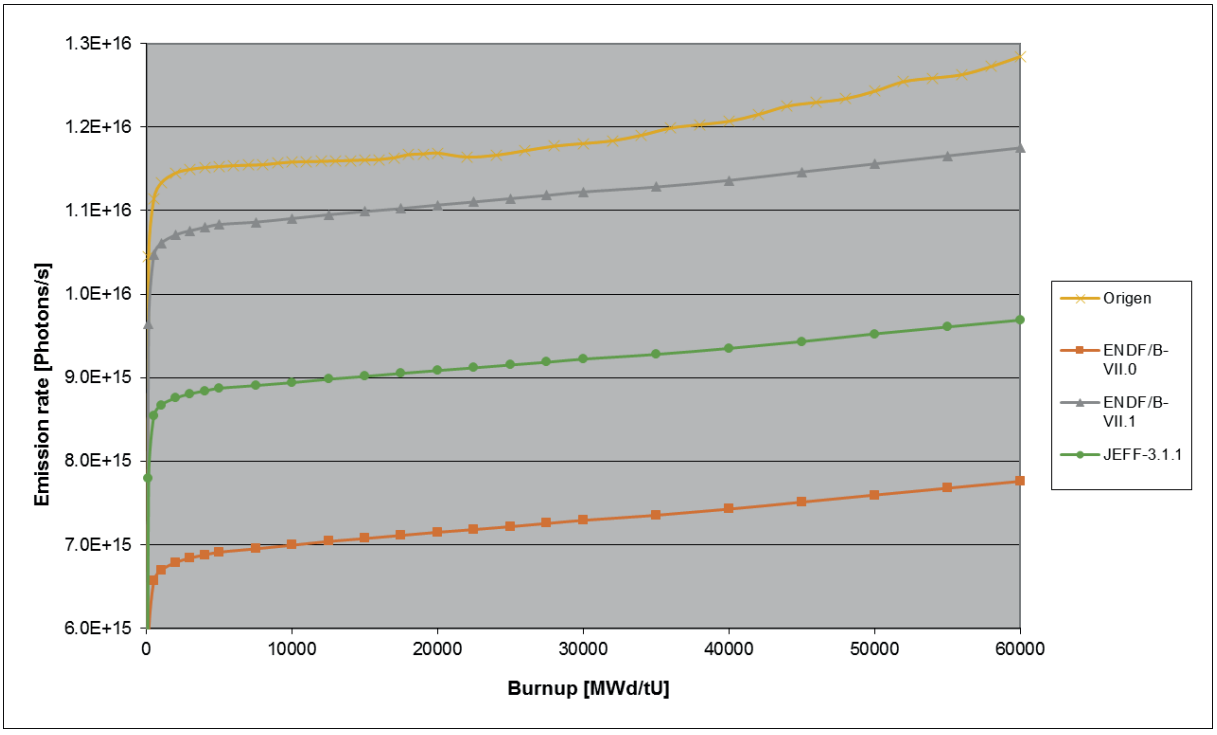


Figure 1: Photon emission rate during fuel burnout

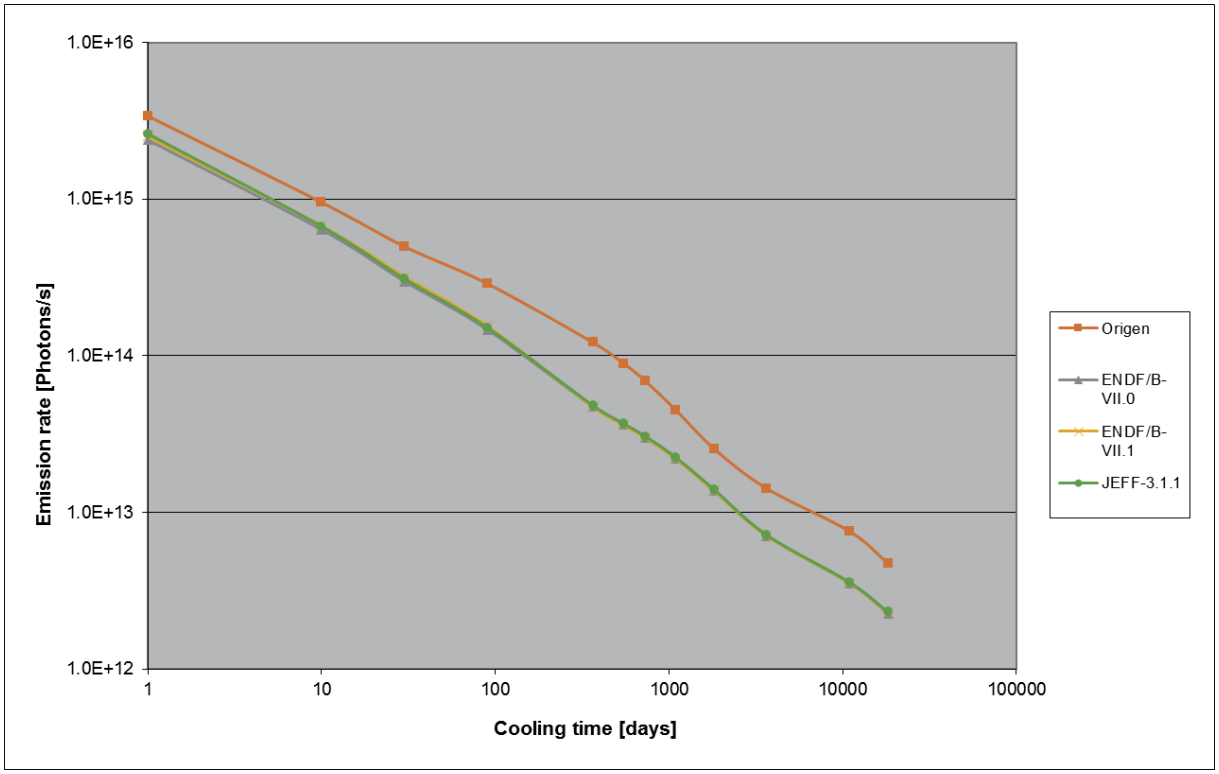


Figure 2: Photon emission rate during fuel cooling

When we tried to estimate neutron emissions, we encountered a few obstacles. Serpent currently predicts neutron emission only from spontaneous fission. There are no models to estimate neutrons from (α, n) and (β, n) reactions. Nevertheless, since spontaneous fission contributes a majority of neutron emissions (roughly 90 %), it is judged that the presented analysis is still representative. Additional drawback is that the Serpent reports only spontaneous fission rates. To get number of neutrons, fission rates have to be multiplied with the average number of neutrons born (nu-bar, $\bar{\nu}$). Since this value differs for different fission nuclides, fission rate for each nuclide had to be multiplied with corresponding $\bar{\nu}$. Values from the ENDF/B-VII.1 library have been taken in all Serpent cases. At the end, it should be noted, that since at longer cooling times only insignificant fractions of the neutron source are caused by the photoneutron reactions, this type of neutron source was neglected in the analysis.

Photon emission comparison of a considered cases is presented in Fig. 3, where neutron emission rate per kg of initial uranium fuel is plotted for the burnups up to 60000 MWd/tU. ENDF/B-VII.0 values are again questionable, since they differ noticeable from other cases at low burnups. Closer examination has shown, that the spontaneous fission rate for the $^{238}$U is 100 times too large due to wrong data in the decay library. Other libraries are more consistent with the Origen code. During the fuel cooling (Fig. 4) JEFF-3.1.1 library is a little closer to the Origen code. ENDF/B-VII.0 and ENDF/B-VII.1 results are almost identical.

In the rest of the paper only values calculated with the ENDF/B-VII.1 library are reported, since the results seem to be the most consistent.

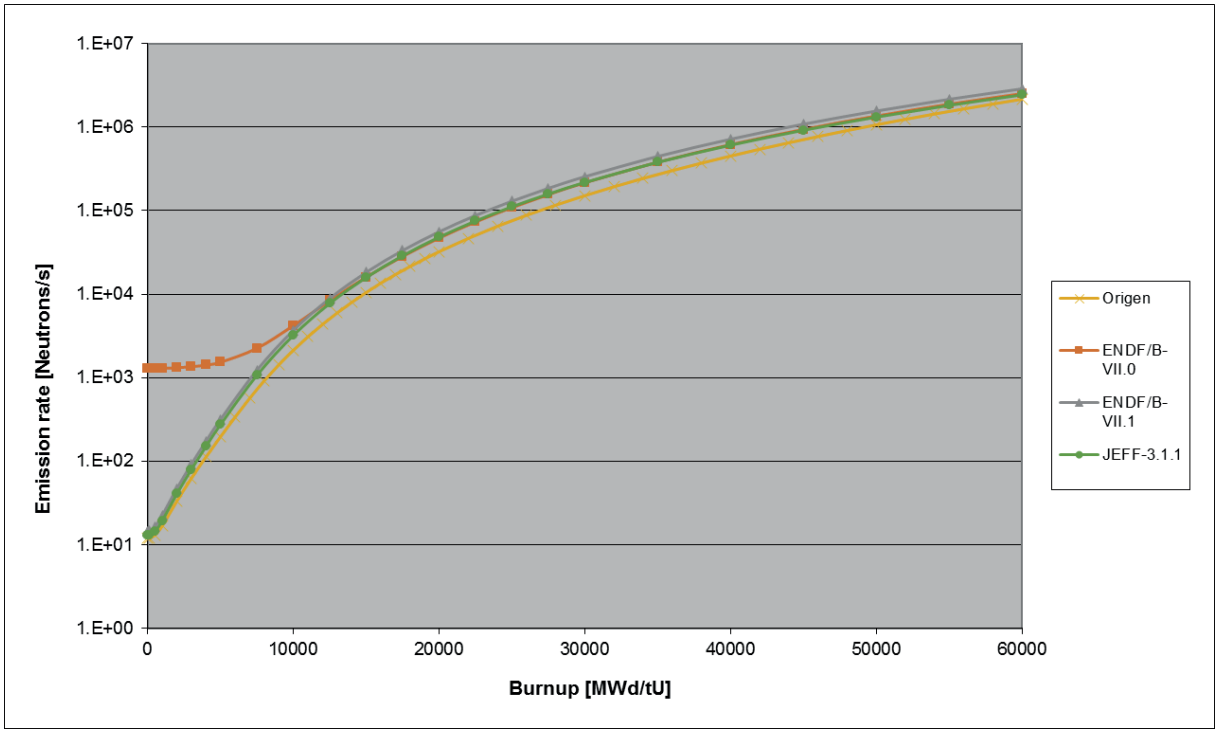


Figure 3: Neutron emission rate during fuel burnout

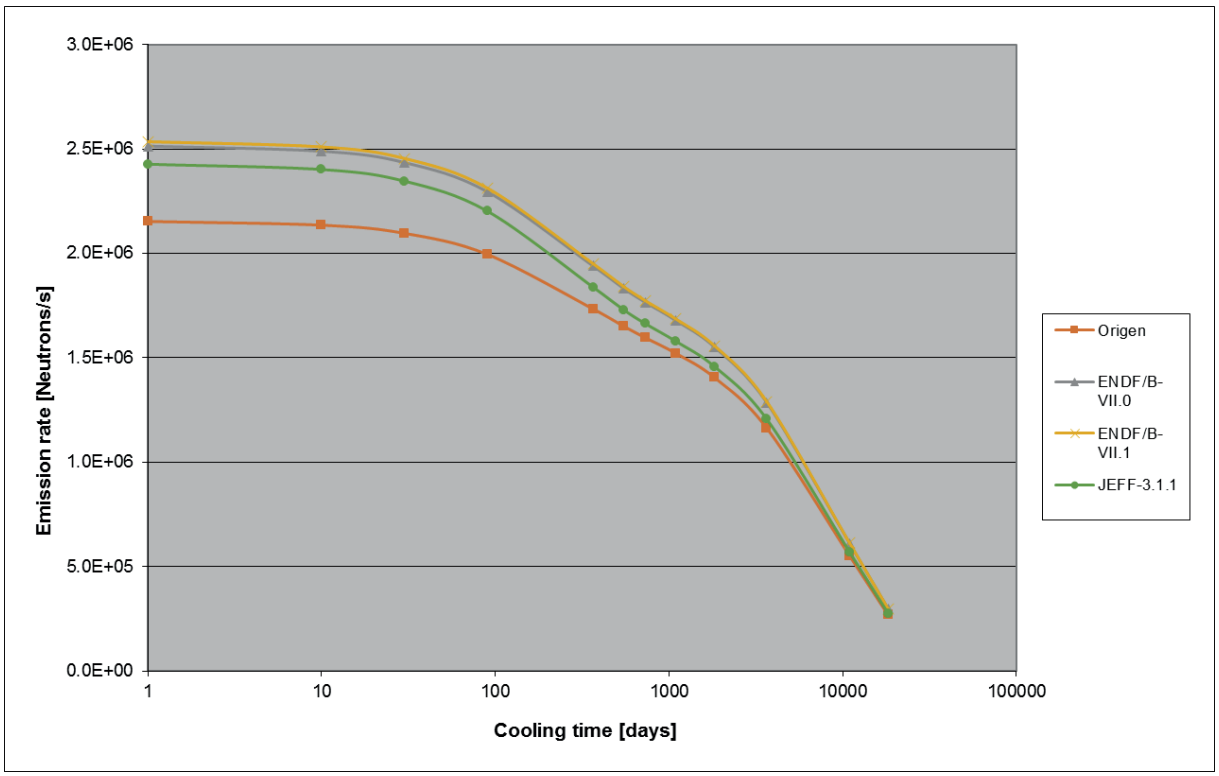


Figure 4: Neutron emission rate during fuel cooling

## 4 SENSITIVITY STUDY

Photons and neutrons in the spent fuel are produced by the radioactive decay of unstable nuclides. Isotopic inventory of these unstable nuclides in the fuel is constantly changing during the reactor operation and is a function of several parameters such as neutron energy spectrum, present fission nuclides inventory etc. Reactor operating conditions (temperatures of the fuel and moderator, water density, neutron absorbers etc.) directly influence neutron spectrum. It is prudent to evaluate effect of these parameters for the development of optimal calculation strategy to achieve desired accuracy. In addition, in the photon and neutron source term evaluations usually some averaging of material properties or conditions is applied. It is not self-evident that such averaging process would yield also an averaged source term value. To verify such assumptions, a sensitivity analysis is needed to confirm such approach or to identify crucial nonlinear parameters.

### 4.1 Burnup

Emission rates versus fuel burnup has already been presented in Figs. 1 - 4. As can be seen from Figs. 1 and 3, changes in the isotopic inventory and consequently emission rates are very high during the fuel burnout. Relative differences in the emission rates for the 40000 MWd/tU and 50000 MWd/tU cases are presented in Figs. 5 and 6. They are rather high and are increasing over cooling time. A curve denoted as "Aver" represents the difference between average of the 40000 MWd/tU and 60000 MWd/tU case relative to the 50000 MWd/tU case. Relative difference is less than 0.6 % for the photon case allowing reasonable averaging process. Situation is very different for the neutron emissions. Fig. 3 is showing increased exponential behaviour (be aware of logarithmic scale), which can clearly not be adequately described by linear function. Therefore, averaging process would produce high errors. "Aver" curve on Fig. 6 is showing errors of almost 25 % for the averaging over ±10000 MWd/tU interval. Closer examination has shown that the major neutron contributors are $^{244}$Cm (80 % – 97 %) and $^{246}$Cm (0.7 % - 3 %) nuclides. Concentration of both nuclides is very sensitive to the fuel irradiation and initial composition.

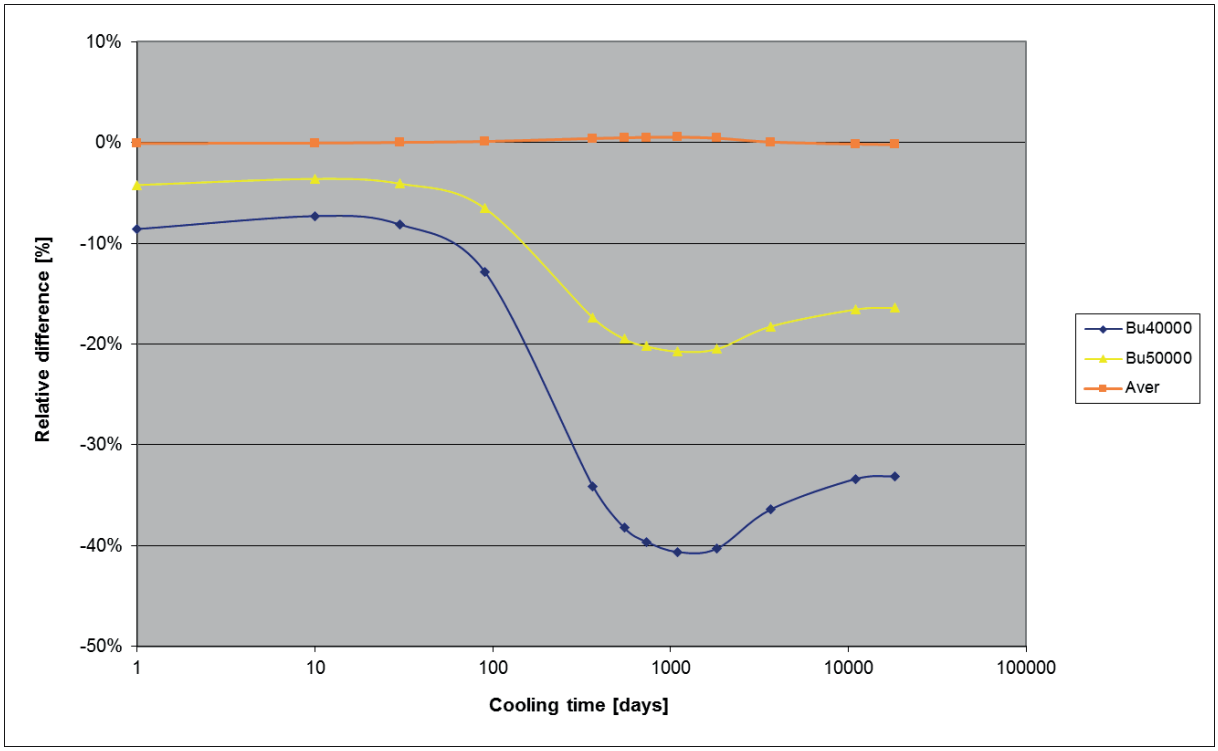


Figure 5: Effect of the burnup on the photon emission rate

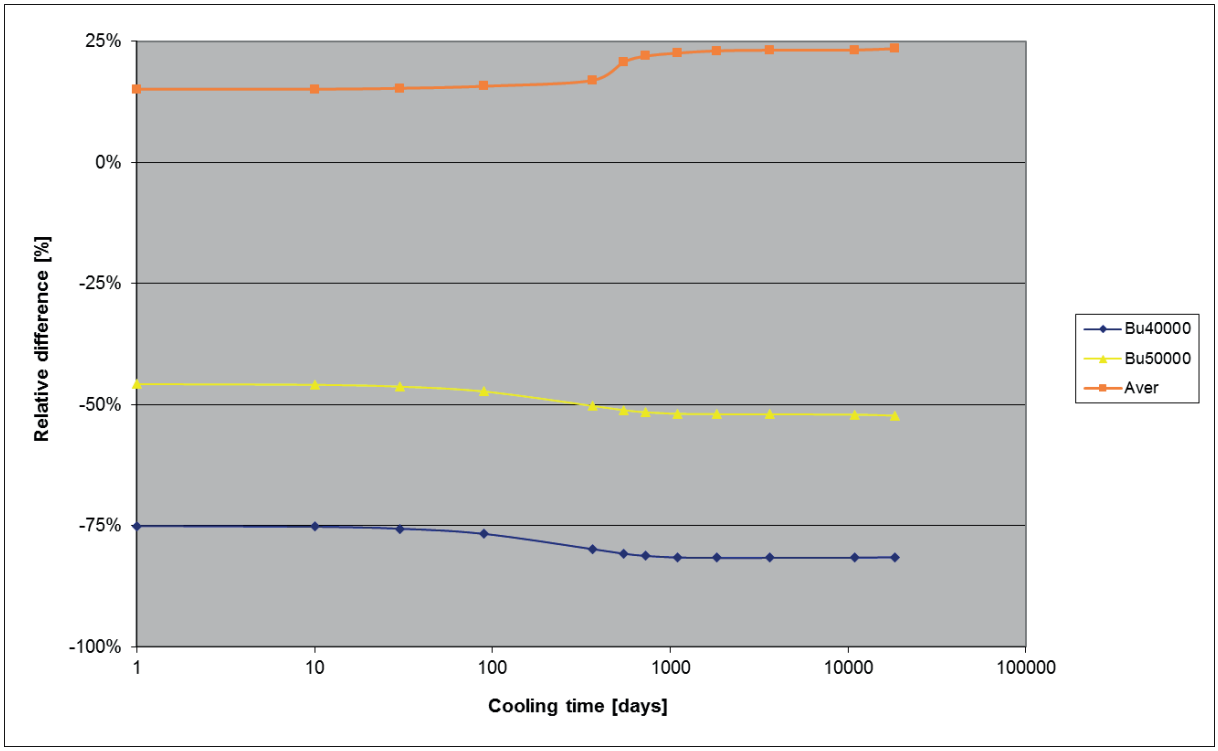


Figure 6: Effect of the burnup on the neutron emission rate

## 4.2 Enrichment

The effect of the fuel enrichment is shown in Figs. 7-8. Two cases (2.1 % and 3.525 %) are compared to the reference 4.95 % case. It can be estimated that a decrease of 1 % in enrichment can induce increase of more than 5 % in the photon emissions rate and 70 % in the neutron emissions. Moreover, the effect is not linear over the cooling period.

As already mentioned, in practice it is a usual procedure to calculate larger fuel areas with some average properties. But strictly speaking, if the fuel assembly is constituted of 2 geometrically equal regions, the one with 2.1 % enrichment and the other with 4.95 %, the average emission rate would not be equal to the emission rate of the fuel with an average 3.525 % enrichment. Differences between the average emission rate of the 2.1 % and 4.95 % fuel region and the emission rate of the averaged 3.525 % region are plotted as “Aver” in Figs. 7 and 8. Differences in photon emission rate of up to 1 % are visible in the 1-10 days region. Much larger differences of up to 15 % are observed for the neutron emission rate confirming unsuitability of the enrichment averaging process for the neutron source term.

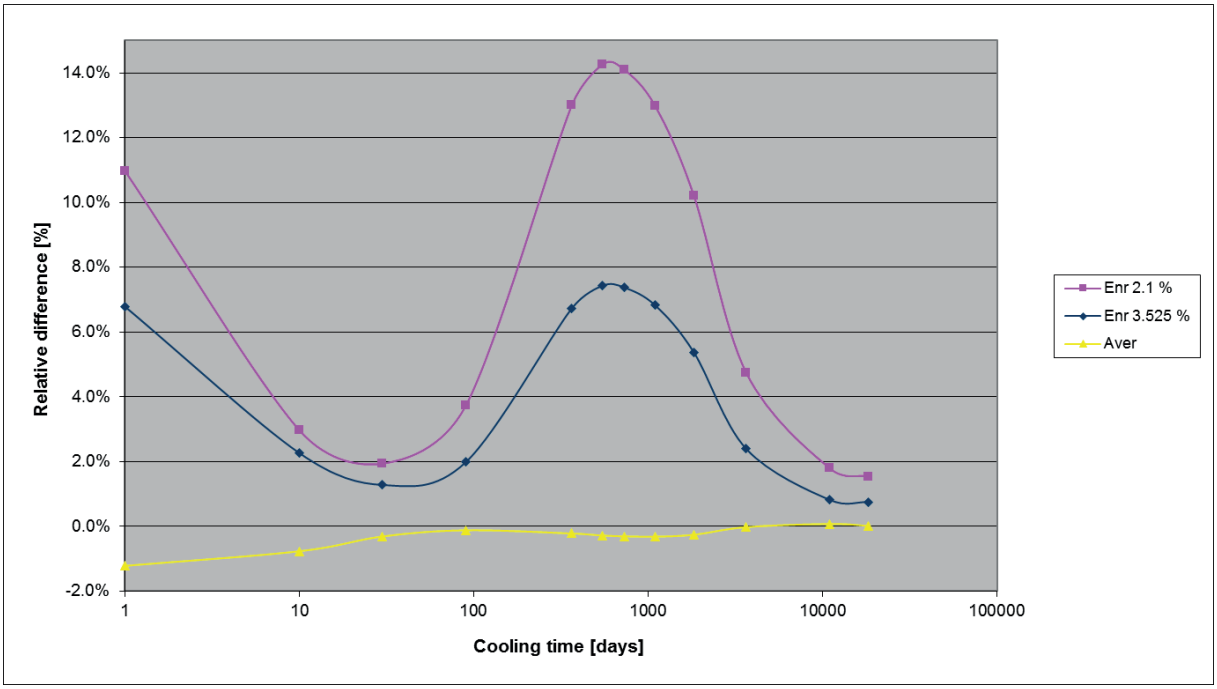


Figure 7: Effect of the fuel enrichment on the photon emission rate

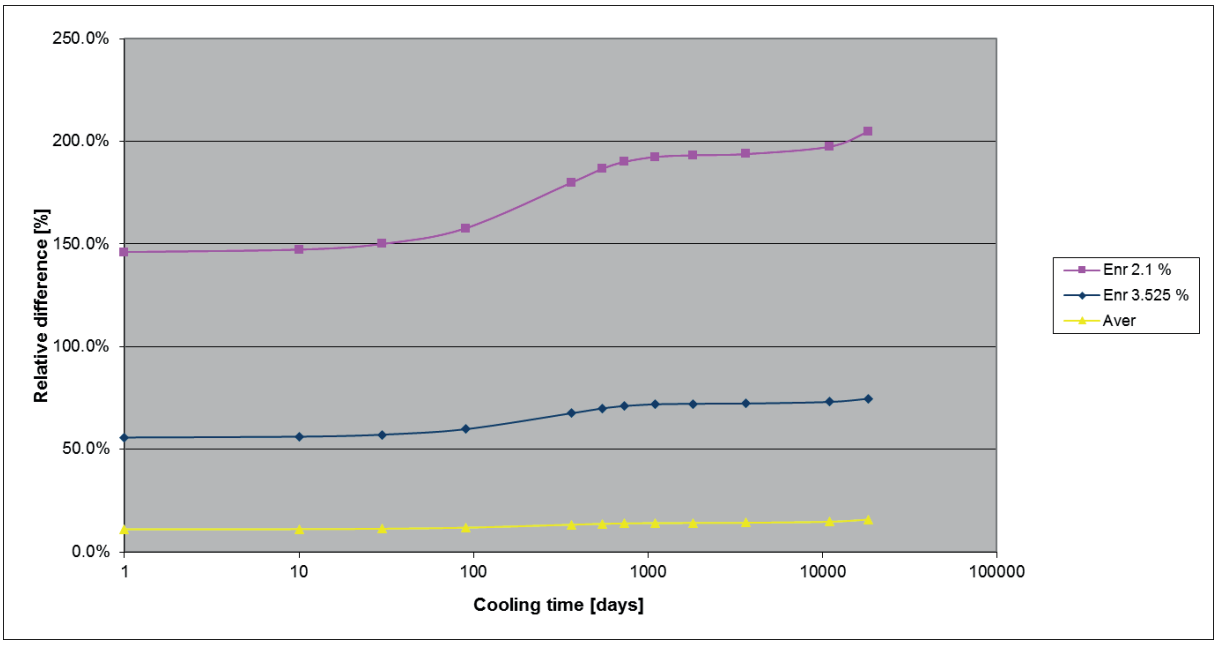


Figure 8: Effect of the fuel enrichment on the neutron emission rate

## 4.3 Fuel temperature

The effect of fuel temperature is shown in Figs. 9 and 10. Two cases (800 °K and 1000 °K) are compared to the reference 900 °K case. Relative differences of both cases are less than 0.25 % for the photon and 0.5 % for the neutron emission rate. Average emissions are very close to the reference case supporting averaging approach.

It should be noticed that in the reality fuel temperature is not constant over fuel pellet but is highest in the centre and decreases towards the cladding due to heat transfer to the moderator. If we assume constant power across the pellet having constant thermal characteristics, we get a parabolic temperature profile. A 10 region annular case was considered assuming a parabolic temperature profile with a pellet average of 900 °K. Obtained results are plotted in Figs. 9 and 10 as “T profile”.

Effect is relatively small and is estimated to be less than 0.2 % in the photon case and 0.3 % for the neutron case.

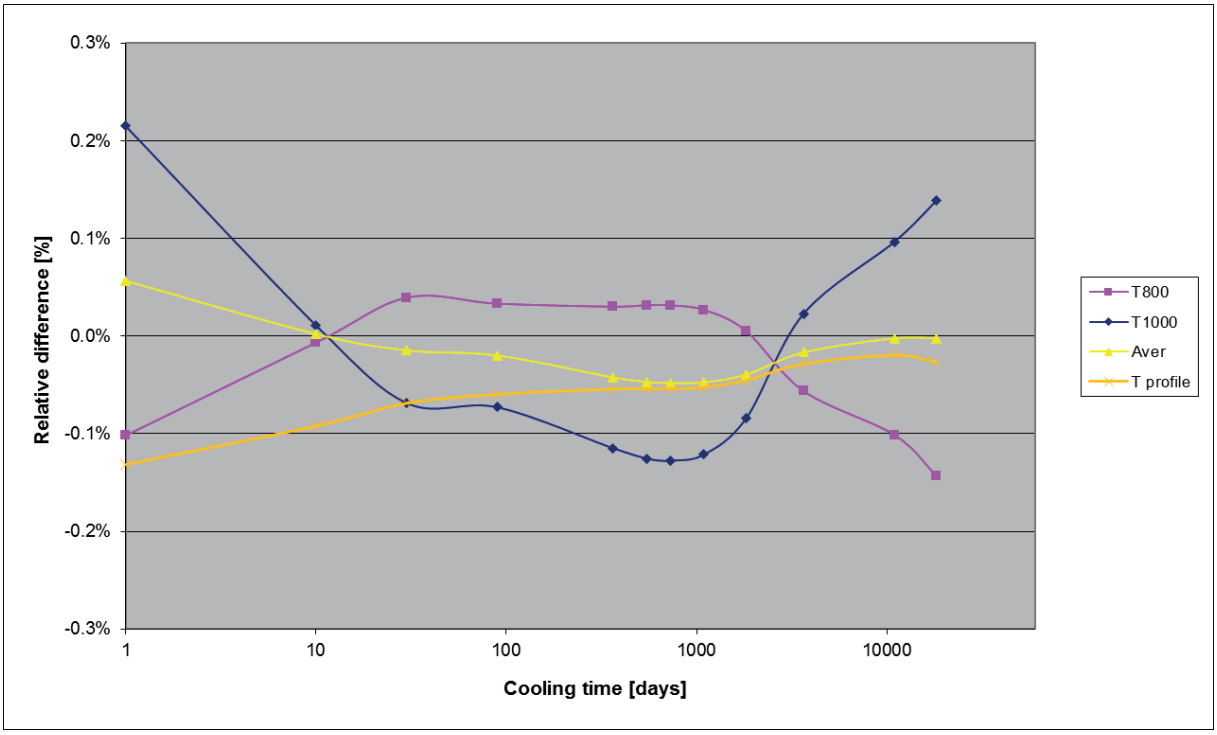


Figure 9: Effect of the fuel temperature on the photon emission rate

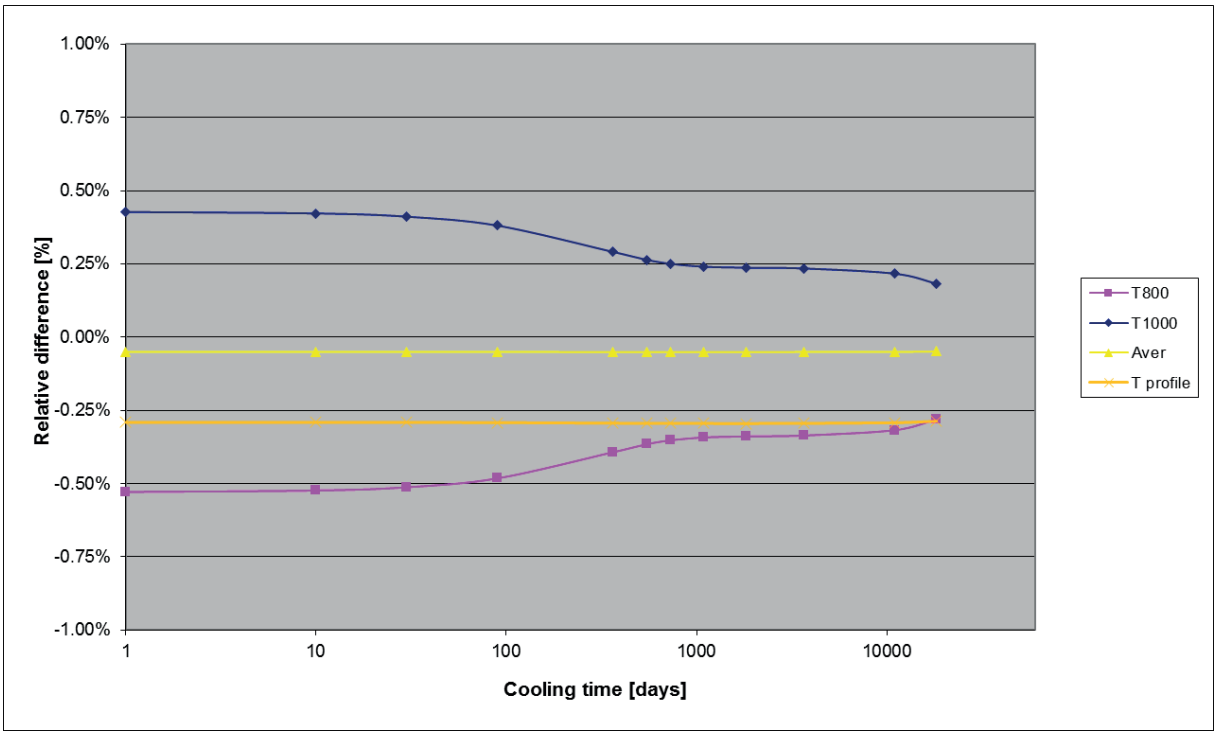


Figure 10: Effect of the fuel temperature on the neutron emission rate

## 4.4 Moderator temperature

Direct influence of the moderator temperature on the emission rates is negligible. However, reactor is operating in the pressure region, where relatively small moderator temperature changes cause

significant differences in the moderator density producing significant differences in neutron moderation and energy spectrum. The effect is shown in Figs. 11 and 12. Temperature was varied for ±20 °K (water density goes from 0.74972 g/cm$^3$ to 0.65642 g/cm$^3$). This is approximately NPP Krško inlet–outlet range at 100 % reactor power. Therefore, upper fuel regions with near core outlet temperatures have up to 3 % higher photon emission and up to 8 % higher neutron emission than bottom regions. Average emissions are up to 0.5 % higher than emissions at average temperature.

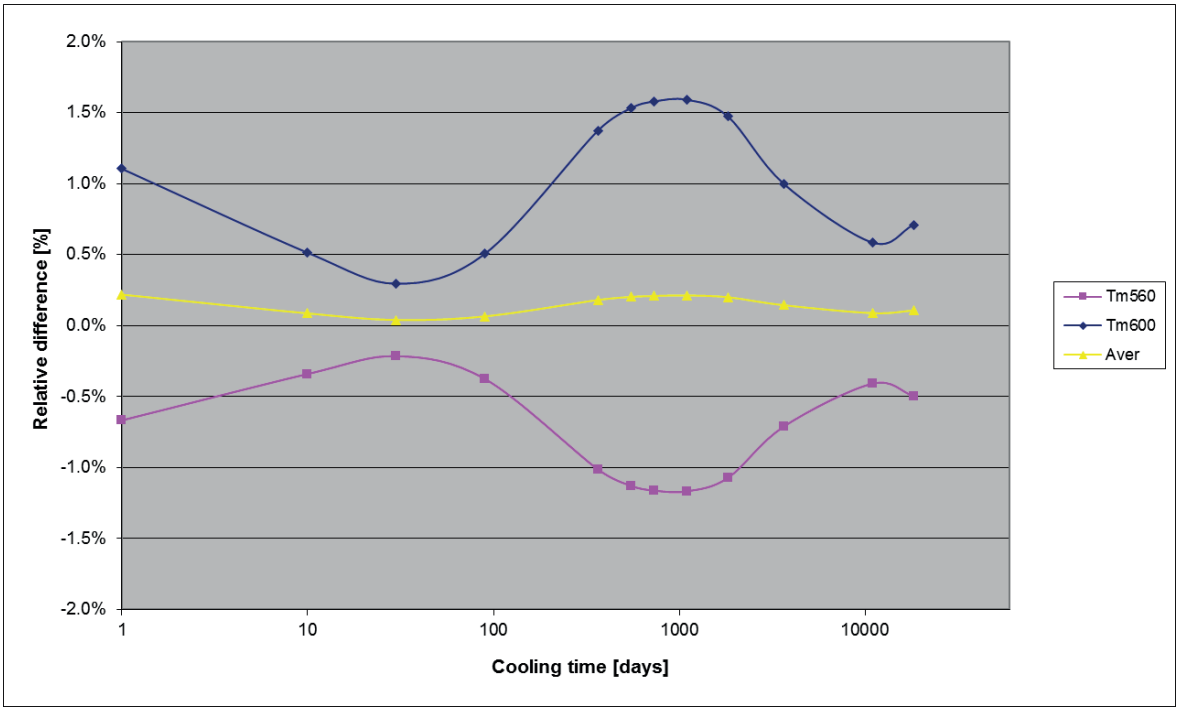


Figure 11: Effect of the moderator temperature on the photon emission rate

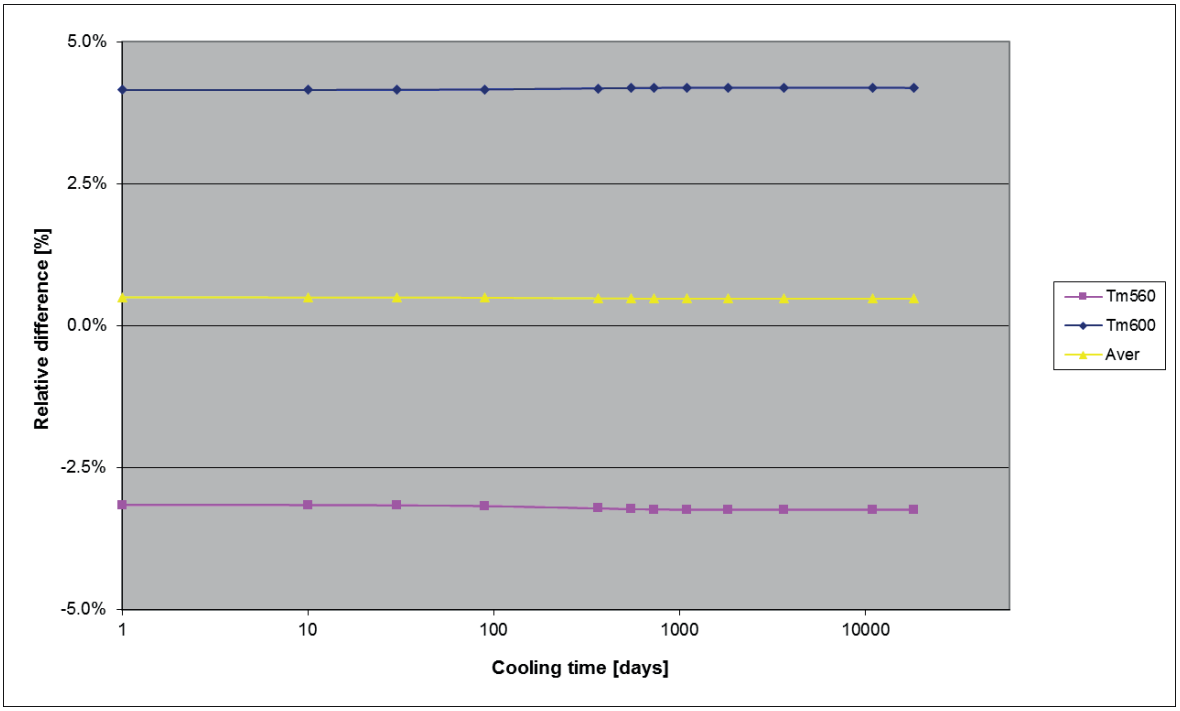


Figure 12: Effect of the moderator temperature on the neutron emission rate


Marjan Kromar, Bojan Kurinčič, Assessment of the Photon and Neutron Source Term for the NPP Krško Spent Fuel, Journal of Energy, vol. 68 Number 2–3, Special Issue (2019), p. 184–198

## 4.5 Soluble boron

The effect of soluble boron present in the moderator is shown in Figs. 13 and 14, where ±500 ppm variations are analysed. Boron concentration increase of 500 ppm can cause up to 1 % higher photon emission and 2.5 % higher neutron emission. Average emissions are almost the same as the emissions at average boron concentration supporting averaging approach.

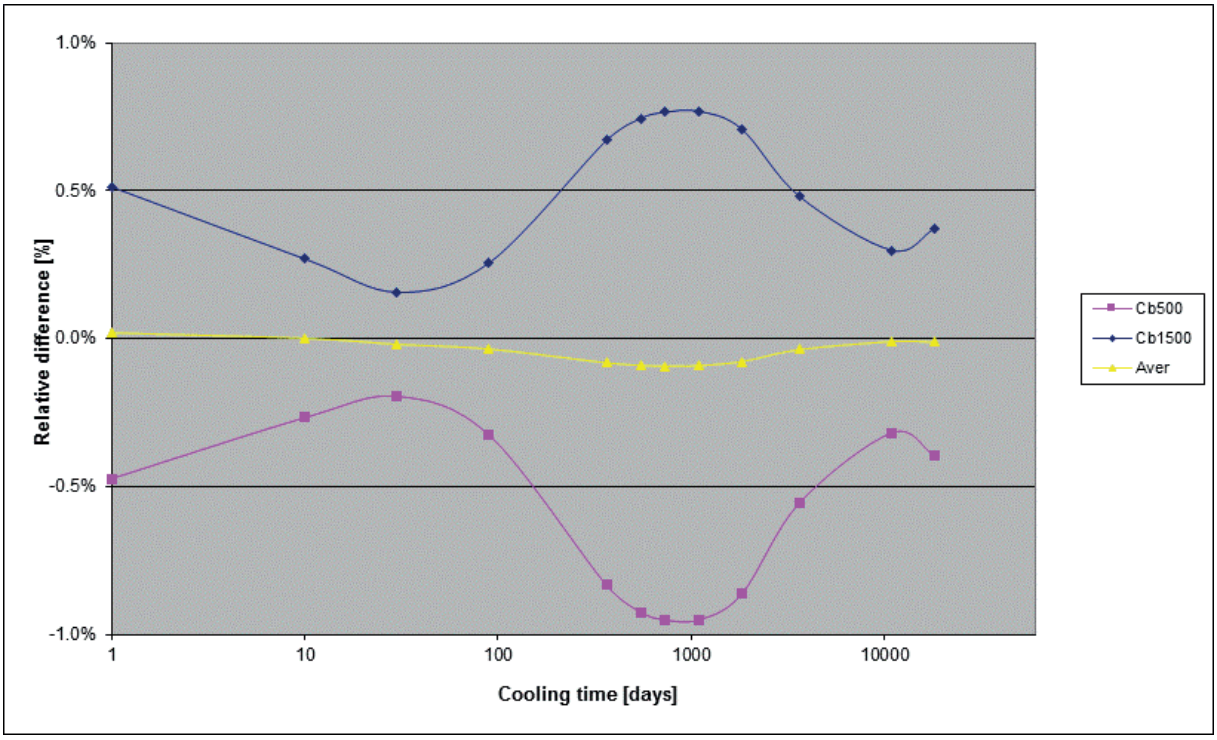


Figure 13: Effect of the soluble boron on the photon emission rate

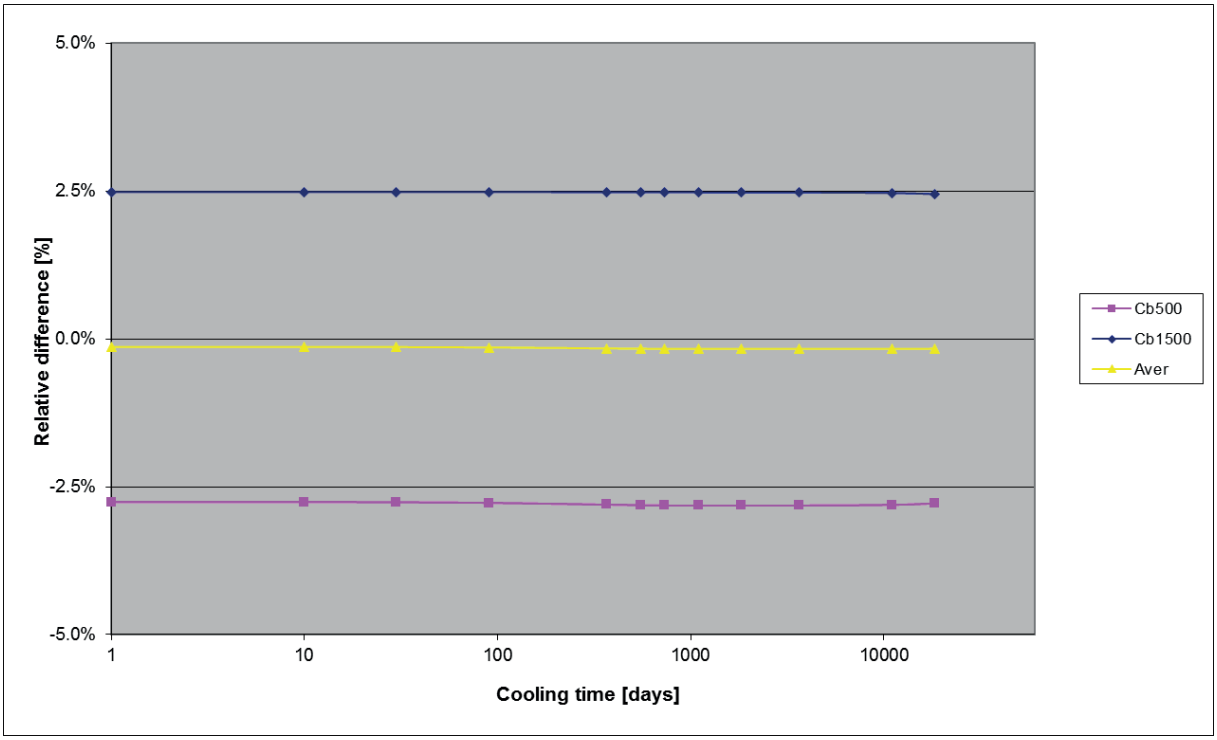


Figure 14: Effect of the soluble boron on the neutron emission rate


Marjan Kromar, Bojan Kurinčič, Assessment of the Photon and Neutron Source Term for the NPP Krško Spent Fuel, Journal of Energy, vol. 68 Number 2–3, Special Issue (2019), p. 184–198

## 4.6 Average power

Cases with 70 % nominal power and 130 % nominal power are presented in Figs. 15 and 16. Photon source term at shutdown is almost proportional to the specific power. 1 % increase in the reactor power results in almost 1 % higher photon emission. That means that the main photon contributors experience some saturation concentration, which is proportional to the specific power. Differences are gradually decreasing over time and are after 10 years cooling approximately 10 times smaller (less than 3 %). Average photon emission is up to 2 % lower than the emission at average specific power. Situation is rather different for the neutron source term (Fig. 16). Emissions are much less dependent on specific power. Differences are less than 2 %. Average neutron emission is up to 0.5 % lower than the emission at average specific power.

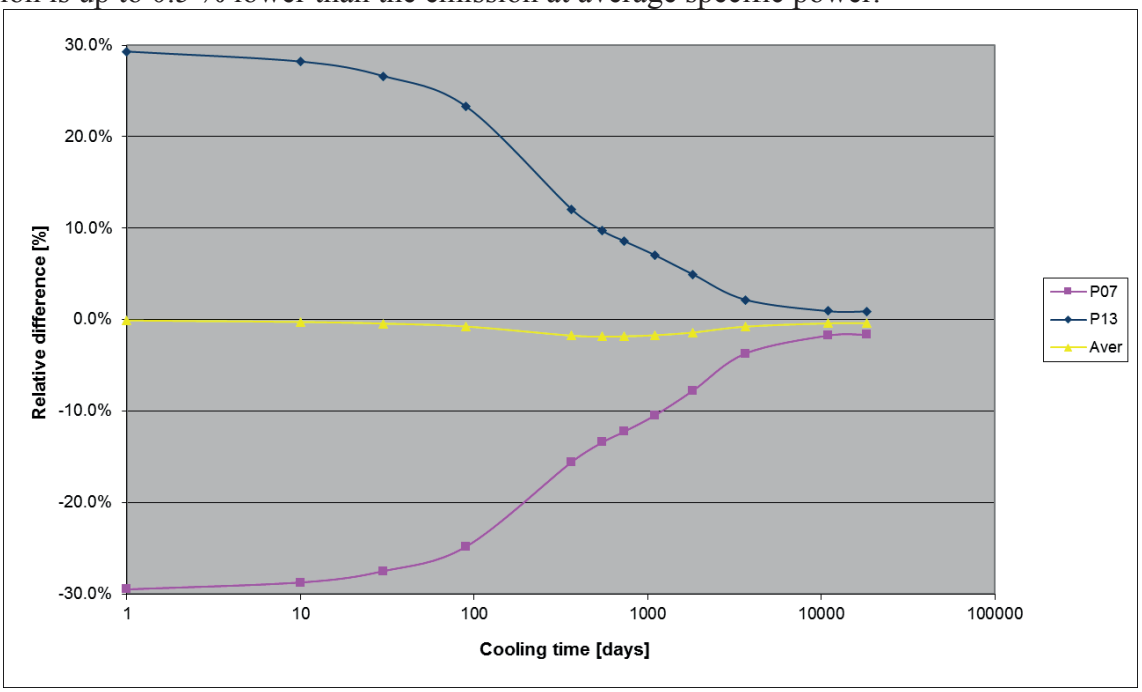


Figure 15: Effect of specific power on the photon emission rate

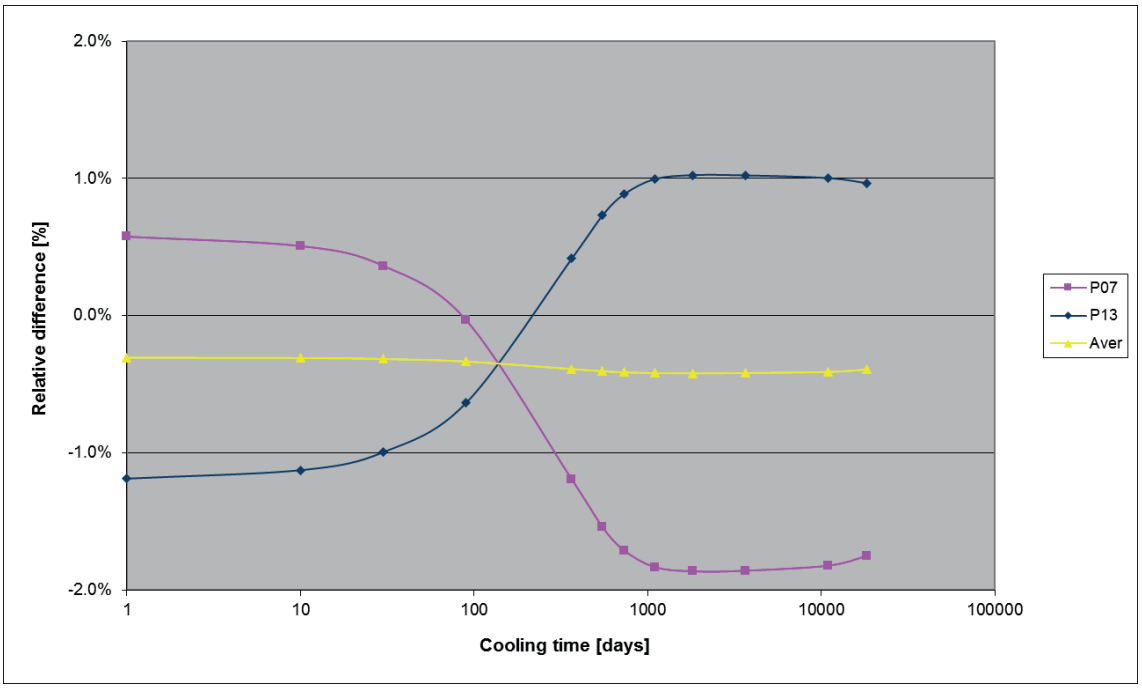


Figure 16: Effect of specific power on the neutron emission rate


Marjan Kromar, Bojan Kurinčič, Assessment of the Photon and Neutron Source Term for the NPP Krško Spent Fuel, Journal of Energy, vol. 68 Number 2–3, Special Issue (2019), p. 184–198

## 4.7 Burnable absorbers

Introduction of burnable absorbers causes spectrum hardening and therefore changes in fuel isotopic composition and consequently increases photon end neutron emissions. The effect is presented in Figs. 17 and 18, where cases with 64 IFBA rods and 116 IFBA rods per assembly are plotted. The fuel with 116 IFBA rods is producing more than 4 % more photons and almost 11 % more neutrons than the fuel with no IFBA rods.

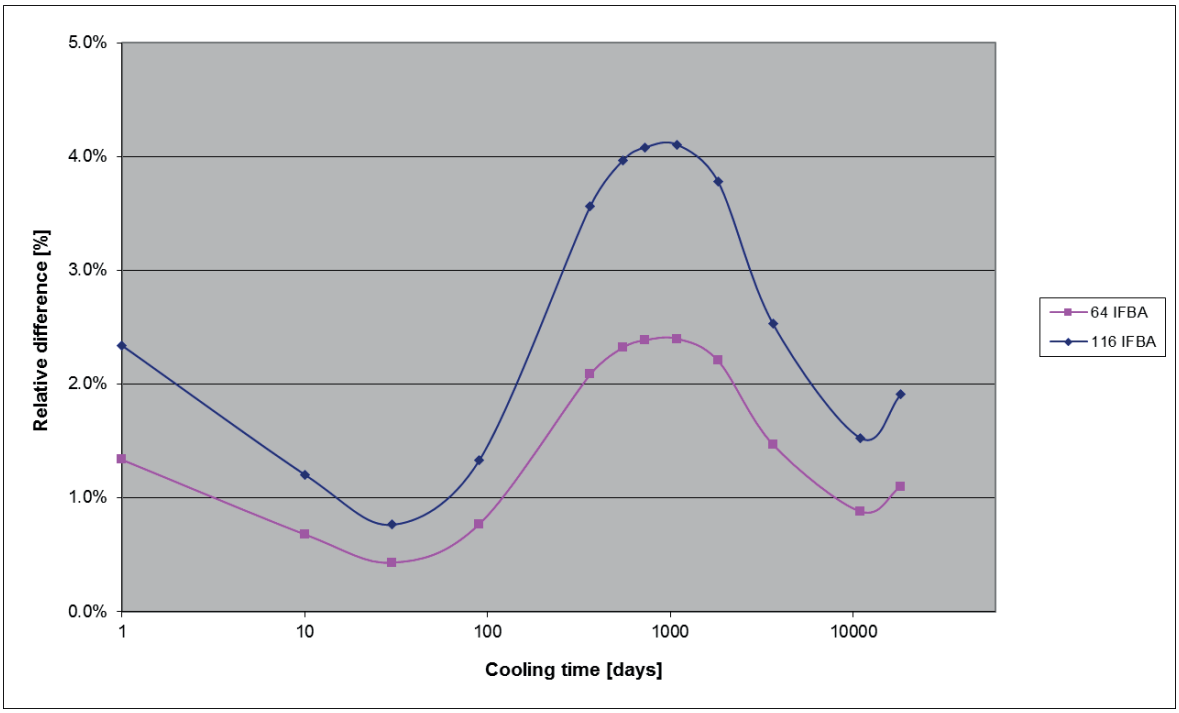


Figure 17: Effect of IFBA rods on the photon emission rate

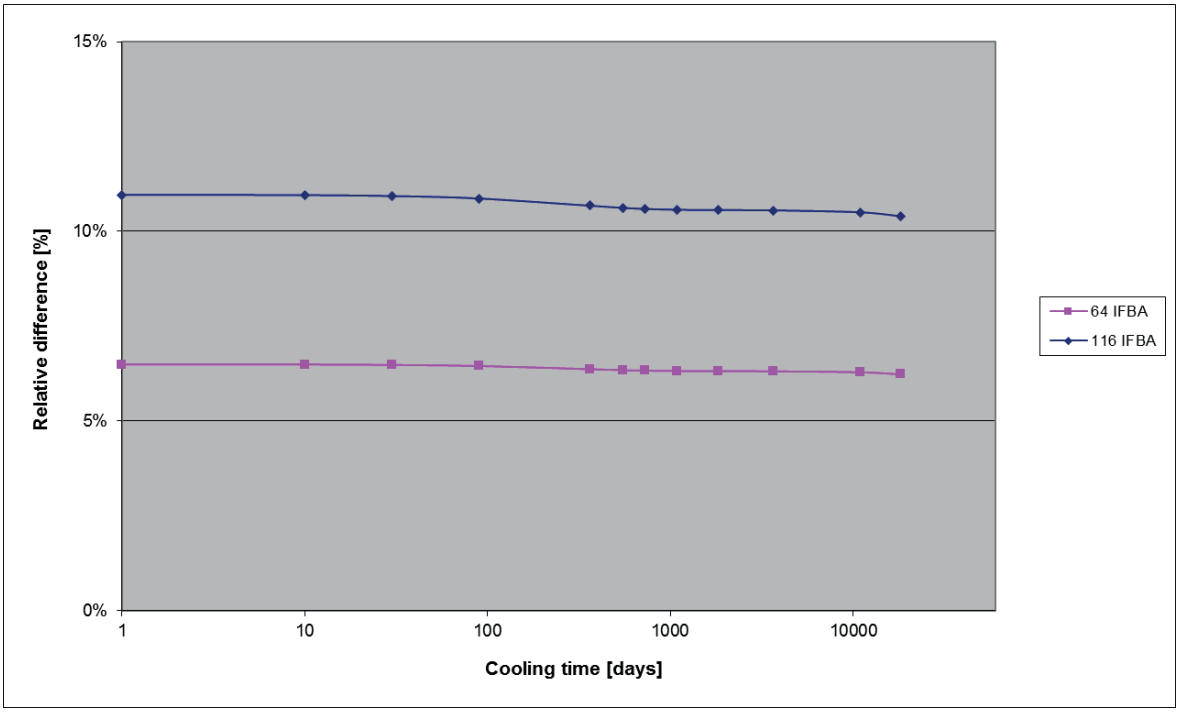


Figure 18: Effect of IFBA rods on the neutron emission rate

## 5 CONCLUSION

Analysis of the NPP Krško photon and neutron nuclear fuel source term with the Serpent code has been performed. Some deficiencies in the supplied ENDF/B-VII.0 decay library have been detected. In addition, it was noticed that the Serpent reports only spontaneous fission rates without (α, n) and (β, n) contributions. To get neutron emission, spontaneous fission rates had to be multiplied with the average number of neutrons born for each particular nuclide manually. Comparison with the Origen code has shown acceptable agreement of the ENDF/B-VII.1 results.

Since the photon and neutron source term are dependent on the fuel isotopic composition and consequently also on neutron flux spectrum, the effect of several operational parameters was examined. Influence of the following parameters on the emissions have been analysed:

1. burnup,
2. fuel enrichment,
3. fuel temperature, profile,
4. moderator temperature,
5. soluble boron concentration,
6. average power,
7. burnable absorbers.

Realistic operating ranges were considered. In addition, it was demonstrated that, except for the burnup and enrichment, averaging of all other parameters is acceptable approach. IFBA fuel should be accounted for explicitly due to relative high impact on the photon and neutron emissions.

## ACKNOWLEDGMENT

The authors acknowledge that the work presented herein was financially supported by the Slovenian Research Agency under the project number L2-8163.

## REFERENCES

[1] J. Leppänen, et al., "The Serpent Monte Carlo code: Status, development and applications in 2013," *Ann. Nucl. Energy*, 82, pp. 142-150, 2015.

[2] J. Leppänen and A. Isotalo, "Burnup calculation methodology in the Serpent 2 Monte Carlo code," *Proceedings, PHYSOR 2012*, Knoxville, TN, Apr. 15-20, 2012.

[3] Allen G. Croff, "Origen2: A Versatile Computer Code for Calculating the Nuclide Compositions and Characteristics of Nuclear Materials," *Nucl. Technol.,* 62, 3, pp. 335-352, September 1983.

[4] M. Kromar and B. Kurinčič, "Determination of the NPP Krško Spent Fuel Activity," *Proceedings, 24th International Conference Nuclear Energy for New Europe - NENE 2015*, Portorož, Slovenia, September 14-17. Ljubljana: Nuclear Society of Slovenia, 2015.

[5] M. Kromar, B. Kurinčič, "Determination of the NPP Krško spent fuel decay heat," *AIP conference proceedings : Thermophysics 2017, 22nd International Meeting of Thermophysics 2017, Terchova, 12-14 September 2017*, (AIP conference proceedings, 1866), American Institute of Physics, pp. 050005-1, 2017.

[6] M. Pusa and J. Leppänen, "Computing the matrix exponential in burnup calculations," Nucl. Sci. Eng., 164, pp. 140-150, 2010.

[7] NEA Data Bank, “ZZ SERPENT117-ACELIB, Continuous-energy X-sec lib., radioactive decay, fission yield data for SERPENT in ACE,” NEA-1854/01, http://www.oecd-nea.org/tools/abstract/detail/NEA-1854/.

[8] J. L. Conlin, et al., “Continuous Energy Neutron Cross Section Data Tables Based upon ENDF/B-VII.1”, Nuclear Data Team, XCP-5, Los Alamos National Laboratory, February 2013.

Journal of Energy
VOLUME 68 Number 2-3 | 2019 | Special Issue
journal homepage: http://journalofenergy.com/

# Influence of Spacer Grids Homogenization on Core Reactivity and Axial Power Distribution

**Radomir Ječmenica, Davor Grgić, Mario Matijević**
University of Zagreb, Faculty of Electrical Engineering and Computing
Unska 3, 10000 Zagreb, Croatia
radomir.jecmenica@fer.hr, davor.grgic@fer.hr, mario.matijevic@fer.hr

## ABSTRACT

The paper presents the influence of spacer grid homogenization during cross section generation on core reactivity and axial power distribution. Homogenization calculation was performed at fuel assembly level using FA2D code. The first approach is to smear uniformly all centrally located spacer grids along 120 inches of fuel assembly and carry out 2D transport calculation. The second approach is to smear spacer grid within 6 inches of fuel assembly and perform homogenization calculation. That composition is then assigned to closest 6 in axial subdivision of the core calculation. The last analysed option is to do additional localization of spacer grids and carry out homogenization within 2 inches of fuel assembly height. The additional subdivision is afterward performed of the closest regular axial core subdivision in nodal core calculation. The core calculation was performed using modified PARCS 2.5 code for NPP Krško cycle 29. The normalized axial power distributions obtained by PARCS for three different ways of spacer grid homogenization are then compared to quantify the influence of modelling. Similar comparison was performed for critical boron concentration. As expected larger influence is present for axial power distribution (more details for fine localization), with some influence on axial power offset and global reactivity.

***Keywords:*** *homogenization, spacer grids, FA2D, PARCS, axial power distribution, axial offset*

## 1 INTRODUCTION

Reactor of NPP Krško is Westinghouse PWR with two cooling loops and consists of 121 fuel assemblies (FA). Each 16×16 VANTAGE+ FA consists of 235 fuel rods, 20 guide tubes and one instrumentation tube. Fuel is in form of uranium oxide, cladding is made of ZIRLO alloy, and IFBA and soluble boron are used for control of excess reactivity. NPP Krško works in 18-month cycles and current cycle is Cycle number 30.

We have tried to quantify the influence of axial homogenization of the spacer grids on usually calculated core operation data and to see is it possible to calculate axial power profiles that can offer similar information as power profiles measured with in-core instrumentation. In addition, we wanted to see if a new approach of smearing of spacer grids can decrease discrepancies between our axial offset (AO) results and measured data and results of reference calculation. That is especially true for sudden increase in Westinghouse BOC axial relative power profile at the middle of active core height. Commonly, six spacer grids are smeared over 304.8 long central part of FA, and one spacer grid was smeared over bottom axial blanket region (15.24 cm), and now they are smeared over 15.24 cm long part of FA (one PARCS axial node).

As shown in Figure 1 there are eight spacer grids in each fuel assembly. Seven of them are within active core height, and one is in upper axial reflector region. The lowest spacer grid is in the

axial blanket region, and remaining grids are inside central region with a nominal fuel enrichment. Spacer grid positions and their heights are shown in Figure 1. Distribution of material compositions and location of spacer grids within them are shown in Figure 1 too. The localization of spacer grids is adjusted to fit original PARCS axial meshing and minimize number of spectral calculations. The spacer grid number 6 is really in material compositions at places 18 and 19. Considering that it requires two additional spectral calculations at FA level and spacer grid number 6 was shifted up by approximately 1 cm. This means that material composition at place 18 is without spacer grid, and material composition at place 19 is with spacer grid.

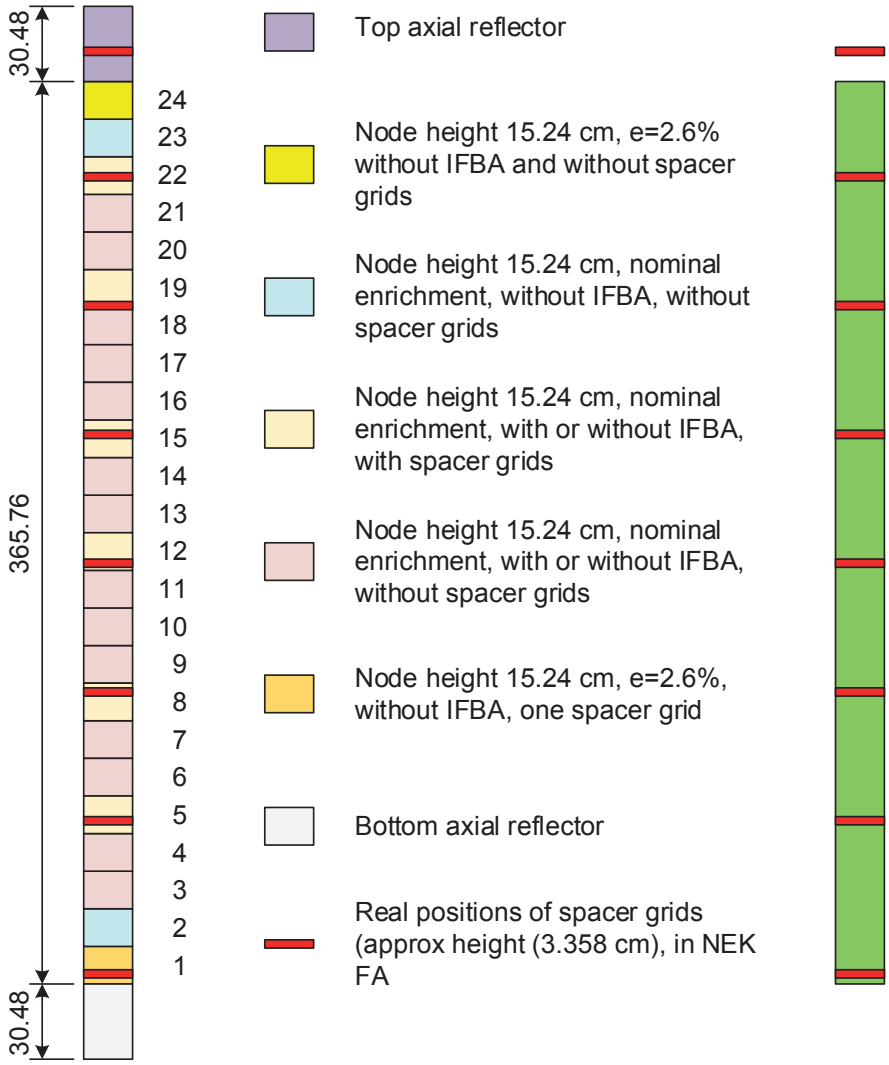


Figure 1 Material compositions and spacer grids positions in NPP Krško FA

## 2 CALCULATIONAL TOOLS

A modified 3D nodal core simulator PARCS v2.5 [1] used to obtain whole-core power distribution and global reactivity. Homogenized few-group constants obtained using two-dimensional collision probability lattice code FA2D [2]. The code is verified by benchmark calculations at fuel assembly level, as well as fuel management calculations for the NPP Krško and two advanced reactors IRIS and I$^2$S-LWR. FA2D was originally developed at the Faculty of Electrical Engineering and Computing, University of Zagreb, but some parts of the code rely on geometrical code package MARSLIB [3] from ORNL (Oak Ridge National Laboratory).

For each material composition heterogeneous depletion calculation was performed at a constant power density of 40.5 W/gU up to burnup of 60 GWd/tU and predictor-corrector method is used during the depletion calculation. The code uses 97-group cross-section library based on ENDF-B/VI.5 data files. The library consists of 290 different isotopes. Assumed state point thermal-hydraulic variables were: effective fuel temperature 810.9 K, gap temperature 810.9 K, cladding temperature 616.5 K, moderator temperature and pressure 15.51 MPa and 580.6 K, boron concentration 500 ppm. Inter assembly gap was explicitly treated but cold nominal dimensions were assumed. Inconel spacer grids are homogeneously mixed with moderator and boron from $ZrB_2$ coating is smeared over the fuel rod gap.

To form collision probability matrix fuel assembly was covered with a mesh of parallel lines, mutually distant 0.05 cm, and having 16 equally spaced angles. The convergence criterion for fundamental mode calculations was 1.0E-6.

Originally NRC's code PARCS was developed for steady-state and transient (RIAs) standalone calculations, or as a part of coupled code together with TRAC or RELAP5 to provide 3D neutronic core information. PARCS 2.5 has been modified at the FEEC and the main modifications of PARCS 2.5 were done to:

1. Provide internal depletion capability
2. Perform multi-cycles fuel management calculations
3. Make possible usage of XS tables prepared by FA2D code
4. Calculate burnup weighted local history variables to be used as independent variable in interpolation routine
5. Calculate burnup dependent fuel temperature to be used in fuel rod model.

All required data for multi-cycles analysis are provided within fuel assembly description Fuel Assembly Specification (FAS) files. Each fuel assembly has one FAS file and it can be updated at the end of each depletion cycle. Integral parts of the FAS files are links to separate files with cross section (XS) tables that describe fuel assembly material compositions. Usually FA consists of several material compositions which vary by number of IFBA pins, fuel and IFBA enrichments and presence of spacer grids. For NPP Krško cycle 29, 30 fuel compositions and 10 reflector compositions are used. Cross-section tables are calculated just once in the life-time of the plant using any cross-section generation code (FA2D in our case).

Branch point calculations were performed at selected burnup points using isotopic compositions calculated during depletion under average conditions. The special post-processing program saves two-group cross section data for each material composition in a format similar to the cross section library format given in the OECD MSLB benchmark [4]. In addition to macroscopic cross section data assembly average neutron fluxes, power form factors, discontinuity factors, corner flux discontinuity factors, fractions and decay constants of delayed neutrons, fission yields of $^{135}I$, $^{135}Xe$ and $^{149}Pm$, number densities of $^{135}I$, $^{135}Xe$, $^{149}Pm$ and $^{149}Sm$ are saved too.

A trilinear interpolation procedure is part of the library implementation. Separate cross section library is used to describe rodded fuel assemblies. There is a separate library with history variables correction too.

## 3 RESULTS

The reference depletion calculation is performed for NEK Cycle 29 core with 24 equdistant axial subdivisions in active core and 2×2 radial subdivisions in each fuel assembly. That calculation uses 18 fuel material compositions (cross section data) with 6 spacer grids homogenized within FA central part (304.8 cm, 120 in) and 10 radial and axial reflector material compositions. It is labeled 5S. The second calculation is performed using cross section dana calculated so that spacer grid is smeared over length of 15.24 cm (6 in). The number of fuel material compositions is now 30. We are still using equidistant axial core subdivision and material compositions with spacers are

assumed in node which contains whole spacer grid (or most of it). The results are labeled with 1S. Last calculation assumes homogenization of spacer grid over length of 5.08 cm (2 in). That node is still longer than actual spacer height (around 3.3 cm). Existing PARCS equidistant nodes are additionaly subidvided in two or three parts (2-4, 4-2, 2-2-2) with one part having homogenized spacer and another is without. Number of fuel materal compositions is the same (30) and number of axial subdivisions within active core length is 34. Label LS is used for those results.

When moved from original homogenization labelled as 5S to homogenization 1S we noticed increase of critical boron concentration for about 40 ppm. The further localization of homogenization (LS) has very small influence on critical boron concentration. Critical boron concentration as found in Nuclear Design Report (NDR) [5] for Cycle 29 is shown in Figure 2 together with our reference calculation (5S) and more localized 1S calculation. 5S calculation gives critical boron concentration very close to Westinghouse one and 1S values are above for between 40 and 20 ppm (depending on burnup). In Figure 3 we have together measured critical boron concentration (flow corrected and B10 corrected values), Westinghouse NDR values and our 1S values. 1S and LS CB values are somewhere between NDR and measured values. It is not completely clear why critical boron concentration increased due to different homogenization length of spacer grids. In both case we have the same amount of material, but flux weighting can result in some change of reactivity.

The expected influence of spacer grids homogenization can be seen in normalized axial power profiles calculated at 150 and 20520 MWd/tU, Figure 4 and Figure 5. When compared with available measured NEK profiles (in-core instrumentation) we can say that rather good prediction was obtained, especially with LS localization, Figure 6. It is clear that measured data use finer spatial raster than calculation. The spacer grids are localized to within 5.08 cm, in LS case, with spacer grid axial position again deviation up to 5.08 cm. The influence of spacer grid homogenization to AO is rather small, going in the direction of less negative AO in the first part of depletion cycle. That is good direction of change compared to measured data, but calculated AO is still more negative than measured plant data.

The influence of spacer grid axial homogenization on radial power distribution is expected to be small. The reference prediction of assembly power is within -3.7 to +5.21% from NDR values for BOC data and within -2.26 to + 4.50% from NDR values for EOC data, Figure 7 and Figure 10. The relative difference between LS and 5S radial power distribution at BOC is within -0.87% and 1.34%, Figure 8. For EOC values the difference between LS and 5S values is within range from -0.33 to 0.49%, Figure 11. Both, for BOC and EOC, the relative difference between LS and 1S radial distributions is within 0.1% for BOC, Figure 9, and within 0.05% for EOC.

The overall experience with this new type of homogenization of spacer grids and capability of PARCS code to perform that type of calculation is positive one and we will continue to use it in parallel with old one. The only drawback of this approach is increased number of spectral homogenization calculations needed in preparation of cross section libraries.

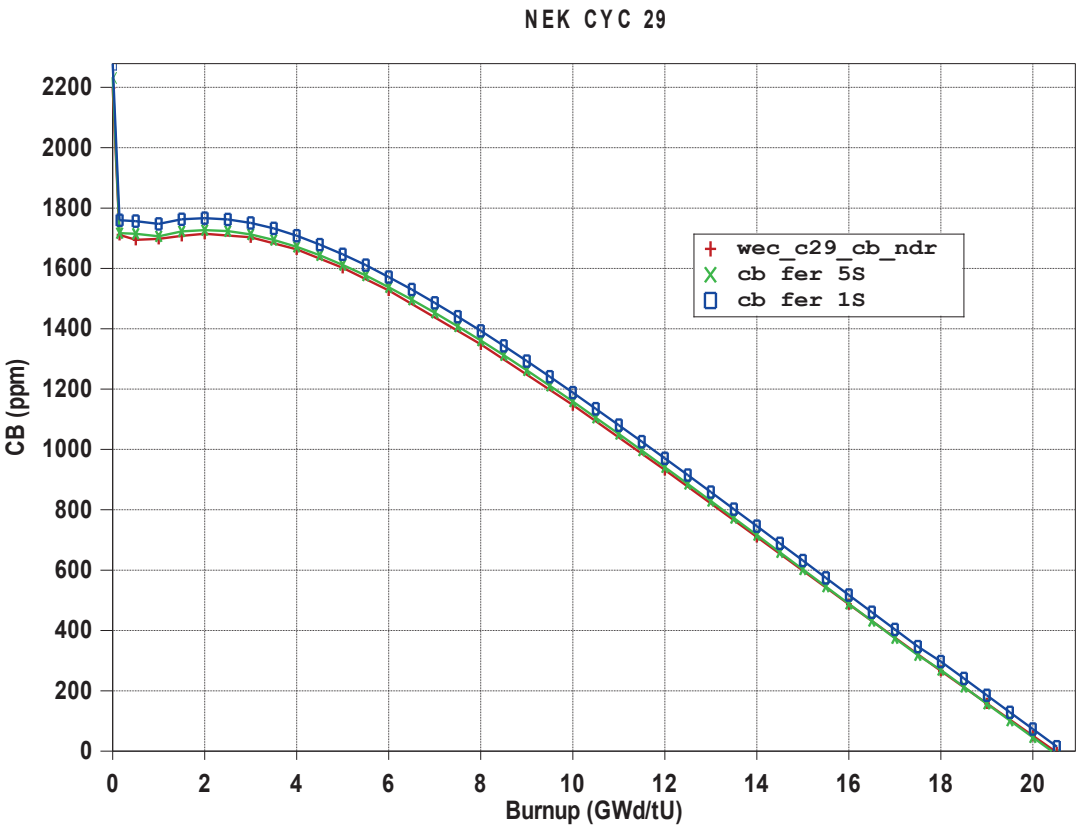


Figure 2 Influence of spacer grid homogenization on critical boron concentration

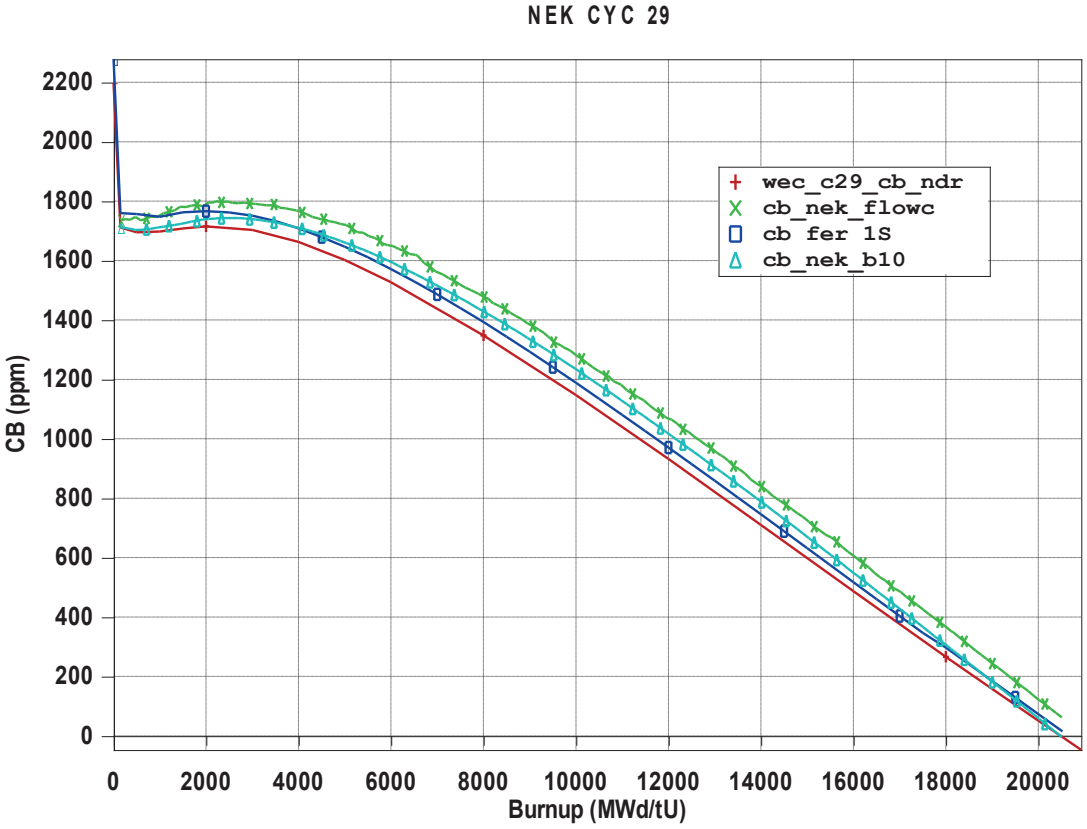


Figure 3 Critical boron concentration depending on burnup

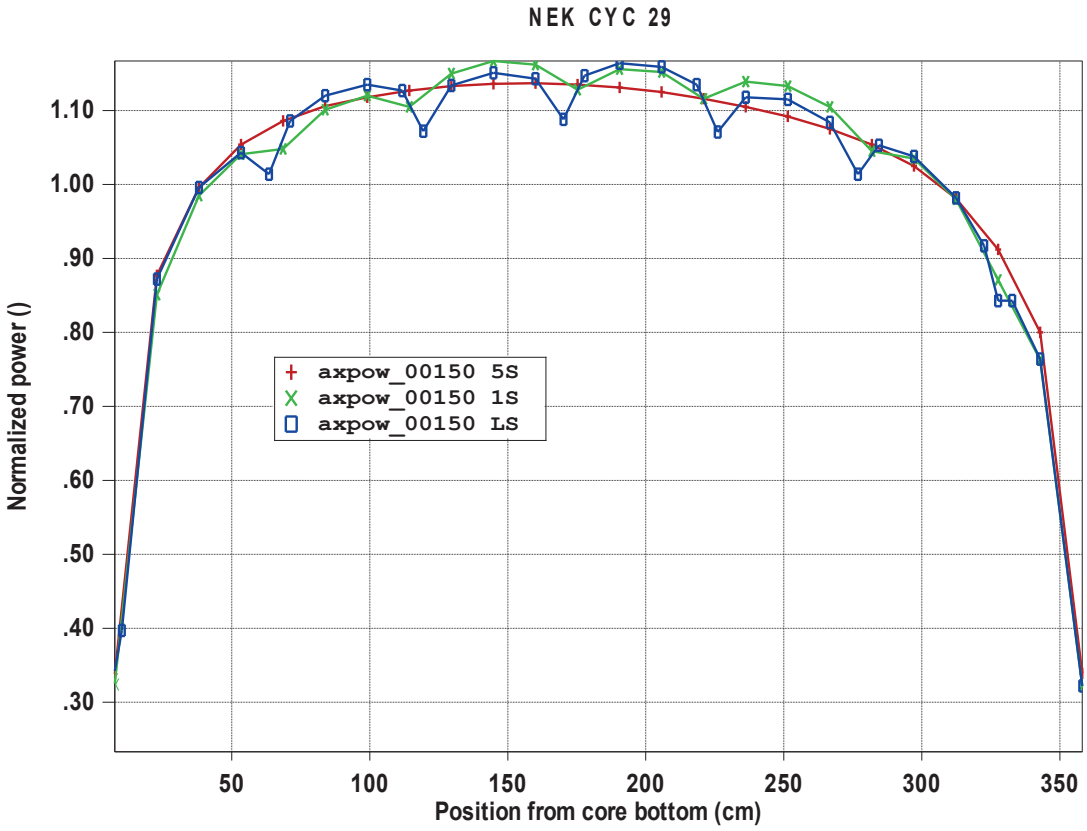


Figure 4 Axial power profile for three different ways of grids smearing - BOC

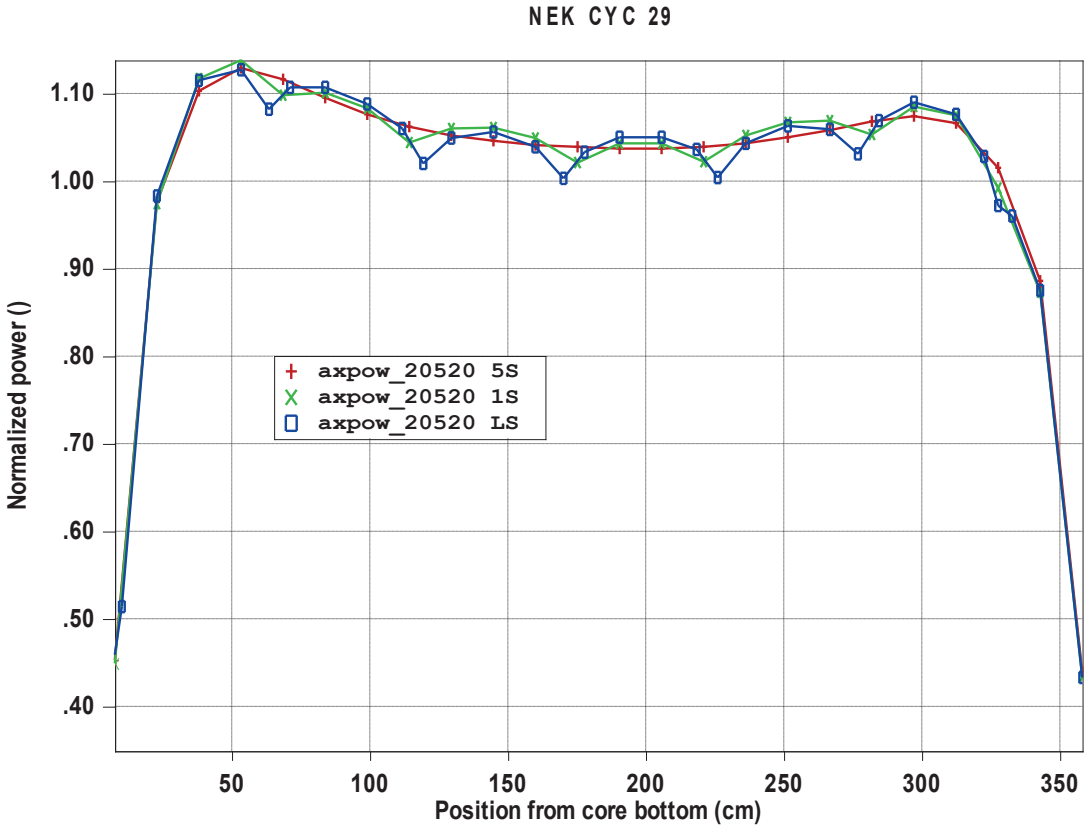


Figure 5 Axial power profile for three different ways of grids smearing - EOC

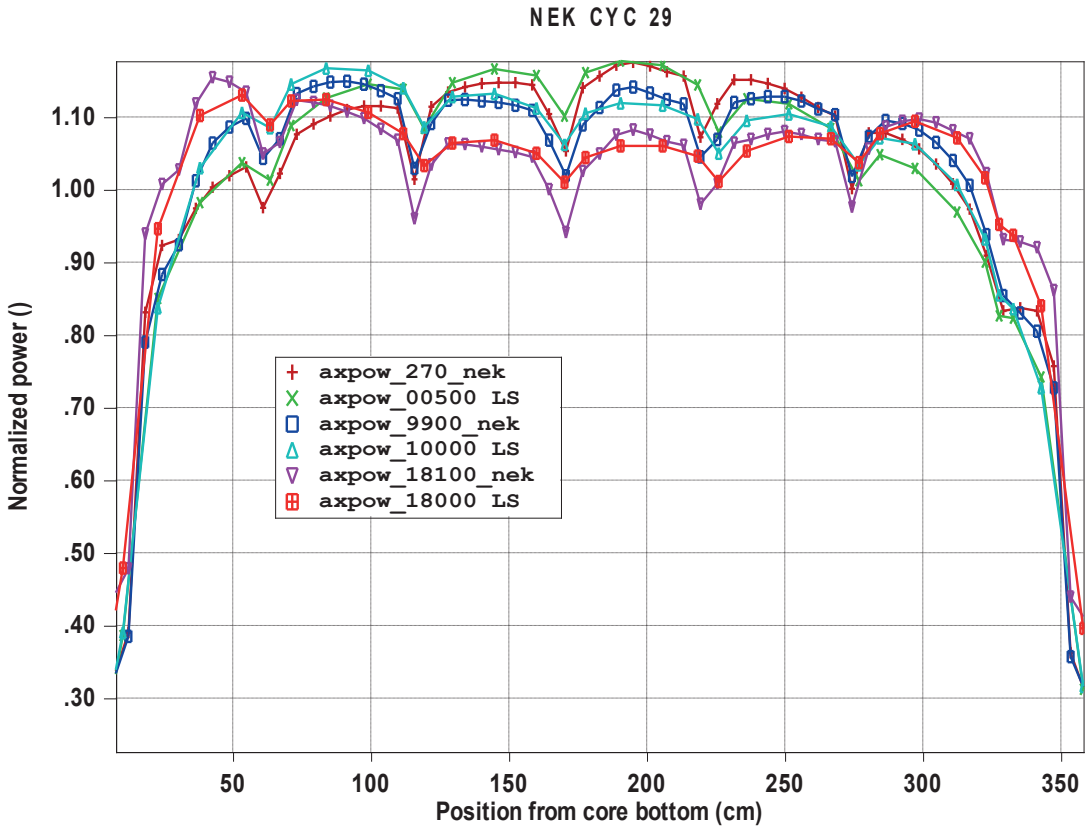


Figure 6 Comparison of axial power profiles with measured data at BOC, MOC and EOC

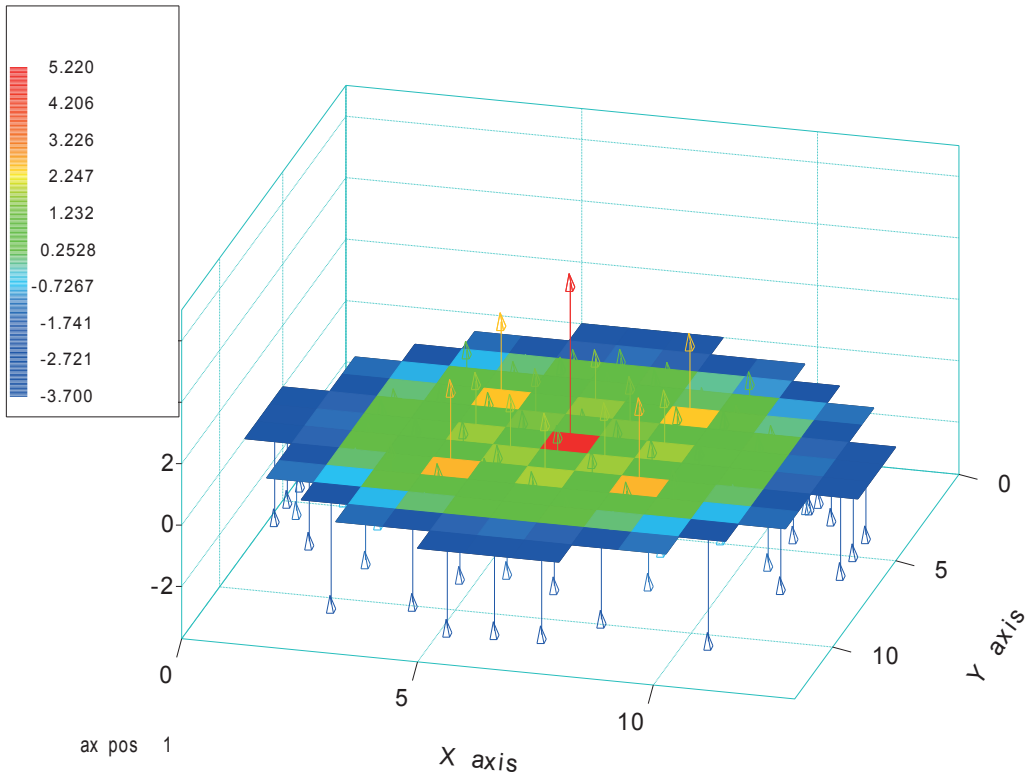


Figure 7 Relative differences of radial power distribution; WEC vs. 5S – BOC


Radomir Ječmenica, Davor Grgić, Mario Matijević, Influence of Spacer Grids Homogenization on Core Reactivity and Axial Power Distribution, Journal of Energy, vol. 68 Number 2–3, Special Issue (2019), p. 199–208

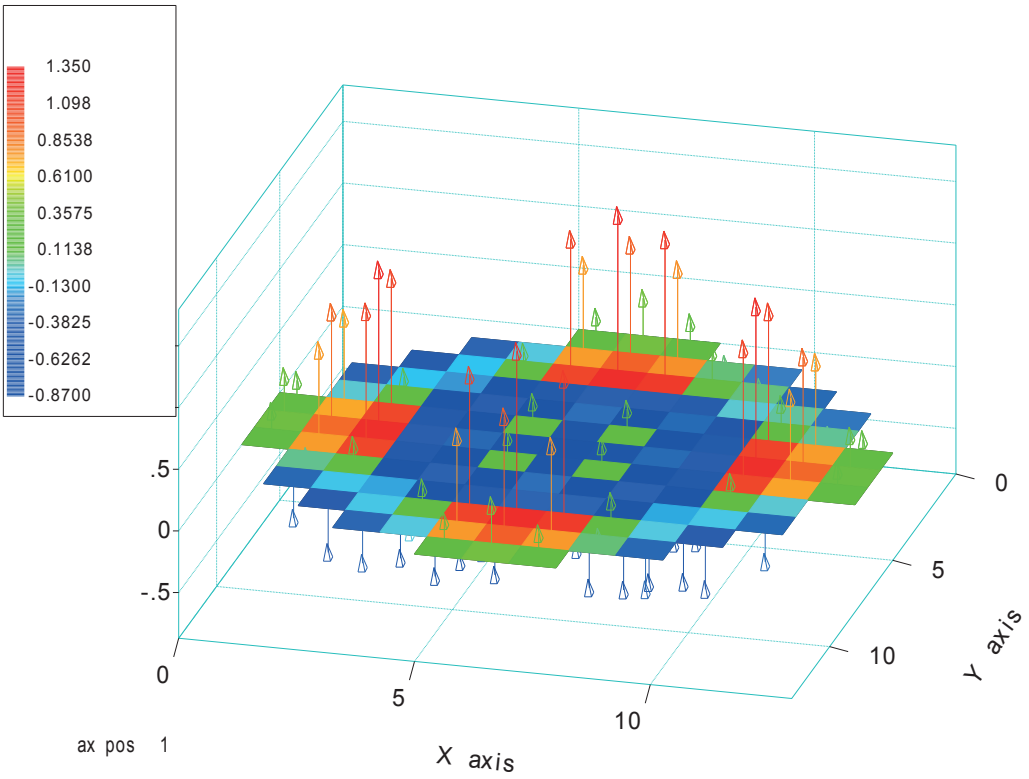


Figure 8 Relative differences of radial power distribution; LS vs. 5S – BOC

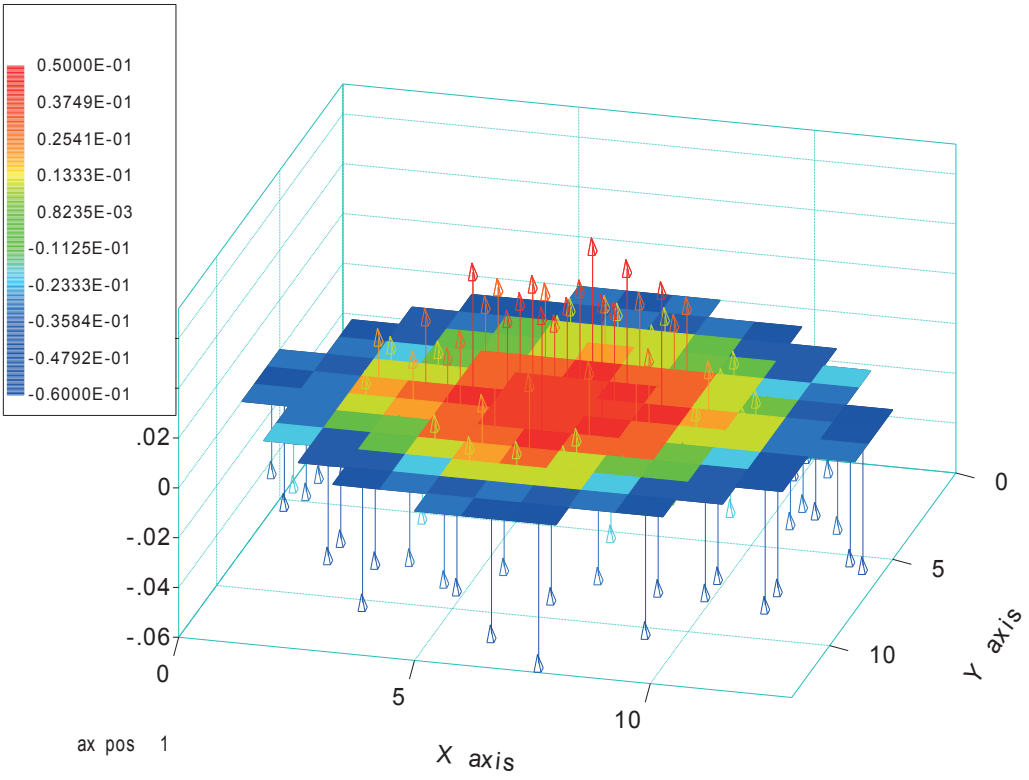


Figure 9 Relative differences of radial power distribution; LS vs. 1S – BOC

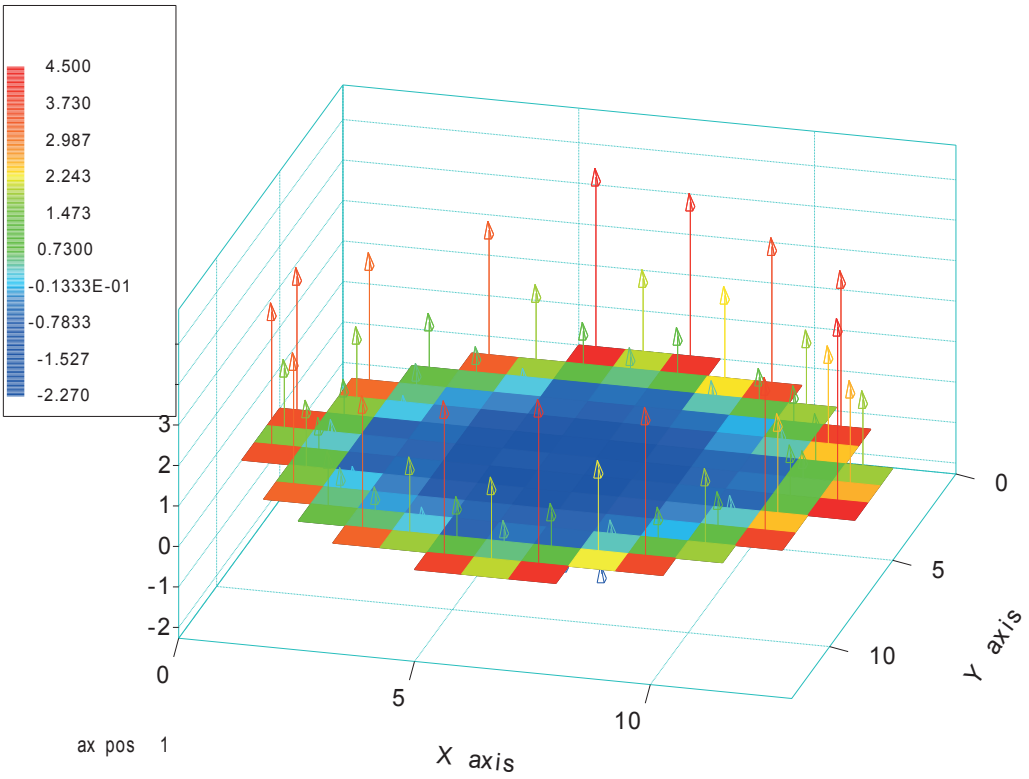


Figure 10 Relative differences of radial power distribution; WEC vs. 5S – EOC

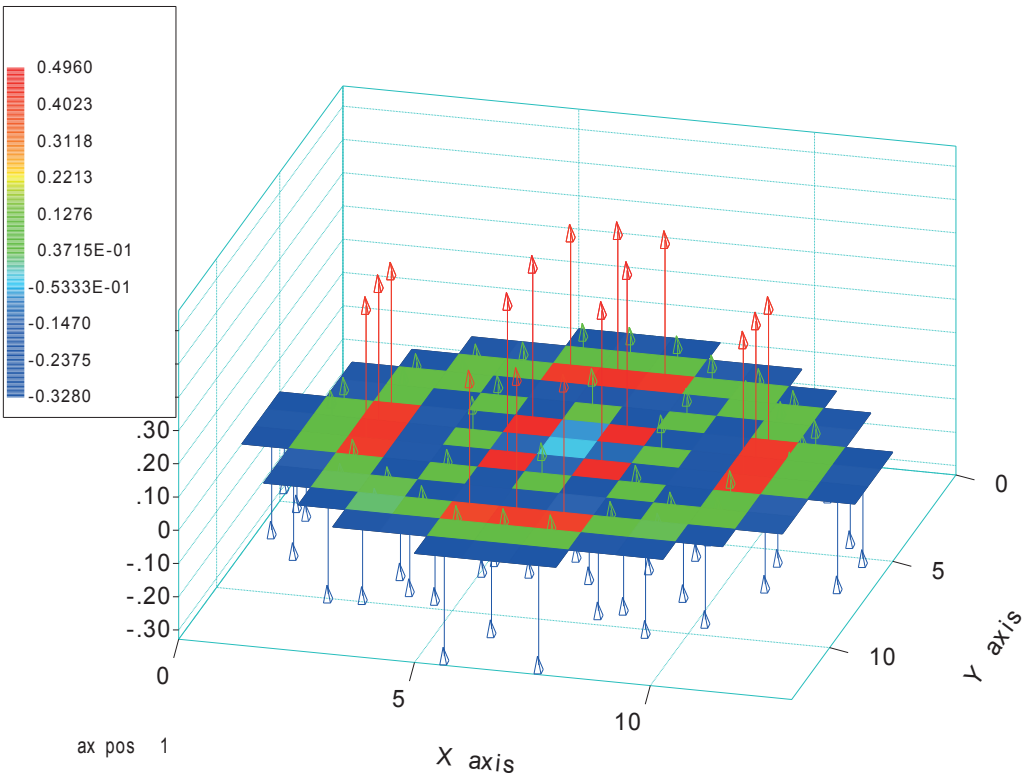


Figure 11 Relative differences of radial power distribution; LS vs. 5S – EOC

## 4 CONCLUSION

3D nodal core depletion calculation usually assumes homogenized spacer grid taken into account within fuel assembly cross section data. Our usual approach is to homogenize 6 spacer grids within central part of NPP Krško fuel assembly (results labelled with 5S). Lowest spacer grid is homogenized within lower axial blanket material composition (15.24 cm, 6 in) and highest is within top axial reflector. We have tried to quantify the influence of axial homogenization of the spacer grids on usually calculated core operation data and to see is it possible to calculate axial power profiles that can offer similar information as power profiles measured with in-core instrumentation. Our reference PARCS 3D nodal calculation used constant axial node size of 15.24 cm (6 in). First logical choice was to homogenize spacer grid (approximate length of 3.3 cm) over that length (1S). Next step was to decrease homogenization length three times, down to 5.08 cm (2 in) (LS). That means, for each combination of enrichment and IFBA number, calculation of two additional homogenized cross section libraries. The material composition was assigned to spatial node closest to spacer grid actual axial position. When moved from original homogenization labelled as 5S to homogenization 1S we noticed increase of critical boron concentration for about 40 ppm. The further localization of homogenization (LS) has very small influence on critical boron concentration. Axial power profiles are reasonably well predicted compared to measured NEK data especially with LS localization. The influence to AO is rather small going in direction of less negative AO in the first part of depletion cycle. AO is still more negative than measured plant data. The influence of spacer axial homogenization on radial power distribution is within 1% when going from 5S to 1S and negligible after that.

The experience with new type of homogenization of spacer grids and capability of PARCS code to perform the calculation is positive one and we will continue to use it in parallel with old one.

**Acknowledgements:**

We would like to express our gratitude to the NPP Krško for providing relevant input and measured plant data.

## REFERENCES

[1] T. Downar, D. Lee, Y. Xu, T. Kozlowski, PARCS v2.6, U.S. NRC Core Neutronics Simulator, User Manual, Purdue University, W. Lafayette, Indiana, USA, 2004.

[2] D. Grgić, R. Ječmenica, D. Pevec, Xenon Correction in Homogenized Neutron Cross Section, *Proceedings of the 20th International Conference o n Nuclear Engineering ICONE 20*, Anaheim, USA, July 30 – August 3, 2012.

[3] J. T. West and M. B. Emmett, MARS: Multiple-Array System Using Combinatorial Geometry, ORNL, Oak Ridge, Tennessee, November 2006.

[4] K. N. Ivanov, T. M. Beam, A. J. Baratta, Pressurized Water Reactor Main Steam Line Break (MSLB) Benchmark, Volume 1, Final Specifications, NEA Nuclear Science Committee and NEA Commitee on Safety of Nuclear Installations, (1999).

[5] E. F. Shockey et al., „The Nuclear and Core Management of the Krško Nuclear Power Plant Cycle 29, Westinghouse Electric Company, 2016.

Journal of Energy
VOLUME 68 Number 2-3 | 2019 | Special Issue
journal homepage: http://journalofenergy.com/

# Effectiveness of SFP Spray Cooling during Loss of Coolant Accidents

**Davor Grgić, Josip Đaković, Siniša Šadek, Štefica Vlahović**
Faculty of Electrical Engineering and Computing, University of Zagreb
Unska 3, Zagreb, Hrvatska
davor.grgic@fer.hr, josip.djakovic@fer.hr, sinisa.sadek@fer.hr, stefica.vlahovic@fer.hr

**Ivica Bašić**
*APoSS d.o.o*
*Repovec 23b, 49210 Zabok, Croatia*
basic.ivica@kr.t-com.hr

## ABSTRACT

For a large Spent Fuel Pool (SFP) loss of coolant accidents, properly sized SFP spray can slowdown or possibly preclude fast heat-up of spent fuel. The MELCOR 2.1 model of NPP Krsko pool was developed and tested for cases of loss of cooling accidents. The simple spray system with spray nozzles distributed at specified location at the top of the pool was added to the model. Different loss of coolant rates where studied for different fuel heat loadings, and different openings and flow rates of the spray nozzles. Traditionally, spray nozzles able to produce larger diameter droplets are used close to the fuel locations with higher heat loadings. According to preliminary results, spray nozzles that will be installed are able to limit or delay long-term heat-up of the spent fuel, but in the case of late actuation it is possible to have temporary high oxidation rates and corresponding production of hydrogen.

***Keywords:*** *SFP, large loss of coolant, MELCOR, spray nozzles*

## 1 INTRODUCTION

In NEK, the SFP is located in separate building near the Reactor Containment, the Fuel Handling Building (FHB). The SFP is generic pool with the depth approx 12 m with concrete walls, thickness approx 2 m, with the stainless steel construction on the inner side of walls. Fuel assemblies (FAs) are located in racks that sustain FAs in the vertical position. Additionally, they have to enable adequate FAs cooling. The rack is divided in cells of appropriate dimensions to enable coolant flow and to disable criticality. Moreover, the subcriticality is achieved with special metal materials for racks (Boraflex) and the boron acid addition in the water. For the safety proposes, the water level above the FAs should be at least 3 m to ensure that the radiation is at the appropriate level for the workers at the operating deck.

During the refueling outage, the FAs are withdrawn from the reactor and there are very radioactive due to the decay heat production that is the main problem with the nuclear fuel. After withdrawal, the FAs are placed in the SFP, therefore, the SFP has to ensure adequate cooling with the heat exchangers and natural circulation. The coolant in the SFP uses natural circulation to cool the FAs, the warm flow rises through the length of the rack, mixes with the cold coolant above the rack and returns down to the bottom of the rack. This process is supported with the cooling system that intakes the warm coolant above the racks and directs it through the heat exchanger (it is cooled with the Component Cooling Water or Essential Service Water). During the loss of SFP cooling, the coolant starts to heatup and it can lead to the fuel rod heatup and therefore to the radioactive release.

The coolant temperature, during normal condition, is below 50 $^0$C and it can rise to max 80 $^0$C, after which the evaporation heat removal starts.

The U.S. Nuclear Regulatory Commission (NRC) has identified nine possible initial events for the SFP accident. Some of those are: loss of power, fire, loss of cooling, loss of coolant, seismic event, airplane crash. They can be sorted in two consequence groups: loss of cooling and loss of coolant inventory. On the other side, they can be sorted from the perspective of the natural coolant circulation to: partial loss of cooling and total loss of cooling. During the total loss of cooling, the natural air circulation is formed, the air is heated through the length of the rack and it cools with the cold air above racks. During the partial loss of cooling, the hot air circulation is disabled leading to the cladding heatup once the water level drops below the half the length of the rack.

The activities that limit the loss of cooling consequences are: the coolant make up, the good fuel distribution in the SFP, the spray system, the FHB ventilation, etc. The coolant make up is the most logical action to limit the accident propagation. This action is efficient only until the water level drops below the 60 % of the active FA length. If the coolant is lost rapidly, the coolant make up can disable the natural air circulation. The worst FAs distribution in SFP is the uniform configuration because the fresh (the hottest FAs) is surrounded by warm FAs. The best configuration (from heat generation point of view) is 1x4 where the fresh FA is surrounded by 4 cold FAs. This way, the radial heat transfer from hot to cold FA, significantly increases the cooling possibility. The spray system possibility will be described later in details. If the FHB ventilation is inappropriate, then the FHB will heatup. Therefore, the ideal ventilation configuration has to intake cold air at the bottom of the FHB and release the hot air at the top of the FHB.

## 2 SPENT FUEL POOL MELCOR 2.1 MODEL

MELCOR code was developed at Sandia National Laboratories and sponsored by U.S. NRC. It is a fully integrated, engineering-level computer code for BWR and PWR severe accident phenomena. MELCOR has been designed to facilitate sensitivity and uncertainty analyses through the use of sensitivity coefficients. Many parameters in correlations, which are made constant in most codes, are implemented as sensitivity coefficients in MELCOR. MELCOR is executed in two parts. The first is called MELGEN and in it the majority of input is specified, processed and checked. When the input checks are satisfied, a Restart File is written containing initial conditions for the next calculation. The second part is MELCOR program itself which executes the problem based on the MELGEN and MELCOR input. In this paper, version 2.1 is used.

The NEK SFP was originally designed to store the limited number of FAs. Those FAs had to be withdrawn, after some cooling interval, due to permanent storing. According the original design, the SFP had to be filled until 2003. This meant that the NEK had to shutdown because the regulatory guides require that the SFP has to have free space for the total core inventory in the emergency (ECU – emergency core unloading). The NEK had to undergo the reracking of the SFP that had to achieve the possibility store all spent fuel during the whole NPP life (40+20 years). The original SFP had 12 racks. During the reracking, 3 of 12 racks were replaced with 9 new racks. At the moment, there are 9 old racks in NEK SFP that have larger rack cell area and contain newly extracted fuel from the core. There are also 12 new racks that have smaller rack cell area and contain older FAs. New racks have smaller rack cell area and higher density because they have special boraflex plates.

The fuel transfer from the reactor core to the SFP is through the Transfer Canal that is flooded to maintain radioactive protection. A part of the SFP is the Cask Loading Area where the fuel is loaded for dry storage. The control volume (CV) 110 represents the volume where the higher power fuel is located (the fresh fuel) and the CV 210 is the associated bypass for that area. CV 120 represents the volume where the old fuel is located and the CV 220 is the associated bypass for that area. The CV 299 is the coolant volume between the rack and the SFP walls (the downcomer). A part of that volume is extracted to model the downcomer above racks (CV 301). The CV 300

models the coolant volume above racks and CV 100 is the coolant volume below the rack's baseplate.

The spent fuel is modeled in similar way as the active core in COR package. The fuel is divided in 3 rings and 14 axial divisions. First 3 axial divisions model part below the baseplate, and next 10 model the active fuel and the last 2 model upper plenum. That is old way of SFP modeling.

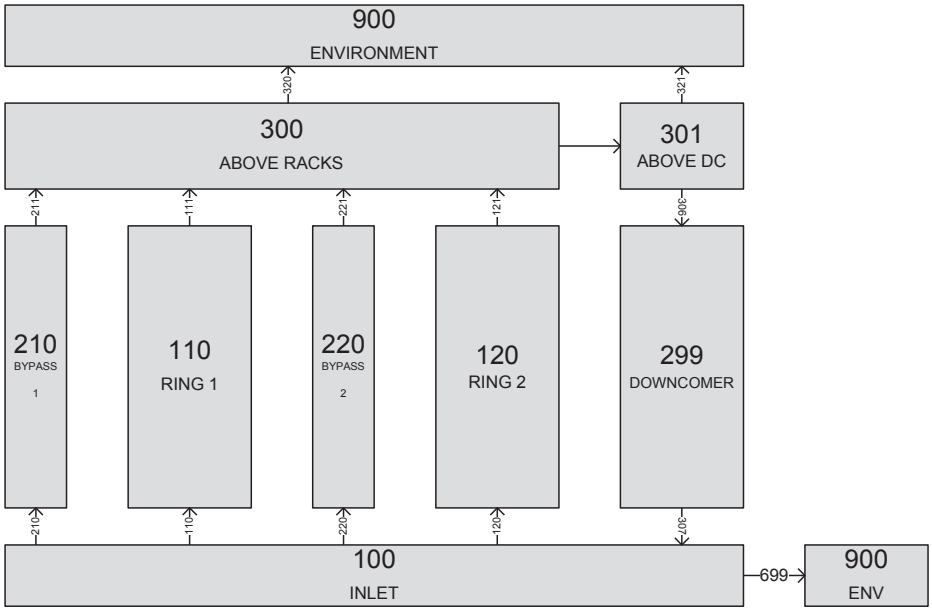


Figure 1: NEK SFP - Control volumes and flow paths

The cooling of the SFP based on spray nozzles will be introduced as part of NEK safety upgrade program [1]. The spray system will be located along the north and south wall of the SFP on the elevation 115.55 m. Both spray lines will have valves for spray pressure control that will discharge water in the SFP when the pressure setpoint is obtained. If all spray nozzles fail, the water will be discharged in the SFP through the relief valves. The water source for spray nozzles will be fire protection water or water from Sava river. The spray system will be divided in low (3 $m^3$/h), medium (25.4 $m^3$/h) and high (59.2 $m^3$/h) mass flow rate nozzles. Every type has 4 nozzles and they are located as shown in Figure 2. Low mass flow rate nozzles are associated with the new racks because there is old cooled fuel. Medium and high flow rate are associated with the old racks where the fresh fuel is located.

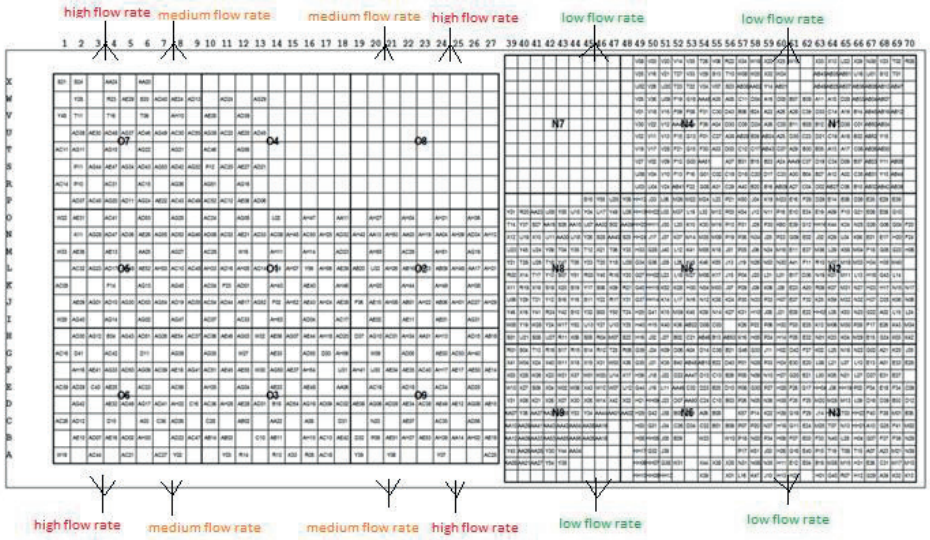


Figure 2: Spray nozzle arrangement above the SFP

The spray system in MELCOR is modeled with two separate sprays, one above the old part of the SFP and another above the new SFP. Spray for the old part of SFP is located in the CV 300 on

the elevation 11.7 m, and its mass flow rate is 84.6 $m^3$/h (that is sum of medium and high mass flow rate nozzles). Spray for the new part of SFP is also on the elevation 11.7 m, and its mass flow rate is 3 $m^3$/h. For both spray, fractions of spray droplets that reach the certain volume are defined through the input cards. The CV 100 is the control volume containing the sump where all water that did not evaporate flows. The spray is controlled with the control function that starts spray at the certain time after the accident initiation.

A control function is also used to model opening of the blow out panels in FHB. Due to the SFP spray operation, a hydrogen production is expected. Therefore, a part of the SFP modification was to install blow out panel in the FHB that could decrease the pressure increase in the SFP due to hydrogen generation. They open at approximately 1800 s and stay opened the whole accident. The ideal ventilation configuration is to intake cold air from the FHB bottom and to exhaust hot air at the FHB top. In the NEK, that is simulated with big FHB door that are used for the fuel transfer and the blow out panels at the top.

Argonne National Laboratory (ANL) has made tests that showed that a smoother change from pre-breakaway to post-breakaway oxide layer gave a better fit to experimental data. The results of the SFP experiments suggest that a maximum lifetime of 1.2 gives a better fit for the default breakaway parameters than 1.0 what was used before. This newly implemented MELCOR model calculates the maximum lifetime for breakaway in each cell using the local cladding temperature. In this paper, the breakaway oxidation was modeled with control functions that compared accumulated damage for clad component in each COR cell with 1.0. The fuel collapse time is defined as the function of cladding temperature and it is applied only when the unoxidized Zircaloy thickness is less than 0.1 mm. When this is satisfied, the model calculates the damaged fuel fraction for every time interval and adds it to the previously calculated damage. When the cumulative fuel damage reaches 100%, the fuel in the SFP MELCOR model collapses.

## 3 CALCULATION RESULTS

The time selected for calculation is 09.10.2016., the moment when the fuel, during the refueling outage, was transferred from the reactor to the SFP. The SFPFA program was used to obtain data for the current SFP inventory, its decay heat and the time to boiling. The program is very easy to use and it uses simple conservative models to estimate basic data for the SFP safety. Figure 3 top shows how many days the spent fuel was in SFP (the span is from 9 to 12150 days), whereas the bottom side shows the spent fuel decay heat. The decay heat for old racks is between 98 W and 52.82 kW (5.71 MW total) and for new racks is between 89 W and 2.03 kW (0.573 MW total).

The first observed transient is loss of coolant due to 1 $cm^2$ break at the SFP bottom. That break size is used in SFP loss of coolant standard analyses. The transient was simulated for 600000 s. Figure 4 shows the start of the fuel heatup for the case without the spray. The fuel temperature distribution is given for every axial division of the active fuel. As expected, the highest fuel division starts to heatup first as the coolant level drops during the accident. Figure 5 shows the comparison of the SFP water level without and with the spray. This figure demonstrates the effectiveness of the spray system in the SFP during the loss of coolant accident. For the case B (with the spray), the water level starts to decrease later than for the case without the spray, therefore the SFP integrity is longer maintained.

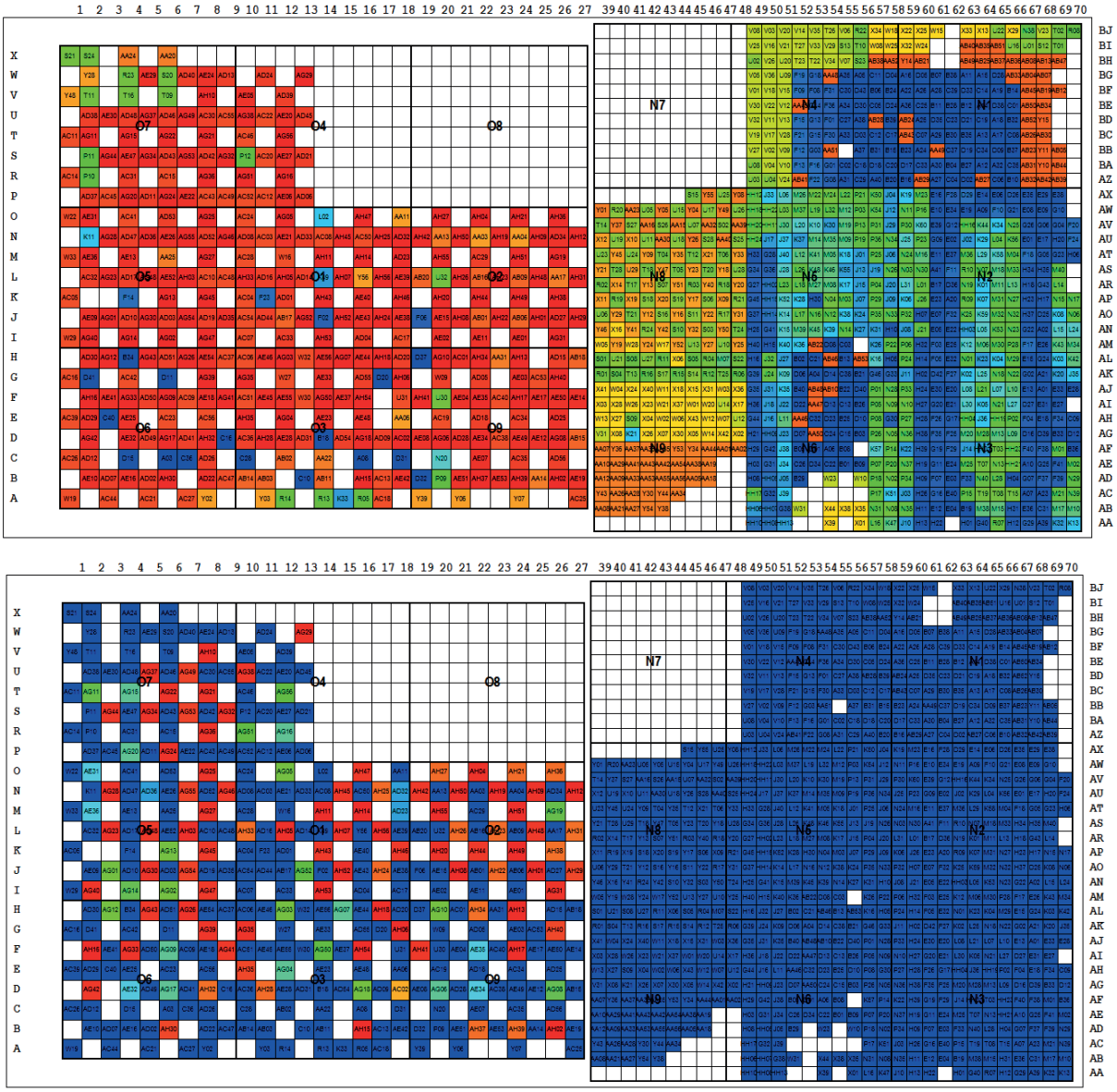

Figure 3: SFPFA calculation results (time and power)

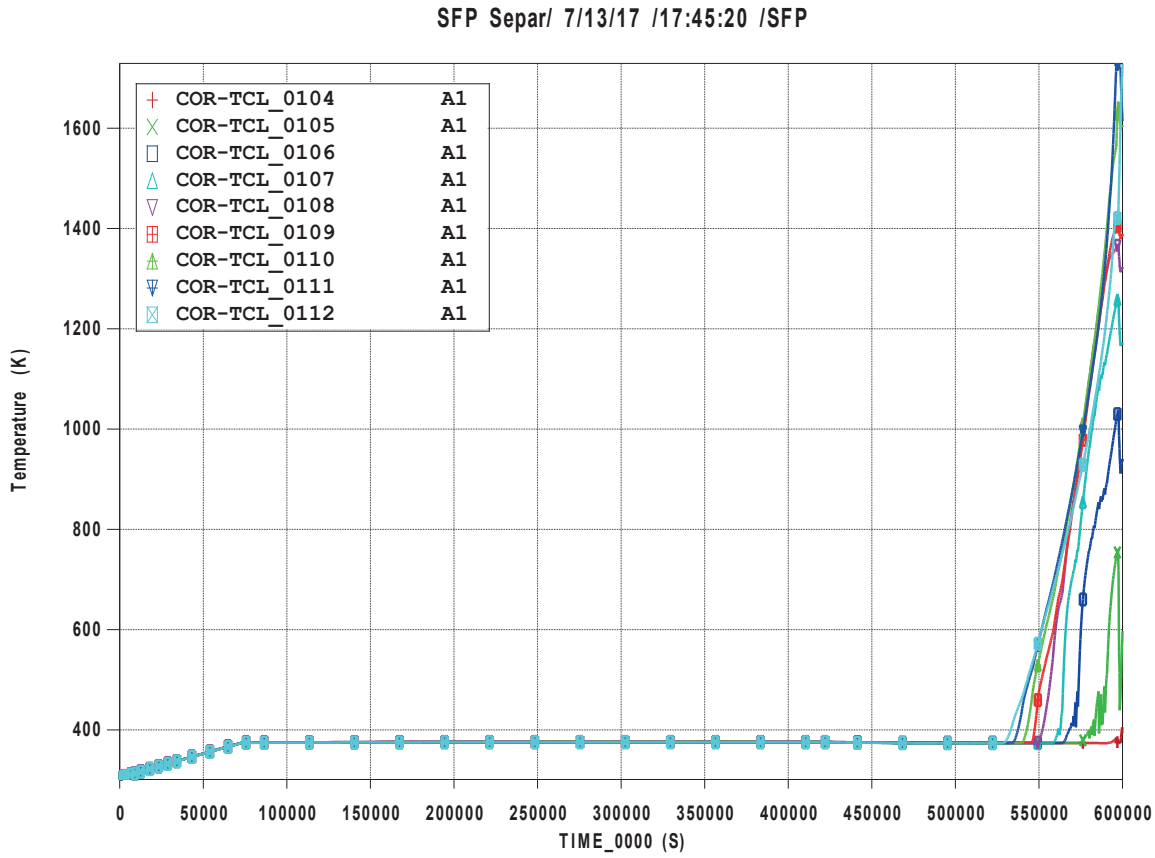


Figure 4: The start of fuel heatup without spray (1 cm$^2$ break)

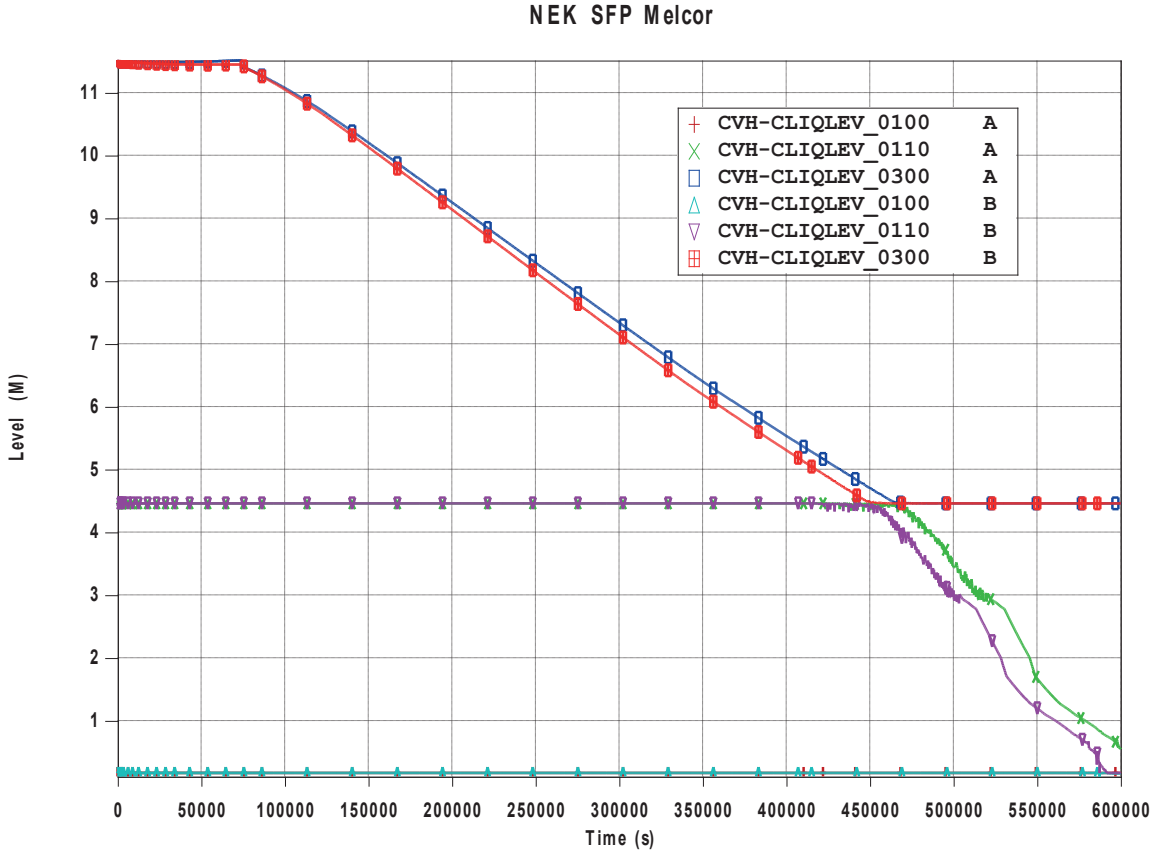


Figure 5: The comparison of the SFP water level without and with the spray (1 cm$^2$ break)

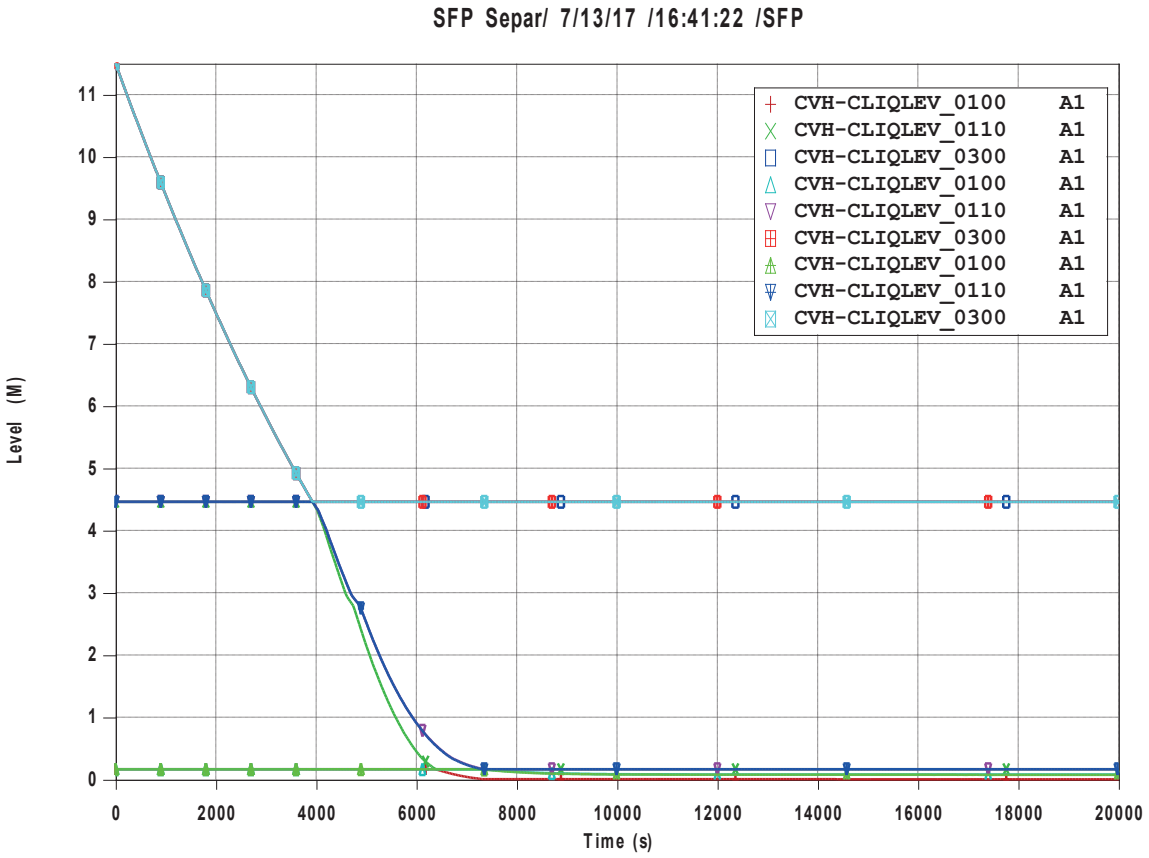


Figure 6: The comparison of the SFP water level without and with the spray (10 cm$^2$ break)

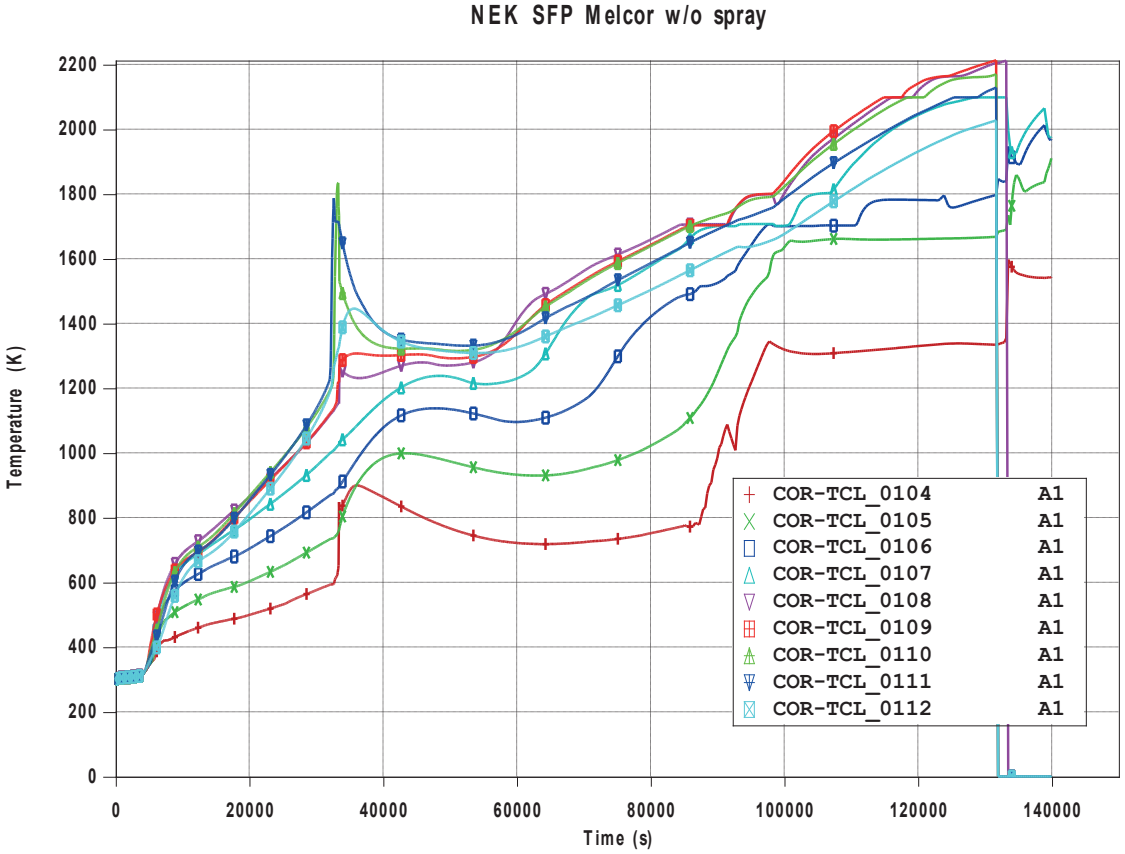


Figure 7: The fuel heatup without spray (10 cm$^2$ break)

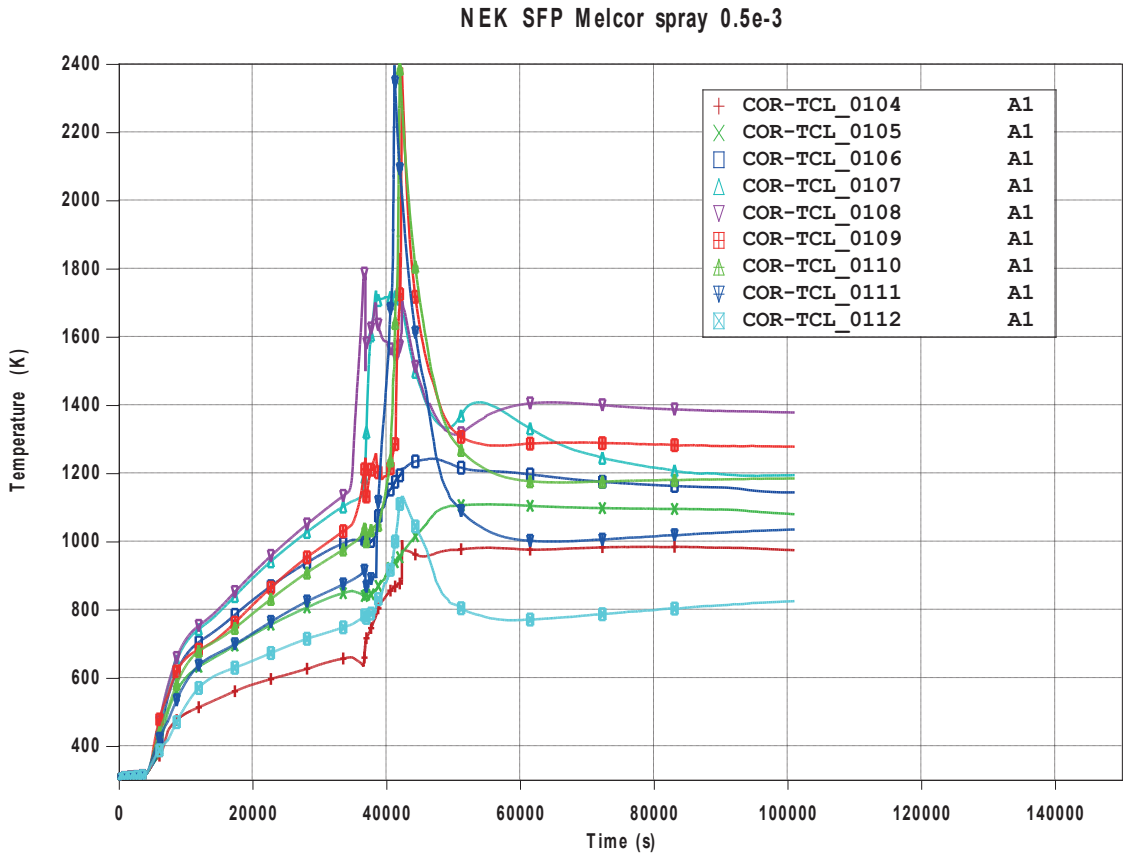


Figure 8: The fuel heatup with spray droplet of 0.5 mm diameter (10 $cm^2$ break)

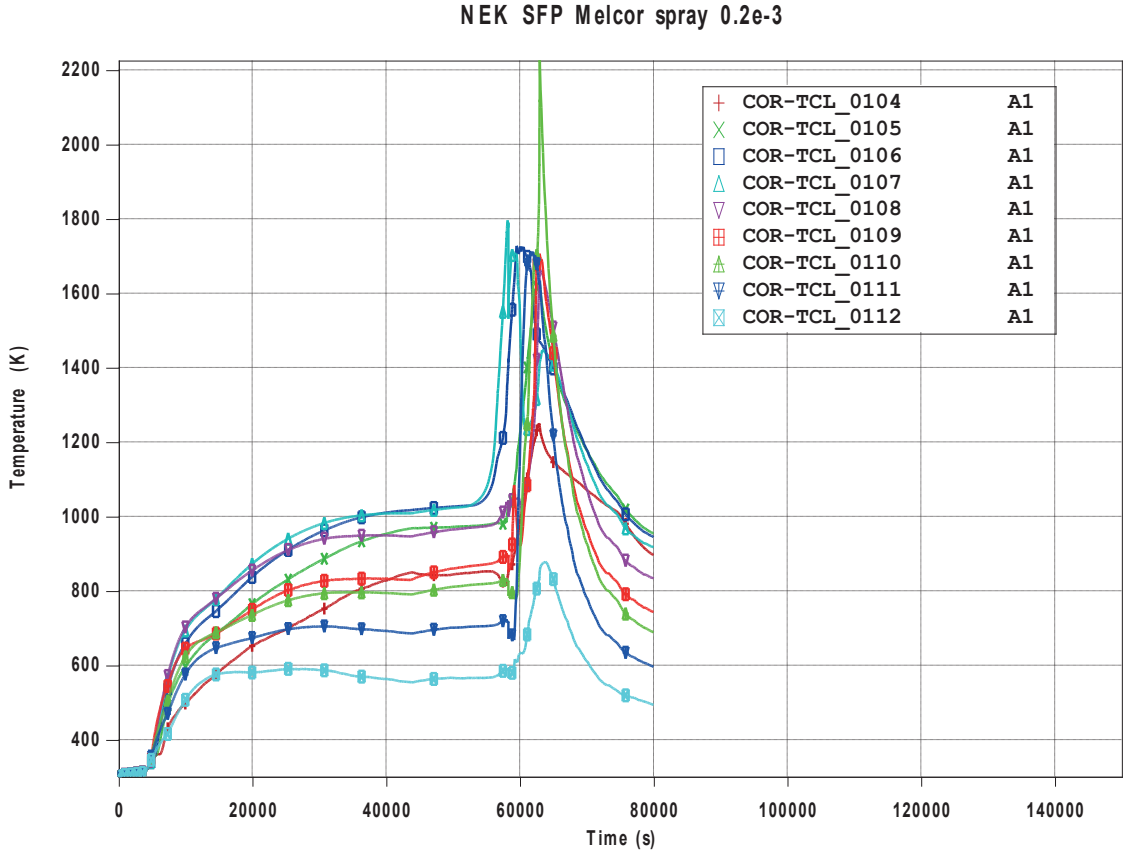


Figure 9: The fuel heatup with spray droplet of 0.2 mm diameter (10 $cm^2$ break)

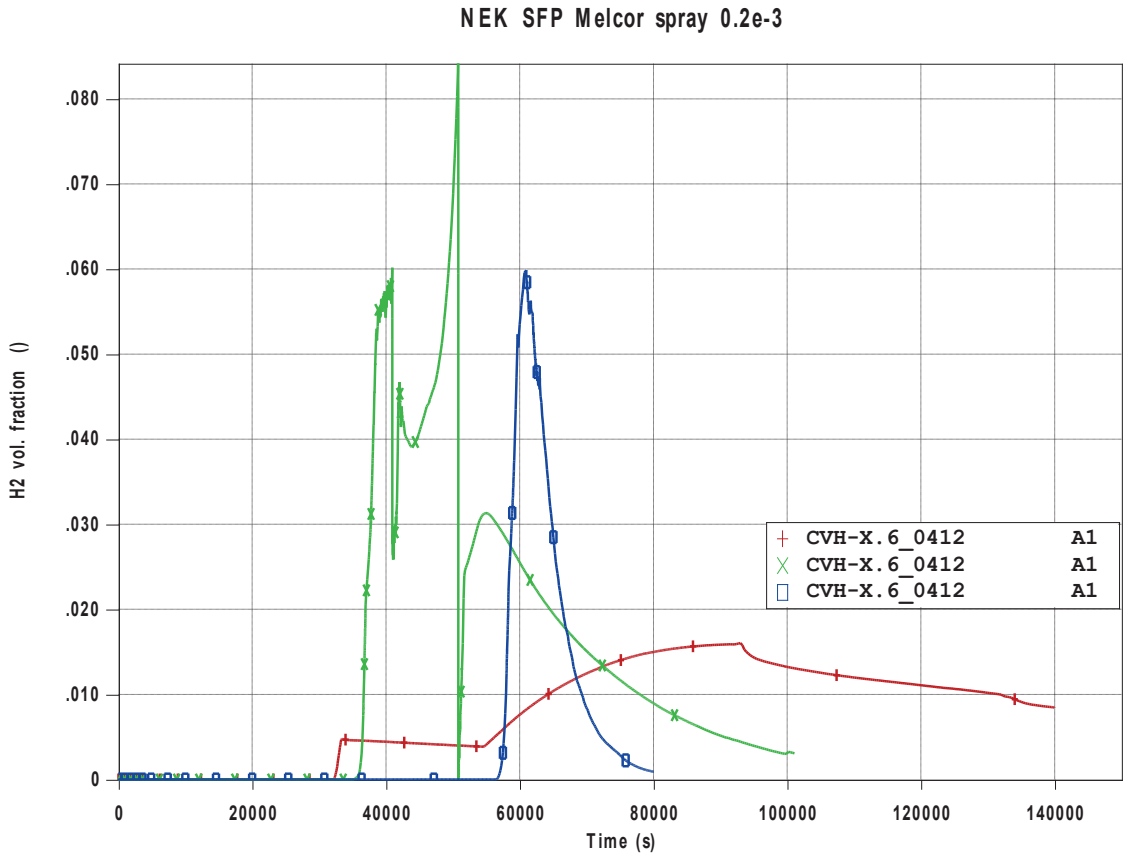


Figure 10: Hydrogen fraction without and with spray - 0.2 and 0.5 mm (10 cm$^2$ break)

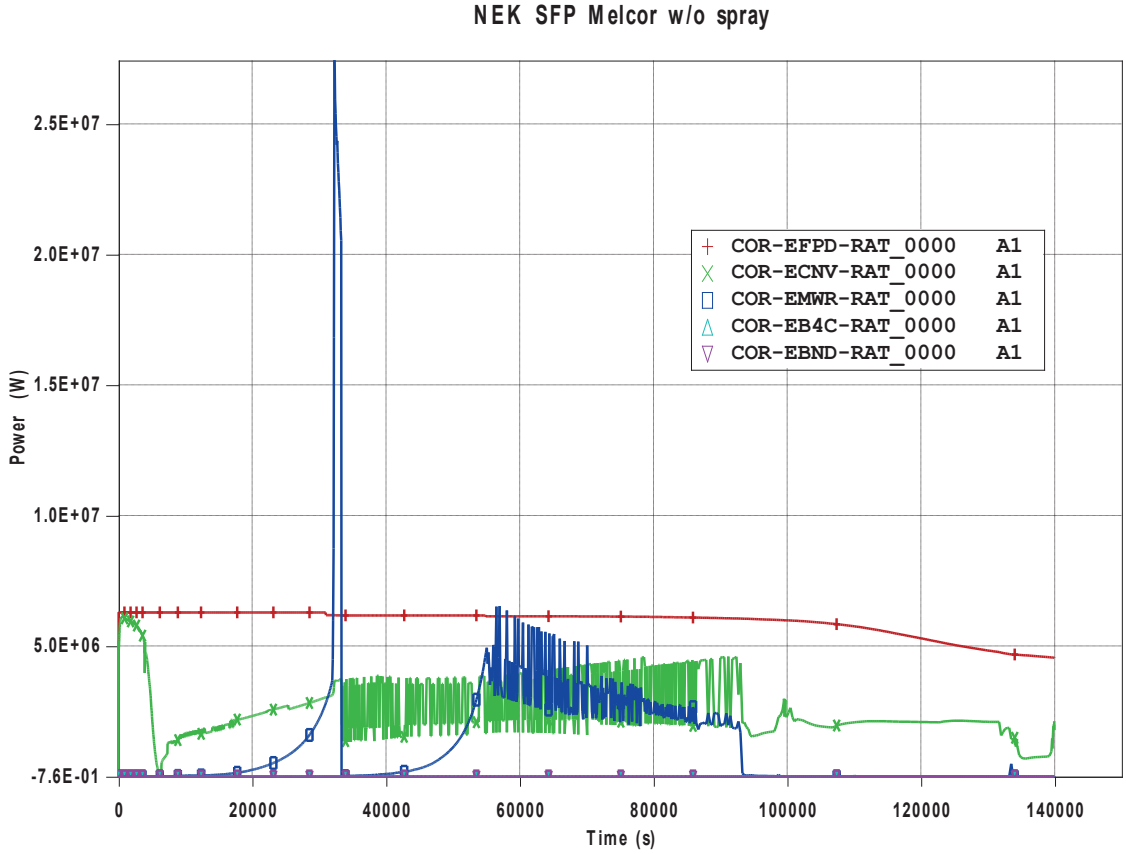


Figure 11: The power distribution for the case without spray (10 cm$^2$ break)

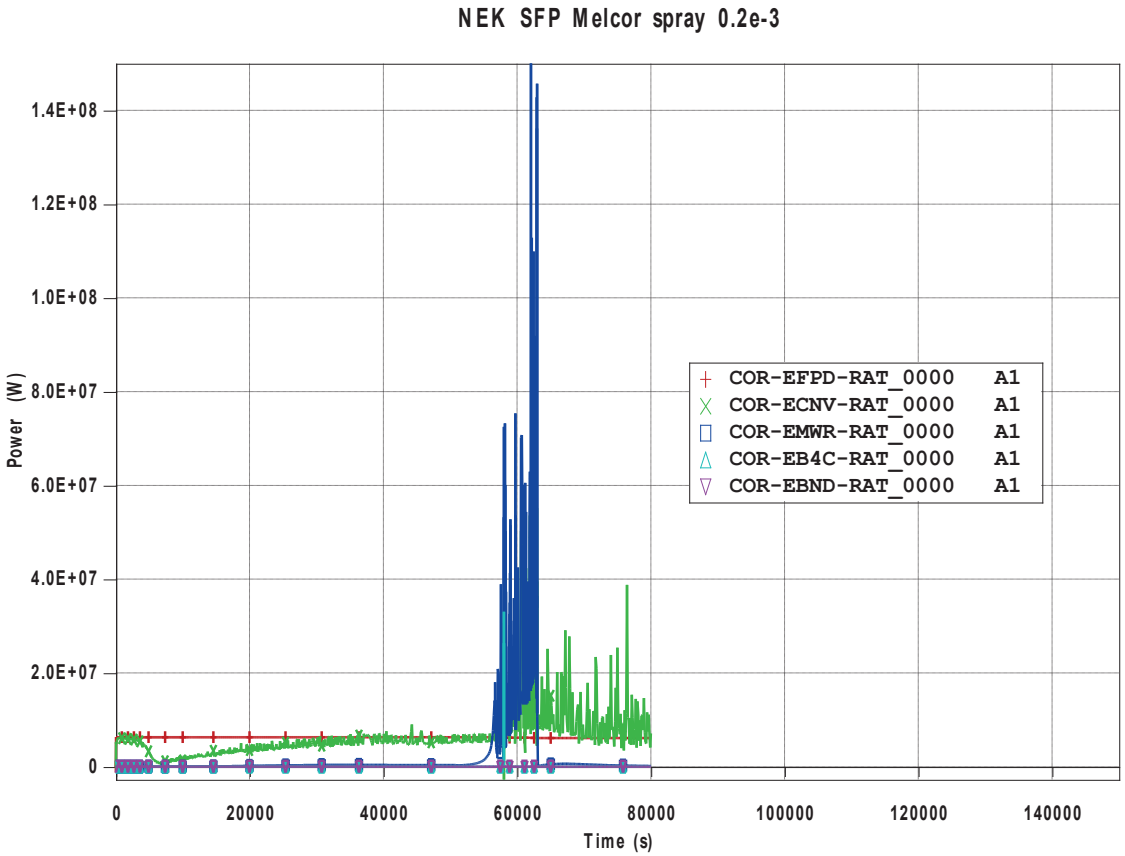


Figure 12: The power distribution for the case with 0.2 mm diameter spray droplets (10 $cm^2$)

The second observed transient is loss of coolant due to 10 $cm^2$ break at the SFP bottom. The transient was simulated for 140000 s. The break flow rate is much higher than in the first observed transient due to larger area break. The comparison of the SFP water level for the case without and with the spray is shown in Figure 6. Like for the 1 $cm^2$ break, the water level starts to decrease later for the case with the spray. The water level in the SFP, due to spray, stabilizes above zero, whereas for the case without the spray, the water drains completely out of the SFP. Figure 7 shows the fuel heatup for the case without the spray. The fuel temperature for all axial division is shown and again the highest divisions start to heatup first. The first peak is reached at approx 30000 s. In that moment, the effect of the breakaway cladding oxidation is noticeable leading to the fuel temperature decrease. Afterwards, the fuel temperature starts to increase until the fuel melts and begins to relocate.

For the same break size, the effectiveness of the spray system was demonstrated. It is initiated with the control function at the 3900 s when the fuel starts to uncover. Figure 8 shows the fuel heatup when the spray system is installed with the spray droplet of 0.5 mm diameter. As expected, the first peak is reached later than in case without spray (at approx 40000 s). This demonstrates that installed spray system can prolong the heatup start and therefore give time to operators to plan an action to prevent severe accident.

For this transient, a case with spray droplet of 0.2 and 0.5 mm diameter was observed to estimate the cooling effectiveness on the droplet size. Figure 9 shows the fuel heatup with spray droplet of 0.2 mm for the same break size. The fuel heatup starts at approx 60000 s that is much later than for the 0.5 mm diameter droplet showing that the smaller droplet can more effectively cool the fuel in the SFP. As a consequence of using the spray, hydrogen is generated due to exothermic steam oxidation. Figure 10 shows the comparison of hydrogen distribution during the accident without spray and with spray droplets of 0.2 and 0.5 mm diameter. In the case without the spray, the smallest amount of hydrogen is generated, whereas the bigger droplet size generates more

hydrogen. Figure 11 and 12 show the power distribution for each type of heat transfer for the case without spray (Figure 11) and for the case with 0.2 mm diameter droplets (Figure 12).

## 4 CONCLUSION

The most critical SFP accidents are loss of cooling and loss of coolant. One of activities that can prolong the fuel heatup in the SFP is spray system. The aim of this paper was to demonstrate the effectiveness of the installed spray system in the SFP. Efficiency of spray system in SFP depends on several parameters, especially on the diameter of spray droplets. The calculations conservative and uses old ring based approach to SFP modelling.

This preliminary calculations show that spray system is eventually capable of limiting fuel temperature increase in SFP, but depending on time of actuation and droplets size can cause hydrogen generation.

**Acknowledgements:**

We would like to express our gratitude to the NPP Krško for providing relevant input data used in calculation and for supporting whole activity.

## REFERENCES

[1] NEK Safety Upgrade Project Design Input and Interfaces, Rev.6

[2] Wagner, K. C. i Gauntt, R. O. Mitigation of Spent Fuel Pool Loss-of-Coolant Inventory Accidents And Extension of Reference Plant Analyses to Other Spent Fuel Pools. Albuquerque, New Mexico 87185 and Livermore, California 94550 : Sandia National Laboratories, 2008.

[3] Barto, et all Consequence Study of a Beyond-Design-Basis Earthquake Affecting the Spent Fuel Pool for a U.S. Mark I Boiling Water Reactor. s.l. : US Nuclear Regulatory Commission, 2013.

[4] Humphries, L.L., B.A. Beeny, F. Gelbard i D.L. Louie, J. Phillips. MELCOR Computer Code Manuals; Vol. 1: Primer and Users' Guide; Version 2.2.9541 2017. Albuquerque, NM 87185-0748 : Sandia National Laboratories, 2017.

[5] Rok Bizjak, Dejvi Kadivnik. SFP water heatup and evaporation. NEK ESD-TR-07/11, Krsko 2011.

[6] Cardoni, Jeffrey. MELCOR Model for an Experimental 17x17 Spent Fuel PWR Assembly. Albuquerque, New Mexico 87185 and Livermore, California 94550 : Sandia National Laboratories, 2010.

[7] Allen G. Croff, A User's Manual For The ORIGEN2 Computer Code, ORNL/TM-7175 (CCC-371), Oak Ridge National Laboratory, July 1980.

[8] Decay Heat Power in Light Water Reactors, ANSI/ANS-5.1-2005

Journal of Energy
VOLUME 68 Number 2-3 | 2019 | Special Issue
journal homepage: http://journalofenergy.com/

# Potential Impact of Reactor Core Damage on Severe Accident Management Actions in Vicinity of Spent Fuel Pool

**Ivica Bašić, Ivan Vrbanić**
APOSS d.o.o.
Repovec 23B, 49210 Zabok, Croatia
basic.ivica@kr.t-com.hr, ivan.vrbanic@zg.t-com.hr,

**Davor Grgić**
Faculty of Electrical Engineering and Computing, University of Zagreb
Unska 3, Zagreb, Hrvatska
davor.grgic@fer.hr

**Mario Mihalina,**
Nuclear Power Plant Krško
Vrbina 2, 8670 Krško, Slovenia
mario.mihalina@nek.si

## ABSTRACT

Fukushima Daiichi NPP accident showed that plant technical support center (TSC) in an extreme and rare external event (design extended condition (DEC)) can have a problem in the case of coincident loss of decay heat removal from the core (possibly resulting in significant core damage) and loss of decay heat removal from spent fuel pool. From the point of view of prioritizing severe accident management strategies it looks like the priority mitigation action should be to reestablish the emergency core cooling in the reactor pressure vessel. The reason is the longer time window available before the water inventory in the spent fuel pool would be evaporated and spent fuel exposed to overheating. However, if such actions would not be successful and reactor core would, consequently, be damaged, potential design basis leakage (or even greater leakage) from the containment to the fuel handling building (FHB) can affect already established TSC measures or operator accessibility to FHB, or it can jeopardize functioning of the systems, structures and components due to radioactive releases and presence of hydrogen (independently of the fact that containment atmosphere can be inerted by steam or that containment may be equipped with passive autolytic recombiners (PARs)). Paper describes an engineering evaluation of possible hydrogen presence in the containment annulus, its flammability and leakages through the penetrations toward FHB in the case of long term station blackout (SBO) without successful restoration of the core cooling in the reactor pressure vessel. SBO accident sequence progression and amount of produced hydrogen is evaluated by MAAP code.

***Keywords:*** *core damage, SFP, SAMG, containment leakage, MAAP*

# 1 INTRODUCTION

One noteworthy feature of typical Westinghouse designed PWRs is that the SFP is located in close proximity to the containment in building named Fuel Handling Building (FHB). According to [1], the investigation of severe accidents for the PWR SFP-Reactor PSA should include the assessment of possible postulated initiating events (PIEs) introducing a challenge to the SFP fuel cooling.

Very generally, the interface dependencies (illustrated by Figure 1) may arise due to the following:

1. Simultaneous failures related to the initiating event (e.g., loss of offsite power, design extension condition (DEC) seismic events, etc.)
2. Reactor severe accident conditions that result in adverse conditions affecting the FHB/SFP structure or SFP cooling/make-up equipment.

Resulting adverse conditions may include the following:

- Hydrogen release that could result in deflagration events that fail structures or electrical/mechanical equipment;
- Containment failures that cause similar effects;
- Fission product releases that inhibit or preclude access to the areas needed for local alignments;
- Failure of all installed equipment may force the TSC staff to decide where to prioritize the use of any remaining portable equipment. Staging for use in one application (e.g., reactor accident mitigation) may preclude its subsequent realignment to the SFP due to local environmental conditions.

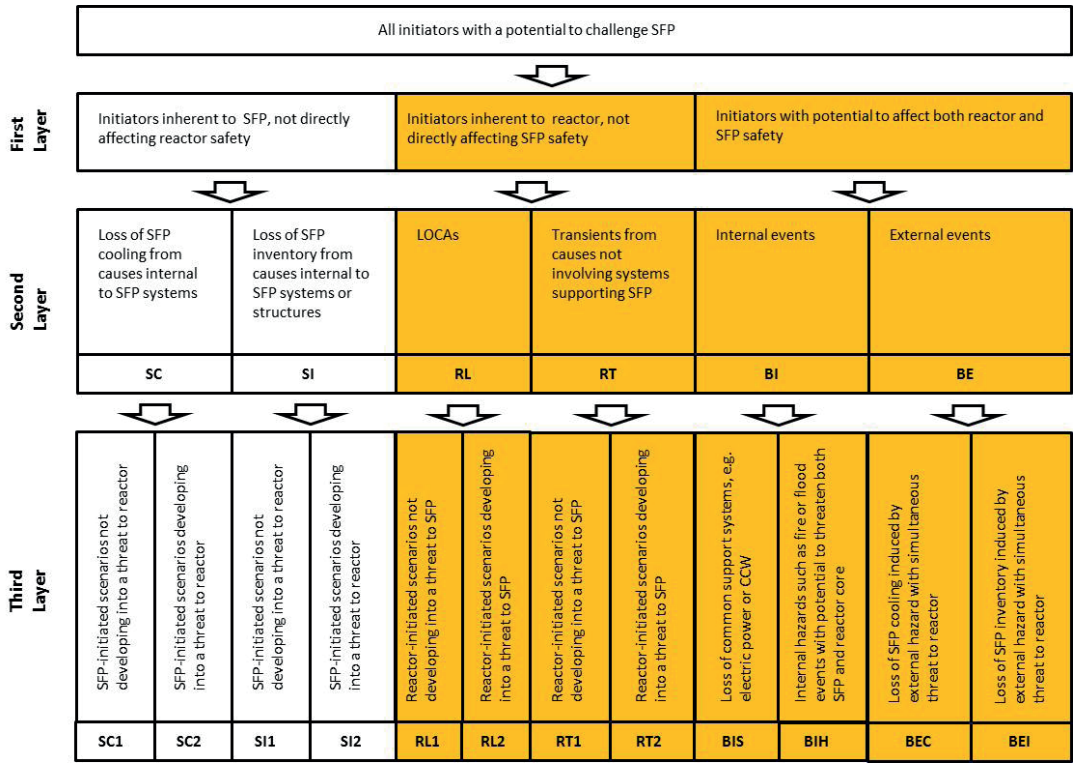


Figure 1: All initiators with potential to challenge SFP

Paper does not intend to discuss the assessment of the full PSA interface study. It describes a simplified engineering evaluation of possible hydrogen presence in the containment annulus, its flammability and leakages through the penetrations toward FHB.

## 2 CONTAINMENT LEAKAGES

Figure 2 presents the typical analytical scheme for leakage paths from the containment (where RB is for Reactor Building (containment); AB is for Auxiliary Building; IB is for Intermediate Building; and FHB is for Fuel Handling Building)). Plant Updated Safety Analysis Report (USAR) analyses of radiological consequences usually take into account the limited total leakage from the containment corresponding to the design leakage rate from the containment ( e.g. 0.2% by weight of the containment air per 24 hours, at $P_a$ = 3.15 kp/cm$^2$ - [5], LCO 3.6.1.2 ). From Figure 2 it can be reasonably concluded that a definition of distribution of leakages to the various adjacent buildings, rooms and spaces can introduce rather large uncertainties. Due to this reason, for simplification of assessment and practical usage, assumption will be used that the total design leakage is always applied to only one possible path. On the other hand, such approach generates problems because assuming that hydrogen or radioactive influents are released only to one particular area gives their unrealistic concentrations in the considered area.

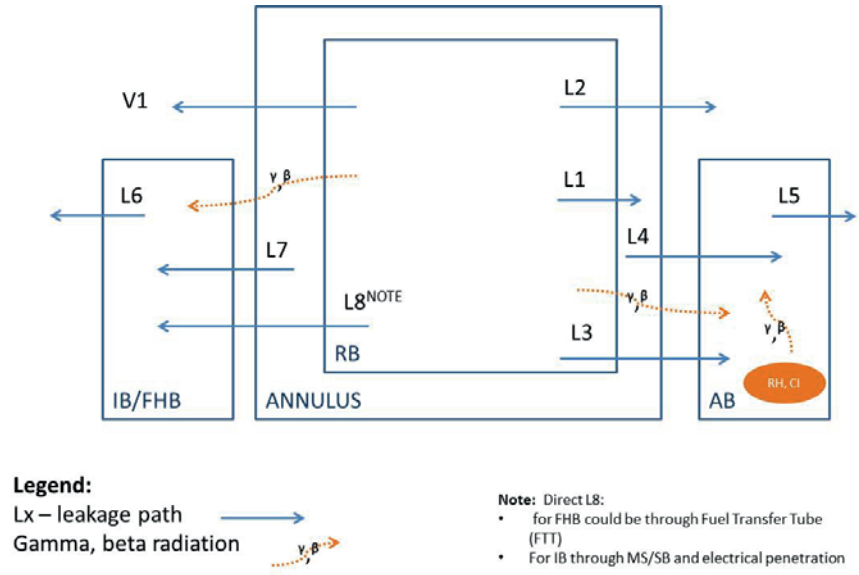


Figure 2: Containment Leakage Scheme

Path L8 on scheme shown in Figure 2 could represent the Fuel Transfer Tube (FTT), used during an outage for direct connection between FHB (fuel Transfer Canal (TC)) and the containment reactor cavity - Figure 3. FTT is isolated during normal operation by a blind flange and a valve.

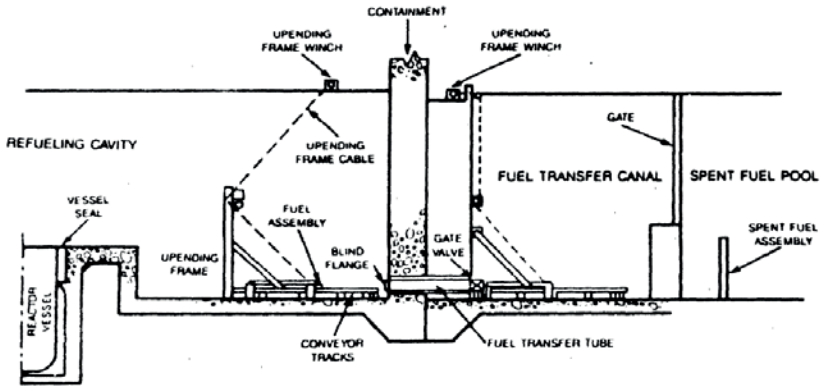


Figure 3: Fuel Transfer System, [7]

## 3 HYDROGEN PRODUCTION AND DISTRIBUTION

In the original Krško NPP Level 2 PSA studies (1995), the production of hydrogen by fuel cladding zirconium oxidation and its distribution in the containment were discussed and evaluated on the basis of principles presented in [8]. Deterministic analyses were performed for the chosen accident scenarios (Station Blackout (SBO), Large Break Loss of Coolant Accident (LLOCA) and Small Break LOCA (SLOCA)) by integral best estimate severe accident code MAAP 3.0B. NPP Krško repeated these analyses by upgraded MAAP 4.0.5 model in the light of the IAEA RAMP (Review of Accident Management Program) mission recommendations. Results were discussed in [4] and are summarized in Table 1 below. From the compared results it can be concluded that the evaluation by the new version of the code resulted with the increased amount of hydrogen released from corium to the containment. Krško NPP is currently preparing the new revision of [8] which will be supported with newer research information on hydrogen production/behavior in the containment, upgraded plant model and improved version of the code (MAAP5.0.3). Distribution of hydrogen in containment for observed scenarios was additionally evaluated by GOTHIC 3D code and documented in [9]. Conclusion was that hydrogen is uniformly distributed around the containment and there is no concentration which would reach the flammability limit within 24h. More recent Krško NPP's analyses (either by MELCOR 1.8.6 or/and MAAP 4.0.7) which assumed an installation and usage of containment passive autocatalytic recombiners (PARs) and Passive Containment Filter Vent (PCFV) were not taken into account in this rough evaluation. PARs recombine the hydrogen as long as all the oxygen in the containment is not consumed (so-called "starvation strategy"). The maximum allowable equivalent hydrogen mass (taking into account in and ex-vessel produced hydrogen and carbon monoxide (CO) produced by molten core concrete interaction (MCCI) ) that can burn by deflagration without exceeding 6 bar abs (5% failure probability, as used in SAMG) is ~408 kg per section 20 of [10]. Therefore, the sizing criterion has been chosen to ensure that PARs reduce the oxygen content such that any combustion is oxygen limited, regardless of CO or hydrogen concentrations. Once when all oxygen is consumed the concentration of hydrogen (and explosive carbon monoxide (CO)) in containment can be potentially increased by MCCI without efficient recombination if there is no mitigative action from the TSC staff with flooding of the reactor containment cavity.

Table 1: Comparison of Hydrogen Production Mass Generated in SBO, LLOCA and SLOCA Accidents

| Run ID | MAAP 3B H2 mass generated in the core at end of the transient (kg) | MAAP4.0.5 H2 mass generated in the core at end of the transient (kg) |
|---|---|---|
| **SBO (HSBO1)** | 255 | 266 |
| **LB LOCA (LLOCA3)** | 103 | 185 |
| **Small LOCA (SLOCA2)** | 280 | 320 |

To simplify the discussion about influence of assumed scenario and timing of hydrogen releases from reactor vessel to containment, for illustration of the methodology described below, it will be assumed that 100% of zircaloy from fuel cladding (11860kg) is oxidized producing 525kg of hydrogen within time frame of 24h and that additional 1000kg of equivalent hydrogen is produced by MCCI. (This also takes into account a production of carbon monoxide. The hydrogen and carbon monoxide (CO) as a mixture have similar flammability limits to the gases considered alone, when expressed as a volume fraction. In addition, hydrogen and CO have similar molar heats of combustion. Thus, on a molar basis, CO and hydrogen may be considered as "equivalent".)

## 4 SIMPLIFIED DETERMINATION OF CONCENTRATION OF HYDROGEN IN THE CONTAINMENT ANNULUS OR/AND FUEL HANDING BUILDING (FHB)

Basic assumptions:

- The mass of hydrogen in the inner rooms of the containment is conservatively assumed at maximum. The work of passive catalytic hydrogen recombines (PARs ) is not considered.
- The assessment is applied in the range of containment pressures below passive containment filter vent (PCFV) opening setpoint. (The passive actuation of the system will occur once the containment pressure exceeds the rupture disk burst pressure of 5 bar differential).
- Due to inability to determine the exact locations of leakages from the containment, the complete free volume of containment annulus or FHB is assumed for calculation. At the same time it is assumed that the environment in the annulus space between the inner metallic liner and outer containment shell is perfectly mixed. Same is valid for the FHB environment.
- Conservatively, it is assumed that only the hydrogen leaks from the containment atmosphere to annulus or FHB. In reality mixture of steam, air, hydrogen and radioactive effluents would leak from the containment to the adjacent buildings and areas as shown in Figure 2 above.
- The maximum containment design leakage from the containment is assumed (0.2% volume).
- Leakages from the annulus space to the adjacent buildings and the surrounding atmosphere are not taken into account. It is always assumed that the total amount of leakage flows to only one area/volume.

Initial data:

- Containment annulus free volume is 11220 $m^3$.
- Fuel Handling Building (FHB) free volume is 26220 $m^3$.
- Design leakage from the containment is 0.2% by weight of the containment air per 24 hours, at $P_a$ = 3.15 $kp/cm^2$ ([5], LCO 3.6.1.2 ).
- Containment annulus and FHB initial pressure is atmospheric, 101325$P_a$.
- Containment annulus and FHB initial temperature $T_{a.s.}$ = 313K.
- The mass of hydrogen in containment could be based on MAAP calculation or conservatively assumed as shown in para 4 above.

Calculation:

It is necessary to determine the volumetric hydrogen concentration in the annulus space between the liner and outer containment shells, $x_{a.s.,H_2}$.

a) Volumetric hydrogen concentration can be determined by equation (1):

$$x_{a.s.,H_2} = 1 - \frac{P_{a.s.,0}}{P_{a.s.}} \quad (1)$$

where:

$P_{a.s.,0}$ represents the initial air pressure in the annulus;

$P_{a.s.}$ represents the pressure of the mixture (air / hydrogen) in the annulus.

b) The pressure of the mixture in the annulus space can be determined by equation (2):

$$P_{a.s.} = \frac{R \cdot T_{a.s.}}{V_{a.s.}} \left( \frac{M_{a.s.,air}}{\mu_{air}} + \frac{M_{a.s.,H_2}}{\mu_{H_2}} \right) \quad (2)$$

where:

$M_{a.s.,air}$ represents the initial mass of air in the annulus space;

$\mu_{air}$ represents the molecular mass of air (29);

$M_{a.s.,H_2}$ represents hydrogen mass released from containment to annulus;

$\mu_{H_2}$ represents the molecular mass of hydrogen (2);

$V_{a.s.}$ represents free volume of annulus;

R represents ideal gas constant (8314kJ/mol-K).

c) The initial mass of air in the annulus space is determined by equation (3):

$$M_{a.s.,air} = \frac{P_{a.s.,0} \cdot V_{a.s.}}{R \cdot T_{a.s}} \cdot \mu_{air} \quad (3)$$

Results of simplified evaluation:

The results of simplified evaluations taking into account maximal concentration of hydrogen without MCCI (525kg) and with MCCI (1500kg) are shown in Table 2. The determined maximum volume concentrations of hydrogen in the annulus and FHB for various initial conditions do not reach flammability limit of 4% in the observed area.

The same method is used to determine at which containment leakages the hydrogen concentration can reach flammable limit (4% for observed area) in annulus and FHB. The summarized results are shown in Table 3. The simplified evaluation shows that 7% volume/day leakage to annulus and 16.5% volume/day leakage would increase hydrogen concentration to flammable limit without MCCI but much smaller leakage is needed for it in the cases with MCCI.

Table 2: Summarized Results: Maximum Concentration of Hydrogen in Observed Area

| | **Calculated volumetric hydrogen concentration** | |
|---|---|---|
| **Case description** | **Annulus** | **FHB** |
| Design Leakage (0.2%volume/day) no MCCI | 0.12% | 0.05% |
| Design Leakage (0.2%volume/day) with MCCI | 0.35% | 0.15% |
| DEC leakage (2 x design leakage), no MCCI | 0.24% | 0.10% |
| DEC leakage (2 x design leakage), with MCCI | 0.69% | 0.30% |

Table 3: Summarized Results: Minimum Containment Leakage Needed for Flammable Limit (4%) in Adjacent Areas

| **Location** | **without MCCI** | **with MCCI** | |
|---|---|---|---|
| **Annulus** | 7% | 2.39% | in-leakage/day |
| **FHB** | 16.50% | 5.60% | in-leakage/day |

## 5 CONCLUSION

Presented simplified engineering assessment shows that hydrogen leakage from containment to annulus and/or FHB should not be safety concern from flammability (4% of hydrogen in volume) point of view if we are talking about the normal design basis leakage (or even its double value, in the light of potentially increased containment pressure during design extension condition (DEC) before passive containment filter vent (PCFV) would be actuated). However, evaluation of minimum containment leakage needed to reach flammable limit show that partial or full loss of containment tightness can cause flammable environment in the FHB and the annulus. The annulus is of particular concern because the fire or detonation can jeopardize containments liner from the outside which cannot be mitigated easily by any kind of TSC mitigative action.

Presented assessment demonstrates how important it can be to adequately address the candidates for a high level action (CHLA) related to ventilation of the auxiliary buildings (3.2.19, [2] and [3]) in the plant specific SAMGs, because it is not possible to completely eliminate the potential for a breach in the containment at the outset of the accident (postulated DEC) or as a consequence of the harsh conditions that develop inside the containment. This is also important from the point of view that presence of flammable concentrations in annulus or FHB is not monitored by the MCR.

As it is recommended by mentioned CHLA, if normal building ventilation is not available or is ineffective at mitigating the buildup of flammable concentrations in the auxiliary buildings, including the FHB and the annulus, alternate strategies must be implemented to control the building ambient conditions before entering (accessing) these areas for any other implementation strategy

(e.g. makeup of SFP by portable means, see Figure 4 in Attachment 1). Examples of alternative methods to reestablish building ventilation can include the following:

- Using alternative power supplies to reestablish power to a minimal but critical set of ventilation system components;
- Using portable power, exhaust, and recirculation equipment;
- Introducing natural circulation pathways through buildings by opening doors, windows, and other barriers at multiple levels of the building;
- Introducing natural circulation flow using a chimney effect by creating openings at the lower and upper levels of the building.

One point of consideration for future work in this area would be to evaluate possible correlations between core damage and plant damage accident sequences with SFP accident sequences, as described in [1]. Also, best estimate deterministic analyses would be needed to evaluate more realistically containment leakages distribution with upgraded MAAP model, including more detailed connections between FHB / SFP and containment, as well as more detailed model of adjacent buildings to decrease all postulated conservatisms described in section 4.

## REFERENCES


[1] EPRI- 3002002691, PWR Spent Fuel Pool Risk Assessment Integration Framework and Pilot Plant Application, June 2014.

[2] EPRI-1025295-V1, Severe Accident Management Guidance Technical Basis Report, Volume 1: Candidate High-Level Actions and Their Effects, October 2012.

[3] EPRI-1025295-V2, Severe Accident Management Guidance Technical Basis Report, Volume 2: Volume 2: The Physics of Accident Progression, October 2012.

[4] Bašić, I., Bilić-Zabric, T., Špiler, J., Hydrogen Behavior in PWR Containment Evaluated By MAAP4.0.5, 5th International Conference on Nuclear Option in Countries with Small and Medium Electricity Grids, Dubrovnik, Croatia, May 16-20, 2004.

[5] Krško NPP Technical Specification, Rev. 166, 2016.

[6] Bašić, I., Dudaš, M., NPP Krško On-Line Low Pressure Containment Tightness Monitoring Implementation, 5th International Conference on Nuclear Option in Countries with Small and Medium Electricity Grids, Dubrovnik, Croatia, May 16-20, 2004.

[7] US NRC Information Notice No. 88-92: Potential For Spent Fuel Pool Draindown, March 2011.

[8] WENX/95/24, IPE of Krško NPP, Level 2 Report, Volume 1, Containment Event Tree Notebook, Part 2, August 1995;

[9] Grgić, D., Fancev, T., Hydrogen Distribution in NPP Krško Containment, NEK-ESD-TR13/10, June 2010;

[10] NEK Updated Safety Analysis Report (USAR), revision 24, 2018;

Attachment 1:

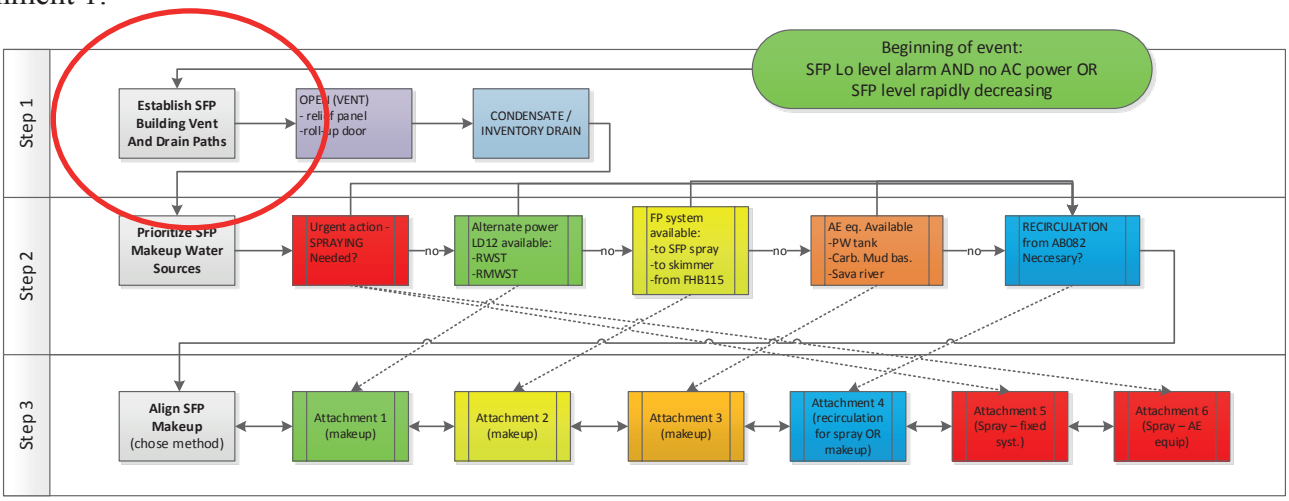


Figure 4: Example for Functional Support Guideline (FSG)

Journal of Energy
VOLUME 68 Number 2-3 | 2019 | Special Issue
journal homepage: http://journalofenergy.com/

# Basic Relation between RAW and RRW and Some of Its Implications on Risk Reduction Strategies

**Ivan Vrbanić, Ivica Basić**
APOSS d.o.o.
Repovec 23B, 49210 Zabok, Croatia
ivan.vrbanic@zg.t-com.hr, basic.ivica@kr.t-com.hr

**Pranab K. Samanta**
Nuclear Science and Technology Department
Brookhaven National Laboratory, Bldg. 130
Upton, NY 11973-5000, United States of America
samanta@bnl.gov

## ABSTRACT

In using risk-informed approaches for ensuring safety of operating nuclear power plants (NPPs), risk importance measures obtained from probabilistic safety assessments (PSAs) of the plants are integral elements of consideration in many cases. In PSA models and applications associated with NPPs the risk importance of a particular feature (e.g. function, system, component, failure mode or operator action) can be, most generally, divided into two categories: importance with respect to risk increase potential and importance with respect to risk decrease potential. The representative of the first category, as used for practical purposes, is Risk Achievement Worth (RAW). Representative of the second category, as mentioned in consideration of risk importance, is Risk Reduction Worth (RRW). It can be shown that the two risk importance measures, RAW and RRW, are dependent on each other. The only parameter in this mutual dependency is probability of failure of the considered feature. The paper discusses the relation between RAW and RRW and some of its implications, including those on the general strategies for the reduction of risk imposed for the operation of the considered facility. Two general risk reduction strategies which are considered in the discussion are: a) risk reduction by decreasing the failure probability of the considered feature; and b) risk reduction while keeping the failure probability of the considered feature at the same level. Simple examples are provided to illustrate the differences between two strategies and point to main issues and conclusions.

***Keywords:*** *probabilistic safety assessment, risk importance measures, risk achievement worth, risk reduction worth*

## 1 INTRODUCTION

In using risk-informed approaches for ensuring safety of operating nuclear power plants (NPPs), risk importance measures obtained from probabilistic safety assessments (PSAs) of the plants are integral elements of consideration in many cases. In PSA models and applications associated with NPPs the risk importance of a particular feature (e.g. function, system, component, failure mode or operator action) can be, most generally, divided into two categories: importance with respect to risk increase potential and importance with respect to risk decrease potential. The

representative of the first category, as used for practical purposes, is Risk Achievement Worth (RAW). Representative of the second category, as mentioned in consideration of risk importance, is Risk Reduction Worth (RRW).

There is a number of other importance measures which were defined and used in reliability and risk analyses. Some of them are defined in relative and some in absolute terms. Most of them are related to each other and some of them produce the same risk ranking. Their theory and use is described in a number of books such as [1], [2] or [3] and studies or engineer's handbooks and guidelines such as [4], [5], [6] or [7]. In this paper we want to focus on those which are most widely used in current PSAs for NPPs and we select the above mentioned two importance measures as representatives.

We will use their definitions from NUREG/CR-3385, [4], which can be considered as one of the early references to establish the use of risk importance measures in PSA applications. Let:

$R_0 =$ the present ("nominal") risk level;

$R_i^+ =$ the increased risk level with feature "*i*" assumed failed;

$R_i^- =$ the decreased risk level with feature "*i*" assumed to be perfectly reliable.

The first importance measure, risk achievement worth (RAW), related to risk increase potential, is defined as ratio:

$$RAW_i = \frac{R_i^+}{R_0} \tag{1}$$

(Besides ratio, NUREG/CR-3385 also defines the RAW on an interval scale as $R_i^+ - R_0$. These two values are related to each other. When one is known, the other can be calculated directly (considering that nominal risk $R_0$ would normally be known).)

The second importance measure, related to risk decrease potential, risk reduction worth (RRW), is defined as ratio:

$$RRW_i = \frac{R_0}{R_i^-} \tag{2}$$

(In the similar fashion, NUREG/CR-3385 also introduces the related RRW on an interval scale, as $R_0 - R_i^-$.)

## 2 THEORETICAL RELATION BETWEEN *RAW* AND *RRW* AND SOME DIRECT IMPLICATIONS

First, two basic terms are introduced which will be used in the considerations to come. Both of them are "events":

*A* Failure or unavailability of component or safety feature, when challenged. (This failure or unavailability is presented in a PSA model by specifically defined single basic event.)

*B* Occurrence of specified top event representing certain damage state of considered system or facility (e.g. reactor core damage).

The probability of top event *B*, i.e. *P(B)*, will be taken as a surrogate for the quantitative risk *R* which was used in the above general expressions for importance measures. This is normally done in PSA models. One issue with this is that some of the most important quantitative risk surrogates

in PSAs are expressed as frequencies rather than probabilities, e.g. core damage frequency (CDF). The frequency is brought into the risk equation by initiators, which are frequency-type events. For the sake of simplicity, we will, without mathematical formalism, "bypass" this issue by assuming that frequency-type event can be interpreted as occurrence within specified time unit, i.e. frequency is interpreted as probability of occurrence within specified time unit interval (which can always be selected as sufficiently small, so that the interpretation is valid).

Particularly, RAW is, in principle, not defined for the initiators, as frequency type events. Setting the frequency to the value of "1" (i.e. occurrence guaranteed), would imply the assumption that initiator occurs once per unit of time considered. With the above interpretation, setting the frequency-type event to logical value of "1" corresponds to assuming that its occurrence is guaranteed within the time unit (or that the probability of its occurrence during the time unit is 1.0).

Based on their above definitions, the RAW importance measure ( $I_{RAW}$ ) and the RRW importance measure ( $I_{RRW}$ ) can, most generally, be defined as:

$$I_{RAW} = \frac{P(B|A)}{P(B)} \tag{3}$$

(i.e. the ratio of the conditional probability of top event under the assumption that considered component or feature would always fail when challenged and the base case top event probability)

$$I_{RRW} = \frac{P(B)}{P(B|\overline{A})} \tag{4}$$

(i.e. ratio of the base case top event probability and the conditional probability of top event under the assumption that considered component or feature would never fail when challenged).

By expanding the above definition of RAW into:

$$I_{RAW} = \frac{P(B|A)}{P(B)} = \frac{P(BA)}{P(B)P(A)} \tag{5}$$

and considering $B = B(A+\overline{A}) = BA + B\overline{A}$ and, consequentially, $P(B) = P(BA) + P(B\overline{A})$, it can easily be shown that:

$$I_{RRW} = \frac{1-P(A)}{1-P(A)I_{RAW}} \tag{6}$$

or:

$$I_{RAW} = \frac{I_{RRW} - 1 + P(A)}{P(A)I_{RRW}} \tag{7}$$

The above relation was discussed, e.g., in [8] which also provides its demonstration by calculations based on a PSA model.

Thus, the importance measures RAW and RRW for particular failure event are related to each other, with probability of considered failure event as a parameter. The first direct and simple implication is that if one of the importance measures RAW or RRW is known, then the other one is determined (assuming that the failure probability is known). It is useful to point out that the above relation is established on the basis of probability theory and is not specific for PSA modeling or for any kind of particular features of PSA model.

Second implication is related to the upper bounds for the two measures. Concerning RRW, its definition given by Eq. (4) implies that it can, theoretically, go to infinity. This would be the case

when the system considered (top event) is represented by the considered feature, such that $B = A$ and $P(B) = P(A)$. In this case, if considered feature $A$ is assumed to be "perfect" (i.e. $P(A) = 0$) the denominator in Eq. (4) would go to zero and RRW would go to infinity. Of course, the assumption is that nominal system failure probability is larger than zero. In the case of RAW, the definition given by Eq. (3) appears to imply that RAW can become arbitrarily large. However, RAW can actually acquire the values only within the interval $\langle 1, \frac{1}{P(A)} \rangle$. This can be clearly seen from Eq. (7) when letting $I_{RRW}$ to go to large values. Figure 1 illustrates the case with $P(A) = 0.1$, which shows that RAW would asymptotically go to $\frac{1}{P(A)} = 10$ .

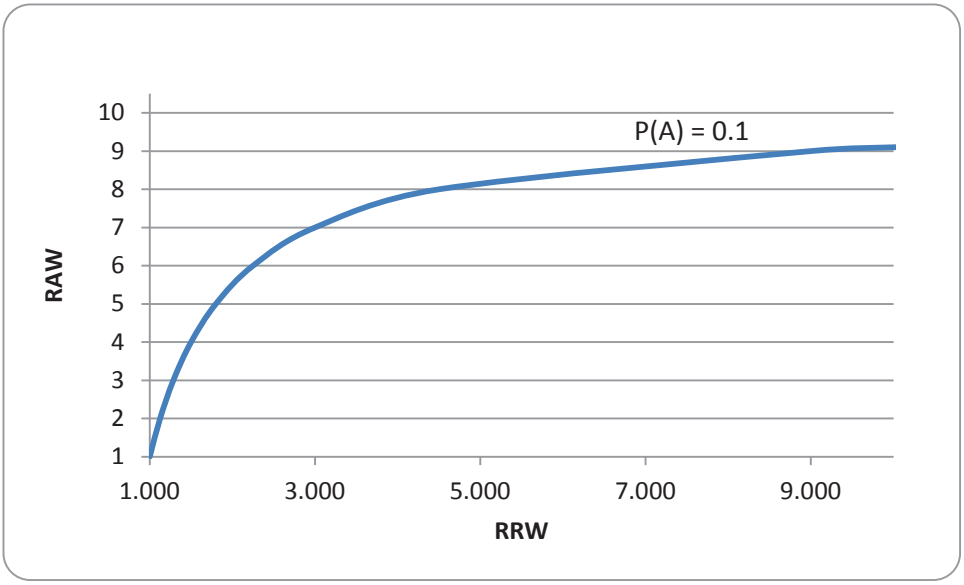


Figure 1: RAW as a Function of RRW with $P(A) = 0.1$ as Parameter

Then, there is third implication which is derived from the second one: large RAW importance measure (possibly implying not well balanced design from the risk perspective) is really a concern with small failure probability events (because RAW is bounded by $\frac{1}{P(A)}$). Non-reliable components cannot have huge RAW. They cannot achieve huge risk because they already are non-reliable (within the nominal risk estimate). On the other hand, a component with very low failure probability (low unavailability) or very high reliability can achieve huge risk (if there are no redundant or diverse means to compensate for its failure). For highly reliable component there is always hazard that its reliability (availability) may degrade. If such a component (or feature or a condition (e.g. failure mode) which may affect multiple components) represents a single line of defense then reliance on its high reliability or availability would reflect as high RAW value and may point to not well balanced risk profile.

This implication is further discussed in the next section through considering two strategies for reducing the overall risk of a system (facility) by reducing the RRW of its particular safety feature (e.g. component).

## 3 TWO STRATEGIES FOR REDUCTION OF FACILITY'S RISK BY CONTROLLING (DECREASING) *RRW* VALUE OF FEATURE *A*

Let us consider a situation where a safety feature (e.g. component) *A* within a system (facility) *B* has significant potential for reducing the system's risk *P(B)*, which reflects in significant value of its RRW measure, i.e $I_{RRW}(A)$.

There are two basic strategies for reducing the risk of the facility *B* with respect to particular feature *A* by controlling (decreasing) the RRW of considered feature *A* (i.e. $I_{RRW}(A)$):

**Strategy I**: *Decreasing the* $I_{RRW}(A)$ *with failure probability P(A) kept at the same level*. In this strategy, the feature *A* and the operational practices associated with it are kept the same. However, some additional feature is introduced into the facility which provides for diversity or redundancy of the feature *A*. In many cases, this strategy may require considerable budget. However, in a number of cases it may be implemented in a relatively affordable way by means of flexible equipment or equipment with relaxed safety requirements.

**Strategy II**: *Decreasing the* $I_{RRW}(A)$ *by decreasing the failure probability P(A)*. Examples of this strategy may include: reducing the test/inspection period; improving testing strategies (e.g. staggered versus sequential testing); extending the scope of inspection; improving the operating procedures or maintenance procedures; extending / improving preventive or predictive maintenance; etc.. In principle, these are, usually, relatively affordable (not so expensive) measures. However, if feature *A* is defined at the level of system's train or even a system as a whole, they may include design changes such as installation of redundant components or even trains (in which case they may require considerable budget).

Important property of the *strategy I* is that RAW value of feature *A* in the new constellation always decreases or, if already close to the asymptote (i.e. $\frac{1}{P(A)}$), remains the same (but never increases). In principle, this means that risk profile of the facility's new status (with lower risk) remains, as far as the feature *A* is of concern, as balanced as it was.

This is illustrated by Figure 2 where the RRW of considered feature *A* is reduced from an old value ($RRW_{old}$) to a new value ($RRW_{new}$) by moving downward through a curve defined by *P(A) = const*. Clearly, the respective RAW value would always decrease. (It should be noted that graphical presentation in Figure 2 is based on the same relation between RAW and RRW as in the case of Figure 1. The only difference is that the axes RAW and RRW have exchanged places and that Figure 2 shows only the segment of the curve corresponding to the RRW values between 1.0 and 1.3. This range of RRW values is more relevant from the perspective of practical applications of PSAs for NPPs.)

On the other hand, in the case of the *strategy II* the RAW value of feature *A* can, in the new constellation, increase. This means that although the overall risk is reduced, the risk profile may become unbalanced in the sense that there is over-reliance on the high reliability / availability of the considered feature *A*.

This is illustrated by Figure 3. In order to achieve the same decrease in RRW value of the considered feature *A* (i.e. from the same $RRW_{old}$ to the same $RRW_{new}$), certain reduction in failure probability or unavailability *P(A)* would be needed. How large, exactly, the reduction in *P(A)* would be required (for the predefined decrease in RRW) would depend on the configuration of the facility or system *B*, i.e. on its elements other than *A*. Figure 3 clearly shows that reduction in *P(A)* from the initial 0.03 to 0.02 already causes the increase in the RAW of feature *A*. (Even smaller reductions in *P(A)* than from 0.03 to 0.02 may cause an increase in the RAW.) If reductions larger than this are needed, an increase in the RAW may be considerable.

The above should be considered in the context where there are already well established and recognized guidelines with safety significance threshold set at RAW > 2 (e.g. NEI 00-04, [9]).

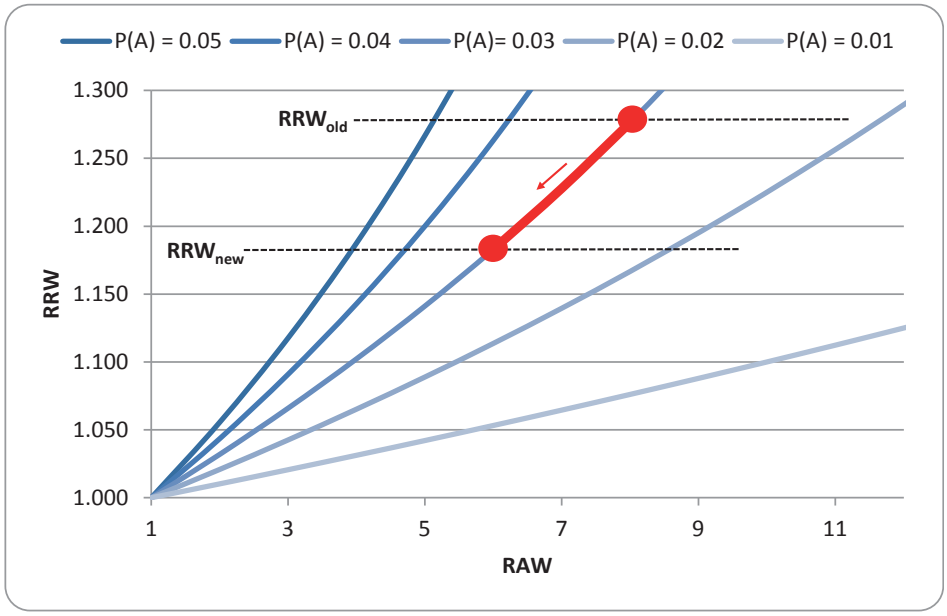


Figure 2: Reducing the Risk with Feature A Involved via Strategy I

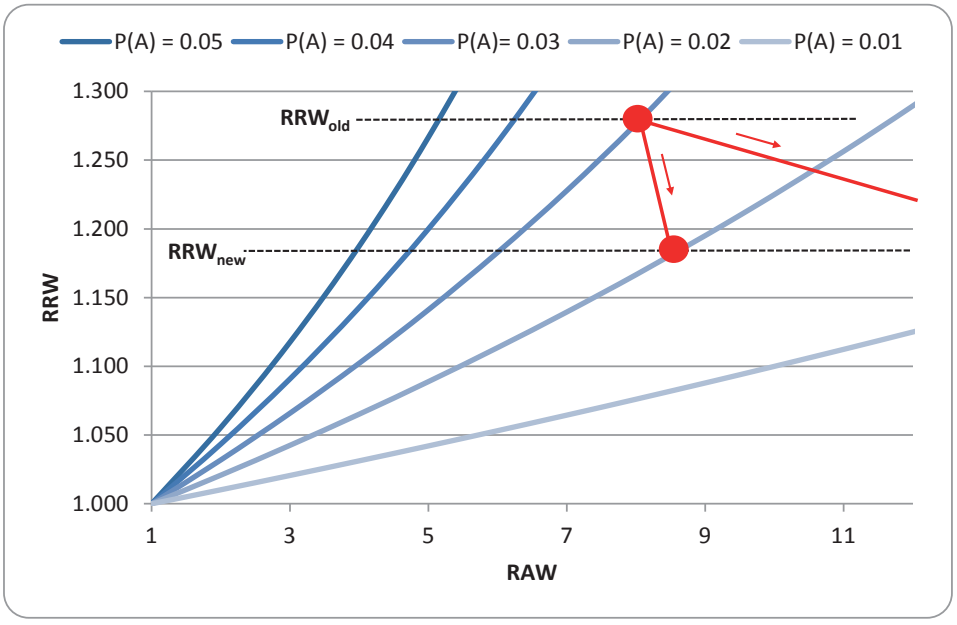


Figure 3: Reducing the Risk with Feature A Involved via Strategy II

The points of discussion will be illustrated on two very simple examples.

## 4 SIMPLE ILLUSTRATIVE EXAMPLES FOR THE TWO STRATEGIES

### 4.1 First Example: Feature "A" Represents Whole System

The first is an example where considered feature *A* represents the whole system (facility), so that its failure represents the failure of the whole system, i.e. *B = A* and *P(B) = P(A)*. Under these circumstances, the RRW asymptotically goes to infinity (since $P\big((B|\bar{A}) = P(B|\bar{B})\big)$ goes to zero) while, according to Eq. (7), RAW becomes $\frac{1}{P(A)}$ (considering $P\big((B|A) = P(B|B) = 1\big)$). Although the example is elementary, it is still good enough to illustrate the point.

The initial value $P(A) = q_0$ will be set to 0.1. The initial *P(B)* is then:

$$P_{init}(B) = q_0 = 0.1 \tag{8}$$

The initial RAW is 10 (i.e. $\frac{1}{P(A)}$).

The two strategies described above are, for this example, illustrated by means of simple reliability diagrams in Figure 4. In the *strategy I* reduction of risk (presented by reduction of the system failure probability) is obtained by adding a new feature *R* as an alternative to the existing feature *A*. New system status is, in terms of the reliability diagram, presented as parallel configuration of the two features. In the case of *strategy II* the overall reduction of risk (reduction of system failure probability) relies solely on reduction of failure probability of the existing feature *A*. There is no alternative "way out" (success path).

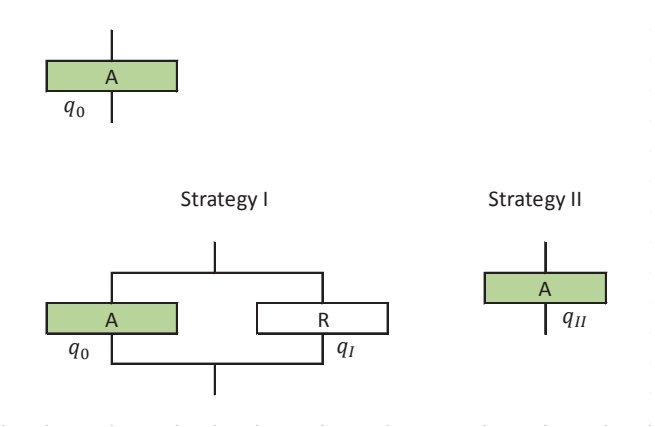


Figure 4: Two Strategies in the First Example

With notation as in Figure 4, the final system failure probability (upon implementation of a strategy) is obtained as

$$P_{fin,I}(B) = P(A)P(R) = q_0 q_I \tag{9}$$
$$P_{fin,II}(B) = P_{II}(A) = q_{II}$$

where indices *I* and *II* refer to the strategies *I* and *II*, respectively. (In the case of the strategy *I* the initial failure probability of feature *A*, *P(A)*, remains as is, in accordance with description of the

strategy. System failure probability (i.e. risk) is controlled by the failure probability of alternative feature *R*.)

Table 1: First Example – Five Cases of Reduced Risk

| Case | $P(B)_{fin}$ | $P(R) = q_I$ | $P_{II}(A) = q_{II}$ |
|---|---|---|---|
| a | 0.09 | 0.9 | 0.09 |
| b | 0.08 | 0.8 | 0.08 |
| c | 0.07 | 0.7 | 0.07 |
| d | 0.06 | 0.6 | 0.06 |
| e | 0.05 | 0.5 | 0.05 |

Table 1 shows five cases ("a" through "e") where failure probability of alternative feature *R* (*strategy I*) and new, reduced, failure probability of the existing feature *A* were selected in such a way that final system probability, *P(B)*, is same for both strategies (i.e. $P_{fin,I}(B) = P_{fin,II}(B)$, considering Equation (9)).

Thus, both strategies are equally successful in quantitatively reducing the overall risk.

However, the point of interest is the new RAW value of the feature *A* (which remains the main safety feature of the system in any case) in the new status of the system. Table 2 shows how the RAW value changes with reducing the risk through the same five cases shown in Table 1. It can be seen that in the case of the strategy *I* the RAW of the feature *A* remains the same whereas at strategy *II* as the risk decreases the RAW of the feature *A* increases. As the risk is cut in half, the RAW of *A* gets doubled. This comes from the fact that the feature *A* is a single line of defense and indicates, in a way, that the risk is not well balanced. It is worth mentioning that the same risk impact is at strategy *I* obtained with additional feature *R* which has relatively low reliability (failure probabilities in the range from 0.5 through 0.9).

Table 2: First Example – RAW Values in Five Cases Considered

| Case | $I_{RAW,I}(A)$ | $I_{RAW,II}(A)$ |
|---|---|---|
| a | 10 | 11.11 |
| b | 10 | 12.50 |
| c | 10 | 14.29 |
| d | 10 | 16.67 |
| e | 10 | 20.00 |

### 4.2 Second Example: Feature "A" As Part of Series Configuration

Second example, illustrated by the reliability diagram in Figure 5, is the case where considered safety feature *A* appears in series with another feature, designated as *L* in the mentioned figure. Therefore, feature *A* is necessary for operability of the system, but is not sufficient. In terms of risk (represented by a failure of the system), the risk cannot be eliminated solely by means of making the feature *A* "perfect" as was the case in the first example.

The initial value $P(A) = q_0$ will be set to 0.01 . The initial value of feature *L* will be set to the same value, i.e. $P(L) = p = 0.01$ .

Under the rare event approximation the initial *P(B)* is:

$$P_{init}(B) = p + q_0 = 0.02 \tag{10}$$

The RRW under the same approximation is $\frac{p+q_0}{q_0} = 2$ , and the initial RAW is $\frac{1}{p+q_0} = 50$ .

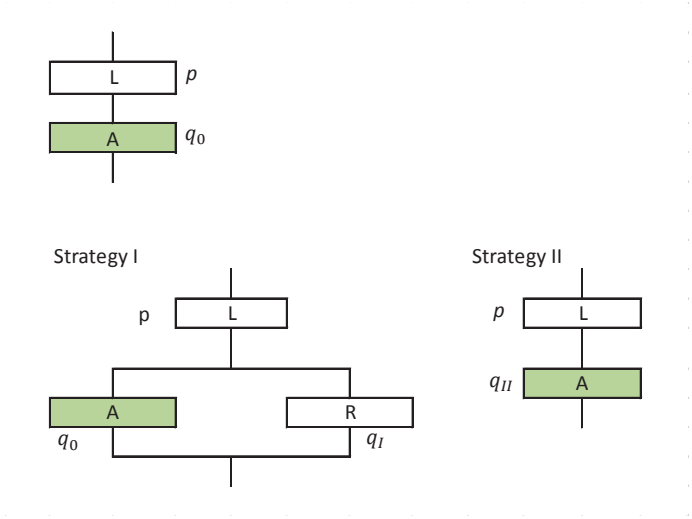


Figure 5: Two Strategies in the Second Example

With notation as in Figure 5 and under the rare event approximation, the final system failure probability (upon implementation of a strategy) is obtained as

$$P_{fin,I}(B) = P(L) + P(A)P(R) = p + q_0 q_I \tag{11}$$
$$P_{fin,II}(B) = P(L) + P_{II}(A) = p + q_{II}$$

where indices *I* and *II* refer to the strategies *I* and *II*, respectively.

In the similar manner as above, Table 3 shows five cases ("a" through "e") where failure probability of alternative feature *R* (*strategy I*) and new, reduced, failure probability of the existing feature *A* were selected in such a way that final system probability, *P(B)*, is same for both strategies (i.e. $P_{fin,I}(B) = P_{fin,II}(B)$, considering Equation (11)).

Thus, as before, both strategies are equally successful in quantitatively reducing the overall risk.

Similarly to the first example, Table 4 shows how the RAW value of feature *A* changes with reducing the risk through the same five cases shown in Table 3. This time it can be seen that, as the overall risk decreases, the RAW of the feature *A* in the case of the strategy *I* decreases also, whereas at strategy *II* it increases again. As the risk is reduced by 25%, the RAW of *A* increases by some 33%. The reason is the same as in the previous case, only that this time the feature A is not a single line of defense on its own: it is only a part of it. The observation, again, indicates that the risk is not well balanced. It is again mentioned that the same risk impact is at strategy *I* obtained with additional feature *R* which has relatively low reliability (failure probabilities in the range from 0.5 through 0.9).

Table 3: Second Example – Five Cases of Reduced Risk

| Case | $P(B)_{fin}$ | $P(R) = q_I$ | $P_{II}(A) = q_{II}$ |
|---|---|---|---|
| a | 0.019 | 0.9 | 0.009 |
| b | 0.018 | 0.8 | 0.008 |
| c | 0.017 | 0.7 | 0.007 |
| d | 0.016 | 0.6 | 0.006 |
| e | 0.015 | 0.5 | 0.005 |

Table 4: Second Example – RAW Values in Five Cases Considered

| Case | $I_{RAW,I}(A)$ | $I_{RAW,II}(A)$ |
|---|---|---|
| a | 47.89 | 52.63 |
| b | 45.00 | 55.56 |
| c | 41.76 | 58.82 |
| d | 38.13 | 62.50 |
| e | 34.00 | 66.67 |

## 5 CONCLUSION

Basic theoretical relation between the RAW and the RRW importance measures was discussed, together with some of its direct implications on risk considerations. In this context, the two basic strategies were discussed for reducing the risk of the facility with respect to particular safety feature by controlling (decreasing) the RRW of considered feature: 1) decreasing the RRW with failure probability kept at the same level, and 2) decreasing the RRW by decreasing the failure probability. It was shown that in the first case the RAW of the considered feature decreases while in the second case it can also increase, depending on the role the considered safety feature has in the facility's configuration. This means that although the overall risk is reduced, the risk profile may become unbalanced in the sense that there is over-reliance on the high reliability / availability of the considered feature *A*.

Even the simplistic examples which were discussed point to the importance of diversification of safety functions. Additional diverse (alternative) features may even not necessarily have particularly high reliability.

In this simple exercise no attempt was made to address the common cause failure potential, but it is considered that it would only strengthen the conclusions.

In some cases, it may be easier to introduce an alternative success path with flexible or/and movable equipment with relaxed safety classification requirements than to demonstrate that certain risk target is achieved through improved testing, inspection, maintenance or quality assurance strategies.

## REFERENCES


[1] Fullwood, Ralph R., Hall, Robert E., Probabilistic Risk assessment in the Nuclear Power Industry, Fundamentals and Applications, Pergamon Press, 1988.

[2] Henley, E.J., Kumamoto, H., Reliability Engineering and Risk Assessment, Prentice-Hall, Inc., 1981.

[3] Barlow, R. E., Proschan, F., Statistical Theory of Reliability and Life Testing: Probability Models, Holt, Rinehart and Winston, Inc., 1975

[4] Vesely, W. E. et al., Measures of Risk Importance and Their Applications, NUREG/CR-3385, Battelle Columbus Laboratories / U.S. NRC, 1983.

[5] Vesely, W. E. et al. Fault Tree Handbook, NUREG-0492, U.S. NRC, 1981.

[6] Papazoglou, I.A. et al., Probabilistic Safety Analysis Procedures Guide, NUREG/CR-2815, Brookhaven National Laboratory / U.S. NRC, 1984.

[7] ASME/ANS RA-Sa–2009, Addenda to ASME/ANS RA-S–2008 Standard for Level 1/Large Early Release Frequency Probabilistic Risk Assessment for Nuclear Power Plant Applications, An American National Standard, The American Society of Mechanical Engineers, 2009.

[8] I. Vrbanic, P. Samanta and I. Basic, Risk Importance Measures in the Design and Operation of Nuclear Power Plants, The American Society of Mechanical Engineers, New York, 2017.

[9] NEI 00-04, 10 CFR 50.69 SSC Categorization Guideline, Revision 0, Nuclear Energy Institute, July 2005 (http://adams.nrc.gov/wba/, Accession No.: ML052900163, as of July 15, 2016)

# ENERGIJA